SPECTROCHIMICA ACTA

COMMENTARIUM SCIENTIFICUM INTERNATIONALE
TRACTANS DE RE SPECTROCHIMICA

PRIMO EDITUM A

A. GATTERER S.J. †
SPECOLA VATICANA CASTEL GANDOLFO

COLLABORANTIBUS

A. BARDÓCZ-BUDAPEST · **C. G. CARLSSON**-STOCKHOLM · **R. CASTRO**-UGINE · **N. D. COGGESHALL**-PITTSBURGH, PA. · **G. H. DIEKE**-BALTIMORE · **J. H. ENNS**-ANN ARBOR, MICH. · **Wa. GERLACH**-MUNICH · **G. HANSEN**-OBERKOCHEN · **G. R. HARRISON**-CAMBRIDGE, MASS · **J. JUNKES S.J.**-CASTEL GANDOLFO · **J. M. LÓPEZ de AZCONA**-MADRID **R. MANNKOPFF**-GÖTTINGEN · **W. MARTI**-WINTERTHUR · **A. E. MARTIN**-NEWCASTLE **O. MASI**-TURIN · **R. MECKE**-FREIBURG · **W. F. MEGGERS**-WASHINGTON, D.C. · **A. C. MENZIES**-LONDON · **FOIL A. MILLER**-PITTSBURGH, PA. · **K. PFEILSTICKER**-STUTTGART · **J. M. PHÉLINE**-UGINE · **W. ROLLWAGEN**-MUNICH · **R. A. SAWYER**-ANN ARBOR, MICH. · **R. SCHMIDT**-AMSTERDAM · **R. O. SCOTT**-ABERDEEN · **B. F. SCRIBNER**-WASHINGTON, D.C. · **D. M. SMITH**-WEMBLEY · **L. W. STROCK**-BAYSIDE, NEW YORK · **F. TWYMAN**-LONDON

VOL.
7
55/56

EDITUM A

R. BRECKPOT — LOUVAIN
V. A. FASSEL — AMES, IOWA
H. KAISER — DORTMUND
E. LOEUILLE — PARIS
R. L. MITCHELL — ABERDEEN
E. H. S. van SOMEREN — LONDON
H. W. THOMPSON — OXFORD

VOLUME VII

1955–6

PERGAMON PRESS LTD · LONDON & NEW YORK

SPECTROCHIMICA ACTA

EDITORS

BELGIUM AND THE NETHERLANDS

Prof. R. Breckpot, Institut de Chimie, 98 Rue de Namur, Louvain, Belgium

FRANCE

E. Loeuille, Laboratoire Central de l'Armament, Place St. Thomas d'Aquin, Paris, France

GERMANY AND AUSTRIA

Dr. H. Kaiser, Institut für Spektrochemie und Angewandte Spektroskopie, Dortmund-Aplerbeck, Marsbruchstr. 186, Bau I, Germany

GREAT BRITAIN AND BRITISH COMMONWEALTH OF NATIONS

Dr. R. L. Mitchell, Macaulay Institute for Soil Research, Craigiebuckler, Aberdeen, Scotland

Dr. H. W. Thompson, F.R.S., St. John's College, Oxford

E. H. S. van Someren, B.Sc., F.Inst.P., 4 Churchfields, Broxbourne, Herts., England

UNITED STATES OF AMERICA

Dr. V. A. Fassel, Iowa State College, Ames, Iowa, U.S.A.

CONTENTS OF VOLUME VII

No. 1

Page

J. K. Hurwitz: Some observations on sparked craters in spectrographic microvolume analysis 1

M. Margoshes and V. A. Fassel: The infrared spectra of aromatic compounds—I. The out-of-plane C-H bending vibrations in the region 625–900 cm^{-1} . . 14

G. Duyckaerts: Contribution à l'analyse quantitative par les spectres d'absorption infrarouge des poudres—I. Examen théorique de la question 25

J. Bonhomme: Contribution à l'analyse quantitative par les spectres d'absorption infrarouge des poudres—II. Etude expérimentale 32

N. W. H. Addink, J. A. M. Dikhoff, Frl. C. Schipper, A. Witmer und T. Groot: Quantitative spektrochemische Analyse mittels des Gleichstrom Kohlebogens . 45

Spectrochemical Notes:

J. Junkes, S.J. und E. W. Salpeter, S.J.: Effektive Linienbreiten in der Spektralphotometrie 60

S. A. Clarke: A drum attachment to a travelling microscope for direct wavelength reading of spectral lines 64

No. 2

Edward C. Y. Inn: Vacuum ultraviolet spectroscopy 65

D. F. C. Morris and F. M. Brewer: The spectrochemical determination of gallium in blende 88

I. Adler and J. M. Axelrod: Internal standards in fluorescent X-ray spectroscopy 91

San-Ichiro Mizushima, Masamichi Tsuboi, Takehiko Shimanouchi and Yoshizo Tsuda: Spectroscopic investigation of the strength of hydrogen bonds formed by amides 100

A. Walsh: The application of atomic absorption spectra to chemical analysis . 108

VOL
7
1955/

Contents

Page

W. J. PRICE: The determination of trace elements in magnesium and its alloys by spectrographic procedures 118

Spectrochemical Notes:

M. NORDMEYER: Über die Ausleuchtung von Spektrographen 128

K. BUNGE: Ein elektronischer Steuermechanismus für einen Niederspannungsfunkenerzeuger 134

No. 3

J. W. KEMP, M. F. HASLER, J. L. JONES and LOUIS ZEITZ: Multichannel instruments for fluorescent X-ray spectroscopy 141

C. M. CUNDALL and J. D. CRAGGS: Electrode vapour jets in spark discharges . 149

J. McK. NOBBS and P. T. BEALE: The use of intensity scales in the microphotometry of spectra 165

VELMER A. FASSEL and HENRY J. HETTEL: Isotopic assay of lithium by means of hydride band emission spectra 175

Book reviews:

"Optische Messungen des Chemikers und des Mediziners" by FRITZ LÖWE (reviewed by R. L. MITCHELL) 179

"L'analyse spectrale quantitative par la flamme" by R. MAVRODINEANU and H. BOITEUX (reviewed by R. L. MITCHELL) 179

"Index to the Literature on Spectrochemical Analysis" by BOURDON F. SCRIBNER and WILLIAM P. MEGGERS (reviewed by E. VAN SOMEREN) 180

"La Spectroscopie d'Emission" by PIERRE MICHEL (reviewed by E. VAN SOMEREN) . . 180

No. 4

WILBUR KAYE: Near-infrared spectroscopy—II. Instrumentation and technique 181

Spectrographic analysis of nominally pure lead 205

G. J. PITT and the late M. F. FLETCHER: The spectrographic determination of germanium in coal and flue dust 214

G. ECKER: Periodische Erscheinungen bei der Metallablösung an der Oberfläche von Mehrstoffsystemen 219

F. T. BIRKS: The spectrographic estimation of sub-microgram quantities of beryllium by the cathode layer technique 231

Á. BARDÓCZ: Electronically controlled spectrographic low-voltage spark, interrupted arc and d.c. arc source 238

Spectrochemical Notes:

F. J. HAFTKA: Zur Bestimmung der Transformationszahl κ 242

W. MARTI: Elektronische Regulierung der Ladespannung von Kondensatoren in Funkenerzeugern 246

Book Reviews:

"Einführung in die Ultrarotspektroskopie" by W. BRÜGEL (reviewed by H. W. THOMPSON) 250

"The Infra-red Spectra of Complex Molecules" by L. J. BELLAMY (reviewed by H. W. THOMPSON) 250

"Quantitative Spectrochemical Analysis of Silicates" by L. H. AHRENS (reviewed by CYRUS FELDMAN) 251

Announcements 252

VOL. 7 55/56

Contents

Page

No. 5

D. H. WHIFFEN: Infra-red summation bands of the out-of-plane C-H bending vibrations of substituted benzene compounds 253

L. HULDT: Zur Deutung spektroskopischer Temperaturmessungen 264

L. CENCELJ and D. HADŽI: Infra-red spectra of polychloronaphthalenes . . 274

JACOB SHERMAN: The theoretical derivation of fluorescent X-ray intensities from mixtures 283

Á. BARDÓCZ: Investigations concerning light sources for spectrum analysis—IV. High-voltage spark source with electronic control and its electrical characteristics 307

No. 6

C. GORDON PEATTIE and L. B. ROGERS: Analytical studies of the fluorescence of samarium in calcium tungstate 321

CYRUS FELDMAN and JANUS Y. ELLENBURG: Contrast changes of Eastman Kodak Spectrum Analysis No. 1. Emulsion during cold storage, and their effect on observed intensity ratios 349

N. LOUNAMAA: Spectrographic analysis of copper-making and lead-making slags for major constituents 358

ALBERT KEIL: Über den Nachweis von Oxydationsvorgängen in der Funkenstrecke 367

H. T. SHIRLEY, A. OLDFIELD, and H. KITCHEN: A comparison of three methods of plate calibration and evaluation for routine spectrographic analysis of low-alloy steels 373

R. MECKE und H. SPIESECKE: Die Infrarot und Ramanspektren hochsymmetrischer Molekule 387

Spectrochemical Notes:

ILANA LEVITAN: Determination of tin in bismuth 395

H. J. EICHHOFF und K. PICARD: Eine Kapillarelektrode aus Metall zur direkten, spektrochemischen Untersuchung von Lösungen 396

Book Review:

"Chemical and Spectrographic Analysis of Magnesium and Its Alloys" by A. MAYER and W. J. PRICE (Reviewed by ERNEST VAN SOMEREN) 398

Announcements 398

In Memoriam 398

Author Index to Volume VII 399

Subject Index to Volume VII 401

Publishing offices: 4 & 5 Fitzroy Square, London, W.1 (EUSton 4455). Subscription per volume (including postage) £5 15s. 6d. (U.S.A. $16). Back numbers £8 ($22.40), per volume.

Distributors: U.K. only—*Hilger & Watts Ltd., (Hilger Division), 98 St. Pancras Way, London, N.W.1.*

U.S.A.—*Pergamon Press Inc., 122 E. 55th Street, New York 22, N.Y.*

All other countries—*I. R. Maxwell & Co. Ltd., 4 & 5 Fitzroy Square, London, W.1.*

PERGAMON PRESS LTD., 4 & 5 FITZROY SQUARE, LONDON, W.1
PERGAMON PRESS INC., 122 E. 55TH STREET, NEW YORK 22, N.Y.

VOL.
7
1955/5

AUTHOR INDEX TO VOLUME VII

ADDINK, N. W. H., DIKHOFF, J. A. M., SCHIPPER, Frl. C., WITMER, A., und GROOT, T.: Quantitative spektrochemische Analyse mittels des Gleichstrom-Kohlebogens. p. 45

ADLER, I., and AXELROD, J. M.: Internal standards in fluorescent X-ray spectroscopy. p. 91

AHRENS, L. A.: Quantitative Spectrochemical Analysis of Silicates. (Rev.) p. 251

AXELROD, J. M.: *see* ADLER, I.

BARDÓCZ, Á.: Electronically controlled spectrographic low-voltage spark, interrupted arc and d.c. arc source. p. 238

BARDÓCZ, Á.: Investigations concerning light sources for spectrum analysis. IV—High-voltage spark source with electronic control and its electrical characteristics. p. 307

BEALE, P. T.: *see* NOBBS, J. McK.

BELLAMY, L. J.: The Infra-red Spectra of Complex Molecules. (Rev.) p. 250

BIRKS, F. T.: The spectrographic estimation of sub-microgram quantities of beryllium by the cathode layer technique. p. 231

BREWER, F. M.: *see* MORRIS, D. F. C.

BRÜGEL, W.: Einführung in die Ultrarotspektroskopie. (Rev.) p. 250

BOITEUX, H.: *see* MAVRODINEANU, R.

BONHOMME, Mlle. J.: Contribution à l'analyse quantitative par les spectres d'absorption infrarouge des poudres. II—Étude expérimentale. p. 32

BUNGE, K.: Ein elektronischer Steuermechanismus für einen Niederspannungsfunkenerzeuger. p. 134

CENCELJ, L., and HADŽI, D.: Infra-red spectra of polychloronaphthalenes. p. 274

CLARKE, S. A.: A drum attachment to a travelling microscope for direct wavelength reading of spectral lines. p. 64

CRAGGS, J. D.: *see* CUNDALL, C. M.

CUNDALL, C. M., and CRAGGS, J. D.: Electrode vapour jets in spark discharges. p. 149

DIKHOFF, J. A. M.: *see* ADDINK, N. W. H.

DUYCKAERTS, G.: Contribution à l'analyse quantitative par les spectres d'absorption infrarouge des poudres. I—Examen théorique de la question. p. 25

ECKER, G.: Periodische Erscheinungen bei der Metallablösung an der Oberfläche von Mehrstoffsystemen. p. 219

EICHHOFF, H. J., und PICARD, K.: Eine Kapillarelektrode aus Metall zur direkten spektrochemischen Untersuchung von Lösungen. p. 396

ELLENBURG, J. Y.: *see* FELDMAN, C.

FASSEL, V. A.: *see* MARGOSHES, M.

FASSEL, V. A., and HETTEL, H. J.: Isotopic assay of lithium by means of hydride band emission spectra. p. 175

FELDMAN, C., and ELLENBURG, J. Y.: Contrast changes of Eastman Kodak Spectrum Analysis No. 1 Emulsion during cold storage, and their effect on observed intensity ratios. p. 349

FLETCHER, M. F.: *see* PITT, G. J.

GROOT, T.: *see* ADDINK, N. W. H.

HADŽI, D.: *see* CENCELJ, L.

HAFTKA, F. J.: Zur Bestimmung der Transformationszahl $\varkappa$. p. 242

HASLER, M. F.: *see* KEMP, J. W.

HETTEL, H. J.: *see* FASSEL, V. A.

HULDT, L.: Zur Deutung spektroskopischer Temperaturmessungen. p. 264

HURWITZ, J. K.: Some observations on sparked craters in spectrographic microvolume analysis. p. 1

INN, E. C. Y.: Vacuum ultra-violet spectroscopy. A review. p. 65

JONES, J. L.: *see* KEMP, J. W.

JUNKES, J., und SALPETER, E. W.: Effektive Linienbreiten in der Spektralphotometrie. p. 60

KAYE, W.: Near infra-red spectroscopy. II—Instrumentation and technique. A review. p. 181

KEIL, A.: Über den Nachweis von Oxydationsvorgängen in der Funkenstrecke. p. 367

KEMP, J. W., HASLER, M. F., JONES, J. L., and ZEITZ, L.: Multichannel instruments for fluorescent X-ray spectroscopy. p. 141

KITCHEN, H.: *see* SHIRLEY, H. T.

LEVITAN, I.: Determination of tin in bismuth. p. 395

LOUNAMAA, N.: Spectrographic analysis of copper-making and lead-making slags for major constituents. p. 358

LÖWE, FR.: Optische Messungen des Chemikers und des Mediziners. (Rev.) p. 179
MARGOSHES, M., and FASSEL, V. A.: The infra-red spectra of aromatic compounds. I—The out-of-plane C-H bending vibrations in the region 625–900 cm^{-1}. p. 14
MARTI, W.: Elektronische Regulierung der Ladespannung von Kondensatoren in Funkenerzeugern. p. 246
MAVRODINEANU, R., and BOITEUX, H.: L'analyse spectrale quantitative par la flamme. (Rev.) p. 179
MAYER, A., and PRICE, W. J.: Chemical and Spectrographic Analysis of Magnesium and its Alloys. (Rev.) p. 398
MECKE, R., und SPIESECKE, H.: Die Infrarot und Ramanspektren hochsymmetrischer Molekule. Mitteilung: Das Infrarotspektrum und die Schwingungsanalyse des Urotropins (1,3,5,7-Tetraazaadamantan). p. 387
MEGGERS, W. F.: *see* SCRIBNER, B. F.
MICHEL, P.: La spectroscopie d'émission. (Rev.) p. 180
MIZUSHIMA, S., TSUBOI, M., SHIMANOUCHI, T., and TSUDA, Y.: Spectroscopic investigation of the strength of hydrogen bonds formed by amides. p. 100
MORRIS, D. F. C., and BREWER, F. M.: The spectrochemical determination of gallium in blende. p. 88
(NOBBS, J. MCK.): Spectrographic analysis of nominally pure lead. (Report of the Lead Analysis Panel of The British Non-Ferrous Metals Research Association Spectrographic Research Committee.) p. 205
NOBBS, J. MCK., and BEALE, P. T.: The use of intensity scales in the microphotometry of spectra. p. 165
NORDMEYER, M.: Über die Ausleuchtung von Spektrographen. p. 128
OLDFIELD, A.: *see* SHIRLEY, H. T.
PEATTIE, C. G., and ROGERS, L. B.: Analytical studies of the fluorescence of samarium in calcium tungstate. p. 321
PICARD, K.: *see* EICHHOFF, H. J.
PITT, G. J., and FLETCHER, M. F.: The spectrographic determination of germanium in coal and flue dust. p. 214
PRICE, W. J.: The determination of trace elements in magnesium and its alloys by spectrographic procedures. p. 118
PRICE, W. J.: *see* MAYER, A.
ROGERS, L. B.: *see* PEATTIE, C. G.
SALPETER, E. W.: *see* JUNKES, J.
SCHIPPER, Frl. C.: *see* ADDINK, N. W. H.
SCRIBNER, B. F., and MEGGERS, W. F.: Index to the Literature on Spectrochemical Analysis. (Rev.) p. 180
SHERMAN, J.: The theoretical derivation of fluorescent X-ray intensities from mixtures. p. 283
SHIMANOUCHI, T.: *see* MIZUSHIMA, S.
SHIRLEY, H. T., OLDFIELD, A., and KITCHEN, H.: A comparison of three methods of plate calibration and evaluation for routine spectrographic analysis of low-alloy steels. p. 373
SPIESECKE, H.: *see* MECKE, R.
TSUBOI, M.: *see* MIZUSHIMA, S.
TSUDA, Y.: *see* MIZUSHIMA, S.
WALSH, A.: The application of atomic absorption spectra to chemical analysis. p. 108
WHIFFEN, D. H.: Infra-red summation bands of the out-of-plane C-H bending vibrations of substituted benzene compounds. p. 253
WITMER, A.: *see* ADDINK, N. W. H.
ZEITZ, L.: *see* KEMP, J. W.

VOL. 7 1955/

SUBJECT INDEX TO VOLUME VII

PAGE

Absorption (*see* also Atomic absorption):
Effects in fluorescent X-ray spectroscopy 92
spectrophotometry in the vacuum UV 75
IR — spectra in powder analysis 25, 32
Alloys, Periodic variations of volatilization during sparking 219
Aluminium:
Detn in slags 358
Detn of traces in Mg and alloys . 121
Amides, Spectroscopic detn of strength of forming H-bonds 100
Announcements:
Colloquium Spectrosc. Intern. VI, Amsterdam 1956 252
Congress on Anal. Chemistry, Lisbon 1956 252
Meetings of Society of Appl. Spectroscopy, New York, Philadelphia . 398
Antimony in pure Pb, Line pairs . . 210
Arc (*see* also Excitation sources):
Constant temperature d.c. — . 45
Aromatic compounds, Out-of-plane C-H bending vibration bands . . . 14
Arsenic in pure Pb, Line pairs . . 210
Atomic absorption:
spectra in spectrochemical analysis 108
and concentration . . . 111
Coefficient of —, Experimental detn 113
Atomic concentration and atomic absorption 111
Background correction in analysis of pure Pb 211
Band specta (*see* also Absorption, Vibration spectra):
Emission — of LiH for isotopic assay 175
Barium, Detn of traces in Mg and alloys 122
Benzene compounds:
Summation bands of the out-of-plane C-H bending vibrations of substituted — 253
Beryllium:
Detn of submicrogram quantities by cathode layer method . . 231
Detn of traces in Mg and alloys . 122
Bismuth:
in pure Pb, Line pairs . . 210
Detn of Sn in — 395

PAGE

Book reviews:
Chemical and Spectrographic Analysis of Mg and its Alloys (MAYER) 398
Chemistry, Optical Measurements in — and Medicine (LÖWE) . . 179
Complex Molecules, IR Spectra (BELLAMY) 250
Flame Method in Spectral Analysis (MAVRODINEANU) 179
Index to Spectrochem. Literature (SCRIBNER) 180
IR Spectra of Complex Molecules (BELLAMY) 250
IR Spectroscopy, Introduction to — (BRÜGEL) 250
Literature Index to Spectrochem. Analysis (SCRIBNER) . . 180
Medicine, Optical Measurements in Chemistry and — (LÖWE) . . 179
Optical Measurements in Chemistry and Medicine (LÖWE) . . 179
Spectrochemical Analysis (MICHEL) 180
by Flame Method (MAVRODINEANU) 179
of Mg and its Alloys (MAYER) . 398
of Silicates (AHRENS) . . 251
Literature Index (SCRIBNER) . 180
Boron, Detn of traces in Mg and alloys 122
C-H, Out-of-plane bending vibrations:
of aromatic compounds in the IR . 14
of substituted benzene compounds in the IR. 253
Cadmium in pure Pb, Line pairs . . 210
Calcium:
Detn in slags 358
Detn of traces in Mg and alloys . 122
Calcium tungstate, Fluorescence of Sm in — 396
Carbon arc of constant temperature for quantitative analysis . . . 45
Cathode layer technique for detn of Be in submicrograms 231
Coal, Detn of Ge in — 214
Complex molecules, IR spectra (rev.) . 250
Concentration, Atomic — and atomic absorption 111
Condenser potential, Electronic control of — in spark sources . . . 246

	PAGE
Constant temperature d.c. carbon arc	45
Cold storage of Eastman Kodak Spectrum Analysis No. 1 Emulsion, Effects on contrast	349
Copper:	
in pure Pb, Line pairs	210
Detn in copper-making and lead-making slags	358
Craters in solid materials by sparking, Formation and shape	1
Detectors:	
for near IR spectroscopy	188
for vacuum UV spectroscopy	73
Effective line widths in photographic photometry	60
Electrodes:	
Capillary metallic — for solution analysis	396
Oxidation effects by sparking of Ag —	367
Electronic control (*see* also Excitation sources):	
of condenser potential of spark sources	246
Enhancement effects in fluorescent X-ray spectroscopy	94
Europium:	
Detn in $CaWO_4$ by fluorescence	342
Effects on Sm fluorescence	336
Excitation (*see* also Excitation sources):	
effects in fluorescent X-ray spectroscopy	94
Excitation sources:	
for near IR spectroscopy	191
for vacuum UV spectroscopy	73
Electronically controlled condenser potential for spark sources	246
d.c. arc	238
high-voltage spark	307
interrupted arc	238
low-voltage spark	134, 238
rectified low-voltage spark	238
Pulse generator of variable frequency	238
Filters for near IR spectroscopy	73
Flame method in spectral analysis (rev.)	179
Flue dust, Detn of Ge in —.	214
Fluorescence, detn of Sm in $CaWO_4$ by —	321
Fluorescent X-ray spectroscopy, *see* X-ray spectroscopy	
Gadolinium, Effect on Sm fluorescence	336
Gallium, detn in blende	88
Germanium, detn. in coal and flue dust	214
High-voltage spark, *see* Excitation sources	
Hydrogen bonds of amides, Detn of the strength of —.	100
Illumination of spectrographs	128
Impurities in pure Pb	205
Infra-red:	
spectra of C-H bending vibrations, of substituted benzenes	253
of aromatic compounds	14
spectra of complex molecules (rev.)	250
spectra of polychloronaphthalenes	274
spectrum of Urotropine	387
Infra-red spectroscopy:	
Instruments and technique in the near —	181
Introduction to — (rev.)	250
Powder analysis by —	25, 32
Instruments (*see* also Electrodes, Excitation sources):	
for fluorescent X-ray spectroscopy	141
for near IR spectroscopy	181
for vacuum UV spectroscopy	68
Capillary metallic electrodes	396
Lens array for slit illumination	132
Mirror systems for illumination of spectrographs	129
Intensities, Theoretical — in fluorescent X-ray spectroscopy	283
Intensity scales in spectral microphotometry	165
Internal standards in fluorescent X-ray spectroscopy	91
Interpretation of spectroscopic temperature measurements	264
Interrupted arc, *see* Excitation sources	
Ionization potentials of molecules:	
Detn by absorption spectroscopy in the vacuum UV	78
Iron (*see* also Steel):	
Detn of — in slags	358
Isotopes:	
Analysis by atomic absorption spectra	116
Detn of Li — by LiH emission bands	175
K value in constant temperature carbon d.c. arc analysis	45
κ in Seidel transformations	242
Lead:	
Analysis of pure —	205
Detn in slags	358
Lens array for slit illumination	132
Light sources, *see* Excitation sources	
Line intensities and temperature	264

VOL. 7 1955/

PAGE

Line widths, Effective — in photographic photometry . . . 60
Lithium:
Detn of traces in Mg and alloys . 125
Isotopic assay by LiH emission bands 175
Lithium carbonate as buffer in detn of Ge 215
Low-voltage spark, *see* Excitation sources
Magnesium:
Analysis of — and its alloys (rev.) 398
Detn in slags 358
Detn of trace elements in — and alloys 118
Measurement of wave lengths using direct reading drum . . . 64
Medicine, Optical measurements in Chemistry and — (rev.) . . . 179
Methods (*see* also Excitation, Photographic photometry, Spectral analysis):
Capillary metallic electrodes for solution analysis 396
Constant temperature d.c. carbon arc 45
Flame — in spectral analysis (rev.) 179
Illumination of spectrographs . 128
Plate calibration in routine low-alloy steel analysis . . . 373
Mirror systems for illumination of spectrographs 129
Molecular spectra, *see* Absorption, Infra-red, Vibration spectra
Near infra-red, *see* Infra-red
Neodymium, Effects on Sm fluorescence 336
Nickel in pure Pb, Line pairs . . 210
Optical materials for near IR spectroscopy 182
Optical measurements in Chemistry and Medicine (rev.) 179
Oxidation effects on Ag electrodes . . 367
Particle size, Effects in fluorescent X-ray spectroscopy 97
Photographic photometry:
by effective line widths . . 60
Contrast changes during cold storage 349
Intensity scales for microphotometers 165
Plate calibration methods for routine low-alloy steel analysis 373
Photoionization of molecules, Detn by absorption spectra in the vacuum UV 82

PAGE

Photometry, *see* Photographic photometry
Plate calibration, *see* Photographic photometry
Powder analysis by IR absorption spectroscopy 25, 32
Polychloronaphthalenes, IR spectra . 274
Pulse generator of variable frequency . 238
Quantometer, X-ray — for research and industry ARL 141
Raman and IR spectrum of Urotropine 387
Rare earths (*see* also Eu, Gd, Nd, Sm):
Detn of traces in Mg and alloys . 125
Routine analysis of low-alloy steel:
Plate calibration and evaluation . 373
Samarium, Detn in $CaWO_4$ by fluorescence 321
Seidel transformations:
Detn of κ value 242
Use in routine low-alloy steel analysis 373
Silicates, Spectrochemical analysis (rev.) 251
Silicon, Detn in slags 358
Silver:
in pure Pb, Line pairs . . . 210
Sparking-off effects on — electrodes 367
Slags: Detn of Al, Ca, Cu, Fe, Mg, Pb, Si, Zn in copper-making and lead-making — 358
Slit (*see* also Illumination, Instruments):
Effect of — width in near IR spectroscopy 191
Solid materials, Crater formation in — by sparking 1
Solution analysis using capillary metallic electrodes 396
Spark (*see* also Excitation sources):
Crater formation in solid materials 1
Discharges 149
Oxidation effects on Ag electrodes 367
Pulse generator of variable frequency for — sources . . 238
Temperature gradients in the — . 264
Spectral analysis (*see* also Instruments, Methods):
by atomic absorption spectra . 108
by constant temperature d.c. carbon arc 45
by flame (rev.) 179
by fluorescence 321
by fluorescent X-ray spectroscopy . 51
in the near IR 181

	PAGE
Spectral analysis—*contd.*	
in the vacuum UV	65
Literature (rev.)	180
of H bonds in amides	100
of isotopes	116, 175
of Mg and its alloys (rev.)	398
of powders by IR spectroscopy	25, 32
of slags from copper and lead making	358
of solutions using capillary metallic electrodes	396
Spectrochemical analysis, *see* Spectral analysis	
Spectrophotometry, Absorption — in the vacuum UV	75
Spectroscopic studies:	
of C-H bending vibrations, of aromatic compounds	14
of substituted benzene compounds	253
of spark temperature	264
Spectroscopy (*see* also Book reviews):	
Review on vacuum UV —	65
Review on near IR —	181
Sources, *see* Excitation sources	
Standards:	
of Pb alloys for detn of impurities in pure Pb	212
Internal — in fluorescent X-ray spectroscopy	91
Steel, Low-alloy —:	
Plate calibration and evaluation in routine analysis of —	373
Storage:	
Effect on contrast by cold —	349
Temperature of spark discharges	264
Tin:	
in pure Pb, Line pairs	210
Detn in Bi	395
Tin dioxide as internal standard for determination of Ge in coal and flue dust	215
Tellurium in pure Pb, Line pairs	210
Thallium in pure Pb, Line pairs	210
Trace elements, Detn of —:	
in Mg and its alloys	118
in pure Pb	205
Transformation value κ in Seidel transformations	242
Urotropine, IR and Raman spectrum	387
UV spectroscopy in the vacuum	65
Vapour jets in spark discharges	149
Vibration spectra:	
of out-of-plane C-H bending, of aromatic compounds	253
of substituted benzene compounds	14
Volatilization rates:	
in solid materials during sparking	12
Periodic variations of — in alloys	219
Wavelength measurements, using direct reading drum	64
X-ray spectroscopy, Fluorescent —:	
Absorption effects	92
Enhancement effects	94
Internal standards	91
Multichannel instruments	141
Particle size effects	97
Quantometer for —	141
Theoretical intensities in —	283
Zinc:	
in pure Pb, Line pairs	210
Detn in slags	358

VOL. 7 1955/5

Spectrochimica Acta, 1955, Vol. 7, pp. 1 to 13. Pergamon Press Ltd., London

Some observations on sparked craters in spectrographic micro-volume analysis*

J. K. HURWITZ
Physical Metallurgy Division, Mines Branch, Department of Mines and Technical Surveys, Ottawa, Ontario, Canada

(*Received* 11 *March* 1954)†

(*Accepted for publication October* 1954)

Summary—The effective spark distribution in a point-to-plane discharge was determined by making depth measurements on sparked craters produced in magnesium, zinc, and cadmium specimens. Of the several distribution functions considered, it was found that a paraboloid of revolution best described the actual distribution. After extending the observations to sparked craters produced in other metals and alloys, several conclusions were made concerning the crater's width and depth and the bulk volatilization rates (mass of material vapourized from the specimen per unit time). In magnesium, the bulk volatilization rate was in effect independent of the traverse speed, but the crater's width and depth varied with this speed. In particular, the width and depth were functions of the reciprocal of the traverse speed. Measurements of the bulk volatilization rates in a large number of metals and alloys revealed trends in which these rates increased as the melting-point and thermal conductivity of the specimens decreased. This result should be applicable to the study of sensitivity limits in the spectrographic analysis of solid specimens.

Introduction

The need to study the shape of sparked craters became evident during the development of a quantitative micro-volume technique for the analysis of segregates and inclusions and for the study of diffusion phenomena in metals and alloys. It was originally assumed [1] that the problem could be dealt with as though the spark-distribution function on the specimen's surface was a circular disc of uniform intensity. However, it was found for steel samples that the traverse theory based on this assumption no longer agreed with experimental results when the specimen was moved at a speed of 0·8 mm per min or less. Microscopic examination of the cross-section of the trough etched into the surface by the discharge suggested that the true spark distribution had given greater emphasis to the centre of the trough than the above assumption did. By assuming that the distribution function was either a paraboloid of revolution or a cap of a sphere [2], excellent agreement between theory and experiment was achieved for all traverse speeds on steel specimens. The reason that the results did not distinguish between these two distributions was that the crater formed in steel was very shallow. There was no *a priori* reason for making either of these assumptions, and it was possible that several other distributions might have been equally good. If a material were found in which the crater was considerably deeper, depth measurements at different points

* Published by permission of the Deputy Minister, Department of Mines and Technical Surveys, Ottawa, Ontario, Canada.

† Received by the publishers 26 October 1954.

in the crater could be made from which information concerning the actual spark distribution might be obtained. Low-melting-point materials, such as magnesium, zinc, and cadium, were found to be suitable for this purpose.

This paper reports the results of the microscopic examination of craters in a large number of metals and alloys to determine the spark distribution, the variation of the crater's depth and width with traverse speed, and the effects of composition and traverse speed on the rate at which material is volatilized from the specimen by the discharge. The influence of these findings on the application of the micro-volume technique to analytical problems is discussed.

Mechanism of crater formation

A crater produced by an electrical discharge is affected by the thermal conditions in and surrounding the specimen. In a discharge, an appreciable portion of

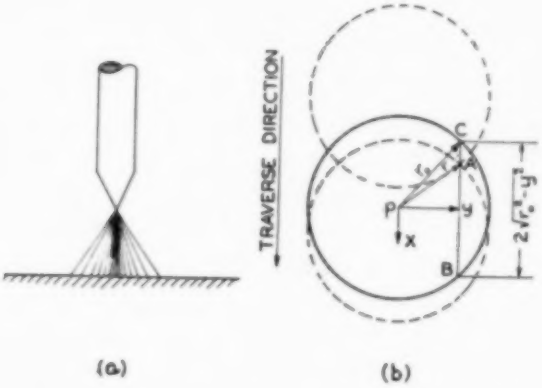

Fig. 1. (a) Schematic sketch of the spark distribution in a point-to-plane spark discharge. (b) Diagram illustrating the formation of a crater in a moving specimen.

the available energy is utilized in heating the specimen. The temperature varies from an extremely high value necessary to vaporize some material in the immediate vicinity of the discharge to temperatures relatively near room-temperature in the bulk of the specimen. This temperate distribution will depend on the thermal conductivity, specific heat, density, size, shape, and environment of the specimen as well as on the discharge characteristics. The width and depth of the sparked crater will be controlled by the rates at which heat is supplied to and conducted away from the crater and therefore by the above properties of the specimen as well as by those of the discharge.

When a spark gap of point-to-plane geometry is used, the discharge is composed of a large number of single discharges distributed in a cone with the apex at the tip of the counter-electrode (Fig. 1a). This spark distribution is circularly symmetrical about the axis of the cone, and determines the ultimate contour of the sparked crater. When the specimen is stationary, each point within the crater is attacked

by the discharge for identical time-intervals, the depth at any point being influenced by the spark distribution on the crater's surface. However, when it is moved, the situation is different, because the points near the edge of the trough are attacked by the discharge for shorter times than those points near the centre line of the trough (Fig. 1b). By assuming that each spark discharge volatilizes a constant amount of material and that the spark distribution for a moving specimen is circularly symmetrical about an axis normal to the surface of the specimen, the cross-section of the trough perpendicular to the direction of traverse may be predicted. There are a few objections to this assumption. In the first place, because of oxidation effects, there might be a difference in the specimen's state between the material immediately in front of the moving discharge and the material which has been passed over. Furthermore, it is conceivable that the amount of material volatilized by a single spark discharge depends on the path it takes to the specimen's surface. Therefore, it appears likely that the total amount of material volatilized would change with traverse speed, especially in low-melting-point materials, because it is conceivable that the crater's radius is dependent upon this speed. There might also be a serious nonsymmetry of the spark-gap geometry in the direction of traverse which might influence the spark distribution. However, these objections are not serious if it can be demonstrated that the mass of material vaporized per unit time (the bulk volatilization rate) is independent of traverse speed. In any case, the spark distribution can be considered to be an effective one instead of the actual distribution.

VOL. 7 65/56

Predicted crater shapes

Consider a few of the possible effective spark-distribution functions that may account for the shape of the trough's cross-section. If this distribution function is a circular disc of uniform intensity with the axis of circular symmetry perpendicular to the specimen's surface, the probability, p, that a given point, A (Fig. 1b), will be attacked by a single discharge is

$$\left.\begin{aligned} p &= a_0, \quad r < r_0 \\ p &= 0, \quad r > r_0 \end{aligned}\right\} \tag{1}$$

where a_0 is a constant which assumes a value necessary to ensure that the total probability is unity, r_0 is the radius of the sparked crater on the surface of the specimen, and r is the distance of the point, A, from the centre of the discharge on the specimen's surface. The total probabilty is

$$\pi r_0^2 a_0 = 1 \tag{2}$$

and

$$a_0 = \frac{1}{\pi r_0^2} \tag{3}$$

Therefore, the depth of the trough, z, etched on a moving specimen at any distance, y, from the centre line is proportional to the integral of the probability over a

straight line parallel to the transverse direction and joining the points A, B, and C (Fig. 1b).

$$z = b_0 \int_{-(r_0^2 - y^2)^{\frac{1}{2}}}^{(r_0^2 - y^2)^{\frac{1}{2}}} p \, dx$$

$$= b_0 \int_{-(r_0^2 - y^2)^{\frac{1}{2}}}^{(r_0^2 - y^2)^{\frac{1}{2}}} \frac{1}{\pi r_0^2} \, dx$$

$$= \frac{2b_0}{\pi r_0} (1 - c^2)^{\frac{1}{2}} \tag{4}$$

where
$$c = \frac{y}{r_0} \tag{5}$$

and takes all values between -1 and $+1$ and b_0 is an arbitrary constant of dimensions length^2.

Therefore,

$$\log z = \log \frac{2b_0}{\pi r_0} + \tfrac{1}{2} \log (1 - c^2) \tag{6}$$

If the effective spark distribution is described by a paraboloid of revolution,

$$\left.\begin{aligned} p &= \frac{a_0}{r_0^2} (r_0^2 - r^2) \\ &= \frac{a_0}{r_0^2} (r_0^2 - x^2 - y^2), \; r \leqslant r_0 \\ p &= 0, \; r > r_0 \end{aligned}\right\} \tag{7}$$

where a_0 has the same meaning as above. The total probability is

$$\pi \int_0^{a_0} r^2 \, dp = \pi \int_0^{a_0} r_0^2 - \frac{p r_0^2}{a_0} \, dp = \frac{\pi r_0^2}{2} \cdot a_0 = 1$$

Therefore,

$$a_0 = \frac{2}{\pi r_0^2} \tag{8}$$

The depth of the trough is

$$z = b_0 \int_{-(r_0^2 - y^2)^{\frac{1}{2}}}^{(r_0^2 - y^2)^{\frac{1}{2}}} \frac{2}{\pi r_0^4} (r_0^2 - x^2 - y^2) \, dx$$

$$= \frac{8b_0}{3\pi r_0} (1 - c^2)^{3/2} \tag{9}$$

and

$$\log z = \log \frac{8b_0}{3\pi r_0} + \frac{3}{2} \log (1 - c^2) \tag{10}$$

VOL.
7
1955/5

If the effective spark-distribution function on the specimen's surface is a cap of a sphere,

$$\left.\begin{aligned} p &= (R^2 - r^2)^{\frac{1}{2}} - (R^2 - r_0^2)^{\frac{1}{2}},\ r \leqslant r_0 \\ p &= 0, \qquad\qquad\qquad\quad r > r_0 \end{aligned}\right\} \tag{11}$$

where R is the radius of the sphere.
The total probability is,

$$\pi \int_0^{R-(R^2-r_0^2)^{\frac{1}{2}}} [r_0^2 - 2p(R^2 - r_0^2)^{\frac{1}{2}} - p^2]\, dp$$

$$= \frac{\pi}{3}[R - (R^2 - r_0^2)^{\frac{1}{2}}][R^2 - R(R^2 - r_0^2)^{\frac{1}{2}} + r_0^2] = 1 \tag{12}$$

Equation (12) is a cubic equation in R which has only one real solution. The depth of the trough is,

$$z = b_0 \int_{-(r_0^2-y^2)^{\frac{1}{2}}}^{(r_0^2-y^2)^{\frac{1}{2}}} [(R^2 - x^2 - y^2)^{\frac{1}{2}} - (R^2 - r_0^2)^{\frac{1}{2}}]\, dx$$

$$= b_0 \left[(R^2 - y^2) \arcsin \frac{(r_0^2 - y^2)^{\frac{1}{2}}}{(R^2 - y^2)^{\frac{1}{2}}} - (R^2 - r_0^2)^{\frac{1}{2}}(r_0^2 - y^2)^{\frac{1}{2}}\right] \tag{13}$$

If $R \gg r_0$, as had been assumed previously [2], equations (12) and (13) may be simplified considerably to

$$z \approx \frac{6b_0}{\pi R}(1 - |c|)(1 - c^2)^{\frac{1}{2}} \tag{14}$$

where $|c|$ is the absolute value of c.
Therefore,

$$\log z \approx \log \frac{6b_0}{\pi R} + \log (1 - |c|)(1 - c^2)^{\frac{1}{2}} \tag{15}$$

It has been suggested by LEAK [3] that a normal distribution may adequately describe this probability.

$$p = a_0 e^{-\frac{r^2}{2\sigma^2}}$$

$$= a_0 e^{-\frac{x^2+y^2}{2\sigma^2}} \tag{16}$$

where a_0 has the same meaning as above and σ is the standard deviation of the distribution. The total probability is,

$$a_0 \int_{-\infty}^{\infty} \int_{-\infty}^{\infty} e^{-\frac{x^2+y^2}{2\sigma^2}}\, dx\, dy = 1$$

Therefore,

$$a_0 = \frac{1}{2\pi\sigma^2} \tag{17}$$

The contour of the trough is,

$$z = b_0 \int_{-\infty}^{\infty} \frac{e^{-\frac{x^2+y^2}{2\sigma^2}}}{2\pi\sigma^2}\, dx = \frac{b_0}{(2\pi)^{\frac{1}{2}}\sigma} e^{\frac{y^2}{2\sigma^2}} \tag{18}$$

and

$$\log z = \log \frac{b_0}{(2\pi)^{\frac{1}{2}}\sigma} - \frac{y^2}{2\sigma^2} \log e \tag{19}$$

These equations are independent of the physical properties of the specimen and the discharge.

Experimental procedure

The traversing equipment and operating procedure for micro-volume analysis have been described elsewhere [1]. The Applied Research Laboratories "Multisource" unit was operated under the following conditions to supply a critically-damped discharge.

capacitance — 2 microfarads
inductance — 50 microhenries
resistance — 10 ohms
discharge-point control — 90 degrees.

The analytical gap spacing was 0·38 mm.

Samples of several materials (Table 1) were polished according to the procedures described in the *Metals Handbook* [4]. After the polished surfaces were traversed over the spark discharge, the specimens were cut open in a plane perpendicular to the traverse direction to reveal a transverse view about half-way along the length

Table 1. *Bulk volatilization rates*

Metal or alloy	*Analysis*	*Traverse speed (mm per min)*	*Bulk volatilization rate (mg per min)*
Aluminium	Al—99·5%	0·356	0·081
Magnesium	Mg—99·98%	0·356	0·14
Zinc	Zn—99·99%	0·356	0·14
Bismuth	Bi—99·99%	0·356	1·2
Lead	Pb—99·9%	0·356	1·7
Tin	Sn—99·9909%	0·356	0·44
Cadmium	Cd—99·99%	0·356	0·21
Magnesium alloy AZ31X	Al—3·4%, Zn—1·0%, Mn—0·49%	0·600	0·21
Low-alloy steel	Fe—92 to 99%	0·444	0·043
Copper	Cu—99·99%	0·356	<0·005
Brass	Zn—1·4 to 30·5%	0·356	<0·005
Bronze (melting stock)	Cu—84·57%, Zn—4·50%, Sn—5·41%, Pb—4·91%, Ni—0·38%	0·600	0·028

of the resultant trough. They were mounted in bakelite to show this new surface, and polished again for metallographic study. Microscopic examination and photomicrographs of the trough's cross-section were made at magnifications in the range from 50 to 140. All experiments described below were performed in quadruplicate.

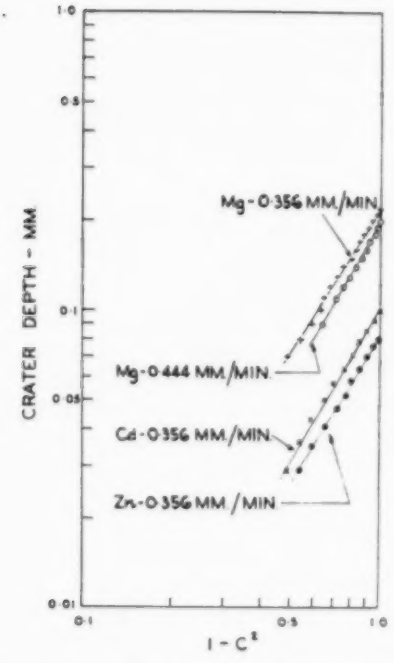

Fig. 2. Curves showing the linear characteristics of the relationship between the logarithm of the crater depth and the logarithm of $(1 - c^2)$.

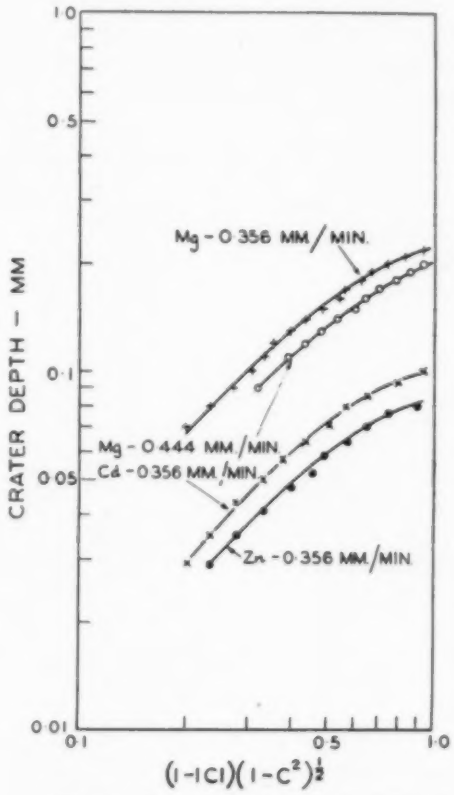

Fig. 3. Curves showing the non-linear characteristics of the relationship between the logarithm of the crater depth and the logarithm of the term $(1 - |c|)(1 - c^2)$.

The effective spark distribution

Theoretical considerations of sparked-crater formation have led to relationships [equations (6), (10), (15), and (19)] for the resultant shapes predicted by four possible spark distributions. To determine which one of these distributions was correct or most nearly fitted the experimental results, it was apparent that the logarithm of the crater depth, z, should be plotted against the logarithm of the expression, $1 - c^2$, $(1 - |c|)(1 - c^2)^{\frac{1}{2}}$ or against c^2 since c was proportional to y (equation 5). If either the circular disc of uniform intensity or a paraboloid of

revolution was the correct distribution function, the graph of $\log z$ versus $\log (1 - c^2)$ would be a straight line. In order to distinguish between these two distributions, the slope of this straight line would be measured and compared with those predicted by equations (6) and (10). If the graph of $\log z$ versus c^2 was found to be linear, the single-spark discharges would be normally distributed. The assumption of a cap of a sphere would be correct if the graph of $\log z$ versus $\log (1 - |c|)(1 - c^2)$ was a straight line.

Depth measurements were made on photomicrographs of craters produced on magnesium, zinc, and cadmium specimens which were traversed at 0·356 mm per min and magnesium specimens which were traversed at 0·444 mm per min. The

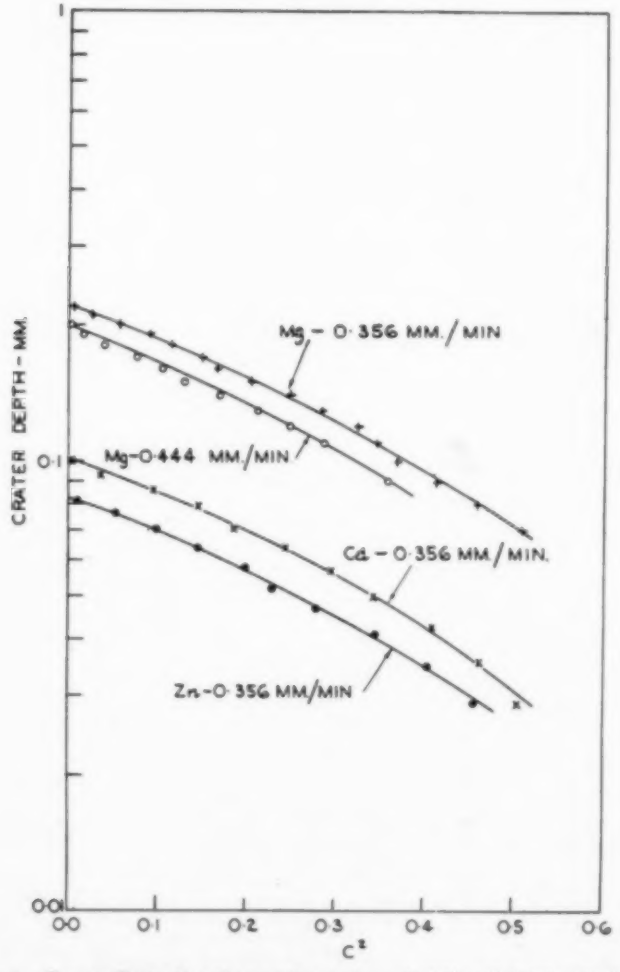

Fig. 4. Curves illustrating the non-linear characteristics of plotting the logarithm of the crater depth versus the square of the distance from the centre line of the trough at which the depth was measured.

data were plotted as described above in Figs. 2, 3, and 4. Straight-line relationships (Fig. 2) were found between $\log_{10} z$ and $\log_{10} (1 - c^2)$ with slopes somewhat greater than 3/2 (Table 2). The "Student's t" statistical test indicated that these slopes

Table 2. Slopes of $\log_{10} z$ *versus* $\log_{10} (1 - c^2)$ *curves*

Metal	*Traverse speed (mm per min)*	*Slope*
Magnesium	0·444	1·74
Magnesium	0·356	1·60
Zinc	0·356	1·66
Cadmium	0·356	1·73

Average slope	1·68
Slope predicted for paraboloid of revolution	3/2
Slope predicted for circular disc of uniform intensity	1/2

differed significantly from this value. Figs. 3 and 4 show that the single-spark discharges were not distributed as described by a cap of a sphere or by a normal distribution, respectively. Of the four assumptions, the paraboloid of revolution gave the best agreement with the experimental results, and the crater shape predicted by the use of this assumption was a very good approximation to the actual shape (Fig. 5). In spite of the fact that the "Student's t" test showed that

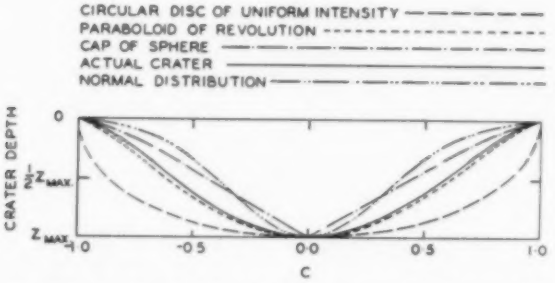

Fig. 5. Predicted and actual crater cross-sections produced in a point-to-plane spark discharge. The predicted crater shapes have been plotted from equations (4), (9), (14), and (18).

the paraboloid of revolution was not the probable distribution, it was close enough for calculation purposes in the micro-volume technique.

The effect of traverse speed

In considering the formation of craters, the assumption was made that the amount of material volatilized by each spark discharge was a constant. For the reasons discussed before, it was suspected that this may not be true, and that the validity

of this assumption could be tested by observing if any alteration in the bulk volatilization rate occurred when the traverse rate was varied over a wide range. The depth of the crater in steel was observed to change with traverse speed [2]. It was possible that the crater width would also vary in a similar way, especially in low-melting-point materials.

Magnesium specimens were traversed at speeds from 0·356 mm per min to 3·0 mm per min. Typical craters which were observed are shown in Fig. 6. The area enclosed by the crater and the original surface of the specimen was measured from the photomicrograph in each case. By multiplying these areas by the corresponding traverse speeds and the density of magnesium, measurements of the bulk volatilization rates were obtained. Within the range of speeds considered, a statistical analysis of the data showed that these rates were not significantly sensitive to changes in traverse speed (Fig. 7). Therefore it was concluded that each spark discharge volatilized a nearly constant amount of material.

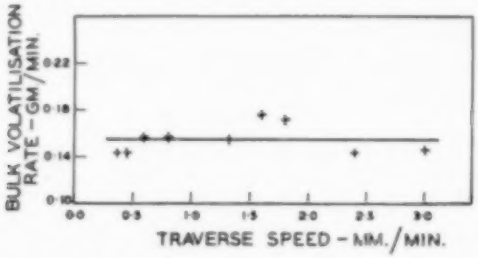

Fig. 7. Variation of the bulk volatilization rate with traverse speed in magnesium.

Examination of the craters revealed that the width and depth depended on the traverse speed (Fig. 6). Plotting the reciprocal of the traverse speed against the radius and the maximum depth of the crater as shown in Fig. 8, it appeared that linear relationships existed between these quantities on a logarithmic basis. Least-squares determinations of the lines of best fit produced the following equations:

$$s = \frac{0{\cdot}040}{z_{\max}\, 1{\cdot}5} \tag{20}$$

$$s = \frac{0{\cdot}22}{r_0\, 4{\cdot}6} \tag{21}$$

and

$$z_{\max} = 0{\cdot}32(r_0)^{3{\cdot}1} \tag{22}$$

where s is the traverse speed in millimetres per minute, $z_{\max}$ is the maximum depth of the crater, and $z_{\max}$ and r_0 were measured in millimetres. Statistical analysis of the data using the "Student's t" test indicated that the exponents of r_0 in equations (21) and (22) were not significantly different from 9/2 and 3 respectively. This result would appear to be a coincidence, since it was found [1, 2] that the radius of the crater in steel was independent of the traverse speed. Therefore, equations (20), (21), and (22) would likely be different for materials other than magnesium. The result that the crater radius increased with decreasing specimen speed meant that

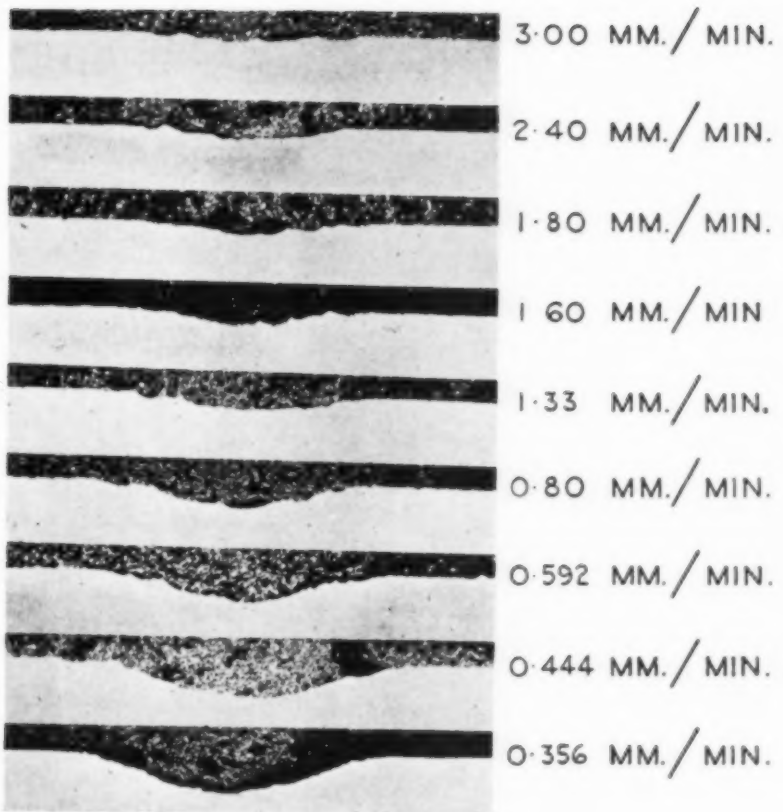

FIG. 6. Cross-sectional views of troughs produced in magnesium at different traverse rates. Specimens were unetched. Magnification ×50.

VOL.
7
1955/5

it would be disadvantageous to choose a low sample speed for the micro-volume analysis of magnesium and other low-melting-point materials. It has been shown [1] that the ability of the micro-volume technique to distinguish between two regions of different composition (the discrimination factor) was a function of the crater radius, the traverse speed, the photographic plate speed and the lengths of the spectrograph and microphotometer slits. For magnesium, a tenfold increase

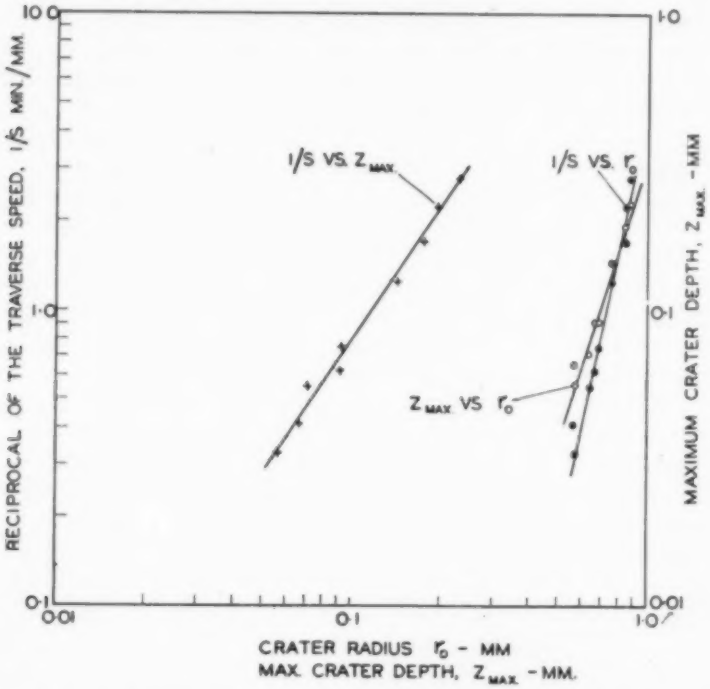

Fig. 8. Curves showing the relationships between traverse speed, crater radius, and the crater's maximum depth in magnesium.

in traverse speed would decrease the effect of the spectrograph and microphotometer slit-lengths on the discrimination factor from about twenty per cent to two per cent for typical values of these parameters. However, the resultant increase in crater radius would cause a fifty per cent increase in this factor, approximately. The maximum crater depth was not important in the traverse theory, but from a practical point of view it would be desirable to know how deep the specimen was sampled by the spark discharge in an analytical problem.

For traverse speeds in the range 0·8 to 3·0 mm per min, the craters had a rough appearance which would seem to indicate preferential sparking. At lower speeds, the craters became relatively smooth. Apparently, at high traverse speeds, a sufficient number of discharges was not available in any plane perpendicular to the traverse direction to produce a smooth crater. Therefore, there was no reason to doubt that the single-spark discharges were at least symmetrically distributed about the centre-line of the trough. This effect was greatly exaggerated in bismuth, lead, and tin.

Bulk volatilization rates

The experiments were extended to obtain measurements of these rates in a large number of metals and alloys (Table 1). Although no quantitative relationships between the bulk volatilization rate and the physical properties of the specimens were found, certain definite trends were observed. Smaller craters were generally produced in high-melting-point materials (iron and copper) than in low-melting-point materials. The crater produced in copper must have been extremely shallow, since it was imperceptible under microscopic examination. The bulk volatilization rate in copper has been estimated to be less than 0·005 mg per min. It would be expected that the rate for copper would be higher than the rate for iron, since the melting-point of copper is less than that of iron. Therefore, some other physical property or properties of these metals must have been important. Since the thermal conductivity of copper is very high compared with that of iron [4], the heat supplied by the discharge was rapidly conducted away in copper, so that very little of the available thermal energy would be used to volatilize material from the crater. Comparison of the bulk volatilization rates for magnesium and aluminium revealed a similar conclusion. Although their melting-points are very nearly identical, the rate in magnesium was greater than the rate in aluminium because of the latter metal's higher thermal conductivity. The addition of alloying elements to magnesium and copper lowers the thermal conductivities of these materials [4] sufficiently so that the bulk volatilization rates for the magnesium alloy AZ31 X, and for the bronze melting stock were greater than those rates for magnesium and copper, respectively. The rates for bismuth, lead, and tin were relatively high because of their low melting-points and low thermal conductivities.

The measurement of bulk volatilization rates would be important in the study of sensitivity limits. These limits might be thought of as being related to the actual amount of material volatilized from the crater and to the chemical environment in the discharge with all other conditions considered equal. Comparison of the traverse spectra emitted by the brass and the magnesium alloy, AZ31 X, revealed that the limit of detection of the spectral line ZnI 3345 Å in brass was six per cent, whereas this spectral line was easily detected at the one per cent level in the magnesium alloy. The bulk volatilization rate in the magnesium alloy was considerably greater than that in brass, and hence greater quantities of zinc were volatilized into the discharge from the magnesium alloy than from the brass.

Conclusions

A series of experiments were performed on magnesium, zinc, and cadmium at different traverse speeds to determine the effective spark distribution in a point-to-plane spark discharge. It was concluded that this distribution function was very close to a paraboloid of revolution. In magnesium specimens, the bulk volatilization rate was essentially independent of traverse speed, and the crater's maximum depth and radius were related to the traverse speed and to each other as described by equations (20), (21), and (22). In general, the maximum depth and radius were functions of the traverse-speed. However, for high-melting-point materials such as steel it was previously observed [1] that the crater's radius was independent

VOL.
7
1955/5

of the traverse speed. The form of these functions would depend on the material from which the specimens were made. Certain definite trends were noticed concerning the variation in the bulk volatilization rate with sample material. In general, this rate was observed to increase as the melting-point and thermal conductivity of the specimen decreased. It was pointed out that the sensitivity limits in solid specimens were also dependent upon the bulk volatilization rates. Experiments are in progress to determine the effect of alloying constituents on these rates.

Acknowledgments—The author wishes to thank Dr. R. L. CUNNINGHAM, Mr. H. H. BLEAKNEY, and Dr. C. M. MITCHELL for their useful comments and interest, and Miss B. CONNOLLY for her assistance in preparing the polished specimens and making crater measurements.

References

[1] HURWITZ, J. K.; *J. Opt. Soc. Amer.* (1952) **42**, 484
[2] HURWITZ, J. K.; *J. Opt. Soc. Amer.* (1954) **44**, 30
[3] LEAK, G. M.; private communication.
[4] *Metals Handbook*, The American Society for Metals, Cleveland (1948).

OL.
7
5/56

Spectrochimica Acta, 1955, Vol. 7, pp. 14 to 24. Pergamon Press Ltd., London

The infrared spectra of aromatic compounds

I. The out-of-plane C-H bending vibrations in the region 625–900 cm^{-1}

M. MARGOSHES* and V. A. FASSEL
Institute for Atomic Research and Department of Chemistry,
Iowa State College, Ames, Iowa

(*Received* 15 *July* 1954)

(*Accepted for publication October* 1954)

Summary—An empirical study has been made of the infrared spectra of aromatic compounds to determine the effect of substituent groups on some of the vibrations of the aromatic nucleus. In this paper particular attention is devoted to the out-of-plane C-H bending vibrations between 625 and 900 cm^{-1}. For monosubstituted benzenes of the type (phenyl)$_n M$, where n is the valence of the substituent atom M, the frequency of the absorption band between 725 and 820 cm^{-1} decreases linearly with the reduced mass of the diatomic group M-carbon. Most monosubstituted benzenes not of the type (phenyl)$_n M$ also show some correlation between the frequency of this band and the mass of the atom attached to the ring, but certain substituents produce anomalous shifts of this band. For disubstituted benzenes the effect of the substituents on the frequencies of some of the out-of-plane vibrations can be correlated with the effect of the same substituents on the 725 to 820 cm^{-1} band in monosubstituted benzenes.

VOL.
7
1955/

1. Introduction

In spite of the relative complexity of aromatic compounds (benzene, the simplest compound in this series has twelve atoms and thirty vibrational degrees of freedom), their infrared spectra have received considerable attention. WILSON [1] has made a complete theoretical study of the normal modes of vibration of the benzene molecule. The most complete assignment of infrared and Raman frequencies to vibrations of benzene has been given by INGOLD and associates in a series of papers [2]. MILLER and CRAWFORD [3] have made a thorough normal co-ordinate treatment of the non-planar vibrations and made frequency assignments on the basis of the calculations. A review of earlier normal co-ordinate treatments on the vibrations of benzene is also given in the paper by MILLER and CRAWFORD.

The lower symmetry of the substituted benzenes makes assignment of their vibrations more difficult than for benzene, but some work has been done on individual molecules. The assignments previously made for benzene can serve as a useful guide to the vibrations of the substituted benzenes. For example, PITZER and SCOTT [4] have made assignments of the vibrations of toluene and some other methyl-substituted benzenes by analogy with the spectrum of benzene rather than by a complete vibrational analysis. PLYLER [5] has studied the spectra of

* Present address: Biophysics Research Laboratory, Peter Bent Brigham Hospital, Harvard Medical School, Boston, Massachusetts.

Contribution No. 343 from the Institute for Atomic Research and Department of Chemistry, Iowa State College, Ames, Iowa. Work was performed in the Ames Laboratory of the Atomic Energy Commission.

twelve substituted benzenes in the 15–40 micron region, and has made assignments based largely on those of PITZER and SCOTT. Similarly, DEPAIGNE-DELAY and LECOMTE [6] have studied the spectra of a series of substituted benzenes from 5 to 8 microns, and have made tentative assignments based on symmetry considerations. BELL, THOMPSON, and VAGO [7] and COLE and THOMPSON [8] have applied a simplified potential function to the calculation of some of the out-of-plane vibrations of benzene and its mono-, di-, and tri-substituted derivatives, and found satisfactory agreement between calculated and observed frequencies.

Other studies on the spectra of aromatic compounds have been designed to find the characteristic frequencies of various groups without necessarily assigning the frequencies to particular vibrations. Thus, the strong absorption bands in the 11- to 15-micron region have been used for several years to determine the arrangement of substituents on the benzene ring. BARNES, LIDDELL, and WILLIAMS [9] appear to have been the first to observe that the frequencies of the absorption bands in this region are primarily determined by the number and position of substituents on the ring rather than by the nature of the substituents. WHIFFEN and THOMPSON [10] and THOMPSON and TORKINGTON [11] improved and extended these correlations. The observed absorption frequencies for benzene rings with various types of substitution have been collected in charts by THOMPSON [12], BARNES, GORE, STAFFORD, and WILLIAMS [13], and COLTHUP [14]. COLTHUP [14] extended the correlations to include non-benzene aromatic systems, such as the naphthalenes and pyridines, by pointing out that the number of adjacent hydrogen atoms appears to be the factor controlling the frequencies of the bands. For example, the same band-structure between 675 and 900 cm^{-1} is shown by pyridine as by a typical monosubstituted benzene. The same observation was made later by CANNON and SUTHERLAND [15], as well as several other significant correlations between the molecular structure and spectra of aromatic compounds. Many condensed ring-systems were included in the study by CANNON and SUTHERLAND [15]. Other important studies on the correlation of characteristic frequencies with structural change in aromatic compounds have been made by MCMURRY and THORNTON [16].

While examining the spectra of a large number of aromatic compounds it became evident to the authors that the frequencies of the bands between 11 and 15 microns did not always correspond to the frequencies established for the various positions of substitution, especially if one or more of the substituents was a nitro or carboxyl group. The same observation has been made by FLETT [17] in the case of substituted benzoic acids, though he did not investigate the matter further nor did he propose any explanation for the anomalies. Since no systematic study has appeared on the effect of the nature of the substituents on these particular frequencies, it appeared desirable to undertake such an investigation.

2. Experimental apparatus

The spectra were recorded on a Baird Associates Model B infrared spectrophotometer [18], using a sodium chloride prism. The spectra of all solids were obtained as mulls in mineral oil. Some of the spectra were also run in solution form. The spectra of liquids were obtained using the pure liquid in 0·1-mm cells or capillary

cells of unknown path-length. Most of the compounds studied were either commercially available or were supplied by members of the Chemistry Department of Iowa State College. These compounds were used without further purification unless doubt existed as to their purity. If purification was necessary, standard methods of distillation and recrystallization were used.

3. Effect of nature of substituents on the out-of-plane C-H bending vibrations

Monosubstituted benzenes. The effect of changing the substituent groups on the frequencies of the benzene-ring vibrations is best studied in the monosubstituted benzenes in order to avoid steric effects and the complications of having two groups act at once. When the effect of changing substituents in monosubstituted benzenes is established it may then be possible to extend the correlations to more complex cases.

In the spectra-correlation charts cited above (12, 13, 14), strong absorption bands are shown for monosubstituted benzenes between 680 and 720 cm^{-1} (13·9 to 14·8 microns) and 725 and 775 cm^{-1} (12·9 to 13·8 microns). The lower frequency band has shown neither pronounced changes in frequency nor significant correlation with the nature of the substituent. In contrast, the higher frequency band showed large variations in frequency with changes in the nature of the substituent. This band has been assigned by PITZER and SCOTT (for toluene) to an out-of-plane C-H bending vibration, which in toluene is identified as vibration number 10b in symmetry class B_2 [4]. THOMPSON *et al.* [7, 8] calculated the frequency of this vibration, using a simplified potential-energy function and a model in which the substituent X is represented by an infinite point-mass which does not move in the vibration. Although details of the mode of vibration obtained by THOMPSON *et al.* differed slightly from the assignments of PITZER and SCOTT, the general good agreement between calculated and observed frequencies justified the use of the simplified model. During a study of this absorption band in compounds of the type $(phenyl)_nM$, where n is the valence of the substituent atom M, it became apparent to us that the frequency showed a significant decrease with increasing mass of the substituent. This is readily apparent from the tabulation of frequencies observed in compounds of this type shown in Table 1. Although no reason can be presently advanced why this frequency should be an inverse linear function of reduced mass (using the mass of carbon as the other vibrating atom), Fig. 1 shows that apparently this relation applies. A possible explanation of these data is that the lighter substituents vibrate along with the ring-carbon atom to which they are attached, although the fact that the change from one element to another involves not only a change of mass but also a change of force-constant and bond-length makes it rather surprising that such a simple relation exists. It is worth noting that the frequency of approximately 725 cm^{-1} observed with the heavy substituents is in excellent agreement with the calculated value of 723 cm^{-1} obtained by THOMPSON *et al.* [7, 8] for an infinitely heavy substituent which does not move during the vibration.

In compounds not of the $(phenyl)_nM$ type, the frequency of this band shows some correlation with the mass of the substituent atom, but certain substituent

VOL. 7 1955/5

groups behave anomalously as shown in Table 2. For example, the frequency of this vibration is 728 cm^{-1} in toluene and 808 cm^{-1} in benzoic acid. Examination of the frequency of these out-of-plane C-H bending vibrations for a large number of compounds has revealed a consistent high frequency of this band in compounds such as benzoic acid, sodium benzoate, ethyl benzoate, benzoylchloride, benzotrichloride, and nitrobenzene. In all of these compounds, the observed frequencies

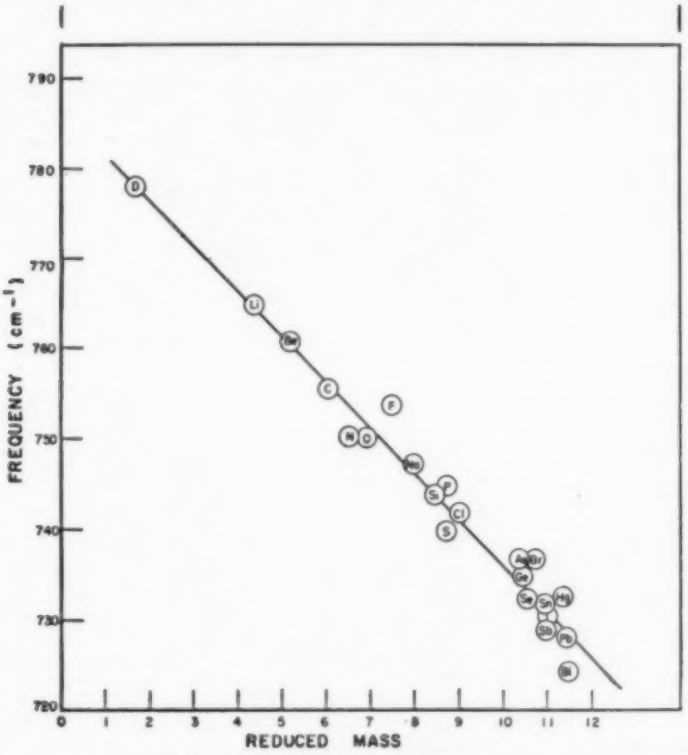

Fig. 1. Frequency of the out-of-plane C–H bending vibration as a function of the reduced mass of the diatomic group *M*-carbon in monosubstituted benzenes.

fall outside of the characteristic frequency range assigned to monosubstituted benzenes. The significance of this anomalous behaviour is examined in Paper II of this series.

Para-disubstituted benzenes. In the structure-spectra correlation charts [12, 13, 14], a strong absorption is shown for para-disubstituted benzenes between 800 and 860 cm^{-1} (11·6 to 12·5 microns). In *p*-xylene, this strong band falls at 796 cm^{-1} and has been assigned to an out-of-plane C-H bending vibration by PITZER and SCOTT [4]. The calculations of THOMPSON *et al.* [7, 8], made in the same manner as outlined above, also characterized this frequency as an out-of-plane C-H bending vibration; the calculated frequency was 837 cm^{-1}. The anomalous behaviour shown by many of the substituent groups in monosubstituted benzene was also exhibited in 1,4-disubstituted benzenes. Direct correlation of

the frequency of this band with the nature of the substituent groups thus was not satisfactory. Some interesting observations by TIERS and TIERS [19] on deuterated benzenes suggested that a correlation of a different type might be useful. TIERS and TIERS noted that the frequency shift of the band in para-disubstituted compounds appeared to be an additive function of the direction

Table 1. *Characteristic frequencies for various substituent atoms in monosubstituted benzene*

Compound	*Substituent element*	*Frequency* (cm^{-1})	*Positive shift in frequency from a base frequency of* 727 cm^{-1}
Deuterobenzene (l)	D	778†	51
Phenyllithium (s′)	Li	765	38
Diphenylberyllium (m)	Be	761	34
Tetraphenylmethane (m)	C	755	28
Triphenylamine (s)	N	750	23
Diphenylether (s)	O	750	23
Fluorobenzene (l)	F	754	27
Phenylsodium (m)	Na	747	20
Tetraphenylsilane (s)•	Si	740	13
Triphenylphosphine (s)•	P	745	18
Diphenylsulphide (l)	S	738	11
Chlorobenzene (l)	Cl	742	15
Tetraphenylgermane (s)•	Ge	735	8
Triphenylarsine (s)•	As	736	9
Diphenylselenide (l)	Se	732	5
Bromobenzene (l)	Br	736	9
Tetraphenylstannane (s)	Sn	733	6
Triphenylstibine (s)•	Sb	729	2
Iodobenzene (l)	I	731	4
Diphenylmercury (s)•	Hg	732	5
Tetraphenyllead (s)	Pb	727	0
Triphenylbismuthine (s)•	Bi	724	−3

l = spectra obtained from liquid sample
m = spectra obtained from Nujol mull
s = spectra obtained from CS_2 solution
s′ = spectrum obtained from diethylether solution
• Spectra of Nujol mull showed splitting of band or structure which degenerated into a single band in CS_2 solution.
† Data of TIERS and TIERS [19].

and magnitude of the frequency shift caused by each of the substituents in monosubstituted benzenes. To make a correlation of this type required the determination of a characteristic frequency shift for the various substituent groups in monosubstituted benzenes. This was simply accomplished by subtracting a selected base-frequency from the observed frequency. The exact frequency used

for the base was immaterial, since different base-frequencies would merely displace the values by a constant amount. The selected base-frequency of 727 cm^{-1} gave the lowest possible shifts for all the groups without the confusion of having

Table 2. Characteristic frequencies for various substituent groups in monosubstituted benzenes

Compound	*Group*	*Frequency (cm^{-1})*	*Positive shift in frequency from a base frequency of 727 cm^{-1}*
Toluene	$-CH_3$	728	1
Benzyl alcohol	$-CH_2OH$	747	20
Ethylbenzene	$-C_2H_5$	747	20
Benzaldehyde	$-CHO$	748	21
Triphenylmethane	$-CH$	762	35
Benzonitrile	$-CN$	763	36
Acetophenone	$-COR$	763	36
t-Butylbenzene	$-C(CH_3)_3$	764	37
Trans-stilbine	$-C=$	767	40
Benzylchloride	$-CH_2Cl$	768	41
Benzamide	$-CONH_2$	771	44
Benzoylchloride	$-COCl$	779	52
Benzotrichloride	$-CCl_3$	805	78
Benzoic acid	$-COOH$	808	81
Ethyl benzoate	$-COOR$	809	82
Sodium benzoate	$-COO^-$	820	93
Aniline hydrochloride	$-NH_3^+$	741	14
Tetraphenyl hydrazine	$-NN-$	747	20
Dimethylaniline	$-N(CH_3)_2$	753	26
Aniline	$-NH_2$	755	28
Nitrobenzene	$-NO_2$	794	67
Phenylacetate	$-OOCR$	752	25
Phenol	$-OH$	753	26
Anisole	$-OCH_3$	758	31
Sodiumbenzenesulphonate	$-SO_3^-$	754	27
Benzenesulphonylchloride	$-SO_2Cl$	757	30

In addition to the above values, a shift in frequency of 9 cm^{-1} for the CH_3 group (except where otherwise noted) and 36 cm^{-1} for the phenyl group was chosen as giving the best fit for the data.

negative shifts for some of the groups (with the exception of bismuth). The data shown in Tables 1 and 2 show the values for the substituent elements and groups obtained in this manner. In a few cases, the monosubstituted benzenes had more than one absorption band in the 720–780 cm^{-1} region; the value then chosen was the one giving the best agreement in the para-disubstituted benzene correlation. A plot of the frequency of the band in para-disubstituted benzenes vs. the sum of the band shifts caused by each of the substituents in monosubstituted

benzenes is shown in Fig. 2. It is apparent that the points scatter about a single line drawn through the origin. Data from compounds containing methyl, carboxylic, and nitro groups gave consistent correlations, even though these substituent groups produced the widely divergent shifts shown in Table 2. The gradient of the line relation in Fig. 2 is less than unity, showing that each substituent produced less of a shift in the para-disubstituted benzenes than in monosubstituted benzenes.

Meta-disubstituted benzenes. Two strong bands at 675 to 730 cm^{-1} (13·7 to 14·8 microns) and 750 to 810 cm^{-1} (12·3 to 13·3 microns) and a moderately strong band at 850 to 900 cm^{-1} (11·1 to 11·8 microns) are listed in the various spectra-correlation charts [12, 13, 14] for meta-disubstituted benzenes. For *m*-xylene, these frequencies fall at 690 cm^{-1}, 770 cm^{-1}, and 880 cm^{-1}. PITZER and SCOTT [4] have assigned

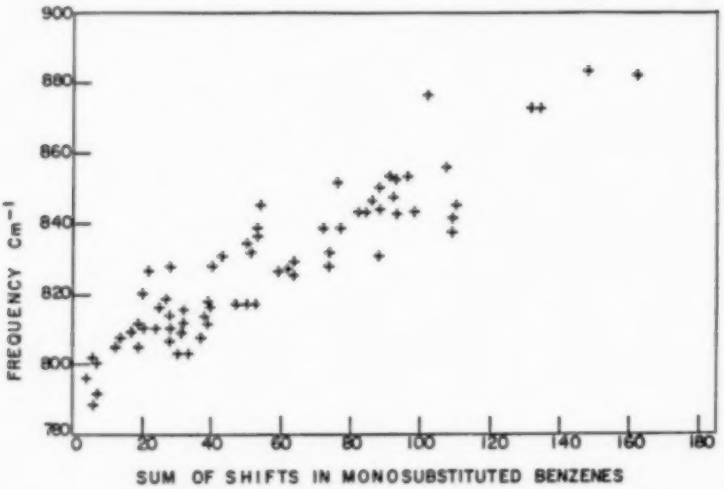

Fig. 2. Variation of the frequency of the 12-micron band of para-disubstituted benzenes as a function of the sum of the shifts caused by the substituents in monosubstituted benzenes.

the 770 cm^{-1} and 880 cm^{-1} bands to out-of-plane C-H bending vibrations. The frequencies calculated by THOMPSON *et al.* [7, 8], for these vibrations gave values of 772 and 937 cm^{-1}. The band at the lowest frequency appeared to be relatively unaffected by changes in the substituents, as was the lower frequency band in this region for monosubstituted benzenes. The other two bands, however, showed regular shifts in frequency with changes in the nature of the substituent groups. The observed frequencies of these bands as a function of the sum of the shifts caused by each of the substituents in monosubstituted benzene are shown in Figs. 3 and 4. The same general trends that were evident for para-disubstituted benzenes appear in the corresponding figure for the meta-disubstituted benzenes, but with some greater scattering of points, particularly for the 850 to 900 cm^{-1} band. In several cases two absorption bands occurred in the same region; these bands are indicated by vertical lines which join the observed frequencies.

Ortho-disubstituted benzenes. According to the spectra-correlation charts [12, 13, 14], ortho-disubstituted benzenes possess a strong absorption band

between 730 and 770 cm^{-1} (13·0 to 13·7 microns). For o-xylene this band falls at 775 cm^{-1}. Although PITZER and SCOTT did not assign this frequency to an out-of-plane C-H bending vibration, the calculations by THOMPSON *et al.* [7, 8] characterized this vibration as an out-of-plane C-H bending with a calculated

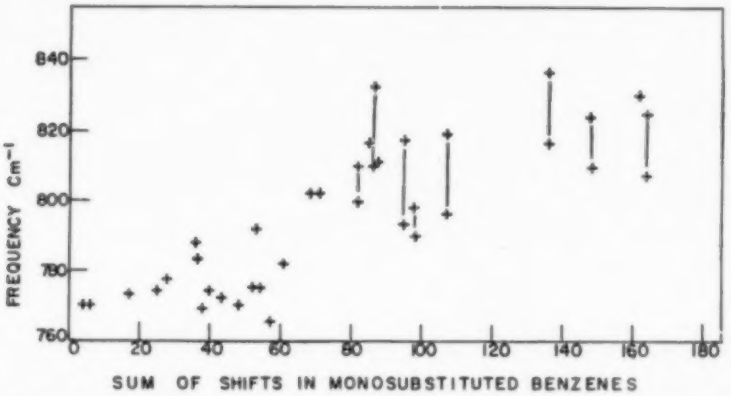

Fig. 3. Variation of the frequency of the 12- to 13-micron band of meta-disubstituted benzenes as the substituents are changed. Vertical lines connect points found for individual compounds when choice of a particular absorption band could not be made.

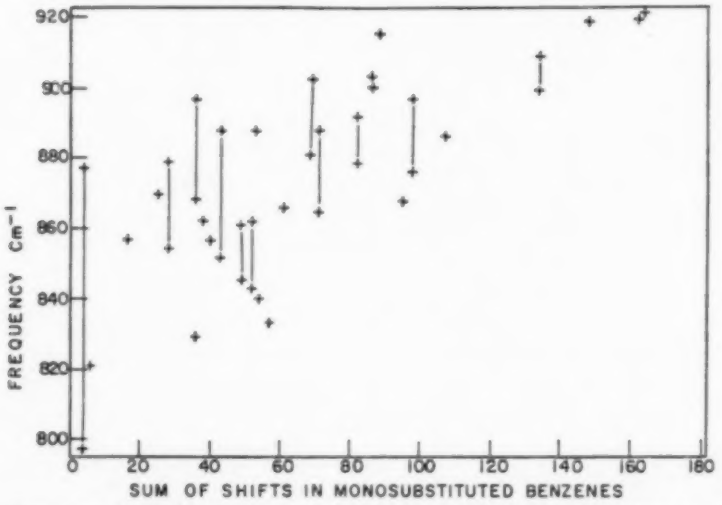

Fig. 4. Frequency of the 11- to 12-micron band in meta-disubstituted benzenes vs. sum of band shifts caused by the substituents in monosubstituted benzenes. Vertical lines connect points found for individual compounds when choice of a particular absorption band could not be made.

frequency of 735 cm^{-1}. The change of frequency of this band as a function of the sum of the shifts caused by each of the substituents in monosubstituted benzene is shown in Fig. 5. The scattering of the points is considerably greater than for the meta- or para-disubstituted benzenes, perhaps because of steric interaction. The points appear to be split into two groups, with most, though not all, of the

points in the lower frequency group belonging to ortho-substituted benzoic acids or esters.

Trisubstituted benzenes. Not enough data have been collected to demonstrate similar correlation for these compounds. Except in the case of symmetrical trisubstitution, steric effects must be considered. Some of the effects of steric interactions will be discussed in greater detail in the second paper of this series.

4. Discussion

Part of the scattering of the points in Figs. 1 to 5 probably arose from the method used for determining the spectra. Spectra of solids were obtained in the form of mineral-oil slurries, and of liquids in the form of thin films between salt plates. Some of the data taken from the literature [8, 10, 19, 20] were from solution

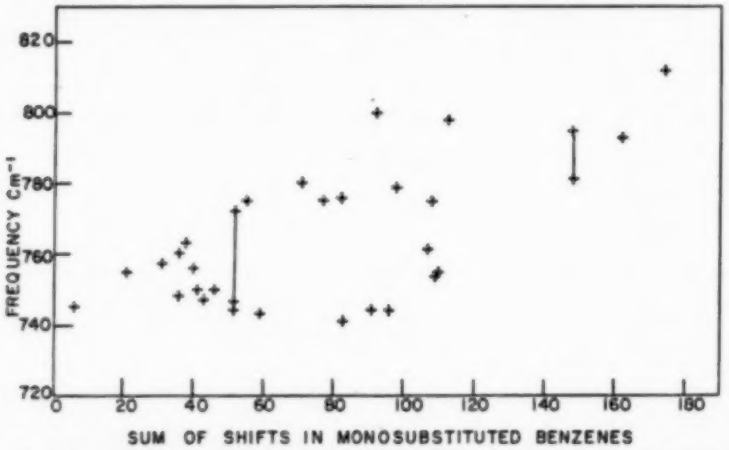

Fig. 5. Variation of the frequency of the 13- to 14-micron band of ortho-disubstituted benzenes as the substituents are changed. Vertical lines connect points found for individual compounds when choice of a particular absorption band could not be made.

spectra. The exact frequency of a vibration depends, in part, on the nature of the medium surrounding the molecule. Ideally, all spectra should be determined with the compound in the form of a vapour, but this is not always possible. Neither is it possible to use a single solvent for all compounds so that the effect of the surrounding medium would be the same for all. Kirkwood [21] has suggested that if there is a simple electrostatic interaction between the vibrating group and the solvent, the frequency shift caused by this interaction should be proportional to $(D - 1)/(2D + 1)$, where D is the static value of the dielectric constant of the solvent. It is possible that the scattering of the points in Figs. 1 to 5 could be reduced by obtaining the spectra of all of the compounds in solution and correcting for the effect of the solvent by Kirkwood's equation or some other applicable relationship.

5. Extra absorption bands found in certain compounds

In addition to the absorption bands expected, aromatic nitro compounds, carboxylic acids, and salts and esters of carboxylic acids sometimes showed an additional

strong absorption band in the region of the out-of-plane hydrogen-bending vibrations. This extra band appeared only for certain substituents and certain symmetries of substitution. Of the various symmetries of substitution studied, an extra band appeared only for para-disubstitution and 1,2,4-trisubstitution, and only when one of the substituents was a nitro or carboxyl group or an ester or salt of a carboxyl group. Fig. 6 shows the spectra from 11·5 to 14 microns of some

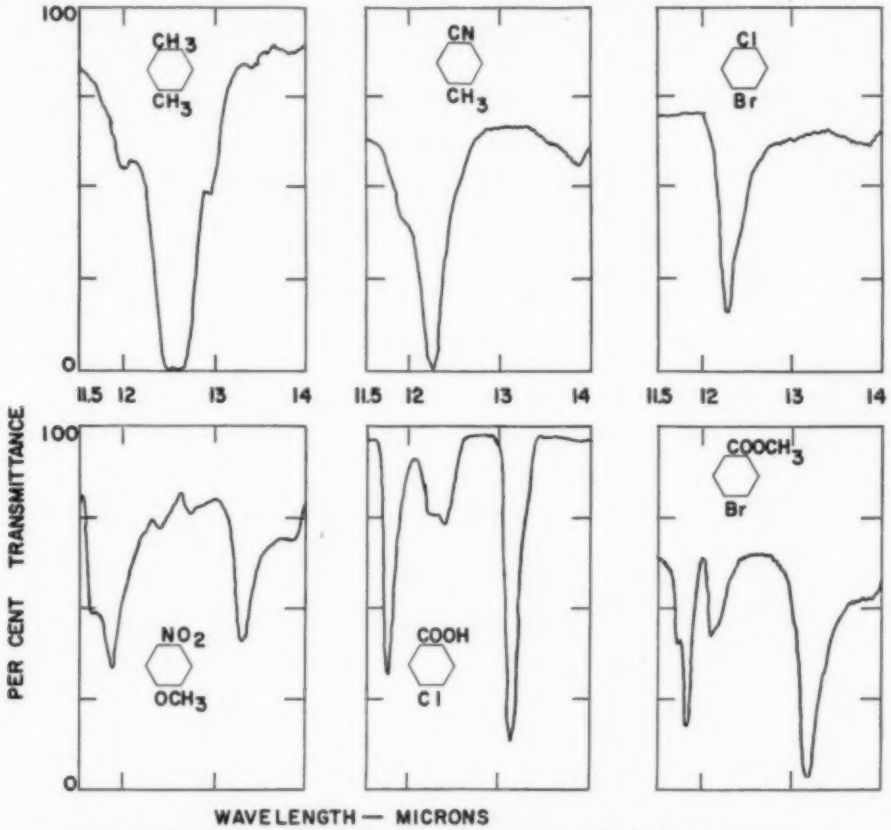

Fig. 6. Spectra from 11·5 to 14 microns of some para-disubstituted benzenes.

para-disubstituted benzenes. The compounds in the lower part of the figure all have a nitro or carboxyl group as one of the substituents and show a strong band just above 13 microns that does not appear in the spectra of the compounds shown at the top of the figure. It is apparent that this extra band cannot be caused by any vibration of the substituents, since these are different in the three compounds shown and because these same substituents do not cause absorption in this region in many other compounds. The absorption frequency must correspond to some vibration of the ring, but the nature of vibration is not known. Mann and Thompson [22] have studied the infrared spectrum of a single crystal of para-nitroaniline, using polarized light, and found that the bands at 755 and 840 cm^{-1} (13·25 and 11·90

microns) both have the dichroism that would be expected for out-of-plane deformations of the benzene ring. This suggests, but does not establish, that the extra band may also be an out-of-plane hydrogen-bending vibration.

The 1,2,4-trisubstituted benzenes also had an extra band at about 13 microns that appeared when the other two substituents were in the 2,4-, 2,5-, or 3,4-positions, with the nitro or carboxyl group in the number 1 position. It is rather strange that this extra band should appear only in these few cases and that it should then be present regardless of the exact arrangement of substituents. In both the para-disubstituted and 1,2,4-trisubstituted compounds the band was not observed if more than one of the substituents was a nitro or carboxyl group.

Acknowledgment

The authors are grateful to Drs. H. Gilman and G. S. Hammond of the Chemistry Department of Iowa State College for supplying pure samples of many of the compounds studied, and to R. Kross for preparing some of the compounds. This work has also been assisted by helpful discussions with Dr. H. Shull and Messrs. R. Kross and R. M. Hedges.

References

[1] Wilson, E. B.; *Phys. Rev.* 1934 **45** 706.
[2] Ingold, C. K., *et al.*; *J. Chem. Soc.* (*London*) **1936** 912, **1946** 222.
[3] Miller, F. A., and Crawford, B.; *J. Chem. Phys.*, 1946 **14** 282.
[4] Pitzer, K. S., and Scott, D. W.; *J. Amer. Chem. Soc.* 1943 **65** 803.
[5] Plyler, E. K.; *Discuss. Faraday Soc.* 1950 **9** 100.
[6] Depaigne-Delay, A., and Lecomte, J.; *J. physique rad.*, Series 8, 1946 **7** 38.
[7] Bell, R. P., Thompson, H. W., and Vago, E. E.; *Proc. Roy. Soc. London* 1948 **A192** 498.
[8] Cole, A. R. H., and Thompson, H. W.; *Trans. Faraday Soc.* 1950 **46** 103.
[9] Barnes, R. B., Liddell, U., and Williams, V. Z.; *Ind. Eng. Chem.* (*Anal. Ed.*) 1943 **15** 659.
[10] Whiffen, D. H., and Thompson, H. W.; *J. Chem. Soc.* (*London*) **1945** 268.
[11] Thompson, H. W., and Torkington, P.; *Trans. Faraday Soc.* 1945 **41** 246.
[12] Thompson, H. W.; *J. Chem. Soc.* (*London*) **1948** 328.
[13] Barnes, R. B., Gore, R. C., Stafford, R. W., and Williams, V. Z.; *Anal. Chem.* 1948 **20** 402.
[14] Colthup, N. B.; *J. Opt. Soc. Amer.* 1950 **40** 397.
[15] Cannon, C. G., and Sutherland, G. B. B. M.; *Spectrochim. Acta* 1951 **4** 373.
[16] McMurry, H. L., and Thornton, V.; *Anal. Chem.* 1952 **24** 318.
[17] Flett, M. St. C., *J. Chem. Soc.* (*London*) **1951** 962.
[18] Baird, W. S., O'Bryan, H. M., Ogden, G., and Lee, D.; *J. Opt. Soc. Amer.* 1947 **37** 754.
[19] Tiers, G. V. D., and Tiers, J. H.; *J. Chem. Phys.* 1952 **20** 761.
[20] Bomstein, J., *Anal. Chem.* 1953 **25** 513.
[21] Kirkwood, J. G., quoted by Jones, L. H., and Badger, R. M.; *J. Amer. Chem. Soc.* 1951 **73** 3132.
[22] Mann, J., and Thompson, H. W.; *Proc. Roy. Soc. London* 1952 **A211** 168.

VOL. 7 1955/5

Spectrochimica Acta, 1955, Vol. 7, pp. 25 to 31. Pergamon Press Ltd., London

Contribution à l'analyse quantitative par les spectres d'absorption infrarouge des poudres

I. Examen théorique de la question

G. DUYCKAERTS

Laboratoire de chimie analytique, et Centre d'analyse spectrale moléculaire
Université de Liège, Belgique

(*Received May* 1954)

(*Accepted for publication August* 1954)

Summary—In a previous paper [5] we have given some preliminary quantitative experimental results about the influence, on the absorption of infrared radiations, of the particle-size of a powder dispersed in a potassium bromide pellet, and we showed that those results were in agreement with a theoretical formula we proposed.

In this part, we give the theoretical considerations which lead to this formula:

(1) In case of a quantity of substance insufficient to give more than one layer, the measured transmission is given by the formula:

$$\frac{I}{I_0} = (1 - \mathscr{F}) + \mathscr{F} \cdot \Theta \tag{1}$$

(I_0, I: intensities of the incident and transmitted light, Θ: transmission of one particle; $\mathscr{F}$: fraction of the surface covered by the powder.)

It follows from (1) that it is the absorption $\left(1 - \frac{I}{I_0}\right)$ and not the extinction $\log\left(\frac{I_0}{I}\right)$ which is proportional to the quantity of substance dispersed in the sample.

(2) In case of a quantity of substance sufficient to give a number n of layers, it has been shown that, for cubic particles, the *absorption* of infrared radiations is given by the following law:

$$E = \log\left(\frac{I_0}{I}\right) = -\frac{m}{Ks\rho d}\log[(1 - K) + K\Theta] \tag{2}$$

(m: mass of substance; ρ: specific weight; s: surface of a section of the pellet normal to the beam; d: cube's edge; K: fraction of the surface covered by a layer.)

In the case of spheres, the relation (2) has to be multiplied by a factor 3/2. The consequences which derive from this relation (2) are:

(a) when kd is large, the measured absorption is independent of the intrinsic absorption coefficient of the substance (k).

(b) when $kd < 0{\cdot}3$, the particle dispersion behaves like a molecular one from the point of view of the *absorption* of radiations.

(c) the measured extinction is proportional to the quantity of substance (equivalent to Beer's Law).

The whole theory was established in the case of the dispersion of a powder in a transparent medium, where all particles are of the same size.

The experimental results obtained in order to test this theory will be given in a second part.

1. Introduction

La prise de spectres infrarouges de substances à l'état solide s'impose très souvent et différentes techniques sont utilisées: film, lame mince, pâte au nujol, aux solvants chlorés ou fluorés, dispersion dans une pastille de bromure de potassium

[1]. Toutes ces techniques rendent de grands services pour l'étude de problèmes de structure et pour l'analyse moléculaire qualitative des substances solides insolubles dans les solvants infrarouges; leur utilisation pour l'analyse quantitative s'est heurtée, jusqu'à présent, à de sérieuses difficultés:

1. S'il est aisé de connaître, dans le cas des liquides ou des solutions, la quantité de substance par unité de surface de la cellule, il n'en est pas de même pour les substances solides où l'épaisseur sera souvent variable d'un endroit à l'autre de la préparation; la technique récente des pastilles de KBr fait cependant exception et elle constitue, à ce point de vue, une méthode aussi commode et précise que celle des solutions; elle possède même vis à vis de cette dernière, l'avantage d'un dispersant parfaitement transparent jusque 25 μ, moyennant certaines précautions; le bromure de potassium finement broyé fixe très rapidement une quantité d'eau gênante pour la prise des spectres et des précautions spéciales doivent être prises lors du broyage et du pastillage.

2. Il faut immédiatement ajouter que les phénomènes optiques qui entrent en jeu dans la prise d'un spectre de poudre sont complexes et que de ce fait leur utilisation en vue d'applications quantitatives se heurtent à de grandes difficultés. Lorsqu'on suit un rayon infrarouge traversant une pastille contenant une poudre finement divisée, on rencontre, à côté de l'absorption proprement dite par la substance dispersée, les réflexions sur les faces de la pastille et surtout les réflexions et les réfractions sur la surface des grains (diffusion).

Tous les spectroscopistes de l'infrarouge savent que, pour obtenir un spectre convenable de poudre, il est avantageux de choisir un dispersant transparent dont l'indice de réfraction se rapproche au maximum de celui de la substance et qu'il est *indispensable* d'amener la substance à un état de finesse *très poussé*.

A. H. Pfund [2] et R. L. Henry [3] ont discuté ces phénomènes et ils ont étudié expérimentalement l'influence de la dimension des grains; la formule proposée par ces auteurs pour interpréter les résultats semble correcte pour les pertes de lumière par diffusion (régions du spectre où l'absorption est faible et continue) mais elle n'a pas encore été contrôlée pour l'absorption proprement dite. Leurs résultats indiquent néanmoins très clairement une influence importante de la dimension des grains sur l'intensité des bandes d'absorption.

Plus récemment, R. N. Jones [4] a mis clairement en évidence les phénomènes complexes inhérents à la spectrophotométrie des poudres et il a attiré l'attention sur les conséquences que cela doit entraîner du point de vue de la loi d'absorption en fonction de la quantité de substance.

Il nous a paru qu'une étude expérimentale et théorique de la question méritait d'être entreprise et que la technique des pastilles était particulièrement adaptée à cette recherche; dans une note antérieure [5], nous avons exposé les premiers résultats expérimentaux de cette étude et nous avons montré que les valeurs de l'absorption proprement dite étaient en bon accord avec une formule théorique que nous proposions.

Nous avons l'intention d'exposer dans cette partie les considérations théoriques qui nous ont conduit à cette formule; une seconde partie sera consacrée à l'exposé de nouveaux résultats expérimentaux obtenus par Mlle Bonhomme et examinés à la lumière de cette théorie.

VOL.
7
1955/5

2. Théorie de l'absorption par les poudres

Nous nous proposons de rechercher la relation existant entre *l'intensité d'une bande d'absorption* infrarouge et la dimension des grains de la poudre dispersée dans un milieu transparent; nous supposerons que ce milieu possède le même indice de réfraction que la substance; dans ce cas, les pertes de lumière par diffusion sont nulles; nous verrons, dans la partie expérimentale, comment il est possible en première approximation de dissocier les résultats expérimentaux en absorption et diffusion et de les confronter avec la théorie proposée pour l'absorption. Nous supposerons également que tous les grains sont uniformes et de même dimension et que la préparation statistique de la poudre est éclairée en rayons parallèles.

Soient s: section de la pastille normale à la direction du faisceau lumineux.
m: masse de substance dispersée dans la pastille.
ρ: poids spécifique de la substance dispersée.
d: diamètre de la particule sphérique ou arête de la particule cubique.
k: coefficient d'absorption intrinsèque moyen de la substance défini par $i = i_0 e^{-kd}$.

1er *cas:* La quantité de substance est insuffisante pour former plus d'une couche complète ($n < 1$).

On conviendra de dire qu'il n'y a pas plus d'une couche lorsque chaque rayon lumineux ne recontrera pas plus d'une particule sur son trajet.

Si l'on projette toutes les particules dispersées statistiquement dans la pastille sur une section normale au faisceau lumineux et si l'on représente par "$\mathscr{F}$" la fraction de la surface couverte, il est aisé de calculer l'intensité de la lumière transmise par unité de surface de la pastille:

$$I = (1 - \mathscr{F})I_0 + \mathscr{F} I_0 \cdot \Theta \tag{1}$$

Θ étant la transmission propre d'un grain (fonction de sa forme, de sa dimension et de son orientation).

La transmission mesurée de la préparation vaut:

$$\frac{I}{I_0} = 1 - \mathscr{F} \cdot (1 - \Theta) \tag{2}$$

Le paramètre "$\mathscr{F}$" dépend de la forme et du diamètre des grains, ainsi que de leur nombre par unité de surface.

Pour des particules sphériques de diamètre "d", on peut montrer que

$$\mathscr{F} = \frac{3}{2} \cdot \frac{m}{s\rho} \cdot \frac{1}{d} \tag{3}$$

La valeur limite de "$\mathscr{F}$" serait atteinte avec des particules serrées les unes contre les autres comme dans un réseau cristallin à deux dimensions et il est aisé de montrer que

$$\mathscr{F}_{\text{lim}} = \frac{\pi}{4} = 0{\cdot}785 \tag{4}$$

indépendamment de la dimension d des sphères.

Pour des particules cubiques d'arête "d," on montre de la même façon que

$$\mathscr{F} = \frac{m}{s\rho} \cdot \frac{1}{d} \tag{5}$$

dans le cas où tous les cubes ont une face perpendiculaire au faisceau.

Il semble logique d'admettre que, dans le cas d'une *distribution statistique des particules* identiques dans le milieu transparent, la valeur maximum de "$\mathscr{F}$" que nous représenterons par "K" soit une grandeur indépendante de la dimension de ces particules et dans certaines limites, de l'épaisseur de la pastille. Il est probable que pour des pastilles très minces ou dans le cas de la sédimentation de la poudre sur une lame, la valeur de K est plus grande.

Si la quantité de substance "m" et le diamètre sont tels qu'il y ait exactement une couche, la transmission lumineuse sera la suivante:

$$\frac{I}{I_0} = (1 - K) + K\Theta \tag{6}$$

A. *Loi d'absorption en fonction de* $\frac{m}{s\rho}$

En remplaçant $\mathscr{F}$ par sa valeur dans l'expression (2), on peut écrire:

$$A = 1 - \frac{I}{I_0} = \frac{3}{2} \cdot \frac{1}{d} \cdot \frac{m}{s\rho} \cdot (1 - \Theta) \tag{7}$$ (sphères)

$$A = 1 - \frac{I}{I_0} = \frac{1}{d} \cdot \frac{m}{s\rho} (1 - \Theta) \tag{8}$$ (cubes)

Il en résulte que, pour une poudre homogène de dimension donnée, ce n'est plus, comme pour les solutions, l'extinction qui est proportionnelle à la quantité de substance par unité de surface (Loi de Beer-Lambert), mais bien l'absorption.

Il est bien entendu que ces deux expressions (7) et (8) ne sont valables que dans les limites d'une quantité inférieure ou égale à une couche c'est à dire pour

$$\frac{m/s\rho}{d} \leqslant K \qquad (9) \qquad \text{(cubes)}$$

$$\frac{m/s\rho}{d} \leqslant \frac{2}{3}K \qquad (10) \qquad \text{(sphères)}$$

Il est d'ailleurs intéressant de constater que $(1 - \Theta)$ représente l'absorption propre d'une particule et que par conséquent, *indépendamment de la forme des particules*

$$A = \mathscr{F} \cdot a \qquad (11)$$

c'est à dire *l'absorption mesurée "A" est égale au produit de l'absorption propre d'un grain "a" multipliée par la fraction de surface couverte par la poudre.*

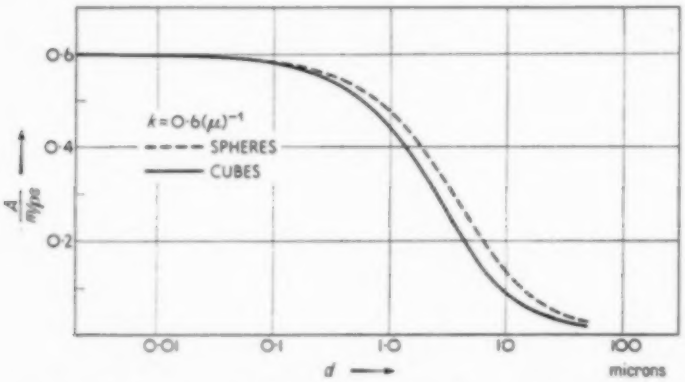

Fig. 1. Variation de l'absorption spécifique d'une poudre de grains uniformes en fonction de la dimension pour une quantité de substance insuffisante pour donner plus d'une couche.

B. *Loi d'absorption en fonction de la dimension et de la forme des grains.*

Cette i eslot donnée implicitement par l'équation (11) et elle dépend évidemment de la forme des particules et, dans certains cas, de leur orientation dans la pastille.

On peut montrer que la transmission d'une sphère isotrope éclairée uniformément en rayons parallèles —en admettant qu'elle soit plongée dans un milieu parfaitement transparent de même indice de réfraction que la sphère—est donnée par l'expression suivante:

$$\Theta = \frac{1 - (kd + 1)e^{-kd}}{k^2d^2/2}. \qquad (12)$$

La transmission d'un cube, dans les mêmes conditions, pour un éclairage normal à une face sera:

$$\Theta = e^{-kd} \qquad (13)$$

On voit ainsi que l'absorption spécifique $A/m/s\rho$, d'une dispersion de cubes, varie avec la dimension suivant la relation:

$$\frac{A}{m/s\rho} = \frac{1}{d} \cdot (1 - e^{-kd}) \qquad (14)$$

Lorsque kd devient très petit, on obtient la valeur limite,

$$\lim_{kd \to 0}\left(\frac{A}{m/s\rho}\right) = \frac{kd}{d} = k \qquad (15)$$

l'absorption spécifique tend vers le coefficient d'absorption intrinsèque de la substance.

Nous avons porté en diagramme la variation de l'absorption spécifique en fonction de la dimension des grains pour les formes cubiques et sphériques et l'on voit que dans l'un comme dans l'autre cas, celle-ci tend vers la valeur du coefficient d'absorption $k = 0{\cdot}6$ choisie arbitrairement.

VOL. 7 1955/5

2ème cas: Conditions donnant $2 \geqslant n > 1$

Dans le cas où un rayon lumineux rencontre 2, 1 ou 0 grains, on peut montrer que la transmission est donnée par l'expression suivante:

$$\frac{I}{I_0} = (1 - \mathscr{K})(1 - K) + [\mathscr{K}(1 - \mathscr{K}) + K(1 - K)]\Theta + \mathscr{K} \,.\, K \,.\, \Theta^2. \tag{16}$$

en admettant les hypothèses simplificatrices suivantes:

(1) toutes les situations dans la pastille sont également probables.

(2) l'absorption d'un rayon qui rencontre deux grains est la même quel que soit le recouvrement de ces deux grains.

K: fraction de surface couverte par la première couche complète.

$\mathscr{K}$: fraction de surface couverte par la seconde couche incomplète.

Lorsque la seconde couche est entièrement formée ($n = 2$), on a $\mathscr{K} = K$ et dans ces conditions

$$\frac{I}{I_0} = [(1 - K) + K\Theta]^2 \tag{17}$$

3ème cas. Nombre de couches n

Il devient maintenant aisé de généraliser la formule dans le cas d'un nombre de couches égal à n et en admettant les mêmes hypothèses simplificatrices:

$$\frac{I}{I_0} = [(1 - K) + K \,.\, \Theta]^n \tag{18}$$

Or, pour des cubes,

$$n = \frac{m}{Ks\rho d} \tag{19}$$

et pour des sphères

$$n = \frac{3}{2} \cdot \frac{m}{Ks\rho d} \tag{20}$$

Il en résulte que:

(a) pour des cubes: $$E = \log\left(\frac{I_0}{I}\right) = -\frac{m}{K\rho s d} \,.\, \log[(1 - K) + K\Theta] \tag{21}$$

(b) pour des sphères: $$E = \log\left(\frac{I_0}{I}\right) = -\frac{3}{2} \cdot \frac{m}{Ks\rho d} \log[(1 - K) + K \,.\, \Theta] \tag{22}$$

Θ étant donné par les relations (12) et (13).

Il va de soi que lorsque d devient très petit, ces formules doivent tendre vers la loi d'absorption d'une dispersion moléculaire (Loi de Beer-Lambert); ainsi, dans le cas de la formule (21), en développant en série le logarithme et l'exponentielle Θ et en ne gardant que le premier terme, on trouve:

$$\lim_{kd \to 0} E = -\frac{m}{K \,.\, \rho s d}\left(-\frac{K \,.\, kd}{2 \cdot 3}\right) = \frac{m \,.\, k}{2 \cdot 3 \rho s} = \frac{m}{s} \cdot \frac{k}{2 \cdot 3 \rho} \tag{23}$$

C'est bien la loi de Beer-Lambert puisque $\frac{m}{s} \equiv c \,.\, l$ et $\frac{k}{2 \cdot 3 \rho} \equiv \varepsilon$ (c = concentration, l = épaisseur de la pastille).

Ce résultat montre que la dispersion équivalente à une solution est atteinte d'autant plus rapidement que le coefficient d'absorption vrai de la bande est plus faible. Nous verrons, dans l'exposé des résultats expérimentaux quelle dimension des grains il faut atteindre pour se retrouver pratiquement dans les conditiones identiques à celles d'une solution, du point de vue des lois d'absorption (condition de dispersion psuedo-moléculaire).

A. *Loi d'absorption en fonction de $m/\rho s$*

On peut voir que, pour une poudre de dimension donnée, l'extinction E devient proportionnelle au produit cl de la loi de Beer ($cl \equiv m/s$), du moment que les conditions soient telles que le nombre n soit élevé; à ce moment, le coefficient d'absorption expérimental $\varepsilon_{exp} = \frac{E}{m/s}$ ne dépend plus que de la dimension des grains, de leur forme et de la répartition.

B. *Loi de variation du coefficient d'absorption expérimental avec "d"*

Les relations ci-dessus (21) et (22) montrent que:

(a) pour des cubes: $$\varepsilon_{exp} = -\frac{1}{Kd\rho} \log[(1 - K) + K \,.\, \Theta] \tag{24}$$

(b) pour des sphères: $$\varepsilon_{exp} = -\frac{3}{2} \cdot \frac{1}{Kd\rho} \log[(1 - K) + K\Theta] \tag{25}$$

Les courbes de la figure 2 ont été calculées au moyen des formules (24) et (25) et elles montrent que:
(1) le coefficient d'absorption expérimental tend vers le coefficient d'absorption intrinsèque de la substance lorsque les grains deviennent très petits et cette valeur limite est d'autant plus vite atteinte que la bande est plus intense.
(2) le coefficient d'absorption expérimental est indépendant du coefficient d'absorption intrinsèque pour les grains de dimension élevée.
(3) l'absorption suit pratiquement la loi de Beer-Lambert avec un coefficient d'absorption égal au coefficient d'absorption intrinsèque lorsque $kd < 0{\cdot}3$ (condition de pseudo-moléculairité).

3. Conclusions pratiques

L'exposé qui vient d'être fait, met en évidence quelques difficultés inhérentes à l'analyse quantitative par la spectrométrie infrarouge des poudres et il nous a permis de dégager, de façon approximative, les lois qui régissent l'absorption d'un milieu discontinu.

En pratique, les conditions expérimentales sont différentes des hypothèses à la base de cette théorie; une poudre finement broyée pour la prise d'un spectre

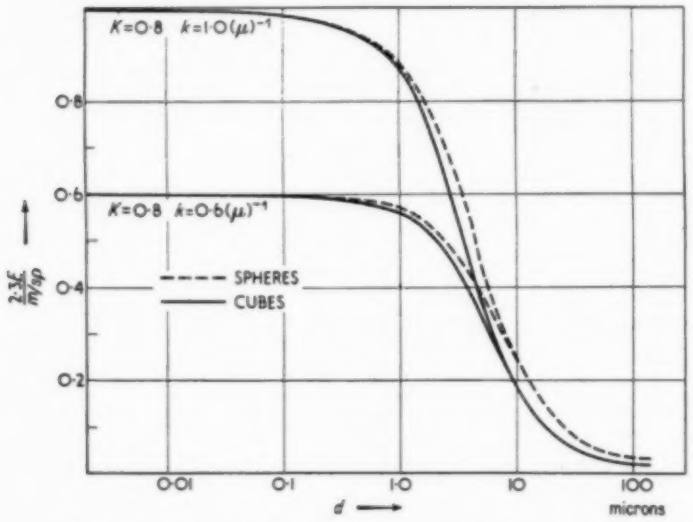

Fig. 2. Variation du coefficient d'absorption expérimental en fonction de la dimension des grains.

est fortement hétérogène du point de vue de la dimension des grains; sa courbe granulométrique dépend d'ailleurs du mode, de la durée et des conditions de broyage.

Il est possible, en principe, de poser les équations régissant l'absorption de la lumière par une poudre possédant une composition granulométrique connue; mais l'intégration des équations se heurte à de grosses difficultés mathématiques. Il semble d'ailleurs, d'après les résultats expérimentaux qui ont été obtenus jusqu'à présent dans mon laboratoire, que la courbe de l'absorption d'une poudre hétérogène en fonction du diamètre du maximum de la courbe granulométrique, conserve la même allure que celle établie pour une poudre homogène; les résultats expérimentaux qui seront exposés dans la seconde partie, semblent indiquer que

l'absorption par une poudre homogène ou non, suit une même loi avec cette différence que les deux constantes K et k de l'équation générale dépendent de la courbe de répartition granulométrique; il est à prévoir que, au fur et à mesure que la courbe granulométrique s'élargit, la valeur de K doit se rapprocher de l'unité puisque les petits grains viennent combler les vides laissés entre les gros grains; k devient alors un coefficient d'absorption fictif.

Du point de vue pratique, il n'est pas question de déterminer la courbe granulométrique pour chaque échantillon à analyser; la seule issue pratique semble être la recherche de conditions de broyage telles qu'on se trouve avec certitude dans les conditions pratiquement équivalentes à une dispersion moléculaire telles que nous les avons définies plus haut.

Des essais effectués dans cette direction sont actuellement en cours.

Bibliographie

[1] Stimson, M. M., *J. Amer. Chem. Soc.* 1952 **74** 1805; Schiedt, U.; *Z. Naturforsch* 1952 **76** 270.
[2] Pfund, A. H.; *Phys. Rev.* 1930 **36** 71; *J. Opt. Soc. Amer.* 1933 175.
[3] Henry, R. L.; *J. Opt. Soc. Amer.* 1948 **38** 775.
[4] Jones, R. N.; *J. Amer. Chem. Soc.* 1952 **74** 2681.
[5] Lejeune, R., and Duyckaerts, G.; *Spectrochim. Acta* 1954 **6** 194.

OL.
7
5/56

Spectrochimica Acta, 1955, Vol. 7, pp. 32 to 44. Pergamon Press Ltd., London

Contribution à l'analyse quantitative par les spectres d'absorption infrarouge des poudres

II. Etude expérimentale

Mlle. J. Bonhomme
Laboratoire de chimie analytique et Centre d'analyse spectrole moléculaire,
Université de Liège, Belgique

(*Received September* 1954)

(*Accepted for publication October* 1954)

Summary—This contribution continues a series of experiments leading to an assessment of the effect of particle size on the intensity of the infrared absorption bands of powdered materials. The material to be tested was meticulously graded by sedimentation, and fractions of known particle-size were mixed with KBr and moulded into discs. The measurements deal with absorption bands of calcite and of Dowex; and they are discussed in connection with the theoretical formulae set out in the previous contribution of this series.

Introduction

On sait que, dans un spectre de poudre, l'influence de la dimension des grains est grande, tant sur l'absorption proprement dite que sur les pertes de lumière par diffusion. R. Lejeune et G. Duyckaerts [1] ont publié une note préliminaire sur l'étude quantitative de ce phénomène portant sur les deux bandes intenses de la calcite à 876 cm^{-1} et 710 cm^{-1}, en s'arrêtant à l'effet de la dimension des grains sur l'absorption proprement dite.

Les résultats se laissent représenter de façon satisfaisante par une formule théorique établie par G. Duyckaerts [2]: l'extinction ($E = \log I_0/I$) d'une dispersion statistique de grains de forme cubique (arête d) dans un milieu transparent est donnée par l'expression suivante, pour un nombre de grains suffisants pour former plusieurs couches:

$$E \equiv \log \frac{I_0}{I} = -\frac{m}{K\rho s d} \log [(1 - K) + Ke^{-kd}]$$

m: masse de substance,

s: surface de la préparation,

ρ: poids spécifique de la substance,

k: coefficient d'absorption intrinsèque moyen de la substance,

K: constante, indépendante de λ, mais fonction des vides relatifs dans une surface de grains tassés.

La valeur de K qui avait dû être adoptée pour le tracé des courbes théoriques, paraît cependant assez surprenante. Cette valeur signifierait que, dans la pastille de KBr, les grains de calcite sont disposés de telle sorte qu'il ne reste pratiquement pas de trous dans les différentes couches de grains projetées sur une surface normale au faisceau lumineux. Or, G. Duyckaerts a montré que, dans le cas

d'une couche de grains sphériques de mêmes diamètres disposés de façon compacte comme dans un réseau à deux dimensions, K c'est à dire la valeur limite de la fraction $\mathscr{H}$ de surface couverte, vaut 0·785. Ce fait semble indiquer que le fractionnement n'avait pas été poussé assez loin et que les petits grains subsistant venaient remplir les interstices entre les plus gros et produisaient un recouvrement plus complet de la surface (K voisin de l'unité).

Il nous a paru intéressant de reprendre cette étude, et d'essayer d'améliorer les résultats en perfectionnant, d'abord la préparation de fractions homogènes de grains de dimensions données et ensuite la préparation des pastilles de KBr.

Nous avons étendu cette étude à la troisième bande intense de la calcite à 1431 cm^{-1}. Nous nous sommes également proposés de vérifier une autre équation établie par G. DUYCKAERTS [2] et donnant la variation de l'extinction d'une dispersion de grains sphériques en fonction de leur dimension. Pour cette étude, nous avons utilisé le Dowex 50, un polystyrène sulfoné, sous la forme ammonique.

1. Préparation de grains de dimensions données

Deux méthodes se présentaient pour la préparation de fractions homogènes de grains de dimensions comprises entre 1 et 30 μ: l'élutrition (entraînement dans un courant d'air) et la sédimentation. Ces deux méthodes sont basées sur la loi de Stokes. L'élutrition est basée sur la vitesse (v) du courant d'air nécessaire pour entraîner verticalement des particules d'un diamètre déterminé:

$$v = \frac{gd^2\rho_s}{18\eta} \qquad \text{(a)}$$

La sédimentation est basée sur la vitesse de chute des particules d'un diamètre déterminé dans un milieu liquide de densité plus faible:

$$v = \frac{gd^2(\rho_s - \rho)}{18\eta} = \frac{h}{t} \qquad \text{(b)}$$

d = diamètre des particules (considérées sphériques),

ρ_s = densité des particules,

η = viscosité de l'air ou du milieu dispersant,

ρ = densité du milieu dispersant,

h = hauteur de chute,

t = durée de sédimentation d'une hauteur h.

Nous avons essayé de préparer par élutrition les particules de diamètre supérieur à 10 μ, en épuisant d'abord la poudre hétérogène en fins $< 10\ \mu$, au moyen d'un courant d'air de vitesse déterminée puis en augmentant légèrement la vitesse pour recueillir les particules de dimension légèrement supérieure. En principe, une telle méthode est susceptible de fournir des fractions très homogènes, mais en fait, on se heurte à plusieurs difficultés:

(1) si le mélange hétérogène initial contient beaucoup de fins, son épuisement exige un temps très long; d'autre part, en partant d'un mélange moins fin, nous avons obtenu des résultats optiques qui ne cadraient pas avec ceux obtenus sur les fractions de sédimentation d'un mélange fin.

(2) l'appareil dont nous disposions ne permettait pas de préparer aisément des échantillons en quantité suffisante pour les essais infrarouges que nous nous proposions d'effectuer.

Nous sommes ainsi revenu à la méthode par sédimentation; les échantillons utilisés par LEJEUNE et DUYCKAERTS [1] avaient été obtenus comme suit: la poudre hétérogène de calcite est mise en suspension dans l'alcool isopropylique contenu dans un récipient d'une trentaine de cm de haut puis on récolte, dans le fond du récipient, dans des petits godets séparés, les fractions sédimentées entre les temps $t_1 - t_2$, $t_2 - t_3$, $t_3 - t_4$, . . . , etc. Cette façon d'opérer ne pouvait donner qu'un premier fractionnement fort imparfait, comme le montrait d'ailleurs l'examen au microscope.

Pour améliorer les résultats, nous avons procédé à une série de sédimentations successives: chaque fraction de la première opération est remise en suspension et sédimentée une nouvelle fois et les opérations sont répétées de 3 à 7 fois suivant les besoins. Lorsque l'examen au microscope indique que la fraction est suffisamment homogène, on prend quelques photos destinées à la mesure précise du diamètre moyen des grains. Les valeurs renseignées dans les tableaux suivants constituent les moyennes des mesures effectuées sur une centaine de particules de chaque fraction.

2. Préparation des pastilles de KBr

Le KBr utilisé pour la préparation des pastilles doit être broyé le plus finement possible, d'abord parce que cela augmente la transparence des lames de KBr et ensuite parce que cela facilite le mélange entre le KBr et la substance à étudier.

Les différentes fractions de KBr obtenues par broyage devant être identiques, les conditions du broyage sont toujours maintenues constantes: 8 g de KBr UCB pour analyse sont broyés grossièrement à la main et séchés 24 h. à l'étuve à 100°, ensuite broyés *sous vide* pendant 24 h. dans un broyeur mécanique tournant à 150 tours/minute. Le KBr broyé est gardé sous exsiccateur. Les multiples précautions prises pour préserver le KBr de l'humidité doivent être strictement observées. Le KBr humide présente en effet des bandes d'absorption intenses gênantes.

Avant la préparation des pastilles, les fractions de calcite et surtout celles de Dowex dont les grains ont tendance à gonfler dans l'eau sont séchées soigneusement à l'étuve à 100°. On pèse exactement un mgr de substance et on l'ajoute à 0·2 g de KBr; le mélange est agité mécaniquement pendant 2 minutes au moyen d'un vibreur, introduit dans un moule et comprimé sous vide pendant 5 minutes avec une charge de 10 tonnes. Les pastilles obtenues ont 12 mm de diamètre et 0·61 mm d'épaisseur. La transmission des pastilles de KBr pur varie entre 95 et 100 per cent dans la région allant de 2500 cm^{-1} à 800 cm^{-1}. Les pastilles, parfaitement transparentes lorsqu'on les retire du moule, se ternissent rapidement à l'air; aussi sont-elles conservées sous exsiccateur.

3. Prise des spectres et mesure des absorptions

Tous les spectres ont été enregistrés au spectrophotomètre Perkin Elmer modèle 21 dans les conditions suivantes:

prisme	NaCl
résolution	935
gain	6·8
réponse	1
fente	117 μ à 1,000 cm^{-1}

La transmission est réglée à 100 per cent après avoir placé une pastille de KBr pur dans chaque faisceau. On enregistre ensuite le spectre de la substance en plaçant une pastille de KBr pur dans le faisceau de référence et la pastille contenant la substance dans le second faisceau.

Dans le cas des deux bandes du Dowex et dans celui des deux bandes à 876 cm^{-1} et 710 cm^{-1} de la calcite, nous utilisons pour la mesure des absorptions la méthode des lignes de base [3], qui consiste à interpoler entre les deux ailes de la bande et à considérer l'absorption de la bande par rapport à cette ligne prise pour 100. De cette manière, on peut espérer dissocier dans la mesure du possible les pertes de lumière par absorption et par diffusion. La bande de la calcite à 1431 cm^{-1}, au contraire, est extrêmement large; une interpolation devient hasardeuse; aussi dans ce cas, nous utilisons la méthode des extinctions compensées [4]: elle consiste à mesurer l'extinction à deux longueurs d'ondes—dans ce cas 1780 et 1431 cm^{-1}—à partir de la courbe de transmission (I_0) obtenue avec une lame de KBr dans chaque faisceau, soit:

$$E' \equiv \log \frac{I_0\ 1780\ cm^{-1}}{I\ 1780\ cm^{-1}}: \text{ extinction due à la substance dans l'aile de la bande.}$$

$$E'' \equiv \log \frac{I_0\ 1431\ cm^{-1}}{I\ 1431\ cm^{-1}}: \text{ extinction au maximum de la bande d'absorption.}$$

$$E = E'' - E' = \text{extinction compensée.}$$

Cette méthode permet également de se libérer dans une certaine mesure des pertes de lumière par diffusion.

VOL. 7 1955/5

4. Résultats

Les résultats expérimentaux que nous allons exposer ont été confrontés avec les équations théoriques établies par G. DUYCKAERTS [2].

Calcite: grains assimilés à des cubes:

$$E = -\frac{m}{K\rho s d}\log\left[(1-K)+K\theta\right] \quad \text{avec } \theta = e^{-kd} \qquad (n \gg 1) \qquad \text{(I)}$$

$$E = -\log\left[(1-\mathscr{H})+\mathscr{H}\theta\right] \qquad \text{avec } \mathscr{H} = \frac{m}{\rho s d} \qquad (n < 1) \qquad \text{(II)}$$

Dowex: grains parfaitement sphériques:

$$E = -3/2\,\frac{m}{K\rho s d}\log\left[(1-K)+K\theta\right] \quad \text{avec } \theta = \frac{2[1-(kd+1)]e^{-kd}}{d^2k^2} \quad (n \gg 1) \qquad \text{(III)}$$

$$E = -\log\left[(1-)\mathscr{H}+\mathscr{H}\theta\right] \qquad \text{avec } \mathscr{H} = 3/2\,\frac{m}{\rho s d} \quad (n < 1) \qquad \text{(IV)}$$

$\mathscr{H}$ = fraction de surface recouverte par la poudre,

n = nombre de couches.

Les autres termes ont la signification signalée dans l'introduction.

A. *Calcite*

En vue de la comparaison des résultats expérimentaux contenus dans le tableau I avec les formules théoriques rappelées ci-dessus, il est nécessaire de rechercher les valeurs des deux constantes k et K:

Le coefficient d'absorption intrinsèque k peut être déterminé par passage à la limite:

$$\lim_{d\to 0} E = \frac{mk}{2{\cdot}3\rho s}$$

Lorsque les valeurs expérimentales ne permettent pas le passage à la limite (bande trop intense), ce coefficient doit être recherché par tâtonnement.

La valeur de K est recherchée par tâtonnement ou par voie graphique. En effet, quand le coefficient d'absorption intrinsèque est élevé, le terme exponentiel dans les formules ci-dessus devient négligeable pour les grands diamètres. Si donc, on porte dans un graphique E en fonction de $m/\rho s d$, on obtient une droite de coefficient angulaire $-1/K \log (1-K)$, qui permet de calculer K; cette méthode a été utilisée pour la bande intense à 876 cm^{-1}.

Les courbes calculées tracées sur les figures 1, 2, 3, et 4 ont été obtenues avec les valeurs suivantes:

1431 cm^{-1};	$K = 0{\cdot}8$;	$k = 3{\cdot}5\ \mu^{-1}$;	$\lim_{d\to 0} E = 4{\cdot}9$
876 cm^{-1};	$K = 0{\cdot}8$;	$k = 0{\cdot}995\ \mu^{-1}$;	$\lim_{d\to 0} E = 1{\cdot}41$
710 cm^{-1};	$K = 0{\cdot}8$;	$k = 0{\cdot}293\ \mu^{-1}$;	$\lim_{d\to 0} E = 0{\cdot}417$

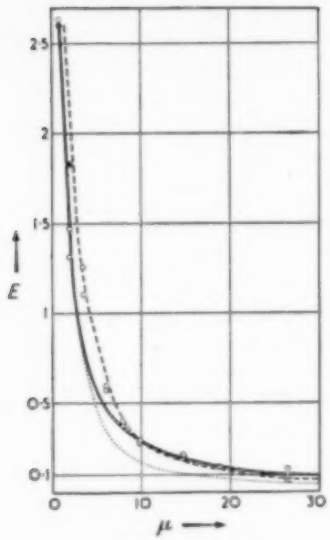

Fig. 1. Calcite.

1431 cm^{-1} $K = 0{\cdot}8$ $k = 3{\cdot}5\ \mu^{-1}$

——— courbe théorique calculée au moyen de l'équation (I)
. . . . . courbe théorique calculée au moyen de l'équation (II)
– – – – courbe théorique calculée au moyen des équations (III) et (IV)
○ points expérimentaux (valeurs obtenues à partir des prises de 1 mg)
● points expérimentaux (valeurs obtenues à partir des prises de 0·5 mg et doublées).

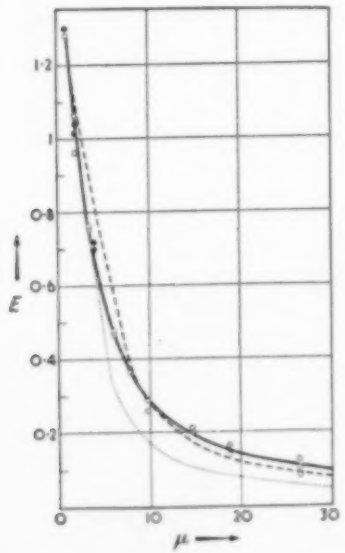

Fig. 2. Calcite.

876 cm^{-1} $K = 0{\cdot}8$ $k = 0{\cdot}995\ \mu^{-1}$

——— courbe théorique calculée au moyen de l'équation (I)
. . . . . courbe théorique calculée au moyen de l'équation (II)
– – – – courbe théorique calculée au moyen des équations (III) et (IV)
○ points expérimentaux (valeurs obtenues à partir des prises de 1 mg)
● points expérimentaux (valeurs obtenues à partir des prises de 0·5 mg et doublées).

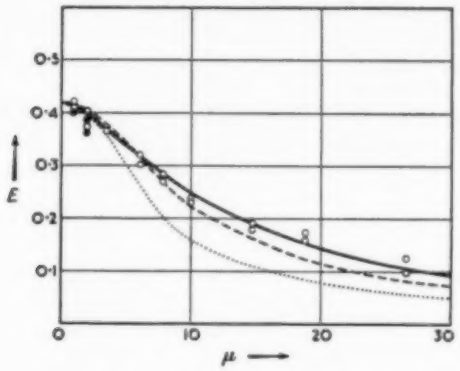

Fig. 3. Calcite.

710 cm^{-1} $K = 0{\cdot}8$ $k = 0{\cdot}293\ \mu^{-1}$

——— courbe théorique calculée au moyen de l'équation (I)
..... courbe théorique calculée au moyen de l'équation (II)
– – – – courbe théorique calculée au moyen des équations (III) et (IV)
○ points expérimentaux (valeurs obtenues à partir des prises de 1 mg)
● points expérimentaux (valeurs obtenues à partir des prises de 0·5 mg et doublées).

OL.
7
5/56

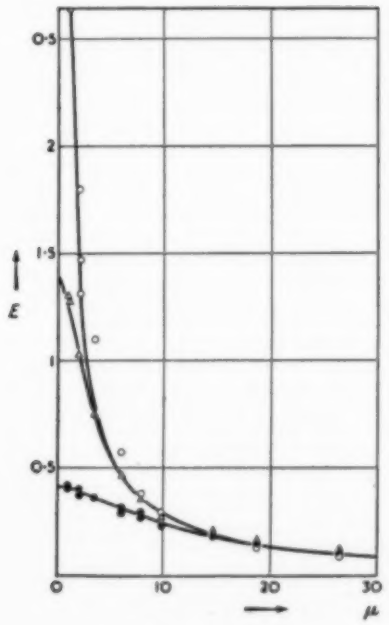

Fig. 4. Calcite.

——— courbes théoriques calculées au moyen de la formule (I)
○ points expérimentaux—1,431 cm^{-1}
△ points expérimentaux— 876 cm^{-1}
● points expérimentaux— 710 cm^{-1}.

Tableau 1. *Calcite*

$m = 1$ mg $\quad s = 1{\cdot}13$ cm^2 $\quad \rho = 2{\cdot}71$ g/cm^3

1. Valeurs expérimentales $\quad$ 2. Valeurs calculées par la formule (I)

Diamètre des grains	$E = \log\left(\frac{I_0}{I}\right)$					
	1 431 cm^{-1}		876 cm^{-1}		710 cm^{-1}	
Microns	1	2	1	2	1	2
26·5	0·072 0·082	0·150	0·085 0·103	0·150	0·099 0·120	0·108
18·8	0·137	0·148	0·140 0·164	0·148	0·159 0·174	0·155
14·7	0·201 0·207	0·195	0·201 0·211	0·195	0·179 0·191	0·192
9·8	0·281 0·290	0·290	0·258 0·287	0·290	0·232 0·235	0·250
7·9	0·384 0·392	0·365	0·365 0·366	0·365	0·268 0·284	0·285
6·1	0·575 0·594	0·475	0·465 0·477	0·470	0·302 0·319	0·318
3·5	1·10	0·840	0·753 0·764	0·760	0·363 0·364	0·365
2·1	1·31 1·47	1·430	0·963 1·11	1·038	0·372 0·402	0·401
1	2·65	2·650	1·28 1·30	1·245	0·408 0·420	0·404
0·5		3·840		1·330		0·407
0·1		4·780		1·390		0·414
0·01		4·940		1·396		0·416
0·001		4·970		1·407		0·417

Si nous examinons d'abord l'ensemble de nos résultats expérimentaux, nous constatons que, dans les grandes lignes, les conclusions générales tirées des résultats préliminaires de la note signalée [1] ne sont pas modifiées:

VOL. 7 1955/5

(1) pour une quantité de substance donnée, l'extinction d'une bande d'absorption augmente lorsque la dimension des particules diminue et elle tend vers une valeur limite aux très faibles diamètres.

(2) cette extinction limite est atteinte d'autant plus rapidement que le coefficient d'absorption intrinsèque de la bande est plus faible.

(3) lorsque la dimension des particules augmente, l'extinction paraît tendre vers une courbe commune à toutes les bandes.

Si, maintenant, nous regardons les nouveaux résultats sous un angle plus quantitatif, à la lumière des considérations théoriques de la première partie, nous pouvons faire les constatations suivantes: tout d'abord, il est possible de représenter de façon satisfaisante les résultats expérimentaux par la formule (I), dans tout le domaine étudié; les nouvelles valeurs de k et K diffèrent très fort de celles obtenues antérieurement; la cause réside dans l'amélioration du fractionnement obtenu dans nos essais; pour un fractionnement imparfait, les petits grains non éliminés viennent remplir les vides laissés entre les gros grains et la valeur de K est augmentée; de même, un fractionnement imparfait doit conduire à un nivellement de la courbe d'extinction en fonction de la dimension. Notons d'ailleurs que la nouvelle valeur de $K = 0{\cdot}8$ se rapproche très fort de la valeur théorique pour les sphères.

D'autre part—et ceci est plus surprenant et plus difficile à interpréter—la formule (I) qui représente de façon convenable l'ensemble des résultats expérimentaux est relative au cas d'une préparation contenant plusieurs couches de particules; or, un calcul approché montre qu'au delà de 5 μ, le nombre de particules est insuffisant pour donner plus d'une couche; il faudrait donc à partir de là utiliser la formule (II) et elle donne un accord beaucoup moins satisfaisant. Il est difficile de savoir, sur la base des résultats expérimentaux dont nous disposons actuellement, si cette anomalie n'est qu'apparente et provient du fait que le petit nombre de grains fins qui subsistent malgré les sédimentations répétées est suffisant pour donner toujours plus d'une couche ou si les considérations théoriques approchées ne cadrent pas de façon suffisante avec la réalité et qu'alors la formule (I) théoriquement établie pour une partie du domaine expérimenté, traduit néanmoins parfaitement l'ensemble des phénomènes observés.

Signalons egalement que dans le cas des deux bandes les plus intenses, nous avons été forcé de réduire la prise d'essai de 1 mg à 0·5 mg pour obtenir des extinctions mesurables avec une précision satisfaisante pour les fractions 3·5–2·1 et 1 μ; les valeurs ainsi obtenues ont été doublées et portées également sur les courbes expérimentales établies à partir des prises de 1 mg. (Nous avons pu montrer que dans cette région, l'extinction est proportionnelle à la quantité de substance jusqu'à des extinctions très élevées.)

B. *Dowex*

Les courbes calculées tracées sur les figures 5 et 6 ont été obtenues avec les valeurs suivantes;

$1028\ \text{cm}^{-1}$; $K = 0{\cdot}8$; $k = 0{\cdot}080\ \mu^{-1}$; $\lim_{d \to 0} E = 0{\cdot}212$

$1001\ \text{cm}^{-1}$; $K = 0{\cdot}8$; $k = 0{\cdot}090\ \mu^{-1}$; $\lim_{d \to 0} E = 0{\cdot}239$

Nous avons adopté, pour le calcul des courbes théoriques, la même valeur de K que dans le cas de la calcite; en effet, cette valeur est proche de la valeur limite théorique et d'autre part, comme les coefficients d'absorption intrinsèques sont faibles, la valeur de K n'a que peu d'influence sur le tracé des courbes.

Pour la concentration de 1 mg de Dowex dans 0·2 g de KBr, il ne peut y avoir

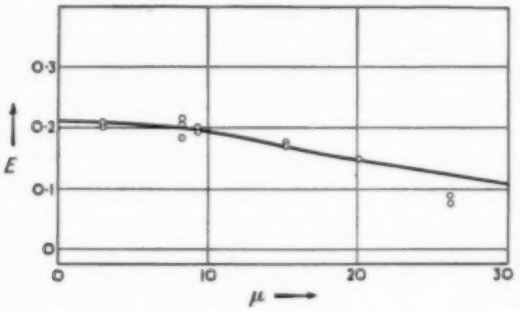

Fig. 5. Dowex.

1028 cm^{-1} $K = 0{\cdot}8$ $k = 0{\cdot}080\ \mu^{-1}$

——— courbe théorique calculée au moyen des équations (III) et (IV)

○ points expérimentaux.

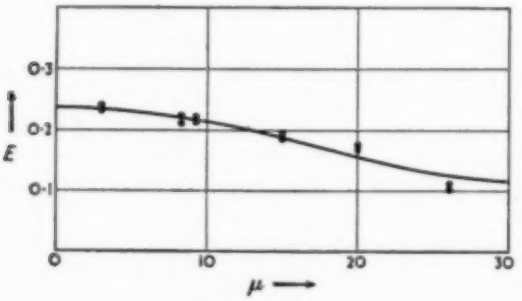

Fig. 6. Dowex.

1001 cm^{-1} $K = 0{\cdot}8$ $k = 0{\cdot}090\ \mu^{-1}$

——— courbe théorique calculée au moyen des équations (III) et (IV)

● points expérimentaux.

une couche complète que pour des valeurs des diamètres des grains inférieures à environ 11 μ:

$$n = 1 \text{ pour } d = 3/2\,\frac{10m}{K\rho s} = 11\ \mu.$$

Jusqu'à 10 μ, la courbe théorique est calculée au moyen de la formule particulière (IV) et en dessous, au moyen de la formule générale (III). La poudre initiale est très pauvre en grains fins: il ne nous a pas été possible de recueillir une fraction suffisante $< 3\ \mu$. Il est donc normal que les valeurs expérimentales concordent mieux avec la formule particulière que dans le cas de la calcite.

La même conclusion que dans le cas de la calcite s'impose; les coefficients d'absorption intrinsèques étant très faibles, la limite des valeurs de l'extinction est beaucoup plus vite atteinte que dans le cas des bandes de la calcite.

Tableau 2. Dowex

$m = 1$ mg $\quad s = 1{\cdot}13$ cm^2 $\quad \rho = 1{\cdot}45$ g/cm^3

1. Valeurs expérimentales 2. Valeurs calculées

Diamètre des grains	$E = \log \frac{I_0}{I}$			
Microns	1,028 cm^{-1}		1,001 cm^{-1}	
	1	2	1	2
26·1	0·092 0·089	0·125	0·108 0·106	0·125
19·9	0·150 0·151	0·150	0·171 0·175	0·150
15·2	0·160 0·168	0·168	0·178 0·188	0·185
9·3	0·195 0·198	0·194	0·214 0·223	0·217
8·3	0·194 0·198	0·195	0·212 0·222	0·220
3	0·200 0·205	0·206	0·235 0·240	0·232
2	—	0·208	—	0·234
1	—	0·210	—	0·236

En général, on peut dire que l'extinction devient pratiquement constante (à 3 pour cent près) pour des valeurs de $kd < 0{\cdot}3$; en effet, voici les diamètres à partir desquels l'extinction atteint pratiquement la valeur limite:

Calcite: $k = 3{\cdot}5\ \mu^{-1}$; $d = 0{\cdot}085\ \mu$; Dowex: $k = 0{\cdot}090\ \mu^{-1}$; $d = 3{\cdot}3\ \mu$

$k = 0{\cdot}995\ \mu^{-1}$; $d = 0{\cdot}3\ \mu$; $k = 0{\cdot}080\ \mu^{-1}$; $d = 3{\cdot}7\ \mu$

$k = 0{\cdot}293\ \mu^{-1}$; $d = 1\ \mu$.

En bref, on peut constater que ce phénomène complique très sérieusement l'utilisation des spectres de poudres pour l'analyse quantitative et que si l'on désire se placer dans des conditions où la granulométrie ne joue pratiquement plus aucun rôle, il est nécessaire de broyer les échantillons jusqu'à un degré de

finesse très grand et d'autant plus grand que les bandes utilisées possèdent un coefficient d'absorption intrinsèque élevé.

C. *Variation de l'extinction avec la quantité de substance*

La théorie montre que, dans le cas où n est inférieur à 1, c'est l'absorption qui est proportionnelle à la quantité de substance par unité de surface tandis que dans le cas où n est supérieur à 1, c'est l'extinction qui devient proportionnelle à cette quantité.

Pour vérifier ce point de la théorie, nous avons préparé des pastilles de calcite et de Dowex de différentes concentrations, dans les deux cas, au moyen de la fraction 20 μ.

Tableau 3. *Calcite*

1. Valeurs expérimentales.
2. Valeurs calculées au moyen de la formule (I).
3. Valeurs calculées au moyen de la formule (II).

Concentration $m/\rho s$ *Volume/unité de surface*	876 cm^{-1}						710 cm^{-1}					
	$E = \log \frac{I_0}{I}$			$A = \left(1 - \frac{I}{I_0}\right)$			$E = \log \frac{I_0}{I}$			$A = \left(1 - \frac{I}{I_0}\right)$		
	1	2	3	1	2	3	1	2	3	1	2	3
0·327	0·145 0·148	0·152	0·083	0·293 0·284	0·299	0·174	0·159 0·162	0·152	0·083	0·306 0·313	0·299	0·174
0·654	0·288 0·334	0·304	0·185	0·485 0·537	0·503	0·347	0·297 0·331	0·304	0·185	0·495 0·533	0·503	0·347
0·981	0·434 0·438	0·456	0·329	0·634 0·649	0·650	0·531	0·447 0·457	0·456	0·329	0·643 0·651	0·650	0·531

Dans les figures 7 et 8, nous avons porté à la fois l'extinction et l'absorption en fonction de la quantité de substance.

On voit pour la calcite que, bien qu'en principe, pour des grains parfaitement homogènes, la quantité soit insuffisante pour former plus d'une couche, c'est néanmoins la proportionnalité entre l'extinction et la concentration qui est observée; d'autre part, les points expérimentaux, en valeur absolue, comme le montre le tableau, satisfont beaucoup mieux à la formule relative à plus d'une couche. Ces deux observations confirment la conclusion antérieure pour la calcite à savoir que le nombre de petits grains qui subsistent est suffisante pour former plus d'une couche. Dans ce cas, c'est l'absorption et non l'extinction qui est proportionnelle à la concentration. Nous nous trouvons dans le cas où n est inférieur à 1.

Les résultats obtenus ci-dessus sont une nouvelle preuve de la validité des équations théoriques.

Cette étude de l'influence de la granulométrie sur l'intensité des bandes d'absorption est naturellement encore très incomplète. Nous nous proposons de l'étendre d'une part dans un domaine plus étendu de longueurs d'ondes et d'autre part à des substances dont les grains ont des formes très différentes de cubes ou de sphères.

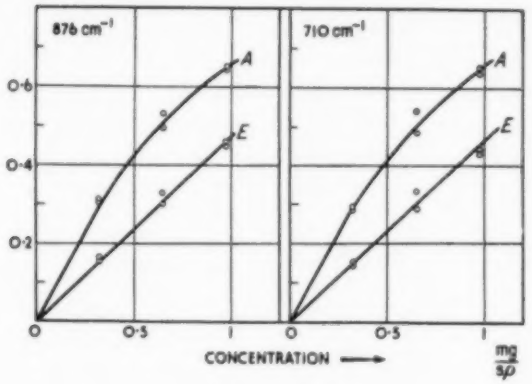

Fig. 7. Calcite.
——— courbes théoriques
⊙ points expérimentaux.

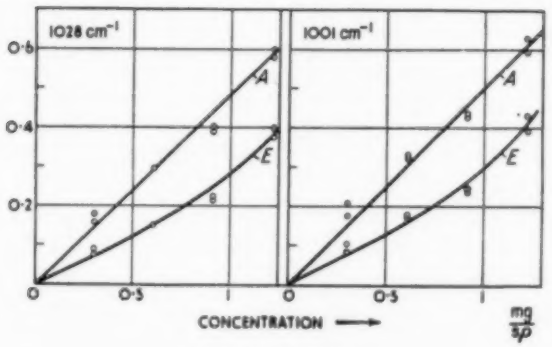

Fig. 8. Dowex.
——— courbes théoriques
⊙ points expérimentaux.

Enfin, des essais sont actuellement en cours en vue de l'application de la technique des pastilles de KBr à l'analyse quantitative.

Il nous est particulièrement agréable d'adresser nos plus vifs remercîments à Monsieur le Professeur G. Duyckaerts qui nous a suggéré ce travail de recherche et qui nous a aidé de ses précieux conseils tout au long de sa réalisation.

Nous tenons aussi à exprimer notre reconnaissance à l'I.R.S.I.A. qui, en nous accordant une bourse de spécialisation, nous a permis d'entreprendre ce travail.

Tableau 4. *Dowex*

1. Valeurs expérimentales.
2. Valeurs calculées au moyen de la formule (IV).

Concentration $m/\rho s$ *Volume/unité de surface*	1028 cm^{-1}				1001 cm^{-1}			
	$E = log \frac{I_0}{I}$		$A = \left(1 - \frac{I}{I_0}\right)$		$E = log \frac{I_0}{I}$		$A = \left(1 - \frac{I}{I_0}\right)$	
	1	2	1	2	1	2	1	2
0·305	0·075 0·087	0·069	0·159 0·181	0·147	0·085 0·102	0·073	0·177 0·209	0·155
0·610	0·150 0·151	0·151	0·292 0·293	0·294	0·171 0·175	0·159	0·325 0·331	0·306
0·915	0·217 0·222	0·251	0·393 0·400	0·439	0·243 0·248	0·267	0·429 0·435	0·460
1·220	0·376 0·399	0·383	0·579 0·601	0·586	0·392 0·432	0·413	0·594 0·630	0·613

VOL. 7 1955/5

Résumé

Cet article relate une série de résultats expérimentaux concernant l'influence de la dimension des particules sur l'intensité des bandes d'absorption infrarouge des substances en poudre.

Ils ont été obtenus au moyen de la technique des pastilles de KBr; la substance absorbante dispersée dans le KBr a été soigneusement calibrée par des sédimentations répétées.

Les données expérimentales sont relatives aux bandes de la calcite à 1,431, 876, 710 cm^{-1}, et aux bandes du Dowex à 1,028 et 1,001 cm^{-1}.

Les résultats sont discutés sur la base des formules théoriques proposées dans la première partie de cet article.

Bibliographie

[1] Lejeune, L. R., et Duyckaerts, G.; *Spectrochim. Acta* 1954 **6** 194–197.

[2] Duyckaerts, G.; *Spectrochim. Acta* 1955 **7** 25-31.

[3] Heigl, J. J., Bell, M. F., et White, J. V.; *Ind. Eng. Chem.* (Anal.) 1947 **19** 293.

[4] Pirlot, G.; *Bull. Soc. Chim. Belge* 1950 **59** 327.

Spectrochimica Acta, 1955, Vol. 7, pp. 45 to 59. Pergamon Press Ltd., London

Quantitative Spektrochemische Analyse Mittels des Gleichstrom Kohlebogens

N. W. H. Addink

unter Mitarbeit von

J. A. M. Dikhoff, Frl. C. Schipper, A. Witmer, und T. Groot

Philips Forschungslaboratorium, N.V. Philips' Gloeilampenfabrieken, Eindhoven-Niederlande

(Vorläufige Mitteilung)*

(*Received* 23 *August* 1954)

Summary—A complete description of the "Constant temperature arc" method of quantitative analysis which has been developed in Eindhoven is given, with tables of the empirically determined K-values announced so that they can be checked in other laboratories. The method consists of completely volatilizing 5 mg of a powdered sample in a shallow anodic crater of a carbon arc, with the addition of materials to modify the rate of volatilization if required. The line intensities are calibrated by comparison with selected Fe-lines so as to get comparable analytical results; the calculations required are illustrated by several examples which also indicate the accuracy of the method.

Allgemeines Prinzip

Physikalisches

Bringt man eine Substanz in einen Lichtbogen, so wird sie in folge der hohen Temperatur in ihre Bestandteile zerlegt; die Bruchteile (Atome oder Moleküle) werden zur Lichtemission angeregt. Zerlegt man das ausgesandte Licht mittels eines Spektralapparates, so nimmt man in Abhängigkeit von der Menge des Stoffes mehr oder wenig stärkere Intensitäten der Spektrallinien wahr. Die vollständige Verdampfung einer relativ geringen Menge Materials (5 mg) liefert eine auf einer Photoplatte integrierte Intensität von Spektrallinien, welche der Konzentration der betreffenden Elemente proportional ist. Um Proportionalität zu erreichen, ist es notwendig geringe Dampfdichte zustande zu bringen, sowie auch relativ geringe Linienintensitäten zu messen (Eliminierung der Selbstabsorption). Wegen der Kathoden- und Anoden-Effekte wird das analysierte Licht nur aus der Mitte des Bogens entnommen (durch eine Blende zwischen Lichtquelle und Spalt, oder mit Hilfe einer Zwischenabbildung), wo die Temperaturverteilung über den Querschnitt als konstant anzusehen ist. Diese Temperatur kann unter konstant gehaltenen Bedingungen nur abhängen von den verdampfenden Substanzen (Elemente mit niedriger Ionisierungsspannung setzen die Temperatur bekanntlich herab). Der Einfluss der verdampfenden Analysensubstanz auf die Temperatur kann aber gering gehalten werden, indem man nur eine relativ kleine Menge verdampft: die Menge des in der Säule befindlichen Kohlenstoffs wird immer relativ gross gehalten durch die richtige Form der Elektroden. Auf

* Auf Anregung in Gesprächen während des vierten Internationalen Kolloquiums für Spektroskopie (Münster, September 1953) mit den Herren Dr. H. J. Eichhoff, Dr. W. Seidel und anderen.

diese Weise kann man von einem Kohlebogen verhältnissmässig konstanter Temperatur sprechen. Diese Massnahme hat zur Folge, dass man—im Gegensatz zu der Harveyschen Methode—den Einfluss der Hauptbestandteile nach den bisherigen Erfahrungen nicht zu berücksichtigen braucht.

Chemisches

Um die Verdampfung auch von hochschmelzenden Substanzen durchführen zu können, werden diese auf die Anode gebracht, da die Anodenbrennflecktemperatur höher ist als die der Kathode. Dann müssen aber notwendigerweise auch Massnahmen getroffen werden um die Verdampfungsgeschwindigkeit der leicht verdampfenden Substanzen entsprechend herabzusetzen. Andrerseits liegen auch Fälle vor, wo die Brennflecktemperatur (etwa 3400°C) immer noch zu niedrig ist, um in einer praktisch zulässigen Zeit von sechs bis acht Minuten die Verdampfung vollständig durchführen zu können. Im ersten Falle verzögert man die Geschwindigkeit der Verdampfung z.B. mittels Quarzpulvers, mit welchem das Untersuchungsmaterial *überschichtet* wird; im zweiten Falle erhöht man sie durch einen Verdampfungsträger, ein relativ leicht aber nicht zu schnell verdampfen des Materials, wie z.B. Nickel, *unterhalb* des Untersuchungsmaterials. Immer wird die Gesamtmasse abgedeckt mit reinem Kohlepulver, damit während des Zündens des Bogens nur Kohlepartikel herausgeschleudert werden können. Falls der Brennfleck nicht auf dem Material haftet, kann man durch Beimischen von anderen Substanzen die Verdampfung doch vollständig machen. Es ist auch möglich, dass das Material während des Brennens spritzt, entweder im festen oder im flüssigen Zustand; in solchen Fällen wird dieses Verhalten durch Zumischung geeigneter Substanzen verhindert (s. Tabelle 1).

Praktisches

Nachdem mittels photometrischer Messungen von bestimmten Fe I-Linien im Gebiete 2450–3500 Å festgestellt worden ist in welchem Masse der verwendete Spektralapparat[1] von demjenigen abweicht, mit welchem die später zu erwähnenden K-Werte bestimmt worden sind—eine Differenz, welche im allgemeinen 10 Prozent nicht überschreitet, wie bis heute gefunden wurde—werden die Entwicklungsbedingungen der Photoplatten, welche verwendet werden sollen, zweckmässig so gewählt, dass die Schwärzungskurve eine Neigung von $\gamma = 1$ aufweist. Die Schwärzungskurve selbst wird so aufgestellt, dass der Schwärzung, $S = 0{\cdot}30$ eine relativ Intensität von 4·0 entspricht.

Die mit einem Mikrophotometer bestimmten Schwärzungen von Spektrallinien und von deren Untergrund werden mit dieser Schwärzungskurve in relative Intensitäten umgerechnet oder diese Intensitäten werden mit einer s-p-d-Skala, welche auf die Schwärzungskurve bezogen ist, ermittelt. Für den weiteren Gang einer Analyse sind zwei Fälle zu unterscheiden:

[1] Die Absicht ist, einer grossen Anzahl Fe I Linien im Gebiete 2450–3500 Å genau bestimmte Intensitäten zu geben. Unter vollkommen gleichen Bedingungen der Lichtanregung im Bogen werden Intensitätsbestimmungen derselben Linien mit dem Spektralapparat, welche zu Verfügung steht, wiederholt. Der Verlauf der Verhältnisse der Intensitätsbestimmungen mittels beider Apparaten ermöglicht das Übertragen von Angaben von einem zum anderen Apparat. Die Untersuchung zusammen mit Dr. Eichhoff ist noch im Gange.

VOL. 7 1955/5

(1) Die Probe besteht nur aus Elementen, die spektrochemisch bestimmt werden (z.B. Metalllegierungen), d.h. die Summe der Prozentgehalte der spektrochemischen Vollanalyse muss 100 Prozent ergeben. In diesem Falle wird entsprechend der Beziehung $C = K \cdot I$ (C = Konzentration in Prozent, K = Proportionalitätsfaktor—"K-Wert," I = Intensität) die Konzentration aller Elemente bestimmt. Ergibt deren Summe nun z.B. 120 Prozent, so werden sämtliche primär erhaltenen Konzentrationswerte durch "innere Normierung," welche in diesem Beispiel in einer Multiplikation mit dem Faktor 100/120 (Normierungsfaktor) besteht, korrigiert.

(2) Die Probe enthält auch spektrochemisch nicht bestimmbare Elemente, oder es wird keine spektrochemische Vollanalyse ausgeführt (z.B. Salze, Minerale, u.s.w.). In diesem Falle wird eine "*äussere Normierung*" vorgenommen. Zu diesem Zweck werden mindestens 2 Aufnahmen von 5 mg reinem Eisen (unter gegebenen Bedingungen, s. Tab. 1) gemacht; die Blende, welche nur das Licht aus der Mitte der Bogensäule passieren lässt (s. Fig. 2), wird so gewählt (Länge 15 mm; Breite etwa 0·5 mm), dass die Eisenlinien 2645·42, 2667·91, 2883·7 und 2815·50 Å eine Schwärzung von $\sim 0{\cdot}3$, d.h. einen Intensitätswert von ~ 4 aufweisen. *Soweit wird dieses Verfahren in allen Fällen angewandt, um die Aufnahmeapparatur grössenordnungsmässig auf die Benutzung der im Folgenden wiedergegebenen Tabelle der K-Werte einzustellen.* Zur vollständigen äusseren Normierung verfährt man nun so, dass man die Intensitäten der genannten Eisenlinien genau bestimmt und unter Anwendung der entsprechenden K-Werte eine Reihe von Konzentrationswerten für das reine Eisen berechnet, aus denen ein Mittelwert gebildet wird. Der Eisengehalt muss zu 100 Prozent gefunden werden. Sollte nun z.B. ein Eisengehalt von p Prozent gefunden werden, der von 100 Prozent abweicht, so werden alle primär gefundenen Intensitätswerte mit dem Normierungsfaktor $100/p$ korrigiert. Alle Spektren, welche auf der gleichen Platte aufgenommen wurden, können nun analysiert werden: man hat nur die korrigierten Intensitäten der Linien mit den zu-gehörigen K-Werten zu multiplizieren.

OL.
7
5/56

Details der Methode

Das Analysenmaterial (homogen und identisch mit der empfangenen Probe) soll immer im feinverteilten Zustand vorliegen, die nichtmetallischen Substanzen pulverförmig, die metallischen Materialien als Feilicht (Teilchengrösse maximal 0·2 mm). Immer soll das Feilicht vor der Einwage mittels eines starken Elektromagneten oder durch Auskochen mit Salzsäure, wenn möglich, vom Eisen der Feile befreit werden.

Präparieren der Elektroden

Die obere Elektrode (Kathode) ist geformt wie Fig. 1 zeigt. Die Unterschneidung soll das störende Emporklettern des Bogens verhindern. Die untere Elektrode, die Anode, ist wie die Kathode aus Graphit hergestellt. Die folgende Liste (Tabelle 1) gibt Beispiele der Füllung der Anode; die getroffenen Massnahmen sprechen für sich selbst.

Bemerkung

Schwer verdampfende Stoffe wie W u. dgl. werden nicht quantitativ aus der Anode verdampft, sicher nicht, wenn sie in verhältnismässig hoher Konzentration anwesend sind. Die Verdampfung der Verunreinigungen in solchen Substanzen ist trotzdem vollständig, wie die Untersuchung ergeben hat. Die Bestimmung der schwer verdampfenden Stoffe selbst wird ausgeführt nach geeigneter Verdünnung (meistens mittels Nickelpulvers). Werden in einem solchen Fall x mg Analysensubstanz zur vollständigen Verdampfung gebracht, so müssen die K-Werte mit $5/x$ multipliziert werden.

Optisches

Es wurden drei Littrow Spektrographen der Firma Hilger (London) benutzt (zwei E 492 und ein E 478). Im allgemeinen wurde eine Spalthöhe von 2 mm gewählt und eine Spaltbreite von 0·025 mm. Die Sammellinse B (s. Fig. 2) sorgt dafür, dass ein scharfes Bild der Elektroden (D) an der Stelle des Prismas (nicht in die Figur aufgenommen) entworfen wird; ihre Brennweite beträgt 29 cm. Das untersuchte Wellenlängegebiet liegt zwischen 2450 und 3500 Å. Im allgemeinen soll dafür gesorgt werden, dass minimale Lichtmengen zum Spektrographen geführt werden. Zu diesem Zweck soll man jedoch nicht das Prisma oder die Sammellinse im Spektrographen abblenden, sondern eine Blende zwischen der Lichtquelle und dem Spalt des Spektrographen anbringen.

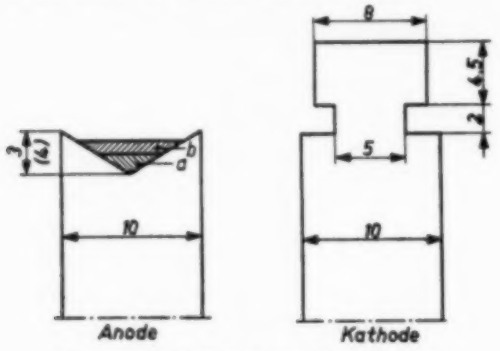

Fig. 1. Die benutzten Graphitelektroden.
Dimensionen in mm. a = Probe; b = Kohlepulverschicht.

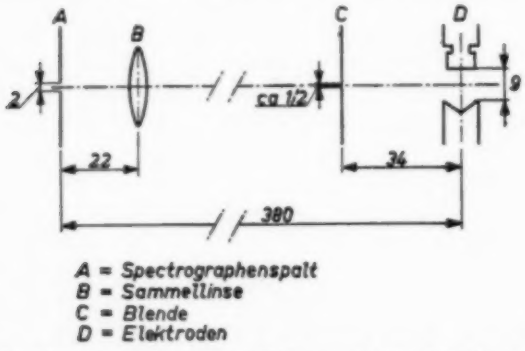

Fig. 2. Optische Anordnung (Lichtbogen-Blende-Sammel-linse-Spalt des Spektrographen).*

* Wenn ein Littrow-Spektrograph verwendet wird, empfehlt es sich die Blende $\frac{1}{2}$ bis 1 mm aus der optischen Achse zu stellen. Reflexionen gegen die optische Oberfläche im Innern des Spektrographen werden alsdann seitwärts gerichtet und grossenteils von der geschwärzten Innenseite des Instrumentes absorbiert.

"*Brennen*" *des Bogens*

Die Zündung geschieht durch Kurzschluss. Der Kurzschlussstrom wird auf einen bestimmten Wert eingestellt (in unserem Fall 16 Amp.). Dann wird die Kathode aufgezogen, bis der Elektrodenabstand $8\frac{1}{2}-9$ mm beträgt. (Während der ganzen Expositionszeit wird dieser Abstand innegehalten und unausgesetzt optisch kontrolliert.) Damit beginnt die Expositionszeit. Im Anfang wandert der Bogen und brennt meistens auf verschiedenen Teilen des Randes der Anode. Während dieser Zeit wird das Analysenmaterial auf höhere Temperatur gebracht, bis dessen Dampfdruck genügend ist, um die Bogenentladung zu tragen. Meistens beträgt

VOL. 7 1955/5

Tabelle 1

Das Füllen der Anoden (einige Beispiele). Es werden immer 5 mg Analysensubstanz abgewogen. Wenn ein Zusatz gemacht wird, wird das in der Tabelle angegeben mit:

(*u*) das heisst: Zusatz-schicht unter der Probe;

(*o*) das heisst: Zusatz-schicht über der Probe;

(*m*) das heisst: Probe und Zusatz werden *in* der Anodehöhlung mit einem kleinen Spatel gemischt. Falls der Zusatz aus 10 mg $BaCO_3$ oder 10 mg H_2BO_3 besteht, wird als Tiefe der Anodenhöhlung 4 mm statt 3 mm gewählt. $5SiO_2$ bedeutet 5 mg SiO_2 u.s.w.

Die Anodenfüllung von Probe und Zusatz wird immer mit einer Schutzschicht aus Kohlepulver (etwa 7 mg) abgedeckt.

Metalle (und Legierungen)	*Zusatz*	*Brennzeit in Minuten*[1]
Ag	$5SiO_2$ (*o*)	6
Al		7
Co		6
Cr	5C (*m*)	7
Cu	$5SiO_2$ (*o*)	7
Fe (und Stahl)	5C (*m*)	7
Fe (Nb, V in Stahl)	5Ni (*u*)	8
Mg	$5SiO_2$ (*o*)	6
Mg-Al-Legierung	$5SiO_2$ (*o*) 1Ni (*u*)	7
Mo	5C (*m*)	8
Ni		6
Ni in Cu, Ag	$5SiO_2$ (*o*)	6
Pb	$5SiO_2$ (*o*)	6
Pt	5Ni (*u*)	8
Sb	$5SiO_2$ (*o*)	6
Si		6
Sn	$5SiO_2$ (*o*)	6
V (Ferro-Vanadin)	5C (*m*)	7
W	5Ni (*u*)	8
W (in Stahl)	5Ni (*u*)	8
Zn	$5SiO_2$ (*o*)	6
Zn (legiert)	1Ni (*u*) $5SiO_2$ (*o*)	6
Zn (legiert mit Ag, Cu, Cd)	$5SiO_2$ (*o*)	6
Verbindungen:		
Carbide von Si		6
Carbonate der Erdalkalien		7
Ferrite	10C (*m*)	7
Phosphate des Al	$10H_3BO_3$ + 5C (*m*)	8
Phosphate	5C (*m*)	7
Oxyde von		
Al	$10H_3BO_3$ + 5C (*m*)	8
Cd	$5SiO_2$ (*o*)	6
Fe	5C (*m*)	7
Mo	$5BaCO_3$ (*m*)	8
Ti	$10BaCO_3$ + 5C (*m*)	8
W	5Ni (*u*)	8
Zn	$5SiO_2$ (*o*)	6
Zr	$10BaCO_3$ + 5C (*m*)	8
Silikate	1Ni (*u*)	7
Sulfate	(eventell 1Ni (*u*))	6 (7)
Sulfide (Zn, Cd)	$5SiO_2$ (*o*)	6
Wolframate (Ca)	5Ni (*u*)	8

[1] Es wurden Graphitstäbe (Johnson Matthey) verwendet (10 mm Diameter; 30 mm Länge). Die chrom-eisernen Elektrodenhalter wurden nicht künstlich mit Wasser gekühlt. Die Brennzeit ist mittels Fahrspektrogrammen bestimmt worden.

die Stromstärke dann etwa 10–12 Amp. Sie wird nicht nachreguliert. Im Falle leichtverdampfender Substanzen setzt die Verdampfung schon nach etwa 10 Sekunden ein, anderenfalls nach 1–2 Minuten. Es ist nicht ausgeschlossen, dass die geschmolzenen Substanzen in die Anode eindringen und deswegen ist es notwendig eine relativ lange Brennzeit einzuhalten (6–8 Minuten!)—Es soll darauf geachtet werden, dass das Brennen des Bogens während der Expositionszeit unausgesetzt (mittels eines dunklen Glases) beobachtet wird: es soll kein Analysenmaterial verspritzen (im Anfang sieht man nur ein geringes Spritzen des Kohlepulvers der oberen Schicht, welche das Material abdeckt). Am Ende der Exposition ist meistens die Stromstärke auf 7–10 Amp. abgefallen. Während dieser Periode werden die letzten Reste des Analysenmaterials verdampft; darauf sind die Schwankungen der Stromstärke zurückzuführen.

Um die Schwankungen so gering wie möglich zu machen und ein Erlöschen des Bogens am Ende der Expositionszeit zu vermeiden, ist es zu empfehlen, den Bogen mit einer Treibspannung von etwa 220 V zu betreiben.

Temperatur der Arbeitsräume

Mittels eines einfachen Temperaturreglers halten wir den Arbeitsraum auf 21 ± 1°C; auch die Temperatur der Dunkelkammer halten wir auf 21 ± 1°C. Trotzdem wird die Temperatur des Entwicklers (doppelwandige Schale) zu Beginn der Entwicklung auf 21·0°C eingestellt. Es wird mit der Hand in zwei senkrechten Richtungen abwechselnd geschaukelt und kein Pinsel während des Entwickelns benutzt. Mehrere Plattensorten sind benutzt worden (Gevaert Superchromosa und Scientia, Ilford Ordinary, Kodak SA2).

Auswertung der Spektren

Wie schon gesagt, kann die Ausmessung der Linienintensitäten mittels eines Photometers oder mittels der s.p.d. Skala (eine ausführliche Diskussion betreffs des Gebrauchs der s.p.d. Skala wird demnächst erscheinen) erfolgen. In beiden Fällen wird für den Untergrund korrigiert.

Im allgemeinen soll die Intensität den Wert 6 bis 10 nicht überschreiten, denn die Gleichung:

$$C = K \times I$$

(Konzentration = K-Wert × Intensität)

gilt nur, wenn die Selbstabsorption keine Rolle spielt. Da man-mit der s.p.d. Skala-ausreichend messen kann im Intensitätsgebiet zwischen $\frac{1}{2}$ und 6 bis 10, so kann man eine Linie in einem Intervall von etwa 1 : 15 gebrauchen. Es ist wünschenswert mehrere Linien zu messen. Trotzdem kann man gezwungen sein, höhere Werte zu benützen. In solchen Fällen steigt der K-Wert und nur dort wo steigende Werte einer Linie (s. die Tabelle 2) erwähnt sind, sind sie geprüft worden. Weiter soll man einen Mittelwert aus möglichst vielen Linienmessungen bilden. Beträgt die Standardabweichung x Prozent, so beträgt die von n Messungen $\frac{x}{\sqrt{n}}$ Prozent. Um Plattenfehler, Abweichungen im Brennen des Bogens zu eliminieren, ist es immer wünschenswert mehrere Aufnahmen zu machen.

Bevor ein Beispiel einer Berechnung gegeben wird, werden zunächst eine Reihe von K-Werten mitgeteilt (Tabelle 2).

Tabelle 2. K-Werte von 235 linien von 38 Elementen

Elemente	*Wellen-länge*, Å	*K-Wert*	*Int.*	*Elemente*	*Wellen-länge*, Å	*K-Wert*	*Int.*
Ag	3280·68 I	0·0011		Cd	2980·62 I	~ 1	
		0·0017	~ 20		2868·26 I	17	
		0·0025	~ 30		2775·04 I	25	
	3382·89	0·0015					
		0·0022	~ 20	Ce[x]	3063·01	0·9	
		0·003	~ 30		3077·64	5	
	2721·76	16					
				Co	3453·50 I	~ 0·007	
Al	3082·15 I	0·011			3465·80 I	~ 0·015	
	2575·10	0·14			2521·36	0·017	
	2567·98	0·16			3044·00	0·022	
	2652·48 I	~ 0·35			2627·64 I	0·7	
	3057·15	~ 4·5			3177·27	2·2	
	2669·16 II	50			2644·77 I	7·3	
As	2780·19 I	~ 0·3		Cr	2677·15 II	0·047	
	2860·45 I	~ 0·5			3013·71 I	0·2	
			bis 400!		2860·93 II	0·23	
B	2497·73 I	0·0053	bis 200!		2731·90 I	0·57	
	2496·77 I	0·011			2653·58 I	~ 0·6	
					2935·13	~ 4·7	
Ba	3071·59 I	1			2622·86	5	
	2785·26 I	36			2913·72	6·5	
	2702·63 I	47			2642·11	7·5	
	2596·67 I	55			2700·59 I	8·7	
					2785·70	10·5	
Be[x]	2650·63 I	0·01					
	2494·55 I	0·025		Cu	3247·54 I	0·0006	3
	2494·57 I				3273·96 I	0·0006	1
						0·001	5
Bi	3067·71 I	~ 0·007				0·0019	20
	2897·97 I	0·07			2824·36 I	~ 0·25	
	2989·02 I	0·08			2961·16 I	~ 0·4	
	2938·29 I	0·12			2766·37 I	1·0	
	3024·63 I	0·15			2997·36 I	3·5	
	2798·68 I	~ 60			3169·68 I	25	
					3156·62 I	30	
Ca	3179·33 II	~ 0·1			2978·27 I	~ 90	
	3158·86 I	~ 0·2					
	3181·27 II	~ 0·6	15–20	Fe	3020·64 I	0·0094	
	3006·85 I	0·65	5–7		2599·39 II	~ 0·02	
	2997·31	1·8			2739·54 II	~ 0·1	
	3009·20 I	~ 2			2628·29 II	~ 0·2	
	2994·95 I	2·4			2735·47 I	0·24	
	2721·64 I	20			2772·10 I	0·3	
					2767·52 I	~ 0·6	
Cd	3261·05 I	~ 0·1			2767·50 II		
	3466·20 I	~ 0·2			2623·53 I	0·6	
	3403·65 I	~ 0·4					

Tabelle 2 (continued)

Elemente	*Wellenlänge*, Å	*K-Wert*	*Int.*	*Elemente*	*Wellenlänge*, Å	*K-Wert*	*Int.*
Fe	2472·34 I	1·6		Mn	2589·70	~ 30	1½
	3200·47 I	1·9			2652·48	~ 40	1
	3205·40 I	2·1					
	3000·45 I	2·4		Mo[1]	3132·59	0·1	
	3215·94 I	2·5			3170·34	0·13	
	3055·26 I	2·8			3193·97	0·14	
	2877·30 I	4·0			2816·15 II	~ 0·2	
	2645·42 I	25			3158·16	~ 0·4	
	2667·91 I	27			2848·23 II	~ 0·4	
	2883·70 II	29			2930·50	~ 0·5	
	2883·73				2807·75	~ 1·8	
	2815·50 I	29			2602·79	5	
	2786·78	~ 75			2854·11	7·5	
Ga[x]	2943·63 I	0·025		Na	3302·32 I	0·35	1
					3302·32 I	0·6	4
Hf[x]	2940·77 I	0·25			3302·32 I	0·9	16
	2964·87	0·5					
	2975·88 II	0·5		Nb[x]	3194·97 II	0·15	
	2833·27	1			3094·18 II	0·15	
					3130·78	0·2	
Li[x]	3232·61 I	0·2			2883·17	0·4	
	2741·31 I	1·3			3028·44	0·5	
Mg	2852·12 I	~ 0·0006					
	2802·69 II	~ 0·0015		Ni	3414·76 I	~ 0·0025	
	2779·83	0·032			3002·49 I	~ 0·005	
	2781·41	0·11			3050·81 I	0·01	
	3332·15 I	~ 0·2			3003·62 I	0·015	
	3091·07 I	0·5			3315·66 I	~ 0·08	
	2942·11 I	~ 1·2	2		2992·59 I	~ 0·09	
	2942·11 I	~ 1·7	6		3105·46 I	0·27	
	2790·78 II	2			3145·71 I	1·3	
	2936·53 II	~ 4·5			2802·27	6·2	
					2540·02 I	7	
Mn	2798·27	0·0015	geringe Int.		3165·50 I	20	
	2801·06	0·002	geringe Int.		3170·71 I	28·5	
	2933·06	0·04			3176·29 I	32	
	3044·5	0·2			2932·62	50	
	2595·76	~ 0·45					
	3073·12	0·45		P	2535·65 I	0·23	2½
	3070·27	~ 0·5			2535·65 I	0·4	7
	2809·10	0·9			2553·28 I	0·5	1
	2610·20	1·9			2553·28 I	~ 0·9	3
	2738·86	~ 9	4		2534·01 I	1·3	
	2639·83	~ 13	3		2554·93 I	1·5	

[1] Wenn oxydisches Material vorliegt, so sollen die *K*-Werte mit 0·45 multipliziert werden.

VOL. 7 1955/5

Tabelle 2 (continued)

Elemente	*Wellenlänge*, Å	*K-Wert*	*Int.*	*Elemente*	*Wellenlänge*, Å	*K-Wert*	*Int.*
Pb[1]	2833·06 I	~ 0·09†		Sr[x]	3307·53 I	4·2	
	2614·17	~ 0·15†			2931·83 I	4·5	
	2873·31	~ 0·45†		Th	2885·04	0·45	
	2663·16	~ 0·6†			2692·42	0·45	
	2628·26 II	~ 12†			2684·42	0·85	
	3220·53	12			2641·49	1·2	
	2657·10	45		Ti	3241·98 II	~ 0·016	
Pd[x]	3142·81 I	3	~ 12		2646·63 I	0·27	
	3009·77 I	5	~ 7		2841·93 II	~ 0·4	
	3218·97 I	9	~ 4		3152·25 II	~ 0·4	
	2593·26 I	35	~ 1		2605·15 I	0·6	
Pt[x]	2794·20 II	20			2534·62 II	0·8	
	2504·04 I	20			2891·06 II	1·8	
	2625·33 II	45			2619·93 I	~ 3	
					2661·97 I	~ 5	
Rh[x]	2555·36 I	0·8			3299·41 I	~ 6	
	2862·93 I	1			2974·93 I	~ 20	
	2652·66 I	1			2812·98	~ 26	
	2728·94 I	1·8		V	3185·39 I	0·014	
Sb[x]	2598·06 I	0·035			3130·26 II	~ 0·06	
	2877·91 I	0·11			2952·08 II	0·12	
	2612·30	2			2882·50 II	0·16	
	2692·25	7			2884·78 II	0·2	
	2727·21	8			2914·92 I	0·4	
	2480·44	13			3231·95	~ 8	
	2510·52	20			2916·01 I	~ 8·5	
	2554·61	27			2830·40	~ 15	
	2474·58	60			3013·10	~ 17	
Si	2516·12 I	0·006		W[2]	2946·98	1·5	
	2506·89 I	0·016			2896·4	2	
	2528·51 I	0·019			2947·38	~ 2·8	
	2631·31 I	~ 0·4			2934·99	~ 3·8	
	2987·64 I	~ 0·5			2896·00	~ 5·3	
	2532·37 I	~ 2·5					
	2568·64 I	~ 15		Zn	3345·02 I	0·12	
	2970·34 I	17			3302·58 I	~ 0·2	
	2577·13 I	40			3072·06 I	2·2	2
					3072·06 I	2·7	4
Sn	3175·01 I	0·01			3072·06 I	3·4	8
	2850·61	0·24			3018·35 I	12	
	2785·03	1·5			2712·48 I	20	
	2812·56	6					
	2787·92	12·6		Zr[x]	3438·23 II	0·05	
					3430·53 II	0·1	
Sr[x]	3464·45 II	0·08			2734·85 II	0·2	
	3351·24 I	1·3			2758·81 II	0·4	
	3329·98 I	2·2					

[1] Da die meisten Bleilinien Selbstabsorption aufweisen und die Neigung der log. Int./log Konz.—Gerade unzureichend genau bekannt ist, sind sämtliche *K*-Werte mit einem ~ versehen worden. Man verwende nur geringe Intensitätswerte. Wenn oxydisches Material vorliegt, so sollen, wo das Zeichen † angegeben ist, die *K*-Werte mit ¼ multipliziert werden.

[2] Wenn oxydisches Material vorliegt, so sollen die *K*-Werte mit 1/7 multipliziert werden.

Allgemeine Bemerkungen zur Tabelle 2:

(1) Im Falle ungenügender Erfahrung mit bestimmten Materialien sind diesbezügliche Elemente mit einem[s] versehen worden.

(2) Wo ein K-Wert unsicher ist, ist das Zeichen $\sim$ benutzt worden.

(3) Im allgemeinen sind Ergebnisse am besten, wenn sie mit niedrigen Intensitätswerten berechnet worden sind. In einigen Fällen sind die Intensitätsgrenzen angegeben, z.B. B 2497·73; $K = 0{\cdot}0053$, sogar wenn $I = 400$ (Anwendung von Filtern u. dgl.).

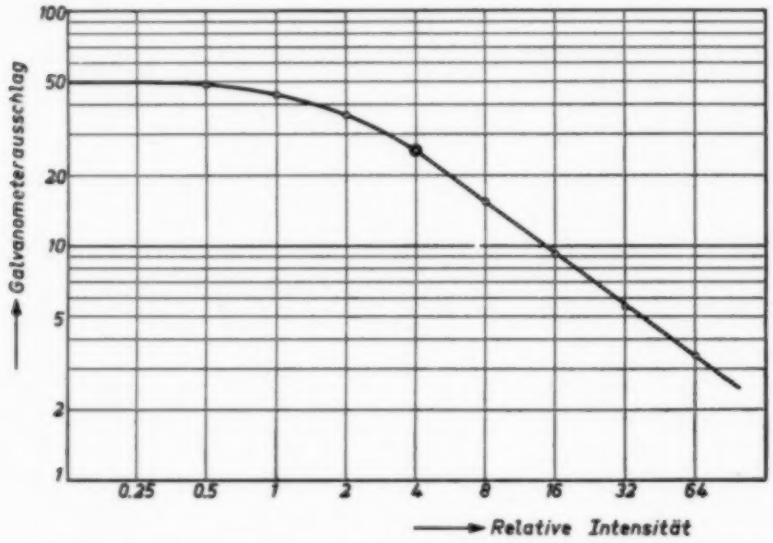

Fig. 3. Beispiel einer Schwärzungskurve (Plattennummer 1435); s. Beispiel I, Seite 55.

(4) Zuweilen ist es nicht möglich höhere Intensitätswerte zu vermeiden; in solchen Fällen hat man den Effekt der Selbst absorption (bei steigender Intensität eine Zunahme des K-Wertes) mit einzubeziehen.

Beispiel: Na-Linie 3302·32 Å. In der Tabelle findet man:

Int.	*K-Wert*	*Konzentration (berechnet)*
1	0·35%	0·35%
4	0·60%	2·40%
16	0·90%	14·4%

Die Figur 4 zeigt dazu die log. Int./log Konz. — Gerade mit einem Neigungswinkel α, wo $tg\alpha = 0{\cdot}7^5$. Man sucht nun mit Hilfe der für jede Platte korrigierten Intensität die zugehörige Konzentration auf. Im Falle einer Vollanalyse wird dann zweckmässig so verfahren, dass man diesen durch äussere Normierung und Anwendung der log I/log C—Kurve bestimmten Konzentrationswert bei der Summenbildung über sämtliche Elementkonzentrationen benutzt und dann noch eine zusätzliche innere Normierung zur Berechnung der endgültig anzugebenden Konzentrationen durchführt. So braucht man aber nur bei K-Werten zu verfahren, die intensitätsabhängig sind.

Beispiel (*I*) *einer Analyse eines Chrom-Nickel-Stahls* (es wurde ein Standardstahl vom "National Bureau of Standards" Nr 101[a] verwendet).

(A) *Photometrische Messungen.* Fig. 3 stellt die Schwärzungskurve dar; die vertikale Achse gibt den Galvanometerausschlag an im logarithmischen Maßstab. Die folgende Tabelle enthält die Messergebnisse und die daraus berechneten Gehalte:

Tabelle 3

Photometrische Auswertung eines Duplikat Spektrums (Plattennummer 1435) von Cr-Ni-Fe. (Breite der Blende zwischen Lichtquelle und Sammellinse—*C* in Fig. 2—0·35 mm.) Es bedeutet:

G_{1+u}: der Galvanometerausschlag der Spektrallinie
G_u: der Galvanometerausschlag des Untergrundes der betreffenden Linie
I_{1+u}: Intensität der Spektrallinie + Untergrund } aus der Schwärzungskurve
I_u: Intensität des Untergrundes } (Fig. 3)
I_1: $I_{1+u} - I_u$
I_{1m}: der Mittelwert der Duplikatspektren
K: der betreffende K-Wert (S. Tabelle 2)
C_1: die berechnete Konzentration $= K \times I_{1m}$, berechnet pro Linie
C_{e1}: Mittelwert der Konzentration, berechnet pro Element
C_e: die endgültige Konzentration nach Korrektur auf 100%.

Element	λ	G_{1+u}	G_u	I_{1+u}	I_u	I_1	I_{1m}	K	C_1	C_{e1}	C_e	*chemisch*
Fe	2645·4	21·9	43·3	5·05	1·12	3·93	4·1	25	102·5	96·05	71·8	71·6
		21·0	44·0	5·30	1·03	4·27						
	2667·9	23·9	44·5	4·40	0·97	3·43	3·47	27	93·8			
		23·8	44·7	4·30	0·95	3·50						
	2883·7	24·3	44·2	4·30	1·00	3·30	3·2	29	92·9			
		25·3	44·7	4·05	0·95	3·10						
	2815·5	24·7	45·1	4·20	0·90	3·30	3·27	29	95·0			
		25·1	45·3	4·10	0·87	3·23						
Cr	2785·7	29·5	44·1	3·06	1·00	2·06	1·98	10·5	20·8	23·1	17·3	18·3
		30·6	44·9	2·82	0·92	1·90						
	2700·59	27·4	45·0	3·50	0·90	2·60	2·52	8·7	21·9			
		28·3	45·4	3·30	0·86	2·44						
	2642·11	26·3	45·2	3·76	0·88	2·88	2·71	7·5	20·3			
		27·4	44·5	3·50	0·97	2·53						
	2913·3	19·7	43·3	5·85	1·12	4·73	4·41	6·5	28·6			
		21·4	43·3	5·20	1·12	4·08						
	2935·1	17·2	39·8	7·00	1·55	5·45	5·08	4·7	23·9			
		18·9	40·6	6·15	1·45	4·70						
Ni	2540·0	26·7	38·5	3·67	1·68	1·99	1·96	7·0	13·7	13·2	9·9	8·98
		27·4	39·5	3·50	1·58	1·92						
	2802·3	28·9	42·5	3·17	1·21	1·96	2·05	6·2	12·7			
		29·0	44·0	3·16	1·03	2·13						
	3145·7	11·0	33·5	12·6	2·37	10·23	10·25	1·3	13·3			
		11·2	34·5	12·5	2·23	10·27						
	Auf dieselbe Weise ist die Summe der Verunreinigungen gefunden, der Kürze halber hier nicht ausgeführt (0·46 Si; 0·6 Mn; 0·05 Mo; 0·1 Cu; 0·09 Co; 0·05 V)									1·35	1·0	0·97
	Summe der C_{e1}									133·7	100·0	

In der Tabelle 4 folgen die Endwerte der Konzentrationen der Verunreinigungen:

Tabelle 4

	spektrochemisch	*chemisch*
Si	0·34	0·34
Mn	0·44	0·47
Mo	< 0·035	0·01
Cu	~ 0·07	0·05
Co	0·07	0·07
V	0·04	0·03

(B) *Messungen mittels der s.p.d. Skala.* Es wurde das Duplikatspektrum, unter (A) angeführt, verwendet (Plattennummer 1435). Die folgende Tabelle zeigt das in einfacher Weise erreichte Resultat:

Tabelle 6

Element	λ	I_1	I_{1m}	K	C_1	C_{e1}	C_e	*chemisch*
Fe	2645·4	3·4–3·8	3·6	25	90·1	92·2	71·0	71·6
	2667·9	3·4–3·7	3·55	27	96·0			
	2883·7	3·0–3·2	3·1	29	90·0			
	2815·5	3·1–3·3	3·2	29	92·8			
Cr	2785·7	2·5–2·4	2·45	10·5	25·7	25·0	19·2	18·3
	2700·59	2·7–2·5	2·6	8·7	22·6			
	2642·11	3·7–3·4	3·55	7·5	26·6			
	2913·3	4·2–3·8	4·0	6·5	26·0			
	2935·1	5·2–5·0	5·1	4·7	24·0			
Ni	2540·0	1·7–1·9	1·8	7·0	12·6	11·4	8·8	8·98
	2802·3	2·1–2·0	2·05	6·2	12·7			
	3145·7	7·0–6·8	6·9	1·3	9·0			
	Summe der Verunreinigungen					1·30	1·0	0·97
	Total					129·9	100·0	

Auf die gleiche Weise wurden für die Verunreinigungen im einzelnen gefunden:

Tabelle 7

	spektrochemisch	*chemisch*
Si	> 0·24*	0·34
Mn	0·49	0·47
Mo	0·018	0·01
Cu	~ 0·08*	0·05
Co	0·06	0·07
V	0·03	0·03

*Diese Zahlen hätten bei Aufnahme mit einem Stufenfilter genauer bestimmt werden können.

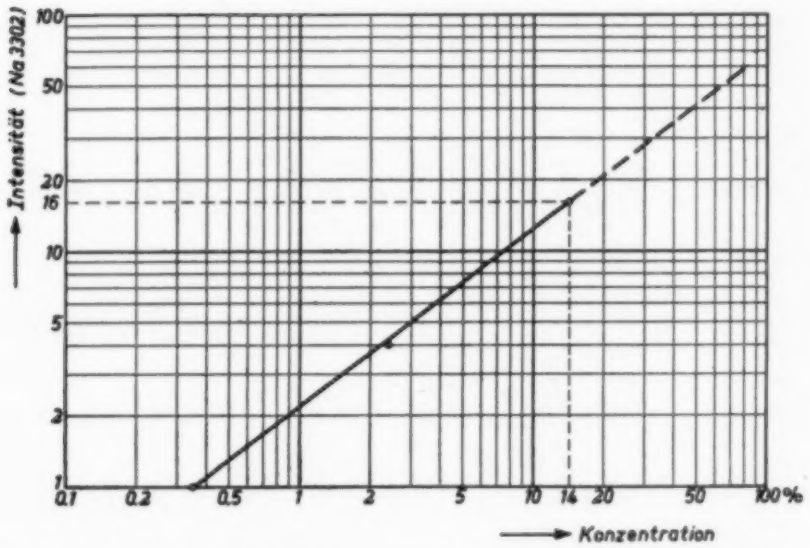

Fig. 4. Doppeltlogarithmische Eichgerade von Na 3302·32; s. Beispiel II, abgeleitet aus den in der Tabelle 2 erwähnten Zahlenwerten für Na.

Beispiel (II) einer Analyse des Natriums in einigen Gläsern mittels der s.p.d. Skala

(A) Ein Borosilikat-Glas (National Bureau of Standards, Nummer 93; Natriumoxydgehalt: 4·16 Prozent). 5 mg dieses Glases (+1 mg Ni) wurden in 7 Minuten zu vollständiger Verdampfung gebracht. Die Duplikatspektren wiesen eine Intensität der Na-Linie 3202·3 Å (gemessen mittels der s.p.d. Skala) von 8·0/8·0 auf. Zur Messung der Borlinien war ein Stufenfilter vorgeschaltet. Der helle Teil dieses Filters schwächte (wegen Reflektion an der Quarz-oberfläche) die Na-Linie um einen Faktor 1·11. Die äussere Normierungsfaktor für die Emulsion dieser Ilford-Ordinary-Platte betrug: 0·56. Die wirkliche Intensität

des ausgesandten Natriumlichtes war also: $8{\cdot}0 \times 1{\cdot}11 \times 0{\cdot}56 = 4{\cdot}97$. Die Figur 4 ergab eine Konzentration 2·95 Prozent. $C_{Na} = 2{\cdot}95 \times 1{\cdot}345 = 3{\cdot}97$ oder abgerundet 4·0 Prozent Na_2O.

(B) Die Analyse eines Natronkalkglases (National Bureau of Standards, Nummer 80; 16·65 Prozent Na_2O) ergab folgendes: Die wirkliche Intensität betrug $3{\cdot}3 \times 1{\cdot}11 \times 6{\cdot}85 \times 0{\cdot}56 = 14{\cdot}0$ (es wurde nun der dunkle Teil des obengenannten Stufenfilters benutzt; Schwächungsfaktor = 6·85). Nach der Figur 4 erhält man so 11·9 Prozent Na oder 16 Prozent Na_2O.

Bemerkung

Relativ grosse Mengen der Alkalien, wie z.B. 20 Prozent Na setzen die Bogentemperatur während der Verdampfung dieser Elemente herab. Dies hat zur Folge, dass Elemente oder Verbindungen, welche gleichzeitig in der Säule angeregt werden eine geringere Intensität aufweisen. Bei den obengenannten Gläsern ist dieser Effekt von geringer Bedeutung, da die Komponenten des Glases praktisch nach einander verdampfen. Wenn man aber z.B. Na_2SnO_3 oder ein Gemisch 1 : 1 von $BaCO_3$-Na_2CO_3 zu analysieren hat (Sn und Ba verdampfen gleichzeitig mit Na) so wurde experimentell gefunden, dass man die in Frage kommenden K-Werte mit 1·5 zu multiplizieren hatte.

Ergebnisse

Als Beispiel für die Zuverlässigkeit des Verfahrens werden hier die Resultate der mit verschiedenen Methoden an gleichen Wolfram-Proben ausgeführten Analysen wiedergegeben (Tabelle 8). Der Vergleich wurde ohne Wissen der einzelnen Laboratorien durchgeführt. Es wurden 6 Proben—I bis VI—auf Si, Mo, Al, und Fe untersucht (sp. bedeutet spektrochemische Analyse, Eindhoven; ch. bedeutet chemische Analyse, Rugby[1])—

Tabelle 8. Die Analyse von Wolfram-Proben

	I		II		III		IV		V		VI	
	sp. %	*ch.* %	*sp.* %	*ch.* %	*sp.* %	*ch.* %	*sp.* %	*ch.* %	*sp.* %	*ch.* %	*sp.* %	*ch.* %
Si	0·03	0·03	0·21	0·21	0·27	0·28	0·27	0·26	0·27	0·28	0·21	0·19
Mo	$0{\cdot}03^6$	$0{\cdot}03^0$	$0{\cdot}03^2$	$0{\cdot}03^5$	0·02	$0{\cdot}00^5$	0·02	$0{\cdot}00^2$	$0{\cdot}04^9$	$0{\cdot}05^0$	$0{\cdot}02^5$	0·03
Al	$0{\cdot}01^4$	$0{\cdot}00^9$	$0{\cdot}00^1$	$0{\cdot}00^2$	$0{\cdot}01^3$	$0{\cdot}01^2$	0·003	0·001	$0{\cdot}02^0$	$0{\cdot}01^5$	$0{\cdot}00^2$	$0{\cdot}00^3$
Fe	0·006	0·005	0·005	0·003	0·004	$0{\cdot}005^5$	0·005	$0{\cdot}004^5$	0·008	0·01	0·007	$0{\cdot}007^5$

[1] Den Herren L. J. DAVIES, Director of Research, the British Thomson Houston Co. Rugby, und L. SCHULTINK, Leiter des W- und Mo-Laboratoriums, Philips, Eindhoven, bin ich sehr dankbar das sie mir obengenannte Zahlen zur Verfügung stellten.

Beim Lesen des Manuskripts hat Dr. H. J. EICHHOFF mir manche guten Ratschläge erteilt, wofür ich ihm sehr dankbar bin. Dr. H. KAISER bin ich sehr erkenntlich für seine Bemerkungen, welche der Klarheit dieser Veröffentlichung zugute kamen.

VOL. 7 1955/5

Zusammenfassung

Die Arbeit bringt eine eingehende Beschreibung des in Eindhoven ausgearbeiteten Analysenverfahrens mit einem Kohlebogen "konstanter Temperatur." Sie enthält Tabellen der vorläufig bestimmten Eichfaktoren K, in der Absicht, deren Nachprüfung an anderer Stelle zu ermöglichen. Das Verfahren beruht darauf, daß eine geringe Probenmenge (5 mg), vermischt mit Zusätzen zur Förderung oder Hemmung der Verdampfung (Vorschriften in Tab. 1) aus einer *flachen* konischen Bohrung der Anode vollständig verdampft wird. Die Intensitäten werden mit Hilfe ausgewählter Eisenlinien normiert, so daß die Eichwerte übertragbar sind. Der rechnerische Gang der Auswertung wird an mehreren Beispielen gezeigt, die zugleich die analytische Leistung des Verfahrens zeigen.

Literatur

[1] Slavin, M. L.; *Ind. Eng. Chem.* (*Anal.*) 1938 **10** 407.

[2] Harvey, C. E.; *A Method of Semi-quantitative Analysis*, Glendale (Calif.) 1947.

[3] Dieke, G. H., and Crosswhite, H. M.; *J. Opt. Soc. Amer.* 1943 **33** 425.

[4] Ahrens, L. H.; *Spectrochemical Analysis*, Cambridge (Mass.) 1950.

[5] Nachtrieb, N. H.; *Principles and Practice of Spectrochemical Analysis*, New York 1950, inbesondere S. 245–251.

[6] Smit, J. A.; Diss. Utrecht 1950.

[7] Addink, N. W. H., and de Groot, W.; *Philips Technische Rundschau* 1951 **12** 341; *Revue Technique Philips* 1951 **12** 341; *Philips Technical Review* 1951 **12** 237. Für weitere Bemerkungen anlässlich der beschriebenen Methode s.:

(a) Addink, N. W. H.; *Rec. trav. chim. Pays-Bas* 1951 **70** 155.

(b) Summarized proceedings of the third international spectroscopy colloquium—Hoddeston, September 1952. *Brit. J. Appl. Phys.* 1952 **3** 369.

(c) Addink, N. W. H.; *Spectrochim. Acta* 1953 **5** 495.

OL.
7
5/56

Spectrochimica Acta, 1955, Vol. 7, pp. 60 to 63. Pergamon Press Ltd., London

SPECTROCHEMICAL NOTES

Effektive Linienbreiten in der Spektralphotometrie

J. JUNKES, S.J., und E. W. SALPETER, S.J.
Laboratorio Astrofisico della Specola Vaticana, Castel Gandolfo

(*Received* 12 *November* 1954)

(*Accepted for publication* 7 *December* 1954)

Summary—The photographic widths of spectral lines are as good for photometric work as their densities, sometimes even better, since they allow one to cover a much wider range of intensities. They are, however, only rarely used in spectrochemical photometry, principally because of lack of an appropriate measuring instrument. Efficient photometers for measuring effective diameters of photographic star images have been recently developed. It is proposed, therefore, to devise an analogous "variable slit photometer" for measuring effective widths of spectral lines.

Die photographische Breite einer Spektrallinie ist in der Hauptsache instrumentell bedingt durch Beugungen und Streuungen des Lichtes an Spalt und Optik und in der photographischen Schicht. Das optische Bild eines feinen Spaltes auf der photographischen Platte wächst nach den Untersuchungen von C. E. K. MEES [10] linear mit dem Logarithmus der eingestrahlten Lichtmenge, was nach späteren Feststellungen von EISENLOHR und ALEXY [5] auch für die monochromatischen Spaltbilder einer Spektralaufnahme gilt. Linienbreiten dürfen also ebenso für photographische Intensitätsbestimmungen verwendet werden wie Schwärzungen, haben aber diesen gegenüber voraus, daß sie auch dort noch sichere Messungen gestatten, wo Schwärzungsmessungen wegen der großen Dichte schon sehr ungenau werden oder gar völlig versagen. Damit lassen sich mit Linienbreiten weit größere Intensitätsintervalle erfassen als mit Schwärzungen.

In der Spektralphotometrie haben Linienbreiten bisher wenig Verwendung gefunden. Die verwaschenen Grenzen des photographischen Bildes einer Spektrallinie erlauben keine sicheren Mikrometermessungen, die irgendwie an die Meßgenauigkeiten der üblichen Schwärzungsmessungen heranreichen. Ein erstes brauchbares Meßverfahren für Linienbreiten geben EISENLOHR und ALEXY [5] an. Sie setzen zunächst eine Standardschwärzung fest, die günstig zwischen Untergrund und Sättigungsschwärzung liegt, und definieren die Breite einer Spektrallinie als den Abstand zwischen zwei Punkten zu beiden Seiten der Zentralschwärzung der Linie, die diese Standardschwärzung aufweisen. Bei Benützung eines Spektrallinien-Photometers mit geeigneter Meßschraube bietet die Bestimmung solcher "photometrischer" Linienbreiten keine grundsätzlichen Schwierigkeiten. Die Ergebnisse können dann genau so zur Aufstellung von Eichkurven benützt werden wie die Schwärzungen, wenn nur beim selben Meßgang die Standardschwärzungen eingehalten werden. Dieses Verfahren wurde von W. GERLACH und W. ROLLWAGEN [6] für eine neue Methode der quantitativen Spektralanalyse angepaßt, die dann P. COHEUR [1, 2] weiter entwickelte und experimentell unterbaute, und die bekannt wurde als die "Methode der photometrischen Linienbreiten." (Vgl. NACHTRIEB [11], S. 133ff.)

Die Doppelbeobachtung der Flankenschwärzungen und die mikrometrischen Messungen sind allerdings nicht so bequem wie einfache Galvanometer- oder Keilablesungen bei Schwärzungsmessungen, sodaß in der Folge auch mit solchen photometrischen Linienbreiten wenig gearbeitet wurde, abgesehen vielleicht von Fällen, wo die üblichen Schwär-

zungsmessungen versagen. Da mit einem immerhin sehr engen Spalt gemessen werden muß, gehen die zufälligen Kornschwankungen der Platte stark in die Meßergebnisse ein.

Nun hat H. SIEDENTOPF [12] schon 1934 ein Verfahren zur Messung "effektiver" Durchmesser von fokalen photographischen Sternbildchen vorgeschlagen, das sich sinngemäß auf die Messung "effektiver" Linienbreiten anwenden läßt. Damit könnten wohl die letzten Hindernisse fallen, die sich einer allgemeinen Verwendung der photographischen Linienbreiten für photometrische Aufgaben noch entgegenstellen, und es dürfte möglich sein, ein Meßverfahren zu entwickeln, das sich mit den gebräuchlichen Intensitätsmessungen über photographische Schwärzungen, was Genauigkeit und Bequemlichkeit betrifft, vorteilhaft vergleichen ließe.

Statt der bisher bei Sternphotometern üblichen festen Blenden zur Photometrierung fokaler Sternbilder verwendet SIEDENTOPF eine veränderliche Irisblende, mit der das Sternbild radialsymmetrisch derart umfaßt wird, daß der durch Blende und photographisches Bild noch durchgelassene Teil des photometrierenden Lichtbündels für alle Durchmesser gleich bleibt. Die Öffnung der Blende ergibt einen "effektiven" Durchmesser, der unmittelbar zu den Sternhelligkeiten in Beziehung gesetzt wird. Einige Jahre später wurde an der Göttinger Sternwarte von H. KIENLE [9] nach diesen Grundsätzen ein äußerst brauchbares Irisblendenphotometer entwickelt, das in den verbesserten Ausführungen von SCHILT und Mitarbeitern [4] und von HAFFNER [7] berufen sein mag, die bisherigen Sternphotometer zu verdrängen. Die Meßfehler sind bedeutend geringer, die Eichkurve wird bei geeigneter Wahl der Blendengröße angenähert eine Gerade, der Untergrund hat wenig Einfluß mehr auf die Meßergebnisse, die Wirkung des Streulichtes ist ganz unbedeutend und das mit einem einzigen Meßgang überbrückte Intensitätsintervall konnte gegenüber den alten Photometern um das Hundertfache erweitert werden.

Die sinngemäße Übertragung der SIEDENTOPFS chen Gedanken auf die Messung "effektiver" Linienbreiten in Spektralaufnahmen bietet keine grundsätzlichen Schwierigkeiten und stellt an die konstruktive Ausführung eines geeigneten Instrumentes weit geringere Ansprüche als ein Irisblendenphotometer. Statt der Iris wird eine Spaltblende benützt,* die genügend weit und meßbar geöffnet werden kann. Durch Einschalten eines Vergleichslichtweges kann das Photometer leicht als Nullinstrument ausgeführt werden, das von den zufälligen Schwankungen der Photometerlampe weitgehend unabhängig ist. Es scheint deshalb der Mühe wert, einmal einige Versuche anzustellen, um sich über die Brauchbarkeit des Verfahrens für spektrochemische Aufgaben und über die Zweckmäßigkeit der Entwicklung und des Baues eines eigentlichen Meßspaltphotometers ein erstes Urteil bilden zu können.

Für diese Versuche wurde ein Zeiss-Spektrallinienphotometer älterer Bauart benützt, dessen Photometerspalt sich allerdings nur auf 2·40 mm öffnen läßt, aber eine Ablesung der Spaltstellung auf 0·01 mm gestattet. Als Meßobjekt diente ein Spektrum des Eisenfunkens, das unter sonst gleichgehaltenen Anregungsbedingungen in geometrisch abgestuften Belichtungszeiten (2·5, 5, 10, 20, 40 und 80 sec) mit dem Q 24 (Spaltbreite 5 μ, Kamera f : 30) aufgenommen wurde. Vermessen wurden einige Fe-Linien, deren relative Intensitäten von den Anregungsbedingungen unabhängig sind und von DIEKE und CROSSWHITE [3] bestimmt wurden. Die 30fach vergrößerten Linien wurden symmetrisch auf den Photometerspalt gebracht und der Spalt so weit geöffnet, bis der für die betreffende Meßreihe festgelegte Normalausschlag des Galvanometers erreicht war. Es wurden drei Meßreihen mit verschiedener "Grundbreite" (0·05, 0·10, und 0·15 mm) ausgeführt, wobei wir mit "Grundbreite" jene Öffnung des Spaltes bezeichnen, die bei klarer Platte den Normalausschlag zeigt, der während der Messungen der Linien konstant gehalten wird. Je größer die Grundbreite, desto mehr wird von dem Saum der Spektrallinien bei den Messungen mitgenommen, desto größer werden also die "effektiven" Linienbreiten.

* Eine solche Meßspaltblende wurde am Göttinger Photometer schon von KIENLE vorgesehen und von Fr. W. JÄGER [8] zur Messung von Gesamtabsorptionen in Absorptionslinien verwendet.

Die Ergebnisse der Messungen sind in der beigefügten Tabelle zusammengestellt, woraus sich nach Bedarf entsprechende Kurven zur Veranschaulichung konstruieren lassen. Zum Vergleich wurden auch die Schwärzungen der Linien beigegeben, die mit einer Öffnung des Photometerspaltes von 0·13 mm nach der üblichen Methode erhalten wurden.

Aus diesen ersten Versuchen geht nun hervor, daß die effektiven Linienbreiten ebenfalls brauchbare Eichkurven für Intensitätsbestimmungen liefern können. Wenn sie auch im Gebiet geringer Schwärzungen etwas weniger zuverlässig sein mögen, sind sie im Bereich

Schwärzungen und effektive Breiten einiger Fe-Linien im Funkenspektrum bei verschiedenen Belichtungszeiten

(Y_{rel}: Log. der relativen Intensitäten nach DIEKE und CROSSWHITE [3]—Eingeklammerte Werte wurden aus Breite:log It-Kurven extrapoliert)

Fe-Linien	Nr λ Y_{rel}	Unter-grund	I 3157·9 0·0	II 3217·4 0·34	III 3200·5 0·52	IV 3222·1 0·89	V 3225·8 1·00	Unter-grund	I 3157·9 0·0	II 3217·4 0·34	III 3200·5 0·52	IV 3222·1 0·89	V 3225·8 1·00
Aufnahme Nr	sec	Schwärzung						Effektive Breiten in 0·01 mm bei Grundbreite 0·05 mm					
1	2·5	0·03	0·08	0·04	0·25	0·52	0·64	5·5	—	—	10	20	25
2	5	0·07	0·18	0·32	0·44	0·82	0·95	7	—	12	16	37	47
3	10	0·23	0·36	0·52	0·70	1·12	1·26	10	13	20	28	66	85
4	20	0·37	0·57	0·79	0·99	1·44	1·55	14	21	32	50	110	131
5	40	0·60	0·81	1·05	1·30	1·74	1·85	22	35	61	86	161	184
6	80	0·80	1·10	1·30	1·48	1·92	2·30	33	57	88	122	200	240
		Effektive Breiten in 0·01 mm bei Grundbreite 0·10 mm						Effektive Breiten in 0·01 mm bei Grundbreite 0·15 mm					
1	2·5	11	—	14	18	34	42	16	17	19	25	47	58
2	5	12	14	20	27	64	79	18	22	30	40	83	103
3	10	15	22	36	54	105	136	20	34	50	71	138	163
4	20	20	36	61	88	166	191	30	53	80	114	190	225
5	40	30	65	107	139	225	(256)	39	90	132	164	(255)	(289)
6	80	40	100	157	188	(295)	(333)	63	140	190	224	(316)	(352)

großer Dichten den Schwärzungen entschieden überlegen. Durch die Wahl der Größe der Grundbreite kann die Eichkurve stark beeinflußt werden; in dem benützten Intervall werden die Kurven steiler und gestreckter, je größer die Grundbreite genommen wird.

Das für diese ersten orientierenden Versuche benützte Meßverfahren hat natürlich noch seine großen Unvollkommenheiten: die Spaltöffnung ist unzureichend, die Ablesungen der Spaltstellung und des Normalausschlages sind unbequem. Dennoch besitzt es alle wesentlichen Elemente, die eine sichere Messung effektiver Linienbreiten gewährleisten, sodaß es im Notfalle ohne weiteres Verwendung finden kann, z.B. wenn wegen zu großer Dichten die Schwärzungsmessungen versagen. Vor allem aber genügt es zur grundsätzlichen Beurteilung der Brauchbarkeit des Verfahrens. Es scheint uns deshalb die Entwicklung und der Bau zweckmäßiger Meßspaltphotometer für spektrochemische Aufgaben hinreichend begründet, mit denen dann weitere Untersuchungen angestellt werden mögen über die Möglichkeiten und Grenzen der Spektralphotometrie mit effektiven Linienbreiten.

Literatur

[1] Coheur, P.; La méthode par largeur photométrique des raies. *Mém. Soc. Roy. Sci. Liège*, 4e série 1942 **5** 1–158.

[2] Coheur, P.; A method of quantitative spectrochemical analysis based on line widths. *J. Opt. Soc. Amer.*, 1946 **36** 498–500.

[3] Dieke, G. H., and Crosswhite, H. M.; The use of iron lines as intensity standards. *J. Opt. Soc. Amer.* 1943 **33** 425–434.

[4] Eichner, L. C., Helt, J. H., Schilt, J., Schwarzschild, M., and Sterling, H. T.; The new photometer of the Rutherford Observatory. *Astron. J.* 1947 **53** 25–31.

[5] Eisenlohr, F., und Alexy, K.; Ein neues Verfahren der quantitativen Emissionsspektralanalyse. I. Über relative Linienverbreiterung. *Z. phys. Chemie* (*A*) 1937 **179** 241–255.

[6] Gerlach, W., und Rollwagen, W.; Ein neuss Photometrierungsprinzip für die quantitative Spektralanalyse. *Naturwiss.* 1937 **25** 570.

[7] Haffner, H.; Das neue Irisphotometer der Göttinger Sternwarte. *Nachr. der Akad. d. Wissensch. Göttingen, Math.-phys. Kl., IIa math.-phys.-chem. Abt.*, Jahrg. 1952, S. 49–65.

[8] Jäger, Fr. W.; Messung von Gesamtabsorptionen schwacher Fraunhoferlinien nach der Methode der effektiven Linienbreiten. *Z. Astrophys.* 1949 **26** 341–373.

[9] Kienle, H.; Grundsätzliches zum Bau von Mikrophotometern. *Mitt. Astr. Gesellsch.* 1950, S. 15–17.

[10] Mees, C. E. K.; On the ratio between the diameter of the photographic image of a point and the exposure which produced it. *Astrophys. J.* 1911 **33** 81–84.

[11] Nachtrieb, N. H.; *Principles and Practice of Spectrochemical Analysis.* McGraw-Hill, New York, 1950.

[12] Siedentopf, H.; Photographisch-photometrische Untersuchungen. I. Über ein neues Photometer zur Schwärzungsmessung von Sternbildern. *Astron. Nachr.* 1934 **254** 33–38.

OL.
7
5/56

Spectrochimica Acta, 1955, Vol. 7, p. 64. Pergamon Press Ltd., London

Spectrochemical Note

A drum attachment to a travelling microscope for direct wavelength reading of spectral lines

S. A. Clarke
British Insulated Callender's Cables Limited, London W.12

This instrument was developed to enable the identification of spectral lines, by their wavelength, to be carried out relatively simply.

A helical expanded distance scale was traced on the drum, which was geared to the thread of the Baker 64 travelling microscope, by fixing a pen to the pointer on the microscope stage (Plate 1). This helix was calibrated for wavelength as follows:

A record was made of the microscope scale-readings of known lines in reference spectra, photographed in juxtaposition. From these a table was constructed, by calculation, of the scale readings corresponding to 10 Å intervals throughout the wavelength range. The nearest two lines, one each side of the wavelength for which the calculation was made, were used. This table was subdivided by simple proportion into smaller units. For example, a drum calibrated for plates exposed on the Bellingham and Stanley medium spectrograph was divided into 0·5, 1·0, 2·0, 5·0 Å intervals in the ranges 2160–2700–3300–4200–6000 Å respectively. This subdivided table was transferred onto the drum, precautions being taken that movement was in one direction only to eliminate the effect of backlash. A scale, fixed rigidly between the curved end-supports, was used as the marking line, and the portion of the helix marked was indicated by the pointer.

The reading line, which was supported by a thin curved perspex sheet fixed on the end-supports as close as possible to the drum surface, was a spring loaded wire attached to runners in the end-supports. The maximum movement of the reading wire round the drum circumference at each end was 7·5 cm, which was equivalent to 3 mm along the plate. This adjustment accommodated the observed variation in the distance between the same spectral lines on different plates.

In use, after the reading wire is set parallel to the drum axis, the drum is rotated until the wire indicates the wavelength of a known line in the low wavelength region. The plate is moved until the line coincides with the hair line of the microscope eyepiece. The drum is rotated until a known line in the high wavelength region coincides with the hair line. The reading wire is then adjusted, at this end of the drum, so that the correct wavelength is indicated. This adjustment will have altered slightly the position of the reading wire at the low wavelength end, so, taking precautions against backlash, the hair line is set again on the first line and the reading wire adjusted at that end so that the correct wavelength is indicated. By repeating the process of adjusting the reading wire at alternate ends of the drum, an optimum position is established when the correct wavelength is indicated with the hair line set on either of the known lines. The wavelength of other lines can now be read directly from the drum.

The average difference between indicated and true wavelength of single readings on many spectral lines was 0·25, 0·55, 0·76, 0·64, 0·50, 0·90 Å in the wavelength ranges: 2160–2400–2700–3000–3300–3600–4700 Å respectively, for a drum calibrated for the medium spectrograph. A similar drum calibrated for the 2700–4450 Å range for the Hilger large quartz spectrograph gave 0.22 Å as the average difference between indicated and true wavelength of single readings on many lines. It was noted that errors were unidirectional and their magnitude changed progressively. It was found possible to make "ad hoc" allowances for these small errors by reference to lines identified previously.

The author wishes to thank the directors of British Insulated Callender's Cables Ltd. for their permission to publish this work.

VOL. 7 1955/5

OL.
7
5/56

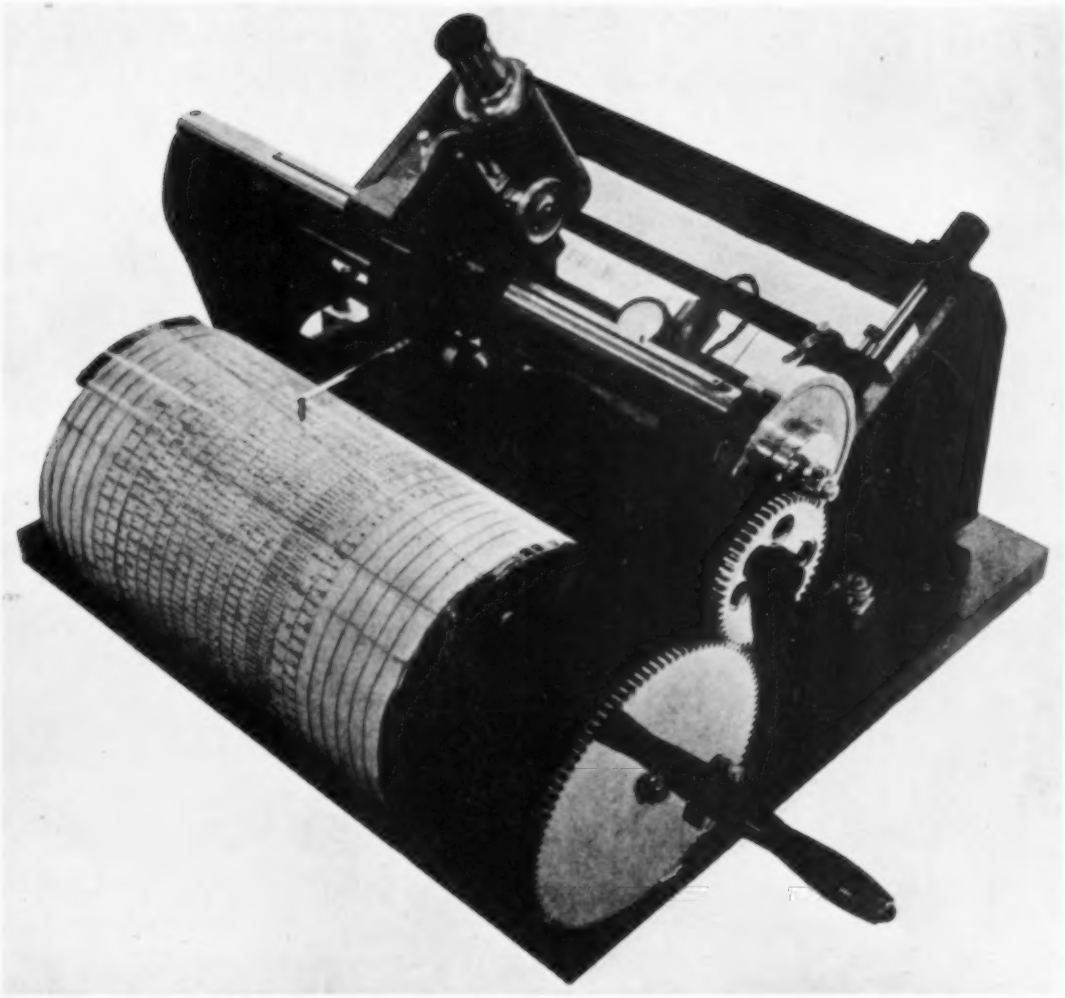

PLATE 1

A drum attachment to a travelling microscope for direct wavelength reading of spectral lines.

VOL.
7
1955/5

Spectrochimica Acta, 1955, Vol. 7, pp. 65 to 67. Pergamon Press Ltd., London

Vacuum ultraviolet spectroscopy*

A Review

EDWARD C. Y. INN†
Geophysics Research Directorate, Air Force Cambridge Research Center,
Air Research and Development Command
Cambridge, Massachusetts

(*Received* 25 *July* 1954)

(*Accepted for publication* 17 *November* 1954)

Summary—Experimental methods and techniques in vacuum ultraviolet spectroscopy are briefly reviewed with emphasis on recent developments in grating monochromators, background light sources and photomultiplier detectors. Recently developed techniques for quantitative absorption spectrophotometry are described. A new method for the measurement of ionization potentials and photoionization cross-section of molecules is also given. Possible applications of vacuum ultraviolet spectroscopy are indicated, especially in problems of molecular structure, the solid state and the upper atmosphere.

OL.
7
5/56

1. Introduction

The spectral region extending from about 2000 Å to shorter wavelengths is usually called the vacuum ultraviolet region (sometimes extreme or far ultraviolet), being bounded at the longer wavelengths by the quartz ultraviolet and at shorter wavelengths by the X-ray region. In a spectroscopic sense the distinction between the conventional and vacuum ultraviolet is arbitrary and determined by the experimental techniques involved. The optical properties of reflecting and refracting materials in the vacuum ultraviolet impose severe limitations and difficulties in experimental techniques and methods. Furthermore, the need for enclosing the optical system of the spectrograph in an evacuated chamber, in order to eliminate atmospheric absorption of vacuum ultraviolet radiation as much as possible, introduces a special problem.

Optical transitions encountered in the vacuum ultraviolet region are primarily transitions of relatively high energies, 6 eV or more. Historically, attention was first focused on spectra of atoms, diatomic molecules and simple polyatomic molecules. However, in recent years spectra of polyatomic organic molecules, e.g., those having chromophoric groups, in the vacuum ultraviolet region have attained increasing importance in the study of electronic structure of molecules. In view of the fact that valence electrons are involved in these optical transitions, it is immediately clear that vacuum ultraviolet spectroscopy has useful application to chemical problems of molecular structure. Since the ionization potentials of most molecules lie above about 6 eV, electronic transitions leading from the ground state of the neutral molecule to the molecular ion (Rydberg transitions) are often observed in this region.

Earlier experimental techniques in vacuum ultraviolet spectroscopy have

* Presented at the 1954 Pittsburgh Conference on Analytical Chemistry and Applied Spectroscopy.
† Now at the U.S. Naval Radiological Defense Laboratory, San Francisco 24, California.

been adequately described by LYMAN [1], BOMKE [2], BOYCE [3], PLATT and KLEVENS [4], and PRICE [5]. Recent advances, especially in spectrophotometric techniques, will be described in some detail in this review. Some of these advances in technique have led to greater precision in measuring absolute absorption intensities in molecular spectra.

2. Experimental problems in technique

A. *Limitations*

In order to appreciate the technical problems of vacuum ultraviolet spectroscopy a brief description of the difficulties will be given. For example, it is well

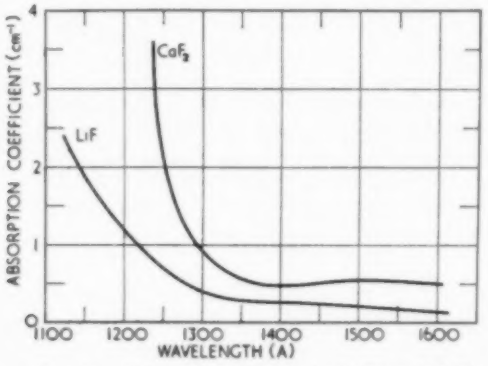

Fig. 1. Absorption coefficient of LiF and CaF_2.

known that air absorbs strongly in this region, so that spectrographs must be placed in evacuated enclosures. In the so-called Schumann region (about 1200–2000 Å) the oxygen molecule strongly absorbs the absorption coefficient [6] at the maximum ($\lambda_{max} \approx 1420$ Å) being about 380 cm^{-1} (see Fig. 7 below). Hence, at this wavelength for optical path lengths of about 1 metre it is necessary to evacuate the spectrograph to partial pressures of oxygen of 1 micron or less in order that the loss of light by absorption be less than 10 per cent. In general, pressures of about 0·1–0·01 microns are maintained in the vacuum spectrograph, thus minimizing any absorption due to residual atmospheric gases, expecially below 1000 Å.

The limitations imposed by the optical materials available introduce an even more serious problem. The only known materials useful in the Schumann region for prisms, lenses, windows, or absorption cells are LiF, CaF_2 (fluorite), and sapphire. The absorption coefficients of CaF_2 and LiF have been measured by POWELL [7] and SCHNEIDER [8], respectively, and are plotted in Fig. 1. In the case of CaF_2 the absorption coefficient increases rapidly at about 1230 Å, indicating a practical limit of transmission at this wavelength. On the other hand, the practical limit of transmission of LiF appears to be below 1100 Å. In Fig. 2 typical transmission curves are plotted for CaF_2 [9] which was 1·9 mm thick and LiF(10) about 1 mm thick. The CaF_2 cut-off appears to be very sharp at 1230 Å while that of LiF much less so (possibly because of the difference in thickness of the samples measured).

In practice, it has been found that the practical limit of transmission of LiF occurs just at about 1050 Å. Thin sapphire windows have been reported to give excellent transmission from the visible region down to about 1435 Å [11].

Extreme care must be taken in the use of all these optical materials. Any deposits of foreign substances on the surfaces can markedly change the transmission characteristics. For example, moisture attacks the surfaces of LiF, resulting probably in an etching action, thus reducing its transmission for vacuum ultraviolet radiation. Furthermore, cleaved surfaces (for windows) show much better transmission than polished ones despite improved polishing techniques. Presumably, this is because of greater scattering by polished surfaces than by cleaved surfaces. It should be mentioned also that LiF fluoresces [12] near its

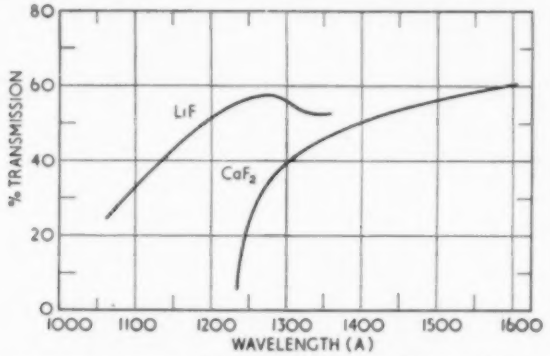

Fig. 2. Transmission curves for LiF (about 1 mm thick) and CaF_2 (1·9 mm thick).

transmission limit so that proper precautions should be taken when used in this wavelength region.

It has been reported recently that thin vacuum tight films of Al and SiO are transparent in the regions 150–400 Å and 150–1200 Å, respectively [13]. The development of such materials for the wavelength regions below 1000 Å will be useful not only as filters but also as windows for absorption cells.

It is well known that reflectivity of gratings becomes increasingly poor on passing to shorter wavelengths, especially at normal incidence. The loss in intensity of the dispersed radiation is a result of the intrinsically low reflectivity of the grating material as well as the subsequent distribution of the dispersed light among many orders. The latter effect is minimized in blazed gratings. From measurements of reflectivities of a large number of metal films in the near and far ultraviolet regions reported by SABINE [14] aluminium surfaces appear to be the best, at least down to about 1000 Å. However, below this wavelength platinum apparently is a much better reflector. SABINE's results for Al and Pt are plotted in Fig. 3. Since these measurements were made on unruled surfaces, it is clear that the actual reflectivity of gratings will be much less than is indicated in Fig. 3.

WATANABE and INN [15] found that an aluminium grating which had become platinized (accidentally) showed a sudden marked improvement in reflectivity below about 1600 Å. This was later confirmed [16] by intentionally platinizing an aluminium grating of low reflectivity. Although some work has been reported

[17] on the effect of various kinds of treatments of gratings and metallic surfaces, it would seem that a systematic investigation on spectral reflectivity in the vacuum ultraviolet region would be highly desirable in view of the obvious benefits derived in improving grating efficiencies.

B. *Vacuum spectrographs*

Prism instruments. Small fluorite prism spectrographs have been used extensively for studying atomic and molecular spectra in the Schumann region. In most designs [2] 60° prisms are used with about 1–2 cm square faces and with 10–20 cm

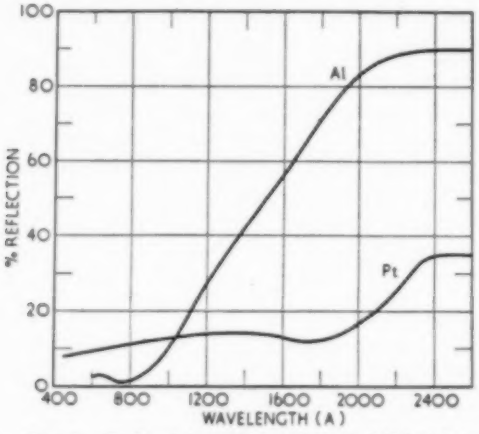

Fig. 3. Reflectivity of Al and Pt at 18° incidence.

focal length collimating and camera lenses. The optical system can then be conveniently enclosed in a bell jar or brass cylinder and a simple vacuum system used to evacuate it. In such an arrangement a rather small and compact vacuum spectrograph can be constructed at low cost. Since the refractive index of fluorite increases rapidly in the Schumann region and because of the necessity for using high plate tilt, relatively high dispersions can be obtained (say, at 1500 Å about 6 Å/mm). As previously noted, spectrographs of this type are limited to wavelengths above about 1300 Å.

Improvements in techniques of polishing and grinding LiF and the commercial availability of synthetic crystals of good optical quality should result in more extensive use of LiF prisms in vacuum ultraviolet spectrographs.

In prism spectrographs the problem of scattered light becomes increasingly important in the vacuum ultraviolet, especially in spectrophotometric measurements. For example, in this region the intensity of scattered light (visible and near ultraviolet) may be several times that of the dispersed radiation. This may be the source of discrepancy in absorption coefficient measurements reported by different investigators. Recently, HAMMOND and PRICE [18] described a photoelectric spectrophotometer which was designed to eliminate the effect of scattered light. Using a fluorite prism in a Littrow arrangement and vibrating the Littrow mirror at 10 cps about a horizontal axis the spectral image was thus focused

VOL.
7
1955/5

on and off the exit slit at the same frequency. Since scattered light was constant over the slit during the vibrations, a photomultiplier detector with a tuned amplifier responded only to the desired vacuum ultraviolet radiation. Preliminary results obtained with this instrument indicated effective elimination of scattered light, thus making the instrument useful for quantitative absorption measurements in the region above 1500 Å.

Grating instruments. Since the pioneering work by LYMAN [1] most of the work in vacuum ultraviolet spectroscopy has been done using concave grating spectrographs. This was in keeping with the necessity for more precise wavelength measurements which could be obtained with grating instruments. Furthermore, for the analysis of rotational structures of molecular bands there was need for spectrographs with greater dispersion and higher resolution.

The conventional type is the normal incidence spectrograph with concave gratings having a radius of curvature between 40 cm and 6 metres, the gratings being ruled with 15,000 or 30,000 lines per inch. The optical system is arranged with grating, slit, and photographic plate on a Rowland circle, the angle of incidence usually being about 14°. The spectrograph is enclosed in thick-walled metal cylinders and the whole system made vacuum tight. Rapid high vacuum pumping systems are used to evacuate the spectrograph and maintain a low pressure. In addition to the usual problems of focusing and alignment of the optical system, problems of leaks and outgassing have to be overcome. Thus, modern methods of leak detection have reduced the difficulties of locating leaks, although very often a supply of alcohol or acetone, a Tesla coil and glyptal is useful for hunting and rectifying the leaks. Pressure measuring devices, such as thermocouple and ion gauges, strategically placed in various parts of the high vacuum system and chamber, are desirable for monitoring the pressure in the evacuated spectrograph. For convenience, various methods have been devised of isolating the slit or plate holder from the main vacuum system, thus allowing any changes to be made externally without letting air into the main chamber enclosing the spectrograph. The practical lower wavelength limit of normal incidence spectrographs is about 500 Å unless extreme measures are taken to increase the light source intensity or reflectivity of the grating.

An interesting method of utilizing higher order spectra with its increased dispersion, without interfering effects of overlapping orders, has been used by BRIX and HERZBERG [19]. This was accomplished by pre-dispersing the light with a small, thin cylindrical LiF lens which focused a narrow band of wavelengths on to the slit of a 3-metre normal incidence spectrograph. The spectrum was observed in the fourth or higher orders. BRIX and HERZBERG reported that it was possible to observe spectra down to 1200 Å, using a 30,000 lines per inch grating, in the fourth, fifth, and sixth orders. Reciprocal linear dispersions of about 0·65, 0·5, and 0·4 Å/mm, resolving powers up to 200,000 were obtained.

A very recent development in vacuum ultraviolet spectroscopy has been the use of échelles for obtaining high resolution. HARRISON [20] has designed a so-called vacuum echelle spectrograph which is essentially a vaccum grating spectrograph crossed with an echelle. The spectrograph was designed in a Wadsworth mount, consisting of a 1·5-metre focal length collimating mirror, a 4 by 8 in. echelle

with 2000 grooves per inch, and a 3-metre radius concave grating with 30,000 lines per inch. The theoretical reciprocal linear dispersion at about 1500 Å was 0·25 Å/mm. Emission spectra of CO (fourth Positive Group) were photographed down to about 1550 Å, the spectra at shorter wavelengths not being observed presumably because of the low reflectivity of the three surfaces. A resolving power of about 150,000 was obtained at about 1700 Å and efforts were being directed to increase this to about 450,000.

Grazing incidence spectrographs [2, 3] have been especially useful for obtaining spectra below 1000 Å and as far down as the soft X-ray region. The advantages of using such spectrographs lie not only in their greater dispersion but also in intensity. With increasing angle of incidence, the shorter wavelengths become more accessible. For example, at 80° and 84·6° incidence the short wavelength limits are 75 Å and 53 Å, respectively. It has been found that resolving power decreases with increasing angle of incidence so that a compromise between resolution and intensity must be made.

During the last twenty years a number of 1-metre vacuum grating monochromators have been reported in the literature [7, 21–27]. Two different techniques have been used for scanning the spectrum. One method is to rotate the grating about a vertical axis through a point on the Rowland circle. The rotation is externally controlled, manually or by means of a synchronous motor which drives a precision screw through a series of reduction gears. Thus, with slits fixed in position special equipment and instrumentation may be conveniently attached without making vacuum connections cumbersome. The disadvantage of this method lies in the defocusing of the spectral image which becomes large as the spectral scanning range is increased.

In the other method the grating is moved tangentially along the Rowland circle, being guided along an accurately-cut groove on the Rowland circle or driven by a lever arm rotating about the centre of the Rowland circle. The advantage of this method is that the spectral image remains relatively in focus on the exit slit throughout the scanning range. However, the disadvantage of this method, though not too objectionable, is that the direction of the dispersed radiation changes as the grating moves along the Rowland circle.

Inasmuch as considerable success has been obtained with the vacuum monochromator reported by TOUSEY, JOHNSON, RICHARDSON, and TORAN [24] a description of it will be given. The instrument was constructed by Baird Associates. The optical system is shown schematically in Fig. 4. The monochromator is of the 1-metre normal incidence type in which the grating moves along the Rowland circle, the grating motion being externally controlled and driven by a synchronous motor. The latter drives a set of gears which communicate the motion through the walls of the vacuum chamber by means of a magnetic clutch to another set of gears and finally to a precision screw. The latter guides a lever arm which rotates about the centre of the Rowland circle, the grating being mounted on the end of the lever arm. With this arrangement various scanning speeds may be pre-set by proper choice of gears and speed of motor, e.g., 300, 100, and 20 Å/min. A Veeder counter is used to indicate the approximate wavelengths for convenient reference. A number of baffles are strategically located along the path of the beam

VOL.
7
1955/5

to eliminate stray and scattered light. The demountable slit assemblies are attached to a heavy end plate by means of vacuum tight flanges, making it possible to replace the exit slit by a camera attachment. The slits are mounted on cylindrical turrets, each turret having three different-sized slits which can be easily interchanged by rotating the turrets while the spectrograph is under vacuum. A vacuum-tight flap valve at the exit slit serves to isolate it from the rest of the system without the necessity of letting air into the evacuated spectrograph. Any light source or special equipment can be readily attached to either slit assembly

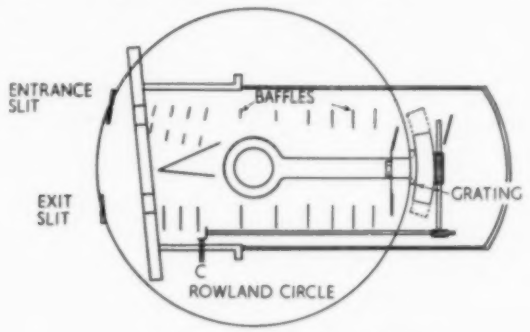

Fig. 4. Schematic layout of 1-metre vacuum grating monochromator.

by means of vacuum-tight flanges. The optical system is thus enclosed in a thick-walled metal bell-jar. The high vacuum system consists of a 6-in. oil diffusion pump backed by a mechanical pump. With this arrangement it is possible to evacuate the system down to 10^{-5} mm Hg in about a half to one hour and maintain this vacuum. The performance of this instrument will be indicated below.

C. *Detectors and methods of detection*

Photographic methods have been used almost exclusively in the vacuum ultraviolet region, especially for precise wavelength measurements and analysis of spectra. In view of the highly absorbing qualities of gelatin for vacuum ultraviolet radiation the problems of photographic detection are generally similar to those encountered in the ultraviolet. Many years ago SCHUMANN [28] developed a technique for preparing emulsions for use in this region, the preparation consisting of an emulsion with very little gelatin and predominantly silver halide grains. Although the recipe for preparing Schumann plates has since been improved, the availability of good quality photographic materials commercially has made it unnecessary to prepare such plates in the laboratory.

Oil-coated emulsions have also been used in the vacuum ultraviolet region. Detailed investigations on the characteristics of photographic plates coated with fluorescent oils have been made by HARRISON [29] and for use in heterochromatic photometry in the vacuum ultraviolet region by HARRISON and LEIGHTON [30, 31]. However, the Eastman Kodak Company has successfully developed ultraviolet sensitized films and plates which have been found quite satisfactory for use in the vacuum ultraviolet. The sensitizer consists of a thin coating of resinous

fluorescent material on the emulsion. The relative quantum efficiencies of the latter have been measured by JOHNSON, WATANABE, and TOUSEY [12] and of sensitized plates by LEE and WEISSLER [32]. These investigators found the relative quantum efficiencies to be appreciably constant over a wide wavelength region. The constant quantum efficiency exhibited by these ultraviolet sensitized emulsions is an extremely desirable property for use in heterochromatic photographic photometry. The undesirable feature, of course, is the necessity for removing the fluorescent coating prior to development.

The Eastman Kodak SWR (short wave radiation) films and plates are recent innovations in vacuum ultraviolet spectroscopy. Tests conducted by SCHOEN and HODGE [33] have shown that these films are somewhat superior in speed and contrast to the Eastman 103-0 ultraviolet sensitized films. The SWR emulsion is very similar to the Schumann type, consisting mostly of silver halide grains with very little gelatin. Other similar types commercially available for use in the vacuum ultraviolet are the Ilford Q and Hilger Schumann plates. Inasmuch as most of these photographic materials are characterized by low gelatin content they are quite fragile and require careful handling.

In quantitative spectrophotometry in the vacuum ultraviolet region photomultiplier detectors have been used with extremely good results. Previously, gas-filled photoelectric cells were used with some success [7, 22, 34], but the rapid development of extremely sensitive and reliable photomultiplier tubes has made superior detectors available for use in this region. The spectral sensitivity characteristics of photomultiplier tubes with quartz envelopes have been studied by DUNKELMAN and LOCK [35] and have been found to be quite satisfactory above the quartz cut-off (about 1550 Å). Satisfactory quantitative absorption spectrophotometric measurements have been made with these quartz photomultipliers [36]. For shorter wavelengths it has been necessary to resort to phosphor-coated photomultiplier tubes. To obtain maximum sensitivity the fluorescent material is usually coated directly on the glass envelope of the photomultiplier tube although coated glass screens placed a short distance from the photomultiplier detector can be used.

In selecting a phosphor for use with a photomultiplier detector it is desirable to select one which has chemical, physical, and optical stability. For example, the phosphor should not react with any of the atmospheric constituents, it should have low water solubility and low sublimation pressure, and it should not undergo photolysis. Furthermore, selection of a phosphor with constant quantum efficiency over a wide spectral range is particularly useful in heterochromatic photometry and in intensity measurements.

Among all the phosphors which have been studied, sodium salicylate [12] seems to be by far the best, possessing most of the desirable properties. To make the coating, a saturated solution of sodium salicylate in a volatile solvent (acetone or methyl alcohol) is prepared and applied (e.g., with an eye-dropper) directly on the glass envelope of the photomultiplier tube. As the solvent evaporates, a thin, almost opaque, uniform coating of the phosphor remains on the glass surface. The coating apparently adheres quite well to the glass surface without the aid of any binding agent. In selecting the photomultiplier tube either the RCA

VOL.
7
1955/5

1P21, 1P28, 5819, or other equivalent commercial photomultiplier tubes may be used, the selection being made on the basis of sensitivity, noise and dark current.

The quantum efficiency of sodium salicylate [12, 15, 37] is practically constant throughout the Schumann region and down to about 850 Å. Below this wavelength the relative quantum efficiency appears to drop by about 15 per cent [15] as indicated in Fig. 5. The use of sodium salicylate as a secondary standard for intensity measurements in the vacuum ultraviolet is based on this property. The

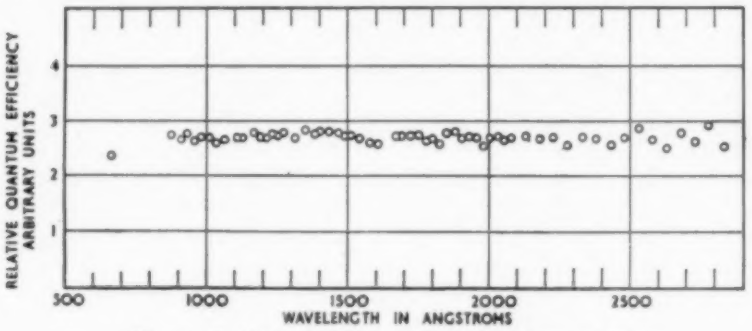

Fig. 5. Relative quantum efficiency of sodium salicylate.

calibration of the secondary standard is usually made with a previously calibrated thermocouple. It has thus been possible to make absolute energy measurements with these secondary standards with an accuracy of about 5 per cent under the best possible conditions and rather easily within 10 per cent.

Recently, windowless vacuum photoelectric cells have been developed which have been successfully used as detectors for vacuum ultraviolet radiation [38]. By suitable choice of cathode material (e.g., Ni, Pt, W) this type of detector is insensitive to wavelengths above the photoelectric threshold. Furthermore, by proper choice of external circuitry (e.g., proper retarding potentials) the response threshold can be controlled and changed to wavelengths shorter than the photoelectric threshold. It has also been found that the photoelectric quantum efficiency in the vacuum ultraviolet region is very high and for this reason these detectors are very sensitive. This type of detector is being further developed and appears to offer great promise.

D. *Light sources*

The types of sources available for absorption studies in the vacuum ultraviolet are very limited in number. It is desirable to use background light sources which have strong continua in the region of interest, and which are continuously operating and stable over reasonable periods of time. These requirements are evidently necessary for reliable quantitative absorption spectrophotometry, but are less stringent for obtaining absorption spectra.

The hydrogen discharge tube is an excellent light source, its emission continuum extending from the visible down to about 1700 Å. The He continuum, discovered by HOPFIELD [39], extends from about 600 to 1000 Å and has been

used for absorption studies in this region. The most widely-used background light source is the Lyman source [1] which has a strong emission continuum extending from the visible down to well below 500 Å. The Lyman continuum is produced by a strongly condensed discharge through a capillary and excited by a high voltage d.c. power supply (about 10–30 kV). Extremely high current densities are obtained in the capillary discharge (estimated by WORLEY [40] to be of the order 60,000 amp/cm^2), giving an extremely bright source. Apparently the continuum is obtained independent of the nature of the gas used.

TANAKA and ZELIKOFF [41] recently reported that under proper excitation conditions a relatively strong emission continuum can be obtained with a Xe source. Thus, at relatively high pressures of Xe (order of 10 mm Hg) and using microwave excitation an emission continuum extending from the resonance line of Xe at 1470 Å up to about 2000 Å was observed. The source was excited by a Raytheon microtherm at 2450 megacycles and operated at about 50–100 watts. It would be extremely valuable if similar continua could be developed using Kr and A, which should then make available background sources for the spectral region extending from 1000 Å up into the visible region.

For quantitative absorption spectrophotometry the hydrogen source has been very useful even for measurements in the region below the emission continuum. using the many-line spectrum as background [6]. The He and Lyman sources have not been used for quantitative absorption measurements although it may be possible to develop special techniques for such measurements with these sources. The Xe source appears to offer definite possibilities for use as reliable background source for quantitative measurements.

A light source of constant emission line spectrum has been developed by LEE and WEISSLER [42] for quantitative absorption measurements. The source is a quenched a.c. low-pressure spark, the constancy and reproducibility depending on the gas composition and breakdown potential. A constancy of about 2 per cent is reported for this source.

3. Applications

A. *Emission spectra of molecules*

Without doubt the contribution of molecular spectroscopy toward elucidation of the structure of molecules, and in particular vacuum ultraviolet spectroscopy to the electronic structure of molecules, has been an important one. Investigations of emission spectra in the vacuum ultraviolet have been somewhat restricted to diatomic molecules in view of the dissociative effects upon excitation in the light source. However, spectroscopy of diatomic molecules is extremely important since the information derived from the spectra of the simplest molecules should contribute much toward development of a more consistent theory of molecular structure.

One example of an emission spectrum in the vacuum ultraviolet which has yielded information of considerable interest is that of the nitrogen molecule. Although the spectrum of N_2 has been studied extensively and in great detail, there has been considerable controversy on the value of the dissociation energy of the molecular ground state. Until recently, from combined spectroscopic,

VOL. 7 1955/5

chemical, and electron impact data, the values reported for the dissociation energy of N_2 have been 9·76 and 7·38 eV [43, 44]. Very recently it was found that consistent interpretations of the results of a series of experiments on the vacuum ultraviolet emission spectra of the nitrogen afterglow can only be made if the higher value for the dissociation energy of N_2 [45] is assumed. Furthermore, these interpretations are also consistent with observations of the nitrogen afterglow spectra in the visible and near infrared [46, 47]. Moreover, the results of these spectroscopic investigations have led to the development of a more plausible theory of the mechanism of the nitrogen afterglow.

In view of the above, it is suggested that investigations on vacuum ultraviolet emission spectra of flames may offer another experimental approach to a study of the mechanism of combustion processes.

B. *Absorption spectrophotometry*

Recent improvements in equipment and techniques have made possible quantitative measurements of absorption intensities, e.g., extinction or absorption coefficients, in the vacuum ultraviolet region using samples in solution, or in the vapour or gaseous state. Not only are these measurements important for developing analytical methods but they are also extremely valuable in the experimental confirmation of theories on oscillator strengths [48]. The latter can be easily calculated from the measured absorption coefficient, k_ν, in the Beer-Lambert law equation,

$$I_\nu = I_{0\nu}\, e^{-k_\nu x}$$

where I_ν and $I_{0\nu}$ are respectively the transmitted and incident intensities and x the optical path length reduced to NTP. Thus, the oscillator strength is given by

$$f = \frac{mc^2}{\pi e^2 N} \int k_\nu \, d\nu,$$

where m and e are the mass and charge of the electron respectively, c is the velocity of light, and N is Loschmidt's number. The integration is performed over the absorption band corresponding to the electronic transition.

Although most of the previously reported absorption coefficient measurements in the vacuum ultraviolet have been made using photographic methods, recent developments in photomultiplier techniques have been so successful that the latter method will certainly be more widely used in heterochromatic photometry in this region. In the photographic method, the absorption cell is usually placed between the light source and slit of the spectrograph or in some cases the spectrograph is filled with the absorbing gas. On the other hand, in the case of the photomultiplier method, the absorption cell is placed between the detector and the exit slit of the monochromator. The immediate advantage of the latter arrangement is that the absorbing gas is irradiated only by monochromatic radiation, hence photochemical effects are minimized.

A brief description of the equipment and technique used in absorption coefficient measurements by the photomultiplier method will now be given [6]. The experimental arrangement is shown schematically in Fig. 6. The optical

system consisted of a Baird 1-metre vacuum monochromator (see above) with a 15,000-lines-per-inch grating, the reciprocal linear dispersion being about 17 Å/mm in the Schumann region, and resolution somewhat less than 1 Å. The

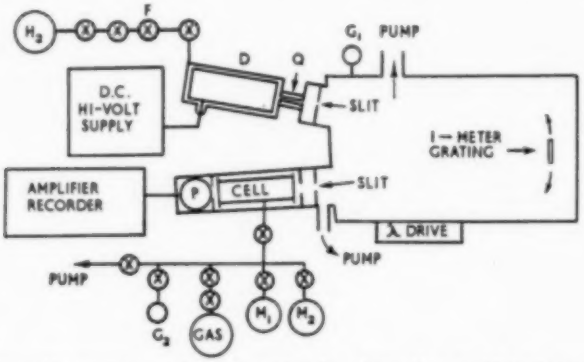

Fig. 6. Schematic arrangement of apparatus for absorption coefficient measurements.

light source was a water-cooled windowless type hydrogen discharge tube, D, with a quartz capillary, Q, used end on. Tank hydrogen flowing through the light source was regulated and monitored by a series of needle valves and an oil manometer, respectively. A 2 KVA d.c. power supply was used to excite the light source.

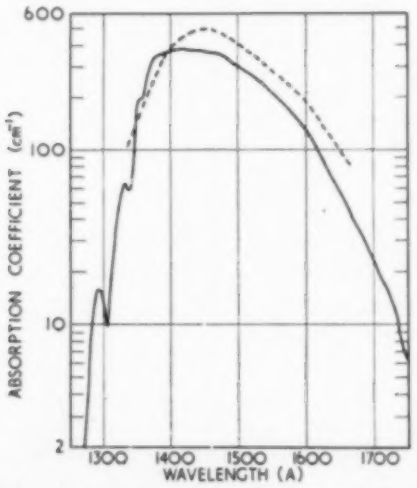

Fig. 7. Absorption coefficient of O_2 in the region of the Schumann-Runge continuum (1300–1750 Å). The dashed curve represents Ladenburg and van Voorhis results.

At the exit slit the absorption cell and photomultuplier detector were enclosed in a vacuum-tight brass box attached to the monochromator. The absorption cell was connected to a high-vacuum gas filling system as shown where M_1 and M_2 are McLeod gauges. Ionization gauges G_1 and G_2 were used to check the pressures of the respective vacuum systems. The absorption cell consisted of a

borosilicate glass ("Pyrex") tube about 20 mm in diameter and 47 mm long, the ends sealed with cleaved LiF windows (about 1 mm thick). The detector was a 1P21 photomultiplier coated with sodium salicylate, using a conventional power supply and amplifier which fed the output into a Speedomax recorder.

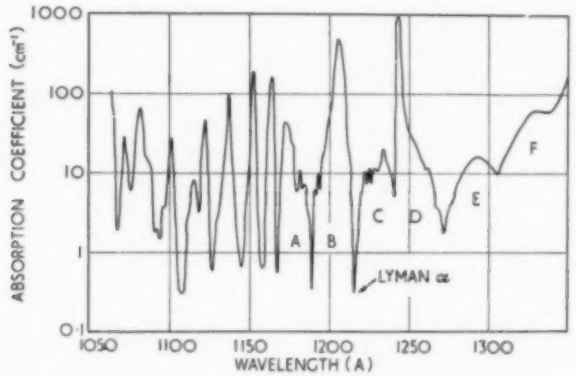

Fig. 8. Absorption coefficient of O_2 in the region 1050–1350 Å.

A slit width of 0·05 mm was used, giving a band width of about 0·85 Å. The scanning speed was 20 Å/min. Wavelengths were determined by comparison with the H_2 spectrum.

The absorption coefficient curves for O_2 shown in Figs. 7 and 8 are typical of

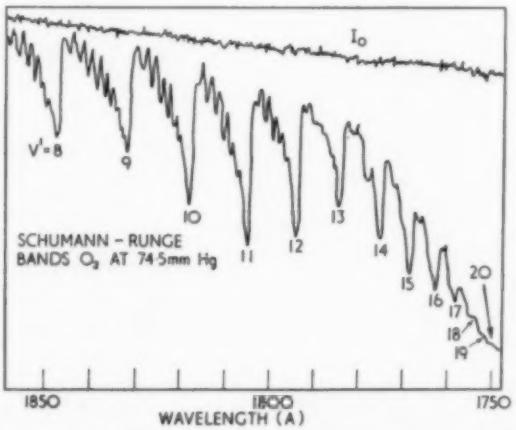

Fig. 9. Reproduction of recorder trace showing Schumann-Runge absorption bands of O_2.

the results obtained using the above technique. In Fig. 7 is shown the Schumann-Runge continuum, the dashed curve representing the results of LADENBURG and VAN VOORHIS [49] obtained by photographic methods. The shorter wavelength region shown in Fig. 8 consists of strong bands and a number of "transparent windows," one of the latter appearing at a wavelength corresponding to the

Lyman alpha line of hydrogen (1216 Å). This "window" has interesting implications in connection with the origin of the *D*-layer in the ionosphere [50].

Fig. 7 indicates that no difficulty was experienced in observing the three sub-maxima on the short wavelength slope of the Schumann-Runge continuum, while photographically they were barely detected [51]. Similarly, it has been possible to detect new bands which presumably could be identified as the 19-0 and 20-0 members of the Schumann-Runge progression as shown in Fig. 9. BRIX and HERZBERG [19] have in fact recently observed and positively identified absorption bands up to 21-0 under much higher dispersion and resolution. From the results of their band analysis they report the new value for the dissociation energy of O_2 to be $5{\cdot}114_8 \pm 0{\cdot}002$ eV.

Absorption coefficients of a number of other molecules such as N_2O, CO_2, O_3, NO, H_2O, and C_2H_4 have been measured by the above method [52–57]. In all these measurements oscillator strengths have been computed for those electronic transitions which could be distinguished from others. New bands have been observed, though it has not been possible to classify them because the method is inherently not suitable for band analysis. However, intensity anomalies can be readily detected by this method.

For quantitative analytical purposes the above method offers definite possibilities, especially for detecting small quantities of impurities in gases. This, of course, implies previous complete data on absorption coefficients of these molecules. For example, it has been possible to detect the presence of H_2O in hydrogen in about 1 part in 10^4, which indicates a greater sensitivity than the conventional analytical mass spectrometer. It should, therefore, be possible to develop a technique specifically for analytical purposes and extend the sensitivity to at least another order of magnitude or more. This method has been used to estimate the amount of CO_2, CO, and O_2 in samples of ozone and also the amount of N_2O impurity in samples of NO. The analysis of mixtures of gases with just a few components is thus in the realm of possibility but much more development in technique is needed to predict any general practical applications. Attempts are being made along this line for organic molecules [36].

VOL.
7
1955/5

C. *Absorption spectra and ionization potentials*

It is generally not possible to give a complete interpretation, from a molecular structure standpoint, of absorption spectra of organic molecules solely from observations in the vacuum ultraviolet region. The spectra in this region are so related to those at longer wavelengths that a complete description would necessarily have to include the combined spectral regions. However, it is intended to confine this discussion to one interesting aspect of absorption spectra of organic molecules appearing almost solely in the vacuum ultraviolet region. Thus, the ionization potentials of molecules as determined from Rydberg transitions in vacuum ultraviolet absorption spectra have been given significance [58–62] in their relation to electronic structure and chemical properties of related molecules.

Since the first ionization potentials of most molecules lie in the vacuum ultraviolet region, it is not surprising that transitions due to excitation and removal of electrons from molecules are observed in absorption spectra in this region. In

these transitions, the more highly excited orbitals are such that the electrons apparently move in atomic-like orbits in much the same way as in atomic Rydberg transitions. The Rydberg series obtained for molecules can be represented by

$$\nu = \nu_\infty - \frac{A}{(n + \delta)^2}$$

where A and δ are constants, n takes successive integral values, ν is the wave number of the corresponding electronic transition and ν_∞ is the series limit or ionization potential. In the case of large polyatomic molecules the lower members of the Rydberg series are usually difficult to observe since the dimensions of the orbitals are of the same order as the molecule and may thus be perturbed.

In ionization the electron involved may be one of three types, namely, bonding antibonding, or non-bonding. An example of each would be, say, the bonding π electron of ethylene, the antibonding electron in NO and the non-bonding lone pair electrons of the halogen atom of hydrogen and alkyl halides. It is apparent that excitation and removal of electrons involved in a bond should result in vibrational excitation of the upper states, hence it is expected, and in fact observed, that vibrational bands accompany the main Rydberg bands. Band shading would thus infer the nature of the molecular orbital from which the electron is excited and removed, i.e., bonding or antibonding. On the other hand, Rydberg transitions involving non-bonding electrons do not generally show this effect. Such observations in the absorption spectra help to establish the molecular orbital from which the electron is excited and removed in ionization.

It is of interest to consider briefly some examples of the information one can obtain from vacuum ultraviolet absorption spectra of related polyatomic molecules and the interpretation made therefrom. For example, the absorption spectra of benzene and some of its derivatives have been studied by HAMMOND, PRICE, TEEGAN, and WALSH [63]. From the observed Rydberg series the following ionization potentials were reported.

Benzene	9·240 eV, 11·7 eV
Toluene	8·820 eV
Ethylbenzene	8·770 eV
iso-propylbenzene	8·760 eV
o-xylene	8·580 eV
m-xylene	8·580 eV
p-xylene	8·480 eV

In the spectra of benzene, short progressions of vibrational bands accompanied the main Rydberg bands. The first ionization potential of benzene, 9·240 eV, is therefore attributed to the removal of one of the six π bonding electrons while the second ionization potential, 11·7 eV, to the more tightly bound π bonding electron according to the respective transitions

$$\chi_1^2\,\chi_{2,3}^4 \rightarrow \chi_1^2\,\chi_{2,3}^3$$

$$\chi_1^2\,\chi_{2,3}^4 \rightarrow \chi_1^1\,\chi_{2,3}^4$$

It is to be noted that there is a general decrease in ionization potential with increasing alkyl substitution, the decrease being interpreted as due to charge transfer or inductive effect. For example, the decrease in ionization potential going from benzene to toluene is interpreted as due to charge transfer from the substituent to the benzene ring. Thus, the greater electron releasing power (less electronegative) of the CH_3 group relative to H results in increasing the electron density in the benzene ring, hence greater repulsion among the bonding electrons and therefore lower ionization potential.

The decrease in ionization potential with alkyl substitution indicates a corresponding long wavelength shift in the Rydberg bands. This seems to be a general characteristic of many absorbing systems, e.g., organic molecules containing chromophoric groups, in which the absorption bands show long wavelength shifts with substitution of related groups of molecules (although short wavelength shifts are also observed). The long wavelength shifts and decrease in ionization potentials of related groups of molecules are usually interpreted as due to charge transfer or hyperconjugation or a combination of both effects.

Another example of interest in absorption spectra of polyatomic molecules interpreted in the light of molecular orbital theory is photoisomerism. The double bond of ethylene in the ground state, N, consists of the strongly bonding σ and less strongly bonding π orbitals. The first ionization potential of ethylene is 10·50 eV* and corresponds to the removal of a π bonding electron [65]. In the absorption spectrum of ethylene the band just below 2000 Å, with a maximum at about 1630 Å, has been interpreted as arising from the $N \rightarrow V$ electronic transition in which one π electron is excited to an antibonding orbital. Thus, in the excited V state, the π electron in the anti-bonding orbital largely cancels the effect of the remaining π electron in the bonding orbital [62] allowing the possibility of rotation about the CC bond. MULLIKEN has shown that a stable configuration with the plane of the two CH_2 groups at 90° is possible [66]. These interpretations suggest the possibility of inducing cis-trans conversions of substituted ethylenes by absorption of vacuum ultraviolet radiation.

The relationship between ionization potential and electronic structure of molecules has been treated by MULLIKEN in a series of papers [67] which provide much of the basis for spectroscopic interpretation of such relationships. On the other hand WALSH [61] has attempted to apply ionization potential data to more specific chemical problems of molecular structure. The basis for these applications lay in the empirical relationship between observed ionization potentials and properties of related groups of molecules. Although these relationships are by no means quantitative, they are certainly indicative and may be useful for qualitative predictions. The following examples illustrate applications of this approach as given by WALSH. It is convenient to discuss the examples according to the type of electrons involved in ionization, namely, non-bonding and bonding.

1. *Non-bonding electrons* (*lone-pair electrons*). On the basis of ionization potential measurements of related groups of molecules it is possible to establish

* All values of ionization potential reported here have been recomputed according to the latest recommendations of physical constants [64].

an order of electronegativity for the substituents. For example, consider some related group of molecules with bond $A—B$, where A represents the substituent and B, an atom possessing lone pair electrons which have negligible interaction with electrons of A other than the bonding electrons of $A—B$. Since the ionization potential of the lone pair electrons of B may be affected by the electron density distribution of the bonding electrons of $A—B$, it follows that any change induced in the latter should cause a corresponding change in the ionization potential of the lone pair electrons. Thus, if A is replaced by a substituent with lower electronegativity, then by charge transfer or inductive effect the electron density in bond $A—B$ will be greater around B. Hence, there will be greater repulsion between the bond electrons of $A—B$ and lone pair electrons of B, and, correspondingly, the ionization potential of the latter will be decreased. From measurements of first ionization potentials it should thus be possible to establish an order of electronegativity for the substituents of certain related groups of molecules. WALSH [61] for example, has listed the following substituent groups in order of decreasing first ionization potential of the lone pair electrons (halide atom), and hence, order of decreasing electronegativity:

H-,	methyl-,	ethyl-,	*i*-propyl,	*t*-butyl,
(12·84)	(11·22)	(10·86)	(10·7)	(10·2)

The first ionization potentials of the substituted chlorides are given in parenthesis below each group [59]. WALSH indicated that this order is confirmed by dipole moment measurements and is also in accordance with other chemical properties.

WALSH [61, 68–70] has also attempted to utilize first ionization potential measurements to determine order of bond polarity. The same type of argument is used to demonstrate this application, in which it is shown that a decrease in first ionization potential implies an increase in bond polarity. Such arguments have been used to establish an order of carbonyl bond polarity. For example, the first ionization potentials of the lone pair electrons of the oxygen atom decrease as follows: CO, CO_2, glyoxal, formaldehyde, and acetaldehyde, which, according to WALSH, establishes an increasing order of bond polarity. Furthermore, WALSH relates empirically ionization potentials with bond polarity and other properties, such as bond length, energy, and stretching force constant. These empirical relationships are: the lower the first ionization potential, the greater the bond polarity, the lower the stretching force constant, the greater the bond distance, and the lower the bond energy. It is emphasized that these relationships imply little or no interaction between the lone pair electrons and electrons other than those on the immediately adjacent bond.

2. *Bonding electrons.* WALSH [61] has indicated the possible usefulness of ionization potential measurements in identifying cis and trans forms of disubstituted olefins. For example, from absorption spectra it has been found that, the first ionization potentials, corresponding to the removal of a π bonding electron of cis and trans isomers of dichlorethylene were 9·65 and 9·95 eV, respectively [71].

In the case of butadiene it has been possible to show the existence of two predicted isomeric forms, the *s*-cis and *s*-trans isomers. The latter refer to isomeric forms with respect to the central "single bond" in butadiene, which according to

molecular orbital theory has some double bond character. The first ionization potentials of the *s*-cis and *s*-trans isomers, corresponding to the removal of a π bonding electron, are 8·75 and 9·06 eV, respectively [72, 73]. This example illustrates the use of ionization potential measurements not only for identifying isomeric forms but also for indicating the existence of those predicted by molecular orbital theory.

D. *Photoionization of molecules*

In view of the applicability of ionization potential measurements to problems of molecular structure another method of measuring them will now be considered. The usual methods of measuring ionization potentials of molecules in the vacuum ultraviolet are electron impact and spectroscopic. The latter procedure gives by far the more precise results, the precision depending on closeness of fit of the spectra to a Rydberg series and the shortness of the extrapolation to the limit. However, frequently it is almost impossible to single out Rydberg series in the spectra due to superposition of bands from other electronic transitions. On the other hand, the electron impact method gives "vertical" ionization potentials (Franck-Condon principle), which are usually greater by a few tenths of a volt than the adiabatic values obtained spectroscopically. The adiabatic ionization potential corresponds to the 0–0 transition from the ground state of the neutral molecule to that of the molecular ion.

A third method [74], recently developed, promises to yield accurate ionization potential data where spectroscopic techniques fail. Although not as precise as the latter, it appears to give more accurate values than is given by electron impact, and it is simple and straightforward. This technique is based on the measurement of the long wavelength limit of photoionization. Thus, by using a cell with parallel plate electrodes, the wavelength corresponding to the appearance and sudden increase in ion current, when the gas or vapour is irradiated with monochromatic radiation, is a direct measure of the first ionization potential. The experimental arrangement [75] is shown schematically in Fig. 10. The "Pyrex" glass cell is enclosed by LiF windows and connected to an external gas filling system. The ion current between the two Pt plate electrodes $C1$ and $C2$ is measured with a Beckman micromicroammeter. The procedure then is to record automatically (Speedomax recorder) the ion current while scanning through the spectral region containing the photoionization threshold. Some of the results obtained by this method are given below [74],

C_2H_4	10·47 ± 0·02	10·50 ± 0·03	(*R*)
		10·62	(*E*)
CH_3I	9·497 ± 0·007	9·535 ± 0·002	(*R*)
		9·1	(*E*)
C_2H_5Br	10·24 ± 0·02	10·29 ± 0·02	(*R*)
		10·0 ± 0·25	(*E*)

where (*R*) and (*E*) represent spectroscopic and electron impact methods, respectively. The good agreement indicates the applicability of the method.

VOL. 7 1955/5

It has been possible not only to measure ionization potentials but also photoionization cross-sections of molecules. These measurements are fairly straightforward in cases where ionization is the only electronic transition, since it is only

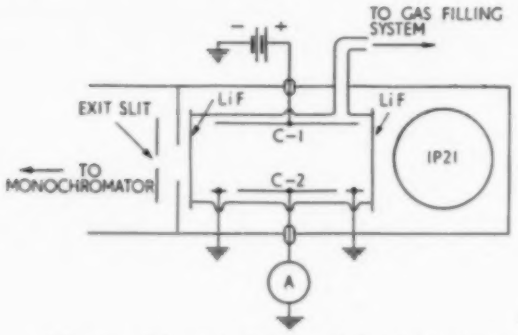

Fig. 10. Schematic diagram of photoionization cell.

necessary to measure the absorption coefficient. However, other absorption processes as well as ionization may occur simultaneously, making it necessary to use a method of measurement which differentiates the ionization process from

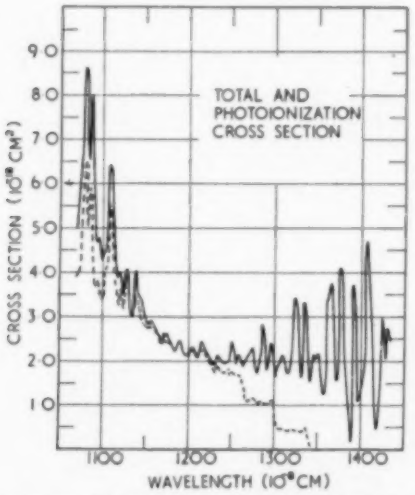

Fig. 11. Photoionization cross-section of NO. The full and dashed curves represent the total and photoionization cross-sections of NO, respectively.

others. Such a method has been developed [75], using the experimental arrangement shown in Fig. 10. Both the ion current and total absorption are measured quantitatively as a function of wavelength. Again the Baird 1-metre vacuum monochromator was used for scanning over the region of absorption. The phosphor-coated 1P21 photomultiplier was calibrated to measure absolute intensities. From these measurements the total and photoionization cross-section can easily

be calculated as well as the quantum efficiency for photoionization. Cross-sections for photoionization of NO have been measured by this method [10, 75] while that for O_2 and N_2 have been measured by a very similar method [76]. In Fig. 11 the total and photoionization cross-section curves are plotted for NO. The fairly sharp long wavelength cut-off of the photoionization cross-section curve is a direct measure of the first ionization potential, 9·23 eV. The step-like structure on this slope has been identified with the higher vibrational levels of the ground state of NO^+.

The sensitivity of this method is shown by the following observation. For a number of polyatomic molecules a long wavelength tail has been observed beyond the photoionization threshold, i.e., ion currents are observed for wavelengths longer than the threshold. Although there is some possibility that these effects could conceivably be due to impurities, the more likely explanation appears to be that the long wavelength tail corresponds to transitions from higher vibrational levels of the ground state of the neutral molecule to the molecular ion. Thus, in accordance with the Boltzmann distribution the higher vibrational levels in the ground state of the neutral molecule may be sufficiently populated to give rise in absorption to measurable transitions to the ground state of the molecular ion.

E. *Application to solid state problems*

Vacuum ultraviolet spectroscopic techniques applied to investigations of the photoelectric effect have revealed some very interesting results. The development of good vacuum ultraviolet radiation detectors using windowless vacuum photoelectric cells has already been mentioned. In connection with absolute energy measurements, extremely high photoelectric yields have been reported [38, 76] for a number of metals, the yields being of the order of 10 per cent in the vacuum ultraviolet region as compared to less than 0·1 per cent in the visible and ultraviolet regions. These high yields apparently cannot be adequately explained by the usual surface photoelectric effect. It has, therefore, been suggested that the "volume" photoelectric effect predominates in the vacuum ultraviolet region, i.e., that the so-called bound electrons are involved in this photoeffect. Such investigations may contribute much to our knowledge of the electronic structure of metals and may suggest another approach to problems in this field.

Absorption spectra of solids have been investigated in the Schumann region, especially for alkali halides and similar crystalline solids [77], to determine the existence of theoretically predicted, non-photoconducting excitation levels lying below the conduction band [78]. In view of recent advances in technique it would seem that much more precise and extensive studies can be made in absorption spectra of solids in this region. The gap between soft X-rays and the ultraviolet has been bridged as regards experimental technique.

Fluorescence studies, especially in solids in which excitation is induced in the vacuum ultraviolet region, should be interesting from the standpoint of the electronic structure of fluorescent solids [79, 80]. Practical applications of fluorescence studies are in the development of vacuum ultraviolet detectors [24]. For example, sodium salicylate exhibits practically constant quantum efficiency throughout a wide wavelength region.

F. *Upper atmosphere problems*

In recent years a promising approach to the study of the upper atmosphere (about 30 miles and upward) has been rocket spectroscopy [81, 82]. It is known that solar radiation passing through the atmosphere contributes a major source of excitation of the atmospheric constituents. This primary absorption process is generally followed by photochemical reactions and collisions which ultimately lead to the composition and structure of the upper atmosphere. One of the most important datum in the study of the upper atmosphere is the quantitative spectral energy distribution of solar radiation. Such data are very limited for regions below 3000 Å and still more so below 2000 Å. Small grating spectrographs have been installed in rockets and flown to obtain solar spectra in the vacuum ultraviolet region. However, very few rocket experiments have been successful, the most significant being the December 1952 flight by the University of Colorado [83]. Using a 50 cm radius concave grating spectrograph mounted for 85° grazing incidence and a sun follower device the solar spectrum was photographed at a rocket height of about 81 km. The successful recording of the Lyman alpha line of hydrogen at 1216 Å in this experiment represents a notable advance in rocket spectroscopy. The line was extremely faint (above scattered light background) with no other emission lines appearing on the film in the region below about 1800 Å. The integrated intensity of this line was estimated to be about 0·05 microwatts/cm² [84]. The results of this experiment give hope of obtaining vacuum ultraviolet band absorption spectra of atmospheric constituents by rocket spectroscopy. In fact, the Naval Research Laboratory has since reported two rocket experiments with even better results. Byram, Chubb, Friedman, and Gaylor [85] using photon counters sensitive to radiation between 1180–1300 Å reported measurements of solar intensity of 0·010–0·002 microwatts/cm² at the top of the atmosphere, the major contribution to this intensity being presumably due to the Lyman alpha line of hydrogen. These results were obtained in Aerobee rocket flights during May 1952, in which maximum altitudes of 128 km were reached. In a more recent experiment reported by Johnson, Purcell, and Tousey [86] new solar spectra were obtained in a rocket flight on February 2, 1954, at altitudes between 80 and 104 km. The Lyman alpha line of hydrogen was obtained in all ten exposures and the solar continuum photographed to 1750 Å. Furthermore, the Schumann-Runge absorption bands of oxygen appeared in the continuum. Traces of the continuum could be seen between 1100–1300 Å at the wavelengths of the O_2 transmission windows. These results should provide much of the data necessary for the assessment of existing theories of the nature of the upper atmosphere.

Vacuum ultraviolet spectroscopic measurements of absorption coefficients of all atmospheric constituents provide the quantitative basis for studying absorption of solar radiation in the atmosphere. Furthermore, measurements of photoionization cross-sections and ionization potentials of these gases is important in the study of the origin of the various ionospheric layers. Of equal significance in studying reactions in the upper atmosphere are the kinetics of photochemical decomposition of atmospheric constituents in the vacuum ultraviolet. It is safe to state that the combined efforts of rocket spectroscopy and fundamental investigations of the interaction of vacuum ultraviolet radiation with atmospheric constituents will contribute much to our knowledge of the upper atmosphere.

OL.
7
5/56

References

[1] LYMAN, T.; *The Spectroscopy of the Extreme Ultraviolet*, 2nd ed., Longmans Green and Co., London, 1928.
[2] BOMKE, H.; *Vakuumspektroskopie*, J. A. Barth, Leipzig, 1937.
[3] BOYCE, J. C.; *Revs. Mod. Phys.* 1941 **13** 1.
[4] PLATT, J. R., and KLEVENS, H. B.; *Revs. Mod. Phys.* 1944 **16** 182.
[5] PRICE, W. C.; *Reports on Progress in Phys.* 1951 **14** 1.
[6] WATANABE, K., INN, E. C. Y., and ZELIKOFF, M.; *J. Chem. Phys.* 1953 **21** 1026.
[7] POWELL, W. M.; *Phys. Rev.* 1934 **45** 154.
[8] SCHNEIDER, E. G.; *Phys. Rev.* 1936 **49** 341.
[9] SCHNEIDER, E. G.; *Phys. Rev.* 1934 **45** 152.
[10] MARMO, F. F.; Ph.D. dissertation, Harvard Univ., 1954.
[11] FRIED, S., MCMURRY, H. L., and ROSENBAUM, E. J.; *J. Chem. Phys.* 1939 **7** 853.
[12] JOHNSON, F. S., WATANABE, K., and TOUSEY, R.; *J. Opt. Soc. Amer.* 1951 **41** 702.
[13] ASTOIN, N., and VODAR, B.; *J. Phys. Radium* 1953 **14** 424.
[14] SABINE, G. B.; *Phys. Rev.* 1939 **55** 1064.
[15] WATANABE, K., and INN, E. C. Y.; *J. Opt. Soc. Amer.* 1953 **43** 32.
[16] WATANABE, K.; *J. Opt. Soc. Amer.* 1953 **43** 318.
[17] PURCELL, J. D.; *J. Opt. Soc. Amer.* 1953 **43** 1166.
[18] HAMMOND, V. J., and PRICE, W. C.; *J. Sci. Instr.* 1954 **31** 104.
[19] BRIX, P., and HERZBERG, G.; *Can. J. Phys.* 1954 **32** 110.
[20] HARRISON, G. R.; Progress Reports Nos. 1–5, Contract No. AF19(604)-506 Mass. Inst. of Technology, 1952–1953.
[21] BAKER, R. F.; *J. Opt. Soc. Amer.* 1938 **28** 55.
[22] LITTLE, E. P., *J. Opt. Soc. Amer.* 1946 **36** 168.
[23] PARKINSON, W. W., and WILLIAMS, F. E.; *J. Opt. Soc. Amer.* 1949 **39** 705.
[24] TOUSEY, R., JOHNSON, F. S., RICHARDSON, J., and TORAN, N.; *J. Opt. Soc. Amer.* 1951 **41** 696.
[25] BOLTON, J. H., and WILLIAMS, S. E.; *Nature* 1952 **169** 325.
[26] JOHNSON, P. D.; *J. Opt. Soc. Amer.* 1952 **42** 278.
[27] FRANKLIN, S. G.; *J. Opt. Soc. Amer.* 1954 **44** 348.
[28] SCHUMANN, V.; *Ann. Physik* 1901 **5** 349.
[29] HARRISON, G. R.; *J. Opt. Soc. Amer.* 1925 **11** 113.
[30] HARRISON, G. R., and LEIGHTON, P. A.; *J. Opt. Soc. Amer.* 1930 **20** 313.
[31] HARRISON, G. R., and LEIGHTON, P. A.; *Phys. Rev.* 1931 **38** 899.
[32] LEE, P., and WEISSLER, G. L.; *J. Opt. Soc. Amer.* 1953 **43** 512.
[33] SCHOEN, A. L., and HODGE, E. S.; *J. Opt. Soc. Amer.* 1950 **40** 23.
[34] PRESTON, W. M.; *Phys. Rev.* 1940 **57** 887.
[35] DUNKELMAN, L., and LOCK, C.; *J. Opt. Soc. Amer.* 1951 **41** 802.
[36] JONES, L. C., and TAYLOR, L. W.; 1954 Pittsburg Conference on Analytical Chemistry and Applied Spectroscopy.
[37] PACKER, D. M., and LOCK, C.; *J. Opt. Soc. Amer.* 1951 **41** 699.
[38] HINTEREGGER, H. E., and WATANABE, K.; *J. Opt. Soc. Amer.* 1953 **43** 604.
[39] HOPFIELD, J. J.; *Astrophys. J.* 1930 **72** 133.
[40] WORLEY, R. E.; *Rev. Sci. Instr.* 1942 **13** 67.
[41] TANAKA, Y., and ZELIKOFF, M.; *J. Opt. Soc. Amer.* 1954 **44** 254.
[42] LEE, P., and WEISSLER, G. L.; *J. Opt. Soc. Amer.* 1952 **42** 80.
[43] HERZBERG, G.; *Molecular Spectra and Molecular Structure. I. Diatomic Molecules*, Prentice-Hall, Inc., New York, 1939.
[44] GAYDON, A. G.; *Dissociation Energies and Spectra of Diatomic Molecules*, Dover Publications, New York, 1950.
[45] TANAKA, Y.; to be published.
[46] REINECKE, L.; *Z. Physik.* 1935 **135** 361.
[47] BROOK, M.; Scientific Report No. 2, Contract No. AF19(122)-453, Inst. of Geophys., Univ. of California at Los Angeles, 1953.

VOL. 7 1955/5

[48] MULLIKEN, R. S.; *J. Chem. Phys.* 1939 **7** 14, 20.
[49] LADENBURG, R., and VAN VOORHIS, C. C.; *Phys. Rev.* 1933 **43** 315.
[50] WATANABE, K., MARMO, F. F., and INN, E. C. Y.; *Phys. Rev.* 1953 **90** 155.
[51] TANAKA, Y.; *J. Chem. Phys.* 1952 **20** 1728.
[52] ZELIKOFF, M., WATANABE, K., and INN, E. C. Y.; *J. Chem. Phys.* 1953 **21** 1643.
[53] INN, E. C. Y., ZELIKOFF, M., and WATANABE, K.; *J. Chem. Phys.* 1953 **21** 1648.
[54] TANAKA, Y., INN, E. C. Y., and WATANABE, K.; *J. Chem. Phys.* 1953 **21** 1651.
[55] MARMO, F. F.; *J. Opt. Soc. Amer.* 1953 **43** 1186.
[56] WATANABE, K., and ZELIKOFF, M.; *J. Opt. Soc. Amer.* 1953 **43** 753.
[57] ZELIKOFF, M., and WATANABE, K.; *J. Opt. Soc. Amer.* 1953 **43** 756.
[58] PRICE, W. C.; *Annual Rep. Chem. Soc.* 1939 **36** 47.
[59] PRICE, W. C.; *Chem. Revs.* 1947 **41** 257.
[60] WALSH, A. D.; *Ann. Rep. on Prog. Chem.* (Chem. Soc. of London) 1947 **44** 32.
[61] WALSH, A. D.; V. Henri Mem. Vol. "Contribution to the Study of Molecular Structure," p. 191 (1947–48). Desoer, Liege.
[62] WALSH, A. D.; *Quart. Revs. Chem. Soc.* (*London*) 1948 **2** 73.
[63] HAMMOND, V. J., PRICE, W. C., TEEGAN, J. P., and WALSH, A. D.; *Discussions of the Faraday Soc.* 1950 **9** 53.
[64] DUMOND, J. W. M., and COHEN, E. R.; *Revs. Mod. Phys.* 1949 **21** 651.
[65] PRICE, W. C., and TUTTE, W. T.; *Proc. Roy. Soc.* (*London*) 1940 **174A** 207.
[66] MULLIKEN, R. S.; *Revs. Mod. Phys.* 1942 **14** 265.
[67] MULLIKEN, R. S.; *J. Chem. Phys.* 1935 **3** 506, 514, 517, 564, 573, 586, 635, 720.
[68] WALSH, A. D.; *Trans. Faraday Soc.* 1946 **42** 56.
[69] WALSH, A. D.; *Trans. Faraday Soc.* 1947 **43** 60.
[70] WALSH, A. D.; *Trans. Faraday Soc.* 1947 **43** 158.
[71] WALSH, A. D.; *Trans. Faraday Soc.* 1945 **41** 35.
[72] SUGDEN, T. M., and WALSH, A. D.; *Trans. Faraday Soc.* 1945 **41** 76.
[73] PRICE, W. C., and WALSH, A. D.; *Proc. Roy. Soc.* (*London*) 1940 **174A** 220.
[74] INN, E. C. Y.; *Phys. Rev.* 1953 **91** 1194.
[75] WATANABE, K., MARMO, F. F., and INN, E. C. Y.; *Phys. Rev.* 1953 **91** 1155.
[76] WAINFAN, N., WALKER, W. C., and WEISSLER, G. L.; *J. Appl. Phys.* 1953 **24** 1318.
[77] SCHNEIDER, E. G., and O'BRYAN, H. M.; *Phys. Rev.* 1937 **51** 293.
[78] FERGUSON, J. N.; *Phys. Rev.* 1944 **66** 220.
[79] MASLEN, V. W., WHITE, N. E., and WILLIAMS, S. E.; *Brit. J. Appl. Phys.* 1953 **4** 303.
[80] BOLTON, J. H., and WILLIAMS, S. E.; *Nature* 1952 **169** 325.
[81] TOUSEY, R.; *J. Opt. Soc. Amer.* 1953 **43** 245.
[82] TOUSEY, R.; *The Sun*, ed. G. P. KUIPER, p. 658, Univ. of Chicago Press, Chicago, 1953.
[83] PIETENPOL, W. B., RENSE, W. A., WALZ, F. C., STACEY, D., and JACKSON, J.; *Phys. Rev.* 1953 **90** 156.
[84] RENSE, W. A.; *Phys. Rev.* 1953 **91** 299.
[85] BYRAM, E. T., CHUBB, T., FRIEDMAN, H., and GAYLOR, N.; *Phys. Rev.* 1953 **91** 1238.
[86] JOHNSON, F. S., PURCELL, J. D., and TOUSEY, R.; *Phys. Rev.* 1954 **95** 621.

Spectrochimica Acta, 1955, Vol. 7, pp. 88 to 90. Pergamon Press Ltd., London

The spectrochemical determination of gallium in blende

D. F. C. Morris and F. M. Brewer
Atomic Energy Research Establishment, Harwell; Inorganic Chemistry Laboratory, Oxford University

(*Received* 11 *December* 1954)

Summary—In order to help to confirm the reliability of the determination of gallium in blende by radioactivation analysis, a spectrochemical method, using zinc as internal standard and the cathode-layer carbon arc, has been employed. The precision of the spectrochemical procedure is such that over a range of 0·005 to 0·02 per cent Ga, the standard deviation incurred is approximately 5 per cent. Agreement between spectrochemical and radioactivation analyses is quite good.

Introduction

The determination of gallium in blende by radioactivation analysis and the geochemistry of the occurrence of the element in the mineral have been described elsewhere (Morris and Brewer [1]). In order to help in obtaining confirmation of figures obtained by the radioactivation method of analysis, an alternative method for estimating the gallium was desirable, and it was decided to attempt a spectrochemical method.

In order to obtain accuracy and precision, it was necessary to select a suitable internal standard. Various quantitative and semiquantitative spectrochemical procedures for determining gallium in blende specimens have been described, but only a few have involved internal standardization. Oftedal [2] has determined gallium together with other trace elements in Norwegian blendes, employing the cathode-layer carbon-arc method, the zinc of the blende being used as an internal standard for gallium. The analysis pair Ga 2943·6 Å and Zn 3282·3 Å was used. Gabrielson [3] has similarly analyzed a large number of Swedish blendes for various trace elements, including gallium. Like Oftedal, he used the cathode-layer carbon arc. Gabrielson carried out semiquantitative analyses, using the line pair Ga 2943·6 Å and Zn 3072·1 Å, and checked the reliability of the procedure by quantitative analyses, involving photometric measurements and employing the line pair Ga 2943·6 Å and Cr 2971·1 Å. A very similar problem has been investigated by Strock [4], who studied the determination of various trace elements in zinc sulphides. Beryllium was used as internal standard for gallium, with the line pair Ga 2943·6 Å and Be 3130·4 Å.

Since zinc in blende volatilizes at a fairly similar speed to gallium with high current cathode excitation, and also because the addition of an internal standard necessitates the weighing of the sample, the weighing of the internal standard, and the thorough grinding of the sample to ensure homogeneity, it was decided to follow Oftedal and Gabrielson and employ zinc as an internal standard. The zinc line at 3035·8 Å was found to be satisfactory as an internal standard line, especially as it is situated fairly close to the gallium line Ga 2943·6 Å. Unfortunately, however, when iron is present to a considerable extent in the blende specimens

an iron line at 3035·7 Å is likely to interfere. It was decided, therefore, to use the line pair Ga 2943·6 Å and Zn 3072·1 Å with a photometric method of analysis.

Apparatus

The spectrograph available was a large Hilger, fully automatic, quartz prism Littrow instrument. The electrodes finally selected for holding the samples were made from pure carbon rods of 5-mm diameter. Pieces 3 cm in length were cut down to a diameter of 3 mm over a length of 17 mm and bored with a recess 4 mm deep and 1/16-in. diameter. When each had been prepared and filled, it was placed in the lower electrode holder and made the cathode. The anodes were similar to the cathodes, but with no bore.

The optical system involved the focusing of an image of the arc on a screen by means of a Hilger F958 quartz lens. Light from 2 mm of the image of the arc-column adjoining the cathode was passed through a diaphragm and on through a Hilger F1025 quartz lens at the slit, being focused at the collimator.

The arc was made by bringing the electrodes together, allowing the current to flow through the closed electrodes for a few sec at 3 amps, then separating them to 4 mm and increasing the current simultaneously to 9 amps. Each exposure was of 40 sec. Ilford Rapid Panchromatic Plates were used, and were developed for 3 min in Ilford ID 2 developer at 18°C.

The line transmissions were measured on a Hilger non-recording microphotometer.

Preparation of standards

As was pointed out by Oftedal [2], it was found that blende has quite different burning characteristics in the arc from precipitated ZnS. For this reason, standards were made by diluting Johnson Matthey Co. Specpure Ga_2O_3 with a blende (No. 17222 in the Oxford University mineral collection) in which no gallium could be detected spectrographically. Standards containing 0·05, 0·02, 0·01, and 0·005 per cent Ga respectively were made by thoroughly grinding and dry-mixing in an agate mortar for thirty minutes to ensure homogeneity of the material.

Photometry and the working curve

The characteristic curve of the emulsion in the required spectral region was determined by placing a step-sector immediately in front of the spectrograph slit, exposing to an iron arc, and measuring with the microphotometer the transmission of each portion of an iron line in that region.

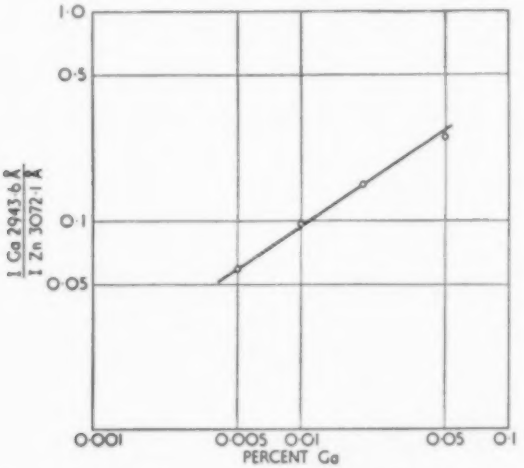

Fig. 1. Working curve for the analysis of gallium in blende. Each point is the mean of four measurements.

The intensities of the analysis line Ga 2943·6 Å and the internal standard line Zn 3072·1 Å were then compared by measuring their transmissions with the microphotometer and employing the characteristic curve. The background intensities were also measured and subtracted from the observed line intensities. The ratio of the corrected intensities of the analysis pair for the series of standard samples was then plotted against gallium percentage composition on log-log co-ordinates to give the working curve, Fig. 1. By measuring the corresponding ratio for the unknown samples, their gallium content could be read directly from the working curve.

Accuracy

In the analysis of samples containing 0·005 to 0·02 per cent Ga the standard deviation incurred was about 5 per cent. Some results obtained on samples in which the gallium had been determined by both the spectrochemical method and by radioactivation analysis are given in Table 1.

Table 1. *Percentage gallium in blende specimens determined by radioactivation and spectrochemical analysis*

Mineral locality	*Gallium content by radioactivation analysis* % Ga	*Gallium content by spectrochemical analysis* % Ga
Threkeld mine, Keswick, Cumberland, England	0·019 0·020 0·020 0·020 Av. 0·020	0·022 0·020 0·023 0·021 Av. 0·022
Force Crag mine, Coledale, Keswick, Cumberland, England	0·0055 0·0059 Av. 0·0057	0·0051 0·0051 0·0051 Av. 0·0051
Brandelhow mine, Keswick, Cumberland, England	0·020 0·020 Av. 0·020	0·021 0·020 0·022 0·023 Av. 0·022

Acknowledgments—The authors wish to express their appreciation to Imperial Chemical Industries, Limited, for apparatus and chemicals used in the analyses.

References

[1] Morris, D. F. C., and Brewer, F. M.; *Geochim. et Cosmochim. Acta* 1954 **5** 134–141.
[2] Oftedal, I.; *Skrif, Norske. Vid-Akad.* (Oslo) 1. *Mat-Nat.* Kl., No. 8, 1940.
[3] Gabrielson, O.; *Sveriges Geol. Undersökn. Ser. C. Avhandl. och Uppsat.*, 1945, No. 468, *Årsbok* 39 No. 1.
[4] Strock, L. W.; *A.I.M.M.E. Tech. Pub. No.* 1866, 1945.

Spectrochimica Acta, 1955, Vol. 7, pp. 91 to 99. Pergamon Press Ltd., London

Internal standards in fluorescent X-ray spectroscopy*

I. ADLER and J. M. AXELROD
U.S. Geological Survey, Washington 25, D.C.

(*Received* 20 *August* 1954)
(*Accepted for publication* 21 *December* 1954)

Summary—The use of internal standards in the analysis of ores and minerals of widely-varying matrix by means of fluorescent X-ray spectroscopy is frequently the most practical approach. Internal standards correct for absorption and enhancement effects except when an absorption edge falls between the comparison lines or a very strong emission line falls between the absorption edges responsible for the comparison lines. Particle size variations may introduce substantial errors. One method of coping with the particle size problem is grinding the sample with an added abrasive.

Introduction

LIEBHAFSKY [1] in a recent review of the fields of both X-ray absorption and emission has pointed out that at the present time "no instrumental method of analysis is growing in popularity so fast as is X-ray emission spectroscopy." A great deal of emphasis has been placed on the development of methods and instrumentation, with the analysis of metals and alloys as the prime objective. Fluorescent X-ray spectroscopy is also a powerful tool for the analysis of ores, minerals, and powders, and it is no exaggeration to say that its potential in this direction has hardly been tapped.

There have been a number of examples of its use in powder analysis. In fact, some of the earliest work with fluorescent X-rays involved the analysis of minerals by such excellent investigators as VON HEVESEY [2], GLOCKER and SCHREIBER [3], and COSTER and NISHINA [4]. More recent examples of such applications are summarized by LIEBHAFSKY [1].

One fact stands out clearly in connection with ore and mineral analysis. Where the matrices are variable, internal standards are of great value. The alternatives to the use of suitable internal standards are very difficult if not impossible to achieve in practice. Briefly, they require either a prior knowledge of each sample and theoretical corrective factors, the determination of which is a problem of considerable magnitude, or a tremendous number and variety of standards along with a complete knowledge of the nature of the samples so that the proper standards may be chosen.

CAMPBELL and CARL [5] have demonstrated the value of molybdenum as an internal standard element for niobium. Similarly, KOKOTAILO and DAMON [6] have used selenium as a control element for the determination of trace amounts of bromine in hydrocarbons. After incorporation of a known amount of the reference element into the sample, the ratio of the intensity of a line of the analytical element to the intensity of a line from the reference element was measured.

The use of internal standards or ratio measurements is, however, subject to

* Publication authorized by the Director, U.S. Geological Survey.

disturbing effects. Problems of selective enhancement or absorption of one of the lines of a line pair must be considered. This subject has been thoroughly treated by von Hevesey [2] and Glocker and Schreiber [3]. The work done by these early workers was thorough and comprehensive. Because the modern spectrograph affords high speed rather than high resolution, a great many of the line pairs used by von Hevesey are not resolvable and therefore it was felt that a systematic examination of element pairs which are neighbours in the periodic chart and provide line pairs which are resolvable should be made. The element pairs chosen ranged from light elements such as chromium and manganese to heavy elements such as thorium and thallium.

Experimental

Instrumentation

The instrumentation used has been described in some detail in a previous publication [7]. It consists essentially of a two channel fluorescent X-ray spectrometer with lithium fluoride analyzing crystals, Geiger counter detection, and simultaneous integration by scalers operating in parallel. The advantages of such a system for investigations of internal standards lie in the greater precision and convenience of measurement resulting from the simultaneous measurement of both lines.

Sample preparation

The analytical methods developed in our laboratory have been based on the use of briquetted samples. We have found that finely divided aluminium powder when mixed in one-to-one ratio with the sample serves very well as a binder [8].

Similarly briquetted samples were used in this investigation of internal standards. The procedure was as follows:

Compounds of the pairs of elements to be tested as control elements for each other were incorporated by grinding under ether into the aluminium powder; the mixture then served as a binder and base material. The concentrations (up to 5 per cent) were chosen so that the intensity ratios of the emitted lines were approximately unity in order to minimize the effects of background, although background corrections were actually made. These base materials were diluted, one part of base material to one part of diluent, with the material or mixture of materials chosen either as an absorber or enhancer. The diluent materials ranged, for every line pair investigated, from 100 per cent lithium carbonate to 100 per cent heavy element or oxide. Lithium carbonate was chosen as being representative of a very light matrix. All materials used were minus 200 mesh or finer.

Internal standards and multichannel spectrometry as a control for power supply fluctuations

The use of internal standards in combination with multichannel spectrometry practically eliminates the need for current and voltage stabilization [7]. This corresponds closely to the situation reported by von Hevesey [2].

Absorption effects

Absorption effects can be divided into two cases:

(a) The change in intensity ratio due to the preferential absorption of the longer wavelength line by an element having an absorption edge on the long wavelength side of the two lines being measured.

(b) The change in intensity ratio due to the presence of an element with an absorption edge between the two lines being measured.

The effects of absorption described in case (a) have been examined analytically by a number of investigators. GLOCKER and SCHREIBER [3] have given a detailed discussion which is repeated by VON HEVESEY [2]. HÁMOS [9] has treated the effects of absorption in connection with his work on an X-ray microanalyzer. More recently SHERMAN [10] has developed a correlation between the intensity of the X-ray spectrum of an element and the concentration of the element in a sample,

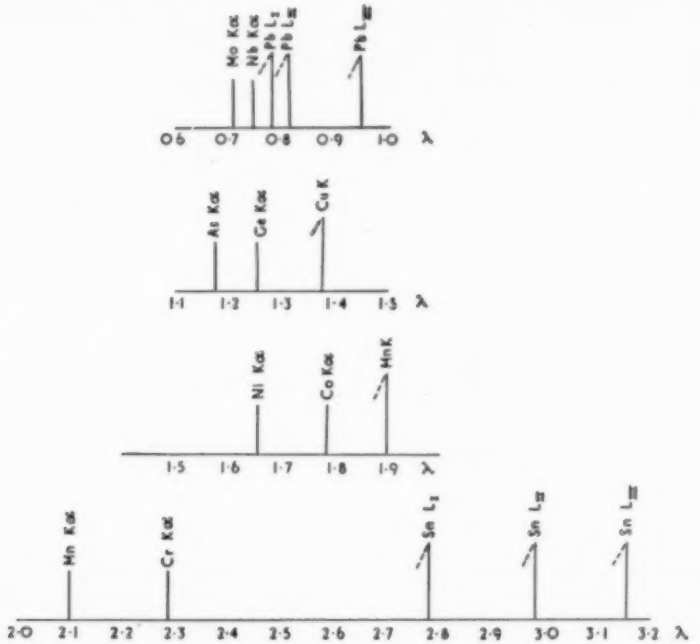

Fig. 1. Relative positions of the measured X-ray lines and absorption edges for the experiments on the effect of an absorption edge on the long wavelength side of all the lines measured.

using statistical considerations, and BEATTIE and BRISSEY [11] have calculated a first-order linear correction for the absorption effects of the various elements in an alloy on fluorescent X-ray intensities.

As indicated in the introduction, the present investigation is concerned with pairs of elements adjacent to each other in the periodic chart. Intensity ratios of the various element pairs have been examined first in the presence of elements having an absorption edge on the long wavelength side of the two comparison lines (Case a). The lines and edges chosen for study are shown in Fig. 1. An effort was made to choose an edge just beyond the longer wavelength line so that the absorption curve would be steep and the absorption coefficients high. It was felt that this would constitute a rather powerful test of the constancy of the ratios. Fig. 2 shows the behaviour of the ratio of niobium Kα to molybdenum Kα in the presence of varying amounts of lead oxide. For purposes of comparison the variation in

ratio of a long wavelength pair such as chromium Kα and manganese Kα in the presence of varying amounts of tin oxide is also shown in the same figure. In the chromium Kα to manganese Kα comparison the concentration of chromium had to be three times that of the manganese in order to get an intensity ratio of approximately unity. This was due to greater absorption in the external air path and the mica window of the Geiger tube, and to the greater end effect in the Geiger tube for the chromium radiation, and yet the ratio is seen to be practically independent of the matrix.

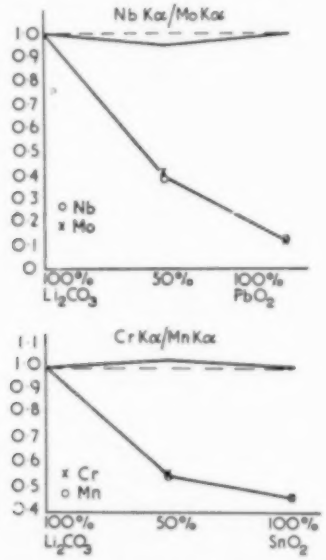

Fig. 2. The effect of an absorption edge on the long wavelength side of all the lines measured on intensity ratio and on absolute intensity. The upper curve in each sketch represents the normalized intensity ratio versus the diluent composition and the lower curve represents normalized absolute intensity versus diluent composition.

The results obtained for other line pairs such as germanium Kα to arsenic Kα, cobalt Kα to nickel Kα, and thallium $L\beta_1\beta_2$ to thorium $L\alpha_1$ were very similar to those shown in Fig. 2. The intensity ratios were practically constant despite three- to fourfold changes in absolute intensities of the individual elements.

The absorption effect described in Case (b) has been adequately treated by von Hevesey [2]. He points out that errors of substantial magnitude can result. By way of illustration it was shown that the intensity ratio of chromium $K\alpha_1$ (2258 XU) to praseodymium $L\beta_1$ (2254 XU) was shifted 63 per cent in favour of the chromium by the presence of titanium when the atomic ratio of titanium to praseodymium was four to one. Since this effect is so obvious no additional work was done.

Excitation effects

Excitation effects may also be divided into two cases:

(a) The line of a third element present occurs between the absorption edges of the two elements to be compared.

(b) A line of the third element is on the short wavelength side, but much closer to the edge of one of the two elements to be compared.

Von Hevesey [2] indicates that Case (a) is a cause for concern only when the line between the edges is a strong one. More will be said about this later.

When an intense line of a third element is on the short wavelength side and nearer one of the edges giving rise to the two lines to be compared, it is conceivable that the element having the closer edge will be more favourably excited. This effect has been shown to be small, even where the edges are widely separated and the exciting line is strong. For example, Glocker and Schreiber [3] found only

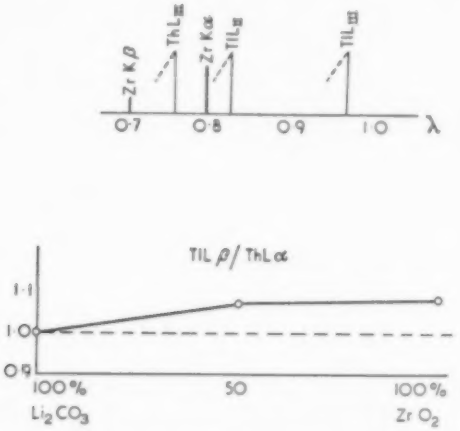

Fig. 3. Enhancement of the intensity of thallium radiation relative to thorium radiation by zirconium. The upper sketch shows the positions of the zirconium lines relative to the thorium and thallium edges involved. For the lower sketch, the ordinate is the normalized Tl/Th intensity ratio and the abscissa is the composition of the diluent added to the base material.

a 4 per cent decrease in intensity of titanium relative to vanadium due to selective enhancement of the vanadium line by iron, which was 80 per cent of the sample by weight. The absorption edges considered were vanadium K (2265 XU) and titanium K (2494 XU) and the line was iron $K\alpha_1$ (1932 XU).

Both these effects have been re-examined by us in terms of modern instrumentation. Fig. 3 shows the effect of zirconium on the intensity ratio of thallium $L\beta_1\beta_2$ (1008 XU, 1013 XU) to thorium $L\alpha_1$ (954 XU). The zirconium line is between the thorium and thallium edges involved. The thallium $L\beta_1\beta_2$ line is seen to be enhanced due to excitation by the secondary zirconium line. It is significant that the enhancement is only approximately 10 per cent for such an extreme case. The effect of absorption of the zirconium $K\beta$ line is much less.

Fig. 4 shows the effect of selenium on the ratio of germanium $K\alpha$ (1253 XU) to arsenic $K\alpha$ (1175 XU). The intensity ratio shows a marked enhancement of the germanium line with respect to the arsenic line as the selenium increases. This, also, is to be expected from the fact that the stronger selenium $K\alpha$ line is on the long wavelength side of the arsenic edge only. Here the individual curves are plotted to show the nature of the enhancement. The lines of both elements are seen to decrease in absolute intensity as the concentration of the selenium increases.

The decrease of the germanium line intensity, however, is not as great, resulting in the rising ratio.

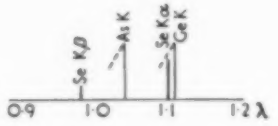

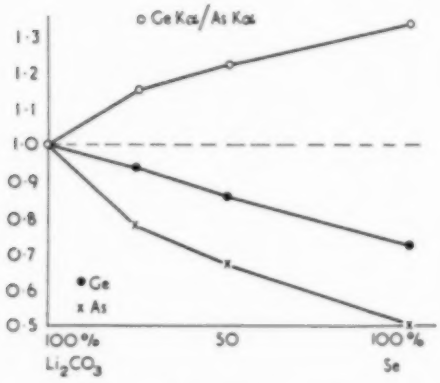

Fig. 4. Enhancement of the intensity of germanium radiation relative to arsenic radiation by selenium. The ordinate in this figure is, for the upper curve, the normalized Ge/As intensity ratio and, for the lower curves, the normalized absolute intensity. The abscissa is the composition of the diluent added to the base material.

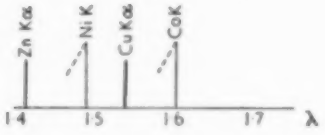

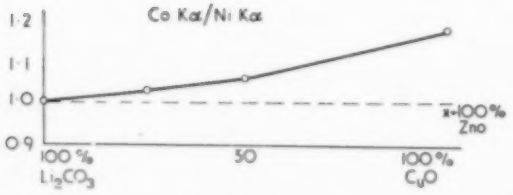

Fig. 5. Enhancement of the intensity of cobalt radiation relative to nickel radiation by copper. The abscissa is, for the curve, the composition of the diluent consisting of lithium carbonate and cupric oxide. The absence of enhancement by zinc is shown by the position of the point for 100 per cent zinc oxide as diluent.

Fig. 5 shows both the effect of a strong line between the absorption edges and the effect of a strong line on the short wavelength side of both absorption edges. The ratio considered in this case is cobalt Kα to nickel Kα in the presence of

VOL. 7 1955/5

varying amounts of copper oxide in one case and in the presence of zinc oxide in the other. The effect of the copper whose Kα line falls between the absorption edges of the nickel and cobalt is, as would be expected from the previous example, to enhance the cobalt Kα line with respect to the nickel Kα line. The zinc Kα line falls on the short wavelength side of both edges, and despite its closeness to the nickel edge, the ratio of the cobalt to nickel Kα lines is seen to be unaffected by a high concentration of zinc.

This effect is shown in even greater detail in Fig. 6, where the chromium Kα to manganese Kα line ratio is studied. The diluent is varied from lithium carbonate

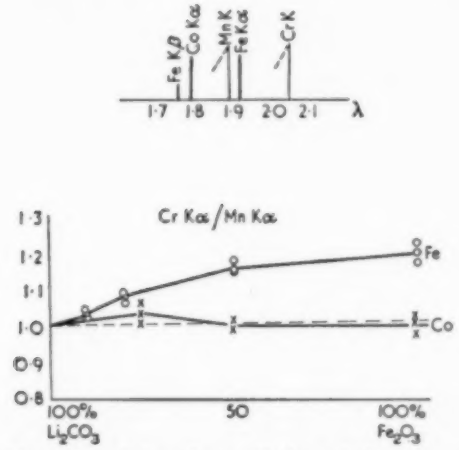

Fig. 6. Enhancement of intensity of chromium radiation relative to manganese radiation by iron and absence of such enhancement by cobalt. The ordinate is the normalized intensity ratio for Cr/Mn and the abscissa is the composition of the diluent added to the base material.

to iron oxide in one case and from lithium carbonate to cobaltic oxide in the other. Again the iron with a strong line between the edges causes enhancement of the longer wavelength line and the cobalt, which has a line on the short wavelength side of both edges, has no measurable effect.

To summarize these findings, neighbouring elements in the periodic chart serve very well as internal standards for each other. They compensate for absorption and enhancement except when there is a strong line between the edges involved or, as discussed by VON HEVESEY [2], an edge between the comparison lines. The closer together the lines chosen, the less is the likelihood of these types of interferences. Where such interference is not likely to occur, adjacent elements are satisfactory.

Particle size effect

The analysis of powders, such as rock samples and ores, poses a serious problem in sample preparation. One important factor that must be considered is the particle sizes of the various components.

Intensity ratios measured on chemically identical samples were found to vary by as much as a factor of 2 between samples made of coarse and of fine materials.

Examples of such an effect are shown in Table 1, where the intensity ratios of the Th $L\alpha_1$ to the Tl $L\beta_1\beta_2$ lines are compared for different particle sizes. The effect of particle size on the Zr Kα/Nb Kα and Fe Kα/Mn Kα (in solid solution) ratios is substantially smaller, as is also shown in Table 1. Mortimore, Romans,

Table 1. *Variation of intensity ratio with particle size*

Mesh	*Th* $L\alpha_1$/*Tl* $L\beta_1\beta_2$			*Zr* Kα/*Nb* Kα	*Fe* Kα/*Mn* Kα*
	A	*B*	*C*	*D*	*D*
200–300	0·88	1·25	0·70	1·34	1·25
300–400	0·92	1·18	1·14	1·33	1·29
–400	1·17	1·14	1·35	1·25	1·39

A 0·1 gram ThO_2, 0·1 gram TlCl, 0·8 gram Al
B 0·1 gram $Th(NO_3)_4 \cdot 4H_2O$, 0·1 grams TlCl, 1·8 grams Al
C 0·4 gram monazite, 0·1 gram TlCl, 1·5 grams Al
D 0·1 gram zircon, 0·1 gram columbite, 1·8 grams Al
* The iron and manganese are known to be mostly in solid solution.

Statistical coefficient of variation based on minimum total count = 1·2 per cent
Estimated variation due to Geiger tube fluctuation = 0·5 per cent

and Tews [12] have reported very large particle size effects in their work on tantalum. The results obtained in the internal standard investigation were on samples which had only been ground long enough to obtain good mixing, and particle size effects are probably the cause of the erratic nature of the ratio curves in Figs. 2 and 6.

Table 2. *Variation of intensity ratio with grinding*

	Ratios:	*Th* $L\alpha_1$/*Tl* $L\beta_1\beta_2$		*Zr* Kα/*Nb* Kα		*Fe* Kα/*Mn* Kα	
Mesh	*Samples:*	*A*		*B*		*B*	
	Grinding time:	0	$\frac{1}{2}$ hr	0	$\frac{1}{2}$ hr	0	$\frac{1}{2}$ hr
200–300		0·90	1·22	1·32	1·24	1·62	1·59
300–400		0·96	1·23	1·34	1·26	1·57	1·60
–400		1·21	1·32	1·24	1·28	1·68	1·62

A briquets contain 0·1 gram ThO_2, 0·1 gram TlCl, 0·5 gram SiC, 0·8 gram Al
B briquets contain 0·1 gram columbite, 0·1 gram zircon, 0·8 gram SiC, 1·0 gram Al

Statistical coefficient of variation based on minimum total count = 1·2 per cent
Estimated maximum variation due to Geiger tube voltage fluctuation = 0·5 per cent

To eliminate these effects it is necessary to prepare homogeneous samples for measurement. Three methods of achieving such homogeneity have been suggested. The first is to grind the components fine enough that particle size is negligible, the second is to incorporate the sample and internal standard into a solid solution, and

the third is to initially dissolve both sample and standard and then coprecipitate the elements to be measured [12].

In this investigation grinding with silicon carbide in an automatic mortar grinder was considered as probably the simplest and most rapid approach. It was felt that the silicon carbide would provide an effective means of grinding all other components equally well and of scouring the mortar so soft material would not stick preferentially to the mortar. The value of such grinding is shown in Table 2. The improvement in constancy of the Th/Tl ratios is most noteworthy.

The technique of grinding for half an hour with carborundum is seen to allow analyses good to about 5 per cent in the worst examples investigated. A more efficient grinding technique might afford even better results. A method of forming the sample and standard into a solid solution should also work well for any sample if a solvent for any and all oxide, sulphide, and silicate minerals could be devised. Lacking these, a solvent or treatment that will result in a homogeneous dispersal of all components should eliminate erratic sample behaviour due to particle size. The method of grinding with an abrasive is offered, however, as the simplest and quickest approach.

OL.
7
5/56

Acknowledgments

The authors gratefully acknowledge the technical assistance of the following colleagues in the U.S. Geological Survey: M. K. Carron for assays of the thoria fractions, David Gottfried for zircon samples, and R. S. Harner for spectrographic analyses of the iron and manganese oxides. Helpful suggestions were made by W. J. Campbell, of the U.S. Bureau of Mines, and G. E. Ashby, then of the J. J. Maguire Company.

References

[1] Liebhafsky, H. A.; *Anal. Chem.* 1954 **26** 26.
[2] Hevesey, G. v.; *Chemical analysis by X-rays and its applications*, 1932, McGraw-Hill Book Co.
[3] Glocker, R., and Schreiber, H.; *Ann. Physik* 1928 **85** 1089.
[4] Coster, D., and Nishina, J.; *Chem. News* 1925 **130** 149.
[5] Campbell, W. J., and Carl, H. F.; *Anal. Chem.* 1954 **26** 800.
[6] Kokotailo, G. T., and Damon, G. F.; *Anal. Chem.* 1953 **25** 1185.
[7] Adler, I., and Axelrod, J. M.; *J. Opt. Soc. Amer.* 1953 **43** 769.
[8] Adler, I., and Axelrod, J. M.; *Anal. Chem.* 1954 **26** 931.
[9] Hámos, L. V.; Arkiv Mat., Astron., Fysik 1944 **31** 1.
[10] Sherman, J.; ASTM Special Technical Publication No. 157, 27–33 (1953).
[11] Beattie, H. J., and Brissey, R. M.; *Anal. Chem.* 1954 **26** 980.
[12] Mortimore, D. M., Romans, P. A., and Tews, J. L.; *Applied Spectroscopy* 1954 No. 1 **8** 24.

Spectrochimica Acta, 1955, Vol. 7, pp. 100 to 107. Pergamon Press Ltd., London

Spectroscopic investigation of the strength of hydrogen bonds formed by amides

San-ichiro Mizushima, Masamichi Tsuboi, Takehiko Shimanouchi, and Yoshizo Tsuda
Chemical Laboratory, Faculty of Science, Tokyo University

(*Received September* 1954)

Summary—The infrared and ultraviolet absorptions have been measured on the ternary systems consisting of a large quantity of nonpolar solvent and small quantities of two polar substances involved in hydrogen bonding. From the shift and the intensity of absorption bands the proton-accepting power of the CO group and the proton-donating power of the NH group of amides have been determined. The effect of solvent on the N—H · · · O=C hydrogen bonds has also been studied.

Introduction

We have been interested in the molecular structure of N-methylacetamide [1], acetylaminoacid N-methylamide [2], etc., which can be regarded as structural units of polypeptide chain, and especially in the *intramolecular* and *intermolecular* hydrogen bonds formed by these molecules.

The strength of the hydrogen bond, X—H · · · Y has been determined in our laboratory as follows [3, 4]. We make a ternary solution consisting of small quantities of two polar substances, a proton donor with X—H group and a proton acceptor with Y atom, and a large quantity of nonpolar solvent. Then we measure the frequency and the intensity of the absorption bands of the specific groups involved in the hydrogen bonding.

Recently this method has been applied to the determination of the proton-accepting power of the C=O group and of the proton-donating power of the N—H group of amides. At the same time the dependence upon solvent of the strength of the hydrogen bond formed by amides has also been determined. The results will be discussed in the present paper.

Experimental

In Table 1 are shown the ternary systems measured in the present experiment. Of the compounds tabulated here, N,N-dimethylacetamide was prepared by heating the mixture of dimethylamine hydrochloride and sodium acetate at 170°C.* N-methylacetamide was prepared by T. Sugita of our laboratory and was purified by vacuum distillation. All other substances used in this experiment are the commercial samples which were purified by us.

The infrared absorptions were recorded with Perkin-Elmer infrared spectrophotometer Model 12C with the NaCl prism, the Baird spectrophotometer with

* A small quantity of acetic acid was added to the mixture to prevent the evaporation of dimethylamine. The reaction product was subjected to fractional distillation and the fraction boiling at 165–167°C was dissolved in ether. To this the potassium carbonate powder was added to remove water and acetic acid from N,N-dimethylacetamide.

the CaF_2 prism, and the reflecting monochromator of our own construction with the LiF prism. The ultraviolet absorptions were measured with a quartz spectrometer, type E_2, and the Beckmann spectrophotometer, Model DU.

Results and discussions

1. *The proton-accepting power of C=O group*

Let us first compare the strength of hydrogen bond formed between C=O of amides and O—H of phenol with that between C=O of acetone and O—H of phenol. As shown in Fig. 1, phenol exhibits only one OH band with a peak at

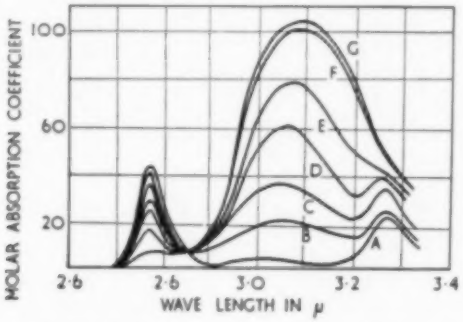

Fig. 1. Infrared absorption curves of phenol in the solutions:
A. CCl_4 + phenol 0·010 mole/l;
B. CCl_4 + phenol 0·010 mole/l + N,N-dimethylacetamide 0·00203 mole/l;
C. CCl_4 + phenol 0·010 mole/l + N,N-dimethylacetamide 0·00406 mole/l;
D. CCl_4 + phenol 0·010 mole/l + N,N-dimethylacetamide 0·0102 mole/l;
E. CCl_4 + phenol 0·010 mole/l + N,N-dimethylacetamide 0·0203 mole/l;
F. CCl_4 + phenol 0·010 mole/l + N,N-dimethylacetamide 0·0508 mole/l;
G. CCl_4 + phenol 0·010 mole/l + N,N-dimethylacetamide 0·102 mole/l.

Table 1. *The ternary systems*

Proton donor	*Proton acceptor*	*Solvent*	*Reference*
Phenol	N,N-dimethylacetamide	carbon-tetrachloride	Fig. 1, Fig. 2 (infrared), Table 2 (ultraviolet)
Phenol	acetone	carbon-tetrachloride	Fig. 2 (infrared), Table 2 (ultraviolet)
Phenol	N-methylacetamide	carbon-tetrachloride	Fig. 3 (infrared)
Phenol	N,N-dimethylacetamide	petroleum ether	
Phenol	acetone	petroleum ether	
Phenol	N,N-dimethylacetamide	iso-octane	Fig. 4, Table 2 (ultraviolet)
Phenol	acetone	iso-octane	Fig. 5, Table 2 (ultraviolet)
Phenol	N,N-dimethylacetamide	cyclohexane	Table 2 (ultraviolet)
N-methylacetamide	ethyl ether	carbon-tetrachloride	Fig. 6 (infrared)
N-methylacetamide	acetone	carbon-tetrachloride	Fig. 6 (infrared)
Ethanol	acetone	carbon-tetrachloride	Fig. 6 (infrared)
Diethylamine	acetone	carbon-tetrachloride	Fig. 6 (infrared)
Aniline	acetone	carbon-tetrachloride	Fig. 6 (infrared)
Phenol	ethyl ether	petroleum ether	
Acetanilide	ethyl ether	petroleum ether	

2·77 μ in carbon-tetrachloride solution at the concentration of 0·01 mole/l. This shows that in this solution almost all the molecules are in the single state and not associated. If, however, we dissolve N,N-dimethylacetamide in this solution, the free OH band at 2·77 μ decreases in intensity and a new OH band appears at 3·04 μ. This is assigned to the OH vibration involved in the hydrogen bond, $C_6H_5OH \cdots O{=}C(CH_3)N(CH_3)_2$ [3].

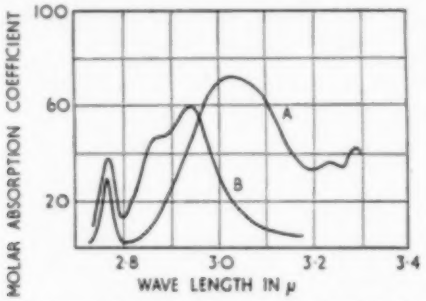

Fig. 2. Infrared absorption curves of phenol in the solutions:
A. CCl_4 + phenol 0·0053 mole/l + N,N-dimethylacetamide 0·01 mole/l;
B. CCl_4 + phenol 0·0053 mole/l + acetone 0·1 mole/l.

Fig. 2 shows the bonded OH absorption of the systems, phenol-N,N-dimethylacetamide and phenol-acetone, both in carbon-tetrachloride solutions. It is seen that the shift of OH frequency on hydrogen-bond formation is much greater in the former than in the latter. Furthermore, the equilibrium constant of the formation

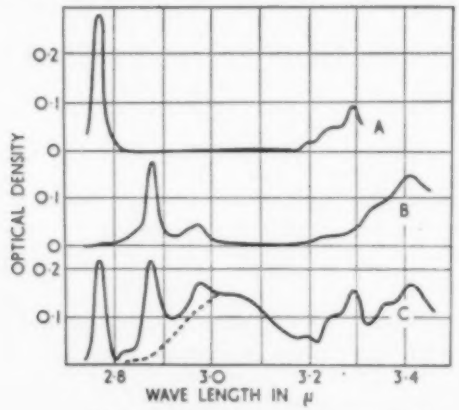

Fig. 3. Infrared absorption curves of:
A. phenol 0·0053 mole/l in CCl_4;
B. N-methylacetamide 0·0050 mole/l in CCl_4;
C. phenol 0·0053 mole/l + N-methylacetamide 0·0050 mole/l in CCl_4.
(The optical path-length is 1·0 cm in each case.)

of the complex is much greater in the former than in the latter. We can, therefore, conclude that the proton-accepting power of the C=O group of N,N-dimethylacetamide is greater than that of acetone.

Fig. 3 shows the infrared absorption for the system, phenol-N-methylacetamide

in carbon-tetrachloride. A, B, and C refer, respectively, to the absorptions of dilute solutions of phenol, N-methylacetamide, and both in carbon-tetrachloride. It is seen that in C there is an absorption band at 3·04 μ which appears neither in A nor in B and, furthermore, the free OH band of phenol decreases in intensity. This shows that the OH group of phenol and the CO group of N-methylacetamide are involved in the hydrogen bond, O—H · · · O=C. From the position and the intensity of the 3·04 μ band, it is concluded that the strength of the hydrogen bond is of the same magnitude as in the system of phenol and N,N-dimethylacetamide.

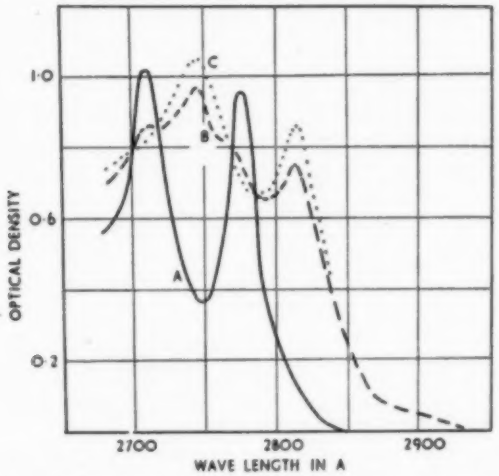

Fig. 4. Ultraviolet absorption curves of phenol in the solutions:
A. iso-octane + phenol 0·00047 mole/l;
B. iso-octane + phenol 0·00047 mole/l + N,N-dimethylacetamide 0·00790 mole/l;
C. iso-octane + phenol 0·00047 mole/l + N,N-dimethylacetamide 0·0158 mole/l.
(Optical path-length: 1·0 cm. Temperature: 9°C)

It should be noted that the free NH band at 2·88 μ and the bonded NH band at 2·97 μ of N-methylacetamide have almost the same intensity in B as in C. This shows that the association of N-methylacetamide is not affected by the presence of phenol in the ternary solution. This is compatible with the conclusion derived in a previous paper [5] that the formation of the hydrogen bond between water and amide is effected by the bond between OH of water and CO of amide and not between O of water and NH of amide.

Nagakura and Baba have shown that when phenol is involved in hydrogen bonding, the ultraviolet absorption band at 2,700 Å is shifted towards longer wavelengths [4]. Similar measurements have been made here for the ternary system consisting of phenol, acetone, and nonpolar solvent. A dilute solution of phenol (0·0004 mole/l) in petroleum ether shows sharp absorption bands at 2,709 and 2,777 Å, which correspond to the $^1A_{1g} \rightarrow {}^1B_{1u}$ absorption of benzene. When acetone is added to this solution, new absorption bands appear at 2,738 and 2,808 Å at the concentration of 0·03 mole/l in addition to the two bands referred to above. All the four bands persist in the concentration range from 0·03 to 0·1 mole/l.

However, when the concentration of acetone becomes higher than 0·1 mole/l, the bands at 2,709 and 2,777 Å disappear and only those at 2,738 and 2,808 Å are observed. (See Fig. 5.) From these experimental results it is concluded that the bands at 2,738 and 2,808 Å arise from the molecular complex of phenol and acetone.

If N,N-dimethylacetamide is added in place of acetone as the third component of the ternary system, the bands due to the complex of phenol and N,N-dimethylacetamide appear at 2,748 and 2,816 Å at the concentration of 0·004 mole/l of the latter substance, and the bands arising from free phenol molecules

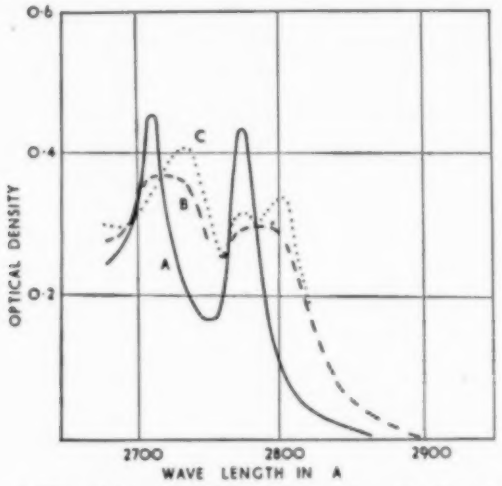

Fig. 5. Ultraviolet absorption curves of phenol in the solutions:
A. iso-octane + phenol 0·0020 mole/l;
B. iso-octane + phenol 0·0020 mole/l + acetone 0·0878 mole/l;
C. iso-octane + phenol 0·0020 mole/l + acetone 0·176 mole/l.
(Optical path-length: 1·0 cm. Temperature: 11°C)

cannot be observed when the concentration is raised to 0·02 mole/l. (See Fig 4.) Therefore, the intermolecular hydrogen bond formed between phenol and N,N-dimethylacetamide is concluded to be stronger than that between phenol and acetone. This is compatible with the observed shift of the ultraviolet absorption band, which is greater for the former system than for the latter. The stronger hydrogen bond in the former system has a larger effect on the electronic state of phenol molecule, which results in greater shift of the absorption band.

The equilibrium constant K and the free-energy difference of the reaction

$$C_6H_5OH + CH_3CON(CH_3)_2 \rightleftarrows C_6H_5OH \cdots OC(CH_3)N(CH_3)_2$$

can now be calculated, if the intensity of infrared and ultraviolet absorptions arising from the free and bonded phenol molecules is measured at different concentrations.* The results of the calculation are shown in Table 2. The table also contains the energy difference ΔE and the entropy difference ΔS of the first system, which was calculated from the temperature dependence of ΔF. This

* As to the method of intensity measurement and the calculation of ΔF, see reference 3.

7·7-kcal/mole figure is compared with the energy difference of 5·7-kcal/mole obtained by NAGAKURA [6] for the complex of phenol and ethyl acetate in petroleum ether. From this comparison the proton-accepting power of the peptide CO group is concluded to be greater than that of the ester CO group.

Table 2. Equilibrium constant K, free energy difference ΔF, energy difference ΔE, and entropy difference ΔS of the complex formation

t°C	K	ΔF (kcal/mole)	ΔE (kcal/mole)	ΔS (E.U.)
Phenol-N,N-dimethylacetamide-iso-octane (ultraviolet absorption)				
9	530	$-3{\cdot}53 \pm 0{\cdot}04$		
20	310	$-3{\cdot}37 \pm 0{\cdot}05$	$-7{\cdot}7$	$-14{\cdot}8$
31	213	$-3{\cdot}25 \pm 0{\cdot}04$		
39	138	$-3{\cdot}07 \pm 0{\cdot}04$		
Phenol-N,N-dimethylacetamide-cyclohexane (ultraviolet absorption)				
19	276	$-3{\cdot}28$		
50	70	$-2{\cdot}75$		
Phenol-N,N-dimethylacetamide-carbon-tetrachloride (infrared absorption)				
20	270	$-3{\cdot}28$		
30	136	$-2{\cdot}98$		
Phenol-acetone-iso-octane (ultraviolet absorption)				
11	15·2	$-1{\cdot}55$		
Phenol-acetone-carbon-tetrachloride (infrared absorption)				
30	8·35	$-1{\cdot}30$		

2. *The proton-donating power of the NH group of amides*

Fig. 6 shows the infrared absorption in the 3-μ region of the systems containing acetone or ethyl ether as proton-acceptor and N-methylacetamide, diethylamine, or aniline as proton-donor. It will be seen from these figures and Fig. 2 that a strong absorption due to the O—H · · · O vibration of phenol appears with a frequency shift of $\Delta\nu = 210$ cm^{-1} or 270 cm^{-1}, when phenol is present with acetone or ethyl ether at a concentration of 0·05 mole/l, while a weaker absorption with a smaller frequency shift $\Delta\nu = 50$ cm^{-1} is observed for N—H · · · O bonded band. Therefore, the proton-donating power of the NH group of amides is much weaker than that of the OH group of phenol. Similarly, from the inspection of the experimental data shown in Fig. 6, the proton-donating power of the NH group of peptide is shown to be of the same magnitude as those of the OH groups of alcohols and the NH group of diethylamine and is greater than that of the NH group of aniline. Furthermore, we have made similar measurements in the ultraviolet region. As referred to above, phenol shows an absorption band at 2,777 Å in petroleum-ether solution. If we add ethyl ether into this solution, a new absorption

band arising from associated molecules appears at 2,810 Å at the concentration of 0·15 mole/l. However, when the concentration of ethyl ether becomes larger than 0.7 mole/l the 2,777-Å absorption band disappears and only the hydrogen-bonded phenol absorption at 2,810 Å is observed.

Similar change in absorption is observed when acetanilide is used as the proton donor in place of phenol. Acetanilide in a dilute solution of petroleum ether shows an absorption band at 2,810 Å, and a new absorption band at 2,825 Å

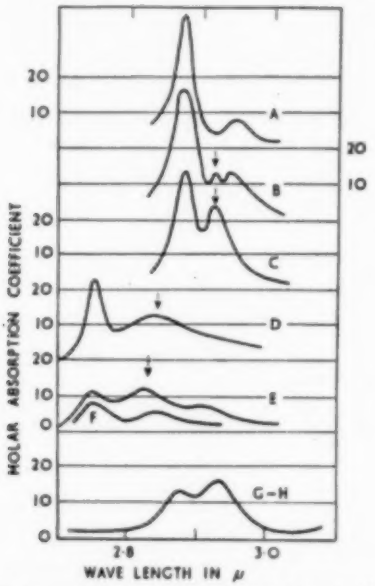

Fig. 6. Infrared absorption curves of N-methylacetamide in the solutions:
A. CCl_4 + N-methylacetamide 0·0050 mole/l;
B. CCl_4 + N-methylacetamide 0·0050 mole/l + ethyl ether 0·10 mole/l;
C. CCl_4 + N-methylacetamide 0·0050 mole/l + acetone 0·10 mole/l;
ethanol in the solution:
D. CCl_4-ethanol 0·0050 mole/l + acetone 0·10 mole/l;
diethylamine in the solutions:
E. CCl_4 + diethylamine 0·015 mole/l + acetone 0·10 mole/l;
F. CCl_4 + diethylamine 0·010 mole/l + acetone 0·07 mole/l;
and aniline in the solutions:
G. CCl_4 + aniline 0·02 mole/l;
H. CCl_4 + aniline 0·02 mole/l + acetone 0·10 mole/l.

arising from associated molecules appears when ethyl ether is added to the solution. In this case the appearance of the absorption due to the associated molecules and the disappearance of the absorption due to the free molecules occur at almost the same concentrations as in the case of the ternary system of phenol, ethyl ether, and petroleum ether. This shows that the proton-donating power of the NH group of anilide is of nearly the same magnitude as that of phenol.

3. *The solvent effect on the N—H ··· O=C hydrogen bond*

As was shown in our previous paper [1], N-methylacetamide in the liquid state is associated through the intermolecular N—H ··· O=C hydrogen bond.

If this is dissolved in carbon-tetrachloride, the amount of the associated molecules becomes less with increasing dilution, until almost all the molecules are in the free state at 0·002 mole/l. All the stages of association can be followed by the intensity measurement of the bands at 2·88 μ (due to free NH) and at 2·96–3·03 μ and 3·22 μ (due to bonded NH). In chloroform solutions the dissociation of associated molecules is much more pronounced, and already at the concentration of 0·02 mole/l only the free NH band at 2·88 μ is observed and the bonded NH bands escape detection. This is due on the one hand to the larger value of the dielectric constant of chloroform, which reduces the hydrogen bonding, and on the other hand to the presence of the C—H group, which has to some extent proton-donating power and which, therefore, reduces further the NH $\cdots$ O=C hydrogen bond referred to above.

In the case of the ether solutions we have quite a different experimental result:— in the concentration range from 0·92–0·02 mole/l we observe a broad band with a peak at 2·96 μ which is independent of concentration in intensity and frequency. This band is explained as due to the N—H $\cdots$ O hydrogen bond formed between the NH group of peptide and the O-atom of ether (solvent).

As shown above, we have obtained in this measurement experimental data useful for the explanation of the nature of hydrogen bond formed in the binary and ternary systems containing amide as one of the components. The results will contribute to the understanding of the *intramolecular* and *intermolecular* hydrogen bonds of the polypeptides and hence also to the reliable prediction of the stable configurations of polypeptide chains [7].

References

[1] Mizushima, S., Shimanouchi, T., Nagakura, S., Kuratani, K., Tsuboi, M., Baba, H., and Fujioka, O.; *J. Amer. Chem. Soc.* 1950 **72** 3490.

[2] Mizushima, S., Shimanouchi, T., Tsuboi, M., *et al.*; *J. Amer. Chem. Soc.* 1951 **73** 1330; 1952 **74** 270, 4639; 1953 **75** 1863; 1954 **76** 2479.

[3] Tsuboi, M.; *Bull. Chem. Soc. Japan* 1952 **25** 60; *J. Chem. Soc. Japan* 1951 **72** 146.

[4] Baba, H., and Nagakura, S.; *J. Chem. Soc. Japan* 1950 **71** 613; 1951 **72** 3. Nagakura, S., and Baba, H.; *J. Amer. Chem. Soc.* 1952 **74** 5693.

[5] Tsuboi, M.; *Bull. Chem. Soc. Japan* 1952 **25** 160.

[6] Nagakura, S.; *J. Chem. Soc. Japan* 1953 **74** 153.

[7] As to the summary of researches made on this problem in our laboratory, see Mizushima, S.; *Advances in Protein Chemistry*, 1954, Vol. IX. See also Mizushima, S.; *Structure of Molecules and Internal Rotation*, Academic Press, New York (1954).

Spectrochimica Acta, 1955, Vol. 7, pp. 108 to 117. Pergamon Press Ltd., London

The application of atomic absorption spectra to chemical analysis

A. WALSH
Chemical Physics Section, Division of Industrial Chemistry,
Commonwealth Scientific and Industrial Research Organization, Melbourne, Australia

(*Received* 18 *January* 1955)

Summary—The theoretical factors governing the relationship between atomic absorption and atomic concentration are examined and the experimental problems involved in recording atomic absorption spectra are discussed. On the basis of the discussions, it is shown that such spectra provide a promising method of chemical analysis with vital advantages over emission methods, particularly from the viewpoint of absolute analysis. It is also suggested that the absorption method offers the possibility of providing a simple means of isotopic analysis.

1. Introduction

The application of atomic spectra to chemical analysis has proved so successful over such a wide field that there is a tendency to overlook some of the basic limitations of existing methods. In spite of the remarkable advances in technique which have resulted in press-button analyses of high precision at fantastic speeds, there has been practically no progress whatsoever in solving the fundamental problem of devising an absolute method, i.e., a method which will provide an analysis without comparison with chemically analyzed standards or synthetic samples of known composition. In routine analysis for production control this problem is of little consequence, since it is only necessary to have a limited number of standards, and in such work modern direct-reading methods leave little to be desired, except on the score of complexity of equipment and associated expense. When analyses of miscellaneous materials are required, the task of providing the required range of standards becomes insurmountable and the spectrochemical method then loses its accuracy, since accurate analyses generally necessitate the use of standards which are closely similar in composition to the sample for analysis. In some analyses it is also essential that the sample and standards be similar as regards physical condition. For example, the intensity of the spectrum of a metal or alloy may vary with the metallurgical history of the sample. This difficulty may be overcome by taking the sample into solution, but accurate and sensitive methods of analyzing solutions are only available for the limited range of elements, having a low excitation potential, which can be estimated by flame photometry. In this method, also, it is necessary to use standard solutions having compositions closely similar to that of the test solution.

The possibility of adapting any of the existing methods to absolute analysis does not appear to be promising. In the first place, there seems to be little prospect of developing a light source which is such that the emission spectrum of a given element is not affected by the presence in the atomic vapour of atoms of other elements. Secondly, even if these interelement effects were eliminated, there remains the problem of absolute intensity measurement and the associated problem

of determining the distribution of atoms over the various energy states. In practice there is the third difficulty that electrical discharges of the type now in use do not give a stable output of radiation; modern methods conceal these erratic variations in output by integrating, photographically or photoelectrically, the radiation over a period of several seconds. Finally, there are other problems arising from self-absorption and self-reversal, and from the fact that the processes of vaporization and excitation are not isolated from each other. A review of these and other aspects of source behaviour has been given elsewhere [1].

At the present stage of its development there is no doubt that the major obstacle to further progress in the technique of spectrochemical analysis is the occurrence of interelement effects, since if these could be eliminated it would be possible to use the same set of standards for the determination of any one element in any material. With existing emission methods the intensity of a given spectrum line due to one particular concentration of an element in different materials varies greatly. For example, PROKOF'EV [2] reports that for the same concentration of silicon the intensity of the silicon lines in the spark spectrum of steel is eight times as great as in brass, and in duralumin the intensity is even less. Many other examples of interelement effects have been published.

OL.
7
5/56

No satisfactory explanation of these effects has yet been given, nor can one be expected, since the phenomena occurring in the arc and spark discharges used as light sources are far too complex to permit of any theoretical analysis, and the approach to the subject seems likely to remain essentially empirical. It seems possible, however, to arrive at certain broad conclusions. Since interelement effects are usually of the same order of magnitude for different spectrum lines of a given element, corresponding to transitions between different energy states, they probably arise from changes in the concentration of atomic vapour rather than changes in the excitation conditions. However, such changes cannot occur in sources in thermal equilibrium at a constant temperature. Thus, if thermal equilibrium is assumed, then interelement effects must necessarily be due to a change in the temperature of the atomic vapour. Whilst the behaviour of the electrical discharges used in spectrochemical analysis shows that it is not justifiable to assume thermal equilibrium or to ascribe a temperature to the discharge, it is instructive to consider the effects of changes in temperature on a mass of atomic vapour in thermal equilibrium.

Consider the emission of a spectrum line due to the transition from an excited state j, of excitation energy E_j, to a ground state of energy $E_0 = 0$. Then if P_j and P_0 are the statistical weights for the excited state and ground state respectively, the number of atoms in the excited state, N_j, is related to the number of atoms in the ground state, N_0, by the relation

$$N_j = N_0 \frac{P_j}{P_0} e^{-\frac{E_j}{kT}} \tag{1}$$

and, neglecting self-absorption and induced emission, the intensity of the emitted line is proportional to N_j.

In order to illustrate the magnitude of N_j/N_0, the calculated values for resonance lines of various elements at different temperatures are given in Table 1.

Table 1. *Values of N_j/N_0 for various resonance lines*

Resonance line	*Transition*	P_j/P_0	N_j/N_0			
			$T = 2{,}000°K$	$T = 3{,}000°K$	$T = 4{,}000°K$	$T = 5{,}000°K$
Cs 8521 Å	$^2S_{1/2} - {}^2P_{3/2}$	2	$4{\cdot}44 \times 10^{-4}$	$7{\cdot}24 \times 10^{-3}$	$2{\cdot}98 \times 10^{-2}$	$6{\cdot}82 \times 10^{-2}$
Na 5890 Å	$^2S_{1/2} - {}^2P_{3/2}$	2	$9{\cdot}86 \times 10^{-6}$	$5{\cdot}88 \times 10^{-4}$	$4{\cdot}44 \times 10^{-3}$	$1{\cdot}51 \times 10^{-2}$
Ca 4227 Å	$^1S_0 - {}^1P_1$	3	$1{\cdot}21 \times 10^{-7}$	$3{\cdot}69 \times 10^{-5}$	$6{\cdot}03 \times 10^{-4}$	$3{\cdot}33 \times 10^{-3}$
Zn 2139 Å	$^1S_0 - {}^1P_1$	3	$7{\cdot}29 \times 10^{-15}$	$5{\cdot}58 \times 10^{-10}$	$1{\cdot}48 \times 10^{-7}$	$4{\cdot}32 \times 10^{-6}$

It will be seen that in nearly all cases the number of atoms in the first excited state is only a small fraction of the numbers of atoms in the ground state. The fraction only becomes appreciable at high temperatures for states of low energy. Since most elements have their strongest resonance line at wavelengths below 6,000 Å, and since we shall be concerned mainly with flames or furnaces having temperatures below 3,000°K, we may regard N_j as negligible compared to N_0. The fraction of atoms in higher excited states is much less than those given above, and thus ΣN_j is also negligible compared with N_0, and the latter can be considered as equal to the total number of atoms, N.

Thus, whilst the number of excited atoms varies exponentially with temperature, the number of atoms in the ground state remains virtually constant and therefore the integrated absorption $\int K_\nu \, d\nu$ due to transitions from the ground state is independent of temperature. (This discussion only applies to atoms having a ground state well removed from the lowest excited state; the case of atoms having a multiplet ground state is discussed in Section 2.)

On the basis of the above discussion it would appear that atomic absorption spectra would have important advantages over emission spectra as a means of chemical analysis. It is therefore surprising to note that the research in this field has been devoted almost exclusively to emission spectra; the annual review [3] of progress in spectrochemical analysis is, in fact, given under the general title of "emission spectroscopy." Apart from the special case of estimating the contamination of room and laboratory atmospheres by mercury vapour, the application of atomic absorption spectra to chemical analysis appears to have been confined to astrophysical work on the determination of the composition of the solar and stellar atmospheres.

The purpose of this paper is to examine the theoretical factors governing the relationship between atomic absorption and atomic concentration and to discuss the experimental problems involved in recording atomic absorption spectra. On the basis of these discussions, it is shown that such spectra provide a promising method of chemical analysis with vital advantages over emission methods, particularly from the viewpoint of absolute analysis. It is also suggested that the absorption method offers the possibility of providing a simple means of isotopic analysis.

VOL. 7 1955/5

2. Variation of atomic absorption with atomic concentration

The relationships between atomic absorption and atomic concentration, under various conditions, are fully discussed in several papers, mainly in astrophysical journals, and in standard reference books [4–6]. For the purpose of this discussion it is sufficient to consider only the most fundamental of these relationships. In this section the discussion will be further restricted by assuming that atomic absorption lines possess no fine structure; the case of isotopic hyperfine structure is discussed later in Section 4.

Consider a parallel beam of radiation of intensity I_{0_ν} at frequency ν incident on an atomic gas or vapour of thickness l cm. Then if I_ν is the intensity of the transmitted beam, the absorption coefficient K_ν of the vapour at frequency ν is defined by

$$I_\nu = I_{0_\nu}\, e^{-K_\nu l} \tag{2}$$

The dependence of K_ν on ν, i.e., the shape of the absorption line, is determined by the nature of the transition involved in the absorption and on the physical conditions such as temperature, pressure, and electrical fields, to which the atoms are subjected during the measurement.

According to classical dispersion theory, the relationship between absorption and concentration is given by

$$\int K_\nu \, d\nu = \frac{\pi e^2}{mc} N_\nu f \tag{3}$$

where e is the electronic charge, m the electronic mass, c the velocity of light, N_ν the number of atoms per cm^3 which are capable of absorbing in the range ν to $\nu + d\nu$, and f, the oscillator strength, is the average number of electrons per atom which can be excited by the incident radiation. Equation (3) is not valid for strong absorption lines, since it assumes that the refractive index is of the order of 1 over the breadth of the absorption line.

For a resonance line due to a transition from a ground state which is well separated from the lowest excited state, N_ν can be considered as equal to N, the total number of atoms per cm^3 (see Table 1). If, however, the transition does not originate in the ground state, or if there is a multiplet ground state, then the number of atoms capable of absorbing is given by

$$N_\nu = N \frac{P_i e^{-\frac{E_i}{kT}}}{\sum P_j e^{-\frac{E_j}{kT}}} \tag{4}$$

where i denotes the initial state involved in the transition, and the summation in the denominator extends over all possible energy states. In practice, of course, the summation can be restricted to the low-lying levels.

In terms of transition probabilities the equation corresponding to equation (3) is

$$\int K_\nu \, d\nu = \frac{\lambda^2 P_j}{8\pi P_i} \cdot N_\nu A_{ji} \left(1 - \frac{P_i}{P_j}\frac{N_j}{N_\nu}\right) \tag{5}$$

where λ is the wavelength at the centre of the absorption line, P_i and P_j are the

statistical weights of the lower and upper states, respectively, involved in the transition, and A_{ji} is the Einstein coefficient of spontaneous emission for the $j \rightarrow i$ transition. N_j is the number of atoms in the upper electronic state, and will generally be negligible compared with N_v, and in this case equation (5) reduces to the well-known relation:

$$\int K_\nu \, d\nu = \frac{\lambda^2 P_j}{8\pi P_i} N_v A_{ji} \qquad (6)$$

In the general case N_v is given by (4), but for resonance lines is equal to N. Similarly, if the transition from the jth to ith state is the only one which can occur, as in the case for resonance lines, $A_{ji} = 1/\tau$, where τ is the mean life of an atom in the excited state j.

Equations (3) and (6) provide simple relationships between absorption and concentration, and it is now necessary to investigate whether they can be applied to a practical method of spectrochemical analysis. Since the intensities of spectrum lines are usually expressed in terms of oscillator strengths, it is convenient to consider equation (3).

Firstly, it is necessary to know whether suitable absorption lines occur in regions of the spectrum which are amenable to measurement. In terms of sensitivity, it is obviously desirable to use the strongest resonance lines, and in general these will correspond to the strongest lines occurring in emission spectra. These are listed in a paper by MEGGERS [7], and reference to this shows that with the exception of the rare gases, hydrogen, mercury, the halogens and the metalloids, all elements have their most sensitive lines in the region 2,000–9,000 Å. Thus the lines for all the more common elements all lie in regions of the spectrum where measurements are simple to make.

The oscillator strengths of some of these lines have been determined, and are listed in Table 2. Theoretical calculation [8–14] of f-values is possible for atoms having simple electronic structures, but has not yet been carried out for heavy atoms having a complex structure. BATES and DAMGAARD [15] have described a simplified theoretical method and have published tables from which the absolute strengths can be rapidly obtained. The method has been shown to give accurate results for all transitions in the lighter simple systems, but there are insufficient experimental data to enable one to judge to what extent the method can be applied to the more complex electronic structures.

It is interesting to note that the oscillator strength for the strongest copper line is approximately the same as for the alkali metals, in spite of the fact that the closed 3d shell of the copper atom is not nearly so tightly bound as the inner electron shells of the alkali metals. By comparison with the f-values of other elements in Group 1, it seems probable that rubidium, silver, and gold will have f-values of the order of 0·7 for their strongest resonance lines. Similarly, the Group 2 elements Zn and Sr may be expected to have f-values of the order of 2 for their strongest lines.

It does not appear possible at the present time to make any corresponding estimates of the oscillator strengths of spectral lines of other elements, particularly those such as iron and cobalt, with complex electronic structures and multiplet

ground states. The possibility of determining approximate f-values for such elements by a simple experimental method is discussed in Section 4.

For those elements for which the oscillator strengths are known, the atomic concentration can be determined from the integrated absorption coefficient, using equation (3); the experimental problems involved in measuring such coefficients are discussed below.

Table 2. List of f-values

Resonance line	*Transition*	*f*	*Reference*
Li 6708 Å	$^2S_{1/2} - {}^2P_{3/2}$	0·50	[9]
Na 5890	$^2S_{1/2} - {}^2P_{3/2}$	0·70	[16]
K 7665	$^2S_{1/2} - {}^2P_{3/2}$	0·64	[17]
Cu 3247	$^2S_{1/2} - {}^2P_{3/2}$	0·62	[18]
Cs 8521	$^2S_{1/2} - {}^2P_{3/2}$	0·66	[19]
Be 2349	$^1S_0 - {}^1P_1$	1·82*†	[11, 13, 14]
Mg 2852	$^1S_0 - {}^1P_1$	1·74*	[13, 14]
Ca 4227	$^1S_0 - {}^1P_1$	2·28*†	[12, 13, 14]
Cd 2288	$^1S_0 - {}^1P_1$	1·20	[20]
Ba 5535	$^1S_0 - {}^1P_1$	2·10	[21]
Hg 1849	$^1S_0 - {}^1P_1$	1·19	[22]
Tl 2769	$^2P_{1/2} - {}^2D_{3/2}$	0·20	[23]
Cr 4254	$^7S_3 - {}^7P_4^0$	0·084	[24]
Ni 3415	$^3D_3 - {}^3F_4^0$	0·02	[25]
Fe 3720	$a^5D_4 - z^5F_5$	0·013	[29]

* Theoretical values.

† Biermann and Trefftz [13] state that these values should be corrected according to the method described in ref. 14. See also the values quoted in ref. 30.

Footnote. Since the purpose of this table is to indicate the order of the f-values for various lines, the values obtained by different observers are not included. They are discussed by Korff and Breit [26] and by Mitchell and Zemansky [4].

3. Experimental determination of atomic absorption coefficients

The shape of an atomic absorption line is determined by (a) the natural width of the line due to the finite lifetime of the excited state; (b) the Doppler contour due to the motions of the atoms relative to the observer; (c) pressure broadening, either by atoms of the same kind giving rise to resonance broadening or to foreign gases;

and (d) Stark broadening due to external electric fields or to neighbouring charged particles. The natural width of an atomic spectral line is of the order of 10^{-4} Å, and for the purposes of this discussion is negligible compared to the width due to other causes.

The Doppler width of a line is given by

$$D_\lambda = 1{\cdot}67 \frac{\lambda}{C} \sqrt{\frac{2RT}{M}} \tag{7}$$

where R is the universal gas constant and M is the atomic weight. Typical values of D_λ are given in Table 3.

Table 3. *Values of* D_λ *at various temperatures*

Element	λ	M	D_λ		
			1,000°K	2,000°K	3,000°K
Na	5890	22·3	0·028 Å	0·039 Å	0·048 Å
Cu	3247	63·6	0·0092 Å	0·0013 Å	0·016 Å
Zn	2139	65·4	0·0060 Å	0·0085 Å	0·010 Å

If we assume that a temperature of 2,000°K is required to produce sufficient vapour, then the Doppler width is of the order of 0·01 Å. The accurate measurement of the profile of such a line would require a resolution of about 500,000, which is beyond the performance of most spectrographs. In addition, if it is desired to use photoelectric methods of intensity measurement, then it is scarcely feasible to use a continuous source, since the energy emitted over such a small spectral slit-width would be too small to give a high enough signal/noise ratio. In the past this difficulty has often been overcome by using the method of total absorption, in which the energy removed from the incident beam is measured. This method has the advantage that the measurement is independent of the resolution of the monochromator, but suffers from the disadvantage of giving a complicated relation between N and f, according to the region of the curve of growth in which the measurement is made. However, if the absorption is so strong that it is not possible to make an accurate measurement of the absorption coefficient, as in astrophysical work, then the curve-of-growth method is the only one available. The method has been successfully applied to the measurement of oscillator strength from furnace absorption spectra by KING [18] and by ESTABROOK [24, 25].

From the point of view of spectrochemical analysis, a more attractive method appears to be to measure the absorption coefficient at the centre of the line, using a sharp-line source which emits lines having a much smaller half-width than the absorption line. If the shape of the latter is determined entirely by Doppler broadening, we have [27]

$$K_{\max} = \frac{2\lambda^2}{D_\lambda} \sqrt{\frac{\ln 2}{\pi}} \cdot \frac{\pi e^2}{mc^2} Nf \tag{8}$$

VOL. 7 1955/

where D is the Doppler width. Thus in this case also there is a linear relation between absorption and concentration.

If such a sharp-line source is used, it is now no longer necessary to use a spectral slit-width of the same order as the half-width of the absorption line. The requirement now is the ability to isolate a selected line from other lines emitted by the source. Thus spectrographs having the same resolution as those used in conventional emission methods are adequate. In many cases it may be sufficient to use filters.

Various methods of producing such sharp-line sources are available. In our work it has been found convenient to use hollow-cathode discharge tubes, and it has proved possible to make sealed-off tubes about the size of a photomultiplier tube.

There is one other experimental difficulty. In many cases vaporization of the sample will result in the emission of radiation at exactly the wavelength where it is desired to make the absorption measurement. This difficulty can be overcome by modulating the incident radiation before it reaches the atomic vapour and amplifying the output of the detector by an amplifier tuned to this modulation frequency. Thus the radiation emitted by the atomic vapour, which is not modulated, produces no signal at the output of the amplifier.

So far it has been assumed that the line shape is determined solely by Doppler broadening, and this is sensibly true if the vapour is produced by a vacuum furnace, such as that used by KING, and if the vapour pressure is so small that resonance broadening is negligible. Another convenient method of vaporizing the sample is to atomize a solution of the sample into the air supply of a Meker burner, as in emission methods of flame photometry. In this case there is broadening due to foreign gases, and, although we have not made accurate measurements for the flame we have used, its magnitude is probably of the same order as that due to thermal motions. Once the broadening due to pressure is known, the corresponding correction to equation (8) can be applied, using the tables published by ZEMANSKY [28]. As an example, if the pressure broadening width is equal to the Doppler width, the maximum absorption is 43 per cent of that due to Doppler broadening alone.

IV. Discussion

The above discussion of atomic absorption spectra has indicated the attractive possibilities of using them for chemical analysis and of developing a method which will provide a useful complement to emission methods and in many cases may well supersede them. One of the main attractions of this absorption method is that, theoretically, it is expected to be much less susceptible to interelement effects. In so far as effects observed in emission are due to variations in the distribution of atoms over the various excited states, they would have no counterpart in absorption where this is due to a transition from the ground state. Similarly, absorption will not be critically dependent on the temperature of the atomic vapour, since the Doppler width only varies as $T^{1/2}$, whereas small changes in temperature produce large changes in the intensity of the emitted radiation. In addition, the integrated absorption coefficient is independent of wavelength, in marked contrast to the emission intensity, which will vary according to Planck's law.

Whilst the discussion has been limited to the ideal case of a vapour in thermal equilibrium, in practice there may be effects due to a sheath of cool vapour. But whereas in emission spectroscopy this causes self-reversal which reduces the peak intensity, in absorption it will contribute to the absorption and will in no sense reduce the sensitivity. Incidentally the self-reversal observed in emission spectra provides a good indication of the sensitivity of the absorption method. Another cause of deviation from thermal equilibrium is chemiluminescence; this may well produce a number of excited atoms, which is comparable with that due to thermal excitation, but will not produce any significant change in the number of unexcited atoms. Thus the effects on the absorption spectrum are negligible compared to those on the emitted radiation.

On the experimental side, the important advantage of the absorption method lies in the fact that the measurement of the absorption coefficient consists of measuring the ratio of two intensities, which is much simpler to achieve than the measurement of emission intensities in absolute units.

The possibilities of absolute analysis have been discussed and the use of a relative absolute method may also be noted. For example, if the sample solution is atomized into a flame, then a calibration for one element would serve to deduce the approximate calibration of other elements, provided the oscillator strengths are known. In this connection it would appear that, using standard solutions, this method could be used to determine oscillator strengths, at least to within an order of magnitude.

Finally, the absorption method may prove suitable for isotopic analysis. If sources emitting spectra of only one isotope are used, then an analysis for this isotope can be obtained directly, since the oscillator strength is the same for each component of the hyperfine structures of the excited level. If no pure isotope is available, then sources having different concentrations of isotopes may be used. Alternatively, an isotopic filter containing the vapour of one or more isotopes may prove satisfactory.

The results of some preliminary experiments have been in full accord with the conclusions arrived at in this paper, and future papers by J. P. SHELTON and the author will describe the construction of an atomic absorption spectrophotometer and its application to various analytical problems.

References

[1] WALSH, A.; Chapter 7 of *Metal Spectroscopy* by F. TWYMAN, Griffin and Co., London, 1951.
[2] PROKOF'EV, V. F.; *C.R. Acad. Sci., U.R.S.S.* 1940 **29** 443.
[3] MEGGERS, W. F.; *Anal. Chem.* 1954 **26** 54.
[4] MITCHELL, A. C. G. and ZEMANSKY, M. W.; *Resonance Radiation and Excited Atoms*, Cambridge Press, 1934.
[5] ROSSELAND, S.; *Theoretical Astrophysics*, Clarendon Press, Oxford, 1936.
[6] UNSÖLD, A.; *Physik der Sternatmosphären*, Springer, Berlin, 1938.
[7] MEGGERS, W. F.; *J. Opt. Soc. Amer.* 1941 **31** 39.
[8] SUGIARA, Y.; *Phil. Mag.* 1927 **4** 495.
[9] TRUMPY, B.; *Z. Physik*, 1930 **66** 720.
[10] VINTI, J. P.; *Phys. Rev.* 1932 **42** 632.
[11] HARTREE, D. R., and HARTREE, W.; *Proc. Roy. Soc. London*, 1936 **A154** 588 and **A156** 45.
[12] HARTREE, D. R., and HARTREE, W.; *Proc. Roy. Soc. London*, 1938 **A164** 167.

VOL
7
1955/

[13] BIERMANN, L., and TREFFTZ, E.; *Z. Astrophys.*, 1949 **26** 213.
[14] TREFFTZ, E.; *Z. Astrophys.*, 1944 **26** 240.
[15] BATES, D. R., and DAMGAARD, A.; *Phil. Trans. Roy. Soc.* 1949 **A242** 101.
[16] MINKOWSKI, R.; *Z. Physik*, 1926 **36** 361.
[17] WEILER, J.; *Ann. Phys.* 1929 **1** 361.
[18] KING, R. B., and STOCKBARGER, D. C.; *Astrophys. J.* 1940 **91** 488.
[19] MINKOWSKI, ,R. and MÜHLENBRUCH, W.; *Z. Physik* 1930 **63** 198.
[20] ZEMANSKY, M. W.; *Z. Physik* 1931 **72** 587.
[21] WESSEL, G.; *Z. Physik* 1949 **126** 440.
[22] WOLFSOHN, G.; *Z. Physik* 1930 **63** 634.
[23] KUHN, W.; *Det. Kgl. Danske Videnskab. Math.—Fys. Medd.* 1926 **7** 12.
[24] ESTABROOK, F. B.; *Astrophys. J.* 1952 **115** 571.
[25] ESTABROOK, F. B.; *Astrophys. J.* 1951 **113** 684.
[26] KORFF, S. A., and BREIT, G.; *Rev. Mod. Phys.* 1932 **4** 471.
[27] See ref. 4, p. 100.
[28] ZEMANSKY, M. W.; *Phys. Rev.* 1930 **36** 919; see also ref. 4, p. 329.
[29] KING, R. B.; *Astrophys. J.* 1942 **95** 78.
[30] KOPFERMANN, H., and WESSEL, G.; *Z. Physik* 1951 **130** 100.

VOL. 7 55/56

Spectrochimica Acta, 1955, Vol. 7, pp. 118 to 127. Pergamon Press Ltd., London

The determination of trace elements in magnesium and its alloys by spectrographic procedures

W. J. PRICE
Spectrographic Laboratory, Magnesium Elektron Limited

(*Received September* 1954)

Summary—A survey on the detection and determination of a number of elements at trace concentrations in magnesium and its alloys is reported.

General techniques for various sample forms are detailed, and linepairs and sensitivities are quoted for all the elements concerned. Aluminium, beryllium, cadmium, calcium, cerium, copper, iron, lanthanum, lead, manganese, nickel, silicon, silver, tin, titanium, zinc, and zirconium may all be determined in a common routine procedure. Special analytical or standardization procedures are given for boron, beryllium, barium, calcium, and lithium, and several working graphs are reproduced by way of illustration.

Concentrations in the range 0·01–0·1 per cent are determinable with a coefficient of variation of about 6–8 per cent of the content. This increases as the range extends lower.

Introduction

The determination, by emission spectrography, of trace quantities of about twenty elements likely to be found in magnesium alloys, either as essential constituents or as impurities, has been investigated. In the following paper, general techniques are first described, while in the second section are subsumed the specific details for each element, and special methods where these apply.

Several papers in the published literature have dealt with the determination of the major alloying constituents of magnesium alloys, but only one [1], as far as the author is aware, has made any contribution to the present subject. Several more elements are now dealt with, and the lower limits of determination of some others have been extended.

Over recent years the range of alloy compositions has much increased, and, in particular, an extensive series of zirconium-containing alloys has been introduced.

Aluminium and zirconium are mutually incompatible in magnesium alloys and when one is present as an essential alloying element, the other cannot be present in solid solution in greater than trace quantities. Magnesium alloys can therefore be broadly subdivided into aluminium- and zirconium-containing alloys.

When zirconium is added to a melt containing aluminium, both elements are thrown out as a Zr/Al complex, which may also contain amounts of iron, manganese, and silicon. The majority of this complex settles to the bottom of the melt before pouring, but a small amount appears in the casting or test block as microscopically visible clusters or inclusions. The effect of this upon spectrographic analysis is an occasional high figure for these elements which, however, can usually be detected through the disagreement of replicate determinations.

Experience has shown that the normally encountered concentrations of zirconium (i.e., below 1 per cent) have a negligible effect on the determination of other elements, except in one or two cases where there is actual line-interference.

The effect of aluminium may be much more pronounced, and does not bear a direct relationship to the amount of aluminium present. It is therefore necessary to provide special standard samples for determinations in the presence of high aluminium concentrations—i.e., from 1 to 10 per cent. The only further alloying element that need be considered is zinc. Its effect on other impurity/magnesium intensity ratios at concentrations below 1 per cent zinc is negligible, but at 3 per cent it appears to have a small effect on magnesium line intensity (see also VAN CALKER and WIENECKE [2]) though, unless the greatest accuracy in trace determination is required, this also can be ignored.

It is outside the scope of the present paper to give a quantitative survey of the effects of alloying elements upon line intensity ratios in magnesium alloys, for the indications are, both here and elsewhere [2], that the magnitude of such effects depends upon the lines employed, and also upon the nature of the excitational discharge. The existence, however, of such effects must be constantly borne in mind and their influence upon analytical results determined in individual cases.

I. General techniques

The methods employed will be familiar to all spectrographic workers, and are summarized as follows:

(i) Solid sample using interrupted arc excitation.

(ii) Solid sample using high-voltage spark excitation.

(iii) Sample in solution, using high-voltage spark excitation.

The choice of technique must depend upon the problems presented by each particular element. A number of elements are most sensitive to arc excitation, while in some cases, the spark is adequate or even preferable (see Tables 2 and 3).

If samples in the form of solid blocks are specified, it is presupposed that the comparison standards in similar form have already been analysed, either chemically, or by way of an independent spectrographic standardization.

Suitable methods of chemical analysis have been set out elsewhere [3], and spectrographic standardization, by the solution technique, will be described here.

For solid metal samples, two electrode systems are in common use, viz., the "point-to-plane" (with graphite counter-electrode) and "pencil self-electrode" systems. It has been found that the former is more convenient for magnesium alloys, as it is extremely difficult to cast a homogeneous and porosity-free pencil. On the other hand, pencil self-electrodes appear to give increased sensitivity of detection for a number of elements, and also obviate the interference of cyanogen band-spectra.

The interrupted arc source which has been employed for the following work is the general-purpose source unit evolved by WALSH [4] and BEALE [5]. The main characteristic of this unit is that it provides a unidirectional discharge with a frequency of 50 c.p.s., the charging and discharging circuits being electrically separated. All the circuit parameters—capacitance, resistance, inductance—are widely variable, the optimum setting being given in Table 1, where details of the simple uncontrolled spark generator are also given.

Metal electrodes

1. *Point-to-plane system.*
   Sample: block not less than one quarter-inch thick, with a *machined* flat surface of at least one square inch for arcing or sparking.
   Counter-electrode: Graphite rod, 4 mm diam. flat-end. Gap width: 4 mm.
   Polarity: Sample negative.

2. *Pencil self-electrodes.*
   Both electrodes: Pencils, 6 mm diam., cast direct or machined from sample block. Sparking ends turned to 4mm diam.
   Gap width: 4 mm.

Table 1

Source unit	*Settings*				
	Secondary voltage	*Capacitance*	*Inductance*	*Resistance*	*Electrode gapwidth*
Spark Source I for block sample	15 Kv	0·005 μF	0·005 mH	nil	4 mm
Spark Source II for solution excitation	8 Kv	0·005 μF	0·135 mH	nil	2 mm
BNF controlled arc source	—	200 μF	0·50 mH	7 ohms	4 mm

Solutions

Solution techniques may be found to be indispensable under certain circumstances. Chemical analysis becomes unnecessary, since synthetic standard solutions are made up from the pure constituents; it follows, therefore, that in cases where chemical analysis is difficult, tedious, or even impossible, suitable solid standards may be calibrated by means of a solution technique. Poor reproducibility of results from solid specimens, which is often caused by heterogeneity, is generally improved by taking such samples into solution.

The procedure recommended is the porous-cup technique originated by FELDMAN [6]. The method of producing the cups was fully described in the work referred to, and it will suffice to state here that these should all conform exactly to the same dimensions. The graphite or carbon used must be chosen according to its purity with respect to the elements being determined. If solutions do not soak through the porous base within fifteen seconds of being introduced, porosity must be enhanced by heating to red heat in a bunsen flame, or by pre-arcing the cup for twenty seconds as the lower, negative electrode in a 10-ampere d.c. arc. The high-voltage spark source when applied to porous cups containing solutions must have a less powerful setting than that used for solids. A compromise has to be sought between the tendency of the solutions to boil over, and the necessity for an inordinately long exposure period. The best setting for excitation of solutions is

given in Table 1. Counter-electrodes must be of graphite of purity equal to, or better than, that of the cups.

An exposure of between 60 and 120 seconds should be arranged—depending, of course, on the spectrograph employed—to attain maximum sensitivity and reproducibility. A pre-spark of 15–20 seconds is desirable for percolation and to allow spark-gap equilibrium to be reached.

Synthetic solutions to be used as standards should be made up from the purest available chemicals. The procedure is as follows:

Dissolve 2 g of spectrographically pure magnesium in 30 ml of hydrochloric acid 50 : 50 (i.e., 50 ml of 11·3N HCl diluted to 100 ml). When dissolution is complete add a further 20 ml of the acid. After the requisite amount of solutions containing the trace elements has been added, make up to 100 ml. A series of about seven standards is sufficient to cover a hundred-fold range of an element (e.g., beryllium 0·001–0·1 per cent), and a number of elements could be added to the same series of standards (e.g., as in this work, beryllium, barium, boron, lithium, etc.).

Solutions of samples for analysis are prepared in an analogous fashion:

Dissolve 2 g of sample in 30 ml hydrochloric acid 50 : 50. When dissolution is complete, add a further 20 ml of the acid and make up to 100 ml.

It is necessary that the final solutions should be at least 1N with respect to free hydrochloric acid—as allowed for in this procedure—in order to avoid both adsorption of some elements (particularly beryllium) on to the walls of the containing vessel, and chromatographic effects in the porous cup itself. Hydrochloric acid is preferred as the solution medium because of the high volatility of metallic chlorides. There is no reason why other acids should not be used, and they may even be better in some circumstances from the point of view of purity. It must be borne in mind, of course, that sulphuric acid is unsuitable for determination by the solution method of calcium, barium, and lead, that nitric acid is undesirable for tin, and that hydrochloric acid cannot be used when silver is to be determined.

The recording and evaluation of spectra

All the determinations listed can be carried out on a "medium" spectrograph (e.g., Hilger E498) provided that rare earths and thorium are not present. When an alloy containing zirconium and any of these elements is being examined, it is necessary to use a higher dispersion instrument (e.g., Hilger E482 or E742). For this reason, at least one line-pair is given for each of the elements normally determined by the solid sample techniques to enable all of these elements to be included in one wavelength setting of a large Littrow spectrograph (viz., 2700–4450 Å).

The photographic plate employed in trace-determinations should have a fairly high contrast in order to maintain sensitivity near the threshold value. (E.g. Kodak "B10" for 2300–3300 Å, and "Uniform Gamma" for 2300–4000 Å.) The method of photometry is necessarily that of individual plate calibration, since very low intensities are frequently encountered. An iron spectrum is photographed through a rotating stepped sector, and the emulsion calibrated at all wavelengths required. Methods of heterochromatic photometry are rendered unnecessary by judicious choice of emulsion or line-pair. Working graphs relating intensity ratio to concentration (usually on a *log-log* basis) are prepared for all elements, such graphs being independent of the photographic emulsion and processing procedure employed. In practice, it should not be found necessary to re-establish the working curves more frequently than once per month, provided that all precautions are taken to maintain constancy of the electrical discharge conditions.

Background correction, and, with solutions, "blank" correction are frequently essential. For the former, the intensity correction method [7] is employed, and for the latter, a method [7, 8] which depends on the fact that the graph of concentration against intensity ratio, not *log-log*, should pass through the origin.

II. Determination of trace elements in magnesium alloys

The methods and line-pairs given in Tables 2 and 3 are those which, after considerable experimentation, were found to give best overall sensitivity to trace quantities. The tables are augmented by the following remarks:

Aluminium. Traces of aluminium occur in "pure" magnesium, zinc- and

zirconium-containing alloys. Figures of 0·01 and 0·02 per cent may be quoted for the first two as typical specification maxima, but there is no actual specification figure for zirconium-containing alloys, as the aluminium is present in "soluble" and "insoluble" forms and may not therefore be evenly distributed.

Boron. The determination of boron is important, since traces of this element present during the electrolytic extraction process for magnesium cause non-coagulation of the metal, and, hence, low recoveries.

Boron is calibrated for and determined by the solution technique. For samples of magnesia, magnesite, or magnesium chloride, the same standards and method as for magnesium metal are employed. For the lowest concentrations, boron-free graphite must be employed for electrodes.

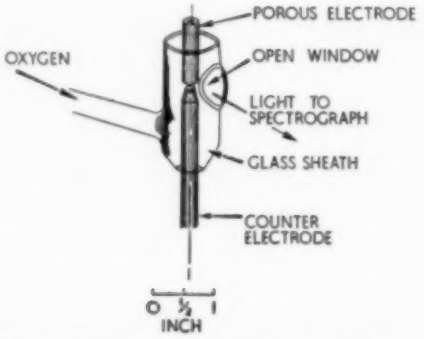

Fig. 1. Excitation of solutions in oxygen.

Barium. Barium can be determined down to 0·01 per cent by the solution technique already given. Below this concentration, a cyanogen band-head at 4553·1 Å causes serious interference with the most sensitive barium line 4554·0. This interference is eliminated by sparking the solutions in an atmosphere of commercially pure oxygen. A simple glass shroud is readily constructed for this purpose (see Fig. 1). Metal samples may also be used, but these must first be calibrated by the above solution technique, and in order to overcome the same band interference, pencil self-electrodes must be employed.

For the estimation of very low concentrations and blanks it may be preferable to plot the intensity ratio Ba 4554·0/underlying background against concentration. A measure of the underlying background is obtained as the average of the background deflexions taken at equal distances on each side of the line.

Examples of working graphs from the solution procedure and from pencil self-electrodes calibrated thereby are given in Figs. 2 and 3.

Beryllium. Beryllium is remarkably sensitive in both arc and spark excitation, and is not easily analysed for by a chemical procedure. Solutions or metal samples may be employed, the latter being standardized by the solution technique. If low concentrations of beryllium are to be determined in the presence of zirconium or the rare earths, a high dispersion spectrograph must be used to overcome the effects of line-interference.

Calcium. The determination of calcium is required in certain "high-purity"

VOL 7 1955/

alloys. There is, for example, a stipulated maximum of 0·02 per cent in specifications DTD118A and DTD140B. The most sensitive lines of calcium occur in the 3934 Å region, where normal plate gamma is too high for accurate evaluation. The

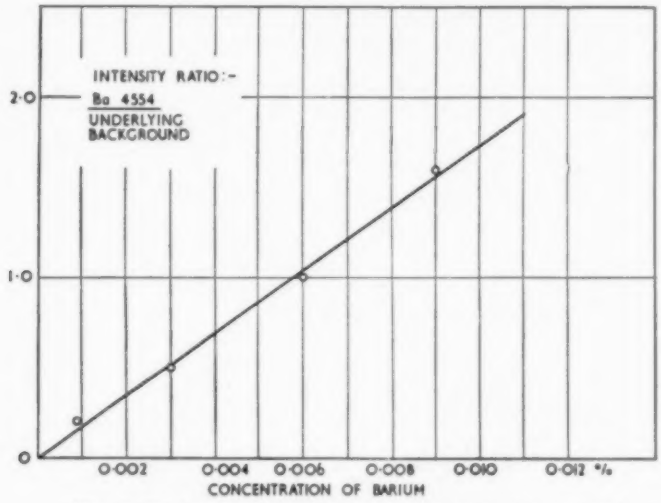

Fig. 2. Barium working graph (solutions excited in oxygen).

use of a uniform gamma plate overcomes this problem, and incidentally simplifies the choice of internal standard line.

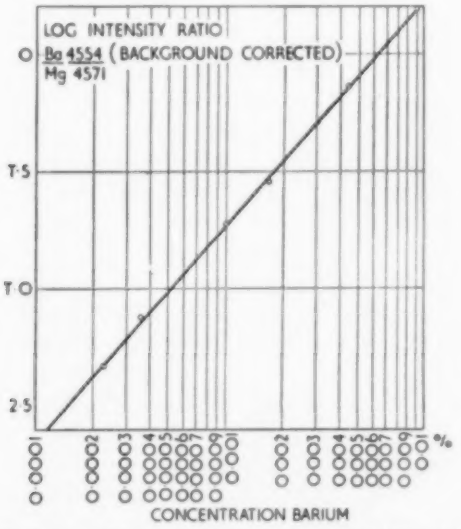

Fig. 3. Barium working graph (pencil self-electrodes—air spark).

As traces of calcium are present in most graphites, counter-electrodes of copper must be employed, unless pencil self-electrodes are used. All sparking surfaces

Table 2

Element	*Sample form*	*Excitation*	*Plate*	*Line pairs*	*Detect. limit %*	*Method of std.*	*Notes*
Aluminium (a)	Block	Arc	U.γ	Al 3961·5* Mg 4057·6	0·001	Chem.	Zr interferes
(b)	Block	Arc	U.γ	Al 3944·0* Mg 4057·6	0·005	Chem.	Th interferes
Boron (a)	Soln.	Spark II	B.10	B 2497·7* Mg 2660·8 or Mg 2776·7	0·005	Spect.	Source unit as Table 1
(b)	Soln.	Spark II	B.10	B 2497·7* Mg 2660·8 or Mg 2776·7	0·001	Spect.	Inductance 0·005 mH
Barium (a)	Soln.	Spark II	Long range spectrum or "I.F."	Ba 4554·0 Mg 4703·0	0·01	Spect.	Sparking in air
(b)	Soln.	Spark II	Long range spectrum or "I.F."	Ba 4554·0* Mg 4703·0	<0·0005	Spect.	Sparking in oxygen
(c)	Pencils	Spark I	Long range spectrum or "I.F."	Ba 4554·0* Mg 4703·0	0·0002	Spect.	Added inductance 0·135 mH
Beryllium (a)	Soln.	Spark II	B.10	Be 3130·4 Mg 3074·0	0·0003	Spect.	
(b)	Block	Spark I	B.10	Be 3130·4 Mg 3074·0	0·001	Spect.	
(c)	Block	Arc	B.10	Be 3130·4 Mg 3074·0	<0·0001	Spect.	
Calcium (a)	Block	Spark I	U.γ	Ca 3933·7 Mg 3329·9 or Mg 3074·0	0·002	Flame-photometer	
(b)	Pencils	Arc	U.γ	Ca 3933·7 Mg 3329·9 or Mg 3074·0	0·0003	Flame-photometer	
Lithium	Soln.	Spark II	Long range spectrum or "I.F."	Li 6707·8 Mg 5528·5	0·002	Spect.	
Rare Earths (a)	Pencils	Arc	U.γ	Ce 3201·7 Mg 3074·0	0·01	Chem.	Total Rare Earths limit: 0·02 per cent
				La 3949·1 Mg 4057·6	0·005	Chem.	
(b)	Block	Arc	U.γ	Ce 3201·7 Mg 3074·0	0·02	Chem.	Total Rare Earths limit: 0·04 per cent
				La 3949·1 Mg 4057·6	0·01	Chem.	

* See note under Table 3.

1955/7 VOL.

must be freshly machined immediately before use in order to minimize contamination from atmospheric dust. Standard samples are conveniently analysed on the flame photometer.

Lithium. Lithium is readily determined and calibrated for by the solution technique, but the occurrence of its strongest line at 6707·8 Å necessitates the use of a panchromatic or special red-sensitive emulsion.

Rare Earths. The spectrographic determination of low concentrations of rare earths is beset by two difficulties, namely the lack of very sensitive emission lines, and the occurrence of most of the lines at wavelengths above 3500 Å—a region of serious cyanogen-band interference. The best sensitivity is therefore obtained with pencil self-electrode samples, and a uniform gamma plate. Calibration is by way of chemical analysis.

Other elements. The foregoing elements have all required individual methods for all or part of the range. A number of elements detailed in Table 3, are sought

Table 3

Element	*Line-pair*	*Lowest limit of detection %*		*Notes*
		Method (1)	*Method* (2)	
Cadmium	Cd 3261·1 Mg 3074·0	0·01	—	
Cadmium	Cd 2288·0 Adj. Bgd.*	0·001	0·0002	
Copper	Cu 3247·5 Mg 3074·0	0·0002	0·00005	
Iron	Fe 3020·6 Mg 3074·0	0·002	0·001	Zirconium interferes
Iron	Fe 2719·0 Mg 3074·0	0·005	0·003	
Iron	Fe 2483·3 Mg 3074·0	0·001	<0·001	
Manganese	Mn 2949·2 Mg 3074·0	0·002	0·002	
Manganese	Mn 2576·1 Mg 3074·0	0·0005	0·0002	
Nickel	Ni 3414·8 Mg 3329·9	0·001	0·001	Zirconium interferes
Nickel	Ni 3002·5 Mg 3074·0	0·002	0·002	
Lead	Pb 3639·6 Mg 3074·0† or Mg 3329·9†	0·002	0·001	† "Uniform γ" plate necessary
Lead	Pb 2614·2 Mg 2736·5 or Mg 3074·0	0·001	0·001	
Silicon	Si 2881·6 Mg 3074·0 or Adj. Bgd.*	0·002	0·002	Background correction of Si line essential
	Si 2516·1 Mg 3074·0 or Mg 2736·5	0·001	0·001	
Silver	Ag 3382·9 Mg 3329·9	<0·001	<0·0001¶	¶ Estimated figure
Tin	Sn 3175·1 Mg 3074·0	0·002	0·001	
Titanium	Ti 3349·0 Mg 3329·9	§	0·002	§ Ordinary graphite contains some Ti
Zinc	Zn 3345·0 Mg 3329·9 or Mg 3074·0† or Adj. Bgd.*	0·002	0·002	† "Uniform γ" plate preferred
Zirconium	Zr 3392·0 Mg 3329·9	0·005	<0·005	

* Adjacent background, where this is reproducible from spectrum to spectrum (e.g., where it originates from closely situated dense magnesium lines) may be employed as an internal standard intensity. The distance from the analysis line at which the background reading is taken must be carefully standardized for each element.

Working graphs for several of these elements are given in Fig. 4.

in the routine examination of all alloys and "pure" magnesium, and are determined using a common set of conditions. Calibration of standard samples for all the following elements is by way of chemical analysis.

Methods: (1) block samples with graphite counter-electrode
(2) pencil self-electrodes

Excitation: interrupted arc

Photographic plate: Kodak B.10.

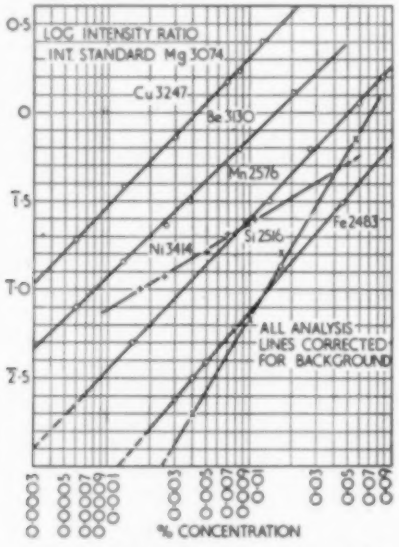

Fig. 4. Trace-element working graphs.

III. General remarks

In order to assess the accuracy with which trace concentrations are determinable under routine conditions, a short series of reproducibility tests was applied to several random samples. The figures quoted in the following table (except for barium) were obtained using the point-to-plane method and arc or spark techniques as previously described. Standard deviations (σ) are calculated from about forty results for each level taken from several plates. The coefficient of variation (v) is the ratio of the standard deviation to the mean expressed as a percentage.

It appears that in the range 0·01–0·1 per cent a coefficient of variation of about 6–8 per cent is to be expected. The higher figures for manganese and silicon may be attributed to the tendency of these elements to segregate to grain boundaries. At lower concentration levels, variabilities increase but can generally be tolerated. Analytical precision can, of course, be improved by replication.

It also appears that the interrupted arc can yield reproducibilities as good as those of the spark. This is not surprising, as excellent reproducibilities have been quoted elsewhere [4] for this particular circuit.

Experience has shown that the variabilities inherent in the pencil self-electrode technique are, in this case, likely to be comparable with those quoted in the table.

The solution technique is usually better, except where the working region is very close to the limit of detection.

The remarkably high sensitivity to spectral excitation of a number of the elements quoted—barium, boron, beryllium, calcium, copper, etc.—provides a method of analysis which may be applied to lower concentrations than known

Table 4

Element	*Concentration level*	σ	*v%*	*Excitation*
Cu	0·05	0·003	6	Spark
Cu	0·005	0·0003	6	Arc
Si	0·07	0·005	7	Spark
Si	0·015	0·002	13	Arc
Zn	0·03	0·002	6	Arc
Mn	0·05	0·005	10	Arc
Be	0·03	0·0025	8	Arc
Be	0·0001	0·00003	30	Arc
Ba	0·0002	0·0001	50	Spark

VOL. 7 55/56

chemical methods. But it must be noted that in other cases the reverse is true: iron, nickel, and some heavy metals can be determined at lower concentrations chemically [3]. The main advantage of the spectrographic procedures lies in the ease and speed with which large numbers of trace determinations can be made once the initial calibration is completed.

Acknowledgment

The author sincerely thanks the Chairman and Board of Directors of Magnesium Elektron Limited for permission to publish this report.

References

[1] Hess, T. M., and Reinhardt, L. G.; *J. Opt. Soc. Amer.* 1944 **34** 104.
[2] van Calker, J., and Wienecke, R.; *Z. angew. Physik* 1952 **4** 210.
[3] Mayer, A., and Price, W. J.; *Chemical and Spectrographic Methods of Analysis of Magnesium and its Alloys.* Magnesium Elektron Limited, Manchester 1954.
[4] Walsh, A.; *Metal Industry (London)* 1946 **68** 235–245, 263–265, 293–294.
[5] Beale, P. T.; British Non-Ferrous Metals Research Assoc., Research Report A915, June, 1951.
[6] Feldman, C.; *Anal. Chem.* 1949 **21** 1041.
[7] Pierce, W. C., and Nachtrieb, N. H.; *Ind. Eng. Chem. (Anal. Ed.)* 1941 **13** 744.
[8] Nachtrieb, N. H.; *Principles and Practice of Spectrochemical Analysis,* McGraw-Hill, New York, 1950.

Spectrochimica Acta, 1955, Vol. 7, pp. 128 to 133. Pergamon Press Ltd., London

SPECTROCHEMICAL NOTES

Über die Ausleuchtung von Spektrographen

M. NORDMEYER
Mitteilung aus dem Staatlichen Materialprüfungsamt Nordrhein-Westfalen, Dortmund

(*Received July* 1954)

Summary—In order to match the optical efficiency of a spectrograph the external light-collecting system should have a light-gathering power not less than that of the spectrograph itself. The geometrical conditions for this are fulfilled by the arrangement of lenses recommended by Zeiss. Improvements are possible by reducing the light-losses in the external system through reflections and through chromatic aberration by substituting a two-mirror system or even a single-mirror system for the lenses. In either case another concave mirror behind the source has advantages for quantitative spectral analysis. Finally the proposal of E. PREUSS to use an array of lenses to eliminate the effect of the movements of the light-source on the illumination of the spectrograph is described.

VOL
7
1955/

BEI den heute immer mehr in Gebrauch kommenden Spektrographen mit großem Auflösungsvermögen gewinnt die Frage einer möglichst günstigen Ausleuchtung erhöhte Bedeutung, weil sich die Lichtstärke bei diesen Geräten naturgemäß verringert und dementsprechend die Belichtungszeiten oft unangenehm anwachsen. Es wird daher für den Spektrochemiker der Praxis vielleicht von Nutzen sein, wenn einmal die wichtigsten geometrisch-optischen Anordnungen zusammengestellt werden, die unter dem Gesichtspunkt einer guten Ausleuchtung zu berücksichtigen sind. Wenn auch das meiste hier zu Sagende nicht neu ist, so ist es doch nicht allgemein bekannt, auch wird dieser Seite von der die Spektrographen liefernden Industrie kaum besondere Aufmerksamkeit geschenkt.

Es ist also die Frage gestellt, wie erfolgt die Lichtvermittlung zwischen der Strahlungsquellen und einem Spektrographen mit vorgegebenemLic htleitwert [1] am günstigsten. Der Lichtleitwert ist die Größe, die den Einfluss der Geometrie eines optischen Systems auf den Strahlungsdurchfluss kennzeichnet. Aus energetischen Überlegungen folgt, daß für eine optimale Ausleuchtung der Lichtleitwert des optischen Vermittlungssystems nicht unter dem des Spektrographen liegen darf. Das bedeutet, die Begrenzungen der optischen Mittel für die Ausleuchtung dürfen nicht die auf ihnen erzeugten Bilder der beiden Hauptblenden des Spektrographen beschneiden.

(A) Als erstes Beispiel sei die Zeiss'sche Anordnung zur Zwischenabbildung der Lichtquelle angeführt [2]. Die Einzelheiten sind aus der Abb. 1 zu ersehen. Wir betrachten die Abbildungsverhältnisse vom Spektrographen beginnend rückwärts.

Die Schriftleitung hat sich zur Aufnahme dieser Notiz in die Spectrochimica Acta entschlossen, obwohl sie, wie der Verfasser selbst sagt, nichts prinzipiell Neues bringt. Diese Übersicht über die korrekten Möglichkeiten zur Ausleuchtung von Spektrographen erschien nämlich sehr nützlich, weil diese Dinge in keinem der verbreiteten Lehrbücher ausführlich behandelt werden; auch wird ihnen in der Laboratoriumspraxis im allgemeinen zu wenig Aufmerksamkeit geschenkt. Bei korrekten Intensitätsmessungen ist ihre sorgfältige Beachtung aber von großer Wichtigkeit.

Die Öffnungsblende des Spektrographen ist durch die Feldlinse III am Spektrographenspalt in die Zwischenbildlinse II abgebildet, der Spalt durch die Zwischenbildlinse in die Linse I, die von der Lichtquelle gleichmäßig ausgeleuchtet wird. Das Bild der Öffnungsblende in der Zwischenbildlinse bildet dann wieder Linse I in die Lichtquelle ab. Die Vorteile der Anordnung sind ersichtlich:

1. Wegen der gleichmäßig ausgeleuchteten Linse I wird auch der Spalt gleichmäßig ausgeleuchtet, so daß dort z.B. ein Stufenfilter angebracht werden kann.

2. Die Zwischenabbildung bei II ist im allgemeinen ein vergrößertes Bild der Lichtquelle, das dann weiter durch die Feldlinse III vergrößert in die Spektrographenöffnung abgebildet wird. Die Zwischenabbildung ist der Ort, an dem bestimmte Bereiche der Lichtquelle, deren Strahlung interessiert, ausgeblendet werden können. Hier werden zweckmäßigerweise auch all die Maßnahmen durchgeführt, die sämtliche Spektrallinien gleichmäßig betreffen sollen, z.B. werden

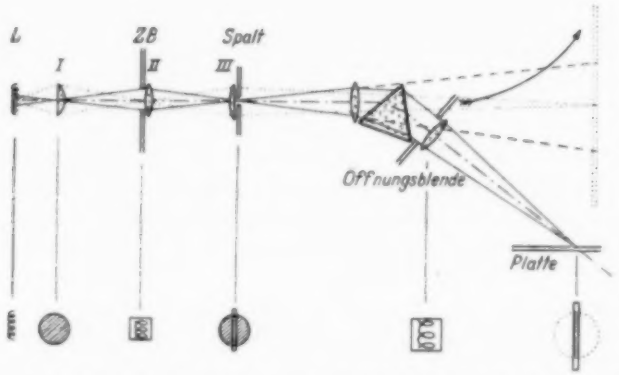

Abb. 1. Zeiss'sche Anordnung zur Zwischenabbildung der Lichtquelle*

am besten Neutralfilter, Netze, etc., hier angebracht. Mit der Zwischenabbildung gewinnt man zugleich einen größeren Abstand zwischen der heißen, oft sprühenden Lichtquelle und dem Spalt.

Gewisse Mängel können bei dieser Anordnung durch den chromatischen Fehler der Linsen auftreten, so daß man bei Aufnahmen größerer Spektralbereiche mindestens für die beiden ersten Linsen Achromate verwenden sollte.

(B) Eine Verbesserung gegenüber der Zeiss'schen Anordnung erhält man nun dadurch, daß man die Linsen durch oberflächenbedampfte Hohlspiegel ersetzt (Abb. 2). Die Spiegel werden in Z-Stellung [3] zur Verringerung des Asymmetriefehlers aufgestellt. Mit diesen Spiegeln ist die Ausleuchtung über den ganzen Wellenlängenbereich gut. Der Einfluß der einzig verbleibenden Linse vor dem Spalt ist in der Horizontalebene, die für das Auslösungsvermögen entscheidend ist, wegen der geringen Spaltbreite (Lochkamera) bedeutungslos. Aber auch für die Vertikalebene ist der chromatische Fehler normalerweise ohne praktische

* Die Abbildung ist der oben zitierten Arbeit von H. KAISER entnommen.

Bedeutung. Der Vorteil gegenüber (A) liegt neben der Wellenlängenunabhängigkeit und den relativ geringen Kosten auch darin, daß Reflektions- und Absorptionsverluste geringer sind.

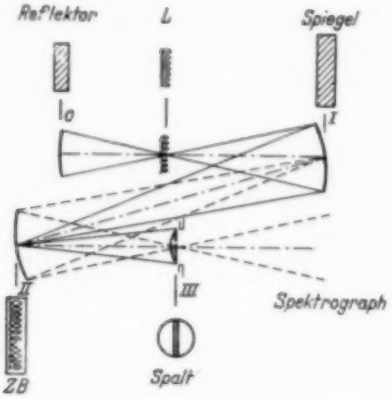

Abb. 2. Anordnung zur Zwischenabbildung der Lichtquelle nach (B). (Horizontalschnitt.)

(C) Eine andere Version mit unbestreitbaren Vorzügen gewinnt man durch Fortlassen des Spiegels II am Ort der Zwischenabbildung (Abb. 3). Er wird durch eine Blende ersetzt, deren Ausschnitt dem vorverlegten Bild der Spektrographenöffnung entspricht. Diese Anordnung dürfte dem von F. TWYMAN [4] erwähnten

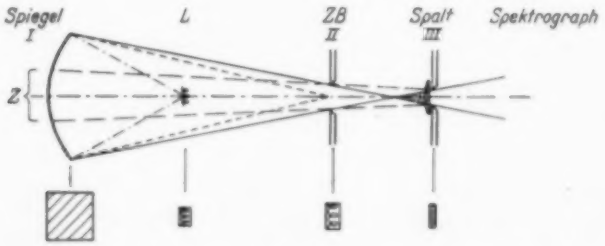

Abb. 3. Anordnung zur Zwischenabbildung der Lichtquelle nach (C). (Vertikalschnitt, *L* befindet sich außerhalb der Zeichenebene).

"mirror system" zugrundeliegen*. Um eine vollständige Ausleuchtung des Spektrographen zu erhalten, muß allerdings der Spiegel I, der die Lichtquelle in die Blende abbilden soll, größer sein als bei (B), und zwar so groß, daß die Verbindungslinie des oberen Spiegelrandes mit der Oberkante der Blende die Unterkante des Spaltes trifft, ebenso die vom unteren Spiegelrand über Unterkante Blende die Oberkante des Spaltes.

Entsprechendes gilt für die seitliche Begrenzung. Der Strahlengang zwischen Blende und Spalt ist dann derselbe wie unter (B). Man kann sich leicht davon überzeugen, daß in dem in der Abbildung 3 schraffierten Teil vor dem Spalt eine

* Ich verdanke Herrn F. J. BRÜNING den Hinweis auf diese vereinfachte Anordnung.

Struktur des Blendenbildes nicht mehr vorhanden ist, da dieser Raum innerhalb der Divergenzkegel sämtlicher in der Blende abgebildeter Punkte der Lichtquelle liegt. Die Vorzüge dieser Anordnung gegenüber (B) sind:

1. Einsparung eines Spiegels (evtl. sogar eines zweiten, weil man gelegentlich wegen der räumlichen Verhältnisse im Falle B) noch einen Umlenkspiegel benötigt), was, von den Kosten abgesehen, im fernen UV einen Energiegewinn etwa bis zum Faktor 2 (bzw. 4) bringt.

2. Variabler Vergrößerungsmaßstab für das Lichtquellenbild. Die Vergrößerung der Zwischenabbildung der Lichtquelle muß verändert werden können, wenn die Größe der Lichtquelle, z.B. bei Änderung des Elektrodenabstandes, variiert. Während die Anordnung unter (B) bei einem solchen Wechsel einen neuen Spiegel mit anderer Brennweite verlangt, brauchen hier nur der erste Spiegel und die Lichtquelle verschoben zu werden. Die Dimensionen des ersten Spiegels müssen für die stärkste vorkommende Vergrößerung berechnet sein. Den Abstand zwischen Blende und Spalt läßt man zweckmäßigerweise immer konstant, so daß weder die Blende noch die Feldlinse vor dem Spalt gewechselt werden müssen.

3. Ungleichmäßigkeiten der Spiegeloberfläche, etwa infolge von Spritzern, werden im mittleren, mit Z bezeichneten Bereich des Spiegels I (s. Abb. 3) die Gleichmäßigkeit der Ausleuchtung des Spaltes nicht beeinträchtigen, erst außerhalb dieses Bereiches liegende Stellen werden verschmiert abgebildet. Im Falle (B) ergibt dagegen jeder Fleck auf Spiegel I ein Bild auf dem Spalt. Der Spiegel I ist daher bei quantitativen Arbeiten, insbesondere bei Benutzung eines Stufenfilters, mit großer Sorgfalt sauber zu halten, und es empfiehlt sich, zwischen Lichtquelle und Spiegel eine kleine Quarzscheibe als Schutz einzuschalten.

Ein geringfügiger Nachteil der Anordnung (C) gegenüber (B) ist ein kleiner Asymmetriefehler bei der Abbildung der Lichtquelle auf die Blende. Außerdem ist zu beachten, daß die in den Spektrographen gelangende Strahlung unter etwas steileren Winkeln aus der Lichtquelle kommt. In der Kameraebene des Spektrographen trägt nämlich allein solches Licht zur Abbildung bei, das durch das Bild des Spaltes gegangen ist, welches der vorm Spalt stehende Spiegel von diesem vor der Lichtquelle entwirft. Im Falle (B) liegt dieses Spaltbild auf dem Spiegel I, im Falle (C) ein entsprechend verkleinertes zwischen Spiegel und Lichtquelle. Bei den praktisch vorkommenden Öffnungsverhältnissen der Spektrographen dürften aber diese Unterschiede kaum meßbar sein, so daß man die Anordnung unter (C) bedenkenlos als die günstigste ansehen kann.

(D) Gegenüber der unter (C) beschriebenen optimalen Ausleuchtungsanordnung ist nun noch ein weiterer Gewinn durch Anbringen eines Reflektorspiegels möglich, der die Lichtquelle in sich selbst in Richtung der optischen Achse des Systems Lichtquelle—Spektralapparat abbildet (in Abb. 2 eingezeichnet). Diese Maßnahme, die natürlich nur bei optisch dünnen Lichtquellen brauchbar ist, eignet sich vorzüglich in der Emissionsspektralanalyse und dort, wo sonst Funken oder Bogen Verwendung finden. Gerade die Spektralanalyse erweist, daß Funken und Bogen optisch durchlässig sind. Wegen der örtlichen Schwankungen der Lichtemission wird das Spiegelbild außerdem die Lichtquelle nur teilweise durchdringen. Bei Linien, die durch Selbstumkehr gekennzeichnet sind,

ist selbstverständlich erhöhte Vorsicht geboten. Tatsache ist, daß bei Verwendung gut reflektierender Hohlspiegel praktisch eine Verdopplung der Strahlungsdichte erreicht wird, so daß bei Aufnahmen mit photographischen Platten die Belichtungszeiten auf die Hälfte verringert werden können.

Die Verwendung des Reflektors ergibt für quantitative Arbeiten folgenden Vorteil: Bei der optimal ausgeleuchteten Apparatur wird die zu untersuchende Lichtquelle in die Öffnungsblende des Spektralapparates so abgebildet, daß diese nach Höhe und Breite gerade vollständig vom Licht erfüllt ist. Örtliche Schwankungen der Lichtquelle haben daher auch Schwankungen in der Ausleuchtung der Öffnungsblende zur Folge. Das Bild der Lichtquelle weicht seitlich aus der Öffnungsblende. Von dieser Veränderung wird das Intensitätsverhältnis zweier Linien aus verschiedenen Teilen des Spektrums im allgemeinen verschieden betroffen werden. Der Grund hierfür liegt in der Tatsache, daß die Strahlungsquerschnitte für die verschiedenen Spektralgebiete unterschiedlich vignettiert werden. Auch die Absorption in der Optik des Spektrographen ist örtlich verschieden. So hat eine örtliche Veränderung in der Ausleuchtung einen unterschiedlichen Einfluß auf die Linienintensität in verschiedenen Bereichen des Spektrums.

Der dadurch entstehende Fehler wird bei Benutzung des Reflektorspiegels fast genau auf die Hälfte reduziert, da das direkte Bild und das Bild der reflektierten Lichtquelle gegenphasig auswandern. Für die meisten praktischen Fälle dürfte die Kompensation mit dem Reflektor ausreichend Abhilfe bieten, zumal wenn man sich über die Größe des Fehlers durch einen Vergleich zweier Aufnahmen mit und ohne Reflektor Rechenschaft gibt.

Das Auflösungsvermögen des Spektralapparates wird von der günstigeren Ausleuchtung des Prismas jedoch nicht betroffen, da zwischen dem direkten Licht der Strahlungsquelle und dem reflektierten keine feste Phasenbexzeihung besteht.

(E) Abschließend soll noch kurz ein Vorschlag erwähnt werden, mit dem E. Preuß [5] den zuletzt besprochenen Fehler praktisch ausgeschaltet hat. Eine stets gleichmäßige Ausleuchtung des Spektrographen wird dadurch erreicht, daß nicht ein einziges Bild der Lichtquelle in der Öffnungsblende erzeugt wird, sondern daß diese mit Hilfe eines Linsenrasters von vielen kleinen Bildern der Lichtquelle gleichmäßig überdeckt wird. Damit fallen unterschiedliche Einflüsse der Vignettierung etc. in den einzelnen Wellenlängenbereichen bei örtlich schwankender Lichtquelle heraus.

Abb. 4 zeigt die Ausleuchtung für den Horizontalschnitt. Die Linse mit dem direkt dahinter befindlichen Linsenraster ($L\ R'\ L'$) entspricht der in den Abbildungen 1 bis 4 mit I bezeichneten Stelle, V (das vor dem Spalt entstandene Vielfachbild der Lichtquelle) der Stelle II und L_2 der Stelle III. Die Linse L_2 ist so berechnet, daß sie das Vielfachbild in die Spektrographenöffnung abbildet. Über Einzelheiten, auch Besonderheiten für die Ausleuchtung des Vertikalschnitts, wird auf die Preuß'sche Arbeit verwiesen. Das Linsenraster läßt sich auch durch ein Raster von kleinen Hohlspiegeln ersetzen.

Abschließend gibt Abb. 5 die Reproduktion einer Platte, auf der unter sonst gleichen Bedingungen das Eisenspektrum zwischen 2234 und 2276 Å mit den Anordnungen (A), (C), und (D) aufgenommen wurde. Sie veranschaulicht recht

VOL
7
1955/

VOL.
7
55/56

Abb. 5, Eisenspektrum zwischen 2234 und 2276Å unter sonst gleichen Aufnahmebedingungen nach Anordnung (A), (C) und (D).

VOL
7
1955/

eindrucksvoll die Vorzüge der beschriebenen Spiegelanordnung sowie die Wirkung des Reflektors.

Zusammenfassung

Das optische System, das möglichst günstig die Strahlungsleistung durch einen Spektrographen mit vorgegebenem Lichtleitwert leitet, muß selbst einen Lichtleitwert haben, der mindestens gleich dem des Spektrographen ist. Diese geometrisch-optische Voraussetzung ist bei der Zeiss'schen Anordnung zur Zwischenabbildung erfüllt. Verbesserungen, die eine Verringerung der Abbildungsfehler sowie der Reflektions- und Absorptionsverluste in den optischen Mitteln bezwecken, können mit einer Zwei-Spiegel-bzw. einer Ein-Spiegelanordnung erreicht werden. Auf die Vorteile bei der Verwendung eines Reflektorspiegels wird hingewiesen. Abschließend ist der Vorschlag von E. PREUSS erwähnt, mittels einer Rasterlinsenanordnung die Ausleuchtung des Spektrographen von den örtlichen Schwankungen der Lichtquelle unabhängig zu machen.

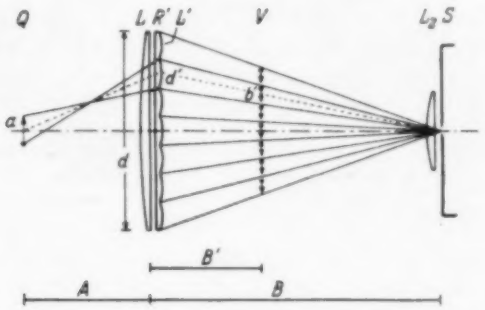

Abb. 4.* Anordnung mit Linsenraster nach E. PREUß.

Literatur

[1] siehe z.B. HANSEN, G.; *Zeiss-Nachrichten* 1941 **IV** (Heft 1).
[2] siehe z.B. KAISER, H.; *Spectrochim. Acta* 1949 **3** 529.
[3] CZERNY, H., und TURNER, A. F.; *Z. Physik* 1930 **61** 192.
[4] TWYMAN, F.; *Metal Spectroscopy*, London, 1951, S. 80.
[5] PREUß, E.; *Die Ausleuchtung von Spektrographen mit Linsenrastern*, Heidelberger Beitrage zur Mineralogie und Petrographie, 1954 **4** 163.

* Die Abbildung ist der oben zitierten Arbeit von E. PREUß entnommen.

Spectrochimica Acta, 1955, Vol. 6, pp. 134 to 154. Pergamon Press Ltd., London

Spectrochemical Note

Ein elektronischer Steuermechanismus für einen Niederspannungsfunkenerzeuger

K. BUNGE
Mitteilung aus dem Institut für Spektrochemie und angew. Spektroskopie, Dortmund

(*Received* 27 *August* 1954)

Summary—An electronic control mechanism is described which initiates condenser discharges at regular intervals at frequencies of 1–200 per second, with results similar to those of the Pfeilsticker type of interrupted arc. The interval between the discharge of the condenser and the recharging can also be adjusted. The timing originates in a variable frequency circuit, which is controlled by two vibrators; and a high-voltage circuit generates the necessary sparks for ignition. With some modifications the circuit might also be used for high-voltage controlled sparks.

Einleitung

Den unmittelbaren Anlass zu der vorliegenden Arbeit gaben Untersuchungen über den Materialabbau an Zinkelektroden beim Übergehen elektrischer Entladungen. Dabei wurden aperiodische Kondensatorentladungen verwendet; die Ladespannung auf dem Kondensator betrug etwa 1 kV. Um den Abbau unter möglichst verschiedenartigen Bedingungen untersuchen zu können, wurde ein besonderer Steuermechanismus gebaut; er erlaubt es, in zeitlich gleichem Abstand aufeinander folgende Entladungen zu erzeugen. Ihre Anzahl pro sec. ("Funkenfolge") kann von etwa 1–200 variiert werden. Bei vielen spektrochemischen Aufgaben, die mit Niederspannungsfunkenerzeugern bearbeitet werden sollen, liegt ebenfalls das Bedürfnis vor, die Funkenfolge zu variieren. In den meisten zur Zeit gebräuchlichen Geräten ist aber die Funkenfolge ursächlich mit der Frequenz des speisenden Netzes verknüpft; deshalt kann sie nicht ohne weiteres geändert werden. Der erwähnte Steuermechanismus soll daher—zumal er sich in einigen wesentlichen Punkten von bisher angegebenen Schaltungen unterscheidet—kurz mitgeteilt werden.

Über elektronische Steuerungen von Funkenerzeugern liegen eine ganze Reihe von Arbeiten vor. Besonders ist auf die neueren Arbeiten von BARDÓC [1] zu verweisen. Ein Variieren der Funkenfolge ist beim Niederspannungsfunkenerzeuger (Teil des Generatore Universale) der Optica (Milano) möglich. Dabei erhält man allerdings keine äquidistanten Entladungen, sondern Funkengruppen mit dazwischen liegenden Pausen. Die Steuerung erfolgt mechanisch.

1. Der Niederspannungskreis

In der vorliegenden Arbeit soll in erster Linie das *steuernde* Glied des Funkenerzeugers behandelt werden. Figur 1 gibt zunächst die Schaltung des *gesteuerten* Teiles, der die Energie für den Analysenfunken liefert, wieder ("Niederspannungskreis"). U (etwa 1 kV) ist die konstante Spannung der benutzten Stromquelle. Von ihr aus kann über das Thyratron Th der Kondensator C aufgeladen werden. Geht ein Zündfunke in der Analysenfunkenstrecke AF über, so entlädt sich C über den Widerstand R, die Induktivität L, den Teslatransformator T und die Funkenstrecke AF. (Grössenordnung der elektrischen Schaltelemente: $C = 1$–$100\ \mu$F, $R = 0$–$200\ \Omega$, $L = 0$–1 mHy.)

Der Steuermechanismus greift in den Niederspannungskreis bei T und am Gitter von Th ein. Durch T wird die den Zündfunken hervorrufende Hochspannung induziert. (Die Zündung kann nach geringen Abänderungen auch als Parallelzündung nach Art des Multisource vorgenommen werden.) Ist C entladen, so zündet ein positiver Steuerimpuls am Gitter das Thyratron, sodaß C wieder auf U aufgeladen wird. Die Zeit zwischen Entladung von C und seiner Wiederaufladung kann eingestellt werden. Das ist wichtig, da man auf diese Weise die höchste unter gegebenen Bedingungen überhaupt mögliche Funkenfolge (sofern diese kleiner als 200 pro sec. ist) erzielen kann. Die obere Grenze

wird dadurch bestimmt, dass die Aufladung von C erst dann beginnen kann, wenn die ihr unmittelbar vorangehende Entladung hinreichend abgeklungen ist.

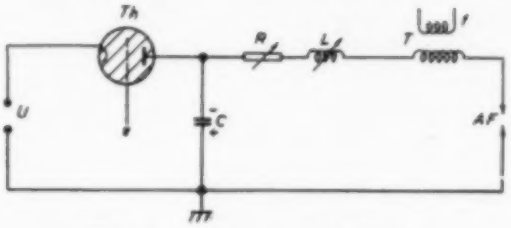

Figur 1. Niederspannungskreis N.

U = 1 kV
C = 1–100 μF
R = 0–200 Ω
L = 0–1 mHy
T prim. ca. 10 μHy
sec. ca. 50 μHy
Th Wahl hängt hauptsächlich von der maximalen mittleren Belastung ab.
AF Analysenfunkenstrecke

2. Blockdiagramm und Prinzip der Schaltung

Das Blockschema des Steuermechanismus findet sich in Figur 2, es besteht aus folgenden Teilen: dem Frequenzgenerator Fr, den Univibratoren U I und U II, dem Hochspannungsteil H und den entsprechenden Speiseaggregaten. (Diese sind im einzelnen nicht aufgeführt.) Die Pfeile zwischen den Bauelementen stellen Hinweise auf die Abfolge der Vorgänge dar. Spannungs- bezw. Stromverlauf an den Verbindungsstellen der Einzelteile sind aus den Diagrammen zu ersehen (schematisch). Im grossen und ganzen funktioniert

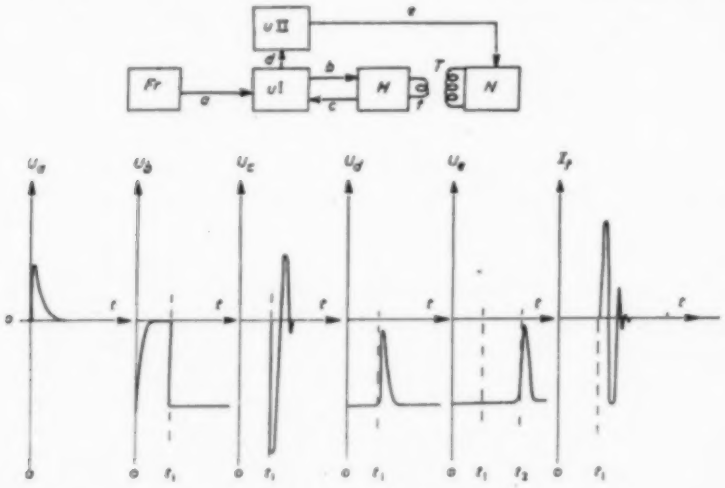

Figur 2. Blockschema.

Fr Frequenzgenerator
U I Univibrator I
U II Univibrator II
H Hochspannungsteil
N Niederspannungsteil
$U_a \ldots I_f$ Bezeichnung der Spannungen bzw. des Stromes, die an den durch die Indizes gekennzeichneten Stellen auftreten. Bedeutung der Zeiten t_1, t_2 siehe Text.

die Anordnung wie folgt: Zu einem bestimmten Zeitpunkt ($t = 0$) liefert der Frequenzgenerator einen Impuls an den Univibrator I. Der Univibrator kippt in seine labile Lage) Das bewirkt Veränderungen im Hochspannungsteil derart, dass zur Zeit t_1 (t_1 etwa 0·5 m sec., ein Funke in ihm erzeugt wird. Der dabei fliessende hochfrequente Strom wird benutzt. um über den Teslatransformator T im Niederspannungsteil eine Spannung zu induzieren, deren Höhe die Durchschlagsspannung der Analysenfunkenstrecke übertrifft. In dieser tritt daher ein energiearmer Zündfunke auf. Ihm folgt die stromstarke Entladung von C, in der das Spektrum angeregt wird. Der zur Zeit t_1 im Hochspannungsteil übergehende Funke erzeugt einen Impuls, der den Univibrator I in seine stabile Lage zurücktriggert; dabei wird der Univibrator II in die labile Lage befördert. Zur Zeit t_2 kehrt er spontan in seine stabile Lage zurück und zündet dabei das Thyratron Th im Niederspannungsteil über dessen Gitter. Die Spannungsquelle U lädt daher den Kondensator C erneut auf.

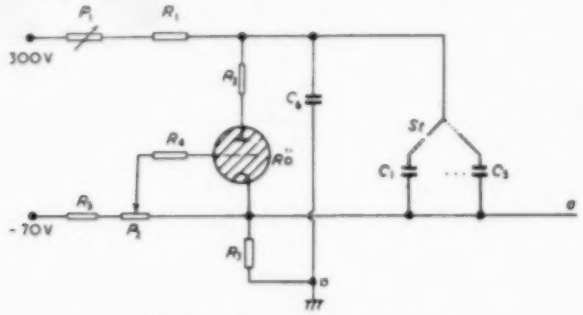

Figur 3. Frequenzgenerator *Fr*

Rö	Thyratron *S* 1/0,2 i II A
St	Stufenschalter
$R_1 = 0{\cdot}3$ M	$C_1 = 10{,}000$ pF
$R_2 = 1$ K	$C_2 = 30{,}000$ pF
$R_3 = 3$ K	$C_3 = 0{\cdot}1$ μF
$R_4 = 0{\cdot}1$ M	$C_4 = 0{\cdot}3$ μF
$R_5 = 10$ K	$C_5 = 1$ μF
$P_1 = 1$ M	$C_6 = 3000$ pF
$P_2 = 5$ K	

Der Frequenzgenerator strebt wieder seiner Ausgangslage zu und beschliesst damit den Zyklus. Dessen Dauer und damit die Funkenfolge wird durch den am Frequenzgenerator (Fig. 3) eingestellten Kondensator C_i ($i = 1 \ldots 5$) und den am Potentiometer P_1 eingestellten Widerstand gegeben.

3. Beschreibung der Einzelteile

Die Figuren 3, 4, und 5 zeigen die Schaltung der Einzelteile. (Die Heizung der Röhren ist nicht mit aufgeführt.) Frequenzgenerator und Univibratoren sind bis auf geringe Abänderungen in konventioneller Weise ausgeführt. (Wegen der elektronischen Schaltungen siehe z.B. [2].) Gewisse Modifikationen waren nötig, um die Schaltung gegenüber hochfrequenten Störungen zu stabilisieren. Solche Störungen treten einerseits in der Anordnung selbst auf (vor allem im Hochspannungsteil); zum anderen können sie von aussen eingestreut werden. (z.B. durch Betrieb weiterer Funkenerzeuger in der Nähe.)

(a) *Der Frequenzgenerator* (Figur 3)

Der in Figur 3 skizzierte Thyratronoszillator liefert positive Impulse an den Univibrator I mit einer Frequenz, die kontinuierlich von etwa 1–200 pro Sekunde variiert werden kann.*

* Bei geeigneter Schaltung könnten auch anders geartete Oszillatoren verwendet werden.

VOL 7 1955/

(b) *Die Univibratoren I und II* (Figur 4)

Beide Univibratoren bestehen aus den gleichen Grundelementen. (Verschieden sind nur die in den gestrichelten Feldern befindlichen Schaltteile.) Die linke Röhre mit ihren Schaltelementen ist die Eingangs- die rechte die Ausgangsstufe. Die beiden mittleren Röhren bilden den eigentlichen Univibrator. In der stabilen Lage leitet die rechte von

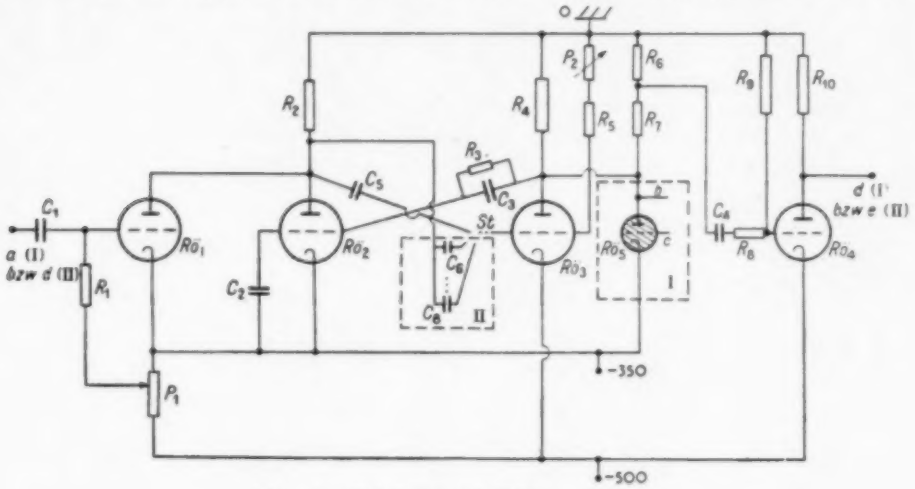

Figur 4. Univibratorteil *U* I bzw. *U* II.

$R_1 = 0{\cdot}3$ M	$R_6 = 0{\cdot}1$ M	$C_1 = 1000$ pF
$R_2 = 40$ K	$R_9 = 0{\cdot}2$ M	$C_2 = 500$ pF
$R_3 = 0{\cdot}3$ M	$R_{10} = 70$ K	$C_3 = 1000$ pF
$R_4 = 40$ K	$P_1 = 0{\cdot}1$ M	$C_4 = 150$ pF
$R_5 = 0{\cdot}3$ M	$P_2 = 5$ M	$C_5 = 3000$ pF
$R_6 = 70$ K		
$R_7 = 15$ K		

St Stufenschalter
$R\ddot{o}_1 - R\ddot{o}_4$ 1/2 ECC 40
In Feld I $R\ddot{o}_5$ Thyratron PL 10
In Feld II C_6 10,000 pF
C_7 0·1 μF
C_8 0·3 μF

ihnen, während die linke sperrt. Der Univibrator wird durch einen positiven Stoß am Eingang in die labile Lage gekippt und liefert beim Zurückfallen einen positiven Impuls am Ausgang.

(A) Beim Univibrator I kommt das in Feld I gezeichnete Thyratron hinzu. (Type PL 10 von Philips. Es handelt sich um ein Thyratron mit einem als Aussenelektrode ausgebildeten Gitter.) In der stabilen Lage des Univibrators kann das Thyratron nicht gezündet werden, da die Anode negativer als die Kathode ist. Wird das Thyratron in der labilen Lage des Univibrators gezündet, so wird dieser in seine stabile Lage zurückgetriggert.

(B) Beim Univibrator II ist der im Feld II gezeichnete Kondensatorsatz zusätzlich angeordnet. Er gestattet es, die Zeit, während der sich der Univibrator in seiner labilen Lage befindet, in Stufen einzustellen.

(c) *Der Hochspannungsteil* (Figur 5)

Der Hochspannungsteil wird von der konstanten Spannungsquelle $V = 10$ kV gespeist. Es sind weiterhin die beiden nahezu identischen Stromkreise R_1, $C(R_2)$, S bzw. R'_1,

$C'(R'_2)R_3$, S vorhanden. (R_3 ist klein gegen R'_1.) Diese beiden Kreise können geöffnet oder geschlossen werden dadurch, dass man das Gitter der Senderöhre S stark negativ macht oder in die Nähe von Null bringt. Bei geöffnetem Kreis entladen sich die Kondensatoren C bzw. C' über die Überbrückungswiderstände R_2 bezw. R'_2, falls sie zuvor aufgeladen waren. Bei geschlossenem Kreis laden sie sich über R_1 bezw. R'_1 so weit auf, bis die Durchschlagsspannung der Funkenstrecke F', die zweckmässig zu etwa 7 kV gewählt wird, erreicht ist. F' schlägt durch, C und C' schalten sich hintereinander, so dass nun auch F, deren Durchschlagsspannung zwischen 7 und 14 kV liegt, durch einen Funken überbrückt wird. In dem nunmehr gebildeten Stromkreis C, F', C', T, F entladen sich die Kondensatoren in hochfrequenten Schwingungen. Der Teslatransformator wird benutzt, um in dem Niederspannungskreis eine zum Überschlagen der Analysenfunkenstrecke hinreichende Spannung zu induzieren. Beim Durchschlagen von F' wird über

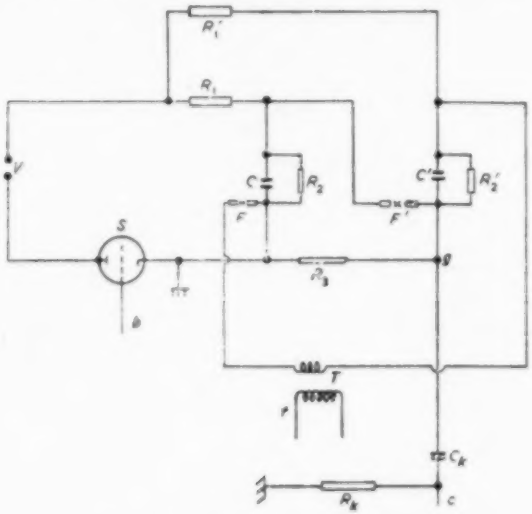

Figure 5. Hochspannungsteil H.

V	= 10 kV	R_k	= 0·3 M
S	Senderöhre *RS* 31	$C; C'$	= 700 pF (Hochspannungskondensator, verlustarm)
$R_1; R_1'$	= 0·5 M	$F; F'$	= Funkenstrecken
$R_2; R_2'$	= 5 M	C_k	= 200 pF (Hochspannungskondensator)
R_3	= 0·1 M		

den Koppelkondensator C_k bei c ein Triggerimpuls an den Univibrator I geliefert. Das Gitter von S ist bei b mit dem Univibrator I verbunden.

Das Hintereinanderschalten der beiden Kondensatoren im Hochspannungsteil (Marxsche Stoßschaltung) wurde vorgenommen, um mit geringer Eingangsspannung auszukommen. Man könnte natürlich auch *einen* Kondensator benutzen, müsste dann aber um denselben Effekt zu erreichen, mit der doppelten Spannung also 14 kV arbeiten.

4. Wirkungsweise der Schaltung

Die Wirkungsweise übersieht man am besten, wenn man einen vollen Operationszyklus ablaufen lässt:

Im Ausgangszustand befinde sich der Frequenzgenerator kurz vor dem Zeitpunkt, in dem er einen Impuls abgibt. Die beiden Univibratoren nehmen ihre stabilen Lagen ein. Demgemäß liegt die Anode von $R\ddot{o}_3$ im Univibrator I auf einer Spannung von etwa −400 Volt. Da diese Anode mit dem Gitter der Senderöhre S im Hochspannungsteil direkt

verbunden ist, sperrt S. C und C' im Hochspannungsteil seien entladen. Im Niederspannungsteil sei der Kondensator C auf die volle Speisespannung U aufgeladen.

Der Zyklus wird in Gang gesetzt durch Zünden des Thyratrons im Frequenzgenerator. Dabei wird an a ein positiver Impuls erzeugt, der zu dem Eingang des Univibrators I geleitet wird. Dieser kippt in die labile Lage, wobei die Spannung der Anode von $Rö_3$ plötzlich bis nahe an Null ansteigt. Da nunmehr auch das Gitter der Senderöhre S im Hochspannungsteil nahe an Null liegt, leitet S. Nun spielen sich die in 3c näher beschriebenen Vorgänge ab: C bezw. C' laden sich auf, schalten sich beim Durchschlag von F' hintereinander und entladen sich über F', den Teslatransformator und F. Über den Teslatransformator wird im Niederspannungskreis die zum Überschlag der Analysenfunkenstrecke nötige Spannung induziert, sodass der Zündfunke übersprigen kann. Die ihm folgende energiereiche Entladung des Kondensators C bildet die Lichtquelle, in der das Spektrum der zu analysierenden Substanz angeregt wird.

Der beim Überschlagen von F' bei g erzeugte Impuls wird über den Koppelkondensator C_k nach c und damit an das Gitter von $Rö_5$ beim Univibrator I geleitet. Er zündet $Rö_5$. Daher sinkt die Anodenspannung dieser Röhre auf etwa -300 Volt ab und der Univibrator wird in die stabile Lage zurückgetriggert. Die Senderöhre S sperrt wieder und der Hochspannungsteil kehrt nach einiger Zeit (< 1 m sec.) in seine Ausgangslage zurück. Beim Zurückfallen des Univibrators I erscheint an dessen Ausgang ein positiver Impuls, der den Univibrator II über dessen Eingang in seine labile Lage bringt. Nach einem Zeitintervall, das durch die Zeitkonstante des am Stufenschalter St eingestellten Kondensators C_i ($i = 5 \ldots 8$) und des am Potentiometer P_2 eingestellten Widerstandes bestimmt wird, kehrt der Univibrator II in seine stabile Lage zurück. Der dabei am Ausgang erscheinende positive Impuls zündet das Thyratron Th im Niederspannungskreis. Der Kondensator C im Niederspannungskreis lädt sich wieder auf die volle Speisespannung U auf und das Thyratron erlischt. Der Frequenzgenerator kehrt gemäss der an ihm eingestellten Frequenz in seine Ausgangslage zurück. Damit befinden sich alle Teile wieder in der Anfangsstellung, so dass der Zyklus geschlossen ist.

5. Störanfälligkeit der Anordnung

Leitender Gesichtspunkt bei der Konstruktion war das Vermeiden möglicher Störungen.

(a) *Stabilität gegen innere Störungen*

Über die Stabilität des Frequenzgenerators und der Univibratoren im allgemeinen ist hier nichts zu sagen, da die entsprechenden Hinweise der einschlägigen Literatur entnommen werden können. (siehe z.B. [2].) Näher soll auf die Funktion von $Rö_5$ im Univibrator I eingegangen werden. Diese Röhre ist überhaupt nur betriebsbereit, wenn der Univibrator sich in seiner labilen Lage befindet. (Nur dann liegt ja eine gegenüber der Kathode positive Anodenspannung an.) Störspannungen an dem als Aussenelektrode ausgebildeten Gitter der Röhre können diese aber auch dann nicht vorzeitig zünden; hierzu wären nämlich relativ grosse Spannungen (mehrere 100 Volt) erforderlich. Die Sperrung der Senderöhre S im Hochspannungsteil erfolgt unmittelbar nach der Zündung von $Rö_5$, da deren Anode direkt mit dem Gitter von S verbunden ist; das Zeitintervall ist allein durch die Aufbauzeit des Plasmas in $Rö_5$ bestimmt. Da $Rö_5$ im gezündeten Zustand eine kleine Impedanz besitzt, wird der Univibrator sehr sicher in seine stabile Lage zurückgetriggert. Beim Zurückfallen wird selbsttätig die Spannung von der Anode von $Rö_5$ genommen, so dass diese wieder erlischt.

Im Hochspannungsteil würde sich eine Änderung der Speisespannung V nur insofern bemerkbar machen als die Zeit zur Aufladung der Kondensatoren C bzw. C' verlängert oder verkürzt würde, was bei nicht sehr grossen Änderungen von V natürlich keine Rolle

spielt. Weiter könnte die Spannung am Gitter von S Schwankungen unterliegen. Für den Betrieb von S kommt es jedoch nur darauf an, dass R_1 gross gegen den Innenwiderstand der leitenden, R_2 klein gegen den der sperrenden Röhre ist. Diese Bedingungen lassen sich natürlich in einem weiten Intervall der am Gitter von S anliegenden Spannung einhalten, so dass selbst grössere Schwankungen dieser Spannung (mehrere 10 Volt) das Funktionieren der Anordnung nicht beeinträchtigen können. Ebenso wenig stören auch geringe Änderungen der Emission von S wie sie z.B. durch Schwankungen des Heizstromes oder durch Verminderung des Emissionsvermögens der Kathode auftreten können.

Etwas wäre noch über ungenaues Einstellen bzw. Abbrand der Elektroden in der Funkenstrecke F' zu sagen. Hierbei wird die Spannung, auf die sich C bezw. C' aufladen, geändert. Das macht sich in der im Niederspannungskreis induzierten Spannung und der Energie des Zündfunkens bemerkbar. Da die induzierte Spannung jedoch nur gross genug sein muss, um die Zündung sicher zu bewerkstelligen, spielen geringe Änderungen keine Rolle. Die Energie des Zündfunkens ist klein gegenüber der Energie derHaup tentladung. Ihr genauer Wert ist aber auch unwesentlich.

(b) *Stabilität gegen äussere Störungen*

Um die Anfälligkeit gegen Störungen wie sie im Spektrallabor auftreten können, zu untersuchen, wurde in der Nähe der Anordnung ein Feussner-Funkenerzeuger mit Trafostufe 4 (15 kV_{eff}), $C = 6500$ pF, "ohne Induktion" betrieben. In einer Entfernung des Funkenerzeugers von mehr als etwa 1 m traten keine nennenswerten Störungen auf. Beim Näherbringen des Funkenerzeugers wurde der Frequenzgenerator beeinflusst, und zwar derart, dass eine Neigung zur Synchronisierung seiner Frequenz mit der Frequenz des Funkenerzeugers bestand. Doch dürfte eine so ungünstige Anordnung im Laboratorium sich wohl immer vermeiden lassen. Es ist zu bemerken, dass keine Vorkehrungen zur Abschirmung getroffen wurden.

VOL
7
1955/

Schlussbemerkungen

Die Funkenfolge des Aggregates wurde gemäss den vorliegenden Erfordernissen von 1–200 in der Sekunde einstellbar gewählt. Sie dürfte sich jedoch, falls es sich als notwendig erweisen sollte, erheblich erhöhen lassen.—Die aus Frequenzgenerator, Univibrator I und Hochspannungsteil bestehende Einheit dürfte nach geringfügigen Abänderungen im Hochspannungsteil (geeignete Dimensionierung der Senderöhre, Kondensatoren usw.) gut als "tandem-gap"-Hochspannungsfunkenerzeuger verwendet werden können. Ein Funkenerzeuger dieser Art vereinigt mit den bekannten Vorzügen der "tandem-gap"-Funkenerzeuger den weiteren, dass er eine äquidistante Funkenfolge liefert. Dies dürfte eine erhebliche Stabilisierung der Durchschlagsspannung mit sich bringen, so dass vielleicht besondere Stabilisierungsmittel, wie Düsen zum Durchblasen von Luft, vermieden werden können. Versuche darüber sind im Gange.

Der Gesellschaft zur Förderung der Spektrochemie und angewandten Spektroskopie und insbesondere Herrn Dr. H. Kaiser danke ich herzlich für die Mittel zur Durchführung der Arbeit.

Zusammenfassung

Es wird ein elektronischer Steuermechanismus für einen Niederspannungsfunkenerzeuger angegeben, der es erlaubt, in zeitlich gleichem Abstand aufeinander folgende Kondensatorentladungen (Pfeilstickerfunken) mit einer Frequenz von 1–200 in der Sekunde zu erzeugen. Ausserdem lässt sich die Zeit zwischen Entladung und Wiederaufladung des Kondensators einstellen. Ein Frequenzgenerator liefert die nötige Frequenz, ein Hochspannungsteil den Zündfunken. Für den zeitlich richtigen Ablauf aller Vorgänge sorgen zwei Univibratoren. Das Gerät dürfte nach geringfügigen Abänderungen auch als Hochspannungsfunkenerzeuger verwendbar sein.

Literatur

[1] Bardócz; *Spectrochim. Acta* **1953** **5** 397–408 (dort auch weitere Literatur).
[2] Elmore and Sands; *Electronics. Experimental Techniques.* New York, 1949, McGraw-Hill.

Spectrochimica Acta, 1955, Vol. 7, pp. 141 to 148. Pergamon Press Ltd. London

Multichannel instruments for fluorescent X-ray spectroscopy

J. W. Kemp, M. F. Hasler, J. L. Jones, and Louis Zeitz
Applied Research Laboratories, Glendale, Calif.

(*Received* 5 *August* 1954)
(*Accepted for publication* 8 *December* 1954)

Summary—Two multichannel instruments for fluorescent X-ray spectroscopy are described in detail, the Applied Research Laboratories' X-ray Research Quantometer and X-ray Industrial Quantometer. Each instrument uses a 60 kV, full-wave, filtered supply with a Machlett OEG-60 tube. The XRQ has been used with multiple flat-crystal spectrometers; the XIQ with multiple flat- and curved-crystal spectrometers. The recording circuits are very similar to those used in the Applied Research Laboratories' line of optical emission Quantometers.

Although the basic principles of fluorescent X-ray analysis have been known for a long time, serious attempts to use this method have been made only in the last three or four years. A review of the current literature indicates that a number of laboratories have studied this method of analysis [1, 2, 3, 4, 5, 6, 7]. Generally, two types of instruments have been used: Commercial diffraction units converted to crystal spectrometers, or special instruments constructed in the various laboratories. Practically all of this equipment provides only single-channel recording.

It was felt that a completely new set of instruments was required to meet the needs of the industrial analyst. A study of this problem over a period of several years has led to the design of the instruments to be described here. The X-ray Research Quantometer (XRQ) was the first instrument to be designed on the basis of this study. Experience with this instrument led to the design of the X-ray Industrial Quantometer (XIQ).

The X-ray tube supply

The basic circuit used is a full-wave rectifier. The usual secondary current meter, flow-sensing switch, master switch, etc., have been used. Since the unit is intended for use with various non-dispersive instruments where accurate voltage control is important, as well as with dispersive units, the supply is filtered and a resistance-type kilovoltmeter in the secondary is used. The specifications for the standard unit are given in Table 1. Since ratios of intensities rather than absolute intensities are measured with the Applied Research Laboratories' X-ray Quantometers,

Table 1. *Power supply specifications*

Input	230 V, 50–60~
Output	60 kV, 30·5 ma or 37·5 kV, 50 ma max.
Rectifier	Two G.E. KR-7 tubes
Filter	0·1 μF
Ripple	3·0 per cent at 37·5 kV 50 ma 10·5 per cent at 10 kV 50 ma
Voltmeter resistors	30—Two megohm $\pm$ 1 per cent pyrolytic carbon resistors
Voltmeter accuracy	2 per cent
Current control	Rheostat in filament transformer primary
Voltage control	Variable transformer in power transformer primary

extreme regulation of the supply is not required. This was demonstrated, as shown in Table 2, by measurement of the precision of stainless-steel analysis with the X-ray Research Quantometer with 0·1 per cent input voltage regulation and with the X-ray Industrial Quantometer with no regulation. Conditions were such that the precision was limited by the maximum intensity allowable with the receivers used, so that other differences between the instruments did not enter into the experiment.

Table 2

Element	XRQ		XIQ	
	Concentration %	*Coefficient of variation** %	*Concentration* %	*Coefficient of variation** %
Iron	71·0	±0·5	72·9	±0·4
Nickel	9·12	±1·0	8·64	±1·0
Chromium	17·48	±1·1	17·14	±1·1
Per cent standard deviation of absolute Fe intensity		±0·7		±10·6

* The coefficient of variation is the standard deviation of the concentration divided by the concentration times 100. It should be noted that the probable error (P.E.), used by some workers, is 0·67 times the standard deviation.

The percent standard deviations and the coefficients of variation were determined from twenty runs of one minute each. Although satisfactory results can be obtained with no regulation, tube filaments should be protected by the use of moderate (1 per cent) regulation. Physically, the supply is housed in a bench-height cabinet (Fig. 6) constructed so that various spectrometers can be mounted on top. The high-voltage section, shown in Fig. 1, is completely oil-immersed and features a hermetically sealed unit containing the power and filament transformers. This sealed portion is filled with a specially processed high-dielectric strength oil and is contained within the same water-cooled tank as the remainder of the high-voltage components. These included the voltmeter resistors, rectifiers, and capacitor terminals. In later models, the entire capacitor has been included in the tank. Connection to the X-ray tube is made with standard X-ray cable, so that no unprotected high-voltage points exist in the unit.

The spectrometers

Three types of spectrometers have been used: non-dispersive, flat-crystal dispersive, and curved-crystal dispersive. Each type has its field of usefulness, although it appears that curved crystals will eventually replace the flat crystals altogether.

The non-dispersive receivers are made up of Geiger counters or scintillators and filter holders; in other words, they serve as X-ray filter photometers. These can be used in simple analytical problems and in thickness gauging. For example, Table 3 gives the data for zinc-dipped steel plate. Here, iron radiation is excited in the base-plate and measured after absorption by the zinc coating. Precision data are given for twenty-one runs on a single area. Due to the non-uniformity of dipped plate, large areas must be integrated to obtain accuracies approaching this precision.

VOL 7 1955/

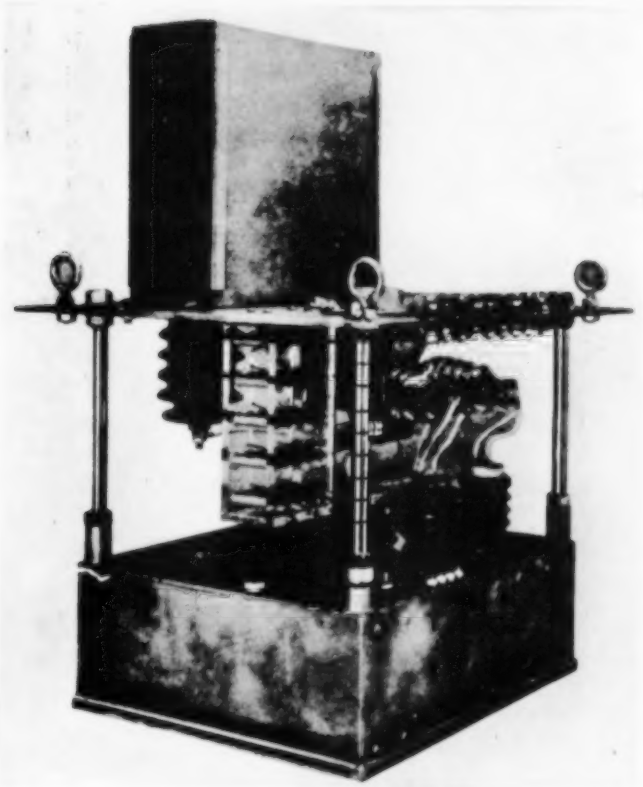

Fig. 1. High-voltage, X-ray tube supply, shown without tank.

VOL.
7
65/56

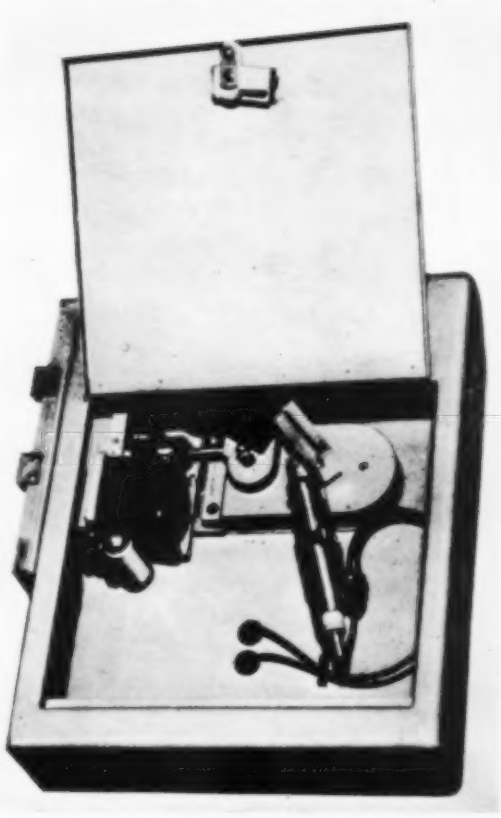

Fig. 3. Motor-driven flat-crystal spectrometer.

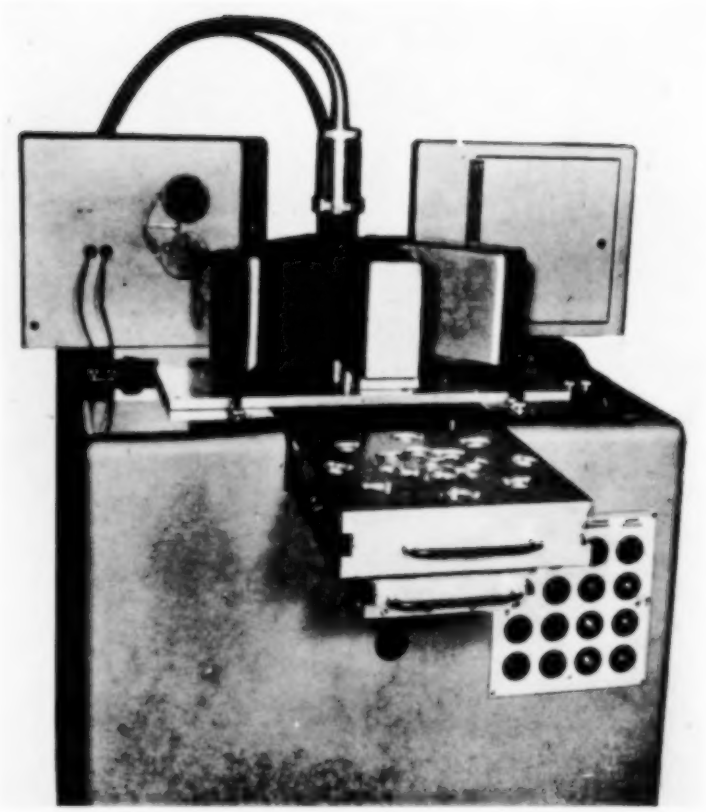

Fig. 5. X-ray Research Quantometer, showing two dispersive spectrometers (right and left) and three non-dispersive units (centre). Filter and sample drawers are shown open.

VOL.
7
1955/

The XRQ was also designed so that samples could be placed in the filter positions and an absorption analysis carried out using a variety of samples as secondary emitters. For all but the simplest analytical problems, dispersive analyzers are required. Most of the work at the Applied Research Laboratories has been done with flat crystals. The general arrangement used is shown in Fig. 2.

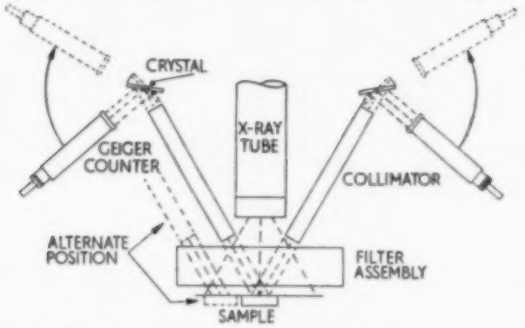

Fig. 2. Schematic drawing of arrangement of multiple flat-crystal spectrometers.

Since high dispersion is desirable, aluminium* or lithium fluoride single crystals are used. The (200) planes of aluminium are roughly equal in intensity and dispersion

Table 3. Zinc plate gauging

Tube	Machlett AEG-50T, Tungsten Target					
Power	15 kV, 20 ma					
Fe Channel Filter	0·0030-cm Fe Sheet					
Exposure	15 sec.					
Receivers	Scintillators					
Precision						
Zn thickness (oz/sq ft)†	0·33	0·55	0·65	1·00	1·22	1·35
Coefficient of variation (%)	0·4	0·3	0·4	0·3	1·9	1·7

to the (200) planes of lithium fluoride. Generally, $\frac{1}{2}°$ collimators are used where possible, and $\frac{1}{4}°$ collimators are available. All flat-crystal spectrometers were designed for the 1- to 3-angstrom range, although they can be used down to 0·7 Å with some loss in intensity due to vignetting. Single, curved LiF or NaCl crystals have been developed for the XIQ-type instrument, whose planes are cylindrically bent parallel to a given radius and the surfaces cylindrically ground to one-half this radius. These crystals are used in focusing spectrometers in the same manner as concave gratings are used in Rowland-type mountings. A 56-cm diameter spectrometer is used from 0·35 to 1·0 Å, and a 20-cm diameter spectrometer from 1·0 to 4·0 Å. Some work has also been done above 4 Å with a 10-cm diameter helium atmosphere unit.

The XRQ is provided with motor- and hand-driven spectrometers (Fig. 3) as well as with only hand-driven units. The XIQ is provided with semi-fixed units designed to be set to a particular wavelength. A scanning arrangement is provided to allow scanning over a few degrees for final alignment.

* Obtainable from Horizons, Inc., Cleveland 4, Ohio.
† Note: 1 oz/sq ft = 30·5 mg/sq cm.

The receivers and recording circuits

On the basis of sensitivity requirements, Geiger-Müller tubes were designed into the original instruments. In this work, the usual procedure for measuring integrated X-ray intensities has been to use a Geiger tube and to record the number of counts in a given time or the time for a predetermined number of counts. It is well known

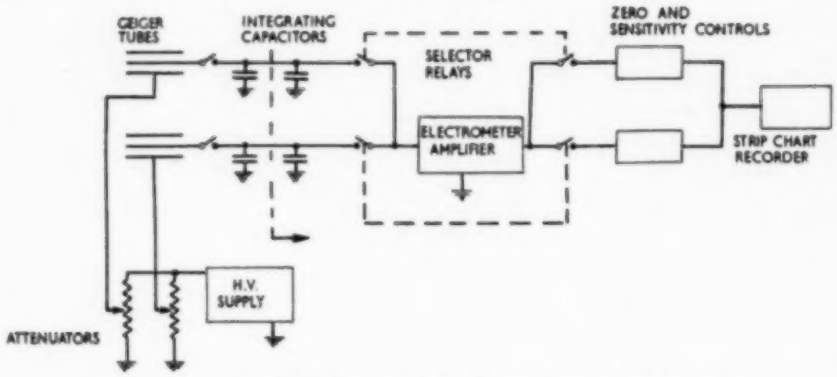

Fig. 4. Simplified diagram of receiving and recording circuits.

that the standard deviation of a total count is the square root of the number of counts. This gives 1 per cent standard deviation for 10,000 counts and 0·3 per cent for 100,000 counts. This applies, however, only when all factors involved—source, power supply, etc.—are held absolutely constant. Since absolute constancy of all factors is difficult to attain in practice, it was decided to use the ratio system that has been used so successfully in optical spectroscopy. A simplified circuit diagram of this system is shown in Fig. 4. All of the Geiger pulses are collected by the integrating capacitors and the voltages attained by the capacitors at the end of the integration period are read by a standard Applied Research Laboratories' Electrometer Amplifier. All of the circuitry to the right of the dotted line is exactly the same as that used in the Applied Research Laboratories' Optical Quantometers. In this circuit, the logarithm of the Geiger-tube output is a linear function of Geiger-tube voltage in the "plateau" region, much the same as the characteristic of a multiplier phototube in the medium-voltage range. The high-voltage supply designed for the X-ray instruments consists of an electronically regulated unit of the same design as that used for the phototubes in the latest optical Quantometers. For high pulse-rates, sensitive, short-dead-time Geiger tubes are required. In order to have reasonable values of integrating capacitance, small average pulse size is desirable. This can be controlled to some extent by attenuation of the Geiger-tube voltage, but only in the plateau region. Capacitance could be reduced by charging to higher than the 4-volt maximum used. This, however, is undesirable, since the integrator voltage reduces the effective Geiger-tube voltage as the charge builds up and contributes to nonlinearity of the system.

A study of commercially available Geiger tubes indicated that approximately 60,000 counts could be integrated over 1 minute, using capacitances of the order of 50 μF. This condition is obtained by using Anton 202T tubes at 1375 volts. In

VOL 7 1955/

VOL.
7
55/56

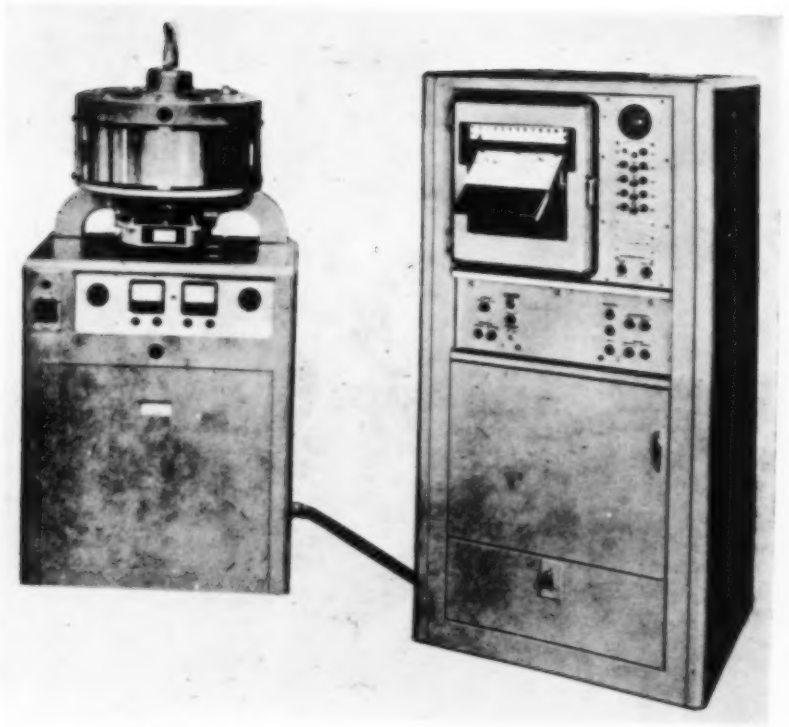

Fig. 6. X-ray Industrial Quantometer, including console.

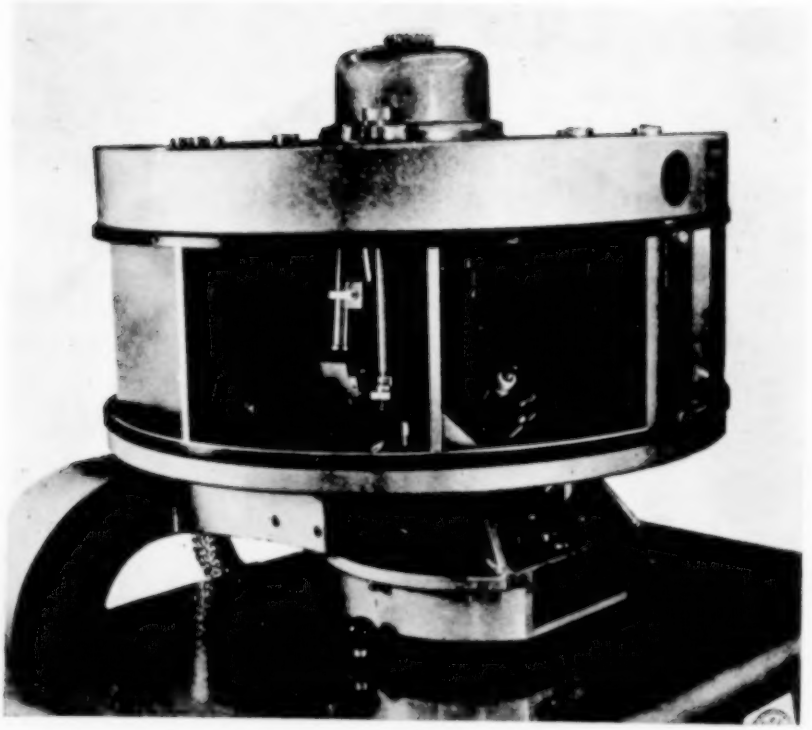

Fig. 7. Spectrometers and sample handling mechanism, X-ray Industrial Quantometer.

VOL.
7
1955/

operation, one Geiger tube receives radiation by some means and utilizes it for control just as the internal standard system is utilized for control in optical emission analysis. In a non-dispersive system, this radiation could be from the sample being analyzed or from a standard sample, with appropriate filters in each case. In a multichannel dispersive system, it could be an internal standard line in the sample, or a line from an external standard sample. The output of this Geiger tube is integrated and recorded during the exposure. Upon reaching a predetermined value, the recorder disconnects all Geiger tubes. Automatic switching then connects each integrator in turn to the amplifier and recorder, switching in the proper sensitivity and zero controls at the same time. Thus, the ratio of integrated intensity of each channel to the standard channel is recorded. This allows the same recording and calibrating techniques to be used that are used with the optical Quantometers. The primary advantage of this system is its ability to record a number of elements in the time required to record one element with the usual scanning spectrometer. A second advantage is the higher precision obtained under industrial operating conditions, as can be seen from the data given in Table 2. There is one disadvantage inherent in this system, however. Intensities should be limited to 60,000 counts per minute because of Geiger-tube non-linearity, and for many problems much higher intensities than this are available. The 60,000-count limit means that the maximum precision of the ratio of two channels obtainable in one minute is $\pm 0{\cdot}6$ per cent standard deviation.

To make full use of the intensities available, a scintillator has been designed consisting of Patterson CB-2 screen material deposited on an RCA 6199 multiplier phototube. Since a non-dispersive head viewing an external standard is generally used for control, there is always sufficient intensity to allow the use of a scintillator in the standard channel. This improves the maximum precision obtainable in one minute to $\pm 0{\cdot}4$ per cent standard deviation. When scintillators can be used in both channels, precision improves to $\pm 0{\cdot}1$–$0{\cdot}2$ per cent standard deviation. Where scintillators can be used, 2 μF rather than 50 μF are required for integration.

The X-ray research quantometer

The XRQ was the first instrument to be designed, and has been used for much of the analytical research in the authors' laboratories. It requires a separate base cabinet, but uses the same power supply and console as the XIQ.

Eight positions have been provided around an end-windowed X-ray tube in which may be placed any combination of dispersive or non-dispersive receivers, as shown in Fig. 5. (A similar instrument has been described by ADLER and AXELROD, [9].) Each receiver is mounted upon a track, so that it may be positioned above either of two ports. The inner port, in each case, receives the radiation from a central sample position directly below the X-ray tube, while the outer port receives radiation from a secondary position which can be used for a reference standard. The ports are provided with automatic shutters to allow removal or replacement of the receivers without danger to the operator. The unknown and reference samples are placed in a sliding compartment which is positioned under the X-ray tube. Fig. 5 shows this compartment pulled out to loading position. A safety shield automatically covers the internal X-ray ports when this compartment is drawn out,

providing complete protection for the operator. Between the sample compartment and the receiver section is another sliding compartment providing for the use of the various filters and apertures which may be required in any of the receivers. In this compartment may also be placed cells for use in absorption work. In conjunction with the sample compartment, these cells may be used in the beam from a secondary emitter. Should it be desirable to have the cells in the primary beam of the X-ray tube, the tube may be placed below the cells and pointing upward. This filter compartment is also provided with an automatic safety shield. The integrating capacitors for the receivers are mounted in the cabinet and the front panel contains switches for selecting the capacitance values for each channel as well as attenuators for controlling the Geiger voltage.

The X-ray industrial quantometer

The complete XIQ, shown in Fig 6, provides for eight channels with any combination of dispersive or non-dispersive receivers. The eight receivers are housed in a single enclosure and the entire spectrometer (Fig. 7) mounts directly on top of the source unit. In the centre of the housing is the end-on OEG-60, tungsten target X-ray tube placed so that its window is 5·6 cm from the horizontal surface of the sample, which is held by spring pressure against a flat aperture plate to assure that the tube-to-sample distance is constant. A lead aperture in front of the window of the X-ray tube permits X-rays to fall only upon the usable area of the sample, thus reducing extraneous scattered radiation to a minimum. The sample surface forms part of the walls of a completely enclosed brass chamber in which the collimators or slits for the eight receivers are mounted.

The ends of these collimators are 5 cm from the centre of the sample and are spaced at equal angles around the X-ray tube. They are placed at an angle of 47° from the axis of the tube. For the flat-crystal receivers, the collimators are of the Soller slit type and consist of thin parallel sheets of phosphor bronze held in a square tube 20·4 cm long with sheet spacings to provide various resolutions as required. The remainder of the flat-crystal receiver consists of a simple and rugged assembly providing for a single flat crystal of lithium fluoride, aluminium, or other material, and a Geiger counter. An external vernier control is provided for rotation of the crystal through a simple linkage, so that after the initial rough setting to a given spectral line, the crystal may be oriented accurately during X-ray excitation to set it upon the peak of the line. Means are provided for adjustment of the position of the collimator in rotation about its own axis for accurate alignment with the axis of rotation of the crystal, so as to insure maximum resolution.

The curved-crystal units designed for use in the XIQ are also of semi-fixed design, with means provided for setting to a particular wavelength. The receiver, shown schematically in Fig. 8, consists of a primary slit, a curved crystal, a secondary slit, and a Geiger counter or scintillator. The primary slit, of fixed design, is provided in various widths to provide a balance between resolution and intensity requirements, and is held in a fixed relation to the sample at a distance of 5·1 cm. The single crystal, of lithium fluoride, rock salt, or other material, is bent, ground, and polished accurately to provide maximum intensity and resolution. The

VOL.
7
1955/5

secondary slit is similar to the primary slit and is also provided in various widths to fit a particular problem. As in the flat-crystal unit, the spectrometer may be scanned through a few degrees for final alignment.

The nondispersive receivers utilize a simple tube collimator to prevent the Geiger tube from "seeing" radiation other than that proceeding from the sample. Filter holders for 1·27 cm diameter briquettes or foil discs are integral with the collimators. Scintillators may be used in place of Geiger tubes.

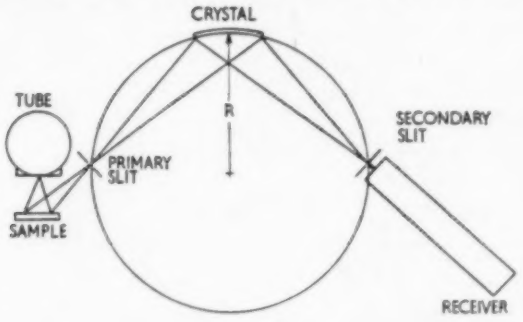

Fig. 8.

One or more positions may be provided for external standard samples for use with either nondispersive or dispersive channels. A specially designed sample-handling mechanism forms an integral part of the spectrometer. This sample changer incorporates a labyrinth path in all directions from the X-ray chamber to insure complete safety for the operator at all times and to avoid the necessity for turning off the X-rays while changing samples. Placement or removal of the sample from its holder requires only a simple one-hand motion to compress the holding spring with the sample. A mirror allows accurate positioning of the sample surface with respect to the X-ray beam. Two positions are provided so that a sample may be placed in its holder while another is being analyzed. It then requires the motion of a single control lever to reverse the positions and allow analysis of the second sample. The high-voltage X-ray cable, X-ray tube water-supply and return, and the Geiger power- and signal-leads are all enclosed within a single sheath which connects the spectrometer to the X-ray source upon which it is mounted. The console containing the electronic supplies and recording circuits is essentially the same as the unit used with the Applied Research Laboratories Optical Quantometers. If desirable, a single console can be used to record the outputs of an optical and an X-ray spectrometer. This suggests the use of a combined optical-X-ray laboratory; the Optical Quantometer for low concentrations and the X-ray Quantometer for high concentrations.

Limitations

These instruments are not suitable in their standard form for the analysis of low concentrations of elements lower than atomic number 20. The limits of detectability obtainable for the remaining elements are a function of the base material as well as of the various instrumental factors involved. The limit, defined as that

concentration at which coefficient of variation of 25 per cent will be obtained, varies from 1 ppm to several thousand parts per million. Precision may be limited by the intensity available, the intensity limitations of Geiger counters, or the precision of the circuits. In the first case, curved crystals offer a considerable advantage, and in simple systems, non-dispersive techniques can be of help. In the second case, the use of curved crystals or non-dispersive techniques can often provide sufficient intensities to allow the use of scintillators. Where scintillators can be used, coefficients of variation of 0·1 to 0·5 per cent can be expected. The electronics used have been shown to provide percent standard deviations of intensity ratios of 0·1–0·2 per cent. Accuracy is a function of instrumentation, excellence of standards, and the care with which working curves are constructed. Where the last two points have been properly considered, accuracies approaching the precision of the system are obtainable.

References

[1] Friedman, H., Birks, L. S., and Brooks, E. J.; A.S.T.M. Special Technical Publication No. 157, p. 3 (1954)
[2] Sherman, J.; A.S.T.M. Special Technical Publication No. 157, p. 27 (1954)
[3] Brissey, R. M., Liebhafsky, H. A., and Pfeiffer, H. G.; A.S.T.M. Special Technical Publication No. 157, p. 43 (1954)
[4] Noakes, Gorden E.; A.S.T.M. Special Technical Publication No. 157, p. 57 (1954)
[5] Carl, Howard F., and Campbell, William J.; A.S.T.M. Special Technical Publication No. 157, p. 63 (1954)
[6] Davis, Elwin N., and Van Nordstrand, Robert A.; *Anal. Chem.* 1954 **26** 973
[7] Mortimore, D. M., Romans, P. A., and Tews, J. L.; *Applied Spectroscopy* 1954 **8** 24
[8] Birks, L. S., Brooks, E. J., and Friedman, H.; *Anal. Chem.* 1953 **25** 692
[9] Adler, Isidore, and Axelrod, Joseph M.; *J. Opt. Soc. Amer.* 1953 **43** 769

VOL
7
1955/

Spectrochimica Acta, 1955, Vol. 7, pp. 149 to 164. Pergamon Press Ltd., London

Electrode vapour jets in spark discharges

C. M. CUNDALL and J. D. CRAGGS
Department of Electrical Engineering, The University of Liverpool

(*Received* 3 *December* 1954)

Summary—A description is given of experimental observations on the properties of the electrode metal-vapour clouds emitted in spark discharges, using a simplified high-voltage supply circuit which provides rectangular current pulses. Measurements of jet propagation velocities and of rates of electrode erosion were made, and are discussed in terms of recent theories of electrode erosion. Image-converter photographs of the metal clouds were taken.

1. Introduction

It is well known that when a spark discharge occurs between metallic electrodes, the latter are eroded and vapour travels into the spark-gap in the form of high-velocity jets. The metal atoms in the jets are excited and emit radiation. The fundamental processes involved in the release of the metal from the electrode surface, the formation of the jets, and the subsequent excitation are not yet understood with certainty, and few relevant measurements have been made. A notable exception is the work of HAYNES [1], who investigated light emission from jets originating at a mercury-pool electrode. A theory of jet production has been put forward by FINKELNBURG [2] which appears to fit the results of HAYNES, and a further theoretical treatment has been published by LLEWELLYN JONES [3]. Some preliminary experiments on the excitation and transport of metal vapour in short sparks in air have been performed by WILLIAMS, CRAGGS, and HOPWOOD [4], using Mg, Cd, and Ba electrodes, and by various other authors.

The aims of the present experiments were to determine the behaviour of the metal-vapour jets from anodes and cathodes composed of various metals for transient (spark) discharges in which the current is maintained at a constant value for a short time (3 to 4 μsec), and then suddenly falls to zero.

The following properties of the jets have been considered:

(a) The velocity of propagation.
(b) The light emission from the jets with both spatial and temporal resolution.
(c) The appearance of the jets using high-speed photographic techniques.
(d) The electrode-voltage drops and the weight of metal eroded from the electrodes per spark, in order to investigate the applicability of some published theories (see above).

The work described here will, it is hoped, be of interest in the spectrochemical analysis of metals where spark-to-spark fluctuations in the light emission from the vapour jet provide a limitation to the accuracies obtainable. Mg, Zn, Cd, and W were the metals chosen for investigation as representing a wide range of physical properties. Single sparks of 600- and 200-amp magnitude and 3- and 3·5-μsec duration, respectively, in hydrogen at about atmospheric pressure were used.

10

2. Description of apparatus

A calibrated spectrometer, photomultipliers, amplifier, and synchronized oscillograph were used to measure the relative intensities of spectral lines as a function of time. This system and the calibration techniques have been already described (TSUI-FANG, CUNDALL, and CRAGGS [6]). Using the optical system of Fig. 1 (in conjunction with a traversing platform on which the spark-chamber was mounted), light could also be examined from narrow regions along the length of the spark.

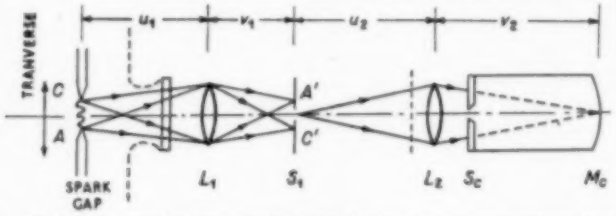

Fig. 1. Optical system for measuring the velocity of vapour propagation, etc., in a spark discharge.

The 600-amp sparks were generated with a modified form of chopping circuit described by DURNFORD and MCCORMICK [5], and the 200-amp sparks by discharging a suitable length of coaxial cable through the spark-gap in series with its characteristic impedance.

The image-converter, the principle of which is described by TURNOCK [7, 8], was used to take $\frac{1}{2}$-μsec duration photographs at various stages in the life of the spark. The shutter of the image-converter required an exposure pulse of $\frac{1}{2}$-μsec duration and 3,500-V magnitude, which had to be applied at a controllable time after the beginning of the spark-current pulse. A block diagram of the control circuit is shown in Fig. 2. The exposure pulse is seen to be initiated, after a variable delay, by a pick-up pulse from the breakdown of the spark-gap. For monitoring purposes, a tapped-off part of the exposure pulse is applied to one Y-plate of the oscillograph, whilst the other plate is left free. The oscillograph trace on which the spark breakdown and the exposure pulse could both be seen, enabled the exact time of exposure relative to breakdown to be measured. Full details of the apparatus are given by CUNDALL [9]. No effort was made to obtain pure gases. The hydrogen used for the main experiments contained up to about 0·5 per cent of oxygen. Some experiments were made with purer hydrogen in which the contamination was due solely to the vacuum-system residuals giving a total impurity content of about 1 in 10^4. It was then found that, despite strong irradiation from radioactive cobalt, the statistical lags were so great and so variable as to make high-speed oscillographic observations difficult, if not impossible. This effect is presumably due to the removal of (oxide?) electrode surface layers in the pure hydrogen, and will ultimately have to be countered in some way, since spark-channel investigations in pure gases are, for many reasons, highly desirable.

3. Experimental procedure

The experiments were all performed using spectroscopically pure metals in rod form. The electrodes were turned in a lathe to form a 60° point, except for Cd,

VOL. 7 1955/5

where rounded electrodes were also used. Irradiation of the spark-gap was found necessary in order to reduce the long statistical time-lags which resulted from the gradual removal of the oxide layers on the electrode surface by the sparks, even in the relatively impure hydrogen mentioned above. This was provided by 10 mg of radioactive cobalt placed near the electrodes. Throughout the work a 7-mm long spark-gap was used.

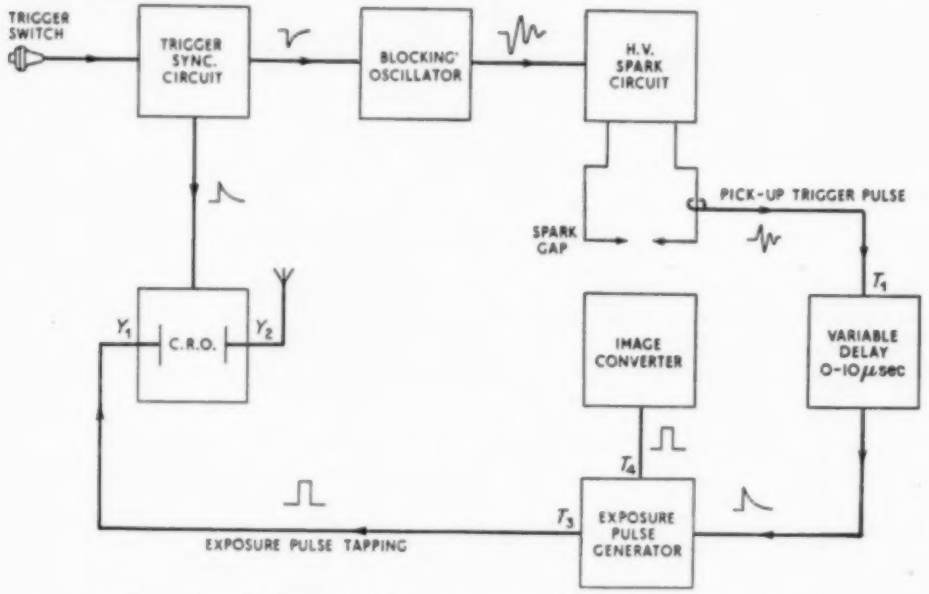

Fig. 2. Block diagram of the image-converter high-speed camera system.

To investigate jet velocities and intensities, using the optical system of Fig. 1, light intensity-time oscillograms of various metal lines were recorded at successive gap positions 1 mm apart. The slit S was 0·23 mm, so that light was taken from 0·12 mm of the total gap-length of 7 mm. The following electrode arrangements were used—

Cathode	Mg	Mg	W	Zn	Zn	W	Cd pointed and rounded	Cd pointed and rounded	W
Anode	W	Mg	Mg	W	Zn	Zn	W	Cd pointed and rounded	Cd pointed and rounded

This enabled the behaviour, for example, of a Mg cathode jet to be investigated both in the presence of a Mg anode jet and with no appreciable anode jet (i.e., with W anode).

The voltage-drop across the gap was measured as a function of time, using the nonlinear voltage divider shown in Fig. 3. Oscillograms were taken of the gap voltage for a range of gap-lengths from 0·2 to 7 mm. The gap-length was altered

between readings by means of a calibrated screw on the spark chamber which drew the rod holding one electrode through a Wilson seal.

The electrode weight changes were measured by weighing the electrodes on a microbalance before and after the passage of 1,000 sparks, which were counted

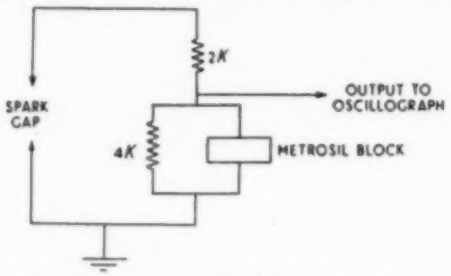

Fig. 3. Nonlinear potential divider circuit.

mechanically. Special handling and weighing techniques had to be employed and careful checks were made to ensure reproducibility of the weight losses.

$\frac{1}{2}$-μsec duration photographs of the sparks were taken, using the image-converter, and recorded on 35-mm filter (5G91), using an f/1 recording camera in

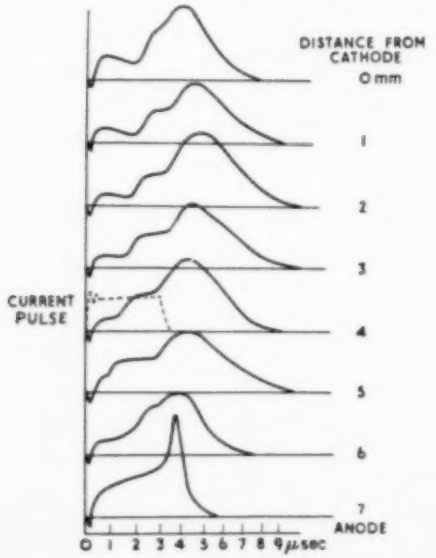

Fig. 4b. Tracings of oscillograms of Mg 3,838-Å radiation for various gap positions, in a 7-mm gap. Mg cathode and W anode.

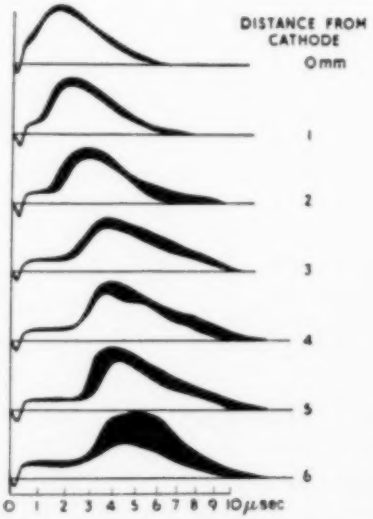

Fig. 4c. Superposed sets of oscillograms for various gap positions to show the fluctuations. Mg cathode, W anode. Radiation: λ3,838 Å (Mg.)

front of the fluorescent screen. The exposures were taken at approximately $\frac{1}{2}$-μsec intervals throughout the visible life of the 600-amp, 3-μsec spark. Simultaneous oscillograph records were made from which the exact time of the exposure with respect to the spark-current pulse was measured.

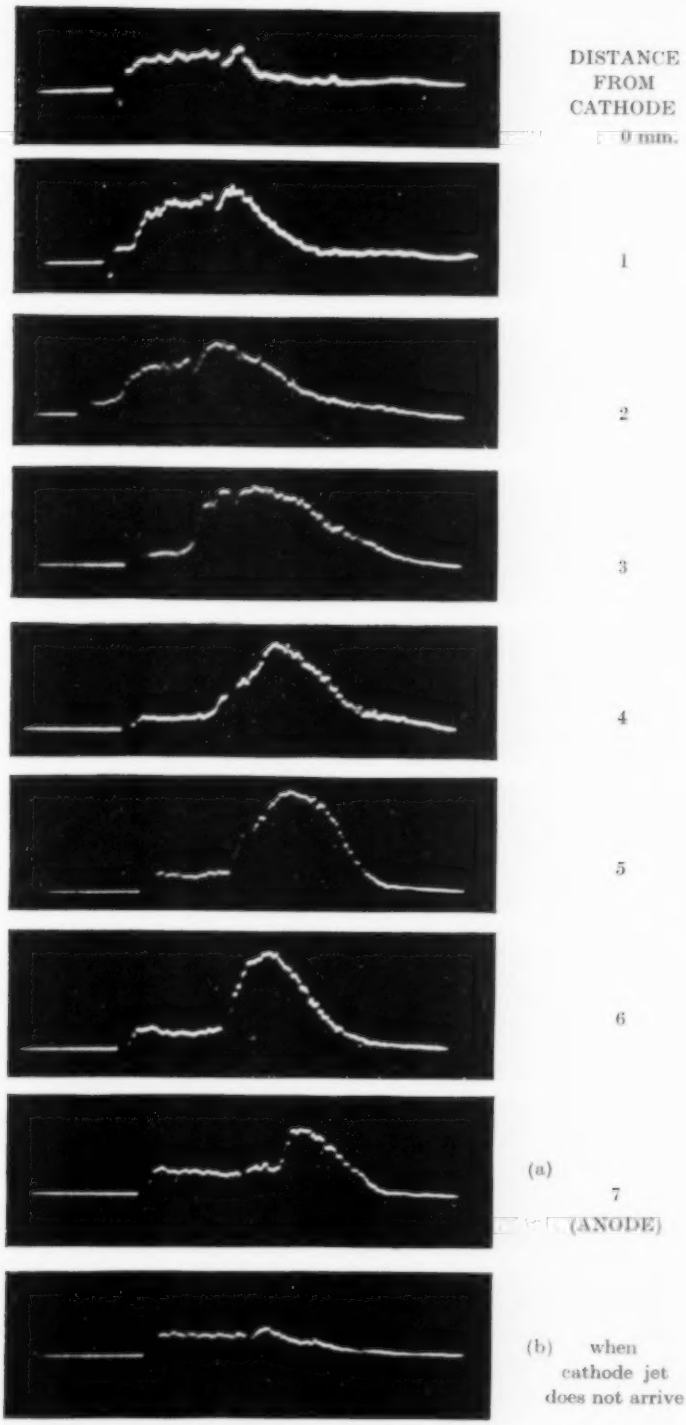

Fig. 4 (a). Oscillograms of the 3838 AU Mg radiation taken at various gap positions in a 7 mm gap. 7 (a) and 7 (b), both taken at the anode, show the extreme fluctuations at that position. The time scale, which is not strictly linear can be deducted from Fig. 4 (b). Approximately 2·4 cm ≡ 4 μsecs.

VOL.
7
1955/5

4. Experimental results

4.1. *Jet velocity measurements*

A typical series of intensity-time oscillograms for the Mg triplet 3,838 Å as a function of gap position, for light from a Mg cathode jet, is shown in Fig. 4a. Oscillograms for anode and cathode jets of other metals are similar, except for the Mg-anode jet (see below). The arrival of the jet at a specific gap position is shown by a sudden increase in the light intensity. In the case of the light from a

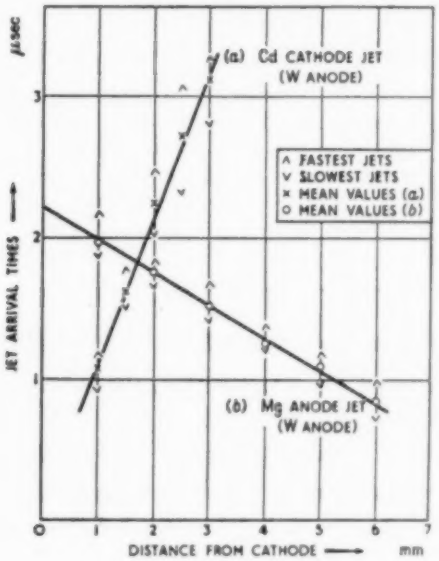

Fig. 5. Data on jet transport.

Mg-anode jet (see Fig. 4b), this increase is small and is followed by a further sudden rise at the end of the current pulse (a possible significance of this is discussed later). The envelopes of the superimposed tracings of ten successive oscillograms similar to Fig. 4a are shown in Fig. 4c. These emphasize that the spark-to-spark fluctuations of a specific line are greatest when measured furthest away from the vapour-emitting electrode. This may have an application to the spectroscopic analysis of metals.

Typical jet-velocity curves are those shown in Fig. 5 for a Mg-anode jet and a Cd-cathode jet. The mean arrival time and the extreme values are plotted for the ten oscillograms taken at each gap position. In these, as in most cases, the curves are approximately linear from 1 mm, indicating a constant velocity through this part of the gap.

Table 1 shows the derived jet velocities. In some cases higher velocities were recorded within 1 mm of the electrode surface, but the sensitivity of the system was not sufficient to measure these accurately.

Table 1. *Vapour jet velocities* (cm/sec)

Metal	*Electrode configuration*	600 amp		200 amp	
		Cathode jet	*Anode jet*	*Cathode jet*	*Anode jet*
Mg	Both Mg	$1{\cdot}7 \times 10^5$	$4{\cdot}0 \times 10^5$	—	—
	Mg-W	$1{\cdot}7 \times 10^5$	$4{\cdot}2 \times 10^5$	$1{\cdot}47 \times 10^5$	$4{\cdot}7 \times 10^5$
Zn	Both Zn	$1{\cdot}3 \times 10^5$	Only just detectable	—	—
	Zn-W	$0{\cdot}96 \times 10^5$	$1{\cdot}95 \times 10^5$	$1{\cdot}02 \times 10^5$	$1{\cdot}45 \times 10^5$
Cd	Cd-W	$1{\cdot}02 \times 10^5$	$1{\cdot}2 \times 10^5$	$1{\cdot}02 \times 10^5$	$1{\cdot}08 \times 10^5$
Cd rounded	Cd (rounded) Cd-W	$2{\cdot}7 \times 10^5$	—	—	—

The following observations may be made on the velocities of Table 1:

(i) The anode jet is in all cases faster than the cathode jet in the same discharge conditions.

(ii) The jet velocities are highest for Mg and lowest for Cd.

(iii) The velocities are lower in the 200-amp discharge.

(iv) Higher jet velocities are recorded for rounded electrodes as compared with pointed electrodes.

4.2. *Luminous intensity of the jets*

A measure of the luminous intensity of the jet as a function of gap position has been obtained by measuring the relative peak light intensity of a specific line at different gap positions, correcting where necessary for background. Some typical curves are shown for the 600-amp discharge in Fig. 6. The accuracy of these intensities is severely limited by the large fluctuations from spark to spark, particularly at large distances from the electrode at which the jet originates (see Fig. 4c). Anode and cathode jets are found to differ considerably. Cathode jets start at a relatively high intensity, which remains approximately constant up to 1, 2, and 4 mm travel for Cd, Zn, and Mg, respectively, and then falls off and reaches zero intensity some 4 μsec later (unless the jets have already reached the anode). The intensity of the anode jet is initially relatively low, and increases as it proceeds into the gap, and only shows any appreciable subsequent decrease in the case of Cd. Similar results were found for the 200-amp discharge. It appears that the intensity of the cathode jets is greater than that of the anode jets (see the image-converter photographs).

4.3. *Voltage drops and weight changes*

The total gap voltage was measured from the oscillograms taken by means of the nonlinear voltage divider (Fig. 3) at 1, 2, and 3 μsec from breakdown. Typical curves of voltage-drop against gap-length for Mg, Zn, and W at 2 μsec are shown

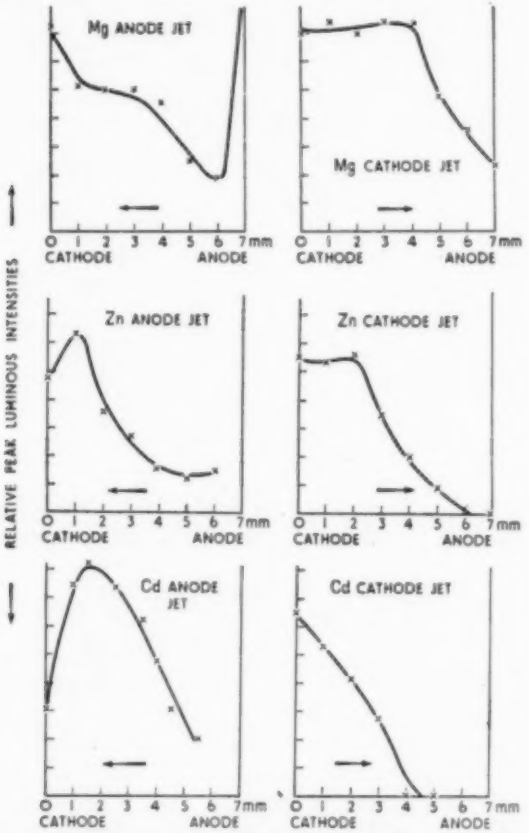

Fig. 6. Curves relating the relative peak luminous intensities in the jets to the gap position for cathode and anode jets. 600-amp 3·5-μsec sparks in hydrogen.

in Fig. 7. These are seen to be similar to those derived by CRAIG [10] for 100-amp, 6-μsec discharges. From about a 1-mm spacing the curves are linear, but at shorter gaps for the metals examined, excepting W, they deviate from the continuation of the linear portion, which is shown dotted. At longer gaps the linear portions almost coincide, and the differences between different metals are most pronounced for the shorter gaps.

The curves have all been extrapolated to find V_0 and V^1 (see Fig. 7), and the results, given in Table 2, show little significant difference for the metals considered. Either V_0 or V^1 (see Fig. 7) and the results, given in Table 2, show little significant difference for the metals considered. Either V or V^1 may be defined as the total electrode drop, although there is no direct evidence in spark or arc discharges

Table 2. Values of V_0 and V^1 (see Fig. 7) for various electrode combinations. 600-amp, 3-μsec sparks in hydrogen.

Electrodes		1		2		3 μsec	
Cathode	*Anode*	V_0	V^1	V_0	V^1	V_0	V^1
Mg	Mg	64	115	32	50	30	47
Mg	W	63	77	35	51	34	49
W	Mg	58	95	26	54	26	50
Zn	Zn	51	76	28	48	28	45
Zn	W	54	97	29	49	27	46
W	Zn	64	76	34	48	31	46
Cd	Cd	67	97	31	45	29	41
Cd	W	67	84	32	44	31	43
W	Cd	48	72	24	36	22	35
Cd (rounded)	Cd	38	75	10	37	7	26
W	W	80	80	44	44	43	43

that V or $V^1 \equiv V_c + V_a$, where V_c and V_a are the cathode and anode voltage drops. It is thought, however, that V probably gives an upper limit to the value of $V_c + V_a$.

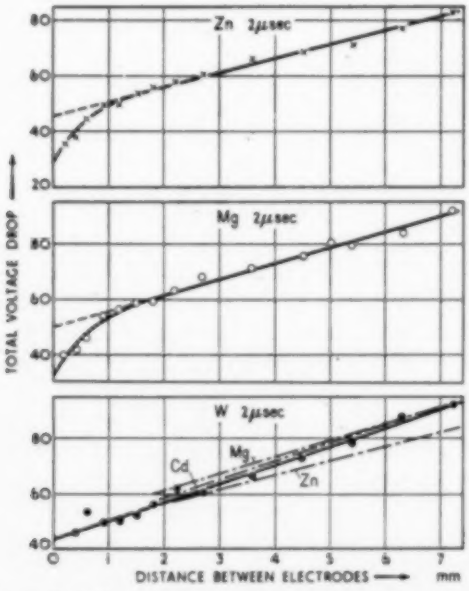

Fig. 7. Voltage-drop curves for 600-amp 3-μsec sparks in hydrogen between Zn, Mg, and W electrodes at 2 μsec after breakdown.

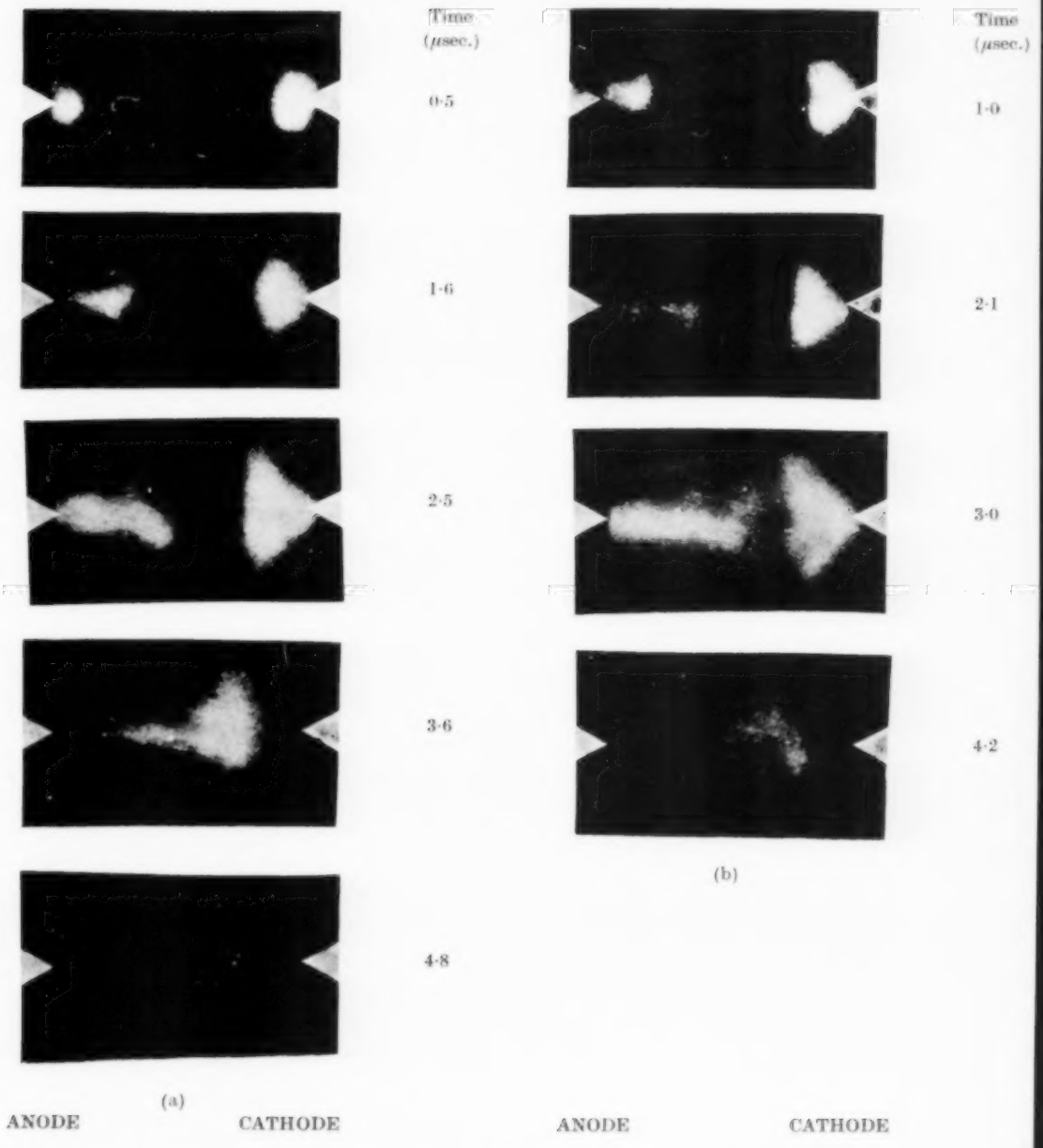

Fig. 8. Image-converter photographs of 600-amp, 3-μsec sparks between Zn electrodes. (0·5-μsec exposure.)

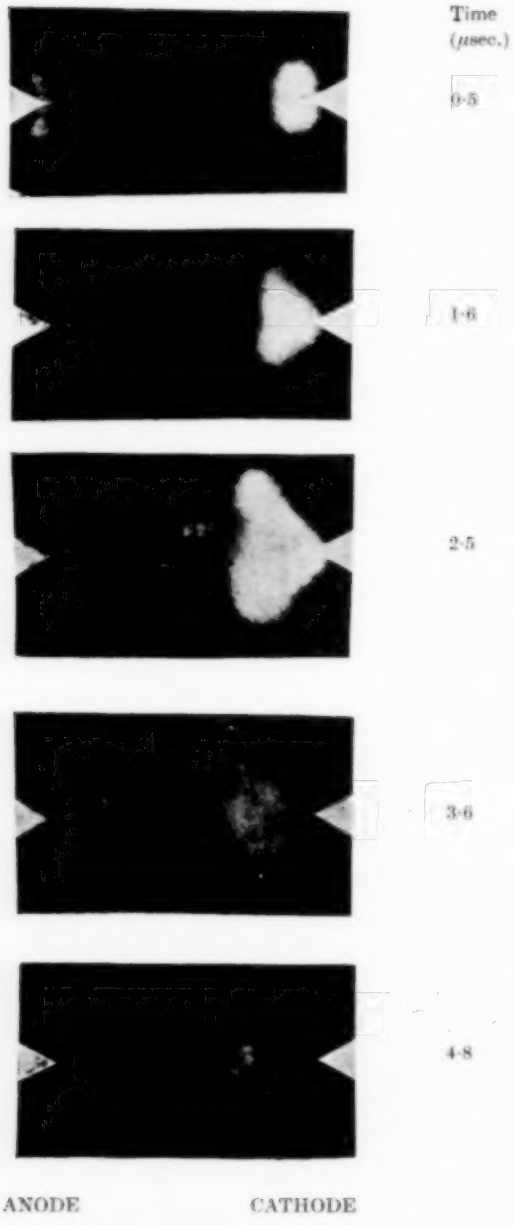

Fig. 9. Image-converter photographs of 600-amp, 3·5-μsec sparks between Zn cathode and W anode. (0·5-μsec exposure.)

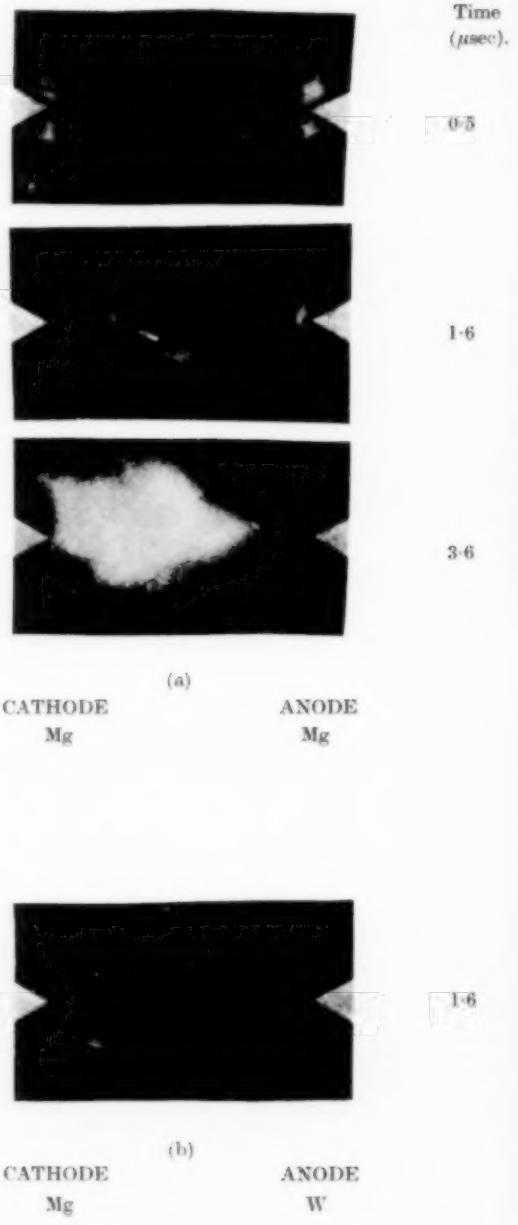

Fig. 10. Image-converter photographs of 600-amp, 3·5-μsec sparks (Mg-Mg or Mg-W electrodes). (0·5-μsec exposure.)

VOL.
7
1955/5

Fig. 11. 0·5-μsec exposure, at 2·1 μsec after breakdown, of a spark between rounded Cd electrodes.

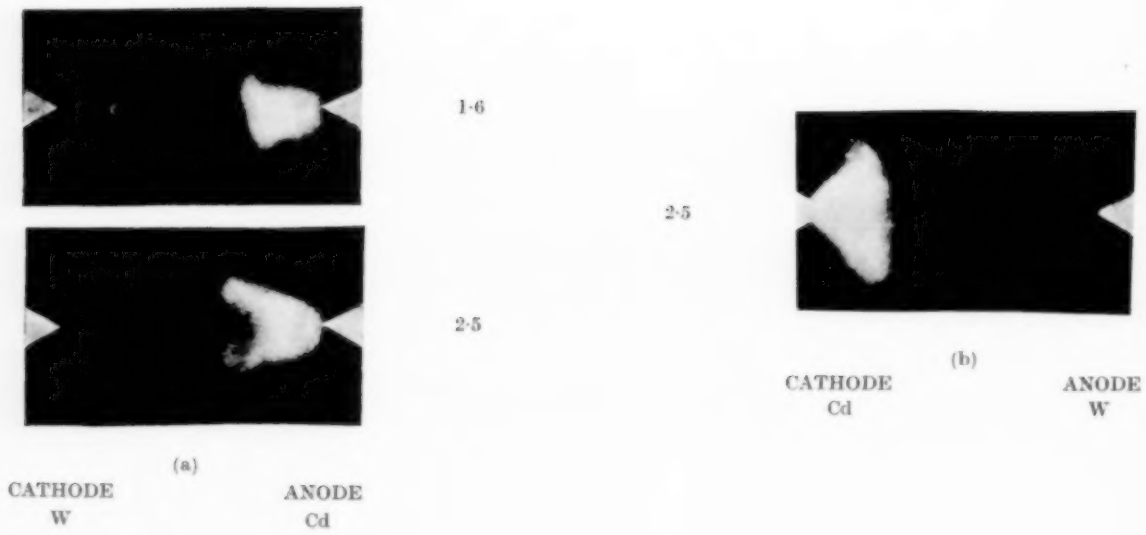

Fig. 12. Image-converter photographs of 600-amp, 3·5-μsec sparks between W-Cd and Cd-W electrodes. (0·5-μsec exposure.)

VOL
7
1955/

The weight changes are given in Table 3. W counter electrodes were used, since the amount of vapour released from them is small compared with that from volatile metals. Even so, there is some loss from W electrodes and particularly from the W cathode. This is in accordance with the fact that jets were observed from W electrodes with the photomultiplier and with the image-converter techniques. It can be seen from Table 3 that in cases where the metal-vapour jet from

Table 3. Measured electrode weight changes (negative for loss of weight) in micrograms per 1,000 sparks. 600-amp, 3-μsec sparks in hydrogen

Metal	*Electrode configuration*		*Change in weights*	
	Cathode	*Anode*	*Cathode*	*Anode*
Zn	Zn	Zn	−95	−18
	Zn	Zn	−95	−11
	W	Zn	−8	−32
	Zn	W	−110	+8
	Zn	W	−113	+17
Mg	Mg	Mg	−15	−56
	Mg	W	−58	−6
	W	Mg	+23	—
	W	Mg	+14	−41
Cd	Cd	Cd	−203	−44
	W	Cd	−6	−37
	Cd	W	−279	−7
Cd (rounded)	Cd	Cd	−162	−36
W	W	W	−20	+2

one electrode reaches the other, metal atoms from the jet are deposited on the latter, causing it either to gain weight or reducing its net loss of weight. For this reason, for example, the 58 μg lost from an Mg cathode with a W anode is reduced to 15 μg when the anode is also Mg. It should be noted as a check on this work that in all cases where the jet from A is known from photomultiplier work not to reach the other electrode B, there is no alteration in the weight-loss at B when A is changed to W (see Fig. 6). Making allowance for the metal transfer as described above, the mean actual loss of metal from the electrodes is given in Table 4.

4.4. *The image-converter photographs of the vapour clouds*

A number of qualitative features of the vapour jets can be ascertained from the image-converter photographs, examples of which are shown in Figs. 8 to 11. (The electrode positions have been superimposed on the prints.)

Fig. 8 shows photographs of sparks between Zn electrodes, in which the light from the vapour jets is recorded in strong contrast with the background radiation from the hydrogen channel. Jets from both electrodes are seen to penetrate further into the gap at successively later times after breakdown, and the jets meet at 3 μsec, i.e., approximately at the end of the current pulse. The jet fronts meet nearer to the cathode, since the anode jet is faster than the cathode jet. After the end of the current pulse, no vapour is seen near the electrodes, but a cloud of excited vapour remains in the centre of the gap and gradually becomes less visible.

Table 4. *Weight of metal eroded from electrodes in micrograms per* 1,000 *sparks (corrected for transfer of metal between electrodes)*

Metal	*Cathode*	*Anode*
Mg	49	58
Zn	110	32
Cd	250	40
W	~15	~5

The jet from a Zn cathode is shown in the absence of any appreciable anode jet in Fig. 9. It still maintains its characteristic conical shape and its front is observed to continue to move forward for about the first $\frac{1}{2}$ μsec of the afterglow. The jet tail simultaneously moves away from the electrode, whilst the cloud as a whole is still approximately conical. The excited W vapour on the anode side of the jet is visible in the records. The jets behave very differently for sparks between Mg electrodes, and some typical records are shown in Fig. 10. Here, particularly in the case of the anode clouds, only the front of the jets is visible, but when the current is cut off the whole of the vapour cloud becomes intensely luminous. This confirms the results obtained with the photomultiplier method (see Fig. 4b).

For sparks between rounded Cd electrodes, the jets from the anode and cathode are seen to have a similar shape (see Fig. 11), although the cathode jet is more intense. In all cases the jets appear to travel perpendicular to the electrode surface (there is some reflected light from the electrode surface beyond the spark). It seems, therefore, that the differences between the anode and cathode jets for pointed electrodes must in part be due to the particular electrode shape. The jets from pointed Cd electrodes (see Fig. 12) are similar to those from Zn, except that the front of the anode jet occasionally has a forked appearance. A further feature with Cd, which has not been observed with any other metal, is the constriction of the hydrogen channel immediately in front of the anode jet in cases where the latter has the forked appearance (Fig. 12, 2·5 μsec).

4.5. *Tungsten vapour*

Mention should also be made of the fact that the presence of tungsten vapour in both 600-amp and 200-amp discharges has been detected. This is of interest,

since W electrodes are often used in experiments where it is desired to examine a discharge channel in sensibly vapour-free conditions. Light from W vapour could be seen in certain image-converter photographs (the contrast is insufficient for reproduction), and W spectral lines were detected during a spectroscopic examination of the comparatively weak hydrogen recombination continuum. The vapour was found to come mainly from the cathode (see Table 4), and the distance along the gap reached by the jet was found to depend on the state of oxidation of the electrode surface; thus the jet did not reach so far when the surface was oxidized. An approximate value for the velocity of a W cathode jet is $2{\cdot}2 \times 10^5$ cm/sec.

5. Discussion

A number of features of the electrode-vapour jets for sparks between pointed electrodes of various metals have been deduced mainly from the light emission of the excited metal vapour. Jet velocities have been found to vary with (a) electrode shape, (b) electrode material, and (c) spark current. Also, the anode jets are in all cases faster than the cathode jets (see Table 1).

Considering (a) first, it is noticed that the cathode jet from a rounded Cd electrode travelled much faster than that from a pointed Cd cathode. This may be due to the fact that the jets from the rounded electrodes have a greater axial velocity component, since the image-converter photographs suggest that jets from a pointed cathode travel inclined to the axis (see later in discussion). FINKELNBURG [2] predicts that the cathode jet velocity varies as $j_c V_c$, where j_c is the cathode current density and V_c is the cathode voltage drop. Thus changes in j_c and V_c with electrode shape would be expected to affect the velocity. Reference to Table 2, however, shows that V_c is less for the rounded electrode, and thus only an increase in j_c in this case could cause the observed increase in velocity.

The effect of the electrode material is seen to be such that the jets are faster for metals of low atomic weight (see Table 1). If all other things such as electrode voltage drop, etc., were equal for the different metals, this would be expected if the jet particles are of atomic size, since the jet energy would vary as MV^2 (atomic weight $\times$ velocity^2).

The velocities are also seen to be faster at higher currents. The electrode current density is thought (CRAIG [11]) to be independent of current, although no accurate measurements have been made and are notoriously difficult; thus, on FINKELNBURG'S theory (see later in discussion) the change in velocity is probably due to a change in the electrode voltage drop. The results of Table 2 confirm that the total electrode drop is greater in the 600-amp spark than in sparks of low current (see CRAIG [10]). It has been suggested—and there is much supporting evidence—that in discharges of the type considered here, excitation of the metal atoms is mainly by electron/atom collisions [12, 13]. For an electron temperature $T_e = 10{,}000°\text{K}$, the mean energy of an electron in the discharge column is $\frac{3}{2}kT_e = 1{\cdot}3$ eV, and these may be taken as typical discharge conditions. Now, the velocity V of the Mg atoms in the anode jet is $4{\cdot}1 \times 10^5$ cm/sec. Thus the translatory energy of such an atom is $\frac{1}{2}MV^2 \sim 2$ eV (M = mass of a Mg atom). Also the energy of the levels involved in the transitions giving rise to the principal

metal lines in the observed spectron is ~3–4 eV. Thus it can be seen that the mean kinetic energy of the atoms in the jet is comparable with the mean electron energy in the discharge, and it is thus possible that atom/atom collisions are important, although the cross-sections involved are not known.

The following features of the jet luminosity have been observed:

(a) The cathode jet intensity remains almost constant as it proceeds for a distance which is least for Cd and greatest for Mg, and then falls to zero at a point reached in about $\frac{1}{2}$ μsec after the end of the circuit pulse.

(b) The intensity of the anode jet initially increases as the jet proceeds, reaches a peak, and commences to fall. The distance travelled before the peak is reached is greatest for Mg and least for Cd. Also, in a 7-mm gap the anode jet always reaches the cathode.

(c) An effect noticed only with the Mg-anode jet (and to a very limited extent with the Mg-cathode jet) is a sudden increase in jet brightness at the end of the current pulse. (See Fig. 10.) It is probably significant that this only occurs for the Mg-anode jet which has the greatest observed velocity.

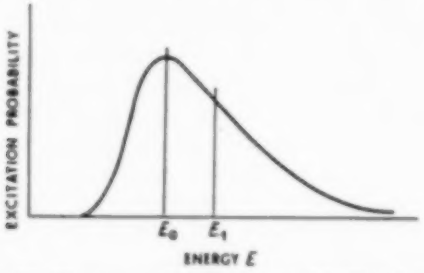

Fig. 13. The energy distribution used in the discussion.

As a possible explanation of some of these effects on the basis of atom/atom collisions, it is suggested that the high anode jet velocities (particularly for Mg) are such that the energy transfer (E_1) involved in a collision is considerably above the energy for the maximum excitation probability (E_0). (See Fig. 13.) The jet, then, as it proceeds, loses kinetic energy and the excitation probability increases, causing the observed increase in the light intensity from the jet. This would also explain (c) above, since there would be a sudden reduction of energy at the end of the current pulse causing a sudden fall in E_1 to the higher excitation probability. The effect is greatest near the anode (see Fig. 4b), where E_1 would be expected to have its maximum value.

For the above effects to be explicable in terms of electron/atom collisions, the variation of jet luminosity must depend on the spatial and temporal variation of the electron energy distribution and/or electron density. Thus (c) would require that the electron temperature, after current flow had ceased, fell from a value too high to give excitation through an optimum value. This is not consistent with Fig. 8a. The electron temperature and electron density may be expected to vary with the amount of metal vapour present and to be lowest where the vapour

VOL 7 1955/

density is highest, because of the high Ramsauer cross-sections of the heavy-vapour atoms [14]. It is probable that the spatial variations in vapour luminosity may be due to this effect, i.e., to spatial variations in the efficiency of excitation by electrons, but further speculation in the absence of vapour density data, etc., in the clouds is pointless.

Shape of the vapour jets

The image-converter records shown in Figs. 9 to 12 provided information on the shape of the vapour jets from both pointed and rounded electrodes. With pointed electrodes, the anode and cathode jets are seen to have very different shapes. In the case of Zn and Cd, the shapes of the cathode jets are similar and consistent with a vapour emission perpendicular to the surface of the electrode (see Fig. 4). When the electrode surface was examined under a microscope, the tip of the cathode had remained pointed, but was observed to be covered with minute pits, and it is thought that the jets originated at these. On the other hand, the anode jets were observed, for Zn and Cd, to travel straight along the discharge axis. When examined, the anode was found to have a sphere of metal at its tip, and there was a complete absence of pits in the surface. It seems possible, therefore, that the vapour comes from this area (molten during the discharge) by simple evaporation. Because of the relatively feeble light emission from both the anode and cathode jets from Mg during the current pulse, it is difficult to determine the shape of the jets in this case. It appears, however, from the limited radiation, that the cathode jet is probably emitted in a similar way to that for Cd and Zn (see above). The anode jet is only luminous at its tip and at isolated points round the edge, and its shape cannot, therefore, be seen. When rounded Cd electrodes were used, the jets were observed (Fig. 11) to travel always perpendicular to the electrode surface. In this case, the jets have a shape similar to that obtained by HAYNES [1] from a flat Hg surface. Also, when the cathode surface was examined it was found to be covered with minute pits similar to those observed round the tip of the pointed cathode. The anode jet was similar in shape (as HAYNES found also) but was less intensely luminous, and the anode surface was covered with minute spheres of molten metal. This suggests that an evaporation process was again operative, at least at the anode.

An attempt has been made to co-ordinate the quantitative results given in the previous sections with the published theories of FINKELNBURG [2] and LLEWELLYN JONES [3]. FINKELNBURG [2] deduces that the weight of metal lost from an electrode

$$w = W/Q \text{ g/sec/cm}^2 \qquad (1)$$

where

$$W = j_c V_c \text{ for the cathode}$$

$$W = j_a(V_a + \phi) \text{ for the anode}$$

(j = current density, V = electrode drop, ϕ = work function). Q is the energy necessary to evaporate 1 gram of electrode material and heat it to the jet temperature (in watt-sec/g). A major part of Q is the energy necessary to heat the metal vapour to the temperature of the jet (which is probably of the order of

10,000°K). Because of the lack of data on the specific heats of metallic vapours over this temperature range, only a tentative value for Q was assumed, namely $Q = 40RT$ watt-sec/mole, where R = gas constant and T = jet temperature-boiling point. (See FINKELNBURG [2], who gives this value for Hg vapour over a similar temperature range.)

If w' = weight of metal lost/spark,

then
$$w = \frac{w'}{tA} \tag{2}$$

where t = the time for which vapour is emitted (assumed equal to the length of current pulse, i.e., 3×10^{-6} sec),
and A = the area over which vapour is emitted (assumed equal to the current carrying area).

Now $W = jV$ ($V = V_c$ at cathode and $V = V_a + \phi$ at anode)

and j = spark current $\div A = 640/A$

Therefore
$$w' = 1{\cdot}92 \times 10^{-3}\, V/Q \text{ g} \tag{3}$$

Values of the weight-loss calculated from equation (3) are given in Table 5, together with the measured results. From these it would appear, considering the

Table 5. Calculated weight losses (Finkelnburg's Theory)

Metal	Mg	Zn	Cd
Cathode			
w_c' calculated (g/spark)	1·4	4·0	$7{\cdot}1 \times 10^{-7}$
w_c (observed (g/spark)	0·49	1·1	$2{\cdot}5 \times 10^{-7}$
Error factor ($= w_c'/w_c$)	2·9	3·6	2·8
Anode			
w_a' calculated (g/spark)	3·3	9·4	$16{\cdot}7 \times 10^{-7}$
w_a observed (g/spark)	0·58	0·40	$0{\cdot}32 \times 10^{-7}$
Error factor ($= w_a'/w_a$)	5·7	23	52

uncertainties in V and Q, that the theory may reasonably account for the production of vapour at the cathode (and at a Mg anode only). This again points to the possibility of a somewhat different process being operative at the anode. FINKELNBURG also deduces the initial jet velocity to be given by

$$u = W/QP = w'/tAP \tag{4}$$

(P = vapour density).

Reliable values of the area of the electrode spot are very difficult to obtain, and no measurements appear to have been published for the metals used here under similar discharge conditions. CRAIG [11] gives the value of $\sim 10^{-4}$ cm^2 for a

Mg-cathode spot in a 100-amp spark, and FROOME has given similar data. Estimates of P have been made, assuming the vapour pressure inside the jet to be equal to that of the surrounding atmosphere and the temperature to be 10,000°K. Using the experimentally derived weight losses and velocities of Tables 1 and 4, values of A were calculated (see Table 6).

Table 6. Calculated electrode spot areas (Finkelnburg's Theory)

Metal	Mg	Zn	Cd
Cathode			
Weight loss w_c g/spark	49	110	250×10^{-9}
Velocity u_c cm/sec	1·7	1·14	$1{\cdot}02 \times 10^{5}$
Calculated area A_c cm²	3·3	4·2	$6{\cdot}2 \times 10^{-3}$
Anode			
Weight loss w_a g/spark	58	32	40×10^{-9}
Velocity u_a cm/sec	4·1	1·95	$1{\cdot}2 \times 10^{5}$
Calculated area A_a cm²	1·6	0·79	$0{\cdot}83 \times 10^{-3}$

The values of A_c in all cases differ from the more probable value of $\sim 5 \times 10^{-4}$ by a factor of $\sim$10. This could possibly be accounted for by (a) the pressure inside the jet being greater than atmospheric, and (b) the initial jet velocity being greater than the value used, which is that found in that part of the gap 1 mm or more from the electrode. The calculated values of A_a are seen to be less than the cathode areas, on the basis of the above theory. This does not agree with the normally accepted fact that the anode-current density is less than the cathode-current density (CRAIG [11], FINKELNBURG [2]). The values of A_a are nevertheless of the correct order of magnitude.

Calculations on the basis of LLEWELLYN JONES [3] theory led to the conclusion that the theory does not seem to be applicable in our case without modification. LLEWELLYN JONES has found it to give satisfactory results with the higher boiling-point metals (Pt, Ni, Fe) for sparking-plug discharges. The conditions in the present sparks used by the authors are very different.

Conclusions

(1) Vapour-jet velocities for anode and cathode jets from Mg, Zn, and Cd electrodes have been determined for 600- and 200-amp, 3-μsec sparks in hydrogen. These have been found to depend on (a) the electrode material with the velocity highest for metals of low atomic weight, (b) the electrode shape, and (c) the spark current, so that the velocity increased with current, other factors remaining constant. Also, for the metals considered, the anode jet is faster than the cathode jet.

(2) The jet velocity is such that the kinetic energy of the metal atoms due to their unidirectional velocity component is comparable with the energy required for excitation.

(3) The relative jet luminosity as a function of gap position has been found to be different for cathode and anode jets of the same metal. In the former case the jet intensity remains constant and then falls to zero at the end of the current pulse, so that the jet is never observed at a particular position unless it has arrived within about $\frac{1}{2}$ μsec of the end of the current pulse. For anode jets the intensity rises as the jet proceeds, reaches a peak, and then, in some cases, falls.

(4) The light intensity in a Mg-anode jet suddenly increases at the end of the current pulse.

(5) The jets from anodes and cathodes of different metals when photographed with the image-converter camera appeared different in shape. Possible explanations of these differences have been put forward.

(6) In order to compare the results with some published theories, the weight of metal eroded from each electrode and the total electrode voltage drops has been measured. The erosion at the cathode was greatest for Cd and least for Mg, but approximately equal weights were eroded at the anode. The total voltage drop was found in all cases to be within the range 22 to 42 volts.

(7) Uncertainties about electrode spot areas, the individual electrode drops, and the variation of specific heat of metal vapour with temperature (up to 10,000°K) rendered theoretical comparisons difficult. It was concluded that FINKELNBURG's [2] theory was probably applicable, particularly at the cathode.

Acknowledgments—The authors wish to thank Professor J. M. MEEK for the interest he has shown in the progress of this work. They are also indebted to the British Iron and Steel Research Association for supporting this work, for the award of a Bursary to one of them (C. M. CUNDALL), and for permission to publish this paper.

References

[1] HAYNES, J. R.; *Phys. Rev.* 1948 **73** 891.
[2] FINKELNBURG, W.; *ibid.* 1948 **74** 1475.
[3] LLEWELLYN JONES, F.; *Brit. J. Appl. Phys.* 1950 **1** 60.
[4] WILLIAMS, G. C., CRAGGS, J. D., and HOPWOOD, W.; *Proc. Phys. Soc.* B 1949 **62** 49
[5] DURNFORD, J., and MCCORMICK, N.; *Proc. Inst. Elect. Eng.* II 1952 **99** 33.
[6] TSUI-FANG, CUNDALL, C. M., and CRAGGS, J. D.; *Spectrochim. Acta* 1953 **5** 452.
[7] TURNOCK, R. C.; Ph.D. Thesis, Liverpool, 1953.
[8] TURNOCK, R. C.; *Proc. Inst. Elect. Eng.* II 1951 **98** 635.
[9] CUNDALL, C. M.; Ph.D. Thesis, Liverpool, 1954.
[10] CRAIG, R. D.; E.R.A. Tech. Rep. L/T.287, 1953.
[11] CRAIG, R. D.; *ibid.* 1/T.260, 1951.
[12] LLEWELLYN JONES, F.; *J. Soc. Chem. Ind.* 1945 **64** 317.
[13] ELENBAAS, W.; *The High Pressure Mercury Vapour Discharge.* North Holland Co., Amsterdam, 1951.
[14] BRODE, R. B.; *Phys. Rev.* 1930 **35** 504.

VOL 7 1955/

Spectrochimica Acta, 1955, Vol. 7, pp. 165 to 174. Pergamon Press Ltd., London

The use of intensity scales in the microphotometry of spectra*

J. McK. Nobbs,† M.Sc., A.R.A.C.I., and P. T. Beale‡
British Non-Ferrous Metals Research Association

(*Received* 2 *January* 1955)

Summary—Investigations have been undertaken into the use of intensity scales for microphotometry, whereby relative intensities are very simply recorded on the microphotometer scale, without continuous reference to a calibration curve, resulting in an appreciable saving of time.

Intensity scales are drawn empirically from plate calibration curves of relative intensity vs. linear galvanometer deflection, and subsequent use of a particular intensity scale is restricted to plates having the same calibration curves. Therefore a number of scales are required when plates of varying contrast factors are used, and a family of intensity scales has been constructed to cover the range of contrasts expected from the type of plates and developing conditions employed. The construction of the scales involved photographic reduction of the original drawing and slight modification of the Hilger galvoscale projector in which they are inserted.

A graph-paper incorporating a modified logarithmic scale (Partial Seidel Transformation) was developed to facilitate the drawing of plate calibration curves, and the family of intensity scales was derived directly from it. This graph-paper extends the density range that can be covered by a straight-line calibration curve and greatly assists in the determination of the correct curve and hence the intensity scale to be used for a particular plate. The appropriate scale can also be selected direct from linear microphotometer readings by means of a slide-rule calculator constructed for the purpose.

Several tests on the accuracy of the scales have been conducted, and no difference has been found between the results obtained with intensity scales and those from the usual methods of plate evaluation. It has been concluded, therefore, that, provided a sufficient number is available, the use of intensity scales introduces no further photometric error and that a simple method has been found for the more rapid microphotometry of plates without loss of accuracy, the method being particularly useful when background corrections are required.

Introduction

An essential feature of spectrographic analysis is the conversion of transmission measurements on lines in the photographed spectra to intensity ratios of the light emitted from the source at the corresponding wavelengths. Unless standards are to be photographed on every plate, an accurate plot of the characteristic curve of the plate emulsion is required. Many ways of obtaining this have been described in the literature, such as employing a rotating stepped sector [1], line groups of known intensity ratio [2], the two-line method [3], stepped filters, and many modifications of these basic methods. The line measurements from the microphotometer can then be converted to relative intensity values by reference to the characteristic curve. Further calculation gives the intensity ratio of analysis line to internal standard line, and this in turn is referred to a working curve, drawn up from analyzed standards, in order to obtain the final analysis.

* The work described in this paper was made available to members of the B.N.F.M.R.A. in a confidential research report issued in February, 1954.

† Investigator seconded from the Defence Standards Laboratories, Adelaide, Australia.

‡ Research Assistant, B.N.F.M.R.A., London.

The procedure can be speeded up by using calculators, the most comprehensive of which is that described by Kaiser [4]. A simpler device has recently been described by Nobbs [5], in which the linear microphotometer scale is replaced by a family of intensity scales and the relative intensities of lines are read directly from the microphotometer scale without reference to a graph.

With all types of spectrographic calculators the several operations outlined above must be carried out on them before an analysis result is obtained from the microphotometer readings, and the efficiency of a calculator is judged by the rapidity with which one operation can follow another without introducing either instrumental or personal errors. In these respects the Kaiser calculator is considered to be the most proficient, but its cost is rather high. By employing intensity scales, the most complex and time-consuming of the operations, that of converting linear galvanometer deflections to relative intensities, is carried out in the microphotometer itself concurrently with the initial line-measurements, and if a calculator is used for the subsequent operations it can be made relatively simple. When background corrections are not required, the number of operations can be reduced to a minimum by employing log-intensity scales, and an added advantage is that intensity scales can be made in quantity at a fraction of the cost of calculators.

This paper describes the construction and application of a family of intensity scales for use in a Hilger galvoscale projector.

VOL
7
1955/

I. The design and construction of intensity scales

The steps involved in the design and construction of a family of intensity scales are as follows:

1. The application of a suitable conversion factor, either empirical [5] or calculated [6], in order to get linear plate characteristic curves from one of the standard methods of plate calibration.

2. Determination of the range of gamma to be expected from plate to plate variations and change of gamma with wavelength.

3. The determination of the intensity graduations associated with the linear galvanometer deflections for each value of gamma, and the preparation of an intensity-scale slide for the microphotometer from a large-scale drawing of the scales giving this relationship.

4. Construction of a simple calculator for the determination of gamma from a set of plate calibration readings; although this may be determined graphically in the usual way.

1. *Plate characteristic curves: derivation of linear curves*

Honerjäger-Sohm and Kaiser [6] have described the application of modified density scales to the construction of characteristic curves in order to obtain linearity over wide density ranges. It has been found that the partial Seidel transformation $(S + D)/2$* of density will give a consistently linear characteristic for the Kodak B.10 plate over the whole density range corresponding to microphotometer deflections 20–490 mm, when the clear plate is 500 mm. It has been noted, however, that some loss of contrast is often evident in the K.B.10 emulsion for densities greater than 1·4 (i.e., deflections < 20 mm).

* Where D is the normal density $= \log\left(\frac{\text{clear-plate deflection}}{\text{line deflection}}\right)$ and S is the Seidel density $= \log\left(\frac{\text{clear-plate deflection}}{\text{line deflection}} - 1\right)$

The plate characteristic can readily be plotted from any of the usual calibration methods by using the graph-paper shown in Fig. 1, where the normal density scale has been replaced by a partial Seidel correction scale marked directly in microphotometer deflections. For convenience in production on a

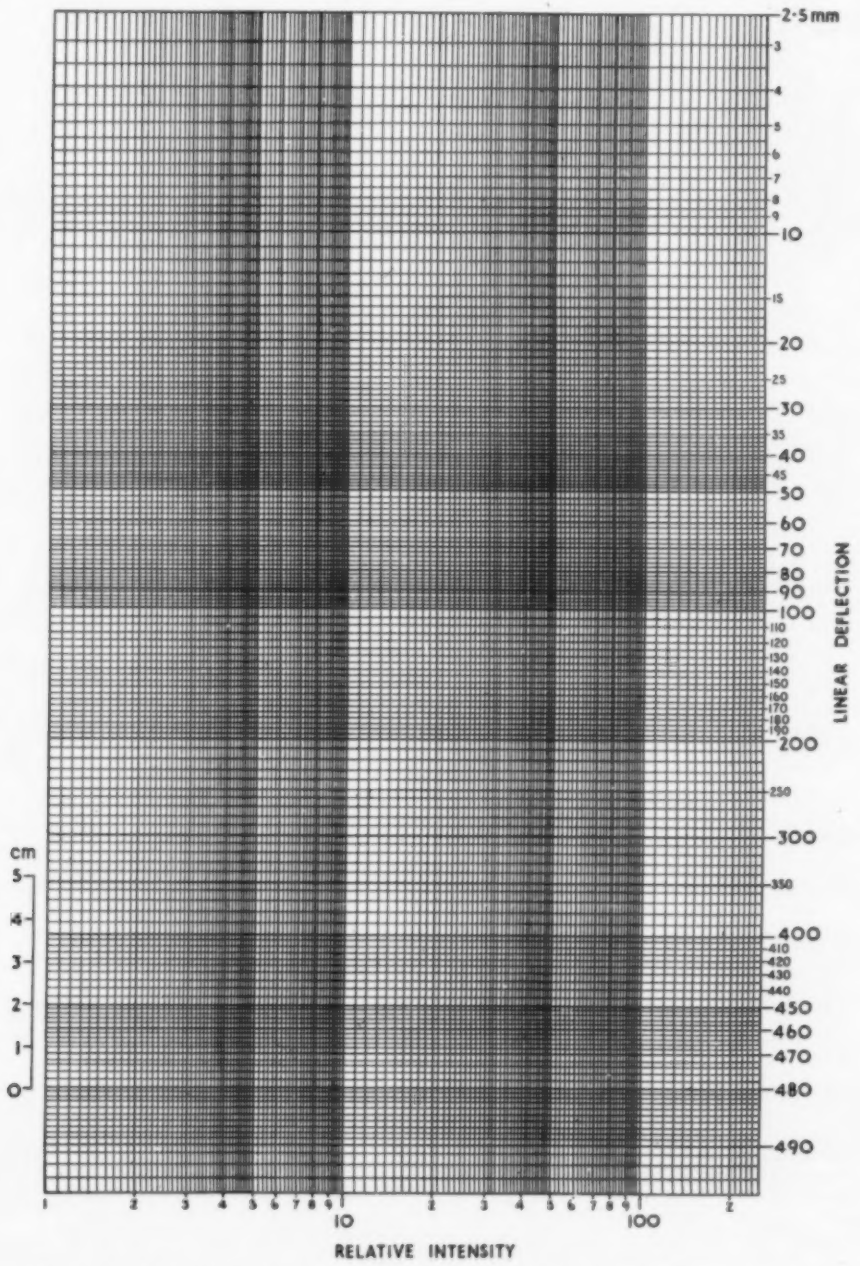

Fig. 1. Seidel graph-paper (linear microphotometer deflection vs. relative intensity).

foolscap sheet, the partial Seidel scale has been modified so that the angle (M) measured on the graph-paper is not the true angle (T) of the characteristic but bears a fixed relation to it;

$$\gamma = \tan T = 0{\cdot}80 \tan M.$$

The intensity calibration pattern used in this work has been a lead spectrum photographed through a rotating stepped sector with six steps and a step ratio of 2. The sector calibration method has the most useful advantage that the contrast can be measured over the whole wavelength range.

2. *Determination of the range of gamma to be covered by intensity scales*

A preliminary survey of Kodak B.10 plates exposed over a period of ten months showed that variations of angle M between 56° and 62°, the average being about 58°, could be expected, and accordingly any group of intensity scales for these plates would have to cover this range. It has also been found that the gamma of the B.10 plate is constant over the wavelength region 2,300–3,200 Å, but always rises above the equivalent of $M = 62°$ at wavelengths higher than 3,200 Å, and since intensity measurements are often required in that region it was clear that scales up to 65° would be desirable. As a result of these observations it was concluded that scales covering the range 56° to 65° would be required.

3. *The construction of the intensity scale slide*

Sinclair [7] described an intensity scale mounted alongside the linear scale of the older-type microphotometer fitted with a lamp and scale giving a reflected spot moving over the fixed scale. Nobbs [5] described advances on this idea and its use in practice. The present report describes the construction of scales for use with the Hilger galvoscale projector, where the image of the scale is reflected by the mirror of the galvanometer, so that deflection of the mirror moves the scale over a fixed index line.

Using the large drawing (~2 × Fig. 1) from which the stencil for the production of the graph-paper (Fig. 1) was made, lines were drawn at 1° intervals from 65°–56° through the arbitrary point "intensity 10, deflection 250 mm." The relative intensity reading corresponding to each deflection was read off from the 56° curve and plotted on a second large drawing alongside a linear scale 50 cm long, as shown in Fig. 4. Similar scales spaced 1 cm apart were plotted for the other angles, so that the area covered was approximately 50 cm × 10 cm. The drawing had then to be reduced on to a slide 1 in. wide by approximately 4 in. long to fit the scale-holder of the galvoscale projector.

The drawing was photographed on a high-resolution plate at 30 ft with a small aperture lens (f 32) to avoid distortion. The negative was 1/10 of the size of the original and was printed on to a strip 1 in. × 4 in. cut from an Ilford thin-film half-tone plate. This was backed by a strip of clear glass, and the slide was mounted in the scale holder of the galvoscale projector.

Adjustment to read from the linear scale or from any one of the intensity scales was made by tilting the mirror of the galvanometer by raising or lowering the rear screw-foot. It was found that tilting the galvanometer to go from the linear to the 65°-scale introduced no errors.

A tendency for the rotation of the screw to move the galvanometer bodily on its stand was corrected by sharply pointing the screw-foot and allowing it to rest in a shallow hole made with the point of a drill in the galvanometer table. This "bearing" is kept oiled, as is the screw passing through the galvanometer base-plate.

4. *Calculator for the determination of angle M from a stepped-sector spectrum*

A simple slide-rule type calculator was devised for the measurement of the slope of the characteristic curve without using the special graph-paper. The slide-rule, as illustrated in Fig. 2, was adapted from a

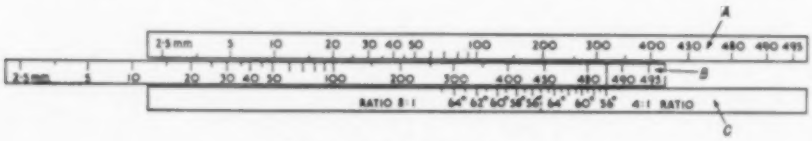

Fig. 2. Slide-rule calculator.

normal calculating type and consists of three scales A, B, and C. Scales A and B are identical with the vertical scale on the "Seidel" graph-paper (Fig. 1), while scale C consists of two sections, each graduated in degrees, which indicate the slope of the calibration curve directly from two microphotometer readings placed on the other two scales; the appropriate section to use is determined from the intensity ratio of the two lines on which the microphotometer measurements were made. On this rule ratios of 4 : 1 and 8 : 1 are employed, corresponding to various combinations of steps on the sector.

When two linear galvanometer deflections are aligned on scales A and B, the two scales are displaced by an amount depending on the intensity ratio of the lines measured and the slope of the plate calibration

curve. When the calibration curve is linear, as it almost invariably is when using the "Seidel" graph-paper, the displacement is the same no matter what density range is used. Therefore, with a fixed intensity ratio the displacement of the scales can be used as a measure of the slope of the calibration curve, and in Fig. 3 are shown the displacements expected from a set of calibration curves, varying from 56° to 64° at 2° intervals, when using both 4 : 1 and 8 : 1 intensity ratios.

The positions of the graduations on scale C (Fig. 2) were derived from Fig. 3 after an indicating mark had been arbitrarily fixed on scale B (Fig. 2). Alternatively, the graduations could have been marked in directly from the displacements of the upper scales as found by applying readings obtained for a fixed intensity ratio of either 4 : 1 or 8 : 1 and varying calibration curve angles.

For the determination of the correct calibration curve angle of a plate, the microphotometer reading obtained on the denser step, of a pair of 4 : 1 or 8 : 1 intensity ratio, is set on scale A, and scale B is moved to align that with the reading obtained on the other step, then, according to which step-ratio has been used, the curve angle is read on scale C.

With a seven-step spectrum it is possible to have five combinations of steps with a 4 : 1 ratio and three at 8 : 1 (although usually only four and two respectively are measurable), and the mean of the results obtained is calculated; the true angle can then be determined to within $\pm\frac{1}{2}°$.

By this method the appropriate intensity scale to use for the microphotometry of a plate can be determined more speedily and accurately than by using the graph-paper.

OL.
7
5/56

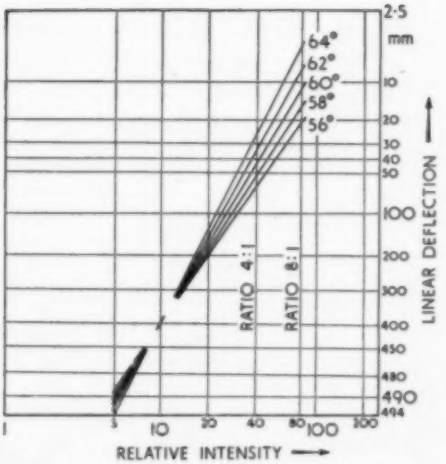

Fig. 3. Showing relation between intensity and calibration curves.

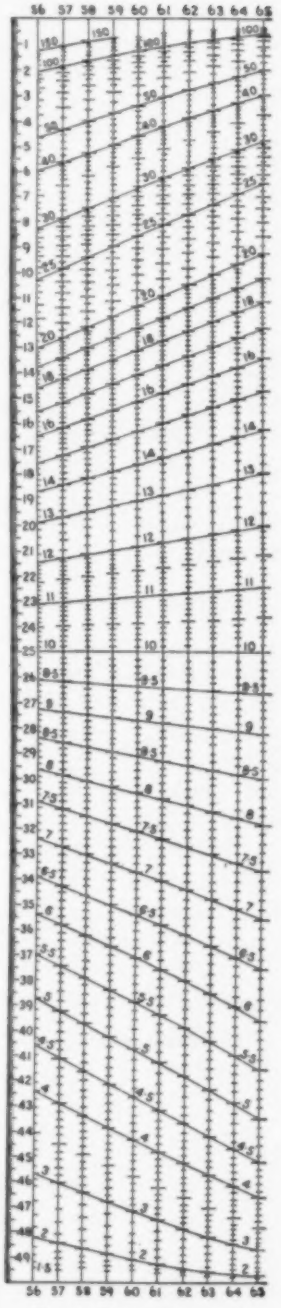

Fig. 4. Intensity scales for Kodak B.10 plate.

II. The application of intensity scales to analysis

1. *Determination of the correct scale to use with a particular plate*

The general procedure in analysis is to measure the calibration spectra on the plate using the linear galvanometer scale. The angle M for the plate is measured from the characteristic curve plotted on the special graph-paper or calculated by means of the slide-rule described above. The appropriate scale is selected and used for all subsequent measurements of lines on the plate, providing they lie in the wavelength region 2,300–3,200 Å and have linear deflections between 20 and 490 mm. Measurements outside these limits can be made on the linear scale, and relative intensity values can be read from the completely plotted characteristic curve. Values read off in this way may be compared with values obtained by using the intensity scales direct. The relative intensities may now be converted to intensity ratios and reference to a working curve, drawn up from analyzed standards, and, relating concentration and intensity ratio, will give the required analysis.

In measuring weak lines it is desirable to apply background corrections in order to get linear working curves of reasonable slope. This can readily be done by measuring, on the appropriate relative intensity scale, the line (plus background) and the background by the side of the line. A simple subtraction gives the relative intensity of the line corrected for background.

2. *Practical test for the use of intensity scales*

The ideal conditions for an analytical procedure usually aim at giving the internal standard deflection approximately 100 mm and the intensity ratio analysis line/internal standard line approximately 2·0 for the maximum percentage content in the range covered and 0·5 for the minimum. In the absence of routine analysis matching these conditions, a simulated control run was obtained by measuring three adjacent steps from a stepped-sector spectrum on all K.B.10 plates used over a period of three months. The middle step was selected to have a deflection of approximately 100 mm, and it was known that the intensity ratio of the three steps should be in the ratio 2 : 1 : 0·5 from the sector angles. The relative intensities of the steps were measured as if carrying out an analysis as described in the previous section. The results of the test are shown in the control chart, Fig. 5.

This chart shows the total error in the measurement of three intensities known to have a fixed ratio, and includes errors from:

(a) Nonuniformity of plate emulsion,
(b) Error in measuring angle N and selection of I scale,
(c) Error in reading intensity scale,

but does not include the errors normally occurring in an analysis:

(a) Heterogeneity of sample,
(b) Irregularity of excitation conditions.

It can be seen that the maximum error is about 5 per cent and the plate-to-plate reproducibility (coefficient of variation) has been found to be 3·3 per cent for a ratio of 2·0 and 3·2 per cent for 0·5, based on thirty-seven readings. Also

VOL
7
1955/

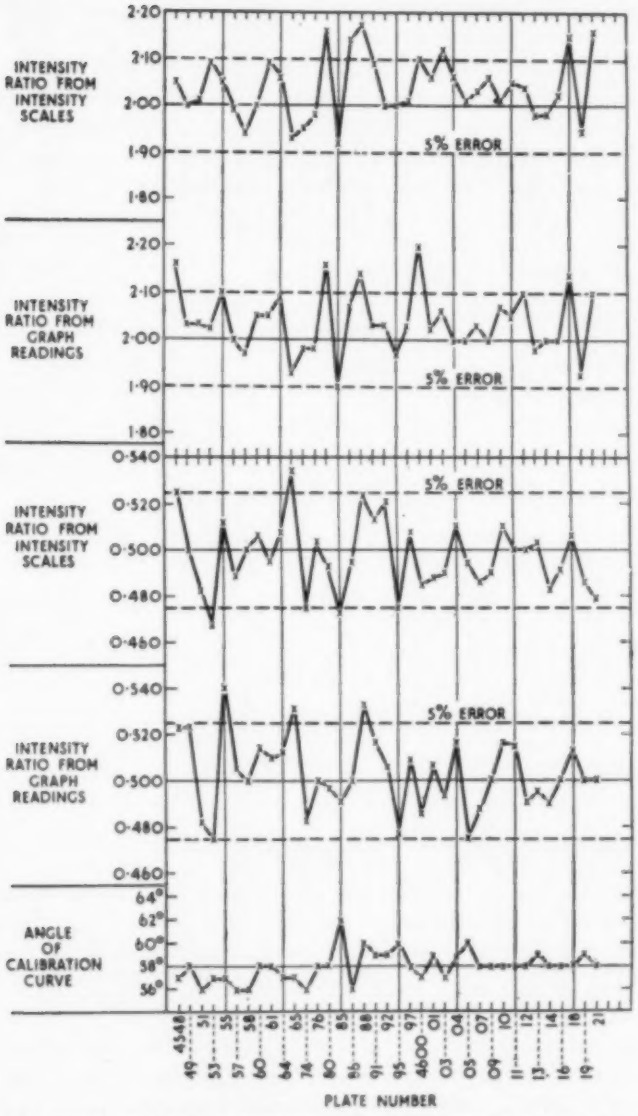

Fig. 5. Control chart showing variations in the measurement of a fixed intensity ratio from plate to plate, as obtained by both intensity scales and from calibration curves, together with variations in the slope of the plate calibration curves.

included in Fig. 5 are the intensity ratios obtained by a straightforward method using measurements made on the normal linear scale converted to intensity ratios by reference to a carefully-plotted characteristic curve using the partial Seidel density and relative intensity. The reproducibility is again about 3 per cent (calculated 3·1 per cent for 2·0 and 3·2 per cent for 0·5), and it is deduced that the

use of intensity scales in the microphotometer has not introduced any appreciable error, although effecting a considerable saving in time.

The chart also shows the variation in measured angle M, and it is seen that the slope of calibration curve has varied from 56° to 62° without affecting the measured intensity ratio, although in some instances, e.g., plate 4585, there is a possible connection between large deviation from the mean intensity ratio and an abnormal calibration angle, but this is by no means consistent.

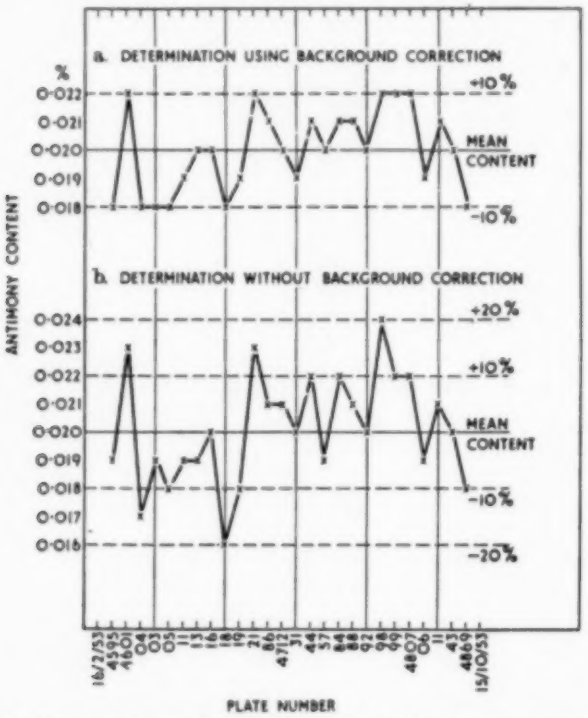

Fig. 6. Control charts showing variation in estimation of the antimony content of a lead sample sparked at intervals over a period of eight months, using a fixed working curve and intensity scales for the line-pair Sb 2311·5, Pb 2712. Each point is the mean of four exposures.

The plate-to-plate reproducibility of intensity-ratio determination is rather high at 3 per cent, and to examine the possibility that additional errors were being introduced by the calibration technique described, a single plate was taken containing fifteen stepped spectra. This plate was measured for three adjacent steps in each spectrum as before, and the reproducibility within the plate was calculated to be 3·3 per cent at the intensity ratio 2·0 and 4·2 per cent at 0·5. These errors were of the same order as the plate-to-plate variation, and it was concluded that the plate calibration and use of intensity scales introduced no additional error. This plate also showed that, under these particular photographic conditions, analytical reproducibility of less than 3 per cent can in general only be expected if the ratio of analysis to internal standard line lies in the range 0·5–2·0,

and clearly the optimum reproducibility will be obtained when this ratio approaches unity.

The possibility of using this method of plate evaluation in conjunction with working curves is illustrated by the control charts shown in Fig. 6. A lead specimen was sparked on a number of plates taken over a period of eight months, and the antimony content (nominally 0·020 per cent) was determined, using working curves derived from five plates containing spectra of standard alloys. A maximum error of ± 10 per cent of content was obtained when background correction was used, compared with ± 20 per cent when background correction was not employed.

The present technique has been confined to the use of the Kodak B.10 plate, but it is anticipated that by using other modifications to the density scale, to get linear characteristics, it could readily be extended to other types of plate and to regions of high or low contrast, corresponding to wavelengths higher or lower than the constant-gamma region.

3. *Errors in intensity ratio measurements arising from selection of the wrong intensity scale*

Using the intensity-scale slide described above, it is possible to have an error of up to 1° in the determination of the characteristic angle M. The corresponding errors in intensity ratio can be easily calculated, and are shown below in Table 1. Two hypothetical cases are considered in which an angle M of 57° and 64° give the correct ratio of 2·0 and 0·5, representing the normal range of intensity ratio. The corresponding relative intensities and ratios have been obtained from scales differing by $\pm \frac{1}{2}°$ and $\pm 1°$ from the true angle M. The internal standard line is given an arbitrary deflection of 100 mm when the clear plate is 500 mm.

Table 1

$M°$	*Deflection (linear scale 500 mm clear plate)*			*Relative intensities*			*Ratios*			
	I.S.	*A.L. (high)*	*A.L. (low)*	*I.S.*	*A.L. (high)*	*A.L. (low)*	*High*	*% error*	*Low*	*% error*
57	100	44	207	24·7	49·5	12·35	2·00	0·0	0·500	0·0
56	100	44	207	25·6	52·5	12·45	2·05	2·5	0·487	2·6
58	100	44	207	23·7	46·5	12·25	1·96	2·0	0·517	3·4†
56·5*	100	44	207	25·1	51·0	12·4	2·03	1·5	0·494	1·2
57·5*	100	44	207	24·2	48·0	12·3	1·98	1·0	0·508	1·6
64	100	34	255	19·7	39·4	9·85	2·00	0·0	0·500	0·0
63	100	34	255	20·2	42·0	9·85	2·08	4·0†	0·487	2·6
65	100	34	255	19·3	37·2	9·85	1·93	3·5†	0·510	2·0
63·5*	100	34	255	20·0	41·0	9·85	2·05	2·5	0·492	1·6
64·5*	100	34	255	19·5	38·5	9·85	1·96	2·0	0·505	1·0

* By interpolation. I.S. = internal standard.
A.L. = analysis line.

† Inaccuracies in drawing the scales contribute to the high magnitudes of these errors. The average error arising from using a scale 1° from the correct angle is 2·6 per cent, and 1·3 per cent at $\frac{1}{2}°$.

From the table it can be seen that appreciable errors in intensity ratio can arise from faulty assessment of the characteristic angle for the plate, and all possible care should be taken over this measurement. It can be seen that measurement of angle M to the nearest $\frac{1}{2}°$ is worthwhile and that scales on the slide at $\frac{1}{2}°$ intervals or a single continuous scale, with a cursor to isolate particular angles or fractions of angles, are necessary for the most accurate work.

Acknowledgment—Acknowledgment is made to the Director and Council of the British Non-Ferrous Metals Research Association for permission to publish this work.

References

[1] Breckpot, R.; *Spectrochim. Acta* 1939 **1** (2) 137–163.
[2] Iron and Steel Inst. Special Report No. 47, September, 1952.
[3] Churchill, J. R.; *Ind. Eng. Chem.* 1944 (November) **16** 653–670.
[4] Kaiser, H.; *Spectrochim. Acta* 1951 **4** 351–365.
[5] Nobbs, J. McK.; *Spectrochim. Acta* 1952 **5** 286–294.
[6] Honerjäger-Sohm, M., and Kaiser, H.; *Spectrochim. Acta* 1944 **2** (8) 396–416.
[7] Sinclair, D. A.; *J. Opt. Soc. Amer.* 1944 **34** 689–693.

VOL
7
1955/

Spectrochimica Acta, 1955, Vol. 7, pp. 175 to 178. Pergamon Press Ltd., London

Spectrochemical Note

Isotopic assay of lithium by means of hydride band emission spectra

VELMER A. FASSEL and HENRY J. HETTEL
Institute for Atomic Research
and Department of Chemistry, Iowa State College, Ames, Iowa

(*Received* 10 *January* 1955)
(*Accepted for publication* 3 *February* 1955)

Summary—A spectrographic method applicable to the determination of the Li^6–Li^7 isotopic ratio is described. The procedure involves the low current d.c. arc excitation of lithium sulphate samples in an atmosphere of 50 per cent H_2–50 per cent He. The intensity ratio of selected Li^6H and Li^7H band lines is plotted against the concentration ratio to yield linear analytical curves of unit slope. Although only the concentration range from 8 per cent to 25 per cent Li^6 is covered by the line pairs used in this investigation, it should be possible to extend the range up to 92 per cent Li^6 using the same line pairs.

VOL. 7 55/56

Introduction

Isotope shifts in atomic spectra have been successfully used for the isotopic assay of several of the very light and very heavy elements in the periodic system [1–5]. Since the isotope shifts in the atomic spectra are very small, it has been necessary to employ high-resolution spectroscopic techniques, such as large grating spectrographs, echelles crossed with spectrographs, or Fabry-Perot interferometers. In contrast, the isotope shift in band emission or absorption spectra of diatomic molecules of the lighter elements is large enough so that moderate dispersion instruments can be employed. For example, whereas the isotope shift in the atomic spectrum of lithium is only 0·154 Å, the isotope shift in the band spectra of Li^6H and Li^7H is as high as 3 Å. Unfortunately, the band emission or absorption spectra of many molecular combinations of the elements are very weak and frequently require elaborate techniques for producing and observing the spectra. The absorption spectra of LiH were obtained by NAKAMURA [6, 7] and CRAWFORD and JORGENSEN [8] by forming LiH in the reaction of lithium metal and hydrogen gas at elevated temperatures. The same investigators obtained the emission spectra of LiH by operating a metallic lithium arc in a hydrogen atmosphere. Exposure periods of up to twenty-four hours were required to give satisfactory intensities.

During some recent studies on the excitation of molecular emission spectra, we observed that the alkali-metal hydride-band spectra could be obtained by simply operating a carbon arc containing salts of the alkali metals in a hydrogen-helium atmosphere. Exposure periods of approximately three minutes were sufficient to produce well-developed spectra. Because of the large isotope shift shown by these spectra, it seemed appropriate to investigate the application of these spectra for isotope abundance ratio determinations.

Contribution No. 359. Work was performed in the Ames Laboratory of the Atomic Energy Commission.

Apparatus and procedure

The initial experiments were conducted by exciting the samples in quartz excitation chambers patterned after the design of OWEN [9]. However, the formation of a lithium glass on the inside walls caused frequent cracking of the chambers. This led to the construction of chambers using furnace tubing made from alundum, since this substance is not only a good electrical insulator, but is also resistant to thermal shock and chemical corrosion.

Fig. 1 shows the construction details of these chambers. The alundum sleeves were 5-cm long. The opposing holes drilled into the tube to accommodate the electrodes were ground

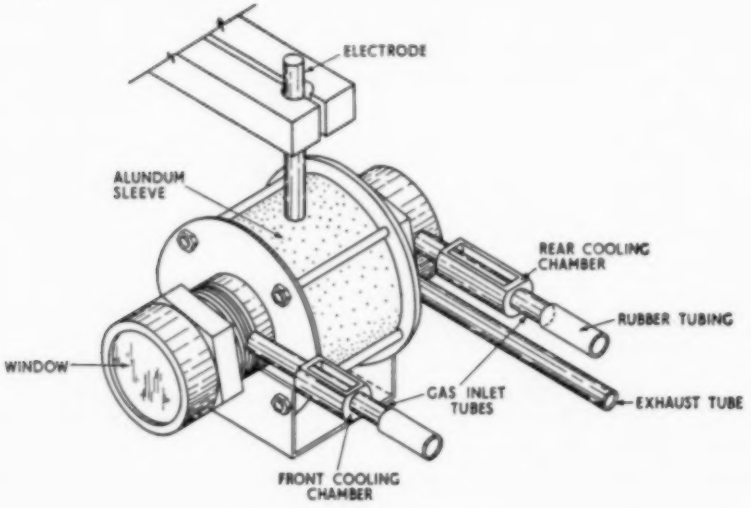

Fig. 1. Excitation chamber

to provide a snug but free fit to the electrodes. The window nacelles were made by drilling 2·4-cm holes through 2·5-cm brass pipe-caps. Radiation passing through the rear window was used to form an image of the electrodes on an auxiliary screen for the purpose of monitoring electrode spacing during the excitation. The cylindrical containers on the gas-inlet arms contained water to prevent the rubber connecting tubing from melting. The rear gas-entry arm prevented the rear window from becoming coated with vaporized sample during the excitation. The bore of the rear arm was about one-third that of the front arm, so that most of the gas flowed from front to rear in the chamber. The hydrogen escaping through the exhaust tube was allowed to burn. The windows were either borosilicate glass (Pyrex) or quartz, depending on the wavelength region to be studied.

The hydrogen and helium were mixed in approximately a 1 : 1 ratio as follows: The hydrogen and helium tanks were connected by means of a T-tube to a flow rate meter, which in turn was connected to the two chamber inlet arms by means of a second T-tube. The helium pressure was adjusted to produce a flow rate of 60 ml per second, and then the hydrogen pressure was adjusted until the total flow rate was 125 ml per second.

Experiments were conducted to determine the optimum flow rate and concentration of hydrogen in the arc chamber. At a flow rate of 125 ml per second, it was found that hydrogen concentrations greater than 50 per cent produced no increase in the lithium

hydride spectrum intensity. Consequently, the lowest optimum hydrogen concentration was used since it produced less flame around the electrode ports and less heating of the chamber.

Lithium sulphate was selected as the sample form, because most chemical forms of lithium may be readily converted to the sulphate by fuming with sulphuric acid.

The supporting graphite electrodes (Fig. 2) were designed to achieve optimum vaporization characteristics of lithium sulphate in a hydrogen-helium atmosphere. During the first thirty seconds of arcing, the molten sulphate vigorously attacked the walls, requiring a sufficiently thick wall to retain the sample. After the decomposition of the sulphate into the oxide, the vaporization proceeded very slowly. In order to reduce the background, the slower vaporization during the later phase of the arcing cycle was accelerated by using the thinner crater walls. Variations of 0·03 mm in wall thickness caused exposure times to vary from two to four minutes.

A summary of other pertinent experimental details is found in Table 1. Photography, microphotometry, and intensity ratio computations followed standard practices. Background corrections were required. The calibration experiments covered the concentration range from 8 to 25 per cent Li^6. The standards were prepared by mixing Li^6-enriched lithium sulphate (obtained from the Stable Isotope Research and Production Division, Oak Ridge National Laboratory, Oak Ridge, Tennessee) with natural lithium sulphate (assumed Li^7/Li^6 abundance ratio of 12·3). To obtain homogeneous standards, the mixtures were dissolved in distilled water, evaporated to dryness, and fused.

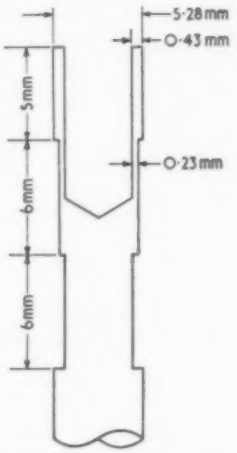

Fig. 2. Dimensions and form of the anode receptacle

The resulting analytical curves were found to be linear with unit slope in the concentration range investigated. Since the Li^7H line at 4,001·7 Å possessed an interference from a component of the NaH band system, an alternate internal standard line, Li^7H 4,000·7, was used when the sodium content was greater than 5 per cent. Although it would be possible to extend the calibration to approximately 92 per cent, using the same line pairs, the lack of sensitive lines in the complex band spectrum of LiH precludes determinations outside of the 8 to 92 per cent range. At the lower limit of determination, i.e., 8 per cent Li^6, the line to background ratio for the Li^6H 4,002·12 line is only 1·15. For this reason, the average deviation of plotted points increases as the analysis line intensity decreases. Thus, the average deviation from the mean for the calibration points was ± 15 per cent for 8 per cent Li^6, ± 7 per cent for 13 per cent Li^6, and $\pm 2{\cdot}5$ per cent for 20 per cent Li^6.

The most serious disadvantage of the procedure is the large sample (approximately 500 mg) required per analysis. This requirement virtually prohibits the extensive analytical use of this technique unless more efficient excitation methods can be devised.

The isotopic assay of lithium by mass and optical spectroscopic methods has been extensively investigated, but discrepancies in the natural abundance ratio values still exist [11]. Since intensity ratios between band components arising from the same transitions in the Li^6H and Li^7H molecule provide useful data on the natural abundance ratio, a special search was made for such related line pairs. However, the combination of very weak line intensities, high background, and interference uncertainties prevented us from obtaining data of adequate accuracy. The actual line pairs employed (see Table 1) for the analytical curve exhibited the best compromise of maximum intensity and freedom from interference, but the transitions producing the lines are not directly related.

Table 1

Operating conditions for obtaining calibration data

Spectrograph	Bausch and Lomb Littrow prism spectrograph, glass optics, reciprocal linear dispersion at 4,002 Å of 4·5 Å/mm.
Line pairs	$\frac{Li^6H\ 4{,}002{\cdot}1}{Li^7H\ 4{,}001{\cdot}7}$ < 5 per cent Na_2SO_4 in samples
	$\frac{Li^6H\ 4{,}002{\cdot}1}{Li^7H\ 4{,}000{\cdot}7}$ > 5 per cent Na_2SO_4 in samples
Upper electrode (cathode)	Graphite rod 6·3 mm diameter 75 mm long, and pointed.
Lower electrode (anode)	Electrode as described and shown in Fig. 2 loaded with 250 mg of powdered lithium sulphate. The spectra of two excitations are photographed in superposition.
Excitation source	250 volts d.c., adjusted to 6 amperes for arc between carbon electrodes in H_2–He atmosphere.
Analytical gap	4 mm
Photographic emulsion	Eastman III-O
Slit	0·02 mm
Spectrograph diaphragm	A focal plane diaphragm must be used to prevent scattered and reflected light from affecting adjacent areas of the plate [10]
Step sector apertures	360°, 237°, 156° (step ratio = 1·52)
Exposure time	Arced to completion

References

[1] BURKHART, L. E., STUKENBROEKER, G. L., and ADAMS, S.; *Phys. Rev.* 1949 **75** 83.
[2] MCNALLY, J. R., Jr.; *Applied Spectroscopy* 1952 **6** (No. 2) 27.
[3] BRODY, J. K., *J. Opt. Soc. Amer.* 1952 **42** 408.
[4] STUKENBROEKER, G. L., SMITH, D. D., WERNER, G. K., and MCNALLY, J. R., Jr., *J. Opt. Soc. Amer.* 1952 **42** 383.
[5] BRODY, J. K., FRED, M., and TOMKINS, F. S., *Spectrochim. Acta* 195 **6** 383.
[6] NAKAMURA, G., and SHIDEI, T.; *Japanese J. Physics* 1931 **7** 33.
[7] NAKAMURA, G.; *Zeits. f. physik* 1930 **59** 218.
[8] CRAWFORD, F. H., and JORGENSEN, T.; *Phys. Rev.* 1934 **46** 746; 1935 **47** 932.
[9] OWEN, L. E., *J. Opt. Soc. Amer.* 1951 **41** 139.
[10] KNISELEY, R. N., and FASSEL, V. A., *J. Opt. Soc. Amer.*, 1954 **44** 390.
[11] BALDOCK, R., and PATTON, J. R.; Atomic Energy Commission Unclassified Document Y-758 (1951).

Book reviews

FRITZ LÖWE: **Optische Messungen des Chemikers und des Mediziners.** 6 Auflage. pp. xx + 364. 1954. Theodor Steinkopff, Dresden und Leipzig. Price: 16s.

THE new edition of LÖWE's well-known book devotes 174 of its 309 pages of text to applied spectroscopy, in addition to shorter chapters on other optical methods such as photometry, refractometry, and interferometry. As is inevitable in a book which first appeared some thirty years ago, descriptions of older methods and equipment occupy a larger space than would be granted them in a completely new book, but the fact that, for instance, FASTIE's modification of the Ebert grating monochromator is illustrated, indicates that recent instrumental developments have not been ignored. The long chapter on spectroscopy is subdivided into sections on types of spectroscopes and spectrographs, absorption spectroscopy, and methods of spectrochemical analysis. The treatment of general principles and apparatus is better than that of specific analytical methods. One searches in vain for reference to such recently introduced but widely employed techniques as FELDMAN's porous cup solution spark method or any of the rotating-disk methods. In general the equipment described is of Zeiss origin, the author being particularly qualified to deal with this, but some illustrations of American apparatus are included.

This is a book for the advanced student or research worker who desires an overall picture of analytical possibilities and the type of apparatus required, rather than a laboratory manual of analytical techniques. The text is well documented, and there is a supplementary bibliography, which has a European bias. Unfortunately, numerous errors in authors' names and page references have been observed: occasional slips are unavoidable, but the number of persistently misquoted references in the literature which obviously originate from bibliographic sources is such that it is apparent that many workers rely on these, instead of consulting the original papers, and compilers of bibliographies must accept a certain responsibility.

R. L. MITCHELL

R. MAVRODINEANU et H. BOITEUX: **L'analyse spectrale quantitative par la flamme.** pp. viii + 247. 1954. Masson & Cie, Paris.

THIS quarto format volume on the use of flame excitation methods in spectrochemical analysis comprises two monographs, one by Dr. R. MAVRODINEANU on the practical aspects of the use of flame emission sources, and the other by Dr. H. BOITEUX on the nature of spectral emission from flames and the chemical equilibria involved.

The initial chapters of the first part deal with the structure, temperature, and stability of flames, the properties of the commoner fuels, particularly acetylene and oxygen, and the devices available for regulating flames. Thereafter different types of burners and sprayers are described in some detail, followed by a consideration of suitable spectrographs, photographic emulsions, and methods of photometry. A discussion of the factors, including interference effects, which in practice influence spectral emission, precedes a short section on flame photometry. Certain subjects are treated quite extensively, others, such as the commercially available flame photometers, are but briefly mentioned. Dr. MAVRODINEANU has, within the limits which he has set, provided a very useful work of reference, bringing together much of the information which has become available in the twenty-five years since LUNDEGÅRDH's early investigations, and presenting in accessible form data on such subjects as the chemical and physical properties of the gases employed, and the behaviour of droplets in a current of air, to name two of the diverse topics covered.

The section by Dr. BOITEUX on the nature of emission from flames is necessarily of a much more theoretical character. After a short discussion of the nature of light and the theory of atomic and molecular spectra, there is a section dealing with the band spectrum, ultraviolet, visible, and infrared, of air- and oxygen-acetylene flames. A long chapter deals with the elements

which can be excited in the flame and presents for each in diagrammatic and tabular form the relevant energy levels and excitation potentials. In conclusion, there is an interesting discussion of thermal equilibria and factors affecting the excitation of elements introduced into the flame. A short table of wavelengths of lines and band heads, and a series of plates of flame spectrograms, are appended.

In this book, which is a publication of the French *Office de la Recherche Scientifique Outre-Mer*, there is much information which would otherwise be difficult to find quickly when required. On the practical side, developments and modifications are being described so abundantly and are of so specialized a nature that any book dealing with such aspects of flame photometry tends to be out of date before it appears; the authors have realized this and refrained from dealing in detail with specific methods. The text is well documented throughout, and only a few minor slips have been noted.

R. L. MITCHELL

SCRIBNER, BOURDON F., and MEGGERS, WILLIAM P.: **Index to the Literature on Spectrochemical Analysis,** Part III, 1946–50. American Society for Testing Materials, 1953, Philadelphia, 226 pp, $4.50

LIKE the previous volumes in this series, this is a standard work of reference for every library which has to serve spectroscopists. It contains over 1,250 references, which are listed alphabetically in five sections, each covering one year. The disadvantages of this time-conscious classification are redeemed by an excellent subject-index and an accurate author-index. Like the second volume of the series this volume contains abstracts of nearly all the papers; some are neat informative abstracts compiled by the Editors, some quoted from Chemical Abstracts or other sources and enriched by varying degrees of detail. There is something to be said for this uneven treatment, which in general provides more detail for papers which would be less accessible to the average American reader. The scope of the subjects is comprehensive, from Meteorites to the sediments of the Tyrrhenian Sea; but a bias towards chemistry rather than physics is shown by the scarcity of papers dealing with details of equipment. It would be unfair to complain of this bias, which is indicated by the title of the work; and all spectroscopists when faced with a sample outside their usual routine will wish to refer to this book.

E. VAN SOMEREN

MICHEL, PIERRE: **La Spectroscopie d'Emission** (Emission Spectroscopy). Armand Colin, Paris, 1953, 224 pp, 260 fr.

THIS is a really concise and selective textbook on analysis by emission spectra; starting from fundamentals and closely reasoned, The author's aim is to provide academic or industrial research workers with a statement of the basic principles of spectroscopy, a few selected examples and an indication of its scope in analysis. Roughly two-thirds of the volume is given to principles and one-third to technique and application, yet the subject is followed through the principles of the calibration of photographic methods of analysis to an outline of the methods recently developed for direct analysis. There is a bibliography admittedly selective, of 44 references, which can be criticized for omitting any bibliographies; and there is an adequate index. Finally, the book is published at a price which would make an American publisher suspect a misprint, and printed in a style which is sober but graceless.

E. VAN SOMEREN

Spectrochimica Acta, 1955, Vol. 7, pp. 181 to 204. Pergamon Press Ltd., London

Near-infrared spectroscopy*

II. Instrumentation and technique

A Review

WILBUR KAYE
Research Laboratories, Tennessee Eastman Company,
Division of Eastman Kodak Company, Kingsport, Tennessee

(*Received* 28 *March* 1955)

(*Accepted for publication* 5 *May* 1955)

Summary—The rapid growth of instrumentation in the field of near-infrared spectroscopy has resulted from the development of rapid and sensitive detectors and from the realization of the many analytical and molecular structure determinations which may be studied in this region of the spectrum. The literature concerning optical materials, detectors, filters, and methods of obtaining automatic relative-transmission operation is summarized. Techniques peculiar to the near-infrared region are discussed. The literature concerning wavelength calibration is tabulated. The sample paths required and the simplified instrumentation possible in the near-infrared region favour the development of production control analyzers. Future developments in near-infrared spectroscopy will probably be concentrated in improving photometric accuracy and in the evolution of inexpensive colorimeter-type instruments.

The near infrared region is considered to cover the electromagnetic spectrum from the visible to a wavelength of about 3·5 μ (2860 cm^{-1}). This region is characterized by absorption bands arising from hydrogenic stretching vibrations, their overtones, and combinations with other modes of molecular vibration [127]. Most of these bands are very narrow in band-width and require monochromators of moderately high resolution. The band intensities vary considerably, so that cell lengths from 0·1 mm to several metres may be required. The advent of the lead sulphide photoconductive detector has opened this spectral region by providing extreme sensitivity with instruments of relative simplicity.

In the following sections the basic factors covering instrumentation for the near-infrared region are summarized and references to more-detailed literature are given. Techniques particularly adapted to the near-infrared region are discussed.

A number of commercial spectrometers which can be used in the near-infrared region are available. The Beckman model DK and Applied Physics Corp. (Cary) model 14 instruments have been specifically designed for use in the near-infrared. The Mervyn-NPL model IRS/A/1 instrument is specifically designed for use in the 2·8–3·6-μ region [143]. The conventional infrared spectrometers manufactured by Beckman (IR-2 and IR-3), Perkin Elmer (models 21 and 112), Baird (model AB2), and Farrand (UVIR) can be used if equipped with SiO_2, LiF, or CaF_2 prisms. Most of these instruments can be obtained with accessory equipment to use the lead sulphide detector. In addition to the above instruments, there are

* Presented at the Fisk Infrared Spectroscopy Institute, Nashville, Tennessee, September 2, 1954.

two grating monochromators available for high-resolution studies. These are the Baird 1-metre monochromator and the Bausch and Lomb Ebert-type monochromator. These instruments require foreprism monochromators for removal of overlapping orders and, in their present state of development, plot energy reception only.

Optical materials

Near-infrared spectroscopy presents its own unique optical requirements. These are further extended by the contemporary desire to use instruments for the near-infrared region in the ultraviolet, visible, as well as infrared regions. A large number of materials are useful in the near-infrared region, although few can be called ideal.

The literature regarding the optical properties of materials is voluminous, and the greater part of this literature was published prior to 1935. The author has found considerable assistance in this compilation from the bulletins prepared by Baird Associates [11] and Harshaw Chemical Co. [102].

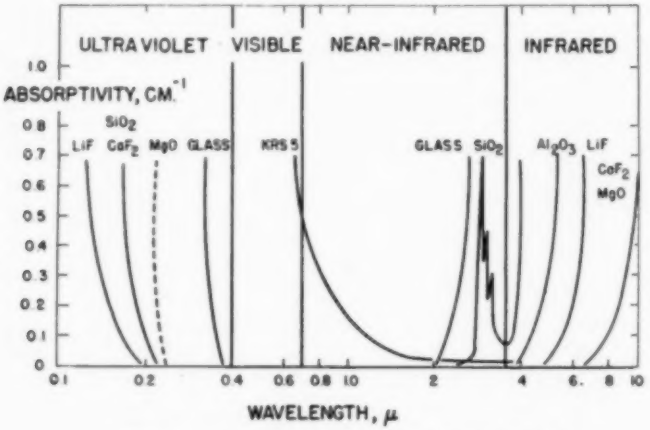

Fig. 1. Absorptivity of useful optical materials.

The optical property of prime importance is transmittance. Fig. 1 shows the transmittance of a number of useful optical materials. Values shown on this graph are not very accurate, since most of these materials show variable absorbance. Fused silica (not shown in Fig. 1) and quartz, in particular, vary widely in the absorptivity around 3 μ. For moderately large prisms an absorptivity of 0·2 to 0·4 may be tolerated, whereas an absorptivity of 0·7 may be acceptable for thin windows.

It is apparent from this graph that almost all of the common synthetic crystals are transparent in the near-infrared. Unfortunately, the most widely-used material, quartz, has a series of moderately intense absorption bands between 2·8 and 3·1 μ. These bands are believed to be due to occluded moisture [61]. These bands are considerably weaker, broader, and occur around 2·75 μ in fused silica. It may be possible to find a method of preparation that will reduce the

intensity of these bands and thus greatly improve the usefulness of quartz and silica in the near-infrared region.

The "glass" shown in Fig. 1 is Pyrex glass. The optical properties of other glass formulations may vary widely in both ultraviolet and near-infrared regions [47]. However, almost all formulations begin absorbing strongly at 2·7 μ. This region of absorption is due to water and carbon dioxide (or carbonates). It has been shown to be possible to eliminate these absorption bands from oxide glasses almost completely by treating the melt in vacuum or dry air [70, 71, 79]. A glass formulation possessing acceptable ultraviolet transmission so treated could make an ideal material for cell windows.

Glasses containing rare-earth oxides frequently possess moderately intense absorption bands in the near-infrared [207]. These bands do not appear to possess sufficient intensity or narrow band-width for filters. Glasses composed of monoxide materials have been prepared. These transmit over a wide spectral range, but possess a high refractive index, thus high reflective loss [74].

A large number of other materials are transparent in the near-infrared region. NaCl, NaF, KCl, KBr, spinel, CsBr, CsI, CdF_2 [91], SrF_2, BaF_2, CaF_2, PbF_2, and $SrTiO_3$ [163] are known to be transparent [117]. Calcite possesses several strong absorption bands at 2·75, 2·50, and 2·3 μ; however, regions exist between and below these wavelengths where calcite is sufficiently transparent for use in polarizing radiation.

The transparency of a material is not only determined by its absorptivity (Fig. 1), but is also determined by its reflectivity. This reflectivity is a function of the angle of incidence of the radiation and the refractive index. At normal incidence the reflectivity is given by the formula

$$R = [(n - 1)/(n + 1)]^2$$

where n is the refractive index at the wavelength in question. Multiple reflections

Table 1. Water solubility and refractive index of optical materials

Material	*Water solubility, g/100 ml/20°C*	*Refractive index (2 μ)*
SiO_2	Insol.	1·52
TiO_2 (rutile)	Insol.	3·2
As_2S_3	0·00005	—
Al_2O_3	0·000098	1·8
AgCl	0·00015	2·00
MgO	0·00062	1·71
$CaCO_3$	0·0014	—
CaF_2	0·0016	1·42
KRS-5	0·05	2·40
LiF	0·27	1·38
NaCl	36	1·53
KBr	65	1·54
CsBr	124	1·67
CsI	44	1·7

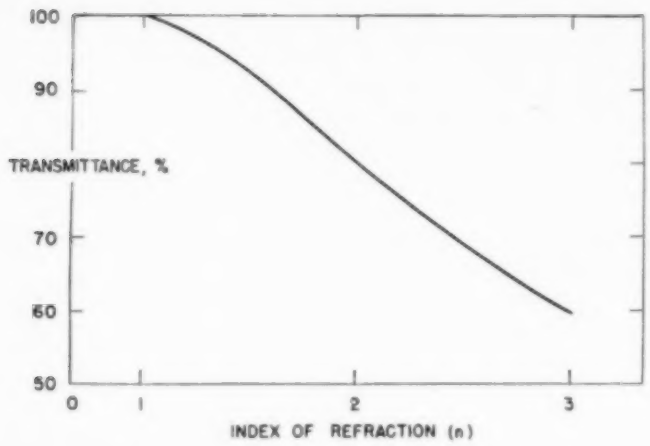

Fig. 2. Transmittance of a plane parallel plate of dielectric without absorption.

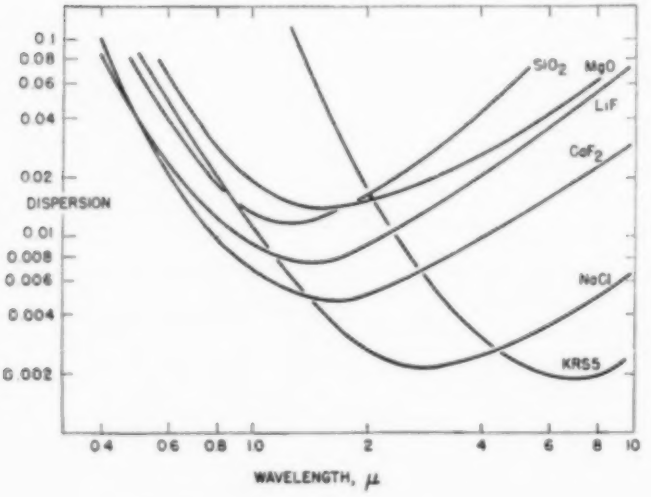

Fig. 3. Dispersion of some common prism materials.

also affect the transmittance, so that non-absorbing materials may best be described in terms of refractive index, using the formula

$$T = 2n/(n^2 + 1)$$

Fig. 2 shows a plot of this formula. Refractive indices of common materials at a wavelength of 2 μ are tabulated in Table 1. Materials such as rutile and KRS-5 have a large light loss because of reflectance.

The solubility and mechanical properties of optical materials must also be considered, especially for sample cells. Most of the materials shown in Fig. 1 are reasonably insoluble in the majority of solvents. Table 1 lists the solubility in water of a number of optical materials. Silica and sapphire (Al_2O_3) possess excellent solubility properties [225]. Magnesium oxide is attacked by atmospheric CO_2 under humid conditions, but is unaffected in dry air [213]. The mechanics and thermal properties of most of the commonly used optical materials have been measured [46].

In selecting a suitable prism material, the dispersion, or change of refractive index with wavelength, is important. Fig. 3 is a plot of the dispersion vs. wavelength for the common prism materials. Under the conditions found in the near-infrared region and using the lead sulphide detector, the resolution achieved with a given spectrometer will be directly proportional to the dispersion (assuming prisms of the same base). Quartz is obviously the best general-purpose prism material readily available, although KRS-5 could be used advantageously between 1 and 2 μ. Fused silica is intermediate between quartz and LiF [191, 192]. When available, MgO may be found to be the best material [8, 211].

Gratings

Recent developments in infrared filters have increased the interest in gratings for dispersing near-infrared radiation. It is possible to achieve a much higher resolution with a good quality grating than is possible with a prism. However, this does not automatically make the grating instrument better than the prism instrument. Many near-infrared spectra taken with gratings are inferior to the best of those taken with prisms. Few prism instruments possess resolving powers in excess of 1000, whereas the double-pass grating instrument of RANK'S design has a reported resolution of 145,000 at 4000 cm^{-1} [183, 186]. The gratings for near-infrared spectroscopy must be blazed properly to concentrate most of the light energy in the desired order of the spectrum. For this reason most grating instruments do not respond well over a wide spectral range. Of course, some means of eliminating unwanted spectral orders must be incorporated in the instrument, but these may be readily eliminated by the use of filters as well as by modifying the sensitivity of the detector [45, 80, 86, 139, 159]. In general, the high resolution of the grating instrument is required only for the study of the rotational spectra of gases, but economical considerations may favour the use of replica gratings for low to moderate resolution applications. Two prism-grating instruments, one manufactured by Applied Physics Corporation and the other by Baird Associates, are on the market to-day. The echellette grating has been considered for use in the near-infrared region in conjunction with the lead sulphide detector [106].

Multi-pass operation

A portion of the high resolution achieved with conventional prism spectrometers is due to the passage of light twice through the prism in the Littrow mounting. It is possible to pass light through the prism more than twice, but this was not considered practical, because of the increase in scattered light, until the advent of fast-responding detectors permitted the use of modulated light. If the light

modulator (shutter) is placed between the second and third (or higher) pass through the prism, a detector tuned to the frequency of modulation will not respond to the light scattered by the prism on its first two passes through the prism, because this scattered light is unmodulated. Since the vastly greater portion of scattered light arises in the first two passes through the prism, this scheme greatly reduces scattered light.

The exact origin of this idea appears obscure [170, 190] but it was first successfully utilized by WALSH [226–229]. The passes through the prism are usually counted in pairs, so that the light in a double-pass monochromator actually traverses the prism four times. Still greater numbers of passes are entirely possible, so that prism instruments can approach the resolution of the grating instrument [230, 95].

Multi-pass operation is not limited to prisms, but may be used with gratings [67, 184, 186].

In some cases double-pass operation is not compatible with double-beam (automatic relative transmission) operation. With instruments similar to the Beckman DK spectrometer, in which light modulation and beam splitting are two separate operations, it is admirably suited.

Resolution is not automatically doubled with double-pass operation, since reflection losses decrease the beam energy. However, if sufficient energy is available so that resolution (for a given noise level and response time) is limited by diffraction or any other time-independent reason, the resolution increase approaches the theoretical value. This situation is frequently encountered in instruments containing the sensitive lead sulphide cell.

VOL.
7
1955/5

Sample cells

Conventional (3–40 μ) infrared spectroscopy requires liquid cells 0·005 to 0·1 cm thick, while gas cells 10 to 100 cm long are usually satisfactory. In the near-infrared it is necessary to use cells many times this length because of the lower absorptivity of the overtone bands. Table 2 lists the approximately optimum cell thicknesses for various wavelength regions. Gas cells for equivalent regions should usually be a hundred times longer than liquid cells. Cells up to 3168 metres in length have been used for studies with gases [23, 231].

The composition of the cell windows is usually determined by spectral transmission and solubility properties, although unusual conditions, such as high

Table 2. Optimum cell thickness

Wavelength (μ)	*Cell length* (*cm*)	*Designation*
3·5–2·7	0·005–0·2	Fundamental
2·7–1·8	0·05–2·0	Combination
1·8–1·4	0·1–1·0	1st overtone
1·4–0·9	1·0–20	2nd overtone
0·9–0·6	10–	3rd and 4th overtones

temperature or pressure, must be considered. In addition to the inorganic materials listed in Table 1, there are a few organic compounds which would be desirable in special cases. Polytrifluorochloroethylene has been recommended in cell construction [204].

If absorbance values must be measured to a high degree of accuracy, considerable attention must be paid to the construction and mounting of the sample cells. Windows must be plane and parallel and readily cleaned without changing cell thickness. Cells must be repositioned accurately and contain no flaws which might distort the optical beam.

Detectors

The spectroscopist is fortunate in having a wide variety of detectors suitable for use in the near-infrared region [114]. Table 3 lists these detectors along with their useful wavelength range and references to pertinent literature. The first four

Table 3. Detectors for use in the near-infrared region

Type	*Useful range (μ)*	*Reference*
Photographic	–1·4	14
Evaporographic	1–9	49, 133
Image converter	0·4–1·5	2, 22, 53, 116, 223
Stimulated phosphorescence	–1·4	220
Temperature-sensitive phosphors	—	221
Photoemissive	–1	43, 128, 131
Pneumatic	wide	84, 85, 205
Bolometer	1–	24, 173
Superconducting bolometer	1–	4, 77
Thermocouple	1–	110, 120
Thermistor	1–	238
Photodiode (Sylvania 1N77A)	0·4–2·0	215
Carbon	1–	141
Thalophide	0·6–1·3	15, 41, 66, 75, 107
Cadmium sulphide	0·3–1·6	83, 208
Lead sulphide	0·3–3·2 (300°K)	68, 152–155, 187, 195, 206, 214
Lead selenide	1·5–5·5 (290°K)	27, 149, 157, 189, 210
	–8 (90°K)	157
Lead telluride	1·5–5·5 (90°K)	68, 130, 155
Indium selenide	0·5–2·0	30

detectors listed in this table are image receivers and their greatest use is in obtaining high-resolution spectrograms. Only the photographic detector is used to any extent in spectroscopy in the near-infrared region. A novel detector combining the image converter with a photomultiplier tube has been reported [116].

The photoemissive and pneumatic detectors differ from the others in responding to the total light energy received rather than to the energy per unit area [118]. As a result the light beam need not be focused upon a small area, and economies in instrument design result. Unfortunately, the photoemissive detectors

do not respond beyond 1·4 μ, and the most sensitive types with built-in multipliers are not made with infrared-sensitive photoemissive surfaces. On the other hand, the pneumatic detector can be used at almost any wavelength (e.g., the Golay cell [84, 85]), and can be made very selective in wavelength, depending upon the absorption properties of the filling gas. The pneumatic detector has been popular in the nondispersing gas analyzers.

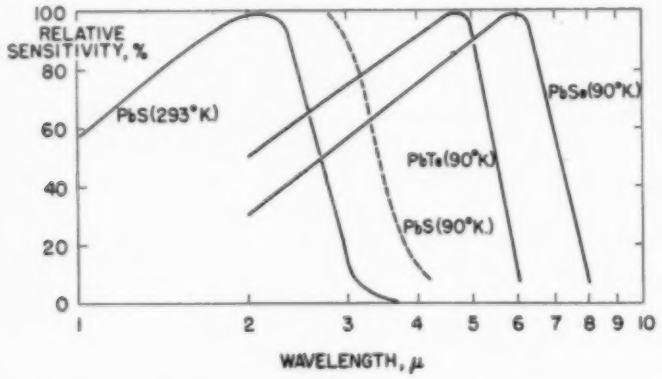

Fig. 4. Response curves of lead sulphide, selenide, and telluride.

The thermocouple and bolometer receivers are essentially heat-sensitive devices. They have the broadest band width and, for this very reason, do not possess high signal-to-noise ratios because of their response to long-wavelength room radiation. It is necessary that they be coated with an absorbing layer of material. They are frequently placed in an evacuated space. In practice they also suffer from an inherently slow response and low impedance, requiring expensive amplifiers; however, they are the most widely used receivers. The thermistor is also a heat-sensitive device, but possesses a high internal impedance ($>$1 meg) and somewhat faster response than the thermocouple [187].

The rest of the detectors tabulated are photoconductive; i.e., their resistance changes in proportion to the intensity of light falling upon them (differentiated from a simple thermal change). The conductance of these detectors depends upon the presence of impurity centres in the crystalline lattice [187] and the wavelength-sensitivity curve depends markedly upon the exact method of preparation [206, 210]. This photoconductivity is a property found in a wide variety of crystals containing impurity centres, and this property (photoconductivity) is being widely used for the study of the solid state. Reference 132 contains a good review of this application along with the early history of photoconductors. Fig. 4 shows the relative response curves of lead sulphide, selenide, and telluride cells. Since the lead telluride cell has no appreciable response at room temperature, its response at liquid-air temperature is shown. The lead sulphide cell is the most widely used photoconductive detector and, in the wavelength range from 1 to 2·5 μ, is by far the most sensitive detector commercially available.

VOL.
7
1955/

In order to understand the reasons for the great sensitivity and low noise of these detectors, it is necessary to consider the black body radiation from all material in the vicinity of the detector [118, 119]. As the detector becomes sensitive to longer wavelengths, it becomes more affected by room temperature. Table 4 lists the percentage of the total power radiated by a black body source which is effective in operating the detector [157]. These detectors thus make

Table 4. Percentage of the total power radiated by a black body source which is effective in operating the cell [157]

Source temperature (°C)	PbS (290°K)	PbTe (90°K)	PbSe (90°K)
300	2·5	25	48
200	0·7	13	34
150	0·25	8	26
100	0·07	5	14
50	0·01	2	11
20	0·004	1	7
0	0·001	0·6	5

OL.
7
5/56

excellent heat-monitoring devices. All of the photoconductors show an increased sensitivity with a shift of the cutoff to longer wavelengths upon cooling; however, if improved signal-to-noise ratio is desired, it is necessary to shield the cell from room-temperature radiation. Fig. 5 shows the marked improvement in the response of the Kodak Ektron (lead sulphide) cell upon cooling.

Two different types of lead sulphide cells with somewhat different characteristics are available [149]. Vacuum deposition of the sulphide in a controlled, low-pressure atmosphere of oxygen results in a detector of short time constant and somewhat inhomogeneous sensitive area. These deposits must be protected from the atmosphere and are usually sealed under a vacuum in a glass envelope. The other method of manufacture consists of chemically depositing the lead sulphide. These cells possess somewhat longer time constants than vacuum-deposited cells and are reported to be slightly more sensitive. They are not so sensitive to the atmosphere and are usually protected only with a thin coating of lacquer. These cells do show an increasing time constant and decreasing resistance with increasing relative humidity.

In all of the photoconductive cells, both the signal and noise increase with increasing bias across the cells. The greater the signal out of the detector the less is the gain required of the amplifier; hence it is desirable to operate the cell with a large bias voltage. The voltage must not be so high as to cause appreciable heating of the detector (approx. 0·01 watt per sq mm). If large signals are received, the amplitude-intensity relationship may become nonlinear owing to appreciable reduction in bias voltage. This situation is seldom encountered in spectrophotometry. Unlike the thalophide cells, the lead sulphide cell does not fatigue upon exposure to intense radiation.

Many factors govern the response of radiation detectors, and these have been carefully examined. As a result, precise definitions and units of response have been developed [35, 118–122]. The detectivity- or responsivity-to-noise ratio for the photoconductive detector has been found to be inversely proportional to the square root of the sensitive area [119]. Thus, the smaller the sensitive area the better, assuming, of course, that this area is filled with concentrated radiation.

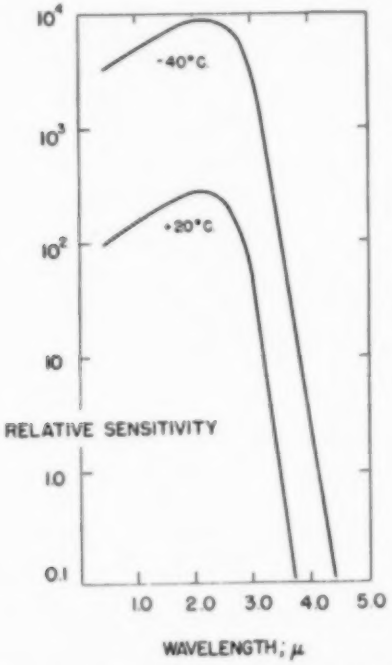

Fig. 5. Response curves for a Kodak Ektron Detector.

When the slit image cannot be effectively focused on the detector by means of a lens or mirror, it is possible to condense the beam on the detector by means of a reflecting cone placed immediately over the detector [237]. The sensitive area of the detector should assume the shape of the slit image in the plane of the detector. Electrodes should be applied to opposite sides of this area either lengthwise or widthwise, depending upon the desired resistance of the cell. If the resistance in either case is not too great to match the input impedance of the amplifier, the position giving the greater impedance should be used. This position will permit the application of greater bias potential and give the greater signal (though with no change in signal-to-noise ratio). The load resistor for the cell should be equal to or greater than the resistance of the cell.

The relation between the speed of response and the detectivity of the lead sulphide cells has been found to be somewhat unusual. The detectivity is found to be relatively little affected by the frequency of light modulation for frequencies greater than the crossover frequency. However, at frequencies of light modulation

less than the crossover frequency the detectivity increases with increasing time constant [121].

Although the lead sulphide detector in its present development is an admirable one, better detectors can be imagined. The greatest fault of the lead sulphide cell is its rapidly decreasing detectivity beyond 2·7 μ. If this cut-off wavelength could be increased to 3·5 μ (at room temperature), it would permit studies in the valuable fundamental hydrogenic stretching region. Lead selenide and telluride cells do respond at this longer wavelength, but for maximum usefulness they must be cooled and so respond to wavelengths beyond 3·5 μ where black body radiation proves a source of noise.

Sources

The conventional sources of infrared radiation, the globar and Nernst glower, are not well suited to near-infrared spectrophotometry. Better sources operating at higher temperatures are available. An ordinary incandescent headlight bulb will serve admirably as a source out to 4 μ [31]. For more intense radiations, one may modify a tungsten source [5, 217] or use an arc lamp of the zirconium type [38, 94] or of carbon [115, 194]. Certain moderately narrow-band sources of infrared energy may be obtained from hot powders (eigenfrequenzen) [171]. A few gaseous discharge emission lines are of interest as sources [145]. (See Calibration section.) *p-n* Junction transistors have recently been shown to emit near-infrared radiation over a narrow band-width and can be electrically modulated [33].

Filters

A number of different methods of filtering near-infrared radiations are available [150]. Such filters are desirable in the near-infrared region to reduce scattered light. If a grating is used as dispersing element, overlapping orders may be eliminated. In the future, instruments for production control (other than the gas analyzer) probably will use filters only to select the wavelength desired. Unfortunately, the analytical possibilities of the near-infrared region have not been widely exploited, and filters for this region have been studied only incidentally in conjunction with conventional infrared spectroscopy studies.

Table 5 contains the main types of filters, the nature of radiations transmitted or reflected, and references to the literature. A band-pass filter will be one absorbing strongly both above and below a given spectral region. The width of the pass band will usually depend upon the thickness of the absorber or the number of interfering elements. Usually the narrower the pass band the lower the efficiency, or percentage of light of desired wavelength transmitted or reflected. Transmission interference filters for near-infrared radiation have recently been prepared by Baird Associates. Fig. 6 shows the excellent nature of these filters. Auxiliary broad-band filters are necessary to remove the side bands from these interference filters. An interference filter designed to pass 700 mμ radiation has been observed in this laboratory to pass radiations acceptably at 1400 mμ.

A high-pass filter transmits (or reflects) all desired wavelengths above a certain cut-off which, for scattering-type filters, depends upon the particle size (or grating space). The Ag_2S filters manufactured by Eastman Kodak Company are good

Table 5. Filters

Type	*Pass*[a]	*Reference*
Absorption-gas	Band-pass	—
liquid	Band-pass	—
film	Band- or low-pass	29
glass	Band- or low-pass	47, 126
crystals	Low-pass	173, 174
Metals		
Bi	High-pass	181, 199
Ge	High-pass	6, 32, 185
Sb	High-pass	181
Se	High-pass	16, 197
Te	High-pass	156, 181
PbS	High-pass	7, 169, 224
PbSe	High-pass	7
PbTe	High-pass	7
ZnS	High-pass	176
InSb	High-pass	216
Ag_2S	High-pass	181
Christiansen	Band-pass	17, 23a, 54, 174, 203
Scattering-transmission	High-pass	16, 101, 105, 174, 181
reflection	High-pass	232
Interference-transmission	Band-pass	12, 89, 90, 94, 99
reflection	Band-pass	89, 90, 94, 95, 99, 222
Birefringent	Band-pass	25, 65, 123
Total reflection	Band-pass	26
Metallic reflection (restrahlen)	Band-pass	173
F-centre (halide)	High-pass	76, 80

(*a*) Refers to wavelength.

examples. The cut-off wavelength can be selected by varying the thickness. The only low-pass filters are those which transmit short-wavelength radiations well and absorb at long wavelengths. Their cut-off is usually not sharp and depends strongly upon thickness. In general, reflection-type filters are more efficient but are not so readily adapted to existing instruments as are transmission filters. Some filters, particularly the birefringent type and, to a lesser extent, the Christiansen and interference filters, are capable of being "tuned" to transmit various wavelengths.

Among the most promising filters for the reduction of scattered light in the important 2·65- to 3·0-μ region are the semiconducting materials [181]. These

materials have absorption bands in the 0·5- to 1·5-μ region and have been the subject of much study in the field of solid-state physics [132]. Unfortunately they possess high indices of refraction which lead to high reflection losses. These

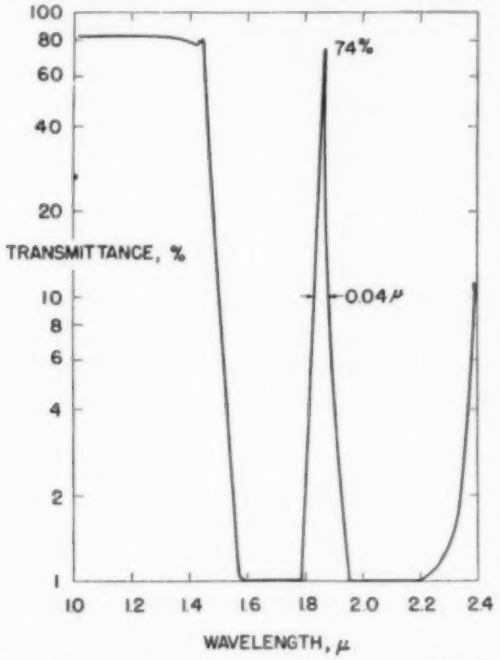

Fig. 6. Absorption curve for a Baird transmission interference filter.

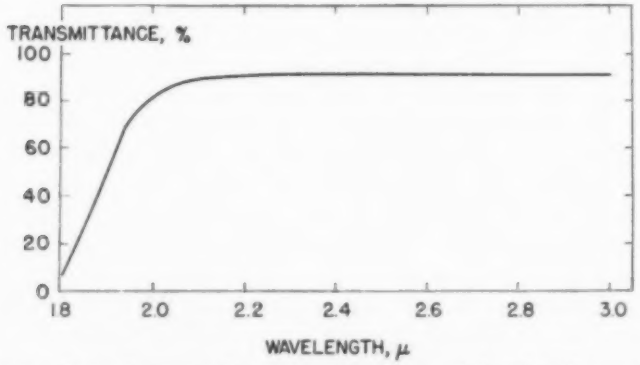

Fig. 7. Absorption curve for a germanium filter coated with antimony trioxide (Baird Associates, Inc.).

reflection losses can be reduced considerably by depositing quarter-wave films on the surface. Fig. 7 shows the absorption curve for one of the best of these filters prepared by Baird Associates, Inc. It is composed of a $\frac{1}{8}$-in. thickness of pure germanium coated with quarter-wave layers (at 2·5 μ) of antimony trioxide.

The cut-off wavelength can be shifted to shorter or longer wavelengths by varying the thickness of germanium. The F-centre halide crystals offer considerable promise as filters since the cut-off frequency can be shifted [76, 89].

Recording

Most of the early spectral data was obtained in the form of point-by-point manual operations. Curves plotted in this manner may be accurate if the instrument is stable for moderate periods of time and if the operator is patient enough. However, for scanning wide spectral regions, particularly in the infrared, the method consumes a prohibitive amount of time. Photographic recording of the displacement of a beam of light by a galvanometer mirror has been used to plot the energy of radiation affecting the detector. An improvement upon this method has been available by using electronic pen recorders such as the Brown Elektronic and the Leeds and Northrup Speedomax. More recently, pen recorders have been modified to plot the ratio of energies transmitted by two cells resulting in transmittance vs. wavelength curves automatically. A large number of schemes for accomplishing this purpose have been published. Table 6 lists the essential factors in these schemes.

The modulation frequency is listed, since it in part determines the speed of operation. With some instruments this modulation frequency must be distinguished from beam alternation between sample and reference paths. The response time of the detector is of prime importance in determining the maximum modulation frequency. In recent years, d.c. operation has been out of favour for infrared instruments because of thermal drift, but this method may regain favour if the total scanning time can be reduced to a period of time over which thermal drift is negligible.

A number of different beam-splitting devices have been used. Those methods which sample different parts of the slit area or source are susceptible to errors in absorption or emission from different parts of the instrument. Oscillating mirrors may readily introduce vibration, which almost eliminates this method when using the microphonic photomultiplier detector. The polarizing prism method possesses many advantages for the visible region, but, as yet, polarizers which are efficient enough are not available for the infrared region. Some of the methods developed depend upon some memory device for maintaining a constant reference or incident energy. The advantage of this method is simplified optics, particularly since only one sample cell is required. The disadvantages are the complexity of the memory device and the requirement of source and dispersion stability. One of the newer promising methods is the rotating sample cell. The author fabricated a device of this sort early in the development of the DK spectrometer. It is one of the simplest methods of obtaining automatic relative transmission operation, but it becomes more difficult as the sample cell size becomes larger. For operation at 3 to 15 μ it should be quite suitable.

There are essentially three methods for balancing the reference and sample beams to record transmittance (or absorbance): the optical null method, the ratio method, and the method of holding the reference constant. The optical null method (best exemplified by the Baird and Perkin-Elmer 21 instruments) places

VOL.
7
1955/5

VOL. 7 5/56

Table 6. Comparison of methods for obtaining relative transmission values automatically

Year	*Author*	*Ref.*	*Modulation frequency*	*Beam-splitting device*	*Balancing system*	*Slit control*	*Monochromator*	*Detector*
1929	A. C. HARDY	97	120	Rotating mirror	Aperture in I_0	Fixed	Custom	Phototube
1935	A. C. HARDY	98	60	Wollaston prism	Rotation of Rochon prism	Cam	Custom	Phototube
		147		Integrating sphere	Rotation of Rochon prism		General Electric	
1939	J. D. HARDY	100	d.c.	1/2 slit	Manual optical null	Manual	Custom	Thermopile (2 arms)
1942	LEHRER	134			Comb			
1943	BAKER	10	1·25	Oscillating mirror	Plots I only	Constant energy	Custom	Bolometer
1945	OETJEN	166			Plots I only	Cam	Custom	
1947	COOR	48	d.c.	1/2 silvered mirror	Ratio	Constant energy	Beckman DU	Photomultiplier (2)
1947	CARY	40			Ratio		Double mon.	Photomultiplier (2)
1947	WRIGHT	239	6	Rotating mirror	Comb	Linear gear	Custom	Bolometer
1947	BAIRD	9	10	Rotating mirror	Comb	Cam	Baird	Bolometer
1947	WILD	235	1/15	Automatic cycling		Servo		
1949	FOREMAN	72	(10)	Manual memory correction by controlling slidewise voltage		Manual	Beckman IR-2	Thermocouple
1949	HALES	92	d.c.	1/2 slit	Ratio	Manual ?	Hilger	Thermopile (2 arms)
1950	SAVITSKY	198	10	1/2 slit	Ratio (90° phase)	Cam	Perkin-Elmer 12B	Golay
1950	HORNIG	111	3	3 rotating mirrors	Ratio	Constant energy	Perkin-Elmer 12B	Thermocouple
1950	WHITE	233, 234	13	Rotating mirrors	Comb	Cam	Perkin-Elmer 21	Thermocouple
1951	DALY	50	1500 (1/10 sec sweep)	Oscillating mirror	Plots I_0–I	Fixed	Unicam	PbS (cathode-ray presentation)
1952	KAYE	126	480	Rotating mirror (12 c.p.s.)	Ratio	Constant energy	Beckman DU	Photomultiplier, PbS
1952	CARY	103	30	Rotating mirror	Pulse ratio	Servo	Applied Physics Lab. 14	Photomultiplier, PbS
1952	MALYSHER	138	9	Rotating mirror	Comb	Cam ?		Bolometer
1952	NORMAND	164	22	Uses two wavelengths	Ratio	Fixed	Dobson	Photomultiplier
1952	GOULDEN	87, 88	16-2/3	Rotating cell	I_0–I plotted	Fixed	Grubb Parsons	
1953	ETZEL	64	35	Mirror (prism)	Ratio	Constant energy	Beckman DU	Photomultiplier
1953	BROCHARD	34	875	Rotating mirror	Rotating Wollaston prism			
1953	DALY	50			Rotating star wheel			
1953	BEITZ	20	(1/180 sec sweep)	None	Graded metallic filter at focal plane of slit	Fixed	American Optical Co.	Photomultiplier (cathode-ray presentation)
1953	COLE	44	External to monochromator		(Type of double pass-double beam operation)		Grubb Parsons	Thermocouple
1953	KING	129	30	1/2 slit (mirror)	Ratio (90° phase)	Constant energy	Perkin-Elmer 12C	Photomultiplier
1953	NELSON	160	60	Collimator	Records I only (no mechanical commutation)	Dynode voltage	Custom	Photomultiplier
1953	CAHN	39	15	2 rotating mirrors	Ratio	Constant energy	Beckman DK	Photomultiplier, PbS
1953	ORR	168	6·5	Rotating mirror for double-pass				
1953	AVERY	5	33	Rotating mirror	Uses I only	Constant energy	Custom	Thermocouple
1953	ZBINDON	242		Rotating mirror	Ratio	Constant energy		
1953	AHLERS	3	13	Rotating cell	Ratio	String	Perkin-Elmer 12C	Thermocouple
1953	HALES	93	8	Rotating mirror	Ratio	Constant energy	Custom	Thermopile (2 arms)
1953	ROYER-WARREN	193a	60	Multiple mirror	Ratio	Constant energy	Beckman DU	Photomultiplier (2)
1953	CAHN	39	1/8	Cell in—cell out	Ratio (cycled)	Constant energy	Beckman DR	Photocell
1954	MERVYN	143	800	None	Adjustable cam on gain	Manual ?	Grating	PbSe
1954	YANG	241	60	Vibrating mirror	Ratio	Fixed (see detector)	Beckman DU	Photomultiplier variable dynode voltage

no requirement of linearity on the amplifiers, but does require precise machining of the comb or other optical attenuating device. One disadvantage of this method is the loss of balancing information at low transmittance due to attenuation of light by the comb as well as the sample. The ratio balancing method has gained favour in recent years because of the improvement in linear amplifiers and the recognition of the greater versatility of the ratio method. Scale expansion, high speed, and differential type operation are readily achieved by this method. The method of holding the reference or incident radiation constant is actually a special case of ratio operation. The memory method of the IR-3 instrument operates by holding the incident energy constant by varying the slit width according to a previously determined (memorized) function. This method may be more cumbersome when the absorber in the reference beam (solvent) varies often. In other methods of holding a constant reference, a cam-operated slit and a graded filter are used. These methods do not permit any compensation for solvent.

Almost invariably the method used to maintain a constant (or nearly constant) reference signal is to vary the slit width and thus let more or less light energy into the monochromator. This is accomplished by programming the slit width with a cam or by monitoring the energy in the reference channel and servo operating the slit for constant energy. Since (among other variables) the slit width determines the resolution, the cam method always reproduces the same instrument resolution. This is not necessarily so of the constant-energy method. Although this represents a disadvantage for the constant-energy method, there are several advantages in its favour. Compensation for solvent absorption is much more readily possible. Cams cannot economically be made to hold the signal energy constant through sharply varying absorption bands such as those from atmospheric water vapour. The servo-operated slit can readily do this as well as control variation in resolution.

The main reason for desiring to reproduce the resolution is to obtain reproducible band intensities. If the band pass of the instrument is appreciably narrower than the width of the absorption band, true band intensities are obtained irrespective of slit width. Thus, as the resolution of the spectrometers increases, the necessity for controlling the slit width decreases. While this situation is not likely to be reached soon for gases, it is being approached for liquids and solids.

It is possible to servo- or cam-operate the instrument gain rather than the slit width, but this method usually leads to an unacceptably large fluctuation in instrument noise and zero level except for photomultiplier operation [241].

Several instruments possess such added features as automatic speed and damping control depending upon the slit width and/or rate of pen motion. Such features conserve scanning time.

A few spectrophotometers have been designed for oscillographic portrayal of the spectrum. Such instruments should be very useful for cursory observation of spectra and particularly for studying fast chemical reactions. It is necessary to weigh scanning time against sample preparation and interpretation time. When this is done, many of the faster pen-type recorders are found to be acceptably fast. High-speed pen recorders of the Sanborn and Brush type have not been used, but will probably be found in future instruments.

VOL. 7 1955/

The requirements of near-infrared spectroscopy do not necessarily dictate a single preferred method of recording. However, the high speed, low noise, and low scattered light possible with lead sulphide detectors lend favour to the ratio-recording method using the constant-energy slit servo. The long cell paths required do not favour motion of the sample cells in the beam.

The relationships between resolving power, noise, slit width, and damping factors in automatic recording have recently been investigated by BRODERSEN [35–37].

Sample handling

Several precautions must be observed in working in the near-infrared region. Since hydrogen bonding effects are readily observed in this region, one must properly interpret concentration effects [13, 58, 78, 124]. Since dilution may cause associating liquids to become more volatile, special precautions are required in preparing solutions [196]. Thin films frequently exhibit interference effects which on linear wavelength plots assume the form of a modulated wave with a crest-to-crest interval proportional to the square of the wavelength of light and inversely proportional to the film thickness. This modulative effect will, of course, be superimposed on any absorption curve. Birefringent materials may produce an effect similar to interference if the spectrometer partially polarizes the light, as most instruments do [63]. When working with mixtures of solids and liquids (mulls), one must watch for unusual effects at wavelengths when the refractive indices of the solid and liquid coincide (Christiansen filter effect) [54, 174, 203].

OL.
7
5/56

Slit-width effects

Except in high-molecular-weight liquids, the band-width of most absorptions in the near-infrared is equal to or less than that passed by quartz monochromators. As a consequence, the observed absorptivity must be corrected if an absolute value is desired [42, 59, 99, 108]. Another error arises in the determination of the wavelength of an absorption. The radiation emerging from the exit slit consists of a finite band-width proportional to the slit width; however, the middle of this wavelength band cannot always be taken as the true average wavelength [37]. The detector may be much more sensitive to the longer (or shorter) wavelength portion of the transmitted band than to other wavelengths transmitted. The extent of this effect may be estimated by obtaining a background energy curve with fixed slit width. The greater the slope of this curve the greater will be the wavelength error for a given slit width. Strong, sharp absorptions produced by water vapour in the instrument may produce an even greater effect than the general background. References [59] and [99] present several ways of correcting for this effect, but do not consider the expedient of inserting a correcting filter into the beam so that the detector is equally sensitive to all wavelengths in a given region [125].

Stray light

At the extreme end of the useful range of any monochromator using a given source and detector, the slit width may be so increased that a large portion of the energy is transmitted through the exit slit at wavelengths other than that indicated on the

wavelength scale [55]. The extent of the "effective" stray light is a function of the source output, monochromator dispersion, fogged or scratched optics, and detector sensitivity. It may be corrected by varying any of these elements (such as temperature of the source) or by filtering. Correction for residual stray light may then be made mathematically [109, 167]. For reducing stray light, double-prism monochromators or double-pass monochromators of the Walsh type are more efficient but more expensive. A somewhat simplified form of double-pass operation useful for reducing scattered light effects has been suggested [96]. In this method the light is modulated by oscillating the Littrow mirror about a horizontal axis. Rotating shutters composed of low-pass filters may be used for reducing scattered light, since only the longer wavelength radiation (where scattered light is serious) is modulated [166]. This method is used in the Beckman IR-2 spectrometers. The Baird spectrometer uses an Ag_2S filter. The filter shown in Fig. 7 should be ideal for the 2- to 3-μ region.

Polarizers

A number of different types of polarizers may be used in the near-infrared region. The Glan-Thompson polarizer possesses excellent polarizing and transmission properties in the region 0·7–3·0 μ along with usable windows of transmission at 4·4 and 4·9 μ (polarizer length one inch) [62]. The Nicol prism can be used in the region 0·7–2·35, 2·47–2·52, 2·65–2·70, and 2·8–2·95 μ (for a one-inch long prism). The Polaroid Corporation produces an oriented polyvinyl chloride polarizer useful to 2·7 μ. Piles of selenium films [60, 175] and silver chloride plates [240] have been used successfully.

Microspectroscopy

The techniques of infrared microspectroscopy [60a] may be applied to the near-infrared region with certain provisions. Only the fundamental and a few overtone and combination bands are likely to possess a sufficiently large absorptivity to produce absorption bands in very small path lengths.

Calibration

Calibration of prism spectrometers is most accurately accomplished by the use of the Friedel-McKinney equations relating frequency to prism rotation [56, 57, 146, 193, 218, 219]. Many absorption bands in the near-infrared are known precisely for points of calibration. Table 7 summarizes the literature on bands which have been recommended for calibration purposes. Some of the earlier reports may be revised in the later studies. The two bands labelled 2·5434 and 2·4944 μ in reference 168 should be corrected to read 2·663 and 2·576 μ, respectively.

The atmospheric-water bands observable in the energy plotted spectrum of most instruments offer the most convenient wavelength (and resolution) check points. These water bands are extremely numerous and sharp, so that it becomes necessary to use as a reference a spectrum obtained on an instrument of nearly the same resolution as that of the instrument being calibrated. The beautifully resolved spectrum obtained at the Bureau of Standards [21] may be unrecognizable in comparison with the spectrum obtained on a prism instrument.

VOL. 7 1955/5

Interference fringes from accurately spaced cell windows [104] or from mica [127] may facilitate calibration.

Care must be exercised to determine whether frequencies in air or in a vacuum are specified [56, 73].

Table 7. Calibration points

Material	λ	*Reference*
H_2O vapour	1·16	158, 182
	1·4	124, 136, 139, 162
	1·9	139, 178, 182
	2·6	18, 21, 139, 159, 177
	3·1	161
NH_3 vapour	1·9	212
	3·0	212
CH_4 vapour	1·1–2·0	158, 165
	1·4–2·6	151, 182
	3·3	180
HCl vapour	1·6	144
	3·2	144
HBr vapour	2	179, 200
	4	179
Hg emission	1·0–2·4	113, 140, 142, 180
Ca emission	1·2–2·3	112
Mg arc	1·2–1·7	69
Polystyrene	3·2–3·5	180
1,2,4-Trichlorobenzene	1·6–2·6	180
Benzene	1–3·6	81, 82, 135, 142
Didymium glass	0·7–2·0	1
Interference filters	—	236

References

[1] Acquista, N., and Plyler, E. K.; *J. Res. Nat. Bur. Standards* 1952 **49** 13–16.

[2] Agnew, J. T., Franklin, R. G., Benn, R. E., and Bazarian, A.; *J. Opt. Soc. Amer.* 1949 **39** 409–410.

[3] Ahlers, N. H. E., and Freedman, H. P.; *Nature* (London) 1953 **172** 260–261.

[4] Andrews, D. A., Milton, R. M., and DeSorbo, W.; *J. Opt. Soc. Amer.* 1946 **36** 518–524.

[5] Avery, D. G., and Hammond, P. H.; *J. Sci. Instr.* 1953 **30** 400–401.

[6] Avery, D. G., and Clegg, P. L.; *Proc. Phys. Soc.* (*London*) 1953 **B66** 512–513.

[7] AVERY, D. G.; *Proc. Phys. Soc.* (*London*) 1954 **B67** 2–8.
[8] AVERY, D. G.; *Research* 1954 **7** 278–285.
[9] BAIRD, W. S., O'BRIAN, H. M., OGDEN, G., and LEE, D.; *J. Opt. Soc. Amer.* 1947 **37** 754–761.
[10] BAKER, E. B., and ROBB, C. D.; *Rev. Sci. Instr.* 1943 **14** 362–367.
[11] BALLARD, S. S., COMBES, L. S., HYDE, W. L., GRIFFITH, G. E., and MCCARTHY, K. Q., Baird Assoc. Inc., Final Rept. on Contract, W-44-009 eng.-473.
[12] BANNING, M.; *J. Opt. Soc. Amer.* 1947 **37** 792–797.
[13] BARCHEWITZ, P.; *Ann. Phys.* 1943 **18** 167–189.
[14] BARNES, J., and FULWEILER, W. H.; *J. Opt. Soc. Amer.* 1927 **15** 331–336.
[15] BARNES, J., and FULWEILER, W. H.; *Phys. Rev.* 1928 **32** 618–623.
[16] BARNES, R. B., and BONNER, L. G.; *J. Opt. Soc. Amer.* 1936 **26** 428–433.
[17] BARNES, R. B., and BONNER, L. G.; *Phys. Rev.* 1936 **49** 732–740.
[18] BARNES, R. B., MCDONALD, R. S., WILLIAMS, V. Z., and KINNAND, R. F.; *J. Appl. Phys.* 1945 **16** 77–86.
[19] Beckman Scientific Instruments, Inc.; IR-3 Instruction Manual, 1951.
[20] BEITZ, R. C.; *J. Opt. Soc. Amer.* 1953 **43** 773–776.
[21] BENEDICT, W. S., and PLYLER, E. K.; *J. Res. Nat. Bur. Standards* 1951 **46** 246–265.
[22] BENN, R. E., FOOTE, W. S., and CHASE, C. T.; *J. Opt. Soc. Amer.* 1949 **39** 529–532.
[23] BERNSTEIN, H. J., and HERZBERG, G.; *J. Chem. Phys.* 1948 **16** 30–39.
[23a] BHAT, M. R.; *Proc. Indian Acad. Sci.* 1953 **38** 67–76.
[24] BILLINGS, B. H., HYDE, W. L., and BARR, E. E.; *J. Opt. Soc. Amer.* 1947 **37** 123–132.
[25] BILLINGS, B. H.; *J. Opt. Soc. Amer.* 1947 **37** 738–746.
[26] BILLINGS, B. H., and PITTMAN, M. A.; *J. Opt. Soc. Amer.* 1949 **39** 978–983.
[27] BLACKWELL, D. E., SIMPSON, O., and SUTHERLAND, G. B. B. M.; *Nature* 1947 **160** 793.
[28] BLOUT, E. R., BIRD, G. R., and GREY, D. S.; *J. Opt. Soc. Amer.* 1950 **40** 304–313.
[29] BLOUT, E. R., CORLEY, R. S., and SNOW, P. L.; *J. Opt. Soc. Amer.* 1950 **40** 415–418.
[30] BODE, D. E., and LEVINSTEIN, H.; *J. Opt. Soc. Amer.* 1953 **43** 1209–1210.
[31] BORST, L. B., BUSWELL, A. M., and RODEBUSH, W. H.; *J. Chem. Phys.* 1938 **6** 61–67.
[32] BRIGGS, H. B.; *J. Opt. Soc. Amer.* 1952 **42** 686–687.
[33] BRIGGS, H. B.; U.S. Patent 2,683,794, 1954.
[34] BROCHARD, J., and JACQUINOT, P.; *J. Phys. Radium* 1953 **14** 131–132.
[35] BRODERSEN, S.; *J. Opt. Soc. Amer.* 1953 **43** 877–881.
[36] BRODERSEN, S.; *J. Opt. Soc. Amer.* 1953 **43** 1216–1220.
[37] BRODERSEN, S.; *J. Opt. Soc. Amer.* 1954 **44** 22–25.
[38] BUCKINGHAM, W. D., and DEIBERT, C. R.; *J. Opt. Soc. Amer.* 1946 **36** 245–250.
[39] CAHN, L., and GALE, GEORGE; *Molecular Symposium*, The Ohio State Univ., 1953.
[40] CARY, H.; *Ind. Eng. Chem.* 1947 **39** 75A.
[41] CASE, T. W.; *Phys. Rev.* 1920 **15** 289–292.
[42] CASTER, W. O.; *Anal. Chem.* 1951 **23** 1229–1236.
[43] CHATTERJEE, S. D., GOSH, N. N., and NAHA, A. M.; *J. Chem. Phys.* 1952 **20** 344.
[44] COLE, A. R. H.; *J. Opt. Soc. Amer.* 1953 **43** 807–808.
[45] COLE, A. R. H.; *J. Opt. Soc. Amer.* 1954 **44** 741–743.
[46] COMBES, L. S., BALLARD, S. S., and MCCARTHY, K. A.; *J. Opt. Soc. Amer.* 1951 **41** 215–222.
[47] Corning Glass Works; *Glass Color Filters*, 1948.
[48] COOR, T., Jr., and SMITH, D. C.; *Rev. Sci. Instr.* 1947 **18** 173–181.
[49] CZERNY, M.; *Z. Physik.* 1929 **53** 1–12.
[50] DALY, E. F.; *J. Sci. Instr.* 1951 **28** 308–313.
[51] DANIEL, J. H., and BRACKETT, F. S.; *J. Opt. Soc. Amer.* 1953 **43** 960–968.
[52] DAVIS, A., CLEVELAND, F. F., and MEISTER, A. G.; *J. Chem. Phys.* 1952 **20** 454–459.
[53] DEJARDIN, G., and FALGON, R.; *C.R. Acad. Sci.* (*Paris*) 1952 **234** 200–202.
[54] DENMARK, H. S., and CADY, W. M.; *J. Opt. Soc. Amer.* 1935 **25** 330–331.
[55] DONALDSON, R.; *J. Sci. Instr.* 1952 **29** 150–153.
[56] DOWNIE, A. R., MAGOON, M. C., PURCELL, THOMASINE, and CRAWFORD, BRYCE; *J. Opt. Soc. Amer.* 1953 **43** 941–951.

[57] DRUMMOND, D. G.; *Nature* 1934 **134** 937.
[58] DUBOIS, J.; *C.R. Acad. Sci.* (*Paris*) 1944 **219** 333–334.
[59] EBERHARDT, W. H.; *J. Opt. Soc. Amer.* 1950 **40** 172–176.
[60] ELLIOTT, A.; *Proc. Roy. Soc.* (*London*) 1952 **A211** 490–499.
[60a] ELLIOTT, A., HANBY, W. E., and MALCOLM, B. R.; *Brit. J. Appl. Phys.* 1954 **5** 377–381.
[61] ELLIS, J. W., and LYON, W. K. (followed by DRUMMOND, D. G.); *Nature* 1937 **139** 70.
[62] ELLIS, J. W., and BATH, J.; *J. Chem. Phys.* 1938 **6** 221–222.
[63] ELLIS, J. W., and GLATT, L.; *J. Opt. Soc. Amer.* 1950 **40** 141–142.
[64] ETZEL, H. W.; *J. Opt. Soc. Amer.* 1953 **43** 87–90.
[65] EVANS, J. W.; *J. Opt. Soc. Amer.* 1949 **39** 229–242.
[66] EWALD, A. W.; *Phys. Rev.* 1951 **81** 607–611.
[67] FASTIE, W. G., and SINTON, W. M.; *J. Opt. Soc. Amer.* 1954 **44** 103–108.
[68] FELLGETT, P. B.; *J. Opt. Soc. Amer.* 1949 **39** 970–976.
[69] FISHER, R. A., and ESHBACH, F. E.; *J. Opt. Soc. Amer.* 1953 **43** 1030–1032.
[70] FLORENCE, J. M., ALLSHOUSE, C. C., GLAZE, F. W., and HAHNER, C. H.; *J. Res. Nat. Bur. Standards* 1950 **45** 121–128.
[71] FLORENCE, J. M., GLAZE, F. W., and BLACK, M. H.; *J. Res. Nat. Bur. Standards* 1953 **50** 187–196.
[72] FOREMAN, R. W., and JACKSON, W., Jr.; *Instruments* 1949 **22** 497–499.
[73] FOX, J. J., and MARTIN, A. E.; *Proc. Roy. Soc.* (*London*) 1938 **A167** 257–281.
[74] FREDRICKS, R.; *J. Opt. Soc. Amer.* 1953 **43** 1153–1157.
[75] FREYMANN, R.; *C.R. Acad. Sci.* (*Paris*) 1931 **193** 656–659.
[76] FRIEDMAN, H., and GLOVER, C. P.; *J. Opt. Soc. Amer.* 1949 **39** 795–796.
[77] FUSON, N.; *J. Opt. Soc. Amer.* 1948 **38** 845–853.
[78] FUSON, N., JOSIEN, M. L., POWELL, R. L., and UTTERBECK, E.; *J. Chem. Phys.* 1952 **20** 145–152.
[79] GARINO-CANINA, V.; *Cahiers de Phys.* 1954 No. 48 72–76; *Sci. Abstr.* 1954 **57** 1040 No. 8180.
[80] GAUNT, J.; *J. Sci. Instr.* 1954 **31** 315–318.
[81] GAUTHIER, G.; *C.R. Acad. Sci.* (*Paris*) 1950 **231** 1453–1455.
[82] GAUTHIER, G.; *J. phys. rad.* 1953 **14** 85–88.
[83] GOERCKE, P.; *Ann. Telecommun.* 1951 **6** 325–331.
[84] GOLAY, M. J. E.; *Rev. Sci. Instr.* 1947 **18** 347–356.
[85] GOLAY, M. J. E.; *Rev. Sci. Instr.* 1947 **18** 357–362.
[86] GOULDEN, J. D. S.; *J. Sci. Instr.* 1952 **29** 215–216.
[87] GOULDEN, J. D. S., and RANDALL, S. S.; *Nature* 1952 **169** 748–749.
[88] GOULDEN, J. D. S., and RANDALL, S. S.; *Nature* 1952 **169** 1108.
[89] GREENLAND, K. M.; *Endeavour* 1952 **11** 143–148.
[90] HADLEY, L. N., and DENNISON, D. J.; *J. Opt. Soc. Amer.* 1948 **38** 483–496.
[91] HAENDLER, H. M., WHEELER, C. M., and BERNARD, W. J.; *J. Opt. Soc. Amer.* 1953 **43** 215–216.
[92] HALES, J. L.; *J. Sci. Instr.* 1949 **26** 359–365.
[93] HALES, J. L.; *J. Sci. Instr.* 1953 **30** 52–57.
[94] HALL, M. B., and NESTER, R. G.; *J. Opt. Soc. Amer.* 1952 **42** 257–258.
[95] HAM, N. S., WALSH, A., and WILLIS, J. B.; *J. Opt. Soc. Amer.* 1952 **42** 496–500.
[96] HAMMOND, V. J., and PRICE, W. C.; *J. Opt. Soc. Amer.* 1953 **43** 924.
[97] HARDY, A. C.; *J. Opt. Soc. Amer.* 1929 **18** 96–117.
[98] HARDY, A. C.; *J. Opt. Soc. Amer.* 1935 **25** 305–311.
[99] HARDY, A. C., and YOUNG, F. M.; *J. Opt. Soc. Amer.* 1949 **39** 265–270.
[100] HARDY, J. D., and RYER, A. T.; *Phys. Rev.* 1939 **55** 1112–1113.
[101] HARRIS, L., MCGINNIES, R. T., and SIEGEL, B. M.; *J. Opt. Soc. Amer.* 1948 **38** 582–589.
[102] Harshaw Chemical Co.; "Synthetic Optical Crystals," 1951, Cleveland, Ohio.
[103] HAWES, R. C., and CARY, H.; *Symposium on Molecular Structure and Spectroscopy*, Ohio State Univ., Columbus, Ohio, June 12, 1952.
[104] HEIDT, L. J., and BOSLEY, D. E.; *J. Opt. Soc. Amer.* 1953 **43** 760–766.

[105] HENRY, R. L.; *J. Opt. Soc. Amer.* 1947 **38** 775–789.
[106] HEPNER, G.; *J. Phys. Radium* 1953 **14** 717–723.
[107] HIPPEL, A. VON, CHESLEY, F. G., DENMARK, H. S., ULIN, P. B., and RITTNER, E. S.; *J. Chem. Phys.* 1946 **14** 355–369.
[108] HISKEY, C. F., and YOUNG, I. G.; *Anal. Chem.* 1951 **23** 1196–1201.
[109] HOGNESS, T. R., ZSCHEILE, F. P., Jr., and SIDWELL, A. E., Jr.; *J. Phys. Chem.* 1937 **41** 379–415.
[110] HORNIG, D. F., and O'KEEFE, B. J.; *Rev. Sci. Instr.* 1947 **18** 474–482.
[111] HORNIG, D. F., HYDE, G. E., and ADCOCK, W. A.; *J. Opt. Soc. Amer.* 1950 **40** 497–503
[112] HUMPHREYS, C. J.; *J. Res. Nat. Bur. Standards* 1951 **47** 262–268.
[113] HUMPHREYS, C. J.; *J. Opt. Soc. Amer.* 1953 **43** 1027–1029.
[114] HYDE, W. L.; *Trans. Instrum. Meas. Conf.* 1952 120–125.
[115] IRT, R. C., and KING, F. T.; *Anal. Chem.* 1952 **24** 1545–1548.
[116] JANIN, J., and PEYRON, M.; *C.R. Acad. Sci. (Paris)* 1954 **238** 224–226.
[117] JONES, D. A., JONES, R. V., and STEVENSON, R. W. H.; *Proc. Phys. Soc. (London)* 1952 **B65** 906–907.
[118] JONES, R. C.; *J. Opt. Soc. Amer.* 1947 **37** 879–890.
[119] JONES, R. C.; *J. Opt. Soc. Amer.* 1949 **39** 327–343.
[120] JONES, R. C.; *J. Opt. Soc. Amer.* 1949 **39** 344–356.
[121] JONES, R. C.; *J. Opt. Soc. Amer.* 1953 **43** 1008–1013.
[122] JONES, R. C.; *Rev. Sci. Instr.* 1953 **24** 1035–1040.
[123] JOOS, G.; *Optik* 1952 **9** 546.
[124] JOSIEN, M. L., and FUSON, N.; *J. Chem. Phys.* 1954 **22** 1169–1177.
[125] KAYE, W.; *J. Opt. Soc. Amer.* 1951 **41** 277.
[126] KAYE, W., and DEVANEY, R. G.; *J. Opt. Soc. Amer.* 1952 **42** 567–571.
[127] KAYE, W.; *Spectrochim. Acta* 1954 **6** 257–287.
[128] KEMPTER, H., and MECKE, R.; *Z. physik. Chem.* 1940 **B46** 229–241.
[129] KING, W. H., Jr.; *J. Opt. Soc. Amer.* 1953 **43** 866–869.
[130] KRENZIEN, O.; *Z. Phys.* 1949 **126** 666–670.
[131] KREUZER, J.; *Z. Phys.* 1941 **118** 325–339.
[132] LARK-HOROVITZ, K.; *The Present State of Physics*, pp. 57–127, 1954, AAAS.
[133] LECOMTE, J.; *J. Phys. Radium* 1949 **10** 27–31D.
[134] LEHRER, E.; *Z. tech. Phys.* 1942 **23** 169–176.
[135] LIDDEL, U., and KASPER, C.; *J. Res. Nat. Bur. Standards* 1933 **11** 599–618.
[136] LIDDEL, U., and WULF, O. R.; *J. Amer. Chem. Soc.* 1933 **55** 3574–3583.
[137] LISTON, M. D., and WHITE, J. U.; *J. Opt. Soc. Amer.* 1950 **40** 36–41.
[138] MALYSHEV, V. I., MARKOV, M. N., and SHUBIN, A. A.; *Dokl. Akad. Nauk SSSR* 1952 **86** 273–276.
[139] MATHIS, R., BOSSON, F., GAUTHIER, G., and LARNAUDIE, M.; *J. Phys. Radium* 1950 **11** 300–304.
[140] MCALISTER, E. D.; *Phys. Rev.* 1929 **34** 1142–1147.
[141] MCMICHAEL, B. D., KMETKO, E. A., and MROZOWSKI, S.; *J. Opt. Soc. Amer.* 1954 **44** 26–30.
[142] MECKE, R., and OSWALD, F.; *Z. Phys.* 1951 **130** 445–448.
[143] Mervyn Instruments; *J. Sci. Instr.* 1954 **31** 349.
[144] MEYER, C. F., and LEVIN, A. A.; *Phys. Rev.* 1929 **34** 44–52.
[145] MCFEE, R. H.; *J. Opt. Soc. Amer.* 1952 **42** 67.
[146] MCKINNEY, D. S., and FRIEDEL, R. A.; *J. Opt. Soc. Amer.* 1948 **38** 222–225.
[147] MICHAELSON, J. L.; *J. Opt. Soc. Amer.* 1938 **28** 365–371.
[148] MILNER, C. J., and WATTS, B. N.; *Nature* 1949 **163** 322.
[149] MILNER, C. J., and WATTS, B. N.; *Research* 1952 **5** 267–273.
[150] MOHLER, N. M., and LOOFBOUROW, J. R.; *Amer. J. Phys.* 1952 **20** 499–515.
[151] MOORHEAD, J. G.; *Phys. Rev.* 1932 **39** 83–88.
[152] MOSS, T. S.; *Nature* 1947 **159** 476.
[153] MOSS, T. S., and CHASMAR, R. P.; *Nature* 1948 **161** 244.

VOL
7
1955/

[154] Moss, T. S.; *Proc. Phys. Soc.* (*London*) 1949 **B62** 741–748.
[155] Moss, T. S.; *J. Opt. Soc. Amer.* 1950 **40** 603–607.
[156] Moss, T. S.; *Proc. Phys. Soc.* (*London*) 1952 **B65** 62–66.
[157] Moss, T. S.; *Research* 1953 **6** 258–264.
[158] Nelson, R. C., Plyler, E. K., and Benedict, W. S.; *J. Res. Nat. Bur. Standards* 1948 **41** 615–621.
[159] Nelson, R. C.; *J. Opt. Soc. Amer.* 1949 **39** 68–71.
[160] Nelson, R. C., and Jenkinson, R.; *J. Opt. Soc. Amer.* 1953 **43** 1181–1183.
[161] Nielsen, H. H.; *Phys. Rev.* 1942 **62** 422–433.
[162] Nielsen, H. H.; *Trans. Instr. Meas. Conf.* 1952 47–51.
[163] Noland, J. A.; *Phys. Rev.* 1954 **94** 724.
[164] Normand, C. W. B., and Kay, R. H.; *J. Sci. Instr.* 1952 **29** 33–39.
[165] Norris, W. V., and Unger, H. J.; *Phys. Rev.* 1933 **43** 467–472.
[166] Oetjen, R. A.; *J. Opt. Soc. Amer.* 1945 **35** 743–754.
[167] Opler, A.; *J. Opt. Soc. Amer.* 1950 **40** 401–403.
[168] Orr, S. F. D.; *J. Opt. Soc. Amer.* 1953 **43** 709–710.
[169] Paul, W., and Jones, R. V.; *Proc. Phys. Soc.* (*London*) 1953 **B66** 194–200.
[170] Perkin-Elmer; PE Instrument News, **1,** No. 4, p. 3, 1950.
[171] Pfund, A. H.; *J. Opt. Soc. Amer.* 1933 **23** 270–273.
[172] Pfund, A. H.; *Phys. Rev.* 1930 **36** 41–76.
[173] Pfund, A. H., and Silverman, S.; *Phys. Rev.* 1932 **39** 64–71.
[174] Pfund, A. H.; *J. Opt. Soc. Amer.* 1933 **23** 375–378.
[175] Pfund, A. H.; *J. Opt. Soc. Amer.* 1947 **37** 558–559.
[176] Piper, W. W.; *Phys. Rev.* 1953 **92** 23–27.
[177] Plyler, E. K., and Sleator, W. W.; *Phys. Rev.* 1931 **37** 1493–1507.
[178] Plyler, E. K.; *Phys. Rev.* 1932 **39** 77–82.
[179] Plyler, E. K., and Barker, E. F.; *Phys. Rev.* 1933 **44** 984–985.
[180] Plyler, E. K., and Peters, C. W.; *J. Res. Nat. Bur. Standards* 1950 **45** 462–468.
[181] Plyler, E. K., and Ball, J. J.; *J. Opt. Soc. Amer.* 1952 **42** 266–268.
[182] Plyler, E. K., Gailar, N. M., and Wiggins, T. A.; *J. Res. Nat. Bur. Standards* 1952 **48** 221–227.
[183] Rank, D. H., Shull, E. R., Bennett, J. M., and Wiggins, T. A.; *J. Opt. Soc. Amer.* 1953 **43** 952–956.
[184] Rank, D. H., Shull, E. R., and Wiggins, T. A.; *J. Opt. Soc. Amer.* 1953 **43** 214–215.
[185] Rank, D. H., Bennett, H. E., and Cronemeyer, D. C.; *J. Opt. Soc. Amer.* 1954 **44** 13–16.
[186] Rank, D. H.; *J. Phys. Radium* 1954 **15** 517–518.
[187] Rittner, E. S.; *Science* 1950 **111** 685–688.
[188] Roberts, A. R.; *J. Sci. Instr.* 1952 **29** 134.
[189] Roberts, V., and Young, A. S.; *J. Sci. Instr.* 1953 **30** 199–200.
[190] Rochester, J. C. O., and Martin, A. E.; *Nature* 1951 **168** 785–786.
[191] Rodney, W. S., and Spindler, R. J.; *J. Opt. Soc. Amer.* 1954 **44** 677–679.
[192] Rodney, W. S., and Spindler, R. J.; *J. Res. Nat. Bur. Standards* 1954 **53** 188–189.
[193] Ross, W. L., and Little, D. E.; *J. Opt. Soc. Amer.* 1951 **41** 1006–1010.
[193a] Royer, G. L., Lawrence, H. C., Kodama, S. P., and Warren, C. W.; *Molecular Symposium*, The Ohio State Univ., 1953; *Anal. Chem.* 1955 **27** 501–506.
[194] Rupert, C. S., and Strong, J.; *J. Opt. Soc. Amer.* 1950 **40** 455–459.
[195] Ryvkin, S. M., and Malakhov, L. N.; *Dok. Akad. Nauk SSSR* 1952 **85,** No. 4, 765–768.
[196] Saier, E. L., and Coggeshall, N. D.; *Anal. Chem.* 1948 **20** 812–817.
[197] Saker, E. W.: *Proc. Phys. Soc.* (*London*) 1952 **B65** 785–787.
[198] Savitsky, A., and Halford, R. S.; *Rev. Sci. Instr.* 1950 **21** 203–212.
[199] Schulz, L. G.; *J. Opt. Soc. Amer.* 1953 **43** 407–408.
[200] Searles, S., and Tamres, M.; *J. Amer. Chem. Soc.* 1951 **73** 3704–3706.
[201] Simpson, O., Sutherland, G. B. B. M., and Blackwell, D. E.; *Nature* 1948 **161** 281.
[202] Simpson, O.; *Proc. Phys. Soc.* (*London*) 1948 **61** 486–487.
[203] Sinscheimer, R. L., and Loofbourow, J. R.; *Nature* 1947 **160** 674.

[204] SMITH, J. S. K., and JONES, E. A.; *J. Opt. Soc. Amer.* 1949 **39** 780–781.
[205] SMITH, V. N.; *Instruments* 1953 **26** 421–427.
[206] SOSNOWSKI, S., STARKIEWICZ, J., and SIMPSON, O.; *Nature* 1947 **159** 818–819.
[207] STAIR, R., and FAICK, C. A.; *J. Res. Nat. Bur. Standards* 1947 **38** 95–101.
[208] Standard Piezo Co.; "CdS Crystal Photocells," 1954.
[209] STANFORD, S. C., and GORDY, W.; *J. Amer. Chem. Soc.* 1941 **63** 1094–1096.
[210] STARKIEWICZ, J.; *J. Opt. Soc. Amer.* 1948 **38** 481.
[211] STEPHENS, R. E., and MALITSON, I. H.; *J. Res. Nat. Bur. Standards* 1952 **49** 249–252.
[212] STINCHCOMB, G. A., and BARKER, E. F.; *Phys. Rev.* 1929 **33** 305–308.
[213] STRONG, J., and BRICE, R. T.; *J. Opt. Soc. Amer.* 1935 **25** 207–210.
[214] SUTHERLAND, G. B. B. M., BLACKWELL, D. E., and FELLGETT, P. B.; *Nature* 1946 **158** 873–874.
[215] Sylvania Electric Products Inc., Eng. Data Sheet 3-54-73A, Electronics Division, Woburn, Mass.
[216] TRANENBAUM, M., and BRIGGS, H. B.; *Phys. Rev.* 1953 **91** 1561.
[217] TAYLOR, J. H., RUPERT, C. S., and STRONG, J.; *J. Opt. Soc. Amer.* 1951 **41** 626–629.
[218] TILTON, L. W., and PLYLER, E. K.; *J. Res. Nat. Bur. Standards* 1951 **47** 25–30.
[219] TOWLER, J. H., and GUY, W.; *J. Sci. Instr.* 1952 **29** 393–397.
[220] URBACH, F., PEARLMAN, D., and HEMMENDINGER, H.; *J. Opt. Soc. Amer.* 1946 **36** 372–381.
[221] URBACH, F., NAIL, N. R., and PEARLMAN, D.; *J. Opt. Soc. Amer.* 1949 **39** 1011–1019.
[222] VASICEK, A.; *Czech. J. Phys.* 1953 **3** 206–222.
[223] VASKO, A.; *Bull. Int. Acad. Tcheque Sci.* 1949 **50** 263–269.
[224] VERNIER, P.; *J. Phys. Radium* 1953 **14** 175–179.
[225] VODAR, B., FREYMANN, R., and TA, Y.; *J. Chem. Phys.* 1940 **8** 349.
[226] WALSH, A.; *Nature* 1951 **167** 810–811.
[227] WALSH, A.; *J. Opt. Soc. Amer.* 1952 **42** 94–95.
[228] WALSH, A.; *J. Opt. Soc. Amer.* 1952 **42** 96–100.
[229] WALSH, A.; *J. Opt. Soc. Amer.* 1953 **43** 215.
[230] WALSH, A., and WILLIS, J. B.; *J. Opt. Soc. Amer.* 1953 **43** 989–992.
[231] WHITE, J. U.; *J. Opt. Soc. Amer.* 1942 **32** 285–288.
[232] WHITE, J. U.; *J. Opt. Soc. Amer.* 1947 **37** 713–717.
[233] WHITE, J. U., and LISTON, M. D.; *J. Opt. Soc. Amer.* 1950 **40** 29–35.
[234] WHITE, J. U., and LISTON, M. D.; *J. Opt. Soc. Amer.* 1950 **40** 93–101.
[235] WILD, R. F.; *Rev. Sci. Instr.* 1947 **18** 436–442.
[236] WILLIAMSON, D. E.; *J. Opt. Soc. Amer.* 1949 **39** 613–614.
[237] WILLIAMSON, D. E.; *J. Opt. Soc. Amer.* 1952 **42** 712–715.
[238] WORMSER, E. M.; *J. Opt. Soc. Amer.* 1953 **43** 15–21.
[239] WRIGHT, N., and HERSCHER, L. W.; *J. Opt. Soc. Amer.* 1947 **37** 211–216.
[240] WRIGHT, N.; *J. Opt. Soc. Amer.* 1948 **38** 69.
[241] YANG, C., and LEGALLIS, V.; *Rev. Sci. Instr.* 1954 **25** 801–813.
[242] ZBINGEN, R., and BALDINGER, E.; *Helv. Phys. Acta* 1953 **26** 111–128.

VOL
7
1955/

Spectrochimica Acta, 1955, Vol. 7, pp. 205 to 213. Pergamon Press Ltd., London

Spectrographic analysis of nominally pure lead*

(*Report of the Lead Analysis Panel of The British Non-Ferrous Metals Research Association Spectrographic Research Committee*)

(*Received January* 1955)

Summary—Co-operative investigations have been carried out by a number of laboratories interested in the spectrographic determination of trace impurities in lead. Methods have been developed for the determination of Ni, Bi, Tl, Cd, Sb, Ag, As, Sn, Cu, Zn, and Te in the range 0·0005–0·005 per cent, with an accuracy of the order of ±10 per cent. The greater sensitivity of the triggered-arc type sources has been demonstrated, although acceptable results can be obtained with simple condensed spark circuits using prolonged exposures.

Introduction

An account is given of the work done and results obtained by a co-operative panel of The British Non-Ferrous Metals Research Association's Spectrographic Research Committee in an investigation of methods suitable for the analysis of minor constituents present in lead in the range 0·0005–0·005 per cent.

Previously lead and lead alloys were analyzed using the methods described by SMITH [1]. These methods suffered from lack of sensitivity of detection for certain elements and since the concentrations were determined by visual comparison of line densities, from greater errors than are nowadays acceptable; with the advent of new types of source unit and a wider use of the microphotometer it seemed probable that more sensitive and accurate methods could be developed.

This paper describes methods which show appreciable advantages over those previously used. A range of standard alloys, prepared in the laboratory and not readily available commercially is required. An account of their preparation is given in an Appendix.

Terms of reference and membership of the Lead Analysis Panel

The Panel had the following terms of reference: "To develop methods for the spectrographic analysis of dilute lead alloys." Its members were:—

Dr. R. TAYLOR (Chairman)	Post Office Engineering Research Station.
Mr. W. H. BANYARD	(Succeeded by February, 1953) W. T. Henley's Telegraph Co. Ltd.
Mr. A. V. GARNER	
Mr. A. N. COFFIN	Pirelli-General Cable Works Ltd.
Mr. W. LESSING	Telegraph Construction and Maintenance Co. Ltd.
Mr. M. MILBOURN	Imperial Chemical Industries Ltd., Metals Division.
Mr. J. C. NORTH	Post Office Engineering Research Station.
Mr. R. H. PRICE	British Insulated Callender's Cables Ltd.
Mr. D. M. SMITH	Johnson, Matthey & Co. Ltd.
Mr. P. T. BEALE	B.N.F.M.R.A.
Mr. J. M. NOBBS	Attached Scientist B.N.F.M.R.A. 1951–1953 (Defence Standards Laboratories, Adelaide, Australia), who prepared the report.

* The work described in this paper was made available to members of The British Non-Ferrous Metals Reseach Association in a confidential research report issued in July, 1952.

Experimental work

A series of binary alloys containing small amounts of arsenic, antimony, tin, and tellurium was prepared by Messrs. Johnson, Matthey & Co. Ltd. The alloys were examined by members of the Panel using a variety of sources and spectrographic conditions and it was found that, with suitable modifications, all the sources were capable of giving limits of detection for these impurities which were substantially lower than those expected from the conventional method [1].

A series of four complex alloys was then prepared, each containing silver, copper, cadmium, bismuth, nickel, antimony, arsenic, tin, tellurium, thallium, and zinc, covering the range 0·0005–0·005 per cent. These are the elements likely to be encountered in nominally pure lead.

The four alloys were prepared, as described in the Appendix, in the Association's Laboratories using a melting technique due to Bannister and Price [2]. After preliminary checks for homogeneity of the alloys had been made in the Association's Laboratory they were examined by other members of the Panel. Their results for (i) limits of sensitivity of detection of the elements, (ii) composition of the standards, and (iii) reproducibility are given below.

(i) *Comparison of sensitivities*

A comparison of the sensitivities of the methods used was made by measuring the line/background intensity ratios of lines for each element at 0·0005 per cent. The results, which are the means of at least ten replicates, are given in Table 1.

It is seen that all the methods are capable of detecting all the elements down to 0·0005 per cent, and even the simple condensed spark can be used for the determination of 0·0005 per cent tellurium, arsenic and antimony if long exposures are tolerated or a short focus condensing lens is used; with the latter the spectra are, under some conditions, out of focus in the extreme wave-length regions, as a result of which laboratory F detected tellurium only at 0·005 per cent. Another objection to the simple condensed spark is the presence of air lines in the spectra, which can be confused with impurity lines.

It has been the experience of the Panel that considerable differences in speed can exist between nominally identical spectrographs, at wavelengths less than 2,500 Å, where various prisms of quartz have different transmissions. Some laboratories have found great difficulty in the detection of Te 2142 and Zn 2138 in the lower standards for this reason.

Investigations carried out with the General Purpose Source Unit (3) showed that no one setting of the unit gave maximum sensitivity for all elements so that it was necessary to compromise with a setting that gave reasonable sensitivity for all elements. When a higher sensitivity is required for a particular element an alternative setting can be used.

It was found that certain thin emulsion plates, such as the Kodak B.10 or Ilford Process, were superior to others tried for detecting lines in the low wavelength region. With a source giving a unidirectional discharge, highest sensitivity was obtained when the sample was negative.

VOL 7 1955/

Table 1. *Line to background intensity ratios for elements at approximately* 0·0005 *per cent*

The ratios given are for $\frac{\text{Line + background}}{\text{background}}$

Laboratory		*A*	*B*			*C*	*D*	*E*	*F*
Source unit		1* 20 μF 4 ohm	1* 20 μF 4 ohm	1* 40 μF 1 ohm	4* 15 kV 0·005 μF	2*	3*	1* 20 μF 5 ohm	4* 12 kV 0·0042 μF
Slit width (mm)		0·025	0·02	0·02	0·02	0·02	0·02	0·025	0·02
Exposure sec. on Kodak B.10		10, 30, 120	30	12	180	30	120	60	20
Source-slit distance (cm)		20	20	20	20	20	38, with FD 28 cm lens	20	38, with FD 6·5 cm lens
Element	*Wavelength*								
Sb	2311	1·08	1·16	1·29	1·36	1·18	1·10	1·15	1·41
As	2349	1·28	1·09	1·33	1·27	1·25	1·13	1·14	1·44
Bi	3067	1·89	1·72	2·29	1·78	2·10	1·40	1·86	1·99
Cd	2265 2144	1·79	1·97	2·20	5·40	6·64	2·74	1·45 2·21	1·77
Cu	3274 2135 2192	6·30	3·70 1·26	4·90 1·34	3·60	1·64	1·13	1·11	
Ni	3050	1·33	1·30	1·87	1·43	1·52	1·13	1·49	1·49
Ag	3382	3·36	5·40	7·70	3·60				
Te	2143 2386	1·15	1·14	1·25	1·38	1·35	1·29	1·13	not detected
Tl	2767	1·34	1·36	1·30	1·30	1·42	1·22	1·24	1·47
Sn	2354 3034 2863	1·07	1·07	1·22	1·30	1·16	1·12	1·15	1·36
Zn	2138 3345	1·44	2·32	2·45	6·1	3·62	1·80	1·80	1·97

* For details, see section on excitation.

(ii) *Composition of standards*

The compositions of the alloys were estimated spectrographically, in each laboratory. It was found that, by applying a background correction, linear calibration curves were obtained and that, if the same method of drawing calibration curves was used in all laboratories, the analyses obtained were, with few exceptions, within ±10 per cent of each other. Results were complicated for some elements by the possibility of heterogeneity. Two rods of each standard were then examined by each laboratory and the mean spectrographic analyses are given in the Appendix.

(iii) *Reproducibility of results*

A survey of the results obtained in each laboratory showed that for all elements one or more of the methods used could give a reproducibility of ±10 per cent at the higher concentrations but that the accuracy of all the methods deteriorated with decreasing concentration of the elements. For analysis to specification a high degree of accuracy may not be necessary for some elements at low concentrations (0·0005 per cent). The following elements at the 0·001–0·002 per cent level can be determined by two or more of the methods employed with a reproducibility of better than ±10 per cent: antimony, bismuth, nickel, cadmium, copper, and silver. Zinc at 0·001 per cent can be determined to better than 15 per cent; tin and arsenic, specified as traces in high grade lead, to better than 20 per cent at 0·0005 per cent; limits for tellurium and thallium are not at present specified.

The methods are applicable to any specification calling for estimation of impurities below 0·005 per cent and in particular to B.S.334 Chemical Lead, type A, of which the maximum impurity limits are given in Table 2.

Table 2. **B.S.334.** *Chemical lead, type A*

Impurity	*Maximum content allowed* (%)
Cu	0·003
Sb	0·002
Bi	0·005
Fe	0·003
Ni + Co	0·001
Ag	0·002
Zn	0·002
Sn	traces
Cd	traces
As	traces
Total impurities not to exceed 0·01 per cent	

No attempt was made to prepare standards for iron or cobalt in lead owing to segregation difficulties.

A comparison of the results received from all laboratories showed that no one method was consistently better or worse than the others.

Methods for the analysis of impurities in lead

It is evident that there is a variety of methods capable of analysing nominally pure lead to specification, although for some elements an improvement in sensitivity would be desirable. The simple condensed spark suffers from the disadvantage that long exposures have to be given to detect elements in the low wavelength regions and the air lines present in its spectra make the detection of some elements difficult; similar air lines are found when the sample is made positive with a unidirectional discharge.

At the present stage the Panel is not in a position to recommend one method as being better than the others and experience seems to show that different elements require different optimum conditions.

The following methods have been employed:

Spectrograph

Medium quartz.
Slit width: 0·02 or 0·025 mm.
Slit length: 1 mm.
Exposure: according to source.

Excitation

1. *B.N.F. general purpose source unit (unidirectional)*
   20 μF, 4 ohm, 0·25 mH or 40 μF, 1 ohm, 0·5 mH if higher sensitivity is required.
   Exposure: 30 sec at source-slit distance 20 cm for 20 μF.
   12 sec at source-slit distance 20 cm for 40 μF.
2. *High-capacity condensed spark*
   15,000 V, 0·0125 μF, 0·12 mH.
   Exposure: 30 sec at source-slit distance 20 cm.
3. *High-voltage spark with Levy trigger* [4]
   1 discharge per $\frac{1}{2}$ cycle, 0·005 μF, 0·12 mH.
   Exposure: 120 sec at source-slit distance 38 cm with lens (focal length 28 cm).
4. *Condensed spark*
   12,000 V, 0·0042 μF, 0·13 mH or 15,000 V, 0·005 μF, 0·13 mH.
   Exposure: 3–4 min at source-slit distance 20 cm or
   20 sec at source-slit distance 20 cm, with lens
   (focal length 6·5 cm) focusing the electrodes near the slit.

Plates

Kodak B.10, or Ilford Process. Development 3$\frac{1}{2}$ min in I.D.2 at 18°C.
Simple dish rocking.
Fixing. Acid hypo for 5 min.

Electrodes

Sample: flat surface (negative)
Counter: graphite rod turned to cone, either sharp or rounded.
or—
Both electrodes sample, either turned to cone or flat strip as recommended by Smith [1].
Gap—4 mm.

Plate calibration

1. Rotating stepped sector.
   Light source: Lead sample v. graphite. G.P.S.U. 20 μF, 4 ohm, 0·25 mH.
   Exposure: 2 min.
   or—
   Light source: Two electrodes sample. Condensed spark, 0·13 mH.
   Exposure: 2 min.

2. Two-line method using 2-step filter [5].
Light source: Iron arc.

It was found that calibration curves were required for three wave-length regions, 3100 A, 2300 A, and 2150 A; the first two differed only slightly in slope.

A Seidel or partial Seidel [6] transformation may be applied to extend the straight line portion of the calibration curve to the lower densities.

Line pairs

A selection of the line pairs given in Table 3 has been found suitable for each method.

Table 3. Line pairs for estimation of impurities

Element	*Analysis line*	*Internal standard line (Pb)*
Ni	3050·8	3087·0
	3050·8	2918·7
	2312·3	2712·5
Bi	3067·7	3087·0
	3067·7	2918·7
	2897·9	2918·7
Tl	2767·7	3087·0
	2767·7	2712·5
Cd	2265·0	2367·7
	2144·4	2145·3
Sb	2311·5	2367·7
	2311·5	2712·5
Ag	3280·7	3240·2
	3382·9	3231·2
	2324·7	2712·5
As	2349·8	2367·7
	2349·8	2712·5
Sn	2354·8	2367·7
	2354·8	2712·5
	3034·1	3087·0
	3034·1	2918·7
Cu	2136·0	2145·3
	3247·5	3240·2
	3247·5	3231·2
	2369·9	2712·5
Zn	2138·6	2145·3
	2138·6	2187·8
	3345·0	3231·2
Te	2142·7	2145·3
	2385·8	2367·7
	2385·8	2712·5

VOL 7 1955/

Note

1. Pb lines 2918·7, 2712·5, 2367·7, and 2145·3 are not listed in M.I.T. Wavelength Tables.
2. Pb line 3087·0 does not appear with some types of source units.
3. The exposures normally used make the lines Cu 3247·5, Ag 3280·7, and Pb 3240·2 too strong to measure accurately: for these a second exposure would be necessary.
4. Bi 3067·7 may be confused with Fe 3067·2 when Fe is present.
5. Tl 2767·9 may be confused with Fe 2767·5 when Fe is present.
6. Sb 2311·5 may be confused with Ni 2310·9.
7. Cd 2265·0 may be confused with Ni 2264·5.
8. Te 2142·7 may be confused with Cd 2144·4.
9. Ag 2324·7 may be interfered with by Ni 2324·6 when Ni is >0·01 per cent.
10. Cu 2369·9 may be interfered with by As 2369·7 when As is >0·005 per cent.

Effect of background corrections

Owing to the high background intensity of the lead spectrum it was necessary to apply background corrections in order to obtain linear working curves. Additional readings on the background near each spectrum line were taken and converted to relative intensities from the plate calibration curve. The corrected line intensity was obtained by subtracting the relative intensity of the background from that of line plus background.

A comparison of reproducibility of results obtained with and without background correction showed some advantage for the former at the 0·0005 per cent level for some elements, where lines are weak relative to background. At the higher contents, the application of background correction appeared to have no consistent effect on reproducibility. However, a long term test has subsequently shown that higher accuracy of analysis can be obtained by the use of background correction and the associated linear working curve.

The form of the test was to construct working curves for antimony in lead at the 0·020 per cent level, both with and without background correction. A single sample was then analyzed, without using standards, on a number of plates taken over a period of eight months by reference to the original working curves. A stepped sector plate calibration was used. Without background correction, the maximum deviation from the mean was found to be ±0·004 per cent Sb and with background correction this was reduced to ±0·002 per cent Sb.

VOL. 7 55/56

Acknowledgments

The members of the panel are indebted to their separate organizations and to the Director and Council of The British Non-Ferrous Metals Research Association for permission to publish this paper. They also wish to acknowledge their appreciation of the co-operation of Messrs. Johnson, Matthey & Co. Ltd., in preparing the binary alloys and of the careful work of Mr. V. E. Carter of the Association's staff in the preparation of the complex standard alloys.

References

[1] Smith, D. M.; Collected Papers on Metallurgical Analysis by the Spectrograph, p. 110. British Non-Ferrous Metals Research Association, London, 1945.
[2] Bannister, L. C., and Price, R. H.; *J. Inst. Metals* 1948 **75** 151.
[3] Walsh, A.; *Met. Ind.* 1946 **68** 243 263 293.
[4] Levy, S.; *J. Opt. Soc. Amer.* 1945 **35** 221.
[5] Churchill, J. R.; *Ind. Eng. Chem.* (*Anal. Ed.*) 1944 **16** 653.
[6] Honerjäger-Sohm, M., and Kaiser, H.; *Spectrochim. Acta* 1944 **2** 396.

Appendix

Preparation of dilute lead alloy standards

Four standard alloys were produced from high purity lead with very small additions of eleven elements. The method adopted was to produce first a series of binary master alloys at the 0·1 per cent level. After chemical analysis, these alloys were used for making the small additions necessary for the final concentrations required.

For production of both master alloys and final alloys the same melting and casting technique was employed, viz:—

The basic lead was melted in a clean salamander crucible heated in an electric muffle furnace and with a reducing gas flame impinging on the surface of the melt to avoid oxidation losses. After melting the required additions were made, the melt stirred, and the temperature adjusted for pouring. The melt was then poured through another reducing gas flame into steel moulds heated to 50–100°C.

A. *Binary master alloys*

Ten of the eleven binary master alloys were made up from a Tadanac lead with the analysis shown in Table 4.

Table 4. *Chemical compositions of pure leads for standards*

Element	*Tadanac lead* %	*High purity lead* %
Copper	0·0002–0·0003	0·0001
Silver	0·0001–0·0003	0·00003–0·0001
Cadmium	0·0001	<0·0001
Arsenic	0·0006	trace
Bismuth	0·0002	0·0001
Antimony	0·0005	0·0001
Tin	0·0002	trace
Nickel	0·000025	nil
Zinc	0·00002	0·0001
Tellurium	0·0006	trace
Thallium	trace	0·0002

The additions of high-purity metal were wrapped in lead foil and the package dropped through the gas flame on to the surface of the molten lead and well stirred into the melt.

Arbitrary allowances of nil for tin, silver, copper, and nickel, 2 per cent for bismuth and 5 per cent for thallium, tellurium, cadmium, zinc, antimony, and arsenic were made for losses on making up and these allowances were proved, on the whole, reasonable by the analysis.

The additions were made at approximately 520–550°C with the exception of copper (700°C), silver (700°C), and arsenic (600°C) and in all cases the temperature was allowed to drop to about 500°C before pouring.

B. *Four standard alloys*

Three of the four standard alloys were made up using the same Tadanac lead as a base. The fourth alloy (with the smallest quantity of additions) was made up using a very high purity lead of the composition shown in Table 4.

For purposes of balancing the total quantity of added elements the eleven elements were grouped according to the following list:

Group A: Copper, silver, nickel, bismuth.

Group B: Arsenic, cadmium, zinc.

Group C: Antimony, tin, thallium, tellurium.

VOL 7 1955/

The four alloys were then made as follows:—

Sample Mark	*Additions*	
I	0·0005 per cent of *all* groups	(Using very high purity lead)
II	0·001 per cent Group A 0·0025 per cent Group B 0·005 per cent Group C	
III	0·0025 per cent Group A 0·005 per cent Group B 0·001 per cent Group C	(using Tadanac lead)
IV	0·005 per cent Group A 0·001 per cent Group B 0·0025 per cent Group C	

Allowance was made for the presence in the basic lead of the element in question (on the analysis figures quoted), but no allowance was made for loss of addition elements through volatilization or oxidation during making up. The metal was cast in the form of 1 in. diameter ingots, which were rolled to $\frac{3}{8}$ in. rods for use.

Compositions of dilute lead alloy standards

The results of the co-operative spectrographic analyses of the two rods of each composition are given in Table 5.

Table 5. Results on master standards

Element	*Per cent concentration*			
Nominal	0·0005	0·001	0·0025	0·005
Nickel	0·00052	0·0011	0·0025	0·0052
Bismuth	0·00055	0·0019	0·0031	0·0054
Thallium	0·0003	0·0016	0·0025	0·0049
Cadmium	0·0004	0·0010	0·0025	0·0050
Antimony	i. 0·00025–0·00057 ii. 0·0004	0·00065	0·0024	0·0050
Silver	0·00037	0·0012	0·0025	0·0052
Arsenic	0·00033	0·00038	0·0016	0·0034
Tin	0·00050	0·0012	0·0032	0·0055
Copper	0·00045	0·0012	0·0026	0·0050
Zinc	0·0005	i. 0·0010 ii. 0·0013	0·0025–0·0045	0·0052
Tellurium	0·0008	0·0005–0·00065	0·0025	0·0049

Results for zinc cannot be relied upon as some rods have shown possible heterogeneity.

An independent check on the compositions of the standards was made against other standards in another laboratory, not represented on the Panel, and good agreement was found.

Spectrochimica Acta, 1955, Vol. 7, pp. 214 to 218. Pergamon Press Ltd., London

The spectrographic determination of germanium in coal and flue dust

G. J. Pitt and the late M. F. Fletcher
National Coal Board, Central Research Establishment I,
Stoke Orchard, nr. Cheltenham

(*Received* 23 *April* 1955)

Summary—A method has been developed for the analysis of germanium in coal and flue dust. The sample is ashed, mixed with lithium carbonate as buffer and a small known amount of tin dioxide as internal standard. Pellets of this mixture are arced to completion in a graphite anode, using direct current. The germanium content is derived from a calibration curve relating the densities of the analysis line and the internal standard line.

The lower limit for detection of germanium is 6 p.p.m. on the ashed sample, but for quantitative estimation the useful range is from 24 p.p.m. upwards, where the coefficient of variation is 5 per cent between exposures on one plate.

1. Introduction

Spectrographic methods for the estimation of germanium have been reviewed by Kraus and Johnson [1], Ahrens [2], and Aubrey [3]. Where the material to be analyzed contains only a small amount of germanium, the use of the d.c. arc would be expected to give the sensitivity required; but the high volatility of germanium compounds tends to prevent the realization of this expectation, and also leads to poor reproducibility. Landergren [4] has claimed improved sensitivity by the use of an interrupted arc, but the source unit necessary in this case is not normally part of the equipment available to the analyst. Goldschmidt and Peters [5] have investigated the use of deep-cavity electrodes (cathode layer technique) to reduce the rate of volatilization, and claim a sensitivity of 10 p.p.m. or better. Aubrey [3] has used a technique in which the sample is mixed with an equal weight of graphite, and the spectra are compared visually with those of synthetic standards; although simple and apparently of adequate sensitivity, this method is not sufficiently accurate for use except in large-scale exploratory work.

Since the development of the method to be described here, three other spectrographic methods have been reported, all of which employ d.c. arc excitation. Of these, the one by Bryson [6] is somewhat similar to the method proposed in this paper and is discussed later. Frederick, White, and Biber [7] use bismuth in the form of Bi_2O_3 as an internal standard, without a spectrographic buffer, and claim a sensitivity of 5 p.p.m.; we have found bismuth less suitable than tin on the evidence of moving-plate spectra. Harris [8] describes a method for the determination of very small amounts (less than 2 p.p.m.) in silicate rocks, which involves a preliminary concentration; tin is used as a carrier and as an internal standard element.

2. Development of method

For our purposes, a method was required which would permit the determination of small amounts of germanium in coals and related materials. In view of the

large number of samples to be analyzed it was desirable that preparation should be reduced to a minimum; high sensitivity and independence of the composition of the matrix were consequently of importance. For these reasons it was decided to investigate the simultaneous use of a buffer and an internal standard in a method based on d.c. arc excitation.

3. Selection of spectrographic buffer

In the first instance, the effect of adding lithium carbonate to germanium dioxide was examined. The rate of volatilization of the germanium was thereby satisfactorily reduced, so that the use of electrodes with shallow cavities became feasible. It is presumed that lithium germanate is formed as an intermediate, and, if this is so, the use of lithium carbonate will have the additional advantage of making the intensity of the germanium line much more nearly independent of the original state of combination of the element. Consequently the preliminary chemical separation suggested by MARKS and HALL [9] will be obviated.

BRYSON has recommended the use of a mixture of one part graphite and two parts lithium carbonate as a buffer, but the addition of graphite does not appear to be necessary.

4. Selection of internal standard element

On the basis of moving-plate spectra from mixtures of germanium dioxide, lithium carbonate, and oxides of the common elements in the B sub-groups of the Periodic Table, the most suitable element found was tin.

The possibility of using lithium as the internal standard element, which has been proposed by BRYSON, was discarded, since there are no lithium lines in this region of the spectrum which would be of suitable intensity from a matrix consisting largely of lithium carbonate, unless a stepped sector were introduced.

5. Spectral lines

The most sensitive germanium line arises from the transition $4p\ ^3P_2 - 5s\ ^3P_2^0$ and has a wavelength 2651·18 Å. The excitation potential, 4·8 eV, is less than that of lithium, 5·4 eV, and the germanium line is therefore not suppressed by the buffer. No interference is likely to be caused by other elements normally present in coal ash; in particular, the iron lines in this neighbourhood are relatively weak. A choice of tin line exists between the line 2546·55 Å arising from the transition $5p\ ^3P_0 - 6s\ ^1P_1^0$ and the line 2571·58 Å arising from the transition $5p\ ^1D_2 - 5d\ ^3D_3^0$. The former is preferable on the grounds that the excitation potential is the same as that of the chosen germanium line, but suffers from the disadvantage that background from an adjoining iron line is liable to overlap with it. The tin line at 2571·58 Å is free from interference by iron, but has a somewhat higher excitation potential (5·9 eV), and was finally rejected in favour of that at 2546·55 Å.

6. Influence of chlorine in sample

Chlorine can occur in coal, but a test in which 1 per cent chlorine (as NaCl) was added to the lithium carbonate, germanium oxide, tin dioxide mixture showed that its effect on volatilization was insufficient to affect the accuracy of the Ge determination.

7. Preparation of sample

From the experimental standpoint, it is quite satisfactory to grind the coal with four parts of lithium carbonate, and arc directly. On the other hand, where the germanium content is expected to be small, it is clearly advantageous to convert the coal to ash, and then arc the mixture of ash plus four parts lithium carbonate. If the ashing is carried out at a temperature not greater than 400°C, the germanium is retained in the ash without detectable loss. The mixture is formed into pellets weighing about 10 mg to be placed in a cavity electrode.

8. Experimental conditions

Item	*Conditions*	*Remarks*
Spectrograph	Large dispersion quartz prism	Hilger E492 or 478
Auxiliary lens	2 cm from slit	Hilger F1025
Waveband setting	2480–3600 Å	
Slit width	0·016 mm	
Arc-gap width	3 mm	Maintained during exposure
Arc current	9 amp	d.c. full-wave rectification (unsmoothed)
Counter electrode (cathode)	Graphite 30°	Johnson, Matthey JM4B
Sample electrode (anode)	3·6 mm cavity; tapered; depth 1·5 mm	6·5 mm diam.
Burning-off time	15 sec	
Exposure time	Time taken for complete consumption of pellet	Approximately 60 sec
Plate	Ilford Ordinary	
Developer	Ilford Developer I.D.2.	
Development time	4 min	This time is greater than the time taken to reach maximum contrast
Developer temperature	67° ± 0·5°F	

9. Calibration

A series of standard mixtures containing from 3 to 200 p.p.m. germanium in the flux (lithium carbonate with 0·1 per cent tin) was prepared, and the spectra used to derive a calibration graph relating the Seidel density difference of the Ge and Sn lines with the Ge concentration. This was checked by means of three other mixtures containing 50, 100, 200 p.p.m. prepared independently. When the Ge content is less than 30 p.p.m., a background correction is applied, based on the assumption that Seidel densities are additive. The calibration graph thus obtained was linear over the concentration range 6 to 200 p.p.m. Ge in flux (slope 1·09; index value 82 p.p.m.).

This graph is used to relate the observed Seidel density difference for a sample being analyzed to the germanium concentration in the flux mixture. If, however, the sample contains more than 7 per cent iron, a background correction becomes necessary to the tin line because of the adjoining iron line at 2545·98 Å.

If the normal ratio of one part ashed sample to four parts flux is used, the lower limit quoted above corresponds to 24 p.p.m. on ashed sample. The lowest detectable germanium concentration is 6 p.p.m. on sample, but the range from 6 to 24 p.p.m. is not considered to be suitable for quantitative work unless more accurate background corrections are applied. From the standpoint of coal analysis

VOL. 7 1955/

this does not constitute a serious disadvantage, since there is a preliminary concentration of the germanium in the ash; if the original coal has 10 per cent ash, a concentration of 24 p.p.m. on ash is equivalent to 2·4 p.p.m. on coal.

The coefficient of variation was estimated from the observations used in preparing the calibration graph. A value of 5 per cent per exposure was obtained between exposures on the same plate.

10. Agreement with chemical methods

Samples of coal ash and flue dust were available which had been analyzed by the colorimetric method proposed by CLULEY [10]. Seven samples of coal ash were analyzed by the spectrographic procedure as described above, duplicate exposures being recorded in each case. Six samples of flue dust were similarly analyzed, except that the flux-sample ratio was increased to 100 : 1 because of the higher concentrations to be expected in these dusts; quadruple exposures were recorded. Two entirely separate determinations were made in each case, and the mean concentrations found are recorded in columns 2 and 3 in the Table. In columns 5 to 7 are recorded individual colorimetric determinations where the data were available, and the mean of two determinations in column 8.

Table. Determination of germanium in coal ash and flue dust

Sample	*Per cent weight germanium in sample*						
	Spectrographic			*Chemical*			
	1	2	*Mean (S)*	1	2	3	*Mean (C)*
Coal ash							
136	0·054	0·052	0·053	0·058	0·058	—	0·058
137	0·020	0·021	0·021	0·024	0·024	—	0·024
147	0·0056	0·0056	0·0056	0·0052	0·0049	—	0·0050
149	0·0042	0·0050	0·0046	0·0051	0·0058	0·0051	0·0053
151	0·0047	0·0049	0·0048	0·0024	0·0026	—	0·0025
153	0·018	0·016	0·017	0·019	0·017	—	0·018
157	0·019	0·018	0·018	0·018	0·018	—	0·018
Flue dust							
268	0·33	0·34	0·34	—	—	—	0·31
269	0·49	0·50	0·50	—	—	—	0·47
270	0·57	0·56	0·56	—	—	—	0·57
271	0·69	0·70	0·70	—	—	—	0·64
272	0·68	0·72	0·70	—	—	—	0·74
273	0·56	0·62	0·59	—	—	—	0·62

The agreement between the two methods is reasonably good. It would appear from the coal-ash results that under the conditions described here, and when the concentration is about 0·050 per cent or lower, the results obtained by the two

methods should not normally differ by more than 0·005 per cent. In the case of the flue dusts, and where the concentrations are in the region of 0·50 per cent, the methods should not normally differ by more than 0·08 per cent.

11. Conclusions

The method described has been found satisfactory for the determination of traces of germanium in coal and flue dust. Sample preparation is relatively simple, and the sensitivity and precision are adequate. Good accuracy has been achieved, both with flue dusts containing at least 0·3 per cent germanium and with coal ashes containing at least 25 p.p.m. germanium.

Acknowledgments—We are grateful to Mr. K. Dixon of the Coal Survey Laboratory, Nottingham, for advice and help with the experimental work, and to Johnson, Matthey and Co. Ltd., for supplying samples of flue dust. The authors also wish to thank the National Coal Board for permission to publish this paper.

References

[1] Kraus, H. H., and Johnson, O. H.; *Analyt. Chem.* 1953 **25** 134–138.
[2] Ahrens, L. H.; *Spectrochemical Analysis*, Chapter 21, Addison-Wesley Press, Cambridge (Mass.) 1950.
[3] Aubrey, K. V.; *Fuel* 1952 **31** 429–437.
[4] Landergren, S., reported by Wickman, F. E.; *Geol. Fören. Stockh. Förh.* 1943 **65** 371–396.
[5] Goldschmidt, V. M., and Peters, C.; *Nach. Ges. Wiss. Göttingen, IV* 1933 **3** 141–166.
[6] Anon; *Chem. Engng. News* 1953 **31** 1083.
[7] Frederick, W. J., White, J. A., and Biber, H. E.; *Analyt. Chem.* 1954 **26** 1328–1330.
[8] Harris, P. G.; *Analyt. Chem.* 1954 **26** 737–739.
[9] Marks, G. W., and Hall, H. T.; Rep. Invest. No. 3965. U.S. Bur. Mines 1946.
[10] Cluley, H. J.; *Analyst* 1951 **76** 523–535.

Spectrochimica Acta, 1955, Vol. 7, pp. 219 to 230. Pergamon Press Ltd., London

Periodische Erscheinungen bei der Metallablösung an der Oberfläche von Mehrstoffsystemen

G. Ecker
Institut für theoretische Physik der Universität Bonn

(*Received* 19 *February* 1955)

Summary—It has been shown experimentally that the volatilization of metal from an electrode of an alloy follows a characteristic time-sequence during which regular periodic variations occur. By excluding irrelevant phenomena a set of simultaneous differential equations can be derived for the volatilization process which permits the evaluation of the variation of the volatilization process with time. Important parameters are the relative volatilization probabilities of the two components of the alloy, the percentage composition, and the probability of energy dissipation in lower layers of the metal beneath the surface layer. A numerical integration of these equations has been carried out for four examples, to show the influence of various parameters. Curves are derived which correspond to observations, and in particular account for the periodic variations.

OL.
7
5/56

Beim Abfunken von Metalloberflächen haben kürzlich H. Kaiser und Mitarbeiter interessante Spektraluntersuchungen der Materialablösung durchgeführt [1]. Sie beobachteten an einem Zweistoffsystem (Cu—Be) mit Hilfe eines photoelektrisch registrierenden Spektrometers das Intensitätsverhältnis einer Cu- und einer Be-Spektrallinie als Funktion der Abfunkdauer. Dabei zeigte sich zu Beginn des Versuches zunächst eine starke monotone Änderung des Intensitätsverhältnisses bis zu einem bestimmten Grenzwert. Überraschenderweise blieb jedoch im weiteren Verlauf des Versuches das Intensitätsverhältnis nicht konstant, sondern führte um den eben genannten Grenzwert periodische Schwankungen von erstaunlicher Regelmäßigkeit aus. A.a.O. wurde darauf hingewiesen, daß diese auffallende Erscheinung durch periodische Aktivierungen der Elektrodenoberfläche verursacht sein könnte.

Unbeschadet dieser interessanten Deutungsmöglichkeit möchten wir in der vorliegenden Untersuchung auf die Tatsache aufmerksam machen, daß schon auf Grund des reinen Ablösemechanismus Periodizitäten der beobachteten Art bei der Stoffablösung von mehrkomponentigen Materialien erwartet werden können. Und zwar läßt sich diese Vorhersage rein formal herleiten, ohne daß eine detaillierte Vorstellung bezüglich der Art des Ablösemechanismus überhaupt erforderlich wäre. Ebenso erübrigt sich die genaue Kenntnis der verschiedenen Stoffeigenschaften und sonstiger physikalischer Parameter. Es genügt vielmehr die Einführung allgemeiner Begriffe, wie beispielsweise der Ablösewahrscheinlichkeit oder des Molekülradius der einzelnen Stoffkomponenten. Mit ihrer Hilfe zeigt eine ganz formale Überlegung, daß die Periodizitäten grundsätzlich bei allen Mehrstoffsystemen zu erwarten sind, sofern die Ablösewahrscheinlichkeiten der verschiedenen Komponenten verschieden groß sind,—eine Annahme, die schon wegen der unterschiedlichen Bindung der Teilchen im Metallverband stets erfüllt sein sollte. Allerdings ist unsere Behauptung noch insofern einzuschränken, als das "grundsätzliche" Auftreten der Schwankungserscheinungen nicht notwendig

ihre Beobachtbarkeit einschließt und in der Tat zeigen die folgenden Ausführungen, daß Periodizitäten der Stärke, wie sie von Kaiser und Mitarbeitern beobachtet wurden, nur unter bestimmten günstigen Bedingungen erwartet werden können.

Die oben erwähnte Allgemeinheit unserer Überlegungen, welche uns den Verzicht auf genauere und möglicherweise unsichere Modellvorstellungen erlaubt, wirkt sich natürlich vorteilhaft auf die Zuverlässigkeit der Resultate aus.

Wir betrachten folgende einfache Anordnung. Auf die ebene Oberfläche eines aus zwei Komponenten (A, B) homogen zusammengesetzten Systems fallen pro Quadratzentimeter eine Anzahl von Ionen, die mit einer gewissen Wahrscheinlichkeit Atome der Sorte A bzw. B aus dem Metall auslösen können.

Um diesen Vorgang zu verfolgen, denken wir uns das Metall durch Ebenen parallel zur Oberfläche in Schichten gleicher Dicke Λ aufgeteilt. Λ sei durch die Bedingung festgelegt, daß eine solche Λ-Schicht bei voller Besetzung "einfach dicht" bedeckt ist. Mit anderen Worten—die Projektionen aller in der vollbesetzten Λ-Schicht befindlichen Atome auf die Oberfläche sollen letztere zwar lückenlos bedecken, sich jedoch gegenseitig nicht wesentlich überlagern.*

Diese Einteilung bildet einerseits eine geeignete Basis für die folgenden Berechnungen. Sie ist aber auch physikalisch sinnvoll, da die Atome einer Schicht für den Ablösevorgang als gleichwertig betrachtet werden können, während die Atome verschiedener Schichten, wie wir noch genauer sehen werden, hinsichtlich des gleichen Vorganges verschiedenes Verhalten zeigen.

Die Teilchenzahlen der Sorten A bzw. B pro cm² der ν-ten Schicht bezeichnen wir mit $N_a^{(\nu)}$ und $N_b^{(\nu)}$. Die mittleren sekundlichen Ablösungsdichten Z_a, Z_b lassen sich mit diesen Dichtezahlen in der Form

$$Z_a(t) = \sum_\nu \frac{dN_a^{(\nu)}}{dt}; \qquad Z_b(t) = \sum_\nu \frac{dN_b^{(\nu)}}{dt} \tag{1}$$

ausdrücken. Um Z_a und Z_b angeben zu können, berechnen wir zunächst die einzelnen Komponenten $dN_{a,b}^{(\nu)}/dt$ als Funktionen der Zeit.

Die Wahrscheinlichkeit, daß durch das Ionenbombardement pro Flächeneinheit der Oberfläche im Zeitintervall dt ein Atom A bzw. B aus der ν-ten Schicht entfernt wird, bezeichnen wir mit $W_a^{(\nu)}\,dt$ bzw. $W_b^{(\nu)}\,dt$. Die Änderung der Besetzungsdichten $N_a^{(\nu)}$, $N_b^{(\nu)}$ der einzelnen Schichten läßt sich damit durch ein System simultaner Differentialgleichungen

$$\frac{dN_a^{(\nu)}}{dt} = -W_a^{(\nu)}; \qquad \frac{dN_b^{(\nu)}}{dt} = -W_b^{(\nu)} \tag{2}$$

beschreiben, wo die Wahrscheinlichkeiten $W_a^{(\nu)}$ und $W_b^{(\nu)}$ vorläufig noch unbekannte Funktionen der Besetzungsdichten sind.

Wir spalten diese Wahrscheinlichkeiten $W_a^{(\nu)}$, $W_b^{(\nu)}$ zweckmäßig in der Form $W_a^{(\nu)} = W_{a1}^{(\nu)}\ W_{a2}^{(\nu)}$ bzw. $W_b^{(\nu)} = W_{b1}^{(\nu)} \cdot W_{b2}^{(\nu)}$ in Anteile $W_1^{(\nu)}$, $W_2^{(\nu)}$ auf. Die Größen $W_1^{(\nu)}$ ($W_{a1}^{(\nu)}$, $W_{b1}^{(\nu)}$) geben die Wahrscheinlichkeit dafür an, daß durch das

* Wir denken uns die Atome innerhalb des Metallverbandes wie üblich als Kugeln vom Radius R_a bzw. R_b gekennzeichnet. In der Projektion erhalten wir damit Wirkungsquerschnitte $Q_a = \pi R_a^2$ bzw. $Q_b = \pi R_b^2$.

Ionenbombardement der Oberfläche einem beliebigen Teilchen der ν-ten Schicht ein Energiebetrag gleich oder größer als seine Austrittsenergie (Potentialdifferenz zwischen dem gebundenen Zustand in der ν-ten Schicht und dem freien Zustand in ausreichender Entfernung von der Oberfläche) mitgeteilt wird. Die Faktoren $W_2^{(\nu)}$ ($W_{a2}^{(\nu)}$, $W_{b2}^{(\nu)}$) dagegen bezeichnen die Wahrscheinlichkeit dafür, daß ein Teilchen der ν-ten Schicht, welchem ein ausreichender Energiebetrag zur Verfügung stehtet, den Mallverband wirklich verläßt.

Beide Wahrscheinlichkeiten $W_1^{(\nu)}$ und $W_2^{(\nu)}$ hängen in komplizierter Weise nicht nur von den verschiedenen Parametern des Metalls und der einfallenden Ionen, sondern insbesondere auch von dem Besetzungszustand der nullten bis $(\nu - 1)$-ten Schicht ab. Wir wollen versuchen, von dieser an sich komplizierten Abhängigkeit ein zwar vereinfachtes, jedoch für unsere qualitativen Überlegungen ausreichendes Bild zu gewinnen.

Beginnen wir mit den Wahrscheinlichkeiten $W_1^{(\nu)}$ und zwar mit der Größe $W_1^{(1)}$ der ersten Schicht. Die Wahrscheinlichkeit $W_1^{(1)}$ hängt natürlich in irgend einer Weise von der Stromdichte, der Masse, der Elektronenhülle und der Energie der einfallenden Ionen, sowie von der Elektronenhülle der gestoßenen Teilchen, ihrer Masse und ihrer Bindungsenergie im Metallverband ab. Jedoch interessiert uns die Abhängigkeit von diesen Parametern, die wir der Kürze halber in der Bezeichnung σ zusammenfassen mögen, hier höchstens insofern, als diese Einflüsse verständlich machen, wieso die Ablösewahrscheinlichkeiten der verschiedenen Komponenten größenordnungsmäßig verschieden sein können. Hingegen ist es wesentlich zu wissen, wie $W_1^{(1)}$ vom Besetzungszustand der Schicht abhängt. Da wir oben die Schichtdicke Λ so definiert hatten, daß jede Schicht im vollbesetzten Zustand nur einfach dicht bedeckt ist, so müssen die Wahrscheinlichkeiten $W_{a1}^{(1)}$ bzw. $W_{b1}^{(1)}$ den Besetzungszahlen $N_a^{(1)}$, $N_b^{(1)}$ proportional sein. Wir erhalten damit die Beziehungen

$$W_{a1}^{(1)} = w_1(\sigma_a) \cdot N_a^{(1)}; \qquad W_{b1}^{(1)} = w_1(\sigma_b) \cdot N_b^{(1)} \tag{3}$$

wo σ_a, σ_b den Einfluß der oben genannten Parameter kennzeichnet.

Bei der zweiten Schicht liegen die Verhältnisse bereits komplizierter, weil jetzt die Wahrscheinlichkeit der Energieübertragung auf ein Teilchen dieser Schicht auch von dem Besetzungszustand der ersten Schicht abhängig ist. Befindet sich kein Teilchen in der ersten Schicht, so gilt natürlich entsprechend Gl. (3) die Beziehung

$$\overline{W}_{a1}^{(2)} = w_1(\sigma_a) N_a^{(2)}; \qquad \overline{W}_{b1}^{(2)} = w_1(\sigma_b) \cdot N_b^{(2)} \tag{4}$$

Mit zunehmender Besetzungsdichte der ersten Schicht nimmt jedoch die Wahrscheinlichkeit der Energieübertragung auf Teilchen der zweiten Schicht ab, da die Energie von den vorgelagerten Teilchen $N_{a,b}^{(1)}$ ganz oder zum Teil abgefangen werden kann. Dieser Einfluß läßt sich in erster Näherung einfach und zugleich anschaulich einleuchtend erfassen, indem wir die Vorstellung verwenden, daß in denjenigen Bereichen, in denen die erste Schicht "dicht besetzt" ist, keine Energie auf die zweite Schicht übertragen wird. In denjenigen Bereichen dagegen, wo die erste Schicht "offen" ist, soll die Ablösewahrscheinlichkeit unbeeinflußt durch

die erste Schicht aus der Formel (4) folgen. Damit würden wir bei beliebigem Besetzungszustand $N_{a,b}^{(1)}$ die Beziehungen

$$\begin{aligned} W_{a1}^{(2)} &= w_1(\sigma_a) \,.\, N_a^{(2)} \,.\, (1 - N_a^{(1)} Q_a - N_b^{(1)} Q_b) \\ W_{b1}^{(2)} &= w_1(\sigma_b) \,.\, N_b^{(2)} \,.\, (1 - N_a^{(1)} Q_a - N_b^{(1)} Q_b) \end{aligned} \tag{5}$$

erhalten, wo Q_a und Q_b die im Vorgang definierten Wirkungsquerschnitte angeben.

Die Beziehungen (5) lassen sich leicht noch etwas allgemeiner halten, wenn wir berücksichtigen, daß möglicherweise der Einfluß der vorgelagerten Schicht nicht einfach durch das Verhältnis von "geschlossener Fläche" zur Gesamtfläche beschrieben werden darf, sondern besser durch eine geeignete Potenz dieses Flächenverhältnisses angenähert werden kann. Auf die anschauliche Bedeutung eines derartigen Potenzansatzes werden wir im folgenden noch zu sprechen kommen. Jedenfalls wollen wir hier um der größeren Allgemeinheit willen die Formeln (5) durch die Beziehungen

$$\begin{aligned} W_{a1}^{(2)} &= w_1(\sigma_a) \,.\, N_a^{(2)} (1 - N_a^{(1)} Q_a - N_b^{(1)} Q_b)^{\gamma_{a1}} \\ W_{b1}^{(2)} &= w_1(\sigma_b) \,.\, N_b^{(2)} (1 - N_a^{(1)} Q_a - N_b^{(1)} Q_b)^{\gamma_{b1}} \end{aligned} \tag{6}$$

ersetzen, in denen das einfachere Modell (5) als Spezialfall $\gamma_{a1} = \gamma_{b1} = 1$ enthalten ist.

Die Verhältnisse bei den folgenden Schichten lassen sich nun leicht übersehen. Wäre die zweite Schicht völlig unbesetzt, so ergäbe sich für $W_1^{(3)}$ entsprechen (6) ein Ausdruck

$$\begin{aligned} \overline{W}_{a1}^{(3)} &= w_{1a} \,.\, N_a^{(3)} \,.\, (1 - N_a^{(1)} Q_a - N_b^{(1)} Q_b)^{\gamma_{a1}} \\ \overline{W}_{b1}^{(3)} &= w_{1b} \,.\, N_b^{(3)} \,.\, (1 - N_a^{(1)} Q_a - N_b^{(1)} Q_b)^{\gamma_{b1}} \end{aligned} \tag{7}$$

Ist dagegen die zweite Schicht ganz oder teilweise gefüllt, so müssen die Ausdrücke (7) noch mit der Wahrscheinlichkeit dafür multipliziert werden, daß die Energieübertragung auf die dritte Schicht nicht durch die zweite behindert wird. Sofern wir allen Schichten einen gemeinsamen mittleren Exponenten $\gamma_{ab,1}$ zuschreiben können, erhalten wir damit

$$\begin{aligned} W_{a1}^{(3)} &= w_{1a} \,.\, N_a^{(3)} \,.\, (1 - N_a^{(2)} Q_a - N_b^{(2)} Q_b)^{\gamma_{a1}} \,.\, (1 - N_a^{(1)} Q_a - N_b^{(1)} Q_b)^{\gamma_{a1}} \\ W_{b1}^{(3)} &= w_{1b} \,.\, N_b^{(3)} \,.\, (1 - N_a^{(2)} Q_a - N_b^{(2)} Q_b)^{\gamma_{b1}} \,.\, (1 - N_a^{(1)} Q_a - N_b^{(1)} Q_b)^{\gamma_{b1}} \end{aligned} \tag{8}$$

und aus der Fortsetzung dieser Schlußweise erkennt man, daß allgemein die Beziehungen

$$\begin{aligned} W_{a1}^{(\nu)} &= w_{1a} \,.\, N_a^{(\nu)} \,.\, \overline{\prod_i}^{1-(\nu-1)} (1 - N_a^{(i)} Q_a - N_b^{(i)} Q_b)^{\gamma_{a1}} \\ W_{b1}^{(\nu)} &= w_{1b} \,.\, N_b^{(\nu)} \,.\, \overline{\prod_i}^{1-(\nu-1)} (1 - N_a^{(i)} Q_a - N_b^{(i)} Q_b)^{\gamma_{b1}} \end{aligned} \tag{9}$$

gelten.

Um die Wahrscheinlichkeiten $W_2^{(\nu)}$ zu formulieren, beginnen wir wieder mit $W_2^{(1)}$. Auch in diesem Fall hängt die Wahrscheinlichkeit dafür, daß ein Teilchen

mit ausreichendem Energiebetrag den Metallverband verläßt, von den Parametern $\sigma\, ab$. Es gilt

$$W_{a2}^{(1)} = w_2(\sigma_a); \qquad W_{b2}^{(1)} = w_2(\sigma_b) \tag{10}$$

Im Gegensatz zu den Größen $W_1^{(\nu)}$ sind jedoch die Wahrscheinlichkeiten $W_2^{(\nu)}$ vom Besetzungszustand ihrer eigenen Schicht weitgehend unabhängig und die Größen $N_{a,b}^{(1)}$ treten daher in (10) nicht in Erscheinung.

Wäre die erste Schicht unbesetzt, so würde für die zweite Schicht entsprechend zu (10) die Beziehung

$$\overline{W}_{a2}^{(2)} = w_{2a}; \qquad \overline{W}_{b2}^{(2)} = w_{2b} \tag{11}$$

gelten. Ist dagegen die erste Schicht ganz oder teilweise besetzt, so kann ein Teilchen der zweiten Schicht nur abgelöst werden, wenn es durch eine Lücke der ersten Schicht austreten kann. Die Wahrscheinlichkeiten $W_2^{(2)}$ stellen sich daher als Produkt aus $\overline{W}_2^{(2)}$ und der Wahrscheinlichkeit $(1 - N_a^{(1)}Q_a - N_b^{(1)}Q_b)$ für die Durchdringung der ersten Schicht dar. Es gilt also

$$\begin{aligned} W_{a2}^{(2)} &= w_{2a}(1 - N_a^{(1)}Q_a - N_b^{(1)}Q_b) \\ W_{b2}^{(2)} &= w_{2b}(1 - N_a^{(1)}Q_a - N_b^{(1)}Q_b) \end{aligned} \tag{12}$$

oder wenn wir um der größeren Allgemeinheit willen auch hier geeignete Potenzen γ_{a2}, γ_{b2} einführen, erhalten wir die Formel

$$\begin{aligned} W_{a2}^{(2)} &= w_{2a}(1 - N_a^{(1)}Q_a - N_b^{(1)}Q_b)^{\gamma_{a2}} \\ W_{b2}^{(2)} &= w_{2b}(1 - N_a^{(1)}Q_a - N_b^{(1)}Q_b)^{\gamma_{b2}} \end{aligned} \tag{13}$$

Die Fortführung dieses Gedankenganges entsprechend den Überlegungen bei den Wahrscheinlichkeiten $W_1^{(\nu)}$ führt unmittelbar zu den allgemeinen Formeln

$$\begin{aligned} W_{a2}^{(\nu)} &= w_{2a}^{\prod_{i}^{1-(\nu-1)}} (1 - N_a^{(i)}Q_a - N_b^{(i)}Q_b)^{\gamma_{a2}} \\ W_{b2}^{(\nu)} &= w_{2b}^{\prod_{i}^{1-(\nu-1)}} (1 - N_a^{(i)}Q_a - N_b^{(i)}Q_b)^{\gamma_{b2}} \end{aligned} \tag{14}$$

Damit gewinnen wir aus (2), (9), und (14) für die Berechnung der Besetzungsdichten das System simultaner Differentialgleichungen

$$\frac{dN_a^{(\nu)}}{dt} = w_a N_a^{(\nu)} \cdot \prod_{i}^{1-(\nu-1)} (1 - N_a^{(i)}Q_a - N_b^{(i)}Q_b)^{\gamma_{a1}+\gamma_a} \tag{15a}$$

und

$$\frac{dN_b^{(\nu)}}{dt} = w_b N_b^{(\nu)} \cdot \prod_{i}^{1-(\nu-1)} (1 - N_a^{(i)}Q_a - N_b^{(i)}Q_b)^{\gamma_{b1}+\gamma_{b2}} \tag{15b}$$

mit

$$w_a = w_{1a} \cdot w_{2a}; \qquad w_b = w_{1b} \cdot w_{2b} \tag{15c}$$

Außerdem gilt die Randbedingung, daß zur Zeit $t = 0$ alle Schichten gleichmäßig und einfach dicht besetzt sind. Das Verhältnis der entsprechenden Teilchendichten N_{a0}, N_{b0} muß natürlich wegen der Homogenität der Probe mit dem Mischungsverhältnis der Komponenten A, B übereinstimmen.

Die uns interessierenden Größen Z_a und Z_b ergeben sich aus (15) durch einfache Summation zu

$$Z_a(t) = w_a \cdot \sum_{\nu} N_a^{(\nu)} \cdot \prod_{i}^{1-(\nu-1)} (1 - N_a^{(i)} Q_a - N_b^{(i)} Q_b)^{\gamma_{a1}+\gamma_{a2}}$$
$$Z_b(t) = w_b \cdot \sum_{\nu} N_b^{(\nu)} \cdot \prod_{i}^{1-(\nu-1)} (1 - N_a^{(i)} Q_a - N_b^{(i)} Q_b)^{\gamma_{b1}+\gamma_{b2}} \tag{16}$$

Damit ist die Berechnung der sekundlichen Ablösungsdichten auf ein rein mathematisches, wenn auch nicht gerade auf ein sonderlich bequemes Problem reduziert.

Das Gleichungssystem (16) formen wir ein wenig um, indem wir als neue unabhängige Variabele x das Produkt $w_a t$ aus der Ablösewahrscheinlichkeit w_a eines A-Teilchens der ersten Schicht und der Abfunkdauer t einführen. Außerdem bezeichnen wir das Verhältnis der Wahrscheinlichkeiten w_b/w_a mit κ. Eine geschlossene analytische Lösung des Systems (16) bereitet erhebliche Schwierigkeiten und aus diesem Grunde haben wir numerische Methoden verwandt. Die Berechnungen, welche sich recht umständlich gestalten, erfassen vier charkteristische Fälle Diese wurden nicht nach experimentellen Anwendungen orientiert, sondern vielmehr so ausgewählt, daß sie die verschiedenen Einflüsse (γ, κ, $N_{b0}Q_b/N_{a0}Q_a$) auf den zeitlichen Verlauf der Materialablösung möglichst weitgehend zu beurteilen erlauben.

In den Fig. 1 und 2 sind die Ergebnisse aufgetragen, wie sie sich aus (16) für den Fall $\gamma_{a1} = \gamma_{a2} = \gamma_{b1} = \gamma_{b2} = 1$ berechnen, wenn κ den Wert 4 bzw. 10 hat und der Bedeckungsquerschnitt $N_{b0}Q_b$ der Teilchen B wesentlich kleiner ist, als derjenige $N_{a0}Q_a$ der Sorte A. Da die Wirkungsquerschnitte der verschiedenen Komponenten sich im allgemeinen nicht wesentlich unterscheiden, entspricht diese Festsetzung einer Anordnung, welche—ähnlich den von KAISER und Mitarbeitern untersuchten Cu-Be-Proben mit 2 Prozent Be—die Komponente B nur als geringe Beimengung enthalten. Der Vergleich der Kurven für $\kappa = 4$ bzw. 10 erlaubt die Bedeutung des Unterschiedes der Ablösewahrscheinlichkeiten (w_b, w_a) abzuschätzen.

Wir hatten im Vorgang darauf hingewiesen, daß die Parameter γ_a, γ_b abweichend von den für die Berechnung der Fig. 1 und 2 zugrundegelegten Verhältnissen, auch Werte größer als 1 besitzen können, wenn aus irgend einem Grunde die Energieübertragung in die ν-te Schicht bzw. der Teilchenaustritt aus der ν-ten Schicht erst dann beachtlich wird, wenn die $(\nu - 1)$-te Schicht bereits weitgehend geöffnet ist. Um den Einfluß einer solchen nichtlinearen Abhängigkeit von der Öffnung der vorgelagerten Schichten beurteilen zu können, gibt die Fig. 3 den Verlauf der Ablösedichte für eine der Fig. 2 entsprechende Anordnung wieder,—nur daß jetzt $\gamma_{a1} + \gamma_{a2} = \gamma_{b1} + \gamma_{b2} = 4$ gewählt wurde.

Schließlich interessiert uns aber auch die Bedeutung des Mischungsverhältnisses der beiden Komponenten A, B für den zeitlichen Verlauf des Materialabbaues. Diese Einwirkung läßt sich mit Hilfe des Parameters $N_{b0}Q_b/N_{a0}Q_a$ erfassen. Das genannte Bedeckungsverhältnis wurde in den ersten drei Figuren wesentlich kleiner als eins vorausgesetzt, während in der Fig. 4, die in allen übrigen Daten mit der Anordnung der Fig. 3 übereinstimmt, die Beziehung $N_{b0}Q_b/N_{a0}Q_a = 1$ verwendet ist.

Fig. 1–4. Relative sekundliche Ablösedichte Z_a/N_{a0} bzw. Z_b/N_{b0} aufgetragen gegen das Produkt aus Abfunkdauer t und Ablösewahrscheinlichkeit w_a der A-Komponente. Die dünn ausgezogenen Kurven kennzeichnen die Anteile der einzelnen Schichten. Die im Text näher erläuterten Parameter κ, γ, und $N_{b1}Q_b/N_{a0}Q_a$ haben in den verschiedenen Figuren folgende Werte.

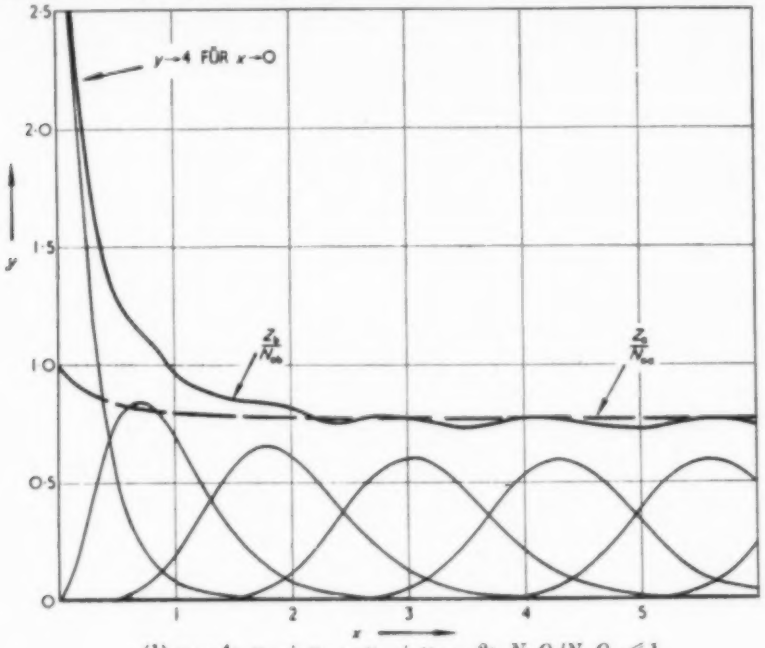

(1) $\kappa = 4$; $\gamma_{a1} + \gamma_{a2} = \gamma_{b1} + \gamma_{b2} = 2$; $N_{b0}Q_b/N_{a0}Q_a \ll 1$

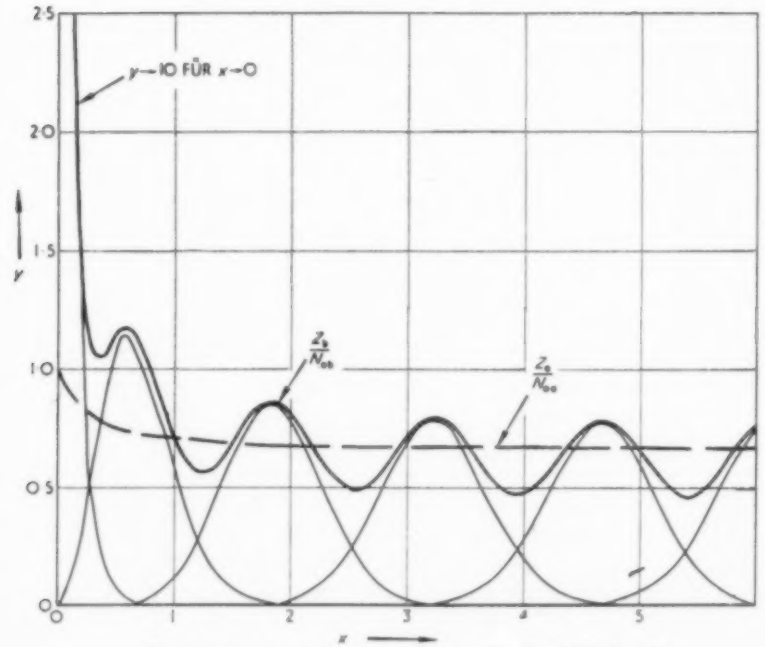

(2) $\kappa = 10$; $\gamma_{a1} + \gamma_{a2} = \gamma_{b1} + \gamma_{b2} = 2$; $N_{b0}Q_b/N_{a0}Q_a \ll 1$

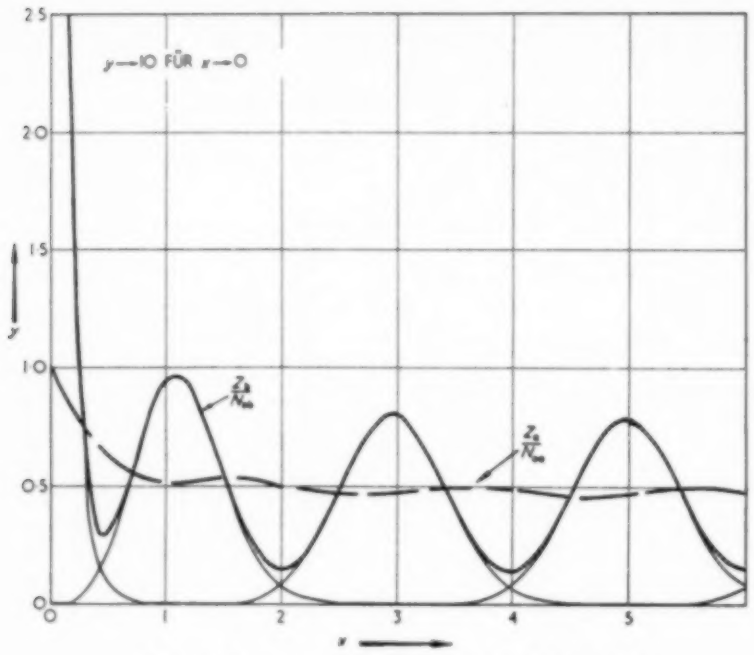

(3) $\kappa = 10$; $\gamma_{a1} + \gamma_{a2} = \gamma_{b1} + \gamma_{b2} = 4$; $N_{b0}Q_b/N_{a0}Q_a \ll 1$

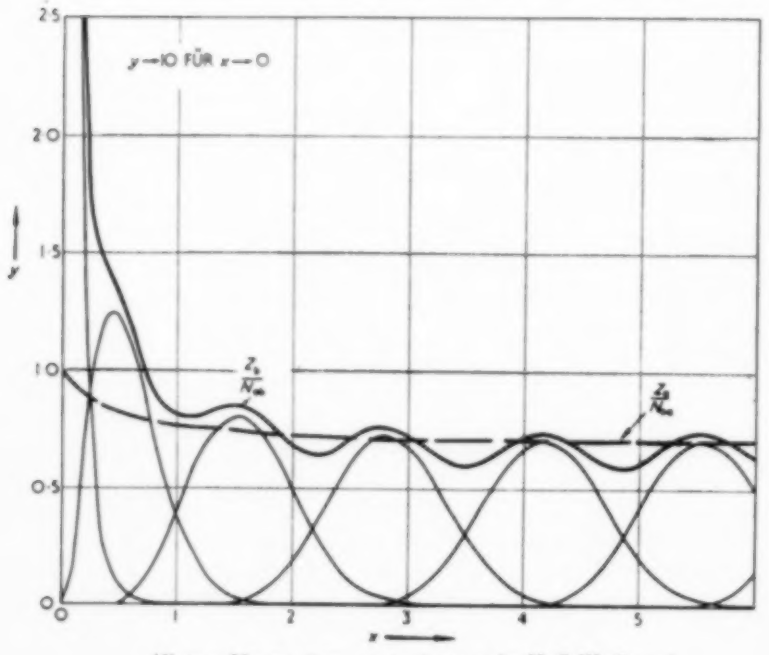

(4) $\kappa = 10$; $\gamma_{a1} + \gamma_{a2} = \gamma_{b1} + \gamma_{b2} = 4$; $N_{b0}Q_b/N_{a0}Q_a = 1$

VOL
7
1955/

Aus dem Kurvenverlauf der genannten Figuren und den Gleichungen (16) lassen sich einige interessante Ergebnisse ablesen. Wir beschränken uns dabei auf qualitative Schlußfolgerungen, von denen wir sicher sein dürfen, daß sie durch unser schematisiertes Modell richtig wiedergegeben werden.

Als wichtigstes und augenfälligstes Ergebnis unserer Überlegung konstatieren wir die Tatsache, daß die sekundliche Ablösedichte in keinem Fall konstant ist, wie dies bei einem Metall mit gleichen Ablösewahrscheinlichkeiten $w_a = w_b$ und $\gamma_{a1} + \gamma_{a2} = \gamma_{b1} + \gamma_{b2} = 1$ zu erwarten wäre. Vielmehr zeigt der Intensitätsverlauf für $w_a \neq w_b$, d.h. für alle praktisch interessierenden Fälle, anfangs einen monoton abfallenden (bzw. ansteigenden) Verlauf, um dann nach einer Art Einschwingvorgang in periodische Schwankungen von beachtlicher Regelmäßigkeit überzugehen. Der Mittelwert dieser Schwankungen nähert sich mit der Zeit asymptotisch einem konstanten Grenzwert, wobei gleichzeitig die Schwingungen in einen stationären Zustand konstanter Amplitude übergehen.

Die Änderung der sekundlichen Ablösedichte im monotonen Kurventeil,—oder genauer gesagt, die Differenz zwischen der Anfangsintensität und dem asymptotischen Grenzmittelwert der Schwankungen, ist bei sonst gleichen Umständen um so größer, je größer das Verhältnis κ der Ablösewahrscheinlichkeiten ist. Die genannte Differenz (gemessen im relativen Maßstab Z_b/N_{b0}, Z_a/N_{a0}) nimmt bei der Komponente größerer Ablösewahrscheinlichkeit (w_b) mit dem Mischungsanteil N_{b0} zu, wohingegen sie für die Komponente kleinerer Ablösewahrscheinlichkeit (w_a) mit sinkendem Mischungsanteil N_{a0} anwächst.

Die Schwankungserscheinungen sind weitaus am deutlichsten bei der Komponente mit der größeren Ablösewahrscheinlichkeit. Hier erreicht die Amplitude der Schwankungen, wie die Figuren zeigen, Werte von der Größe der mittleren Ablösedichte selbst. Demgegenüber bleiben bei der Komponente mit der geringeren Ablösewahrscheinlichkeit die Abweichungen vom Mittelwert teilweise unterhalb der Zeichengenauigkeit. Die Schwankungen sind ferner bei sonst gleichen Umständen um so ausgeprägter, je größer das Verhältnis der Ablösewahrscheinlichkeiten $\kappa = w_b/w_a$ ist, und zwar nimmt die Amplitude, von κ gleich eins anwachsend, zunächst nur langsam, später aber sehr schnell zu. Zunehmendes γ begünstigt die Periodizitäten ebenfalls stark und bedingt gleichzeitig eine Vergrößerung der "Schwingungsdauer." Mit zunehmendem Bedeckungsquerschnitt $N_{b0}Q_b$ der Komponente hoher Ablösewahrscheinlichkeit nimmt die Deutlichkeit der Periodizitäten stark ab, während sich die "Schwingungsdauer" gleichzeitig verkürzt.

Die relativen sekundlichen Ablösedichten (Z_b/N_{b0}, Z_a/N_{a0}) beider Komponenten streben einem gemeinsamen asymptotischen Mittelwert zu, der um so niedriger liegt, je größer γ ist. Er wächst hingegen mit zunehmendem Anteil des leichter ablösbaren Bestandteiles, während er bei einer Vermehrung des schwerer ablösbaren Bestandteiles absinkt. Die Identität der relativen asymptotischen Mittelwerte besagt natürlich nichts anderes, als daß im stationären Endzustand die beiden Komponenten entsprechend dem Mischungsverhältnis N_{b0}/N_{a0} abgebaut werden,—ein Ergebnis, wie man es auch auf Grund allgemeiner Betrachungen erwarten würde.

Überhaupt scheint es verlohnend, kurz darauf hinzuweisen, wie die Periodizitäten

—die hier rein formal mathematisch begründet wurden—in physikalischer Hinsicht zu verstehen sind. Der grundlegende Vorgang ist einfach. Unter dem Bombardement der einfallenden Ionen werden aus der Oberfläche der Probe Atome beider Komponenten A, B ausgelöst und zwar verhalten sich die relativen Ablösedichten zur Zeit $t = 0$ wie die Ablösewahrscheinlichkeiten w_a, w_b. Gilt nun beispielsweise $w_b \gg w_a$, so hat dies zur Folge, daß in der obersten Schicht der Probe sehr rasch eine Verarmung an Teilchen der Komponente B gegenüber den Teilchen der Komponente A auftritt. Dies gilt umso mehr, wenn die Komponente B nur eine geringfügige Beimengung zur Komponente A darstellt. Die genannte Verarmung hat natürlich zur Folge, daß die Ablösedichte der B-Komponente praktisch auf Null absinkt. Erst dann, wenn auch die Komponente A aus der obersten Schicht so weitgehend abgebaut ist, daß jetzt die tiefer liegenden Bereiche dem Zugriff zugänglich werden, wächst die Ablösedichte der Komponente B wieder in stärkerem Maße an. Sobald allerdings dieser Anstieg begonnen hat, macht sich auch schon wieder die höhere Ablösewahrscheinlichkeit geltend und es tritt nach kurzer Zeit—wie oben—eine neuerliche Verarmung und damit ein Absinken der Intensität ein. Dieses Wechselspiel läßt das Auftreten regelmäßiger Schwankungen ohne jede weitere Rechnung verstehen, wenn auch der genauere Verlauf—beispielsweise die experimentell beobachtete sinusähnliche Kurvenform —nur an Hand der obigen mathematischen Auswertung bestätigt werden kann. Die im Vorgang beschriebene Abhängigkeit von den γ-Parametern und der Bedeckungsfläche $N_{b0}Q_b$ ist dagegen ebenfalls schon aus unserer rein qualitativen Überlegung verständlich. Mit zunehmendem γ wird das Aufbrechen der tieferen Schichten und damit die Nachlieferung der B-Teilchen aus dem Inneren erschwert, was natürlich eine Verzögerung des Anstieges der Intensität und damit eine stärkere Trennung der Ablösemaxima zur Folge hat. Eine Erhöhung des Mischungsanteiles der Komponente B und die damit verbundene Vergrößerung der Bedeckungsfläche $N_{b0}Q_b$ bedingt bereits eine Öffnung der tiefer liegenden Schichten durch den Abbau der Komponente B selbst. Dies hat zur Folge, daß die Ablösedichte durch Nachlieferung aus dem Inneren schon wieder anwächst, ehe der Anteil der obersten Schicht abgeklungen ist, wodurch natürlich die Deutlichkeit der Schwankungen verringert wird,—wie es die Fig. 3 und 4 demonstrieren.

Die im Vorgang beschriebenen Ergebnisse über den zeitlichen Ablauf des Ablösevorganges wurden—angeregt dürch eine mündliche Mitteilung von Herrn Prof. Kaiser—gewonnen, ohne daß wir eine Kenntnis des experimentell gemessenen Verlaufes besessen hätten. Um so überraschender erschien uns bei dem späteren Vergleich die gute qualitative Übereinstimmung zwischen dem Kurvenverlauf der Fig. 1 bis 4 und den a.a.O. wiedergegebenen Registrierkurven des Intensitätsverhältnisses der Spektrallinien. Diese Übereinstimmung drängt die Frage auf, inwieweit die hier berechneten Schwankungserscheinungen für die gemessenen Periodizitäten verantwortlich zu machen sind, bzw. ob es möglich ist, ihren Einfluß mit Sicherheit auszuschließen. Auf den ersten Blick mag es scheinen, als sei die bei den experimentellen Beobachtungen gefundene spezifische Empfindlichkeit für Sauerstoff ein ernster Einwand gegen die beschriebenen Vorstellungen. Man hat jedoch zu beachten, daß die Deutlichkeit der Schwingungen—wie wir sahen—in entscheidender Weise von den Faktoren γ und $\varkappa$

bestimmt sind, die durchaus einen spezifischen Einfluß von Seiten der Sauerstoffionen erfahren können, so daß auch diese spezifische Empfindlichkeit für Sauerstoff nicht notwendig außerhalb des Rahmens unserer Überlegungen liegt.

Natürlich muß man sich zur Durchführung des Vergleiches zwischen den theoretischen Resultaten und den experimentellen Ergebnissen den Zusammenhang zwischen unserer Modellvorstellung des raum-zeitlich homogenen Ionenbombardements und dem experimentellen Vorgang des Abfunkens klar vergegenwärtigen und bei der Auswertung in folgender Weise berücksichtigen.

Ein einzelner Funke erfaßt einen Bereich ΔF_0 der Gesamtoberfläche F_0. Er erstreckt sich über ein Zeitintervall Δt_0 und dementsprechend über ein Intervall $\Delta x = w_a \cdot \Delta t_0$. Wir unterteilen nun die Abszisse unserer berechneten Ablösekurven (Fig. 1 bis 4) in gleiche Abstände Δx, die wir ausgehend vom Nullpunkt mit dem Index k numerieren. Zu jedem Δx_k bestimmen wir die zugehörige mittlere Intensität $\mathfrak{J}_k$. Der Funkenansatz setzt im Laufe der Zeit natürlich an allen möglichen Stellen der Metalloberfläche an. Sind für die Auswahl des Ansatzpunktes nur die Gesetze des Zufalles maßgebend, so läßt sich relativ einfach angeben, wie oft bei einer Gesamtzahl von n Funken der Ansatz keinmal, einmal, zweimal usw. an der gleichen Stelle angesetzt hat. Damit ist dann auch die Wahrscheinlichkeit dafür bestimmt, daß der nächste, der $(n + 1)$-te Funken, an einer Stelle ansetzt, wo der Funken bereits vorher k-mal angesetzt hat und wir können mit der so bekannten Häufigkeitsverteilung die wahrscheinliche Ablösedichte des $(n + 1)$-ten Funkens berechnen. Über die Funkenfrequenz erhalten wir damit die wahrscheinliche Intensität als Funktion der Zeit. Diese wahrscheinliche Intensität sollte der gemessenen entsprechen, wenn ein Zeitbereich Δt, innerhalb dessen wir die wahrscheinliche Intensität als konstant betrachten können, eine große Zahl von Funken einschließt, anderenfalls Abweichungen nach Maßgabe der Halbwertsbreite der genannten Häufigkeitsverteilung zu erwarten wären.

Die letztgenannte Bedingung für die Funkenfrequenz ist bei den Untersuchungen von KAISER und Mitarbeitern befriedigt, so daß der Abfunkvorgang eine gute Realisierung unserer Modellvorstellung liefern sollte und der Vergleich zwischen den Fig. 1–4 und den Meßresultaten insofern unbedenklich vorgenommen werden kann.

Dagegen hätte man für eine genauere Analyse der experimentellen Ergebnisse wahrscheinlich zu beachten, daß die zylindrischen Proben im Anfang des Abfunkprozesses ihre Form ändern, indem sie sich der sog. "natürlichen Elektrodenform" [2] annähern, die sie während des gesamten weiteren Vorganges beibehalten. Der Verformungsvorgang bedeutet natürlich nichts anderes, als daß der Funkenansatz in dem genannten Anfangsstadium seinen Ansatzpunkt im Gegensatz zu der obigen Voraussetzung nicht ausschließlich nach den Gesetzen des Zufalles wählt. In diesem Stadium können nicht alle Aufpunkte der Elektrodenoberfläche für den Funkenansatz als gleichqualifiziert betrachtet werden. Aus diesem Grund ist während der Verformungszeit eine gewisse Verschmierung der Periodizitäten zu erwarten, indem die Mittelung, welche die wahrscheinliche Intensität liefert, jetzt ausnahmsweise einen größeren Abszissenbereich der Kurven 1–4 erfaßt. Es scheint nicht ausgeschlossen, daß die mangelhafte Deutlichkeit der beobachteten

Schwankungen während des Anfangsstadiums auf Einflüsse dieser Art zurückgeführt werden kann.

Herrn Prof. Dr. Kaiser danke ich für die mündliche Mitteilung seiner Meßresultate vor der Veröffentlichung, sowie für eine kritische Diskussion der vorliegenden Ergebnisse. Frau Fassbender bin ich für die Ausführung der numerischen Rechnungen zu Dank verpflichtet.

Zusammenfassung

Experimentelle Untersuchungen haben gezeigt, daß bei der Materialablösung an Mehrstoffelektroden die sekundliche Ablösedichte als Funktion der Zeit einen charakteristischen Verlauf aufweist, bei dem besonders das Auftreten regelmäßiger Schwankungen beachtenswert erscheint. Unter bewußter Vernachlässigung aller anderweitigen Einflüsse (Rückdiffusion, Oxydations- und Reduktionsprozesse) ergibt die Berechnung des reinen Ablösevorgangs ein System simultaner Differentialgleichungen zur Bestimmung der Zeitabhängigkeit der Ablöseintensität. Als Parameter gehen u.a. das Verhältnis der Ablösewahrscheinlichkeiten der beiden Stoffkomponenten, das prozentuale Mischungsverhältnis und die Wahrscheinlichkeiten der Energieübertragung nach und der Austrittsmöglichkeit aus tiefer gelegenen Schichten ein. Die numerische Integration wird für vier Beispiele durchgeführt, die die Einflüsse der Parameter abzuschätzen erlauben. Es ergeben sich Kurven, die dem beobachteten Verlauf entsprechen und insbesondere deutliche periodische Schwankungen aufweisen.

References

[1] Rosendahl, F., und Kaiser, H.; *Naturwissenschaften* 1954 **41** 497.
[2] Kaiser, H., und Sohm, M.; *Spectrochim. Acta* 1942 **2** 258–263.

VOL. 7 1955/5

Spectrochimica Acta, 1955, Vol. 7, pp. 231 to 237. Pergamon Press Ltd., London

The spectrographic estimation of sub-microgram quantities of beryllium by the cathode layer technique

F. T. Birks
Atomic Energy Research Establishment, Harwell

Summary—0·02 milligamma ($2·0 \times 10^{-11}$ gram) of beryllium is estimated by the cathode layer technique, using a quartz Littrow spectrograph, while 0·01 mμg is detected if the line contour of Be 2348·61 and of the background structure is traced by means of a recording microphotometer. Fe 2348·30 and 2348·10 interfere if present in large amount, but 0·05 mμg of Be is detected in the presence of 50 micrograms of iron.

Traces of beryllium were sought in three different sources of high-purity graphite, but they were all below the detection limit.

1. Introduction

If the light from a direct-current arc between carbon electrodes is focused on to the slit of a spectrograph, the lines in the resulting spectrum vary in intensity along their length. In the region of the negative electrode or cathode, greatest intensity is shown by those derived from the metals whose ions are positively charged. In the cathode layer method [1], an image of the arc is projected on to an opaque screen, which has an aperture sited so as to allow the transmission of light from only a portion of the arc column. If that portion adjacent to the cathode is selected, then the lines from the metals are obtained with the least continuum or molecular band structure arising from cyanogen emission.

The method has not been widely used in recent years owing to the critical alignment that is necessary in order to obtain quantitative results, but it is justified when the amount of sample available is very small. This is the case when it is desired to analyze samples of biological origin for minute traces of beryllium, a metal which is being used to an increasing extent in industry, and which in certain forms is highly toxic. Cholak and Hubbard [2] have used a normal spectrographic method, first concentrating the beryllium by a chemical separation, then estimating it over the range 0·25–2 micrograms spectrographically, with thallium as internal standard. Subsequently [3] they applied the cathode layer method, and extended their detection limit down to 0·25 mμg with a working range of 1–60 mμg.

Barnes *et al.* [4] detected 1 mμg of Be by a conventional method using a 16-ampere arc between carbon electrodes. Goldschmidt and Peters [5] found that the smallest quantity of beryllium that they could detect by the cathode layer method was 0·001 per cent, using Be 2348 Å, which works out at 1 mμg on a sample weight of 0·1 milligram. With the copper-spark technique Fred *et al.* [6] detected 0·2 mμg of Be.

It was decided to investigate the cathode layer technique in an attempt to measure quantities of beryllium of the order 10^{-10} g (0·1 mμg).

2. Experimental

The Be I line at 2348·61 Å, with an intensity of 2000 [7], was selected for the measurements, since it has the highest sensitivity of detection, and it is in a region

where the background contribution from carbon is low. Plate 1 shows the effect of focusing the light on the slit of the spectrograph, and the Be emission is seen to be concentrated near the cathode, while the background emission extends over the whole length of the arc column.

For the preparation of standards a stock solution of beryllium was made by dissolving 390·7 milligrams of anhydrous beryllium carbonate in N hydrochloric acid and diluting to 25 ml. By chemical analysis this solution was found to contain 1·96 mg of Be per ml. Dilutions with N hydrochloric acid were made from the stock solution as follows:—

Solution 2. 0·1 ml stock solution diluted to 10 ml ≡ 20 μg Be per ml.
Solution 3. 0·2 ml solution 2 diluted to 10 ml ≡ 400 mμg Be per ml.
Solution 4. 0·1 ml solution 3 diluted to 10 ml ≡ 4 mμg Be per ml.

Solution 2 was stored for not more than a few days, and solutions 3 and 4 were freshly prepared each day, to avoid any losses by adsorption on to the glass containing vessel at these great dilutions.

The cathode layer masking screen was a brass disc with jaws adjustable in the vertical plane, and was covered with matt-black paint to prevent reflections.

The first plates were taken on a Hilger Medium quartz spectrograph, and several optical arrangements were tried in order to find the best operating conditions. The best results were obtained with the conditions listed under section 3 procedure.

More light could be put through the spectrograph by placing a front-surface aluminized concave mirror behind the source, so that an erect image was formed on the screen in addition to the inverted lens image, but the density of the background was increased as well as of the beryllium line, and the additional complication was therefore not considered justified. The arc gap was adjusted by projecting an image of the electrodes on to the masking screen by means of an auxiliary lamp. The setting must be reproduced as closely as possible for each exposure. Increasing the exposure time from 15 to 30 sec made no difference to the beryllium sensitivity. The arc was struck by drawing a length of pure graphite across the electrodes rather than by closing the gap momentarily, since the latter procedure causes the gap to be variable during the important first few seconds of the exposure. Higher sensitivity was obtained using carbon (6·5 mm dia.) rather than graphite for the cathodes, probably because of the greater potential drop across the gap, 78 against 60 volts for a current of 10 amp. With 0·1 mμg of Be on the electrodes the sensitivity was doubled by using carbon. It was not possible to re-use the carbon electrodes by burning away the beryllium from the surface, but short lengths of the carbon were used only once by fitting them on to a support pedestal of 3·2 mm diameter graphite.

The samples and standard solutions were loaded into shallow cavities in the electrodes (1 mm deep) on to which one drop of 5 per cent w/v Apiezon M grease in AR petroleum ether had been evaporated, in order to avoid penetration of aqueous solutions into the electrode. If penetration does take place there is a considerable reduction in sensitivity.

It is known that an excess of sodium chloride enhances the intensity of the 6103·6 Å lithium line, and by analogy with the Group I series it was thought that

VOL. 7 1955/5

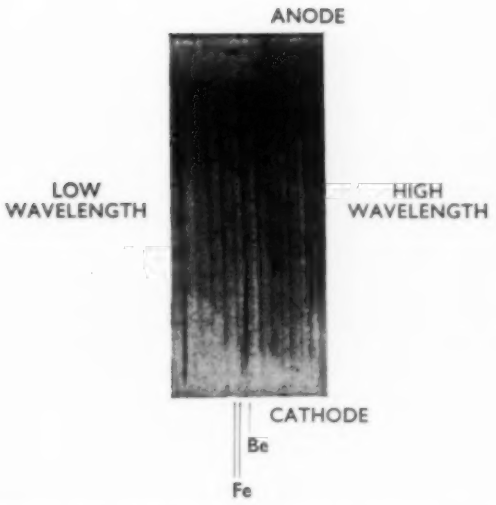

Plate 1. 0·2 milligamma (2×10^{-10} gram) Be focused on Littrow slit, magnification 7 ×.

VOL.
7
1955/5

enhancement of beryllium by other members of its series might be possible. The excitation potentials are compared in Table 1.

Table 1

Element	*Wavelength*	*Excitation potential volts*	*Ionization potential volts*
Li	6707·8	1·84	5·37
Na	5895·9	2·1	5·12
K	7664·9	1·6	4·32
Be	2348·6	5·40	9·28
Mg	2852·1	4·3	7·61
Ca	3933·7	3·1	6·09

A solution of magnesium in hydrochloric acid was prepared which contained 100 mμg of Mg in 0·01 ml, and by adding 100 mμg to prepared electrodes containing 0·2 mμg of Be it was found that the sensitivity of beryllium increased almost by a factor of 2. Blanks on the magnesium solution showed Be to be absent. This quantity of Mg was added to all subsequent standards and samples.

Interfering elements

In Table 2 are set out the wavelengths and arc intensities [7] of those elements which may interfere with Be 2348·6.

Table 2

Element	*Wavelength*	*Arc intensity*	*Element*	*Wavelength*	*Arc intensity*
Bi	2349·10	10	Be	2348·610	2000
U	2348·91	2			
La II	2348·86	2	Zr	2348·586	15
Mo	2348·84	3	W	2348·56	2
Mn	2348·83	3	Pt II	2348·548	3
Cu II	2348·82	15	Ru	2348·327	50
Re	2348,80	9	Fe II	2348·303	5
Nb	2348·748	3	Ir	2348·301	20
Ni	2348·74	10	W	2348·151	8
Nb	2348·61	3	Fe II	2348·099	5

Cholak and Hubbard [2] state that iron interferes even at the dispersion of the large Littrow spectrograph, but do not mention the effect of iron when the more sensitive cathode layer technique is used [3]. If much iron was present they separated it by a cupferron extraction into chloroform from hydrochloric acid solution.

To check for possible interference, a number of electrodes were loaded with 0·1 mμg of Be, and aliquots of 0, 0·1, 1, 10, and 50 micrograms of Cu, Bi, Ni, and

Fe added. Exposures taken on a Hilger Medium quartz spectrograph indicated that the major interfering element was iron. The maximum amount of iron that could be tolerated in the presence of 0·1 mμg Be was 0·1 microgram. By focusing the arc image on the slit of the spectrograph it was shown (Plate 1) that the lines arising from ionized Fe, viz., 2348·303 and 2348·099, were emitted from a region nearer to the cathode than the Be radiation, but there was an overlap which prevented the isolation of the Be line by masking-out a portion of the cathode layer. The greater dispersion of the Hilger Littrow quartz spectrograph was tried with the same optical conditions, and it was found that much more iron could be present before there was interference. With 50 micrograms of Fe added, it was possible to detect 0·05 mμg of Be.

3. Procedure

Spectrograph	Hilger Medium Quartz, or preferably Large Littrow Quartz set on range 2220–2900 Å.
Spectrograph slit	15 microns.
Plate	Ilford ordinary.
Distance from slit of source	38 cm, lower electrode negative.
Distance from slit of Hilger F958 lens (f 6·7 cm)	About 26 cm, adjusted to focus an image of the source on to the masking screen.
Distance from slit of masking screen	8 cm.
Arc gap	4 mm. The gap of the image formed on the masking screen from this is 6 mm.
Masking screen gap	2·4 mm, height adjusted so that the incandescent cathode is masked but the part of the arc adjacent to the cathode is transmitted, i.e., the mask transmits 2·4/6 of the total arc length.
Electrodes	Lower Matthey 6·5 mm dia. carbon, upper 3·2 mm NCC graphite preburned with reversed polarity for 30 seconds at 10 amp.
Current	10-amp d.c. arc.
Exposure time	15 sec.
Sample form	Powdered solid, preferably not more than 1 mg, or solution evaporated on to electrode greased with 1 drop of Apiezon M grease, 5 per cent in petroleum ether. 100 mμg of Mg added before arcing.

4. Results

In Fig. 1 the density difference Be 2348·6 — background is plotted against the quantity of beryllium in milligammas on the electrode. These results were obtained from the Medium spectrograph. In Fig. 2 are plotted the corresponding data for the Littrow. In the absence of much iron the useful working range is from 0·02 to greater than 1 milligamma. It was found that greater accuracy could be obtained at the low end by reading the line densities on a Hilger H670 recording microphotometer. This gave a contour record of the Be 2348·6 line and the surrounding

VOL. 7 1955/5

background from which a consistent estimate of the background could be obtained. Visual comparison of the trace with the blank revealed the presence of 0·01 mμg of beryllium, but measurements could not be made at this level with any accuracy.

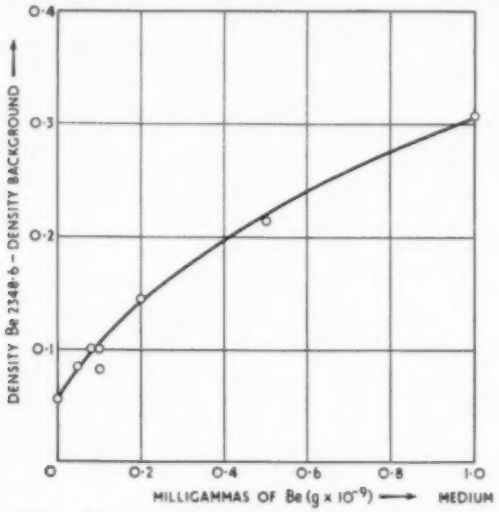

Fig. 1. Plot of Be 2348·6 obtained from Medium quartz spectrograph.

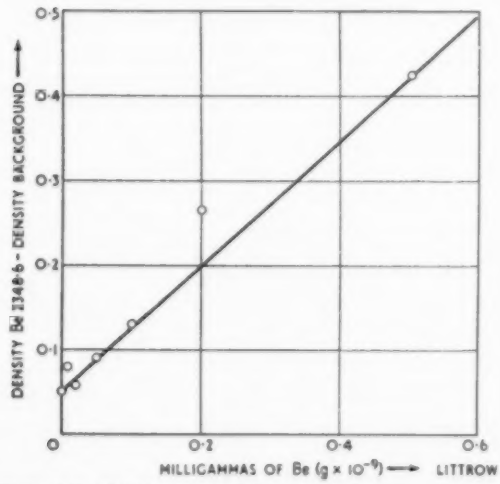

Fig. 2. Plot of Be 2348·6 obtained from large Littrow quartz spectrograph.

Fig. 3 shows the traces obtained from 0, 0·01, 0·025, 0·05, and 0·1 mμg of Be respectively.

Microphotometer traces of the same wavelength region from spectra obtained using copper and silver electrodes, show that the background is largely due to air lines. A slight increase in sensitivity may be obtained if these lines could be eliminated or reduced by arcing in an air-free atmosphere.

Todd obtained recording microphotometer traces from the normal arc spectra of three different sources of graphite, viz., Matthey HS, high-purity NCC, and 6·4 mm diameter rods machined from Harwell Pile graphite. The instrument used for the measurements was a standard Hilger H451 non-recording microphotometer modified by Gillieson and Todd by substituting a photomultiplier for the

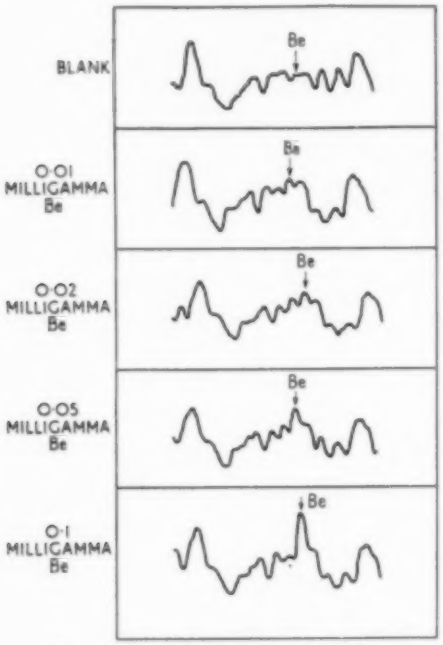

Fig. 3. Recorder traces of Be 2348·6—Littrow.

photocell and feeding the amplified output into a Cambridge recorder. From his results he concluded that minute traces of beryllium may be present in these graphites in different amounts, and confirmed its presence in his batch of HS graphite by ignition of a complete rod and analysis of the ash. However, none could be detected in the ash from the pile graphite. An attempt was made to confirm these results by the cathode layer method, but no significant difference was found between HS and NCC graphites. The line coincident with Be 2348·61, which appears in the blanks of both sources of graphite and also of high-purity carbon electrodes, was further examined by focusing an image of the arc between freshly broken ends of the rods on to the spectrograph slit. From the resulting spectrum, microphotometer traces were then obtained which corresponded to different sections across the arc gap between the cathode and the anode. No concentration of the line at 2348·61 into the region of the cathode was found, but it was strongest in the central zone of the arc. From these results it is concluded that the background line is due to carbon itself, since it is absent from the spectra of copper and silver, and therefore not due to air components.

VOL 7 1955/

Acknowledgment—The author wishes to thank the Director, Atomic Energy Research Establishment, Harwell, for permission to publish this paper.

References

[1] Mannkopff, R., and Peters, C.; *Z. Phys.* 1931 **70** 444.
[2] Cholak, J., and Hubbard, D. M.; *Analyt. Chem.* 1948 **20** 73
[3] Cholak, J., and Hubbard, D. M.; *Analyt. Chem.* 1948 **20** 970.
[4] Barnes, E. C., Piros, W. E., Bryson, T. C., and Wiener, G. W.; *Analyt. Chem.* 1949 **21** 1281.
[5] Goldschmidt, V. M., and Peters, C.; *Nach. Ges. Wiss. Göttingen, Math-Phys. K*1. 1932 **2** 360.
[6] Fred, M., Nachtrieb, N. H., and Tomkins, F. S.; *J. Op. Soc. Amer.* 1947 **37** 279.
[7] M.I.T. Wavelength Tables, John Wiley and Sons Inc., New York, 1939.

VOL. 7 55/56

Spectrochimica Acta, 1955, Vol. 7, pp. 238 to 241. Pergamon Press Ltd., London

Electronically controlled spectrographic low-voltage spark, interrupted arc and d.c. arc source

Á. Bardócz
Hungarian Academy of Sciences, Central Research Institute for Physics,
Department of Spectroscopy, Budapest, Hungary

(*Received* 13 *September* 1954, and in revised form 22 *May* 1955)

Summary—A variable-frequency electronically controlled low-voltage spark, interrupted arc, and d.c. arc source is described, which is capable of producing direct and alternating polarity sparks and interrupted arcs, rectified sparks and arcs, and d.c. arc. The ignition is provided by a new-type spark source of electronic control, which is operated by a variable frequency pulse generator. The pulse generator also controls the charging circuit of the source.

Both in research and practical spectroscopy it is highly inconvenient that, in many cases of interrupted arc and low-voltage spark excitation, the current intensity or the condenser capacity cannot be increased to a desired extent, due to the excessive heating and eventual melting of the electrodes. Thus, in the choice of the excitation energy, a compromise must be made at the expense of the analytical requirements. Owing to this heating, the analysis of solutions is still more difficult. Thus, high-energy excitation is in most cases hopeless, and experience shows that the high-energy facilities of arc and spark sources are generally unexploited. In addition, the control of low-voltage spark and interrupted arc sources provided by synchronous rotary switches or stationary spark gaps is not always satisfactory. In such experiments, control can be maintained only at comparatively low condenser energies, i.e., at low current intensities, because owing to the heating of the electrodes and the resulting thermionic effect, the arc or the spark ignites spontaneously. The case of the low-voltage condensed spark is somewhat more favourable, because, the duration of the discharges being shorter than in the case of the interrupted arc, the heating of the electrodes is also moderate. At higher condenser energies, however, the electrodes may warm up to such an extent that the high-frequency ignition again ceases to be controllable. In the case of a low-voltage condensed spark it is also inconvenient that, if the condenser discharge is of a long duration due to the operating conditions in the discharge circuit, there is time for an arc current to develop in the charging circuit, which makes the condenser discharge continue as an arc discharge lasting till the end of the half-cycle. This can be eliminated by controlling the charging circuit by means of a rectifier [1, 2, 3]. The problem cannot be completely solved in this way, however, because at high capacity values the electrodes are excessively heated, and, owing to the thermionic effect, the analytical gap fires before the condenser can reach its peak charging voltage.

Previous experiments of the author [4, 5, 7] have shown that, in interrupted arc sources, electronic control offers much more favourable setting conditions than those obtained by control equipment used before. The present paper describes the application of electronic control to sources suitable for the production of low-voltage sparks, interrupted arcs, and d.c. arcs.

Electronic control makes possible the excitation of any material under selected conditions. The control system employed enables the number of discharges per unit of time, and with it the heating of the electrodes, to be set as desired, so that the excitation energy can also be selected at will. The adjustment of the excitation conditions is quite independent of the melting-point of the electrodes, the nature of their material, etc.

VOL
7
1955/

In the source to be described, the spark and arc are ignited as usual by high-voltage, high-frequency currents. In contrast to previous practice, the igniting currents are produced by a new type of electronically controlled spark source [6]. This spark source is controlled by a pulse generator [5]. The source consists of three main parts: the arc and spark circuit, the ignitor circuit, and the pulse generator circuit. The wiring diagram of the arc and spark circuit, and that of the ignitor, are shown in Fig. 1. Fig. 2 shows the block diagram of the pulse generator circuit.

The arc and spark circuit is indicated by the heavy line in Fig. 1. This circuit is fed from transformer $T2$ in Fig. 1. The voltage of the transformer can be adjusted to the desired value by the toroid (Variac) transformer $T1$. With the aid of relays MW, MX, and MY operated by the three-position switch $K5$ and their respective contacts $W1$–$W4$, $X1$,$X2$, and $Y1$,$Y2$ in the arc and spark circuit, the source can be set to various operating conditions.

Tubes $V1$ and $V2$, the latter a thyratron, serve partly for rectification and partly for control of the charging circuit. The charging circuit is controlled by controlling the grid of $V2$. $L1$ and $R2$ denote an ironcore self-inductance and an ohmic resistance respectively. Both are used for the suitable adjustment of the operating conditions of the charging circuit. By means of contact $E1$ of relay ME, choke coil $L1$ can be disconnected from the circuit. In producing rectified arcs, condenser $C2$ (Fig. 1) does not suffice to ensure current flow through tubes $V1$ and $V2$. In such cases, the ohmic resistance $R9$, inserted in the circuit by relay ME simultaneously with the disconnection of $L1$, serves to ensure current flow. $C1$, $L2$, and $R3$ are the usual elements of the discharge circuit. The high-frequency currents are transferred to the arc gap I by air-core autotransformer T and condenser $C2$.

The fundamental data as regards the charging voltage, condenser capacity $C1$, and self-inductance $L2$, of Fig. 1, are roughly the same as those of the "Multisource" described by Hasler and Dietert [3]. The data of the various elements of the circuit are given in the legend of Fig. 1.

The high-voltage, high-frequency currents for the ignition of the discharge gap I in Fig. 1 are supplied by the ignitor circuit in the lower, lightly drawn part of Fig. 1. The ignitor circuit consists of a voltage-doubling circuit ($T5$, $V3$, $V4$, $C3$, $C4$), which charges condenser $C5$, and of a discharge circuit ($C5$, T, S), through which the discharge of condenser $C5$ takes place. The mode of operation of this circuit is described in [6].

The grids of the thyratron tubes $V2$ and $V5$ of Fig. 1 are controlled by a pulse generator, the block diagram of which is shown in Fig. 2. This pulse generator supplies voltage signals of a maximum frequency of 100 cps or of frequencies corresponding to subharmonics of the 50-cps mains. The phase of this signal can be set at will with respect to the 50-cps mains signal with the aid of the first multivibrator in the block diagram of Fig. 2. The signal coming from point y' of the pulse generator controls tube $V2$ in the charging circuit; that coming from point y controls tube $V5$ in the ignitor circuit. By proper setting of the switch k of the pulse generator, arcs or sparks with positive, negative, or alternating polarity can be produced [5]. The thyratron tubes $V2$ and $V5$ are biased from the bias source built in the pulse generator.

The operating conditions of the source are comparatively the simplest when switch $K5$ in Fig. 1 is in position X. This time the switching contacts $X1$ and $X2$ of the magnet switch close, and the tubes $V1$ and $V2$ are disconnected from the circuit. With this setting, the circuit is capable of generating direct and alternating polarity sparks and interrupted arcs.

With switch $K5$ of Fig. 1 in position Y, the switching contacts of relay Y close; i.e., tube $V1$ is disconnected, and tube $V2$ operates. Owing to the presence of tube $V2$ in this

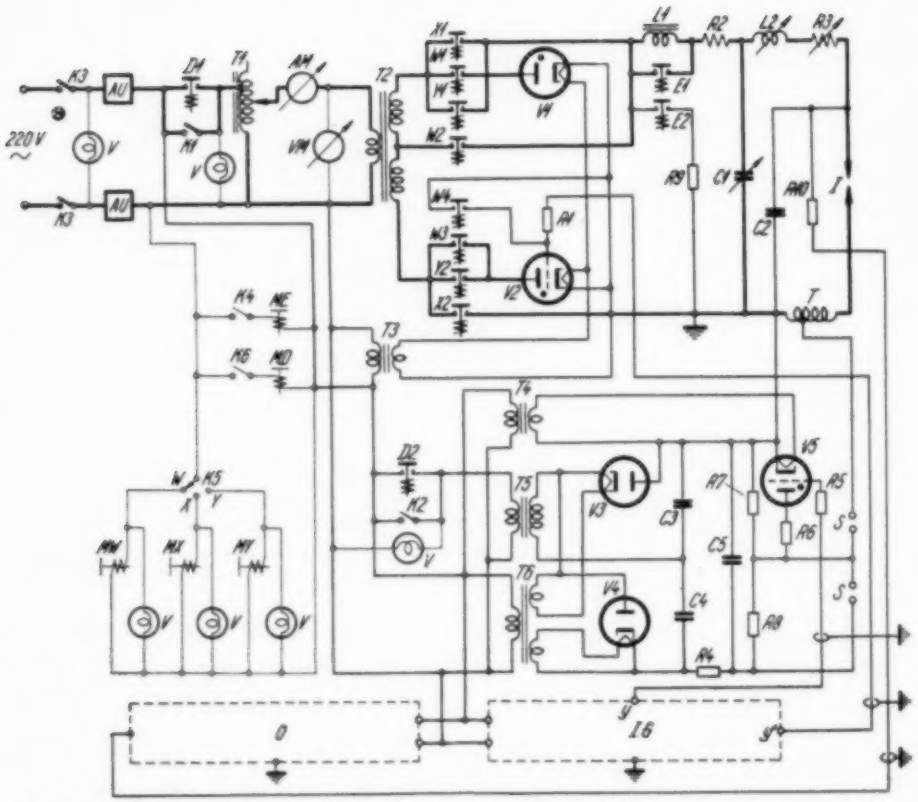

Fig. 1. Wiring diagram of the electronically controlled low-voltage spark, interrupted arc, and d.c. arc source. Heavily drawn part: arc and spark circuit; medium part: ignitor circuit; thin part: control circuit.

AM = ammeter, 40-amp full scale
AU = safety switch 35 amp
C1 = condenser bank (1000/3000 volts), two 1 microfarad, two 2 microfarads, one 4 microfarads, one 10 microfarads, two 20 microfarads units (total 60 microfarads)
C2 = condenser, 0·05 microfarad, 1200/3500 volts
C3, *C4* = condensers, 0·1 microfarad, 6000 volts
C5 = condenser, 0·0025 microfarad, 12,000 volts
D1, *D2* = contacts of relay *MD*
E1, *E2* = contacts of relay *ME*
I = arc and spark gap
IG = pulse generator
K1–*K6* = switches
L1 = iron-core choke coil 10 amp, 0·15 henry at 5 amp
L2 = self-inductance, altogether 500 microhenrys, tapped at 20, 70, 160, 330, and 500 microhenrys
MD, *ME*, *MX*, *MY*, *MW* = relays
O = oscilloscope
R1 = carbon resistor, 5 kohms, 0·25 watts
R2 = wire resistor, 22 ohms, 10 amp
R3 = wire resistor, 250 ohms, tapped at 0·5, 1, 2, 5, 8, 16, 32, 60, 125 ohms
R4 = carbon resistor, 750 kohms, 10 watts
R5 = carbon resistor, 5 kohms, 0·25 watt
R6 = carbon resistor, 0·6 kohms, 3 watts
R7, *R8* = carbon resistors, 16·5 megohms, 3 watts
R9 = wire resistor, 20 kohms, 130 watts
R10 = carbon resistor, 2 × 0·2 megohm, 0·5 watt, in oil
S = twin controlling spark gap
T = air-core autotransformer, 8 turns on 250 mm diameter, winding spacing 9 mm, number of primary turns 1, wire diameter 3 mm
T1 = toroid transformer (Variac), 220/270 volts, 7 kVA
T2 = transformer 220/2 × 350 volts, 7 kVA
T3 = transformer 220/5 volts, 100 VA
T4 = transformer 220/5 volts, 50 VA
T5 = transformer 220/4000 volts, 250 VA
T6 = transformer 220/2 × 6·3 volts, 50 VA, with filament coils insulated for high voltage
V1 = rectifying diode
V2, *V5* = thyratron tube GRG4
V3, *V4* = rectifying diode, V22/7000
V = pilot lamps
VM = voltmeter
X, *Y*, *W* = positions of the switch *K5*
X1, *X2* = contacts of relay *MX*
u = control signal of tube *V5*
u' = control signal of tube *V2*
Y1, *Y2* = contacts of relay *MY*
W1, *W2*, *W3*, *W4* = contacts of relay *MW*

VOL 7 1955/

setting, only d.c. arcs and sparks with a maximum repetition rate of 50/sec can be generated. Current flow in the charging circuit is possible only if thyratron tube $V2$ is ignited by the positive voltage signal coming from the pulse generator. An interesting way of producing interrupted arcs is offered at this setting of the source. If the selector switch k in Fig. 2

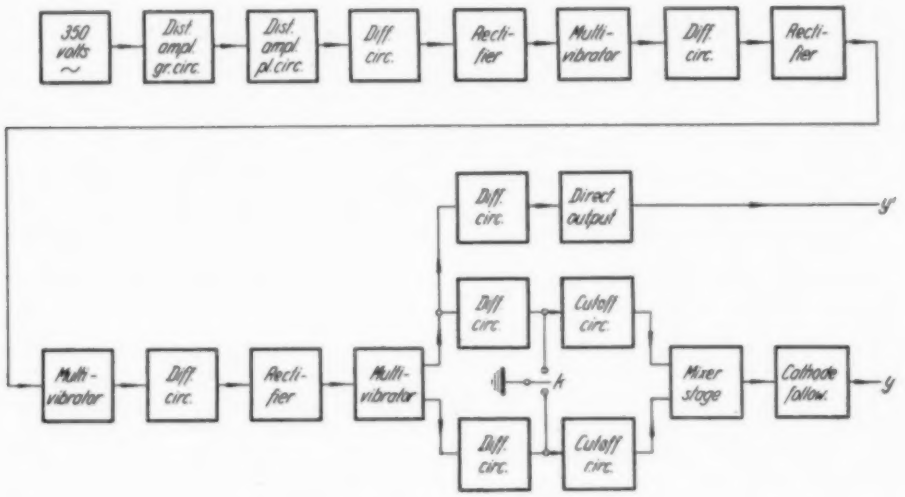

Fig. 2. Block diagram of the pulse generator.

is in the lower position, the ignition of tubes $V2$ and $V5$ takes place almost simultaneously. In the case of such interrupted arcs, no voltage is present on the electrodes at all except during the arcing time. Thus, with this adjustment, "forced" arcing can be obtained, while full control is maintained.

Switch $K5$ of Fig. 1 being in position W, the contacts $W1$–$W4$ of relay MW close. Thus both tubes $V1$ and $V2$ are effective, and the circuit itself is a double-wave rectifier. This circuit is capable of producing rectified sparks and arcs at a maximum repetition rate of 100/sec. At this setting, the source is also capable of generating d.c. arcs. In this case an additional condenser must also be inserted in the circuit.

Further details of the source will be published elsewhere [8].

References

[1] Schmidt, R., *Rec. Trav. Chim. Pays-Bas* (1941) **60,** 378.
[2] Schmidt, R., and Schuringa, A., *Rec. Trav. Chim. Pays-Bas* (1945) **64,** 349.
[3] Hasler, M. F., and Dietert, H. W., *J. Opt. Soc. Amer.* (1943) **33,** 218.
[4] Bardócz, Á., *J. Opt. Soc. Amer.* (1952) **42,** 357.
[5] Bardócz, Á., *Spectrochim. Acta* (1953) **5,** 397.
[6] Bardócz, Á., *Nature* (1953) **171,** 1156.
[7] Bardócz, Á., *Acta Physica Hungarica* (1954) **4,** 91.
[8] Bardócz, Á., *Acta Technica Hungarica* (to be published).

Spectrochimica Acta, 1955, Vol. 7, pp. 242 to 245. Pergamon Press Ltd., London

SPECTROCHEMICAL NOTES

Zur Bestimmung der Transformationszahl $\varkappa$

F. J. HAFTKA

(*Received* 21 *January* 1955)

Summary—In the determination of transformation value κ, care must be taken that the random errors of the values of the blackening used do not contribute too great a systematic error to the relative intensity determinations. A formula is given for obtaining the variance of the values from the variance of the emulsion density, where this is known. For the graphical evaluation of results, suitable values of the step ratio of the filter and of the blackenings to be used are stated, so as to minimize the errors.

Bei der Auswertung spektrochemischer Analysen kann es von Vorteil sein, die gekrümmte Kennlinie der photographischen Emulsion durch eine geeignete mathematische Transformation für einen bestimmten Schwärzungsbereich in eine Gerade zu verwandeln. Von den möglichen Transformationen interessieren uns hier die von H. KAISER [1, 2] angegebenen verallgemeinerten Seidel'schen Transformationen, die wir in 1 Näherung für den praktisch gebräuchlichen Schwärzungsbereich von 0·2 bis 1·2 verwenden wollen.

Die durch Linearkombination der Schwärzung S und der Seidel'schen Schwärzung W entstehende verallgemeinerte Seideltransformation lautet:

$$P = S - \kappa D \tag{1}$$

κ = Transformationszahl, sie bestimmt die Art des Durchhangs der Schwärzungskurve

$D = S - W$.

Der lineare Teil der transformierten Kennlinie kann dann mit Hilfe der Gradation γ und der Empfindlichkeit Y_E durch folgende Gleichung ausgedrückt werden:

$$P_\varkappa = \gamma_P(Y - Y_E) \tag{2}$$

Y = Logarithmus der Intensität.

Zur Bestimmung von κ benutzen wir eine von Seith [2] angegebene Formel:

$$\kappa = \frac{{}^a\Delta S - {}^b\Delta S}{{}^a\Delta D - {}^b\Delta D} \tag{3}$$

Hierin bedeuten:

$${}^a\Delta S = {}^aS_1 - {}^aS_2$$

$${}^b\Delta S = {}^bS_1 - {}^bS_2$$

${}^aS_1$ = Schwärzungswert einer Linie in Filterstufe 1 bei der Belichtung (a)

${}^aS_2$ = Schwärzungswert derselben Linie in Filterstufe 2 bei der Belichtung (a)

${}^bS_1$ = Schwärzungswert derselben Linie in Filterstufe 1 bei der Belichtung (b).

${}^bS_2$ = Schwärzungswert derselben Linie in Filterstufe 2 bei der Belichtung (b).

Für die ΔD gelten analoge Bezeichnungen.

In der oben zitierten Arbeit [2] wird erwähnt, daß die Bestimmung von κ infolge doppelter Differenzbildung recht ungenau ist. Es erscheint daher zweckmäßig, dies in einer näheren Betrachtung zu untersuchen. Zur besseren analytischen Behandlung der

Formel (3) führen wir statt der Schwärzung S eine neue Variable r durch die Beziehung

$$S = \log r \qquad \text{ein.}$$

Die Bestimmungsgleichung für κ lautet dann:

$$\kappa = \frac{\log \dfrac{{}^{a}r_1 \, {}^{b}r_2}{{}^{a}r_2 \, {}^{b}r_1}}{\log \dfrac{{}^{a}r_1({}^{a}r_2 - 1)({}^{b}r_1 - 1){}^{b}r_2}{({}^{a}r_1 - 1){}^{a}r_2({}^{b}r_2 - 1){}^{b}r_1}} = \kappa({}^{a}r_1, {}^{a}r_2, {}^{b}r_1, {}^{b}r_2) \tag{4}$$

Bilden wir die für die Gauß'sche Fehlergleichung notwendigen Differentiale und partiellen Differentialquotienten, so erhalten wir folgende Fehlergleichung für den mittleren absoluten Fehler (abs. Standardabweichung) von κ

$$s_\kappa = \frac{s_s}{A}\sqrt{\Sigma\left(1 + \frac{\kappa}{r-1}\right)^2} \tag{5}$$

wobei die Summe über alle r zu nehmen ist und

A den Nenner von κ in Gleichung (4)

s_s den mittleren Fehler eines Schwärzungswertes bedeuten.

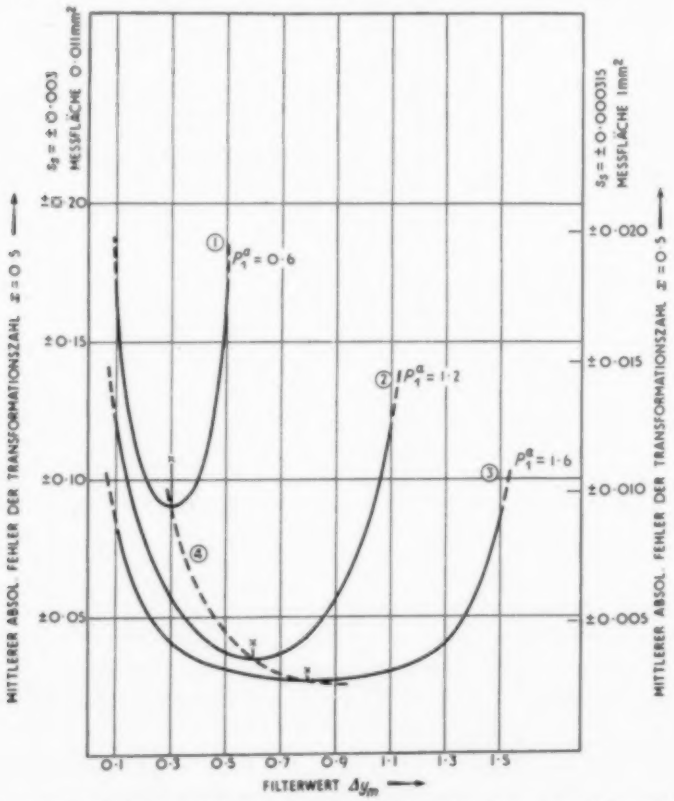

Abb. 1. Abhängigkeit des mittleren absoluten Fehlers der Transformations-zahl κ vom Filterwert ΔY_m und dem höchsten Schwärzungswert S_1^a.

Der Fehler in der Bestimmung von κ hängt naturgemäß von den Fehlern der Meßgrößen ${}^aS_1$, ${}^aS_2$, ${}^bS_1$, und ${}^bS_2$ ab. Nun ist der Fehler einer geschwärzten Emulsionsstelle s_s von der Größe des Schwärzungswertes [3] und der Meßfläche abhängig. Für den praktisch benutzten Schwärzungsbereich von 0·2 bis 1·2 nehmen wir in erster Näherung an, daß die Abhängigkeit von S keine Rolle spielt. Bei brauchbaren Emulsionen liegt s_s zwischen $\pm$0·003 und $\pm$0·006 für eine Meßfläche* von 0·011 mm², der Wert $\pm$0·003 gilt für besonders gute Fabrikate. Auf 1 mm² Meßfläche umgerechnet erhalten wir hierfür den Wert $\pm$0·000315.

Da die Fehlergleichung (5) nur unter Schwierigkeiten in allgemeiner Form analytisch diskutiert werden kann, untersuchen wir sie für einen praktisch wichtigen Fall ($\kappa = 0{\cdot}5$, $\gamma = 1$), ohne auf wesentliche Ergebnisse verzichten zu müssen. Zunächst befassen wir uns mit der Abhängigkeit des Fehlers s_κ von der Lage der vier S-Werte, zwei davon sind durch die beiden anderen und den Filterwert festgelegt. In der Abbildung ist der Fehler von κ als Funktion des Filterwertes aufgetragen. Als unterster S-Wert gilt für alle Kurven 0·209 (${}^bP_2 = 0$), der oberste S-Wert ist für die 1. Kurve 0·654 (${}^aP_1 = 0{\cdot}600$), für die zweite Kurve 1·214 (${}^aP_1 = 1{\cdot}200$) und für die 3. Kurve 1·605 (${}^aP_1 = 1{\cdot}600$). Bei der 3. Kurve ist der Systematik halber der Wert für s_s beibehalten worden, obwohl er in dem höheren S-Bereich merklich ansteigt. In allen Fällen ergeben sich die mittleren S-Werte ${}^aS_2$ und ${}^bS_1$ als Funktion der gewählten Filterwerte.

Die Kurven zeigen alle ein ausgeprägtes Minimum für den Filterwert

$$\frac{{}^aP_1 - {}^bP_2}{2\gamma}$$

Bei diesem Filterwert fallen die beiden mittleren S-Werte zusammen. Es ist jedoch falsch zu glauben, mit drei S-Werten für die κ-Bestimmung auskommen zu können, denn ein Fehler des mittleren S-Wertes macht sich nach der Fehlertheorie mit doppeltem Gewicht bemerkbar. Demgegenüber gehen gleich groβe Fehler zweier gleich groβer, aber unabhängiger S-Werte nur mit dem Faktor 1·4 ins Ergebnis ein. Die bei Verwendung von nur drei S-Werten sich ergebenden Fehler sind durch Markierungen oberhalb der zugehörigen Minima kenntlich gemacht.

Aus dem Verlauf der Verbindungslinie (4) der Minima erkennt man, daß keine wesentliche Steigerung an Genauigkeit erzielt werden kann, wenn ${}^aS_1 > 1{\cdot}2$ wird. Ähnliches kann für die Verkleinerung von ${}^bS_2$ gezeigt werden. Erst recht können wir keine Vorteile erwarten, wenn wir noch berücksichtigen, daß der Fehler s_s für extrem hohe und tiefe S-Werte ansteigt.

Wenn wir unter Beibehaltung der Minimumbedingung, des γ-Wertes sowie des P-Bereiches und damit des Filterwertes zu größeren κ-Werten übergehen, so stellen wir für den κ-Bereich 0·5 bis 2 fest, daß der relative Fehler den Wert $\pm$0·07 in etwa beibehält. Behalten wir statt des P-Bereiches den S-Bereich bei, so vergrößert sich der optimale Filterwert und der relative Fehler sinkt mit steigendem κ. Steigt bei gleichem κ und gleichem S-Bereich die Gradation, so verkleinert sich der durch die Minimumbedingung geforderte Filterwert, der relative Fehler in der κ-Bestimmung bleibt dann unverändert. Bestimmte bisher noch wenig untersuchte funktionelle Zusammenhänge zwischen κ und γ blieben hierbei unberücksichtigt.

Das Ergebnis der Untersuchung kann nun allgemein folgendermaßen formuliert werden. Um die Transformationszahl möglichst genau zu bestimmen, lege man den obersten S-Wert in die Nähe von 1·2 und den untersten in die Nähe von 0·2. Die für die verschiedensten Fälle günstigsten Filterwerte, die in der Tabelle angegeben werden, liegen dann vor,

* Meßfläche beim Zeiss'schen Schnellphotometer, Spaltbreite 0·5 mm, Spalthöhe 20 mm, Vergrößerung 30-fach.

VOL. 7 1955/5

wenn die beiden mittleren S-Werte zusammenfallen. Damit erreicht man auch eine Verteilung der S-Werte, die für die Anwendung der verallgemeinerten Seideltransformationen in der 1 Näherung günstig ist. Arbeitet man stets mit den extremen P-Werten 0 bis 1·2, so ist für alle κ-Werte zwischen 0·5 und 2 der günstigste Filterwert 0·6, wobei noch unter Berücksichtigung von $s_s = \pm 0{\cdot}003$ mit einem fast konstanten relativen Fehler von $\pm 0{\cdot}07$ gerechnet werden kann.

Tabelle :

κ	ΔY_m (für $\gamma = 1$)	ΔY_m (für $\gamma = 2$)	$\frac{s_\kappa}{\kappa}$
0·5	0·6	0·3	0·071
1·0	0·7	0·35	0·050
2·0	0·9	0·45	0·047

Nun können wir abschließend auch die Frage beantworten, ob es bei Serienanalysen mit genau festgelegten Vorschriften für die Behandlung des photographischen Materials sinnvoll ist, κ von jeder Platte neu zu bestimmen. Nach den bisherigen Erfahrungen muß diese Frage verneint werden, denn die Streuung der wahren κ-Werte von Platte zu Platte übersteigt im allgemeinen bei einem Zeitraum von einigen Monaten nicht den mittleren Fehler der κ-Bestimmung auf einer Platte. Es empfielt sich daher, bei den Eichplatten eine möglichst genaue Bestimmung des κ-Wertes vorzunehmen. Der Mittelwert wird dann als Arbeitskenngröße bis zur nächsten Kontrolle nach einigen Monaten oder Wochen benutzt.

Zusammenfassung

Die Bestimmung von κ muß mit Sorgfalt durchgeführt werden, damit die rein zufälligen Fehler der Schwärzungen, die für die κ-Bestimmung benutzt werden, nicht zu großen systematischen Fehlern in der Bestimmung der Intensitätsverhältnisse führen. Es wird eine Formel angegeben, die nach Kenntnis des Plattenfehlers die Berechnung der Streuung der κ-Werte gestattet. An Hand der graphischen Darstellung wird gezeigt, wie die Schwärzungswerte und der Filterwert zu wählen sind, damit das Optimum an Genauigkeit erzielt werden kann.

Literaturangaben

[1] M. Honerjäger-Sohm, H. Kaiser; *Spectrochim. Acta* 1944 **2** 396.
[2] H. Kaiser; *Spectrochim. Acta* 1948 **3** 159.
[3] Vaucouleurs; Origines et corrections des erreurs locales en photométrie photographique. Contr. Institut d'Astrophys., Paris A no 24, *Rev. Opt.* 1948 **27**.

Spectrochimica Acta, 1955, Vol. 7, pp. 246 to 249. Pergamon Press Ltd., London

Spectrochemical Note

Elektronische Regulierung der Ladespannung von Kondensatoren in Funkenerzeugern

W. MARTI
Physikalisches Laboratorium, Gebrüder Sulzer AG., Winterthur

(*Received* 22 *January* 1955)

Summary—A circuit for controlling the charging potential of the main condenser of a spark source unit is described, in which the charging is interrupted at the required value by an inertia-free electronic switching device.

Nach ENNS und WOLFE [1] verschiebt sich eine spektrochemische Eichkurve mit Aenderungen der Anregungsenergie bzw. der Netzspannung, wenn die Anregungsspannungen der beiden Spektrallinien verschieden sind. Bei photographischen Verfahren kann man in den meisten Fällen für die verschiedenen Analysenlinien eine passende Linie des Grundmetalles mit ähnlicher Anregungsspannung finden. Bei direkter Ablesung wird man jedoch nur eine Grundlinie verwenden, um Photozellen einzusparen, weshalb eine konstante Betriebsspannung erwünscht ist.

Man kann nun irgendeinem Funkenerzeuger einen Wechselspannungsregler vorschalten oder dafür sorgen, dass die Funkenenergie durch gleichmässige Ladespannungen des Arbeitskondensators konstant gehalten wird, z.B. nach FOWLER und WOLFE [2] durch Serieschaltung der Analysenfunkenstrecke mit einer angeblasenen Hilfsfunkenstrecke.

Im folgenden wird eine einfache, spontan wirkende Spannungsregulierung gezeigt, die sich in 1½-jährigem Betriebe mit einem A.R.L. Industrial Research Quantometer bewährt hat. Abb. 1 zeigt den Ladekreis eines Niederspannungsfunkenerzeugers nach

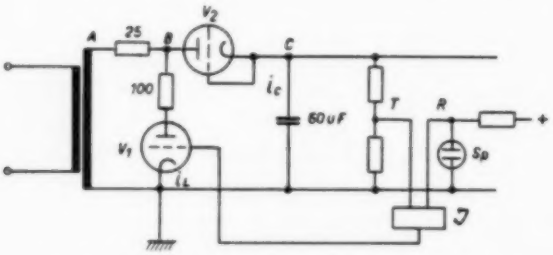

Abb. 1. Regulierung der Ladespannung des Kondensators C. Beim Erreichen der Sollspannung am Kondensator C zündet der Impulsgenerator J das Thyratron V_1, worauf die Ladung durch V_2 abbricht.

HASLER [3]. (Der Entlade- und Zündfunkenkreis wurden der Uebersichtlichkeit halber weggelassen.) Der 50-mal pro sec aufzuladende Kondensator (Abb. 1 C) kann Werte von 2 bis 60 μ F annehmen und soll nach jeder Entladung wieder genau auf 1000 Volt aufgeladen werden. Die Spannung A des Ladetransformators wird so ausgelegt, dass die Kurve A in Abb. 2 bei der kleinsten Netzspannung die Spitze 1 der Kurve B-B überragt. Der Kondensator Abb. 1 C wird nun während des Spannungsanstieges über 25 Ω und den Xenon-Gleichrichter V_2 (Philips PL 5544) aufgeladen.

Die Kurve B ist gegenüber der Kurve C um die Brennspannung des Gleichrichters V_2 höher. Die Ladespannung wird über den Spannungsteiler Abb. 1 T in jedem Moment mit einer Spannungsreferenzröhre Sp (Philips 85A2) verglichen. Sobald $C = 1000$ Volt bzw. $T = 85$ Volt erreicht, wird in einem elektronischen Impulsgenerator Abb. 1 J ein positiver Impuls ausgelöst, welcher ein Xenon-Thyratron V_1 (Philips PL 5544) zündet. Der dabei entstehende "Löschstrom" wird durch den Widerstand 100 Ω begrenzt und erzeugt im Widerstand 25 Ω einen Spannungsabfall. Dadurch wird die Spannungskurve B von

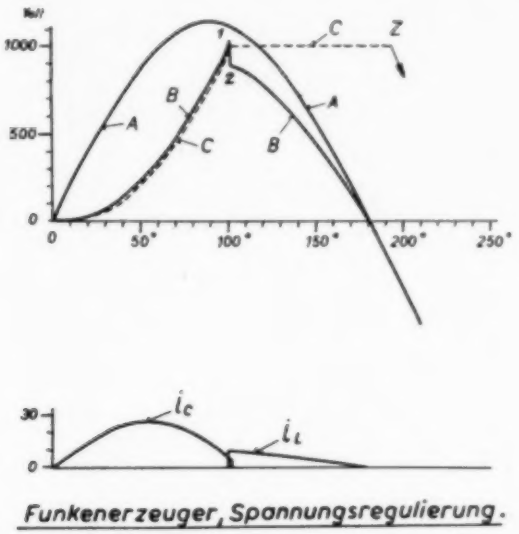

Funkenerzeuger, Spannungsregulierung.

Abb. 2. Oszillogramme der Spannungen und Ströme.

1 auf 2 gesenkt, womit die Ladung des Kondensators C sofort aufhört. Er bleibt solange geladen, bis seine Ladung durch den Zündfunken über den Entladekreis in die Analysenstrecke gelangt.

Der "Löschstrom" i_L (Abb. 2) bleibt bis zum nächsten Nulldurchgang von A bestehen und seine Leistung ist verloren. Die Widerstände 25 und 100 Ω sind so zu dimensionieren, dass die Transformatorspannung A bei der tiefsten Netzspannung die Spitze 1 der Kurve B noch nicht berührt und der Punkt 2 bei der höchsten Netzspannung noch unterhalb 1000 Volt bleibt. Bei kleinen aufzuladenden Kapazitäten verschiebt sich der Punkt 1 nach links ohne die Regulierung zu beeinflussen.

Der Impulsgenerator (Abb. 3) vergleicht in der ersten Gleichstrom-Verstärkerstufe die Ladespannung mit der Spannung der Röhre 85A2. Die gewünschte Ladespannung kann mit dem Potentiometer 50 K noch etwas justiert werden. Die Spannungsdifferenz wird in einer zweiten, direkt angekoppelten Verstärkerstufe weiter verstärkt und einer Kippstufe zugeführt (Amplitudendiskriminator oder Schmidt-Trigger). Beim Erreichen der Sollspannung entsteht im Schmidt-Trigger ein Spannungssprung, der differenziert als Impuls einer vierten Verstärkerstufe und als positiver Impuls dem Thyratron V_1 (Abb. 1) zugeführt wird. Die Anoden- und Kathodenspannungen werden einer Glimmlampenkette (Abb. 4) entnommen.

Die Spitzenwerte der Ladespannungen werden mit einem üblichen Röhrenvoltmeter kontrolliert. Bei der Inbetriebnahme zeigte sich eine Drift mit der Erwärmung des

Impulsgenerators durch die benachbarten Regulier- und Entladungswiderstände. Durch Zufuhr von Luft konstanter Temperatur aus dem Laboratorium konnte dieser Effekt behoben werden. Bei einer Aenderung der Netzspannung um 10 Prozent ändert sich die Ladespannung nur noch ca 0·5 Prozent. Diese restliche Unkonstanz konnte bis jetzt noch nicht abgeklärt werden.

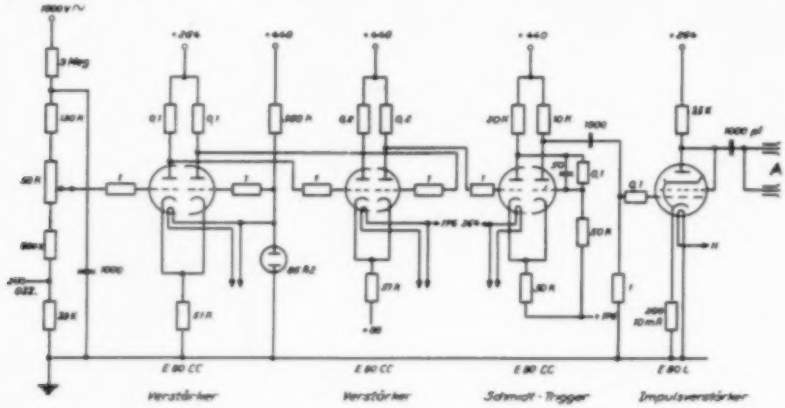

Impulsgenerator

Abb. 3. Impulsgenerator.

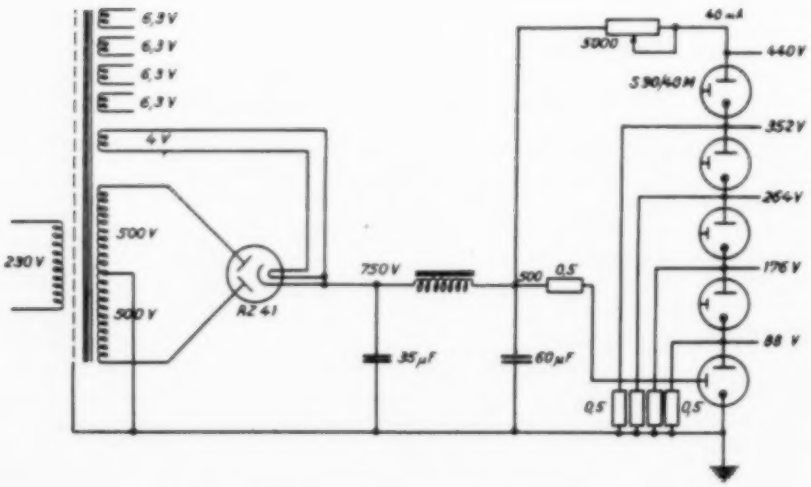

Stromversorgung zum Impulsgenerator

Abb. 4. Stromversorgung des Impulsgenerators.

Die Regulierung höherer Ladespannungen, z.B. von 18'000 Volt für Hochspannungs- bzw. Zündfunken würde ein Thyratron mit hohen Sperrspannungen erfordern. Versuche haben gezeigt, dass das "Löschthyratron" (V_1 in Abb. 1) ebensogut auf der Primärseite arbeiten kann, da sich der Spannungssprung 1–2 auf der Sekundärseite abbildet. Der

Spannungsteiler ist hochspannungstechnisch und mit kapazitiver Abgleichung sehr sorgfältig herzustellen.

Zusammenfassung

Es wird eine Schaltung angegeben, welche die Ladespannungen des Arbeitskondensators von Funkenerzeugern konstant hält, indem die Aufladung bei einer gewünschten Spannung durch trägheitslose, elektronische Einwirkung abgebrochen wird.

Literatur

[1] Enns, J. H., and Wolfe, R. A.; *J. Opt. Soc. Amer.* 1949 **39** 298.
[2] Fowler, R. G., and Wolfe, R. A.; *J. Opt. Soc. Amer.* 1945 **35** 170.
[3] Hasler, M. F., and Dietert, H. W.; *J. Opt. Soc. Amer.* 1943 **33** 218.

VOL. 7 55/56

Book reviews

W. BRÜGEL: **Einführung in die Ultrarotspektroskopie.** Published by Dietrich Steinkopff, Darmstadt, 1954. 343 pp. with references and index. Price DM.46.00

This treatise can be regarded as a "tour de force," and a valuable one. It covers an immense amount of ground, and in many instances the recent experimental techniques and results which are included are so up to date as to be remarkable. Perhaps the most important point is that it is essentially a book for chemists, physical, organic or analytical. Although the essential principles of molecular vibrational theory are quite adequately explained, as well as their implications for the more physical work on such aspects as rotational analysis, the emphasis is upon the newer applications of infrared measurements in qualitative and quantitative analysis and structural diagnosis which have become so important in a vast range of chemical problems.

The book will be equally useful to experts and to those beginning work in this field. It is well planned, and deals successively with the theory of vibrational spectra, experimental techniques and instruments, results and applications. It contains the most thorough modern account of practical methods yet assembled, with many illustrative photographs of the best known commercial spectrometers and accessories. Anyone seeking technical guidance will find in this book useful hints and explicit instruction. The large collection of data includes the survey of frequency correlation rules for key groups, and spectra of many simple and complex inorganic molecules, among which polymers are treated at some length. The exhaustive collection of references provides a background of great value. In a few cases, the author, in following up later work so thoroughly has perhaps not mentioned or given full historical credit to the original papers dealing with some particular new ideas and technical developments.

The book is somewhat expensive, and this may prevent a sale as large as its content deserves. It is definitely an important compilation in the spectroscopic field.

H. W. THOMPSON

VOL
7
1955/

L. J. BELLAMY: **The Infra-red Spectra of Complex Molecules.** Methuen and Co., London. Price 35s.

This book has a somewhat misleading title, for the text deals with only one aspect of molecular spectra. However, this single aspect—the structural diagnosis based upon correlation of molecular vibration frequencies with key groups—is so important and extensive in its application that the book is sufficient in itself, and represents a landmark in the field. From time to time during the past ten years, as new results were obtained, some of us who were engaged in applying infrared absorption spectroscopy to chemical problems brought together the frequent correlation rules as charts or tables for general use. A more thorough compilation has long been overdue, the more so since most of the basic information of value seems now to have been obtained. Dr. BELLAMY has done the job well. No one concerned with this kind of work can afford to be without this book, whether he be needing a guide to the background or to have a ready list of references to almost everything concerned.

The various diagnostic rules are considered in classes, C—H, O—H, C=O and other important bond types being discussed in detail. Among many groups of substances considered are the amides and peptides, aromatic and heterocyclic rings, organo-phosphorus and organo-silicon compounds, as well as inorganic ions. In fact, the whole range of interest is fully covered. The author has illustrated the principles of structural diagnosis by reference to actual spectra which are reproduced and this may be useful for those called upon to carry out such work without previous training. It is important for them, and indeed for everybody, to realize that great caution is often necessary in applying this method to the elucidation of organic structures if the correct decision is to be made between ambiguous solutions. However that may be, this book provides all the available factual equipment for the search. It is possible that the first edition may well be sold out before this review appears.

H. W. THOMPSON

L. A. AHRENS: **Quantitative Spectrochemical Analysis of Silicates.** Pergamon Press, Ltd., London, 122 pp. (1954). 25s.

A detailed table of contents of this book is given on Cover III of Spectrochemica Acta, Vol. 6, No. 5/6. It is primarily a book of supplemental background material and procedures for specialists in this field, but other serious students of spectrochemistry will find many useful suggestions about the practical aspects of performing and interpreting spectrochemical analyses. This book gives abundant evidence that excellent precision and accuracy can be achieved in the difficult field of spectrochemical silicate analysis if—and only if—careful attention is devoted to every step of the procedure. Since almost all of the experimental results reported were obtained by DR. AHRENS and his students at the Cabot Laboratory (Massachusetts Institute of Technology), there is unfortunately only passing reference to the novel and highly interesting techniques of HEGEMANN and his colleagues at Münich. The discussions are always specific and helpful, and written in the clear yet elegant style which have always made Dr. AHRENS' publications a pleasure to read.

CYRUS FELDMAN

VOL.
7
55/56

ANNOUNCEMENTS

Congress on Analytical Chemistry 1956

PROFESSOR I. M. KOLTHOFF, President of the Analytical Section of the International Union of Pure and Applied Chemistry, has announced that the Congress on Analytical Chemistry, to be held in Lisbon, September 9–16, 1956, will be under the patronage of the International Union of Pure and Applied Chemistry. Professor FERNANDO PIRES DE LIMA, Minister of Education, has appointed Professor D. ANTONIO PEREIRA FORJAZ to be President of the Organizing Committee. Arrangements for the meeting are in the hands of Prof. PIERRE A. LAURENT, Instituto Superior Tecnico, Avenida Rovisco Pais, Lisbon, Portugal. Inquiries regarding plans for the meeting should be directed to him. It is intended that the Congress cover broadly all aspects of analytical chemistry. Further details will be published as soon as they become available.

Colloquium Spectroscopicum Internationale VI Amsterdam, 1956

The Sixth International Spectroscopical Colloquium will be held in 1956 at Amsterdam in the Netherlands, from May 14th till May 19th, that is, the week preceding Whitsuntide.

The Colloquium is being organized under the auspices of the Koninklijke Nederlandse Chemische Vereniging and of the Nederlandse Natuurkundige Vereniging; further information may be obtained by writing to the Secretary, F. Freese, at the Laboratorium voor Analytische Chemie, 125 Nieuwe Achtergracht, Amsterdam C-4.

VOL
7
1955/

ERRATUM

The paper by A. WALSH on "The application of atomic absorption spectra to chemical analysis" which appears on pages 108 to 117 of Volume 7 (1955), was received on 19th *November* 1954 and not, as stated, on 18th *January* 1955.

Spectrochimica Acta, 1955, Vol. 7, pp. 253 to 263. Pergamon Press Ltd., London

Infra-red summation bands of the out-of-plane C-H bending vibrations of substituted benzene compounds

D. H. WHIFFEN
The Chemistry Department, The University, Edgbaston, Birmingham 15

(*Received* 16 *July* 1955)

Summary—Evidence is presented to show that the stronger infra-red absorption bands from 1650 to 2000 cm^{-1} in benzene derivatives normally arise from summation tones of the out-of-plane C-H bending vibrations. The assignments not only explain the magnitudes of the individual frequencies, but also explain the characteristic pattern as a function of substitution type, as observed by YOUNG, DUVALL, and WRIGHT [1]. The regularity with which the summation bands appear in the spectrum enables them to be used in the assignment of fundamental frequencies when these are in doubt.

1. Introduction

NORMALLY the spectral region 1650 to 2000 cm^{-1} is not very interesting unless carbonyl groups or triple bonds are present, but this region has been used by YOUNG, DUVALL, and WRIGHT [1] for the characterization of substituted benzene compounds, and its usefulness has been confirmed by BELLAMY [2]. The bands appear to be summation† bands arising from the out-of-plane C-H deformation fundamentals. This adds interest to the region, since it is not always easy to obtain a complete set of C-H deformation frequencies from the fundamental spectra. This is because some of the vibrations are forbidden to appear in the infra-red spectrum, often being in the A_2 class of a molecule with C_{2v} symmetry. Very often weak absorption does occur as a result of the violation of the selection rules in condensed phases. The missing frequencies may be permitted in the Raman spectrum, but they are all weak, and the Raman shifts are not commonly observed.

2. Benzene

A restatement of the facts from the spectrum of benzene interpreted by INGOLD and co-workers [3] will help to establish that the out-of-plane C-H deformation summation tones may appear quite strongly in infra-red absorption. For benzene there are four such C-H deformation fundamental frequencies, two of which are degenerate, and there are three binary combinations which are permitted in the infra-red spectrum [4]. With the class nomenclature of HERZBERG [5] these are:—

$671\ (A_{2u}) + 849\ (E_{1g}) = 1520\ (E_{1u})$ Observed 1529 cm^{-1}

$849\ (E_{1g}) + 970\ (E_{2u}) = 1819\ (E_{1u})$ Observed 1808 cm^{-1}

$970\ (E_{2u}) + 985\ (B_{2g}) = 1955\ (E_{1u})$ Observed 1965 cm^{-1}

These are three of the most intense bands in the infra-red spectrum, apart from those assigned to permitted fundamentals.

† "Summation" is used in this text to indicate both overtones and combination tones in contexts where it is not desired to distinguish between them.

3. Mono-substituted benzenes

Benzene with one substituent has C_{2v} symmetry, if the symmetry of the substituent itself be disregarded. There are then three infra-red active C-H out-of-plane deformation vibrations in the B_2 class, and two infra-red inactive in the A_2 class. All summation tones derived from these five modes belong to either the A_1 or B_1 classes and are infra-red active, and so there are fifteen permitted frequencies. Since many of the mono-substituted benzene vibration modes, especially the A_2 modes, approximate in form to modes of benzene itself, it is reasonable to expect that the strong infra-red summation bands correspond to the active benzene combination bands quoted above.

The average C-H deformation frequencies have been given by RANDLE and WHIFFEN [6], and are repeated in the second column of Table 1. The first column of this table gives the designation following Fig. 1 of reference [6], while the last column gives the vibration of benzene to which it is the closest approximation. The degeneracy of benzene is lifted by the substitution and, corresponding to the first of the benzene combinations, that observed at 1529 cm^{-1}, there are two strong bands expected, namely $f + g$ and $f + i$; corresponding to the benzene combination at 1808 cm^{-1} there are two strong bands expected, namely $g + h$ and $i + h$; corresponding to the third benzene frequency, 1965 cm^{-1}, $h + j$ would be expected to appear. Vibration i is compounded from the $E_{1g b}$ benzene mode and appreciable amount of the $E_{2u b}$ mode, and as a result of this latter admixture the summations $g + i$, $i + i$, and $j + i$ might be expected to appear in the summation spectrum. The experimental evidence is that only the first of these is normally apparent. The observed bands have been labelled with Greek letters, in Table 1 and elsewhere, for identification. The lowest, α, lies near 1588 cm^{-1}, and is normally overlaid by the fundamental frequencies in this region. β, near 1659 cm^{-1}, may also be overlaid, though usually it is apparent; but it is below 1670 cm^{-1}, which is the limit of the range discussed by YOUNG, DUVALL, and WRIGHT [1]. The four bands quoted by them are labelled ζ, ε, δ, γ, and are seen to agree well with the sums of the corresponding fundamental frequencies, especially since both figures are averages which are derived from different ranges of compounds.

However, these authors and BELLAMY [2] stress that it is the pattern of bands, and not the exact frequencies, which is characteristic of the substitution type. This is to be expected, since electron-attracting groups, which raise the C-H deformation frequencies, will consequently cause the whole summation band pattern to be raised; similarly heavy substituents which lower the B_2 frequencies [7] will shift the pattern to lower frequencies. It therefore strengthens the argument for the assignments to show the agreement for a range of compounds, and figures for toluene, phenol, benzonitrile, chlor-benzene, and nitro-benzene, are given in Table 1. The spectral frequencies are taken from the references indicated, and the fundamental assignments are based on the work of RANDLE and WHIFFEN [6]. The agreement is satisfactory, and it can be seen that the higher fundamental frequencies of benzonitrile relative to phenol are reflected in the higher summation frequencies. Modes h and j in particular may be very weak in the fundamental infra-red spectra, and in three cases given in parentheses in Table 1 their values have been deduced from the summation spectra. The 842-cm^{-1} frequency of

VOL 7 1955/

nitrobenzene is similarly deduced, since in both the infra-red and the Raman spectra its presence is masked by the C-N stretching vibration [9] at 854 cm^{-1}.

The argument as regards expected intensities cannot be taken to be precise, but it is probably significant that the second highest fundamental, given as row *h*,

Table 1. *Mono-substituted compounds*

Substituent	*Average*	CH_3	OH	CN	Cl	NO_2	*Class*	*Like* D_{6h} *class*
Reference	[6, 1]	[8]	[8]	[8]	[8]	[10, 1]		
Fundamentals								
f	751	728	753	757	740	797	B_2	A_{2u}
g	837	844	824	847	830	(842)	A_2	E_{1g}
i	908	896	882	928	902	938	B_2	E_{1g}
h	962	966	952	975	965	(980)	A_2	E_{2u}
j	982	982	973	(985)	985	(1010)	B_2	B_{2g}
Summation Bands								
α	—	—	—	—	—	—		
$f + g$	1588	1572	1577	1604	1570	1639	B_1	
β	—	•	—	1686	1647	1740		
$f + i$	1659	1624	1635	1685	1642	1735	A_1	
γ	1730	1736	1705	1770	1736	1780		
$g + i$	1745	1740	1706	1775	1732	1780	B_1	
δ	1790	1802	1770	1818	1795	1815		
$g + h$	1799	1810	1776	1822	1795	1822	A_1	
ε	1860	1855	1835	1900	1873	1925		
$i + h$	1870	1862	1834	1903	1867	1918	B_1	
ζ	1945	1941	1930	1970	1949	1990		
$h + j$	1944	1948	1925	1970	1950	1990	B_1	

Key to symbols in Tables 1 *to* 8. ( ) value of fundamental infra-red from summation bands; — overlaid by fundamentals or otherwise not observed; • weak absorption present but the exact frequency is uncertain.

is required for three strong combination bands which is reasonable for the E_{2u}-like vibration, but not for the B_{2g}-like vibration, which would not give a strong combination band with *g* under the present assumptions. This is the reason for

Table 2. Ortho-substituted compounds

Substituents	*Average*	CH_3, CH_3	CH_3, OH	CH_2, CN	Cl, Cl	*Class*
Reference	[6, 1]	[8]	[8]	[8]	[8]	
Fundamentals						
a	751	742	751	758	748	B_2
b	865	860	844	872	868	A_2
c	934	932	933	949	941	B_2
d	977	(970)	(967)	987	978	A_2
Summation Bands						
α	—	—	—	—	—	
$a + a$	1502	1484	1502	1516	1496	A_1
β	—	—	—	1629	—	
$a + b$	1616	1602	1595	1630	1616	B_1
γ	1690	1675	1680	1712	1701	
$a + c$	1685	1674	1684	1707	1689	A_1
δ	—	1698	•	•	1721	
$a + d$	1728	1712	1718	1745	1726	B_1
ε	—	1718	•	•	1745	
$b + b$	1730	1720	1688	1744	1736	A_1
ζ	1785	1788	1769	1821	1802	
$b + c$	1799	1792	1777	1821	1809	B_1
η	1815	1828	•	•	1842	
$b + d$	1842	1830	1811	1859	1846	A_1
θ	1860	1862	•	1905	1897	
$c + c$	1868	1864	1866	1898	1882	A_1
ι	1900	1897	1883	1946	1927	
$c + d$	1911	1902	1900	1936	1919	B_1
κ	1930	1942	1934	1980	1961	
$d + d$	1954	1940	1934	1974	1956	A_1

VOL 7 1955/

the assignment of the lower fundamental to the A_2 class and the higher to the B_2 class; this point was left uncertain in reference [6].

YOUNG, DUVALL, and WRIGHT [1] quote six anomalous compounds in the mono-substituted series; namely fluorbenzene, anisole, phenetole, propoxybenzene, styrene, and nitrobenzene. In the first four the anomalous band lies between 2000 and 2100 cm^{-1} and is therefore too high for a C-H deformation summation tone, but the frequency in each case is consistent with a combination of the X sensitive frequencies q and r of Table 2 of reference [6]. In some other cases the corresponding band appears, but it is commonly weaker in intensity, e.g., toluene observed 1988 cm^{-1} [8], $q + r = 1996$ cm^{-1}. For characterization of substitution types the range above 2000 cm^{-1} is best disregarded. For styrene, BELLAMY [2] has explained the extra band at 1818 cm^{-1} as the overtone of the out-of-plane deformation of the vinyl group at 910 cm^{-1}. The nitrobenzene spectrum is plausibly explained in Table 1, the anomaly residing in the unusually high frequencies of f and i, so that the band β appears at 1740 cm^{-1} instead of below the range 1670 to 2000 cm^{-1}.

4. Ortho-substituted benzenes

Again the summation bands from 1670 to 2000 cm^{-1} can be explained as being derived principally from out-of-plane C-H deformations as indicated in Table 2. The fundamental vibration modes do not resemble those of benzene very closely, so that there is no a priori guide to the intensities, and the table indicates the evidence for the ten possible summation bands. Those labelled κ, ι, θ, η, ζ, and γ correspond to the six peaks of YOUNG, DUVALL, and WRIGHT [1]. δ and ε are normally weaker than γ, and do not always appear as distinct frequencies. They are clearly resolved in the A.P.I. curves [8] for o-xylene and o-dichlor-benzene, though not in the o-dichlor-benzene curve of reference [1]. The band β is normally lost under a fundamental frequency, though it may appear when it is much above 1600 cm^{-1} as in o-toluenitrile. The highest of the required fundamental frequencies for o-xylene and o-cresol are obtained from the summation frequencies. The fundamental spectra show absorption at 985 and 987 cm^{-1} respectively, which would mask the forbidden A_2 frequencies; these frequencies themselves are unlikely to be the required fundamentals in view of their considerable intensity in both the infra-red and Raman effect, and they are more probably X-sensitive frequencies.

5. Meta-substituted benzenes

In meta compounds also the benzene spectrum is little guide to the summation band intensities, and any of the ten summations from the four fundamental frequencies might appear, and appeal must be made to the experimental results which are shown in Table 3. From this it would appear that the five bands indicated by YOUNG, DUVALL, and WRIGHT [1] are those designated κ, ι, θ, ζ, and δ, and that the band γ is normally strong though just below their range. However, the pattern may sometimes be slightly different, as θ does not always appear distinctly resolved and it is normally weak; also η sometimes appears distinctly resolved from ι, rather than as a broadening of this band as indicated in Fig. 5 of reference 1. ε does not appear strongly, and since its frequency usually lies between ζ and δ, it would

Table 3. Meta-substituted compounds

Substituents	*Average*	CH_3, CH_3	CH_3, OH	CH_3, CN	Cl, Cl	*Class*
Reference	[6, 1]	[8]	[8]	[8]	[10]	
Fundamentals						
a	782	769	769	785	772	B_2
b	876	875	882	885	868	B_2
c	904	906	928	918	892	A_2
d	964	971	966	(980)•	969	B_2
Summation Bands						
α	—	•	—	—	—	
$a + a$	1564	1538	1538	1570	1544	A_1
β	—	1655	—	—	1622	
$a + b$	1658	1644	1651	1670	1640	A_1
γ	—	1689	1698	1712	1671	
$a + c$	1686	1675	1697	1703	1664	B_1
δ	1730	1745	1733	1761	1737	
$a + d$	1746	1740	1735	1765	1741	A_1
ε	—	1745?	—	1761?	1737?	
$b + b$	1752	1750	1764	1770	1736	A_1
ζ	1770	1773	1812	1795	1786	
$b + c$	1780	1781	1810	1803	1760	B_1
η	—	1852?	1842	•	•	
$b + d$	1840	1846	1848	1865	1837	A_1
θ	•	1808	—	—	1786?	
$c + c$	1808	1812	1856	1836	1784	A_1
ι	1850	1852	1880	1898	1860	
$c + d$	1868	1877	1894	1898	1861	B_1
$\varkappa$	1925	1930	1919	1965	1925	
$d + d$	1928	1942	1932	1960	1938	A_1

VOL 7 1955/

be difficult to observe plainly if it were weak. β and α are commonly overlaid by fundamental bands.

6. Para-substituted benzenes

For para compounds, even with different substituents, the V_h symmetry-group selection rules are likely to be a good guide to the appearance of C-H vibrations, and in this case only four relevant summation bands are permitted in the infra-red spectrum. Three of the four fundamentals are forbidden in the infra-red, and although two of these are permitted in the Raman spectrum, they are too weak

Table 4. Para-substituted compounds

Substituents	*Average*	CH_3, CH_3	CH_3, OH	CH_3, CN	Cl, Cl	*Class*
Reference	[6, 1]	[8]	[8]	[8]	[10, 1]	
Fundamentals						
a	817	794	818	815	818	B_{1u}
b	840	835	(811)	(838)*	(825)	B_{2g}
c	(940)	935	927	951	932	B_{3g}
d	961	962	952	970	948	A_u
Summation Bands						
α	—	1628	—	*	—	
$a + b$	1657	1629	1629	1653	1643	B_{3u}
β	1730	*	*	*	*	
$a + c$	1757	1729	1745	1766	1750	B_{2u}
γ	1785	1792	1757	1802	1770	
$b + d$	1801	1797	1763	1808	1773	B_{2u}
δ	1890	1890	1869	1919	1878	
$c + d$	1901	1897	1879	1921	1880	B_{3u}

to find in many cases. Consequently the summation bands have to be used to obtain the values of several of the fundamentals, and others are obtained from their appearance in the spectra of liquids or solids in violation of the strict selection rules. Nevertheless Table 4, which presents the evidence, is seen to be self-consistent. The assignment of the highest frequency to the A_u fundamental and the next highest to the B_{3g} class is not clearly established, and is based partly on the greater intensity of the lower frequency in *p*-cresol and *p*-toluenitrile when it becomes permitted in the infra-red spectrum when C_{2v} selection rules are considered; this is in contrast to the A_u fundamental which remains forbidden. Also force constant calculations [12] suggest that the A_u frequency should be the higher. It is clear

that δ and γ are the two stronger bands of Young, DuVall, and Wright [1], and that the weaker β-band may or may not be apparent.

7. Tri-substituted benzenes

The position for the tri-substituted compounds is given in Tables 5, 6, and 7, where the average bands and the assignments for the trimethyl benzene and one xylenol are given in each case. For 1 : 2 : 3 substitution the four bands of Young, DuVall,

Table 5. 1 : 2 : 3-substituted compounds

Substituents	*Average*	CH_3, CH_3, CH_3	CH_3, OH, CH_3	*Class*
Reference	[6, 1]	[8]	[11, 1]	
Fundamentals				
a	770	766	761	B_2
b	893	890	(890)	A_2
c	958	(960)•	950	B_2
Summation Bands				
α	—	•	—	
$a + a$	1540	1532	1522	A_1
β	1660	1655	•	
$a + b$	1663	1656	1651	B_1
γ	—	1720	1711	
$a + c$	1728	1726	1711	A_1
δ	1780	1775	1780	
$b + b$	1786	1780	1780	A_1
ε	1845	1845	1845	
$b + c$	1851	1850	1840	B_1
ζ	1920	1910	1911	
$c + c$	1916	1920	1900	A_1

and Wright [1] are clearly ζ, ε, δ, and β, while γ is weaker and may not always be apparent. For 1 : 2 : 4 substitution the commonly observed bands are ζ, ε, and δ and γ together. The latter pair are normally predicted to lie within 10 cm^{-1}, and are not resolved. For 1 : 3 : 5 substitution the $A''_2 + A''_2$ overtone is forbidden, and the remaining bands are degenerate. But if the substituents are not identical the degeneracy is removed, and the curves of Young, DuVall, and Wright [1] show a slight splitting of the lower band α.

VOL 7 1955/

Table 6. 1 : 2 : 4-*substituted compounds*

Substituents	*average*	CH_3, CH_3, CH_3	OH, CH_3, CH_3	*Class*
Reference	[6, 1]	[8]	[8]	
Fundamentals				
a	816	806	816	*A″*
b	868	873	877	*A″*
c	929	943	930	*A″*
Summation Bands				
α	—	—	—	
$a + a$	1632	1612	1632	*A′*
β	—	1680	•	
$a + b$	1684	1679	1693	*A′*
γ	1740	1745	1757	
$a + c$	1745	1749	1746	*A′*
δ	1740	1745	1757	
$b + b$	1736	1746	1754	*A′*
ε	1810	1820	1812	
$b + c$	1797	1816	1807	*A′*
ζ	1870	1875	1869	
$c + c$	1858	1886	1860	*A′*

Table 7. 1 : 3 : 5-*substituted compounds*

Substituents	*Average*	CH_3, CH_3, CH_3	CH_3, CH_3, OH	*Class*
Reference	[6, 1]	[8]	[11, 1]	
Fundamentals				
a	845	835	827	A_2''
b	937	928	946	*E″*
Summation Bands				
α	1760	1760	1760	
$a + b$	1782	1763	1773	*E′*
β	1905	1875	1920	
$b + b$	1874	1856	1892	*E′*

VOL. 7 55/56

8. Poly-substituted benzenes

For tetra-substituted benzenes the tables of RANDLE and WHIFFEN [6] do not fully assign the out-of-plane C-H deformations, and Table 8 has been confined to the methyl compounds. It can be seen that for 1 : 2 : 3 : 4 substitution there should be two well-separated bands, β and γ, but that for 1 : 2 : 3 : 5 substitution the two bands lie very much closer together and might often appear to be single. For 1 : 2 : 4 : 5 substitution only one band is permitted, and this is commonly near 1730 cm^{-1}. The single overtone with penta-substitution should also lie here, being twice the fundamental near 871 cm^{-1}. There are, however, weaker

Table 8. *Tetramethyl benzenes*

Substitution positions	1 : 2 : 3 : 4	1 : 2 : 3 : 5	1 : 2 : 4 : 5
References	[8]	[8]	[8]
Fundamentals			
a	804 (B_2)	847 (B_2)	864 (B_{1u})
b	936 (A_2)	878 (A_2)	(876) (B_{3g})
Summation Bands			
α	—	•	
$a + a$	1608 (A_1)	1694 (A_1)	(A_g)
β	1735	1725	1740
$a + b$	1740 (B_1)	1725 (B_1)	1740 (B_{2u})
γ	1865	1754	
$b + b$	1872 (A_1)	1756 (A_1)	(A_g)

bands in the observed spectra [1], and there are some weak bands in the hexa-substituted compounds. It remains true that the permitted out-of-plane C-H deformation summations are often strong, but it is hardly to be expected that they could account for all the observed bands in this range in such complex molecules.

9. Conclusion

Although for the individual bands discussed it may be possible to find alternative assignments, the total weight of evidence for all types taken together is sufficient to make it reasonably certain that the proposed interpretations are correct. As a consequence the region may be used to determine, or at least add certainty to, the assignments of the out-of-plane C-H deformations. This is especially valuable for the frequencies above 900 cm^{-1}, where the fundamental bands are commonly very weak in the infra-red absorption. Since the fundamental C-H pattern depends on substitution type, providing the substituent only produces small changes of

VOL 7 1955/

force-constant and effective mass, the summation bands must similarly depend on substitution type. Consequently the analysis for this type, based on the region 1670 to 2000 cm^{-1}, rests on a satisfactory foundation.

The existence of infra-red absorption in summation bands implies either cubic terms in the potential function or quadratic terms in the dipole-moment function, when these are expressed in terms of displacement co-ordinates. The summation bands agree quite closely with the sum of the fundamental frequencies, which suggests that the potential function does not contain exceptionally large cubic terms, and it is more reasonable to suppose that the reason for the large intensity in the present case lies in the dipole-moment function. In this instance the most important quantity is the coefficient of the square of the angular displacement in the function expressing the dipole moment along the equilibrium C-H direction, i.e., $\partial^2\mu/\partial\gamma^2$. It is noteworthy that the out-of-plane deformations of ethylenic hydrogen atoms, and the deformation of acetylenic hydrogens, also provide strong summation bands, e.g., ethylene [5] 1890 cm^{-1}, acetylene [5] 1328 cm^{-1}, methyl acetylene [5] 1260 cm^{-1}, substituted acetylenes generally [2] 1200 to 1300 cm^{-1}, vinyl compounds generally [2] 1800 to 1865 cm^{-1}. A large value of $\partial^2\mu/\partial\gamma^2$ is thus seen to be characteristic of the out-of-plane deformations of C-H bonds with sp^2 hybridization of the carbon atoms as in ethylenes and benzenes, and deformations of C-H bonds with sp hybridization at the carbon atom as in acetylenes.

VOL. 7 55/56

References

[1] Young, C. W., DuVall, R. B., and Wright, N.; *Analyt. Chem.* 1951 **23** 709.
[2] Bellamy, L. J.; *The Infra-red Spectra of Complex Molecules*, Methuen, London, 1954.
[3] Herzfeld, N., Ingold, C. K., and Poole, H. G.; *J. Chem. Soc.* (*London*) 1946 316.
[4] Bailey, C. R., Ingold, C. K., Poole, H. G., and Wilson, C. L.; *J. Chem. Soc.* (*London*) 1946 222.
[5] Herzberg, G.; *Infra-red and Raman Spectra*, Van Nostrand, New York, 1945.
[6] Randle, R. R., and Whiffen, D. H.; *Molecular Spectroscopy, Report on the conference held in London in October*, 1954 *by the Institute of Petroleum.*
[7] Margoshes, M., and Fassel, V. A.; *Spectrochimica Acta* 1955 **7** 14.
[8] *American Petroleum Institute, Research Project* 44. *Catalogue of Infra-red and Raman Spectra.*
[9] Randle, R. R., and Whiffen, D. H.; *J. Chem. Soc.* (*London*) 1952 4153.
[10] Measurements in this Laboratory.
[11] Whiffen, D. H., and Thompson, H. W.; *J. Chem. Soc.* (*London*) 1945 268.
[12] Whiffen, D. H. Discussion following reference [6].

Spectrochimica Acta, 1955, Vol. 7, pp. 264 to 273. Pergamon Press Ltd., London

Zur Deutung spektroskopischer Temperaturmessungen

L. HULDT
Physikalisches Institut der Universität Stockholm

(*Received* 3 *August* 1955)

Summary—The spectroscopic method of measuring temperature in spark discharges is discussed, bringing out the significance of the cooler zones which lie between the hottest part of the discharge and the surrounding air. A calculation of the relationship between line intensities and temperatures, with the conventional assumptions, leads to the result that most of the spectrum lines measured have their peak emission at between 5000 and 10,000°K. A more precise calculation for a selected example shows that the spectroscopically estimated temperature is independent of a doubling of the peak temperature; and peak temperatures cannot be correlated with experimentally observed temperatures. Consequently no such measurements can lead to reliable conclusions as to the highest temperatures in spark discharges; these can only be estimated using lines of highly ionised atoms whose transition probabilities are calculable.

Einleitung

Aus dem Intensitätsverhältnis zweier Spektrallinien, von der gleichen Atom- oder Molekülart emittiert, kann bekanntlich unter gewissen Bedingungen die Temperatur der Lichtquelle ermittelt werden. Sind die absolute Temperatur T und die Intensitäten der beiden Spektrallinien I_1 und I_2, so gilt

$$\frac{I_1}{I_2} = \frac{A_1 g_1 \nu_1}{A_2 g_2 \nu_2} e^{(E_2 - E_1)/kT} \tag{1}$$

wo k Boltzmannsche Konstante, ν und A Frequenz, bezw. Uebergangswahrscheinlichkeit der Linie, E und g Energie bezw. statistisches Gewicht des oberen Quantenzustandes sind. Die Indizes beziehen sich auf zwei Linien desselben Atoms oder Moleküls.

Für die Gültigkeit der Gleichung (1) müssen folgende Bedingungen erfüllt sein:

1. Thermodynamisches Gleichgewicht muss annähernd verwirklicht sein, sodass die Besetzungszahl n_E des angeregten Niveaus gegeben ist durch

$$n_E = n \frac{g_E e^{-E/kT}}{\sigma(T)} \tag{2}$$

wo n die Gesamtzahl der Moleküle und $\sigma(T) = \Sigma g_E e^{-E/kT}$ ist.

2. Die Linien müssen selbstabsorptionsfrei sein, damit die Proportionalität zwischen I und n_E besteht. Für grössere optische Dicken hängt die Beziehung zwischen I und n_E von der Form der Linie ab.
3. Der Teil der Lichtquelle, welcher auf dem Spalt abgebildet wird, muss über sein ganzes Gebiet dieselbe Temperatur haben, da sonst die aus Gl. (1) berechnete Temperatur ein schwer zu definierender Mittelwert des Bereiches wird. Liegt ausser der Inhomogenität auch Selbstabsorption vor, entsteht die als Selbstumkehr wohlbekannte Erscheinung. Der Einfluss dieser räumlichen Inhomogenität auf spektroskopische Temperaturmessungen wird in dieser Arbeit näher untersucht.

SMIT [1] hat einen zusammenfassenden Bericht über Messungen in Lichtbogen veröffentlicht. Die Bedeutung der Bedingungen 2 und 3 für die Temperaturermittlung ist von LOCHTE-HOLTGREVEN und MAECKER [2] klargemacht und diejenige der Inhomogenität und deren Beseitigung oft, auch von Astrophysikern [3], untersucht worden.

Die erörterte Methode ist für den Wechselstrombogen [1] sowie neuerdings auch für nieder- und hochfrequente Funkenentladungen [4], [5], [6], [7], [8], [9] angewandt worden, wobei zur Zeitauflösung entweder Vervielfacherzellen mit Oscillograph oder Drehspiegel mit photographischer Platte benutzt worden sind. Die dabei erhaltenen Werte der Temperatur sind aber erstaunlich niedrig, meist geringer als 10.000°K. Auch wenn die Bedingung 1 (thermodynamisches Gleichgewicht, das zwar nur Maxwellverteilung der Elektronengeschwindigkeiten zu umfassen braucht) nicht erfüllt ist, könnte man mit Rücksicht auf die im Funken entwickelte Leistung weit höhere Temperaturwerte erwarten. Dafür spricht auch die bekannte und spektrochemisch bedeutungsvolle Tatsache, dass schwer anregbare Linien insbesondere Ionenlinien in Funkenspektren stark sind. Ein Versuch zur Deutung dieser Diskrepanz zwischen erwarteter und beobachteter Grössenordng der Funkentemperaturen wird unten vorgenommen.

VOL. 7 55/56

Bedeutung des Temperaturabfalles im Entladungskanal

Bei der eingehenderen Interpretierung spektroskopischer Intensitätsmessungen muss darauf geachtet werden, dass die Temperatur nicht konstant ist, sondern sowohl im Raume als auch (z.B. bei Wechselstromentladungen) mit der Zeit veränderlich ist. So zeigen die verschiedenen Phasen einer kondensierten Entladung variierende Eigenschaften, die auf eine durch Abkühlung abnehmende Temperatur zurückzuführen sind.

Während es gelungen ist, mit recht guter Auflösung Funkenentladungen zeitlich zu zerlegen, stösst ein Studium der Lichtemission von Punkt zu Punkt im Funken auf erhebliche experimentelle Schwierigkeiten. Die Methode der Abbildung des Entladungskanals quer zum Spektrographenspalt, durch welche bei stationären Entladungen die Temperatur und andere Parameter als Funktion des Abstandes von der Achse bestimmt werden können, ist bis heute bei Funkenentladungen nicht angewandt worden. Die mit der räumlichen Inhomogenität zusammenhängenden Verhältnisse sind jedoch von grösster Bedeutung, da jedes Lichtbündel, das in den Spektralapparat gelangt, auf seinem Wege Gebiete verschiedener Temperaturen durchsetzt. Es ist nicht wahrscheinlich, dass nur die Gebiete der höchsten Temperatur Spektrallinien emittieren; wie unten gezeigt wird, trifft für die hier in Frage kommenden Fälle das Gegenteil zu.

Um eine Auskunft über diese Fragen zu erhalten, wird ein Modell des Funkens entworfen. Um dieses Modell realistisch zu machen, fassen wir einen speziellen Fall ins Auge: die Elektroden sind aus Magnesium, die Entladung findet hauptsächlich in Magnesiumatmosphäre statt. Der Elektronenpartialdruck p_e berechnet sich nach der Saha-Gleichung unter Berücksichtigung der einfachen und zweifachen Ionisation des MgI zu MgII bezw. MgIII, sowie der Ionisation des Füllgases (Luft). Der Einfachheit halber ersetzen wir doch die genaue Rechnung [10] durch die Verwendung einer Interpolationsformel der Form

$$p_e = CT^{5/4}e^{-X/kT} \tag{3}$$

Den gesamten Partialdruck P des neutralen, ein- und zweifach ionisierten Magnesiums nehmen wir mit 10^{-3} Atm an (konstant im ganzen Entladungsraum). Änderung einer Zehnerpotenz in P beeinflusst das Endresultat nicht beträchtlich.

Anpassung der Gl. (3) zur Ionisation bei 5000°K und 10.000°K ergibt die Konstanten

$$C = 1{,}47 \cdot 10^{-6}\ \text{Atm Grad}^{-5/4}, \qquad X = 2{,}48\ \text{eV} \tag{4}$$

Die so erhaltene Interpolationsformel gilt als befriedigend auch für $T = 20.000°\text{K}$, wenn ein Druck der Luft um etwa 0,5 Atm postuliert wird. Es wird sich herausstellen, dass die Daten für die höchsten Temperaturen nicht entscheidend sind. Nach diesen Feststellungen ist das Vorkommen anderer Elemente für die folgenden Ueberlegungen belanglos.

Es sollen nun die Intensität des Triplettes 3^3P–4^3S (5167/73/84 Å) mit der Anregungsenergie $E_1 = 5{,}106$ eV und die der Linie 3^1P–7^1S (4354,5 Å), $E_2 = 7{,}191$ eV, von MgI in diesem Entladungsplasma als Funktion der Temperatur berechnet werden. Es wird zu vernachlässigende Selbstabsorption vorausgesetzt, sodass

$$I_i \sim n_i \sim [\text{MgI}]e^{-E_i/kT} (i = 1{,}2)$$

im Sinne Gl : n (1) und (2) ist.

Für die Ionisation des Magnesiums gilt

$$\frac{[\text{MgII}]}{[\text{MgI}]} = \frac{S_{\text{MgI}}(T)}{p_e} = A \tag{5a}$$

$$\frac{[\text{MgIII}]}{[\text{MgII}]} = \frac{S_{\text{MgII}}(T)}{p_e} = B \tag{5b}$$

$$[\text{MgI}] + [\text{MgII}] + [\text{MgIII}] = P/kT \tag{5c}$$

$$\text{mit } P = 10^{-3}\ \text{Atm} \approx 10^3\ \text{dyn cm}^{-2}$$

Die eingeklammerten Symbole bezeichnen die Konzentration der betreffenden Atom- bezw. Ionenart. Für die Saha-Funktionen S gilt

$$S_X(T) = 6{,}6 \cdot 10^{-7} \frac{\sigma_{X+1}}{\sigma_X} T^{5/2} e^{-E_X/kT} \text{Atm Grad}^{-5/2} \tag{6}$$

E_X ist die Ionisationsenergie des Atomes oder Ions, σ_X seine Zustandssumme, σ_{X+1} die für die nächste Ionisationsstufe. $E_{\text{MgI}} = 7{,}644$ eV und $E_{\text{MgII}} = 15{,}03$ eV.

Aus dem Gleichungssystem (5) erhält man

$$[\text{MgI}] = \frac{P}{kT} \cdot \frac{1}{1 + A + AB}$$

$$[\text{MgII}] = \frac{P}{kT} \cdot \frac{A}{1 + A + AB} \tag{7}$$

woraus durch Multiplizieren mit dem Boltzmannfaktor die mit der Spektrallinienintensität proportionale Grösse n_i zu erzielen ist.

In Abb. 1 ist

$$n_1 = [\text{MgI}]e^{-E_1/kT} \text{ und } n_2 = [\text{MgI}]e^{-E_2/kT} \tag{8}$$

VOL 7 1955/

gegen die Temperatur aufgetragen. Die Besetzungszahl jeder dieser Energiniveaus wächst nicht unbegrenzt mit der Temperatur sondern gelangt bei etwa $T = 6300°K$ bezw. $T = 9000°K$ wegen des Zerfalls durch Ionisation zu einem Maximum. Das Vorhandensein einer solchen optimalen Temperatur ist von LARENZ und BARTELS [11] für eine Bogenentladung nachgewiesen und von ihnen zur Temperaturermittlung verwendet worden. Die Strahlungsdichte einer Spektrallinie

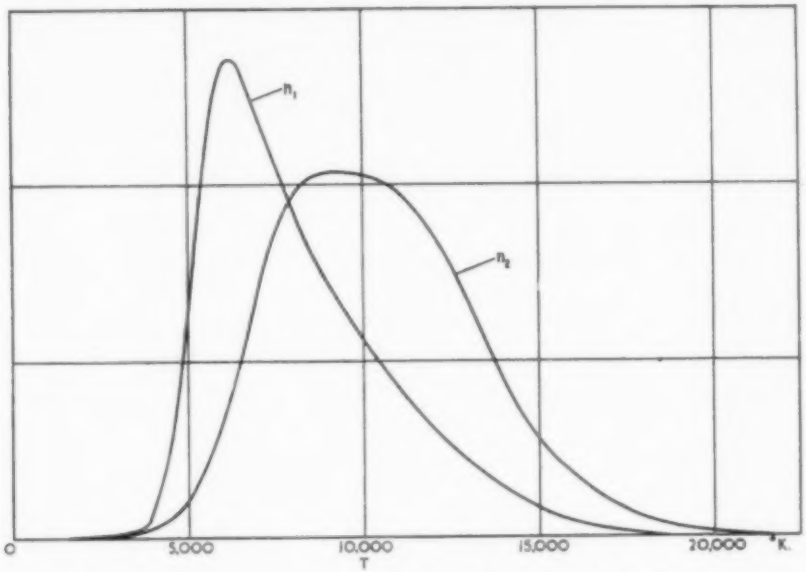

Abb. 1. Konzentration angeregter MgI-Atome (Intensität der Spektrallinien) in Abhängigkeit von der Temperatur.
$n_1 : E_1 = 5{,}106$ eV (λ5167/73/84 Å)
$n_2 : E_2 = 7{,}191$ eV (λ4354,5 Å)

erreicht ihr Maximum bei derselben Temperatur wie die Besetzungszahl n_E ihres Oberniveaus E. Wenn nun die Maximaltemperatur der Lichtquelle im Bereich 15.000–20.000°K liegt, fällt die Temperatur stetig vom Maximum bis auf Zimmertemperatur herab. Es lässt sich kaum eine Laboratoriumslichtquelle vorstellen, die bei 15.000° eine Scheidewand besitzt, welche den Mg-Dampf gegen den unvermeidlichen Temperaturfall abgrenzt. Die Sehlinie des Spektrographen durchsetzt folglich Gebiete mit sehr verschiedenen Temperaturen. Es ist auf Grund der Kurven der Abb. 1 sehr unwahrscheinlich, dass nicht das Temperaturgebiet 15.000°–5000° in der Linienemission überwiegen würde, selbst wenn $T_{max} >$ 15.000° wäre; folglich werden Temperaturen, höher als, sagen wir 15.000°, überhaupt nicht durch dieses Linienpaar indiziert werden.

Um diese Zusammenhänge näher zu veranschaulichen, wird für das obige Funkenmodell eine besondere Annahme über den räumlichen Temperaturverlauf gemacht werden. Wir setzen für die Temperatur als Funktion des Abstandes ρ zur Symmetriachse des Entladungskanal

$$T = \frac{T_0}{1 + \rho^4} \tag{9}$$

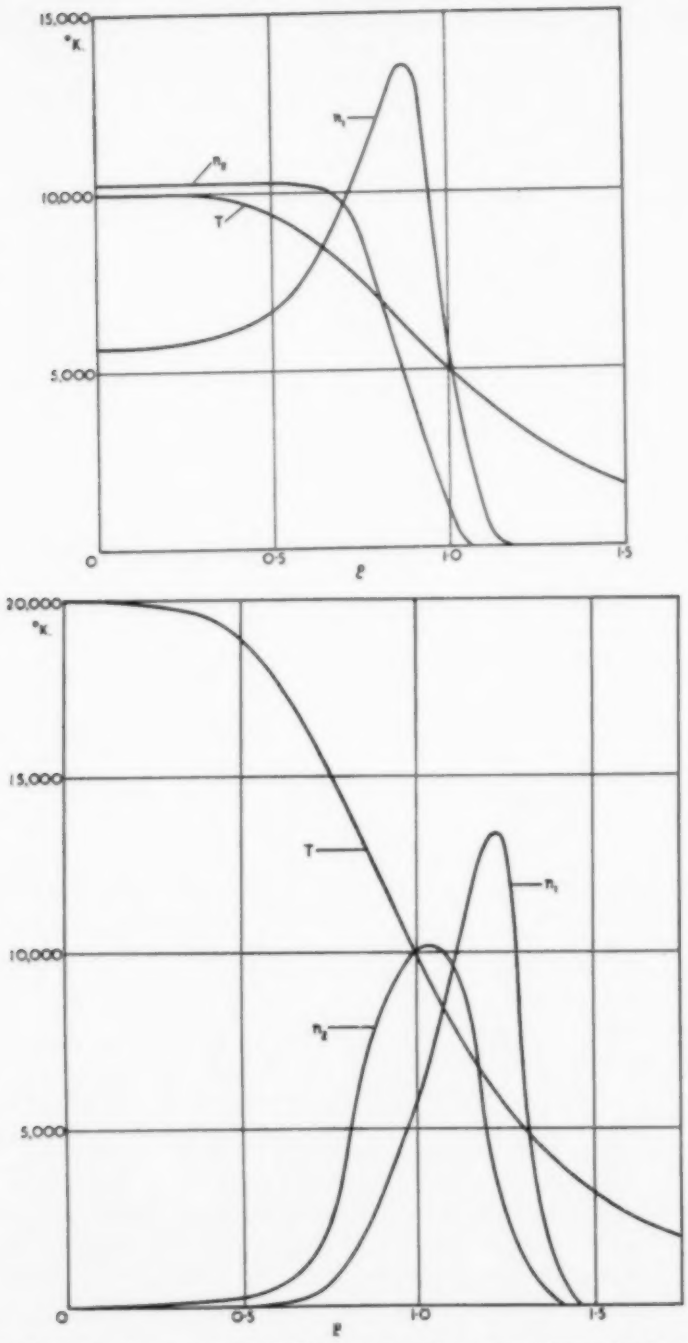

Abb. 2. Konzentration angeregter MgI-Atome, n_1 und n_2, sowie Temperatur in Abhängigkeit von dem Abstand ρ zur Symmetrieachse. $T = T_0/(1 + \rho^4)$.
(a) $T_0 = 10.000°$K; (b) $T_0 = 20.000°$K.
Der Masstab von n_2 ist der zwanzigfache des von n_1 in Abb. 1 und Abb. 2.

Die Einheit von ρ ist somit der "Halbwertsradius." Dieser Ansatz stimmt mit dem für stationäre Bogenentladungen gefundenen flachen Verlauf von T überein. Gl. (9) ist theoretisch von ROMPE, THOURET und WEIZEL [12] für die achsennahen Teile des Bogens als gültig befunden.

Abb. 2 gibt Gl. (9) wieder, sowie n_1 und n_2 in Abhängigkeit von ρ, und zwar für $T_0 = 10.000°\text{K}$ bezw. $T_0 = 20.000°\text{K}$.

Wenn der ganze Entladungskanal z.B. auf die Kollimatorlinse des Spektrographen abgebildet wird, ergibt sich die Intensität einer Linie proportional

$$N = 2\pi \int_0^\infty \rho n_E \, d\rho \tag{10}$$

(Die obere Grenze ∞ ist eine in der Praxis zugelassene Extrapolation.) Wird statt dessen der Kanal auf den Spalt zentrisch abgebildet, gelangt in den Spektrographen nur Licht von einen Streifen durch die Achse, und die Intensität wird dann proportional

$$N = \int_0^\infty n_E \, d\rho \tag{11}$$

Die gemessene "mittlere" Temperatur $\bar{T}$ ergibt sich in beiden Fällen gemäss

$$\ln \frac{N_1}{N_2} = \frac{E_2 - E_1}{k\bar{T}}$$

Aus numerischer Integrierung der bezüglichen Kurven in Abb. 2 ergibt sich

		Gemäss Gl. (10)	Gemäss Gl. (11)
aus Abb. 2a mit $T_0 = 10.000°\text{K}$	$\bar{T} =$	7500°K	8300°K
aus Abb. 2b mit $T_0 = 20.000°\text{K}$	$\bar{T} =$	7700°K	8100°K

Wir sind somit, welche Art der Abbildung auch immer gewählt wird, zu dem Ergebnis gelangt, dass die spektroskopische Temperaturmessung etwa dieselbe Höhe der Temperatur ergeben wird, unabhängig von der Maximaltemperatur, ja sogar, dass die Verdopplung der Maximaltemperatur die gemessene scheinbare "Temperatur" erniedrigen kann.

Dieses willkürlich gewählte Beispiel zeigt die starke Begrenzung der Methode der Temperaturermittlung aus Spektrallinienintensitäten. Da das Strahlenbündel fast immer Gebiete verschiedener Temperaturen durchsetzt, wird die Intensität des Bündels nicht von dem heissesten Bereich bestimmt, sondern von demjenigen, welcher den grössten Beitrag zur Intensität liefert.

Ähnlich wie Mg, das STETTER [8] sowie CRAGGS und Mitarbeiter [5], [6] zur Temperaturermittlung benutzt haben, verhalten sich Cu und Fe, die von STETTER [8] bezw. BLITZER und CADY [7] verwendet sind. Diese drei Elemente haben alle ungefähr dieselbe Ionisierungsenergie, 7,6–7,9 eV. Für Stoffe mit niedrigeren Ionisierungsenergien liegt das Optimum bei niedrigeren Temperaturen. In Abb. 3 ist für BaI mit $E_I = 5{,}209$ eV die Emission der Linie $\lambda 5826{,}21$ Å mit einer Anregungsenergie von 3,54 eV gegen die Temperatur abgetragen, sowie die Emission zweier Linien von BaII mit $E_I = 10{,}00$ eV. Zur Berechnung sind auch hier die Gl : n (3) bis (8) herangezogen worden, nur mit den Daten für Ba

statt mit denjenigen für Mg. Die Lagen der Maxima der Kurven für BaI, MgI (in Abb. 1), und BaII stimmen mit den von Craggs u.a. [5], [6] für die verschiedenen Linien gefundenen Temperaturen überein, soweit die grosse Streuung der Messwerte bestimmte Schlussfolgerungen zulassen.

Um auch das Verhalten eines Molekülspektrums zu untersuchen, wird die Dissoziation und Anregung von CN ebenfalls berechnet. Dieses Molekül ist von Langstroth und McRae [13] herangezogen, um den radialen Temperaturverlauf eines Funkenkanals zu untersuchen. Wir rechnen hier mit Luft von 1 Atm Druck

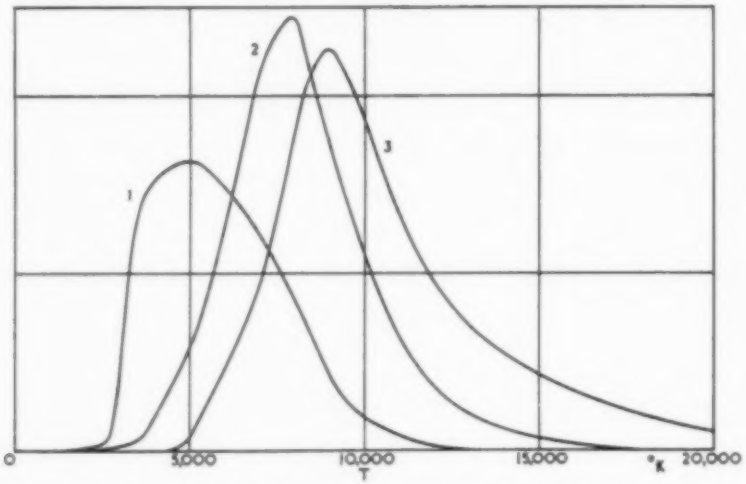

Abb. 3. Konzentration angeregter BaI- und BaII-Atome in Abhängigkeit von der Temperatur.
1. BaI Anr.-Energie 3,52 eV (λ5826,3 Å)
2. BaII Anr.-Energie 2,51 eV (λ4934,1 Å)
3. BaII Anr.-Energie 5,25 eV (λ4525,0 und 4900,0 Å)

und zwar mit vollständiger Dissoziation von N_2 in N. Das Massenwirkungsgesetz ergibt dann [10]:

$$\frac{p_C \cdot p_N}{p_{CN}} = K(T) \sim T^{3/2} e^{-D/kT} \tag{12}$$

wo der entscheidende Faktor im rechten Glied $e^{D/kT}$ ist (D = Dissoziationsenergie von CN). Wenn sowohl p_N als auch p_C als konstant angenommen werden—was berechtigt ist, solange $p_{CN} \ll p_N$—ist p_{CN} proportional $e^{D/kT}$ und die Intensität einer Bande mit der Anregungsenergie E ist:

$$I \sim n_E \sim T^{-5/2} e^{(D-E)/kT}.$$

Für die Dissoziationsarbeit D, die nicht mit Sicherheit bekannt ist, setzt Gaydon [14] als wahrscheinlichsten Wert 8,2 eV an. Damit und mit $E = 3{,}2$ eV für das violette Bandensystem ergibt sich die Kurve, die in Abb. 4 eingetragen ist. Ein abgeänderter D-Wert enthält hauptsächlich nur eine kleine Veränderung des T-Masstabes. Für die Verfolgung der Kurve zu niedrigeren Temperaturen hin, muss Rücksicht auf die umstrittene Grösse der Dissoziationsenergie von N_2

sowie auf den Dampfdruck des Kohlenstoffes genommen werden. Es zeigt sich jedoch immerhin, dass das Maximum der Emission des violetten CN-Systemes bei einer Temperatur $<8000°$ liegt. Bei der Temperaturermittlung aus der Intensitätsverteilung in einer Bande oder in einem Bandensystem kommt somit dem Bereiche der Niedrigeren Temperaturen das grösste Gewicht zu, ähnlich wie bei den oben erörterten Atomlinien. Dies steht mit den Ergebnissen der Utrechter Untersuchungen an Bogen [1] im Einklang. Ausserdem erweist sich, dass auch LANGSTROTH und MCRAE [13] unfähig waren, mit ihrer Methode Temperaturen

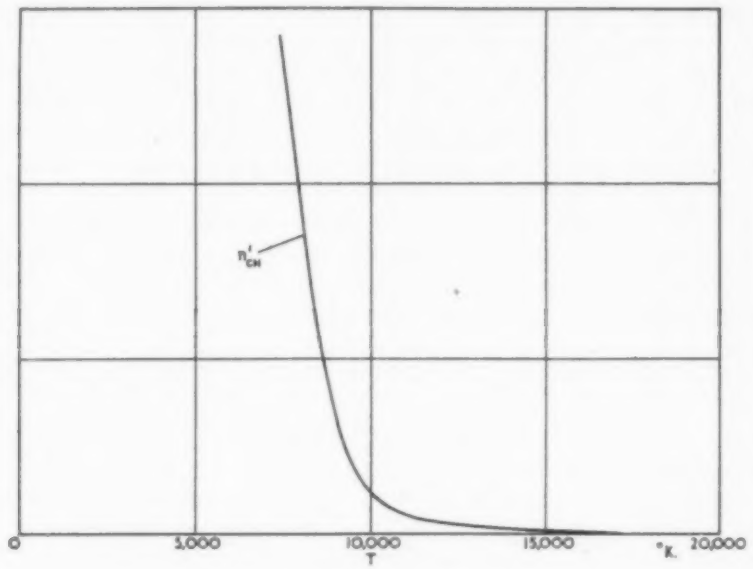

Abb. 4. Konzentration angeregter CN-Moleküle (Oberniveau der violetten Banden) in Abhängigkeit von der Temperatur.

höher als etwa 10.000° zu messen. Die von diesen Forschern vorgenommene Berücksichtigung der Inhomogenität ist unzureichend, da die Dissoziation vernachlässigt ist.

Schlussbemerkungen

Aus den oben durchgerechneten Beispielen sind folgende Schlüsse zu ziehen:

Die bisher angewandten Methoden für das spektroskopische Studium der Anregung in Funken sind nicht imstande, die zu erwartenden hohen Temperaturen zu messen. Statt dieser wird eine Temperatur indiziert, die gewissermassen für das strahlende Atom, Ion oder Molekül spezifisch ist: der Temperaturbereich, in welchem Licht emittiert wird, ist unten durch abnehmende Anregung, oben durch Zerfall des strahlenden Atomes usw. begrenzt. Nur durch Untersuchung räumlich zerlegter Funken, würde es möglich sein, den Einfluss der äusseren "kälteren" Teile der Entladung auszuschalten.

Die oben erwähnten Atome, Ionen, und Moleküle haben alle ziemlich niedrige

optimale Temperaturbereiche. Durch Linien hochionisierter Atome könnten höhere Temperaturen gemessen werden, wenn die Uebergangswahrscheinlichkeiten zu ermitteln wären.

Die zur Zeit vorliegenden Untersuchungen nach der hier erörterten Methode scheinen nicht endgültig die Frage beantwortet zu haben, ob es thermische Funkenentladungen gibt, und wie hoch in solchem Falle die Höchsttemperatur ist. Schlüsse über die Grösse der Ionisation, welche auf andere Art gezogen sind [4], deuten auf viel höhere Temperaturen hin.

Die obigen Ueberlegungen scheinen jedoch folgendes erwiesen zu haben: *Wenn* in einer Entladung quasithermodynamisches Gleichgewicht herrscht, *dann* führen unvermeidlich Versuche zur Messung der Temperatur nach der hier erörterten Methode zu den oben angeführten Komplikationen. Das entworfene Funkenmodell kann natürlich in quantitativer Hinsicht diskutiert werden; weitere experimentelle Untersuchungen werden sicherere Daten ergeben. Die Messwerte scheinen jedoch die erwartete Tendenz zu zeigen. Sofern die von verschiedenen Forschern berichteten Ergebnisse durch eine Temperatur beschrieben werden, so ist es keinesfalls sicher, dass die gemessene Temperatur die maximale ist.

Die Wirkung einer zeitlichen Änderung der Temperatur ist ähnlich wie die der räumlichen Inhomogenität. Ein Spektrogramm, das mehrere Phasen z.B. einer Funkenentladung umfasst, wird eine Temperatur indizieren, die keineswegs die maximale ist, auch nicht eine "Mitteltemperatur" sondern eine Temperatur, die oberhalb einer gewissen Grenze sehr wenig von der Maximaltemperatur abhängt.

VOL.
7
1955/5

Zusammenfassung

Die spektroskopischen Messungen der Temperatur in Funkenentladungen werden erörtert. Es wird auf die Bedeutung der unvermeidlichen kälteren Zonen, welche den Uebergang zwischen Höchsttemperatur und Zimmertemperatur vermitteln, hingewiesen. Eine Berechnung der Emissionsintensität in Abhängigkeit von der Temperatur führt unter plausiblen Annahmen zu dem Ergebnis, dass sämtliche bisher für Temperaturmessung herangezogenen Spektrallinien ihre maximale Emission zwischen 5000° und 10.000°K haben. Die genauere Durchrechnung eines speziellen Beispiels zeigt, dass die spektroskopisch sich ergebende Temperatur gegenüber der Verdopplung der Maximaltemperatur unempfindlich ist, und dass Maximaltemperatur und experimentelle Temperatur nicht immer korrelieren. Man kann deshalb aus derartigen Messungen noch keine Schlüsse für die höchsten Temperaturen in Funkenentladungen ziehen. Um dies zu erreichen, müssen Linien von hochionisierten Atomen und bekannter Uebergangswahrscheinlichkeiten herangezogen werden.

Literaturverzeichnis

[1] Smit, J. A.; *Physica* 1946 **12**, 683
[2] Lochte-Holtgreven, W., und Maecker, H.; *Z. Phys.* 1937 **105**, 1
[3] Rosseland, S.; *Theoretical Astrophysics*, Oxford 1936
[4] Craggs, J. D., and Meek, J. M.; *Proc. Roy. Soc.* 1946 **A186**, 241
[5] Braudo, C. J., Craggs, J. D., and Williams, G. C.; *Spectrochim. Acta* 1949 **3**, 546
[6] Williams, G. C., Craggs, J. D., and Hopwood, W.; *Proc. Phys. Soc.* 1949 **B62**, 49
[7] Blitzer, L., and Cady, W. M.; *J. Opt. Soc. Amer.* 1951 **41**, 440

[8] STETTER, A.; *Spectrochim. Acta* 1953 **5**, 350
[9] STETTER, A.; *Spectrochim. Acta* 1953 **5**, 460
[10] HULDT, L.; *Ark. f. Mat. Astr. o. Fys.* 1947 **34A**, Nr 30; Dissertation, Stockholm. Uppsala 1948
[11] LARENZ, R. W., und BARTELS, A. H.; *Naturwissenschaften* 1950 **37**, 164
[12] ROMPE, R., THOURET, W., und WEIZEL, W.; *Z. Phys.* 1944 **122**, 1
[13] LANGSTROTH, G. O., and MCRAE, D. R.; *Canad. J. Research* 1938 **A16**, 17
[14] GAYDON, A. G.; *Dissociation Energies*, 2nd ed. London 1953

VOL.
7
5/56

Spectrochimica Acta, 1955, Vol. 7, pp. 274 to 282. Pergamon Press Ltd., London

Infra-red spectra of polychloronaphthalenes

L. Cencelj and D. Hadži
University Chemical Laboratory and Institute Boris Kidrič, Academy, Ljubljana, Yugoslavia

(*Received* 8 *August* 1955)

Summary—Infra-red spectra between 1650 and 660 cm^{-1} of the complete range of dichloro- and trichloronaphthalenes, and nine of the isomers of tetrachloronaphthalenes, are presented. The possibility of applying correlation rules valid for benzene substitution in the naphthalene series is briefly discussed.

The published infra-red spectra of substituted naphthalenes are limited mainly to monosubstituted [1], [2], [3], and disubstituted [4], [5] naphthalenes respectively. Spectra of some polymethylnaphthalenes were published by Mosby [6]. No general correlation rules between the bands and the type of substitution were established. This is not surprising in view of the small number of available spectra and the large number of bands displayed by individual substituted naphthalenes. The present authors have collected a number of spectra of polychloronaphthalenes in the course of a study of the chlorination of naphthalene, and it is believed that these spectra might be of some use for similar analytical work.

Experimental

Most of the tri- and tetra-chloronaphthalenes came from the collection of the late Prof. W. P. Wynne, and were donated to us by the Imperial Chemical Industries, Dyestuffs Division. The authors wish to express their indebtedness to them for this generous gift. Di-, and some tri-chloronaphthalenes and 1,4,5,8-tetrachloronapthalene were prepared by one of us (L. C.), and had melting-points as described in the literature [7]. The spectra were recorded on a Perkin-Elmer Model 21 double-beam spectrophotometer, equipped with a NaCl prism. Parallel runs of each substance were made in the solid state (nujol mull) and in solution. Carbon tetrachloride was used in the region from 1650–835 cm^{-1}, and cyclohexane from 835—660 cm^{-1}; the thickness of the cell was 0·2 mm, and the solutions were 0·2 molal approximately.

The spectra of the solids are presented in Fig. 1. The exact positions of strong and medium bands are given in Table 1. In most cases there is little difference between the position of the bands in the solid and the solution respectively, but in some instances, e.g., 1,5-, 1,7-, 2,3-dichloronaphthalenes, etc., the difference for some bands is considerable, and there are even differences in the number of bands observed, as 1,3-, 1,6-, 2,7-dichloronaphthalenes and others.

Discussion

The discussion of the spectra will be limited to the region between 900 and 690 cm^{-1}. In this region, a number of strong bands appear in the spectra of substituted

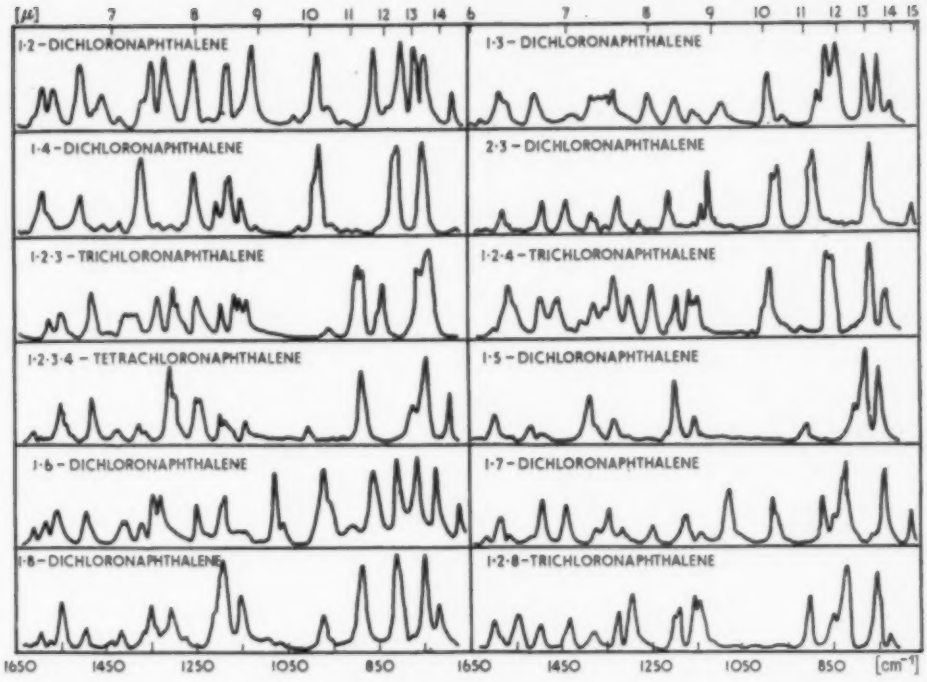
[μ] 7 8 9 10 11 12 13 14 6 7 8 9 10 11 12 13 14 15
1·2 – DICHLORONAPHTHALENE
1·3 – DICHLORONAPHTHALENE
1·4 – DICHLORONAPHTHALENE
2·3 – DICHLORONAPHTHALENE
1·2·3 – TRICHLORONAPHTHALENE
1·2·4 – TRICHLORONAPHTHALENE
1·2·3·4 – TETRACHLORONAPHTHALENE
1·5 – DICHLORONAPHTHALENE
1·6 – DICHLORONAPHTHALENE
1·7 – DICHLORONAPHTHALENE
1·8 – DICHLORONAPHTHALENE
1·2·8 – TRICHLORONAPHTHALENE
1650 1450 1250 1050 850 1650 1450 1250 1050 850 [cm⁻¹]

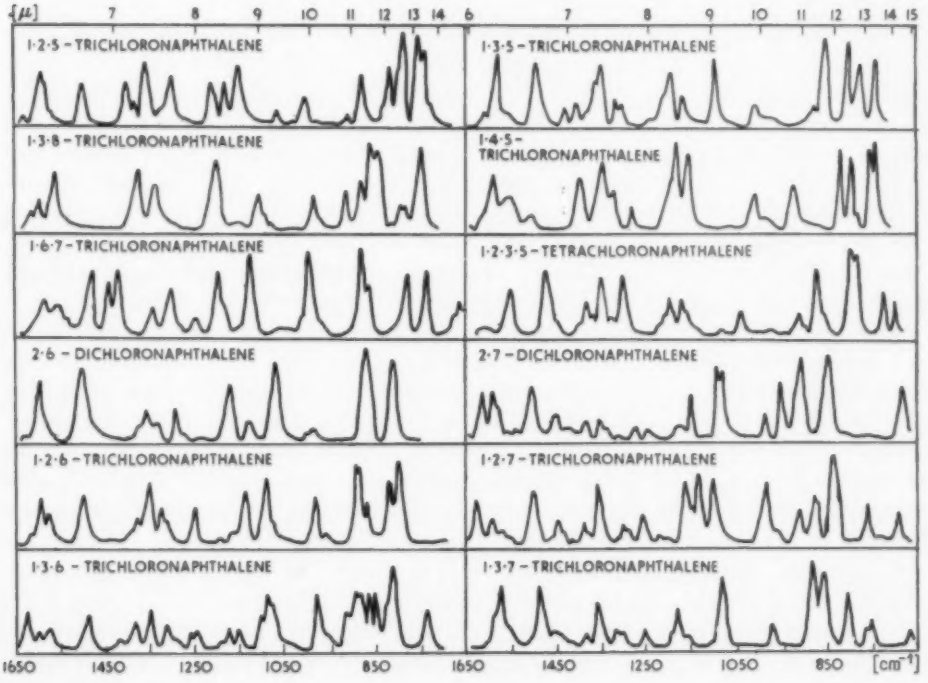
[μ] 7 8 9 10 11 12 13 14 6 7 8 9 10 11 12 13 14 15
1·2·5 – TRICHLORONAPHTHALENE
1·3·5 – TRICHLORONAPHTHALENE
1·3·8 – TRICHLORONAPHTHALENE
1·4·5 – TRICHLORONAPHTHALENE
1·6·7 – TRICHLORONAPHTHALENE
1·2·3·5 – TETRACHLORONAPHTHALENE
2·6 – DICHLORONAPHTHALENE
2·7 – DICHLORONAPHTHALENE
1·2·6 – TRICHLORONAPHTHALENE
1·2·7 – TRICHLORONAPHTHALENE
1·3·6 – TRICHLORONAPHTHALENE
1·3·7 – TRICHLORONAPHTHALENE
1650 1450 1250 1050 850 1650 1450 1250 1050 850 [cm⁻¹]

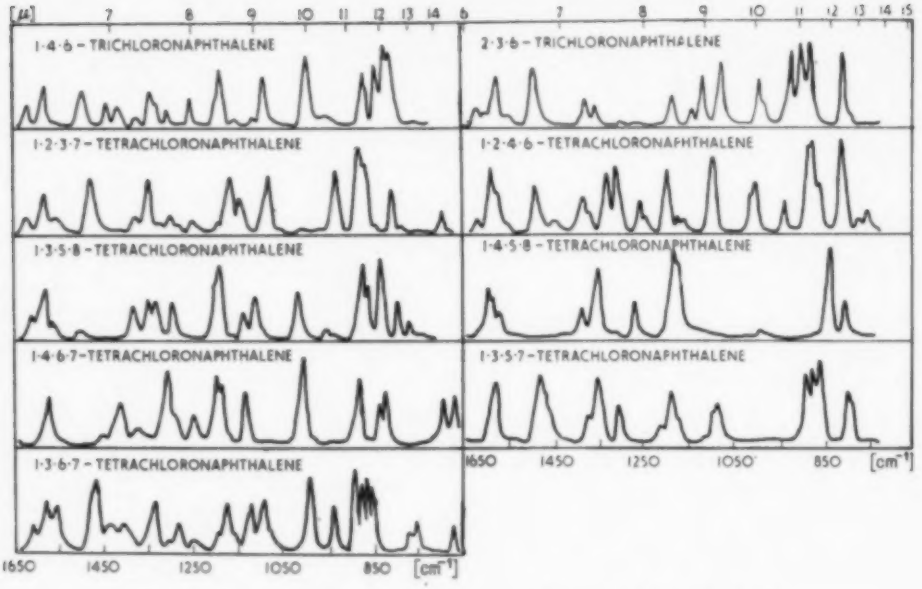

Fig. 1. Infra-red spectra of polychloronaphthalenes (mulled with Nujol) in the range between 1650 and 660 cm^{-1}.

naphthalenes, as in other aromatics. These are known to arise from the out-of-plane deformation vibrations of the hydrogen atoms attached to the rings. Amongst the various attempts at a correlation of the band positions with the substitution pattern, the most promising one seems to be along the lines developed for the benzene series by THOMPSON and his co-workers [8], and summarized by COLTHUP [9] and, recently, by BELLAMY [10]. The band positions are correlated with the number of adjacent hydrogen atoms remaining round the ring. The comparison of the band positions in chloronaphthalenes, and the corresponding methylnaphthalenes, as well as some other disubstituted naphthalenes, shows a relatively good agreement with these correlation rules. This is illustrated by some examples in Table 2. The pattern followed by the bands in this region seems to be characteristic of the type of substitution, independent of the nature of the substituents. In general, the number of bands present considerably exceeds that expected on the basis of these rules. This is a serious limitation to the applicability of the correlation rules for the determination of the type of substitution. The presence of a band is *not* a sufficient proof of the presence of the corresponding group of hydrogen atoms. However, the absence of a band required by a certain type of substitution seems to exclude it. As an example, the band appearing between 770 and 735 cm^{-1} might be taken. This band is characteristic of four adjacent hydrogen atoms, and it could be expected to appear in the spectra of naphthalenes containing one unsubstituted ring. In fact, a strong band is present in the expected interval in all such cases, but it is also present in many other substituted naphthalenes (e.g., 1,5-, 1,6-, and 1,7-dichloronaphthalenes). Similarly, a band between 900 and 860 cm^{-1} is expected to appear for one isolated hydrogen atom, but it is shown

Table 1. Infra-red strong and medium bands of di-, tri-, and tetrachloronaphthalenes in nujol(N) and in solution (S) in cm^{-1}

1,2-dichloro-		1,3-dichloro-		1,4-dichloro-		2,3-dichloro-	
N	S	N	S	N	S	N	S
1590	1590	1618	1626	1590	1592	1575	1580
1565	1563	1585	1587	1504	1505	1493	1497
1506	1506	1563	1563	1456	1458	1437	1439
1456	1458	1495	1502	1370	1374	1344	1344
1370	1370	—	1361	1255	1256	1316	1318
1353	1353	1355	1350	1203	1203	1269	1266
1321	1325	1344	—	1190	1192	1202	1202
1256	1256	1333	1335	1182	1186	1136	1139
1171	1172	1248	1252	1156	1159	1121	1120
1131	1133	1190	1196	1145	1145	971	973
983	985	1149	1151	1031	1031	962	952
862	865	—	1143	986	987	895	887
803	805	1093	1099	952	952	889	881
765	767	1083	1089	901	901	758	744
741	741	975	978	821	822	663	662
677	677	952	952	816	816		
		873	880	755	756		
		—	862	677	676		
		855	853				
		841	844				
		763	766				
		744	745				
		737	—				
		713	712				

1,2,3-trichloro-		1,2,4-trichloro-		1,2,3,4-tetrachloro-		1,5-dichloro-	
N	S	N	S	N	S	N	S
1580	1575	1621	1621	1560	1548	1600	1595
1555	1550	1577	1577	1486	1488	1511	1506
1488	1488	1499	1499	1316	1321	1493	1493
1410	1412	1446	1447	1304	1309	1392	1389
—	1401	1406	1404	1259	1258	1364	1361
1346	1344	1351	1355	1250	1250	1330	1330
1318	1319	1337	1338	1205	1205	1215	1212
1299	1304	1302	1302	1192	—	1198	1200
1252	1253	1252	1253	1152	1153	1152	1151
1206	1206	1202	1200	895	896	—	1057
1167	1165	1167	1167	778	778	906	—
1153	1149	1156	1151	755	757	794	794
1140	1142	1144	1143	698	697	778	779
953	954	1003	—			744	745
895	897	996	995				
879	880	858	864				
849	849	853	856				
843	—	760	758				
761	764	720	718				
—	757						
745	745						

Table 1—*continued*

1,6-dichloro-		1,7-dichloro-		1,8-dichloro-		1,2,5-trichloro-	
N	S	N	S	N	S	N	S
1618	1623	1618	1621	1600	1597	1621	1618
1585	1592	1587	1603	1558	1553	1590	1587
1560	1563	1560	1560	1427	1422	1499	1493
1495	1497	1493	1497	1362	1361	1401	1401
1412	1416	1433	1435	1319	1325	1350	1351
1350	1351	1353	1351	1198	1198	1316	1318
1330	1335	1318	1319	1155	1153	1307	1304
1250	1250	1245	1247	977	977	1212	1214
1198	1200	1193	1195	888	891	—	1200
1189	1190	1183	1183	813	813	1174	1172
1080	1084	1081	1085	730	751	—	1155
1058	1060	979	982	726	726	1144	1140
969	971	865	877			1071	1070
866	870	843	849			1015	1015
—	817	828	826			883	882
812	810	820	823			819	816
779	781	741	741			791	792
737	741	667	670			754	755
674	676					745	739

1,2,8-trichloro-		1,3,5-trichloro-		1,3,8-trichloro-		1,4,5-trichloro-	
N	S	N	S	N	S	N	S
1600	1595	1590	1585	1610	1615	1585	1590
1546	1543	1488	1490	1587	1592	1555	1555
1499	1499	1441	1437	1553	1550	1497	1511
1431	1431	1404	1404	1330	1330	1391	1395
1325	1323	1370	1368	1196	1196	1350	1353
1295	1297	1359	1359	1111	1114	1326	1330
1205	1200	1321	1319	978	980	1285	1285
1196	—	1306	1304	905	910	1198	1199
1157	1159	1211	1212	873	—	1183	1188
1145	1144	1202	1200	855	862	1157	1159
899	906	1161	1155	848	848	1005	1008
840	835	1107	1107	792	—	916	919
822	823	1014	1018	786	786	821	821
749	750	872	865	749	750	797	800
726	729	858	853			758	759
		796	798			744	747
		774	775				
		732	737				

Table 1—continued

1,6,7-trichloro-		1,2,3,5-tetrachloro-		2,6-dichloro-		2,7-dichloro-	
N	S	N	S	N	S	N	S
1585	1582	1577	1577	1587	1587	1618	1626
1560	1558	1475	1477	1497	1497	1582	1587
1481	1481	1381	1393	—	1368	1493	1497
1441	1441	1346	1346	1359	1359	1355	1355
1420	1420	1295	1294	1333	1332	1319	—
1344	1342	1212	1214	1266	1266	1264	—
1304	1304	1202	1200	1175	1176	1230	1238
1244	1245	1170	1171	1139	1135	1181	1172
1200	1198	1159	1156	1131	—	1136	1139
1126	1127	1033	1034	1071	1075	1087	1082
999	995	911	911	874	873	1078	1078
—	903	872	874	811	800	971	—
879	881	796	794			945	946
862	870	789	787			906	—
785	781	735	735			901	901
738	738	699	697			—	891
677	676					841	834
664	663					665	662

1,2,6-trichloro-		1,2,7-trichloro-		1,3,6-trichloro-		1,3,7-trichloro-	
N	S	N	S	N	S	N	S
1592	1587	1621	1618	1621	1621	1595	1592
1563	1555	1585	1582	1587	1587	1585	1582
1493	1490	1497	1497	1560	1560	1563	1567
1389	1374	1439	1439	1490	1493	1490	1488
1351	1347	1353	1351	1416	1416	1441	1439
1318	1317	1294	1294	—	1408	1353	1351
1305	1307	1250	1248	1348	1344	1321	1319
1252	1250	1155	1153	1321	1321	1311	1309
1168	1163	1145	1147	1242	1253	1250	1248
1148	1147	1135	1135	1196	1198	1196	1196
1134	1135	1095	1090	1183	1183	1183	1182
1086	1086	987	990	1149	1149	1083	1085
983	985	907	907	1101	1103	988	988
884	882	875	876	1087	1089	876	877
879	877	871	—	976	978	858	864
861	861	833	833	909	912	840	845
815	817	753	755	891	890	805	802
800	799	683	683	885	—	761	760
				866	866	752	754
				861	—		
				846	844		
				810	817		
				719	720		

Table 1—*continued*

1,4,6-trichloro-		2,3,6-trichloro-		1,2,3,7-tetrachloro-		1,2,4,6-tetrachloro-	
N	S	N	S	N	S	N	S
1618	1618	1621	1626	1616	1618	1616	1613
1587	1587	1580	1590	1582	1577	1582	1577
1495	1497	1488	1488	1548	1548	1567	1563
1437	1439	—	1439	1484	1481	1490	1490
1416	1418	1379	1381	—	1408	1435	1433
1344	1348	1346	1348	1346	1346	1381	1385
1333	1337	1181	1179	1292	1294	1323	1321
1300	1299	1139	1143	1250	1250	1304	1304
1250	1252	1121	1122	1167	1168	1250	1252
1190	1193	1080	1080	1143	1143	1188	1185
1188	1188	975	974	1089	1088	1167	1167
1147	1152	920	919	932	932	1092	1093
1106	1107	897	894	880	878	1009	1005
1087	1089	885	880	873	—	1000	997
990	990	810	801	852	853	930	930
872	877			807	801	884	881
845	845			775	773	876	—
824	820			679	679	864	867
817	—					817	817
						769	769
						752	753

1,3,5,8-tetrachloro-		1,4,5,8-tetrachloro-		1,4,6,7-tetrachloro-		1,3,5,7-tetrachloro-		1,3,6,7-tetrachloro-	
N	S	N	S	N	S	N	S	N	S
1605	1603	1587	1580	1577	1582	1580	1580	1618	1618
1577	1585	1570	1563	1475	1475	1473	1475	1582	1585
1555	1550	1538	1546	1416	1418	1361	1370	1553	1555
1488	1486	1344	1346	—	1399	1300	1302	1473	1475
1376	1376	1266	1264	1302	1305	1205	1205	1414	1414
1342	1342	1178	1176	1292	1295	1188	1188	1337	1339
1326	1326	1170	—	1247	1247	—	1181	1282	1285
1287	1287	826	827	1198	1198	1094	1094	1196	1195
1195	1192	796	794	1188	1188	1087	1087	1181	1182
1188	1188			1133	1134	884	—	1126	1130
1130	1130			1008	1009	880	881	1095	1096
1107	1107			882	884	865	870	996	998
1016	1016			832	—	794	—	939	939
932	933			826	821	784	786	891	894
867	868			691	690			881	880
857	855			669	668			866	868
826	823							851	853
789	787							845	—
765	765							—	762
								748	744
								667	670

VOL. 7 1955/5

Table 2. Infra-red absorption bands of some substituted naphthalenes between 900 and 690 cm^{-1}

1,2-dichloro-	1,2-dimethyl-	1-chloro-2-acetamino-	2-nitro-1-naphthol-	Number of adjacent ring H-atoms	Expected bands
862 m.	865 s.	826 w.	809 s.	2	860–800 v.s.
803 v.s.	808 s.	794 w.	797 m.		
765 s.	786 s.	784 s.	769 s.	4	770–735 v.s.
741 s.	743 s.	781 s.	736 s.		
	723 m.	738 s.			
		719 s.			

1,7-dichloro-	1,7-dimethyl-	1-nitro-7-amino-	1-nitro-7-chloro-	Number of adjacent ring H-atoms	Expected bands
865 m.	870 m.	858 s.	875 s.	1	900–860 m.
843 w.	—	843 s.	833 s.	2	860–800 v.s.
828 m.	823 s.	823 s.	804 m.		
820 s.	—	794 s.	794 s.	3	810–750 v.s.
741 s.	752 s.	746 s.	743 m.		
	719 s.	734 s.	734 m.		

1,8-dichloro-	1,8-dimethyl-	1,8-diamino-	1,8-dinitro-	Number of adjacent ring H-atoms	Expected bands
888 s.	886 w.	889 w.	840 s.	3	810–750 v.s.
813 s.	814 s.	866 m.	806 s.	3	
750 s.	800 m.	814 m.	755 s.	3	
726 m.	789 m.	776 m.	733 m.	3	726–680 m.
	773 s.	765 s.	694 m.	3	
		758 s.			

1,3,5-trichloro-	1,3,5-trimethyl-	1,3,8-trichloro-	1,3,8-trimethyl-	Number of adjacent ring H-atoms	Expected bands
872 w.	—	873 s.	879 w.	1	900–860 m.
858 v.s.	854 v.s.	856 s.	855 v.s.	1	
796 v.s.	796 s.	848 s.	—	3	810–750 v.s.
774 s.	746 s.	792 m.	791 m.	3	
732 s.		786 m.	—	3	
		749 s.	762 v.s.	3	

1,3,5,8 tetrachloro-	1,3,5,8-tetramethyl-	1,4,6,7-tetrachloro-	1,4,6,7-tetramethyl-	Number of adjacent ring H-atoms	Expected bands
867 s.	881 w.	883 s.	870 s.	1	900–860 m.
857 m.	852 v.s.	840 s.	816 s.	2	860–800 v.
826 s.	812 s.	830 s.	—	2	
789 m.	785 m.				

1,4,5,8-tetrachloro-	1,4,5,8-tetramethyl	Number of adjacent ring H-atoms	Expected bands
826 v.s.	817 v.s.	2	860–800 v.s.
796 m.	768 m.		

also by substituted naphthalenes in which no such atom is present. These conclusions are in a good agreement with the ones advanced by Bellamy [10].

The above results have been applied to the analysis of commercial mixtures of polychloronaphthalenes used as insulating waxes in the production of condensers. A sample of "Nibren D88" has been separated into twenty-two fractions by chromatography on a column of activated alumina, using light benzine as solvent and light benzine with 1 per cent benzene as eluent. The spectra of each fraction were recorded after the evaporation of the solvent. The first three fractions contained 1,3,5,7-tetrachloronaphthalene. In the next six fractions 1,4,6-trichloronaphthalene was the main component. Fractions 10–15 contained mainly 1,4,5-trichloronaphthalene and fractions 16–22 mainly 1,4,5,8-tetrachloronaphthalene. The details of this analysis will be dealt with elsewhere.

Acknowledgements—The authors wish to express their gratitude to Dr. Delia J. Agar for a critical reading of the paper, and to the Farbenfabriken Bayer, Leverkusen, for a sample of Nibren.

References

[1] Lecomte, J.; *Compt. Rend.* 1939 **208** 1636. *J. Phys. et Radium* 1939 **10** 423.
[2] Anderson, D. G., and Smith, J. C.; *J. Inst. Petrol.* 1952 **38** 424.
[3] Ferguson, J., and Werner, R. L.; *J. Chem. Soc.* (London) 1954 3645.
[4] Cannon, C. G., and Sutherland, G. B. B. M.; *Spectrochimica Acta* 1951 **4** 373.
[5] American Petroleum Institute, Catalog of Infra-red spectral Data.
[6] Mosby, W. L.; *J. Amer. Chem. Soc.* 1952 **74** 2564.
[7] *Elsevier's Encyclopaedia of Organic Chemistry* 1948 **12B** 301.
[8] Thompson, H. W.; *J. Chem. Soc.* (London) 1948 329.
[9] Colthup, N. B.; *J. Optical Soc. Amer.* 1950 **40** 397.
[10] Bellamy, L. J.; *The Infra-red Spectra of Complex Molecules*, pp. 64–67.

Spectrochimica Acta, 1955, Vol. 7, pp. 283 to 306. Pergamon Press Ltd., London

The theoretical derivation of fluorescent X-ray intensities from mixtures*

JACOB SHERMAN
Philadelphia Naval Shipyard, Philadelphia 12, Pennsylvania

(*Received* 4 *August* 1955)

Summary—A mixture of elements irradiated by a sufficiently energetic X-ray beam absorbs the incident X-rays and re-emits other X-rays, the wavelengths of which are characteristic of the elements in the sample, and the intensities of which may be correlated with their concentrations. The problem is to correlate I_{fi}, the intensity of the X-ray spectrum emitted by an element of atomic number Z_i with c, μ, and τ (concentration, absorption coefficient, and emission coefficient, respectively) of the elements in the sample. The correlation is complicated by the fact that the fluorescent radiation from elements of higher Z will excite additional radiation from elements of lower Z.

Using integral methods, a mathematical analysis of the absorption–re-emission process yields explicit closed formulae, when the incident beam is monochromatic, for $I_{fi}(c, \mu, \tau)$ in terms of logarithms and ψ-functions. A preliminary investigation suggests that the theory of means may offer a theoretical solution when the incident beam is polychromatic. Graphical methods make it possible to invert the formulae and express c in terms of I_{fi}, which makes chemical analysis possible. The use of a reference sample of known composition in the same elements as the sample in question, makes it possible to derive a close approximation to the chemical analysis when the incident beam is polychromatic. A brief comparison of computed and measured intensities from samples of known composition shows a good agreement.

The report closes with appendices giving mathematical details, a numerical table of $\psi(x)$, $(0 \leq x \leq 1)$, and the fluorescence yields for some elements.

1. Introduction

THE intensity of the characteristic X-ray spectrum emitted by an element in a mixture irradiated by a sufficiently energetic X-ray beam of fixed intensity is, in general, not simply a function of the concentrations and absorption coefficients of the various elements in the mixture. There is, in general, an additional dependency on the differences between the atomic numbers of the elements. This effect, often termed the "mutual enhancement effect," is due to the fact that the characteristic spectra of elements of higher atomic numbers are sufficiently energetic to excite the spectra of elements of lower atomic numbers. The added contribution to the intensity of the spectra of lower atomic number, or enhancement, may be highly significant. Indeed, under certain conditions, the enhancement may be greater than the intensity due to the primary incident beam.

By imposing certain conditions, which are really not too restrictive, it is possible to derive closed formulae correlating fluorescent X-ray intensity with composition of the mixture. Although some of the formulae are rather lengthy, the only functions involved are logarithms, with one exception. The exception is the Abel-Legendre χ function, which is easily tabulated. A short table of $\psi(\chi)$ is given in an appendix to this paper.

* The views expressed by the author are his own and do not necessarily represent those of the Department of the Navy.

2. Preliminary considerations, conditions, and nomenclature

Consider a three-component mixture of elements, M, of atomic numbers Z_1, Z_2, Z_3 ($Z_1 < Z_2 < Z_3$) with concentrations c_1, c_2, and c_3, respectively, ($c_1 + c_2 + c_3 = 1$). (For a specific representation one may regard Z_1, Z_2, Z_3 as 24, 26, and 28, i.e., Cr, Fe, and Ni.)

Referring to Fig. 1, the incident beam enters the sample at a fixed entrance angle θ', while the fluorescent beam is measured at exit angle θ''. The angles are measured with respect to the normal to the surface of the mixture. The incident beam may be traced as follows. It is partly absorbed at depth l by an elementary thickness dl with emission of the characteristic spectra of Z_3, Z_2, and Z_1. The spectrum of Z_3 is emitted at l over all space angles, and is partly

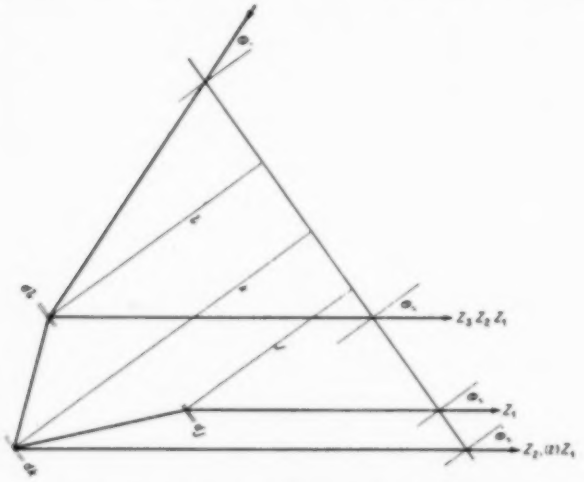

Fig. 1. Absorption and re-emission of X-rays.

absorbed at depth κ by an elementary layer $d\kappa$ with emission of the spectra of Z_2 and Z_1. In like manner, the spectrum of Z_2 emitted at l is partly absorbed at κ by an elementary layer $d\kappa$ with independent emission of the spectrum of Z_1. Similarly, the spectrum of Z_2 is emitted at κ over all space angles, and is partly absorbed at j by an elementary layer dj with emission of the spectrum of Z_1. The fluorescent spectra emitted at all layers are measured at angle θ''.

The following considerations are to be noted:

(1) The final intensities of the spectra of Z_3, Z_2, and Z_1 are the sums of one, two, and four components, respectively.

(2) The entrance and exit beams may be considered well collimated (in particular the window of the detector subtends a small angle at the radiator), and hence may be treated according to "narrow beam" theory.* However, the interior beams are distributed isotropically over all space angles and must be treated according to "broad beam" theory.

* The change from a collimated beam to a broad or divergent beam, as in curved crystal spectrometers is discussed in Section 4(6).

(3) To obtain quantitative estimates for the intensities of the various spectra at the surface of an "infinitely thick" specimen, it is necessary to integrate the elementary contributions from dl, $d\kappa$, and dj over the interval $(0, \infty)$,* and, for the interior beams, over all space angles. It is to be anticipated that the depth effects will involve functions of $|l - \kappa|$ and $|j - \kappa|$.

In order not to involve the mathematical analysis with unnecessary difficulties, the following conditions are imposed on the problem:

(1) The intensities of the incident and fluorescent beams are to be measured only at the surface of the specimen.

(2) The range of atomic numbers (Z) will be limited from 22 to about 50 (Ti to Sn), so that only the κ spectra of the elements are involved.

(3) The κ spectrum of an element will be considered as consisting of only one line, $\kappa\alpha$.

(4) The incident beam is monochromatic with an energy not more than 50 kV, so that the photoelectric effect is the only interaction that need be considered.

(5) Diffuse scattering will be neglected.

(6) The mixture will consist at most of three elements, or, the mixture will be analysed only for the elements of the three highest atomic numbers. While the nomenclature or symbolism used in papers on radiation transfer is not standardized, the following usage is rather common:

Z_i the atomic number or name of an element.

c_i the concentration of Z_i in the mixture; $\Sigma c_i = 1$.

θ' θ'' entrance and exit angles, respectively.

μ_{ij} the absorption coefficient of element Z_i for a beam of wavelength λ_j. The units of μ are cm^2/g. μ is equal numerically to values tabulated as μ/ρ, or mass absorption coefficient. As is customary in radiation theory, length will be measured as mass/cm^2, or superficial density. Frequent use will be made of

μ_{ij_j} the absorption coefficient of element Z_i for the fluorescent ($\kappa\alpha$) line of element Z_j.

ω_i the fluorescence yield of element Z_i, i.e., the ratio of the number of photons of X-radiation emitted by an atom to the number of photons absorbed from the exciting beam. ω_i is always less than 1 and independent of λ (5, 9).

r_i the "κ" jump for Z_i, i.e., the ratio of the absorption coefficients on the high-frequency and low-frequency sides of the κ discontinuity for Z_i. For elements considered in this paper, r_i is about 8 or 9 (5, 9).

I_i the intensity of a beam of wavelength λ_i measured as the rate of flow of photons.

μ', μ'' $\mu/\cos\theta'$ and $\mu/\cos\theta''$, respectively.

Consider an elementary slab of M of thickness dl at a distance l from a source of exciting monochromatic radiation of wavelength λ_j and of unit intensity (number of photons per unit of time). λ_j is less than the wavelength of the κ

* For a thin sample the interval is $(0, t)$.

absorption discontinuity of Z_i. Then the absorption by the elementary slab is $I(l)\mu_{\cdot j}\,dl$, where $I(l)$ is the intensity of the incident beam at l and $\mu_{\cdot j}$ is the absorption coefficient of M for λ_j. But $\mu_{\cdot j} = c_1\mu_{1j} + c_2\mu_{2j} + c_3\mu_{3j}$. Hence, the absorption by component Z_i in the elementary slab is $I(l)c_i\mu_{ij}\,dl$. It is well known that, under these conditions, the intensity of the fluorescent X-ray spectrum emitted by Z_i is $I(l)c_i\omega_i\left(1 - \frac{1}{r_i}\right)\cdot\mu_{ij}\,dl = I(l)\tau_{ij}\,dl$, where τ_{ij} may be considered as an emission coefficient corresponding to μ_{ij} as the absorption coefficient.

The intensity of the exciting beam at l will depend whether it is considered as a "narrow" or "broad" beam. If it is a *narrow beam* (i.e., subtending an elementary solid angle), propagated at an angle θ' with respect to l, then the intensity at l is $e^{-\mu l/\cos\theta'}$, the absorption is $(\mu_{ij}/\cos\theta')\cdot e^{-\mu l/\cos\theta'}\,dl$, and the fluorescent emission is $\tau'_{ij}e^{-\mu' l}\,dl$ (the primes indicate division of the symbol by $\cos\theta'$).

If the exciting beam is *broad*, isotropically distributed over all solid angles (spherical symmetry), the mean value of $I(l)$ is $\int_0^{\pi/2} e^{-\mu l/\cos\beta}\sin\beta\,d\beta$ and the corresponding emission will be measured by $\tau_{ij}\,dl\int_0^{\pi/2} e^{-\mu l/\cos\beta}\,(\sin\beta/\cos\beta)\cdot d\beta$. Substitution of $x = \sec\beta$ in the integral will transform it to $\tau_{ij}\,dl\int_1^\infty \frac{e^{-\mu l x}}{x}\,dx$. The functions $\int_1^\infty e^{-tx}x^{-n}\,dx$ are called integro-exponential functions (1; 4) of order n, and are usually written as $E_n(t)$. (The integral representation of $E_n(t)$ is valid only for $t > 0$.) Hence, the fluorescence intensity is $\tau_{ij}\,dl\cdot E_1(\mu l)$.

To summarize, the element of intensity of fluorescent radiation (1) for a *narrow* beam is $\tau'_{ij}e^{-\mu' l}\,dl$, and (2) for a broad beam is $\tau_{ij}E_1(\mu l)\,dl$.

3. Fluorescent intensity integrals

The integrals for the fluorescent beam intensities from M may now be written directly by reference to Fig. 1.

The following conditions will be recalled:

(a) The incident beam is monochromatic with wavelength λ_j sufficiently small to excite the spectra of Z_1, Z_2, Z_3. It is to be considered as of unit intensity at the surface of the specimen.

(b) The incident and exit (fluorescent) beams are narrow. The interior beams are broad.

(c) The atomic numbers are sufficiently far apart for the $\kappa\alpha$ lines of the elements of higher atomic numbers to be shorter than the absorption edges of the elements of lower atomic number.

(d) The specimen is "infinitely" thick.

$$I_{f3} = \tau'_3\int_0^\infty dl\cdot e^{-(\mu'+\mu'')\rho l} \tag{1}$$

$$I_{f2} = \tau'_2\int_0^\infty dl\cdot e^{-(\mu'+\mu'')\rho l} + \tau'_3\tau_{2f3}\int_0^\infty dl\int_0^\infty d\kappa\cdot e^{-(\mu' l+\mu''\rho\kappa)}E_1(\mu_{f3}\,|l-\kappa|) \tag{2}$$

VOL 7 1955/

$$I_{f1} = \tau'_1 \int_0^\infty dl \, . \, e^{-(\mu' + \mu''_{f1})l} \tag{3}$$

$$+ \tau'_3 \tau_{1f3} \int_0^\infty dl \int_0^\infty d\kappa \, e^{-(\mu' l + \mu''_{f1}\kappa)} \, E_1(\mu_{f3} \, |l - \kappa|)$$

$$+ \tau'_2 \tau_{1f2} \int_0^\infty dl \int_0^\infty d\kappa \, e^{-(\mu' l + \mu''_{f1}\kappa)} \, E_1(\mu_{f2} \, |l - \kappa|)$$

$$+ \tau'_3 \tau_{2f3} \tau_{1f2} \int_0^\infty dl \int_0^\infty d\kappa \int_0^\infty dj \, e^{-(\mu' l + \mu''_{f1} j)} \, E_1(\mu_{f3} \, |l - \kappa|) \, . \, E(\mu_{f2} \, |\kappa - j|)$$

Except for the considerations discussed below, these integrals can be evaluated by direct computation, using the ordinary techniques of interchanging the order of integration (when E_1 is in the integrand), and integration by parts. However, the computation is rather lengthy, so the details of the computation will be reserved for Appendix I.

However, two difficulties arise in the reduction of the integrals, and these may be resolved as follows:

(1) Depending on the particular numerical value of the parameters, E_1 may occur in an integrand with a negative argument in the reduction of (3). The definition of $E_1(t) = \int_1^\infty \frac{e^{-tx}}{x} \, dx$ holds only for $t > 0$, since $E_1(t)$ has a logarithmic singularity at the origin ($t = 0$). However, the definition of $E_1(t)$ can be extended to negative values of t as follows. The exponential integral is defined as follows:

$$\mathcal{E}i(t) = \int_{-\infty}^{t} e^x x^{-1} \, dx, \tag{4}$$

which is valid for $t > 0$ provided that, when $t > 0$, $\mathcal{E}i(t)$ is interpreted in the sense of the Cauchy principal value

$$\mathcal{E}i(t) = \lim_{\delta \to 0} \left[\int_{-\infty}^{-\delta} e^x x^{-1} \, dx + \int_{\delta}^{t} e^x x^{-1} \, dx \right].$$

It follows from the definitions that

$$E_1(t) = \int_1^\infty \frac{e^{-tx}}{x} \, dx = \int_t^\infty \frac{e^{-x}}{x} \, dx = \int_{-t}^{-\infty} \frac{e^x}{x} \, dx = -\int_{-\infty}^{-t} \frac{e^x}{x} \, dx = -\mathcal{E}i(-t) \tag{5}$$

$$E_1(-t) = -\int_{-\infty}^{t} \frac{e^x}{x} \, dx = -\int_{-\infty}^{-t} \frac{e^x}{x} \, dx - \int_{-t}^{t} \frac{e^x}{x} \, dx \qquad (t > 0)$$

$$= \int_t^\infty \frac{e^{-x}}{x} \, dx + \int_{-t}^{t} \frac{e^{-x}}{x} \, dx$$

$$= \int_1^\infty \frac{e^{-tx}}{x} \, dx + \int_{-1}^{1} \frac{e^{-tx}}{x} \, dx$$

$$E_1(-t) = E_1(t) + S(t) \qquad (t > 0) \tag{6}$$

Where $S(t)$ is defined in the sense of a principal value.

Most computations of (3) bring in, in the same formula, either the function $E_1(t)$ or $-\mathcal{E}i(-t)$, according as $t > 0$ or $t < 0$. It is therefore convenient to consider $E_1(t)$ as defined for all values of t, in spite of the fact that the positive branch ($t > 0$) is not the analytic continuation of the negative branch ($t < 0$). Tables of numerical values of $E_n(t)$ have been computed, but there is no need for them in the present application, since E_1 occurs only in an integrand, not in the final formula.

(2) The reduction of (3) makes frequent use of integrals of the form

$$\int \frac{\log (a + bx)}{x}\, dx.$$

These integrals are not expressible in terms of the commonly used transcendental functions. It is convenient, for present purposes, to define the Abel-Legendre ψ-function as follows:

$$\int \frac{\log (a + bx)}{x}\, dx = \begin{matrix} \log a \log x - \psi\left(-\frac{bx}{a}\right) \\ \frac{1}{2}\log^2 bx + \psi\left(-\frac{a}{bx}\right) \end{matrix} \tag{7}$$

The ψ-function has been defined in other ways, the more usual ones being

$$\psi(x) = -\int_0^x \frac{\log (1 - t)}{t}\, dt$$

$$\psi(-x) = -\int_1^{1+x} \frac{\log t}{t(1 - t^{-1})}\, dt \qquad (x > 0)$$

$$\psi(x) = \sum_1^\infty \frac{x^n}{n^2} \qquad (|x| \leq 1). \tag{8}$$

Some useful identities involving the ψ-function will be given in the Appendix I.

Since the ψ-function remains in the final formulae, an abbreviated table of numerical values of $\psi(x)$, $(0 \leq x \leq 1)$ is presented in Appendix II.

4. Formulae for the fluorescent intensity

The intensity integrals in the previous paragraph may be evaluated by the use of the reduction formulae developed in Appendix I.

Since the explicit formulae are rather lengthy, they will be written in the following manner:

(i) The concentrations c_i will be implicitly contained in the absorption (or emission) coefficients; for example

$$\mu = c_1\mu_1 + c_2\mu_2 + c_3\mu_3$$

$$\tau'_i = \omega_i\left(1 - \frac{1}{r_i}\right) c_i\mu'_i \qquad \text{[reference 5, 9]}$$

(ii) For a free element, the intensity is I_{f3}, $(c_1 = c_2 = 0)$.

(iii) For a binary mixture, Z_3, Z_2, the intensities are I_{f3} and I_{f2}, respectively, ($c_1 = 0$).

(iv) For a three-component mixture Z_3, Z_2, Z_1, the intensities are I_{f3}, I_{f2}, and I_{f1}, respectively.

(v) The complete expression for I_{f1} involves a resolution of the general case into one of four exclusive cases, depending on certain functions of the absorption coefficients. In applying the formula, it is necessary to determine which one of the cases applies.

(1) Z_3. $$I_{f3} = \frac{\tau'_3}{\mu' + \mu''_{f3}}$$

*(2) Z_2. $$I_{f2} = \frac{\tau'_2}{\mu' + \mu''_{f2}} + \frac{\tau'_3 \tau_{2f3}}{\mu' + \mu''_{f2}} \left\{ \frac{1}{\mu'} \log \left(\frac{\mu'}{\mu_{f3}} + 1 \right) + \frac{1}{\mu''_{f2}} \log \left(\frac{\mu''_{f2}}{\mu_{f3}} + 1 \right) \right\}$$

Let

$$\mu' + \mu''_{f1} = A_1 \qquad \mu_{f2} + \mu_{f3} = c_1$$
$$\mu' + \mu_{f2} = A_2 \qquad \mu''_{f1} + \mu_{f2} = B_2$$
$$\mu' + \mu_{f3} = A_3 \qquad \mu''_{f1} + \mu_{f3} = B_3$$
$$\mu_{f2} - \mu''_{f1} = D_2 \qquad \mu_{f3} - \mu' = D_3$$

There are four cases, depending on the signs of D_2 and D_3

	Case 1	Case 2	Case 3	Case 4
D_2	+	−	+	−
D_3	+	+	−	−

(3) Z_1. $$I_{f1} = \frac{\tau'_1}{A_1}$$
$$+ \frac{\tau'_2 \tau_{1f2}}{A_1} \left\{ \frac{1}{\mu'} \log \frac{A_2}{\mu_{f2}} + \frac{1}{\mu''_{f1}} \log \frac{B_2}{\mu_{f2}} \right\}$$
$$+ \frac{\tau'_3 \tau_{1f3}}{A_1} \left\{ \frac{1}{\mu'} \log \frac{A_3}{\mu_{f3}} + \frac{1}{\mu''_{f1}} \log \frac{B_3}{\mu_{f3}} \right\}$$
$$+ \frac{\tau'_3 \tau_{2f3} \tau_{1f2}}{\mu' \mu''_{f1}} \left\{ \right.$$
$$+ \frac{1}{A_1} \left\{ \log \frac{A_3}{|D_3|} \log \frac{B_2}{A_2} - \log \frac{B_2}{|D_2|} \log \frac{B_3}{|D_3|} \right\}$$
$$+ \frac{1}{\mu''_{f1}} \log \frac{B_2}{|D_2|} \log \frac{B_3}{\mu_{f3}} + \frac{1}{\mu'} \log \frac{A_3}{|D_3|} \log \frac{A_2}{\mu_{f2}}$$
$$+ \frac{1}{\mu_{f2}} \log \frac{c_1}{\mu_{f3}} + \frac{1}{\mu_{f3}} \log \frac{c_1}{\mu_{f2}} + \text{(one of the following four cases):} \left. \right\}$$

* This formula has been previously reported, without proof, by GILLAM and HEAL [7].

Case 1. ($D_2 > 0$, $D_3 > 0$; $D_2 + B_3 = D_3 + A_2 = \mu_{f2} + \mu_{f3} = c_1$)

$$-\frac{1}{\mu'}\left\{-\psi(1) + \log\frac{c_1}{D_3}\log\frac{c_1}{\mu_{f2}} + \psi\left(\frac{\mu_{f3}}{c_1}\right) + \psi\left(\frac{A_2}{c_1}\right)\right\}$$

$$-\frac{1}{\mu''_{f1}}\left\{-\psi(1) + \log\frac{c_1}{D_2}\log\frac{c_1}{\mu_{f3}} + \psi\left(\frac{\mu_{f2}}{c_1}\right) + \psi\left(\frac{B_3}{c_1}\right)\right\}$$

$$+\frac{1}{A_1}\left\{-\psi(1) + \log\frac{c_1}{D_2}\log\frac{c_1}{D_3} + \psi\left(\frac{A_2}{c_1}\right) + \psi\left(\frac{B_3}{c_1}\right)\right\}$$

Case 2. ($D_2 < 0$, $D_3 > 0$; $|D_2| + c_1 = B_3$, $D_3 + A_2 = \mu_{f2} + \mu_{f3} = c_1$)

$$-\frac{1}{\mu'}\left\{-\psi(1) + \log\frac{c_1}{D_3}\log\frac{c_1}{\mu_{f2}} + \psi\left(\frac{\mu_{f3}}{c_1}\right) + \psi\left(\frac{A_2}{c_1}\right)\right\}$$

$$-\frac{1}{\mu''_{f1}}\left\{\tfrac{1}{2}\log^2\frac{B_3}{|D_2|} - \tfrac{1}{2}\log^2\frac{|D_2|}{\mu_{f3}} + \tfrac{1}{2}\log^2\frac{c_1}{\mu_{f3}} + \psi\left(\frac{|D_2|}{B_3}\right) + \psi\left(\frac{\mu_{f2}}{c_1}\right)\right\}$$

$$+\frac{1}{A_1}\left\{\tfrac{1}{2}\log^2\frac{B_3}{|D_2|} - \tfrac{1}{2}\log^2\frac{|D_2|}{D_3} + \tfrac{1}{2}\log^2\frac{c_1}{D_3} + \psi\left(\frac{|D_2|}{B_3}\right) + \psi\left(\frac{A_2}{c_1}\right)\right\}$$

Case 3. ($D_2 > 0$, $D_3 < 0$; $D_2 + B_3 = \mu_{f2} + \mu_{f3} = c_1$, $|D_3| + c_1 = A_2$)

$$-\frac{1}{\mu'}\left\{\tfrac{1}{2}\log^2\frac{A_2}{|D_3|} - \tfrac{1}{2}\log^2\frac{|D_3|}{\mu_{f2}} + \tfrac{1}{2}\log^2\frac{c_1}{\mu_{f2}} + \psi\left(\frac{|D_3|}{A_2}\right) + \psi\left(\frac{\mu_{f3}}{c_1}\right)\right\}$$

$$-\frac{1}{\mu''_{f1}}\left\{-\psi(1) + \log\frac{c_1}{D_2}\log\frac{c_1}{\mu_{f3}} + \psi\left(\frac{\mu_{f2}}{c_1}\right) + \psi\left(\frac{B_3}{c_1}\right)\right\}$$

$$+\frac{1}{A_1}\left\{\tfrac{1}{2}\log^2\frac{A_2}{|D_3|} - \tfrac{1}{2}\log^2\frac{|D_3|}{D_2} + \tfrac{1}{2}\log^2\frac{c_1}{D_2} + \psi\left(\frac{|D_3|}{A_2}\right) + \psi\left(\frac{B_2}{c_1}\right)\right\}$$

Case 4. ($D_2 < 0$, $D_3 < 0$; $|D_2| + c_1 = B_3$, $|D_3| + c_1 = A_2$, $\mu_{f2} + \mu_{f3} = c_1$)

$$-\frac{1}{\mu'}\left\{\tfrac{1}{2}\log^2\frac{A_2}{|D_3|} - \tfrac{1}{2}\log^2\frac{|D_3|}{\mu_{f2}} + \tfrac{1}{2}\log^2\frac{c_1}{\mu_{f2}} + \psi\left(\frac{|D_3|}{A_2}\right) + \psi\left(\frac{\mu_{f3}}{c_1}\right)\right\}$$

$$-\frac{1}{\mu''_{f1}}\left\{\tfrac{1}{2}\log^2\frac{B_3}{|D_2|} - \tfrac{1}{2}\log^2\frac{|D_2|}{\mu_{f3}} + \tfrac{1}{2}\log^2\frac{c_1}{\mu_{f3}} + \psi\left(\frac{|D_2|}{\mu_{f3}}\right) + \psi\left(\frac{\mu_{f2}}{c_1}\right)\right\}$$

$$+\frac{1}{A_1}\left\{\psi(1) + \tfrac{1}{2}\log^2\frac{A_2}{|D_3|} - \tfrac{1}{2}\log^2\frac{|D_3|}{|D_2|} + \tfrac{1}{2}\log^2\frac{B_3}{|D_2|}\right.$$

$$\left. + \psi\left(\frac{|D_2|}{B_3}\right) + \psi\left(\frac{|D_3|}{A_2}\right)\right\}$$

The formula for I_{f2} will be said to represent the total intensity as the sum of a primary component and a mutual or enhancement component.

Similarly, the formula for I_{f1} will be considered to represent the total intensity as the sum of a primary component, a mutual component due to Z_2, a mutual component due to Z_3, and a third-order component.*

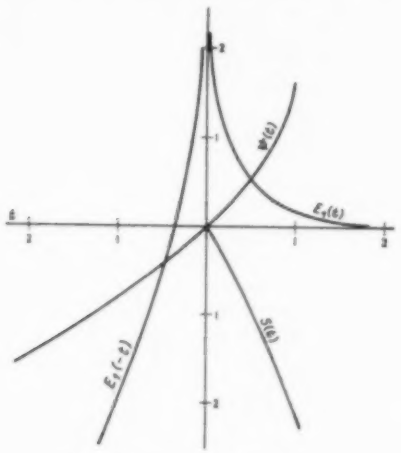

Fig. 2. Graphs of functions.

4.1. *Thin specimen*

If the specimen is thin, thickness t, in g/cm², the interval of integration becomes $(0, t)$ and the formula for the intensity of the radiation from Z_2 in a mixture Z_2Z_3 may be written as follows:

$$F_1 = \mu' + \mu''_{f2}$$

$$G_1 = \mu_3 - \mu' \qquad H_1 = \mu_{f3} + \mu'$$

$$G_2 = \mu_{f3} - \mu''_{f2} \qquad H_2 = \mu_{f3} + \mu''_{f2}$$

$$K_1(t) = \log \frac{|G_1|}{\mu_{f3}} + E_1(G_1 t) \qquad L_1 = \log \frac{H_1}{\mu_{f3}} + E_1(H_1 t)$$

$$K_2(t) = \log \frac{|G_2|}{\mu_{f3}} + E_1(G_2 t) \qquad L_2 = \log \frac{H_2}{\mu_{f3}} + E_1(H_2 t)$$

$$M = e^{-\mu' t} + e^{-\mu'' t} \qquad N = E_1(\mu_{f3} t)$$

$$I_{f2} = \frac{\tau'_2}{F_1}(1 - e^{-F_1 t})$$

$$+ \frac{\tau'_3 \tau_{2f3}}{F_1}\left\{\frac{1}{\mu'}[e^{-F_1 t}\kappa_1 + L_1 - MN]\right.$$

$$\left. + \frac{1}{\mu''_{f2}}[e^{-F_1 t}\kappa_2 + L_2 - MN]\right\}$$

* Graphs of $E_1(t)$, $E_1(-t)$, $S(t)$, $\psi(t)$ are shown in Fig. 2.

4.2. *Remarks*

It is to be noted that the increasing complexity of the formulae as one proceeds from I_{f3} to I_{f1} is due to two factors, namely:

(1) The final intensity is the resultant of a chain of radiative transfers (mutual or enhancement effect). This effect increases the order of integration.

(2) The change from a narrow or collimated beam to a broad or divergent beam. This effect changes the functions in the integrand from exponential, e^{-x}, to integro-exponential, where E_1 and E_2 apply to absorption and transmission effects respectively.

As an example of the latter effect one may consider the formula for I_{f3}. Then, if the incident and emergent beams are cones with 90° half-angle around the axes of symmetry, that is, full π geometry,

$$I_{f3} = \tau \int_0^\infty E_1(\mu\kappa) E_2(\mu_f\kappa)\, d\kappa$$

$$= \frac{\tau}{2}\left[\frac{1}{\mu}\left(1 - \frac{\mu_f}{\mu}\log\left(1 + \frac{\mu}{\mu_f}\right)\right) + \frac{1}{\mu_f}\log\left(1 + \frac{\mu_f}{\mu}\right)\right]$$

The similarity of this explicit expression to that obtained for the mutual effect in a binary system is to be noted.

If the cones subtend arbitrary half-angles, γ and β respectively, then

$$I_{f3} = \int_0^\gamma d\eta \int_0^\beta d\xi \, \frac{\tau \cos\xi}{\mu\cos\xi + \mu_f \cos\eta} \sin\eta \sin\xi$$

Although this integral can be reduced by elementary methods, the explicit formula is cumbersome and lengthy.

The extension of the analysis to I_{f2} and I_{f1}, using divergent incident or emergent beams, may well be left for another occasion.

5. Comparison with experiment

Strictly speaking, one cannot compare fluorescent intensities computed for monochromatic excitation with measured intensities excited by a polychromatic beam. There is, however, a certain amount of regularity in a practical sense. For example, fluorescent radiation intensities computed for a series of mixtures of the same elements for a range of wavelength of incident radiation are, for any one element, proportional to each other (linear on a logarithmic scale), if the variations in concentrations are not too great. Hence, it is better to make comparisons with a reference mixture of similar composition, not at all necessarily closely similar, than with the extreme case of comparison with the intensity of the radiation from the free element. A close study of wavelength effects is made difficult by the unreliability or lack of precision in the available estimates of the fluorescence yields for the various elements (see Appendix III).

In some instances, a comparison of computed and observed results may be expected to show agreement to a reasonable extent. If one were to use the white beam from a tungsten target tube, operated at about 50 KVP, the presence of the tungsten L-spectrum will result in a high concentration of energy in the region

VOL 7 1955/

around 1·0 to 1·2 A. Hence, for mixtures of elements from iron to zinc, computed intensities for an incident beam of assumed wavelength 1·0 to 1·2 should show reasonable agreement with observed values.

The following comparison of computed and observed intensities is to be considered as indicating the reasonableness of the formulae rather than proving them. (The experimental conditions were excitation at 50 KVP for the incident beam with $\theta' = 30°$, $\theta'' = 60°$. The total count for each measurement was at least 150,000.)

5.1. *Binary Mixtures*

Table 1. $ZnO—Fe_2O_3$. Computed for incident beam at $\lambda = 1{\cdot}20$. Intensity ratio of $\kappa\alpha$ line. $\theta' = 30°$, $\theta'' = 60°$.

c_2	c_3	Zn		Fe			
		Computed	Observed	Computed			Observed
				Primary	Mutual	Total	
0·95	0·05	0·029	0·033	0·923	0·040	0·963	0·965
0·90	0·10	0·059	0·066	0·851	0·075	0·926	0·932
0·85	0·15	0·091	0·100	0·782	0·106	0·888	0·890
0·80	0·20	0·124	0·136	0·717	0·134	0·851	0·856
0·50	0·50	0·362	0·377	0·388	0·220	0·608	0·600
0·20	0·80	0·695	0·685	0·137	0·161	0·298	0·296
0·15	0·85	0·764	0·744	0·101	0·133	0·234	0·235
0·10	0·90	0·837	0·825	0·066	0·098	0·164	0·164
0·05	0·95	0·916	0·906	0·032	0·054	0·087	0·088

It should be noted that at lower concentrations the contribution of the mutual component to the total intensity is more significant than that from the primary one. A computation for the limiting value, for other mixtures, i.e., $c_1 \to 0$

$$\omega_2 \frac{\mu_{2i}}{\mu_{1i}} \left\{ \frac{\mu_{1/2}}{\mu'_{1i}} \log \left(\frac{\mu'_{1i}}{\mu_{2/2}} + 1 \right) + \frac{\mu_{1/2}}{\mu''_{2/1}} \log \left(\frac{\mu''_{2/1}}{\mu_{2/2}} + 1 \right) \right\},$$

indicates that the ratio of mutual to primary component in some instances may approach 3·5.

A change in the incident wavelength will introduce a significant change in the value of the fluorescent spectrum. The primary component of Z_2 is constant for all λ less than the absorption discontinuity for Z_3 (ratio from mixture to free element), but the mutual component ratio decreases markedly with increase in wavelength of the incident beam.

Attempts to compute the (relative) intensity of the incident spectrum from comparison of computed values at various wavelengths with observed ratios by the method of least squares (multiple regression) were unsuccessful, since the inverse matrix is of the order of 10^{-6} compared with the absorption coefficients.

5.2. *Three-component Mixtures*

Table 2. ZnO—NiO—Fe_2O_3. Computed for incident beam at $\lambda = 1{\cdot}20$. Intensity ratio of Fe—$\kappa\alpha$.

Composition ($c_1c_2c_3$)	112	121	211
Primary component	0·1870	0·1968	0·4127
Mutual component			
Ni	0·0561	0·1217	0·0935
Zn	0·0974	0·0407	0·0907
Third-order process	0·0331	0·0267	0·0221
Total	0·374	0·386	0·619
Experimental values	0·362	0·374	0·629

Table 3. Cr—Fe—Ni. Complete analysis of alloys (metal). Incident beam: $\lambda = 1{\cdot}2$.

(a) *Inconel*

Element	Concentration	Component or process	Intensity ratios	
			Computed	Observed
Ni	0·79	Primary	0·605	0·597
Fe	0·065	Primary	0·0424	
		Mutual	0·0445	
		Total	0·087	0·083
Cr	0·145	Primary	0·1003	
		Mutual Fe	0·0082	
		Mutual Ni	0·1078	
		Third-order process	0·0164	
		Total	0·233	0·227

(b) *Alloy Type* 310

Element	Concentration	Component or process	Intensity ratios	
			Computed	Observed
Ni	0·205	Primary	0·088	0·095
Fe	0·550	Primary	0·3341	
		Mutual	0·0428	
		Total	0·377	0·384
Cr	0·245	Primary	0·1956	
		Mutual Fe	0·1234	
		Mutual Ni	0·0210	
		Third-order process	0·0207	
		Total	0·361	0·365

6. Effect of a polychromatic incident beam

Even a cursory examination of the formulae in Section 4 will show that the extension to a polychromatic beam introduces great difficulties for a rigorous solution. The following discussion is to be considered as only an introduction to the problem.

For Z_3

$$I_{f3} = \tau'_3/\mu'_i + \mu''_{f3}, \tag{1}$$

which may be expanded to show c_i explicitly.

$$I_{f3}(c_1c_2c_3) = \frac{c_3\omega'_3\mu'_{3i}}{c_1(\mu'_{1i} + \mu''_{1f3}) + c_2(\mu'_{2i} + \mu''_{2f3}) + c_3(\mu'_{3i} + \mu''_{3f3})} \tag{2}$$

The expression for free Z_3, i.e., $c_1 = c_2 = 0$, becomes

$$I_{f3}(001) = \frac{\omega'_3\mu'_{3i}}{\mu'_{3i} + \mu''_{3f3}} \tag{3}$$

A linear expression in c_i may be obtained by dividing (3) by (2).

$$Q = \frac{I_{f3}(001)}{I_{f3}(c_1c_2c_3)} = 1 + \left(\frac{c_1}{c_3}\right)\frac{\mu'_{1i} + \mu''_{1f3}}{\mu'_{3i} + \mu''_{3f3}} + \left(\frac{c_2}{c_3}\right)\frac{\mu'_{2i} + \mu''_{2f3}}{\mu'_{3i} + \mu''_{3f3}} \tag{4}$$

Instead of measuring intensity of a beam, with a Geiger counter, as counts per second, it is advantageous to represent the intensity by the reciprocal of the counting rate, i.e., time required for the counter to reach a predetermined fixed count.

Let
$$T_3 = \frac{1}{I_{f3}}$$

Then

$$Q = \frac{T_{f3}(c_1c_2c_3)}{T_{f3}(001)} = 1 + \left(\frac{c_1}{c_3}\right)\frac{\mu'_{1i} + \mu''_{1f3}}{\mu'_{3i} + \mu''_{3f3}} + \left(\frac{c_2}{c_3}\right)\frac{\mu'_{2i} + \mu''_{2f3}}{\mu'_{3i} + \mu''_{3f3}} \tag{5}$$

or

$$T_{f3}(c_1, c_2, c_3) = u_0 + \left(\frac{c_1}{c_3}\right)u_1 + \left(\frac{c_2}{c_3}\right)u_2 \tag{6}$$

where u_i depends on the absorption coefficients of the elements in the mixture and the counting rate of the free element, parameters which are independent of the composition of the mixture.

The problem for the analysis involving a polychromatic incident beam of an arbitrary spectrum is to derive good linear approximations, similar to formula (6), which will present Q, the ratio of the intensity of the spectrum of Z_3 in a mixture to the intensity of the spectrum from free Z_3, which will be explicitly independent of the spectrum of the incident beam.

One may rephrase equation (3) for a polychromatic beam as

$$I_{f3} = \int_{\lambda_0}^{\lambda_c} I_0(\lambda)\omega'_3 \frac{\mu'_{3i}(\lambda)}{M_{33}(\lambda) + \frac{c_1}{c_3} M_{13}(\lambda) + \frac{c_2}{c_3} M_{23}(\lambda)} d\lambda \tag{7}$$

$$I_{f3}(r_{13}, r_{23}) = \int_{\lambda_0}^{\lambda_c} I_0(\lambda)\omega'_3 \frac{\mu'_{3i}(\lambda)}{M_{33}(\lambda)} \frac{1}{1 + r_{13}\frac{M_{13}(\lambda)}{M_{33}(\lambda)} + r_{23}\frac{M_{23}(\lambda)}{M_{33}(\lambda)}} d\lambda \tag{8}$$

where (λ_0, λ_c) is the range of wavelength in the polychromatic beam capable of exciting the spectrum of Z_3.

$I_0(\lambda)$ is the intensity (number of photons) in the incident beam of wavelength λ.

$$M_{13} = \mu'_{1i} + \mu''_{1f3}; \quad M_{23} = \mu'_{2i} + \mu''_{2f3}$$

$$r_{13} = c_1/c_3; \qquad r_{23} = c_2/c_3$$

$$I_{f3}(0, 0) = \int_{\lambda_0}^{\lambda_c} \frac{I_0(\lambda)\omega'_3\mu'_{3i}(\lambda)}{M_{33}} d\lambda \tag{9}$$

If

$$f = 1 + r_{13}\frac{M_{13}}{M_{33}} + r_{23}\frac{M_{23}}{M_{33}} = 1 + r_{13}u_1 + r_{23}u_2 \tag{10}$$

$$p = I_0(\lambda)\omega'_3 \frac{\mu'_{3i}(\lambda)}{M_{33}} \tag{11}$$

Then

$$Q = \frac{\int_{\lambda_0}^{\lambda_c} p\, d\lambda}{\int_{\lambda_0}^{\lambda_c} \frac{p}{f} d\lambda} = \left(\frac{\int_{\lambda_0}^{\lambda_c} pf^{-1}\, d\lambda}{\int_{\lambda_0}^{\lambda_c} p\, d\lambda}\right)^{-1} \tag{12}$$

That is, Q is the harmonic mean of f with respect to p as a weight or distribution function.

There is no loss of generality if Q were to be normalized in the sense that $\int p\, d\lambda = 1$. Hence,

$$Q = (\int pf^{-1})^{-1}. \tag{13}$$

By definition, a mean of f with respect to p of order r is

$$\mathscr{M}_r(f; p) = \left(\frac{\int pf^r}{\int p}\right)^{1/r} \qquad (r \neq 0) \tag{14}$$

or in normalized form

$$\mathscr{M}_r(f, p) = (\int pf^r)^{1/r}. \tag{15}$$

The properties of power means have been extensively investigated. Some of the applicable properties are

$$\mathscr{M}_r(ku) = k\mathscr{M}_r(u) \qquad (k = \text{const}) \tag{16}$$

$$\mathscr{M}_r(u) \geqslant \mathscr{M}_s(u) \qquad (r > s) \tag{17}$$

VOL. 7 1955/5

If $\mathscr{Q}(u)$ is the arithmetic mean, i.e., $r = +1$, and $\mathscr{H}(u)$ the harmonic mean ($r = -1$), it follows that

$$\mathscr{Q}(u) \geqslant \mathscr{H}(u) \qquad (u \neq 0) \tag{18}$$

with equality only if the set $\{u\}$ is constant.

From MINKOWSKI's inequality it follows that

$$\mathscr{Q}(1 + u) = 1 + \mathscr{Q}(u) \tag{19}$$

$$\mathscr{H}(1 + u) \geqslant 1 + \mathscr{H}(u) \tag{20}$$

From these inequalities it follows that

$$\mathscr{Q}(1 + r_{13}u_1 + r_{23}u_2) = 1 + r_{13}\mathscr{Q}(u_1) + r_{23}\mathscr{Q}(u_2) > \mathscr{H}(1 + r_{13}u_1 + r_{23}u_2) \tag{21}$$

and

$$r_{13}\mathscr{Q}(u_1) + r_{23}\mathscr{Q}(u_2) > \mathscr{H}(1 + r_{13}u_1 + r_{23}u_2) \tag{22}$$

$$-1 > r_{13}\mathscr{H}(u_1) + r_{23}\mathscr{H}(u_2)$$

or

$$Q \geqslant 1 + r_{13}\mathscr{H}(u_1) + r_{23}\mathscr{H}(u_2). \tag{23}$$

Since u_1, u_2 do not depend on composition, but only on the absorption coefficients of the elements and the spectrum of the incident beam, any particular case can be analysed or computed to see how far (17) departs from equality.

The advantage of (17) over the representation of Q as an integral is that the theory of means is a much more powerful mode of attack than integration. The question of analyticity of distribution of u_i does not enter the problem, for the set $\{u_i\}$ may be arbitrary to any extent (except that $u \neq 0$), and (17) will still hold. This problem of suitable approximation in particular instances cannot be answered in general, but must be considered for each particular set of elements in a mixture.

In general, it may be expected that, over significantly important ranges of r_{ij}, for many mixtures the resultant inequality (17) will be practically indistinguishable from equality.

As an experimental check on the formulae, the following test was made. Assuming a binary mixture, then

$$Q_3 = 1 + r_{13}M_{13}/M_{33}.$$

It is also assumed that the K and L branches of the absorption curve of Z_3 and Z_1 are parallel, particularly with respect to Z, i.e., the empirical formulae for the absorption coefficients are

(1) on the K branch: $\mu = aZ^m\lambda^n$

(2) on the L branch: $\mu = bZ^m\lambda^n$.

Then

$$\frac{M_{13}}{M_{33}} = \left(\frac{Z_1}{Z_3}\right)^m \frac{\lambda^n + \lambda_{f3}{}^n}{\lambda^n + \dfrac{b}{a}\lambda_{f3}{}^n}$$

Then, for a fixed Z_3, if for various $Z_i < Z_3$ mixtures are made so that $r_{13}\frac{M_{13}}{M_{33}}$ is constant, the resultant Q_3 will be constant, i.e., the measurement of Z_3 will take the same time for a fixed count.

Experiment proved that there was reasonable constancy, but only if the concentrations were computed on an atomic basis, that is, if

$$c_1 = \text{const} \times \frac{A_1}{Z^{2.75}}$$

where A_1 is the atomic weight of Z_1. This will have no effect on the usual mode of analysis, since the exponent of Z does not enter explicitly into the formulae.

Some of the experimental data are given below as examples of the order of precision. The numbers are seconds for the counter to record $N = 2^{17}$ counts for Z_3 mixed with various Z_i. The mixtures were made of oxides.

Z_1 \ Z_3	Sr	As	Zn
Ti	235	150	117
Cr	245	148	118
Fe	256	155	121
Zn	259	151	
As	254		

There is no relation between columns; constancy is to be expected only within each column.

7. The inverse problem

The formulae in Section 4 may be considered as the rigorous solution to the direct problem under the assumption of a monochromatic incident beam. The inversion of the formulae to show c_i as explicit functions of the intensities or intensity ratios is clearly impossible in a rigorous sense.

Various approximations and graphical methods may be devised, but this problem is not the subject of this paper.

8. Summary and remarks

Under assumptions of a monochromatic incident beam and a one-line fluorescent spectrum, formulae have been derived for the intensities of the fluorescent spectra of three-element mixtures.

A suggestion is presented for a useful extension to the treatment of a polychromatic incident beam.

The restriction to a one-line fluorescent spectrum is theoretically a trivial one. For example, referring to the real K spectrum, it is only necessary to repeat the analysis for the β line with proper allocation of ω. The extension to L spectra

VOL. 7 1955/5

is similar. If the absorption coefficients and the location of the absorption discontinuities are known, it is only necessary to repeat the analysis for each added line.

The restriction to a monochromatic beam is difficult to remove in an analytical sense, since the incident spectrum has no analytical properties correlated with the absorption properties of the mixture.

The restriction of the mixture to no more than three components is a practical one. As may be anticipated, the formulae, in closed form, for many components, become increasingly lengthy and laborious to compute. As a practical consideration, it is questionable whether it is necessary to consider any usual mixture as containing more than four major components (elements). With the increase of the number of components, it becomes more important to develop a good analytic approximation to the exact closed form.

APPENDIX I

Reduction of the intensity integrals

All necessary formulae for the evaluation of the fluorescent intensity integrals are computed in this appendix. In reducing the various integrals, principal parts will be used whenever necessary. There seems to be no essential value in a general specification of the range of the parameters for which the formulae are valid. In any particular application, the formula to be used must be such that the following two conditions hold,

(1) the argument of a logarithmic term is positive, and

(2) the argument of a ψ-term is ≤ 1.

Care should be taken in the use of formulae involving E_1 terms, since the sign of arguments depends on concentration of Z_i as well as on the wavelengths of the various beams.

It will be noted that formulae have not been computed for the limiting case where the argument of an E_1 function vanishes. The computation is rather lengthy and the reduction is of no practical interest, since even small changes in concentration will make the arguments non-vanishing.

It will be noted that logarithms, when they occur in formulae, are all natural logarithms.

1. *Definitions*

(1) $$E_1(t) = \int_1^\infty \frac{e^{-tx}}{x}\,dx \qquad (t > 0)$$

(2) $$S(t) = \int_{-1}^1 \frac{e^{-tx}}{x}\,dx \qquad (t > 0)$$

(3) $$E_1(-t) = E_1(t) + S(t) \qquad (t > 0)$$

(4) $$\psi\left(-\frac{bx}{a}\right) = \log a \log x - \int \frac{\log (a + bx)}{x}\,dx$$

$$\psi\left(-\frac{a}{bx}\right) = -\tfrac{1}{2}\log^2 bx + \int \frac{\log (a + bx)}{x}\,dx$$

$$\psi(x) = \sum_1^\infty \frac{x^n}{n^2}$$

2. *Useful Identities Involving* $\psi(x)$

$$\psi(1) = \tfrac{1}{6}\pi^2 \qquad \psi(0) = 0 \qquad \psi(-1) = \tfrac{1}{12}\pi^2 \tag{5}$$

$$\psi(-x) = -\tfrac{1}{6}\pi^2 + \psi\left(\frac{1}{1+x}\right) - \log(1+x)\log x + \tfrac{1}{2}\log^2(1+x) \tag{6}$$

$$\psi(-x) = -\tfrac{1}{2}\log^2(1+x) - \psi\left(\frac{x}{1+x}\right) \tag{7}$$

$$\psi(x) + \psi(1-x) = \tfrac{1}{6}\pi^2 - \log x \log(1-x) \tag{8}$$

$$\psi(-x) + \psi\left(-\frac{1}{x}\right) = -\tfrac{1}{6}\pi^2 - \tfrac{1}{2}\log^2 x \tag{9}$$

$$\psi(x) + \psi(-x) = \tfrac{1}{2}\psi(x^2) \tag{9a}$$

3. *Table of Integrals*

(*Elementary Forms*) $k, l > 0$

$$k\int_1^\infty \frac{dx}{x(k+lx)} = \log\left(\frac{k}{l} + 1\right) \tag{R1}$$

$$k\int_1^\infty \frac{dx}{x(k-lx)} = \log\left|\frac{k}{l} - 1\right| \tag{R2}$$

$$k\int_{-1}^1 \frac{dx}{x(k+lx)} = \log\frac{|k-l|}{(k+l)} \tag{R3}$$

$$k\int_{-1}^1 \frac{dx}{x(k-lx)} = \log\frac{(k+l)}{|k-l|} \tag{R4}$$

$$\int_{-1}^1 \frac{\log(k+lx)}{x}\,dx = \psi\left(\frac{l}{k}\right) - \psi\left(-\frac{l}{k}\right) \qquad (k > l) \tag{R5}$$

$$k > l, \quad m > n, \quad k, l, m, n > 0, \quad \Delta = kn - lm$$

$$n\int_{-1}^1 \frac{\log(k+lx)}{m+nx}\,dx = \log\frac{\Delta}{n}\log\frac{m+n}{m-n} + \psi\left(-\frac{l}{\Delta}(m-n)\right) - \psi\left(-\frac{l}{\Delta}(m+n)\right);\ (\Delta > 0) \tag{R6, i}$$

$$= \tfrac{1}{2}\log^2\frac{l}{n}(m+n) - \tfrac{1}{2}\log^2\frac{l}{n}(m-n) + \psi\left(-\frac{\Delta}{l(m+n)}\right) - \psi\left(-\frac{\Delta}{l(m-n)}\right) \tag{R6, ii}$$

$$m\int\frac{\log(k+lx)}{x(m+nx)}\,dx = \int\frac{\log(k+lx)}{x}\,dx - n\int\frac{\log(k+lx)}{m+nx}\,dx \tag{R7}$$

VOL 7 1955/

(R8) $$m\int_1^\infty \frac{\log(k+lx)}{x(m+nx)}\,dx = \tfrac{1}{2}\log^2\frac{l}{n}(m+n) - \tfrac{1}{2}\log^2 l + \psi\left(-\frac{\Delta}{l(m+n)}\right) - \psi\left(-\frac{k}{l}\right)$$

$E_1(ax)$. $(a, b, p > 0)$

(R9) $$p\int_0^\infty e^{-px}\,dx = 1$$

(R10) $$p\int_0^\infty e^{-px}E_1(ax)\,dx = \log\left(\frac{p}{a}+1\right)$$

(R11) $$p\int_0^\tau e^{px}E_1(ax)\,dx = e^{p\tau}E_1(a\tau) - E_1\{(a-p)\tau\} - \log\left|\frac{p}{a}-1\right|$$

(R12) $$\int_0^\infty E_1(ax)E_1(bx)\,dx = \frac{1}{b}\log\left(\frac{b}{a}+1\right) + \frac{1}{a}\log\left(\frac{a}{b}+1\right)$$

(R13) $$p\int_0^\infty e^{-px}E_1(ax)E_1(bx)\,dx = -\psi(1) + \log\frac{p+a+b}{a}\log\frac{p+a+b}{b} + \psi\left(\frac{p+a}{p+a+b}\right) + \psi\left(\frac{p+b}{p+b+a}\right)$$

$S(ax)$

(R14) $$p\int_0^\infty e^{-px}S(ax)\,dx = \log\frac{|p-a|}{p+a}$$

(R15) $$p\int_0^\infty E_1(ax)S(bx)\,dx = \psi\left(\frac{b}{p+a}\right) - \psi\left(-\frac{b}{p+a}\right) - \psi\left(-\frac{p-b}{a}\right) + \psi\left(-\frac{p+b}{a}\right)$$

(R16) $$p\int_0^\infty e^{-px}S(ax)S(bx)\,dx = \psi\left(\frac{b}{p-a}\right) - \psi\left(-\frac{b}{p-a}\right) - \psi\left(\frac{a}{p+b}\right) + \psi\left(\frac{a}{p-b}\right) - \psi\left(\frac{b}{p+a}\right) + \psi\left(-\frac{b}{p+a}\right) + \psi\left(-\frac{a}{p+b}\right) - \psi\left(-\frac{a}{p-b}\right)$$

$E_1(-ax)$

(R17) $$p\int_0^\infty e^{-px}E_1(-ax)\,dx = \log\left|\frac{p}{a}-1\right|$$

(R18) $$p\int_0^\infty e^{-px}E_1(ax)E_1(-bx)\,dx = \tfrac{1}{2}\log^2\frac{p+a}{b} - \frac{1}{2}\log^2\frac{b}{a} + \psi\left(\frac{b}{p+a}\right) - \psi\left(-\frac{p-b}{a}\right)$$

$$(R19)\quad p\int_0^\infty e^{-px}E_1(-ax)E_1(-bx)\,dx = \psi(1) - \frac{1}{2}\log^2\frac{p-a}{b} + \frac{1}{2}\log^2\frac{p-b}{a} - \frac{1}{2}\log^2\frac{b}{a} + \psi\left(\frac{a}{p-b}\right) + \psi\left(\frac{b}{p-a}\right)$$

$$(R20)\quad p\int_0^\infty e^{-px}E_1(a\,|t-x|)\,dx = e^{-pt}\log\frac{p+a}{|p-a|} - e^{-pt}E_1\{(a-p)t\} + E_1(at)$$

For thin specimens

$$(R21)\quad \int_1^\infty \frac{e^{-\kappa t}}{(l+mt)}\,dt = \frac{1}{m}\left\{e^{\frac{\kappa l}{m}}E_1\left[\frac{\kappa}{m}(l+m)\right]\right\}$$

$$(R22)\quad \int_0^\tau e^{pt}E_1(at)\,dt = \frac{1}{p}\left\{-\log\left|\frac{p}{a}-1\right| + e^{p\tau}E_1(a\tau) - E_1[(a-p)\tau]\right\}$$

$$(R23)\quad \int_0^\tau e^{-pt}E_1(at)\,dt = \frac{1}{p}\left\{\log\left(\frac{p}{a}+1\right) - e^{-p\tau}E_1(a\tau) + E_1[(a+p)t]\right\}$$

$$(R24)\quad \int_0^t e^{-px}E_1[a(t-x)]\,dx = \frac{1}{p}\left\{-e^{-pt}\log\left|\frac{p}{a}-1\right| + E_1(at) - e^{-pt}E_1\{(a-p)t\}\right\}$$

$$(R25)\quad \int_t^\tau e^{-px}E_1[a(x-t)]\,dx = \frac{1}{p}\left\{e^{-pt}\log\left|\frac{p}{a}+1\right| - e^{-p\tau}E_1(a(\tau-t)) + e^{-pt}E_1[(a+p)(\tau-t)]\right\}$$

4. *Computation of Reference Integrals*

$$\Delta = kn - lm$$

$$(R8)\quad \lim_{u\to\infty}\int_1^u \frac{\log(k+lx)}{x}\,dx = -\psi\left(-\frac{k}{l}\right) - \tfrac{1}{2}\log^2 l + \lim_{u\to\infty}\tfrac{1}{2}\log^2 lu$$

$$\lim_{u\to\infty}\int_1^u \frac{\log(k+lx)}{m+nx}\,dx = -\psi\left(-\frac{\Delta}{l(m+n)}\right) - \tfrac{1}{2}\log^2\frac{l}{n}(m+n) + \lim_{u\to\infty}\tfrac{1}{2}\log^2 lu\left(1+\frac{m}{nu}\right)$$

$$\lim_{u\to\infty} m\int_1^u \frac{\log(k+lx)}{x(m+nx)}\,dx = -\psi\left(-\frac{k}{l}\right) - \tfrac{1}{2}\log^2 l + \psi\left(-\frac{\Delta}{l(m+n)}\right) + \tfrac{1}{2}\log^2\frac{l}{n}(m+n) + \tfrac{1}{2}\lim_{u\to\infty}\left\{\log^2 lu - \log^2 lu\left(1+\frac{m}{nu}\right)\right\}$$

but

$$\lim_{u\to\infty}\left\{\log^2 lu - \log^2 lu\left(1+\frac{m}{nu}\right)\right\} = \lim_{u\to\infty}\left\{-2\log lu\log\left(1+\frac{m}{nu}\right) - \log^2\left(1+\frac{m}{nu}\right)\right\} = 0$$

since $$\log\left(1+\frac{1}{u}\right) = O\left(\frac{1}{u}\right).$$

(R10) $$p\int_0^\infty e^{-pz}E_1(ax)\,dx = p\int_0^\infty dx\,e^{-pz}\int_1^\infty dt\,\frac{e^{-axt}}{t}$$

$$= p\int_1^\infty \frac{dt}{t}\int_0^\infty dx\,e^{-(p+at)x} = p\int_1^\infty \frac{dt}{t(p+at)}$$

(R9, R1)

(R11) $$p\int_0^r e^{px}E_1(ax)\,dx = p\int_0^r dx\,e^{px}\int_1^\infty dt\,\frac{e^{-axt}}{t}$$

$$= p\int_1^\infty \frac{dt}{t}\int_0^r dx\,e^{(p-at)x} = p\int_1^\infty \frac{e^{(p-at)r}}{t(p-at)}\,dt - p\int_1^\infty \frac{dt}{t(p-at)}$$

$$= \int_1^\infty dt\,\frac{e^{(p-at)r}}{t} + \int_1^\infty a\,dt\,\frac{e^{(p-at)r}}{p-at} - p\int_1^\infty \frac{dt}{t(p-at)}$$

$$= e^{pr}\int_1^\infty dt\,\frac{e^{-art}}{t} - \int_1^\infty \frac{e^{-(a-p)rt}}{t}\,dt - p\int_1^\infty \frac{dt}{t(p-at)}$$

(def. E_1 and R_2)

(R12) $$\int_0^\infty E_1(ax)E_1(bx)\,dx = \int_1^\infty \frac{dt}{t}\int_0^\infty e^{-btx}E_1(ax)\,dx = \frac{1}{b}\int_1^\infty \frac{dt}{t^2}\log\left(\frac{bt}{a}+1\right)$$

(R13) $$\int_0^\infty e^{-pz}E_1(ax)E_1(bx)\,dx = p\int_1^\infty \frac{dt}{t}\int_0^\infty dx\,e^{-(p+bt)x}E_1(ax)$$

$$= p\int_1^\infty \frac{\log\left(\frac{p+a}{a}+\frac{b}{a}t\right)dt}{t(p+bt)} = \tfrac{1}{2}\log^2\frac{p+b}{a} - \tfrac{1}{2}\log^2\frac{b}{a} + \psi\left(-\frac{a}{p+b}\right) - \psi\left(-\frac{p+a}{b}\right)$$

(R10, R8)

To obtain (R13), use identities in ψ (5, 6, and 7).

(R15) $$p\int_0^\infty e^{-pz}E_1(ax)S(bx)\,dx = p\int_{-1}^1 \frac{dt}{t}\int_0^\infty e^{-(p+bt)}E_1(ax)\,dx$$

$$= p\int_{-1}^1 \frac{\log\left(\frac{p+a}{a}+\frac{b}{a}t\right)}{t(p+bt)}\,dt$$ (R10, R6,i)

(R17, 18, 19) Combine appropriate forms for $E(-ax) = E(ax) + S(ax)$ and reduce by the use of the identities in $\psi(x)$.

(R20)
$$J = \int_0^\infty e^{-pz} E_1(a\,|t-x\,|)\,dx$$
$$= \int_0^t e^{-pz} E_1(at-ax)\,dx + \int_t^\infty e^{-pz} E_1(ax-at)\,dx$$
$$aJ = \int_0^{at} e^{-\frac{p}{a}x} E_1(at-x)\,dx + \int_{at}^\infty e^{-\frac{p}{a}x} E_1(x-at)\,dx$$
$$y = at - x \qquad\qquad y = x - at$$
$$J = \frac{1}{a} e^{-pt}\left\{\int_0^{at} e^{\frac{p}{a}y} E_1(y)\,dy + \int_0^\infty e^{-\frac{p}{a}y} E_1(y)\,dy\right\}$$

(R11, R10)

5. *Reduction of Intensity Integrals*

The evaluation of the intensity may be reduced to combinations of the following forms.

(J1)
$$\int_0^\infty dl e^{-pl}$$

(J2)
$$\int_0^\infty dl \int_0^\infty d\kappa e^{-(pl+gk)} E_1\{a\,|l-\kappa\,|\}$$

(J3)
$$\int_0^\infty dl \int_0^\infty d\kappa \int_0^\infty dj e^{-(pl+gj)} E_1\{a\,|l-\kappa\,|\}\,.\,E_1\{b\,|k-j\,|\}.$$

The first typical integral (J1) is elementary, and is evaluated in R9.

The second typical integral (J2) may be written as

$$\text{J2} = \int_0^\infty dl e^{-pl} \int_0^\infty d\kappa e^{-gk} E_1\{a\,|l-\kappa\,|\}.$$

The inner integral is evaluated in R20. The second integration may be evaluated by the use of the reduction forms for $E(ax)$ and $E(-ax)$.

The third typical integral (J3) may be written as

$$\text{J3} = \int_0^\infty d\kappa \int_0^\infty dl e^{-pl} E_1\{a\,|l-\kappa\,|\} \int_0^\infty dj e^{-gj} E_1\{b\,|k-j\,|\}$$

which, on reducing by use of R20, becomes

$$\text{J3} = \frac{1}{pg} \int_0^\infty d\kappa \left\{e^{-p\kappa} \log \frac{p+a}{|p-a|} - e^{-p\kappa} E_1\{(a-p)k\} + E_1(ak)\right\}$$
$$\times \left\{e^{-g\kappa} \log \frac{g+b}{|g-b|} - e^{-g\kappa} E_1\{(b-g)k\} + E_1(b\kappa)\right\}$$

Expansion of the product in the integrand will reduce J3 to a sum of nine integrals, the values of which are given in R9 to R13 and R17 to R19. The resultant expressions may then be reduced to simpler forms, depending on the particular

VOL. 7 1955/5

combinations of the parameters. The sign of the arguments of the E_1-function will depend not only on the particular elements, Z_i and the wavelength of the incident beam, but also on the concentrations of the elements in the mixture.

APPENDIX 2

$$y(x) = \sum \frac{x^n}{n^3}$$

χ	0·00	0·01	0·02	0·03	0·04	0·05	0·06	0·07	0·08	0·09
0·0	0·0	0·01003	0·02010	0·03023	0·04041	0·05064	0·06092	0·07126	0·08166	0·09211
0·1	0·10262	0·11318	0·12381	0·13449	0·14523	0·15603	0·16690	0·17783	0·18882	0·19988
0·2	0·21100	0·22219	0·23345	0·24478	0·25618	0·26765	0·27920	0·29082	0·30251	0·31428
0·3	0·32613	0·33806	0·35007	0·36216	0·37434	0·38661	0·39896	0·41140	0·42393	0·43656
0·4	0·44928	0·46210	0·47502	0·48804	0·50117	0·51440	0·52774	0·54119	0·55476	0·56844
0·5	0·58224	0·59616	0·61022	0·62440	0·63887	0·65316	0·66775	0·68248	0·69736	0·71239
0·6	0·72767	0·74294	0·75846	0·77416	0·79003	0·80608	0·82233	0·83878	0·85543	0·87229
0·7	0·88943	0·90670	0·92425	0·94206	0·96013	0·97847	0·99710	1·01603	1·03528	1·05486
0·8	1·07482	1·09510	1·11581	1·13694	1·15852	1·18058	1·20317	1·22632	1·25009	1·27453
0·9	1·29971	1·32573	1·35268	1·38068	1·40993	1·44064	1·47680	1·50790	1·54580	1·58863
1·0	1·64493									

APPENDIX 3

$\omega(K)$

	Ref. [5]	*	Ref. [8]
24 Cr	0·22	0·241	0·27
26 Fe	0·28	0·303	0·34
27 Co	0·31	0·336	(0·38)
28 Ni	0·34	0·368	0·42
29 Cu	0·37	0·400	0·46
30 Zn	0·40	0·432	0·49
33 As	0·49	0·523	(0·58)
34 Se	0·52	0·551	0·60
35 Br	0·54	0·578	0·63
38 Sr	0·62	0·650	0·71
42 Mo	0·71	0·727	0·77
47 Ag	0·79	0·796	0·83
50 Sn	0·83	0·827	0·86

* AREND's formula—$\omega(k) = \dfrac{0{,}957Z^4}{0{,}984 \times 10^6 + Z^4}$

References

[1] KOURGANOFF, V.; *Basic Methods in Transfer Problems*, Oxford, 1952.
[2] KOURGANOFF, V.; *Annales des Astrophysique* 1947 **10** 282; 1948 **11** 329.
[3] BUSBRIDGE, I. W.; *Quarterly Journal of Mathematics* 1950 **1**, 176.
[4] CHANDRASEKHAR, S.; *Radiative Transfer*, Oxford, 1950.
[5] BURHOP, E. H. S.; *The Auger Effect*, Cambridge, 1952.
[6] HARDY, LITTLEWOOD, and POLYA; *Inequalities*, Cambridge, 1934.
[7] GILLAM, E., and HEAL, H. T.; *Brit. Jour. Appl. Physics* 1952 **3** 353.
[8] FANO, U.; *Nucleonics* 1953 **11** 10.
[9] COMPTON, A. H., and ALLISON, S. K.; *X-rays in Theory and Experiment*, New York, 1935.

VOL
7
1955/

Spectrochimica Acta, 1955, Vol. 7, pp. 307 to 320. Pergamon Press Ltd., London

Investigations concerning light sources for spectrum analysis—IV*

High-voltage spark source with electronic control and its electrical characteristics

Á. BARDÓCZ
Hungarian Academy of Sciences, Central Research Institute for Physics,
Department for Spectroscopy, Budapest, Hungary

(*Received* 30 *June* 1954; *revised version* 4 *October* 1954)

Abstract—The experiments on the improvement of the operating conditions of high-voltage spectroscopic spark sources resulted in an electronically controlled spark source. The control of the source is carried out by a thyratron tube-operated control spark gap, which can be single or double. The electrical circuit of the system is of such a design that the excitation energy does not pass through the thyratron tube, the only role of which is to operate the control spark gap. The thyraton tube is controlled by a pulse generator, owing to which the number of spark discharges/sec can be varied. The new design spark source is suitable for producing low-energy ignitor sparks as well as high-energy excitation sparks. The electrical characteristics of the spark source are described.

Introduction

In present spectrographic practice, rotary-gap or stationary-gap controlled high-voltage spark sources are almost exclusively used. The purpose of the control is, on the one hand, to increase the excitation energy stored in the condenser, and on the other to secure for the condenser the same charging before each discharge. Neither of the two above spark-source systems, however, satisfies these requirements completely. In rotary-gap-controlled sources the energy stored in the condenser is always the same, but, owing to the fact that the length of the control gap keeps varying, it has the disadvantage that the ratio of the energies dissipated in the control gap and in the analytical gap respectively, and consequently the conditions of the analytical gap, may also vary. The advantage of the stationary-gap controlled spark source is that the ratio of the discharge energies falling on the analytical and the controlling spark gap is constant. Its disadvantage, however, is that it is rather sensitive to adjustment, and a change in its length owing to burning or other reasons results in changing the excitation conditions, the charging voltage of the condenser being a function of the conditions of this gap. In addition, if the discharge circuit contains a larger self-inductance, the extinguishing of the spark gap is difficult owing to the longer duration of the discharge. From this point of view the rotary-gap control is more advantageous, because, in addition to control, this gap breaks the eventual short

---

*This paper forms Part IV of a series of articles, the previous parts being:

Part I: Á. BARDÓCZ: Interrupted arc source for spectrum analysis. *Acta Phys. Hungarica* 1952, **1**, 247.

Part II: Á. BARDÓCZ: Electronically controlled A.C. operated D.C. interrupted arc source. *Acta Phys. Hungarica* 1953, **2**, 265. *See also*: Electronically controlled A.C. interrupted arc source for spectrographic purposes. *J. Opt. Soc. Amer.* 1952, **42**, 357.

Part III: Á. BARDÓCZ: Electronically controlled A.C. operated A.C. interrupted arc source. *Spectrochim. Acta* 1953, **5**, 397.

circuit of the charging circuit through the analytical and the control gap initiated by the discharge of the condenser.

In both spark-source systems the frequency of the spark discharges is determined by the mains frequency and it generally equals its double value. Spark discharges of lower frequency are necessary in ignitor spark sources for interrupted arcs and low-voltage condensed sparks, while a higher sparking rate is desirable in the case of high-voltage condensed sparks. A version of stationary-gap controlled spark sources is the air-interrupter controlled type, which is suitable for producing more than one spark during a half-period of the mains [1, 4].

Recently, spectroscopic practice seems to prefer stationary-spark-gap controlled systems.

The trend of the development of the above almost unique electrical control methods is due to the fact that switching elements better than spark gaps were not available to operate the relatively high instantaneous energies occurring in spectroscopic practice. The first experiment to control the excitation energies in some other way was carried out by Malpica and Berry [5], who applied an ignitron as controlling element. In some other similar experiments the switching element was the trigatron tube [6] developed during the last war, which is also suitable for controlling high instantaneous energies [7, 8]. The latter spark sources were also designed for constant-frequency operation.

The author's experiments on the improvement of spark sources resulted in a system controlled by a double control spark gap operated by a thyratron tube [9]. This circuit is, in addition to securing the advantages of electronic control, in principle suitable for controlling unlimited condenser energies and it possesses the advantages of the stationary control spark gap. The control gap can be switched in a *forced* way, independently of its conditions and, with certain restrictions, of its dimensions. In this electronically controlled spark-source system the frequency of the discharges can be set within wide limits below and above the mains frequency.

VOL.
7
1955/5

The new electronically controlled spark source

The basic circuit of the new electronically controlled spark source is shown in Fig. 1, which is a slightly modified form of the circuit described in [9]. In Fig. 1 the thin-line part on the left-hand side of condenser C is the charging circuit, and the right-hand side thick-line part is the discharge circuit. The thin-line part inside of the discharge circuit is the control circuit.

The condenser C [Fig. 1] supplying the excitation energy is charged by transformer Tr through the rectifying diode $V2$. In the circuit, $S2$ and F denote the double control gap and the analytical gap, respectively. $R4$ is an ohmic resistance used in general to shunt the analytical gap. The high-value resisters $R1$ and $R2$ divide the voltage of condenser C equally between the two spark gaps of $S2$. $R1$ and $R2$ can be replaced by condensers. The presence of $R4$ does not interfere with this voltage division, as its resistance is negligible as compared to the resistances of $R1$ and $R2$. In the circuit, $V1$ denotes a thyratron tube whose anode circuit contains the ohmic resister $R3$. The thyratron tube $V1$ is blocked by a negative bias through its grid. L is the usual self-inductance in the discharge circuit.

The circuit in Fig. 1 operates in the following way. The double control gap $S2$ must be set so that condenser C being charged, it is just prevented from breakdown. If a positive-voltage signal is applied to the grid of the thyratron tube $V1$, the tube fires, and owing to this the point b of the circuit practically comes to the potential of the point a. This means, however, that the whole charging voltage of the condenser C appears on the upper part of the control gap $S2$, causing it to break down. Afterwards condenser C begins to discharge through $R4$, the upper part of $S2$, $R3$, and $V1$. In this state of the system $R3$ shunts the lower part of $S2$; consequently of the spark gap F and the lower part of $S2$, the one shunted with the

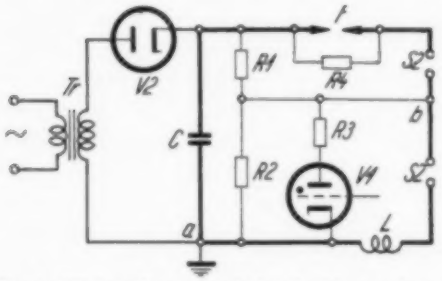

Fig. 1. Wiring diagram of the double spark-gap type electronically controlled high-voltage spark source. C = condenser; F = analytical spark gap; L = self-inductance; $R1$, $R2$ = voltage-divider ohmic resisters; $R3$, $R4$ = ohmic resisters; $S2$ = double control gap, Tr = high voltage transformer; $V1$ = thyratron tube; $V2$ = rectifying diode. The thick-line part is the discharge circuit.

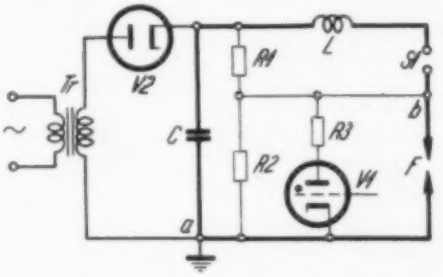

Fig. 2. Wiring diagram of the single spark-gap type electronically controlled high-voltage spark source. C = condenser; $S1$ = control gap; F = analytical spark gap; L = self-inductance; $R1$, $R2$ = voltage divider ohmic resisters; $R3$ = ohmic resister; Tr = high-voltage transformer; $V1$ = thyratron tube; $V2$ = rectifying diode. The thick-line part is the discharge circuit.

greater resistance breaks down first. If, as usual, $R4$ is larger than $R3$, the breakdown of the upper part of $S2$ is followed by that of F. The discharge of condenser C continues through F, the upper part of $S2$, $R3$, and $V1$. Under such conditions the entire charging voltage of condenser C appears on the terminals of $R3$, i.e., on the lower part of the double-spark gap $S2$, which latter breaks down too. Then condenser C discharges through F, $S2$, and L, supplying the excitation energy. The thyratron tube extinguishes either at the end of the discharge of condenser C or before it, depending on the electrical data of the circuit F, $S2$, L. The case of $R3 = R4$ and that of $R3$ larger than $R4$ will be treated below.

The positive-voltage pulses necessary to operate the thyratron tube $V1$ are fed in either by means of a mechanical switch, or electrically. The operation of the apparatus is correct if condenser C is charged during one half-period of the mains voltage and discharged during the other.

The operation of the circuit is illustrated in Fig. 16, to which we shall return below.

A modification of the circuit in Fig. 1 is shown in Fig. 2, which differs from the former in that the spark gap denoted by F in Fig. 1 with shunt resister R4 is missing from it. Thus Fig. 2 contains two spark gaps altogether, one-half of the double control gap of Fig. 1 becoming the analytical spark gap F. The operation of the circuit in Fig. 2 is clear according to the above.

The experimental arrangement

The experimental arrangement employed to determine the electrical characteristics of the electronically controlled spark source is described below.

The transformer Tr [Figs. 1 and 2] is of 220/15,000 volts. To vary the charging voltage of condenser C, a voltage-regulating transformer is inserted before the transformer Tr. In the primary circuit of transformer Tr there is a resistance of about 3 ohms to limit the current flow when the spark gaps F and S are short-circuited. $V2$ are rectifying vacuum diodes of an operating voltage of 20,000 volts and an inverse voltage of 40,000 volts, maximum load 1 amp. $V1$ are gas-filled triodes (thyratron) of an operating voltage of 10,000 volts, peak anode current 16 amps. For the condenser C partly Minos, partly Dubilier mica condensers were used. $R1 = R2$ are 100 MΩ, each composed of 30-piece 3·3 MΩ, 5-watt radio-resisters. $R3$ and $R4$ are 100-watt resisters, the values of which are given below.

The spark gaps $S2$ and $S1$ in Figs. 1 and 2 have been formed of three zinc or carbon discs in symmetrical arrangement. The diameter of the middle disc is 58 mm, its thickness 27 mm: the two outer discs are 45 mm in diameter and 23 mm thick. The surfaces of the zinc discs facing each other are centrally ribbed, while the carbon discs are flat. The distance between the outer and the middle discs can be regulated. Owing to the suitable construction, the distance can also be adjusted while the voltage is on the apparatus. To avoid heating and, at the same time, to increase the reproducibility of the measurements, the zinc discs were water-cooled during operation. In these measurements the b points of Figs. 1 and 2 were earthed, thus the middle disc of the spark gap could be directly connected to the water mains. As in such a circuit the outer discs of the control gaps $S1$ and $S2$ are at high voltage, the cooling was carried out with the aid of vessels placed on insulators. The temperature of the mains water circulating in the discs varied between 14 and 17°C. If one control gap was operated, one of the outer discs was conductively connected to the middle disc. In Figs. 4–7 the single spark gap was marked by two discs (lettering $S1$), and the double spark gap in Figs. 8–13 by three discs (lettering $S2$). If no water-cooling is desired, the zinc discs of the control gaps can well be replaced by carbon or graphite discs. The investigations have shown that the cooling has only negligible influence on the operating conditions of the source.

The electrodes employed in the analytical spark gaps F of Figs. 1 and 2 were in every case spectroscopically pure flat-ended rods 6 mm in diameter. The analytical spark gaps were always ionized by an ionizing needle, which had important influence on the operation of the source.

The grids of thyratron tube $V1$ in Figs. 1 and 2 was controlled by a pulse generator [10, 12]. The negative bias blocking the tubes is also supplied by the pulse generator. The pulse generator produces voltage signals at a rate of 100/sec, or lower. The frequency of the voltage signals of a lower rate is equal to a subharmonic of the mains frequency. The operation of the pulse generator is synchronous with the mains frequency. All the characteristic curves to be described below were taken at a sparking frequency of 50 Hz.

During the investigation the correctness of the adjustment and the regularity of the operation of the apparatus were controlled by a cathode-ray oscilloscope, by observing the voltage variation on the terminals of condenser C.

VOL 7 1955/

Electrical characteristics of the single control gap source

To study the electrical characteristics of the new source we have investigated what influence the capacity of condenser C in Fig. 2, the charging voltage U_C, the ohmic resistance $R3$, the electrode separation d_{S1} of the control gap $S1$ and d_F of the analytical gap F, respectively have on the operating conditions. The relations between these five parameters have been determined by measurements.

If in the spark source in Fig. 2 (the analytical electrode separation d_F being fixed) the electrode separation d_{S1} of the control gap is varied, we find that there is a lower and an upper d_{S1} electrode separation, within which the system operates regularly. In the following we shall name this electrode separation difference Δd_{S1} the *operating range*.

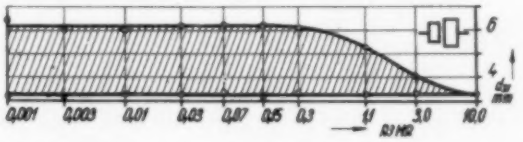

Fig. 3. Operating range of the single control-gap type spark source. d_{S1} = electrode separation of the control gap; $R3$ = ohmic resistor; d_F = 3-9 mm; U_C = 18,000 volts; C = 10,000 pF. Sparking frequency = 50/sec. The operating range is hatched.

The purpose of the first group of measurements was to determine the influence of the ohmic resister $R3$ on the operating range and the most adequate value of this resister. The results of the measurements are displayed in Fig. 3. With d_F = 3·0, 6·0, and 9·0 mm electrode separations of the analytical gap F, the resister $R3$ being varied, the figure shows the control-gap electrode separations d_{S1} at which the source operates regularly. By regular operation we mean that the oscilloscope shows the picture in Fig. 16a, no ignition is missing, and the spark gaps do not all ignite themselves irregularly, i.e., without control. It must be noted that we carried out all the following experiments with the analytical electrode separations d_F = 3·0, 6·0, and 9·0 mm.

On the abscissa of Fig. 3 the values of $R3$ are plotted on a logarithmic scale against the distance d_{S1} of the control spark gap $S1$ on the ordinate. The measurements show that if the charging voltage of condenser U_C = 18,000 volts, C = 10,000 pF, and the separation d_F of the electrodes of the analytical gap F varies between 3–9 mm, by varying the value of resister $R3$ between about 0·001 and 0·2 MΩ, a safe operating range is obtained if the electrode separation d_{S1} of the control gap $S1$ is between 3·3 and 6·2 mm. If the value of $R3$ is still increased, the upper value of d_{S1} decreases, and in the neighbourhood of about 10 megohms the operating range shrinks to a single point. Consequently, the operation of the circuit in Fig. 2 is safe if the current flowing through the thyratron tube $V1$ exceeds a certain minimum.

In Fig. 3 the operating range Δd_{S1} is hatched.

Further measurements were made to determine how the operating range Δd_{S1} varies as a function of the analytical electrode separations d_F, the charging voltage U_C, and the capacity of condenser C. The resistance $R3$ was selected according to Fig. 3, and a value of 0·02 megohms was kept constant during the investigations.

For the capacity values $C = 1000$, 5000, 10,000, and 20,000 pF the results are displayed in Figs. 4, 5, 6, and 7, where on the two abscissae the charging voltage U_C and the analytical electrode separation d_F are plotted, respectively. The ordinate is

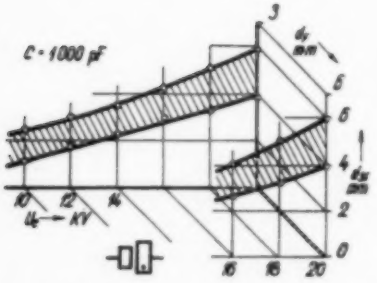

Fig. 4. Operating range of the single control-gap type spark source as a function of the charging voltage U_C and the analytical gap electrode separation d_F. $C = 1000$ pF; $R3 = 0{\cdot}02$ MΩ, sparking frequency = 50/sec. The operating ranges are hatched.

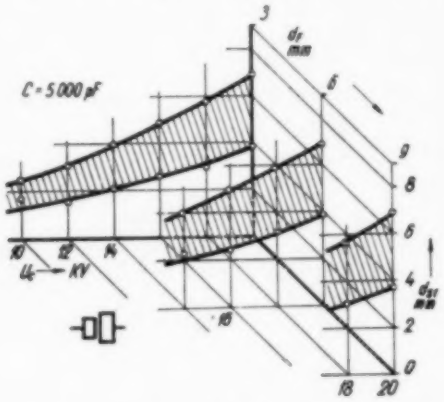

Fig. 5. Operating range of the single control-gap type spark source as a function of the charging voltage U_C and the analytical electrode separation d_F. $C = 5000$ pF; $R3 = 0{\cdot}02$ MΩ; sparking frequency = 50/sec. The operating ranges are hatched.

the electrode separation d_{S1} of the control gap. To interpret the figures, let us start from Fig. 6, showing the conditions for the capacity value $C = 10{,}000$ pF. Fig. 6 consists of three parts, for $d_F = 3$ mm, $d_F = 6$ mm, and $d_F = 9$ mm, respectively.

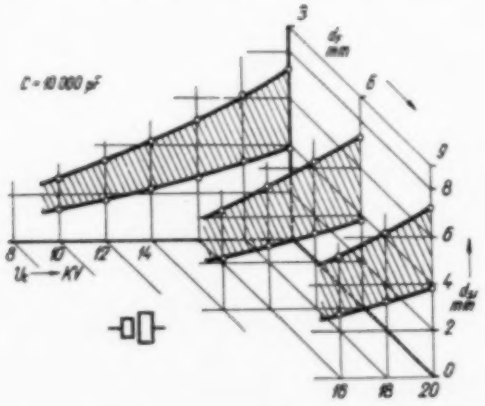

Fig. 6. Operating range of the single control-gap type spark source as a function of the charging voltage U_C and the analytical electrode separation d_F. $C = 10{,}000$ pF; $R3 = 0{\cdot}02$ MΩ; sparking frequency = 50/sec. The operating ranges are hatched.

The initial parts of the curves are similar, but at higher analytical gap lengths d_F the operating range vanishes at comparatively much higher voltage values. In general, at given analytical electrode separation d_F the control-gap electrode

separation d_{S1} decreases with decreasing condenser-charging voltage U_C, as expected, and the width of the operating range Δd_{S1} also decreases. When the charging voltage U_C of condenser C has decreased to such an extent that the source is no more capable of breaking down the distances d_F and d_{S1} during operation, condenser C cannot discharge any more. Consequently, with given d_F and d_{S1} gap lengths there is a minimum voltage below which the source cannot operate.

Comparing Figs. 4, 5, 6, and 7, it can be stated that the source of the curves is

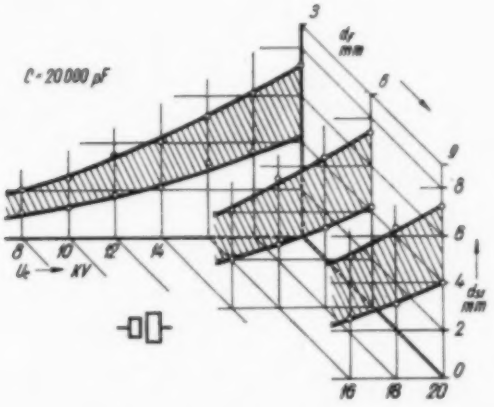

Fig. 7. Operating range of the single control-gap type spark source as a function of the charging voltage U_C and the analytical electrode separation d_F. C = 20,000 pF, $R3$ = 0·02 MΩ; sparking frequency = 50/sec. The operating ranges are hatched.

in general the same for every capacity value. The deviation is that at lower capacity values of condenser C the operating range narrows, and that at lower capacity values, if the analytical electrode separations d_F are greater, the source is no more capable of operation.

Electrical characteristics of the double gap controlled source

In this case the purpose of the first investigations was to determine the most favourable values of the resisters $R3$ and $R4$ in Fig. 1. The results are summarized in Figs. 8 and 9, showing the variation of d_{S2} and Δd_{S2}, with the various values of $R3$ and $R4$ for the analytical electrode separations $d_F = 3$ and $d_F = 6$ mm. By the electrode separations of the double control gap we always mean the sum of the electrode separations of the two half-gaps.

In Fig. 8 the two abscissae are the values of $R3$ and $R4$ in a logarithmic scale, on the ordinate the sum of the double control-gap electrode separations d_{S2} is plotted. In the measurements C = 10,000 pF, U_C = 18,000 volts, d_F = 3 mm. According to the figure, both $R3$ and $R4$ must not exceed a certain maximum value to enable Δd_{S2} to be large, i.e., the operating range to be wide. From Fig. 8 it can be stated that, if the value of $R3$ is between 0·001 and 0·15 megohms, and that of $R4$ is between 0·02 and 0·15 megohms, the surface has a plateau, within which the operating range is the widest. Here the value of d_{S2} is between 7·2 and 11·4 mm. Outside of the area covered by this plateau the operating range Δd_{S2} decreases.

If, under the above experimental conditions, the length of the analytical gap d_F is increased from 3 mm to 6 mm, the conditions in Fig. 9 are obtained. It is clear from the figure that with $d_F = 6$ mm the widest operating range is between the values 7·2 and 10·2 mm of d_{S2}. It is also remarkable that the surface is crossed by a valley where the operating range Δd_{S2} narrows so much that the system ceases to operate. The appearance of the valley can be explained by the following.

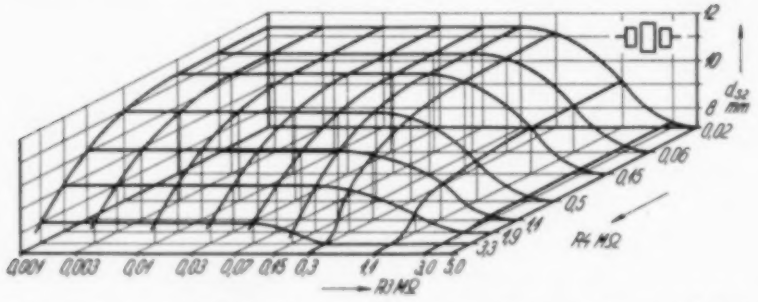

Fig. 8. Operating range of the double control-gap type spark source. d_{S2} = total electrode separation of the double control gap; $R3$ and $R4$ = ohmic resisters; $d_F = 3$ mm; $U_C = 18{,}000$ volts; $C = 10{,}000$ pF; sparking frequency = 50/sec.

We have mentioned above that when the one part of the control gap $S2$ has already broken down during the operation of the circuit in Fig. 1, the charging voltage U_C of condenser C is distributed between the resistances $R3$ and $R4$. The analytical spark gap being $d_F = 6$ mm, the charging voltage $U_C = 18{,}000$

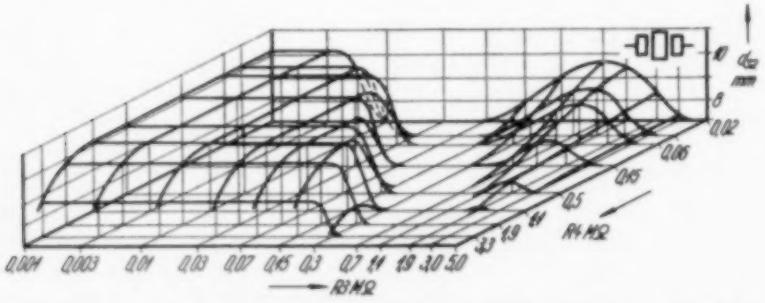

Fig. 9. Operating range of the double control-gap type spark source. d_{S2} = total electrode separation of the double control gap; $R3$ and $R4$ ohmic resisters; $d_F = 6$ mm; $U_C = 18{,}000$ volts; $C = 10{,}000$ pF, sparking frequency = 50/sec.

volts of condenser C cannot cause break-down if the resisters $R3$ and $R4$ divide the voltage U_C between the two spark gaps almost equally. As a consequence of this, in Fig. 9 the valley appears in the neighbourhood of resistance values at which $R3$ and $R4$ are approximately equal. To enable the lower part of $S2$ and F to break down when the upper part of the controlling spark gap $S2$ has already broken down, the values of $R3$ and $R4$ must differ considerably. If $R4$ is larger than $R3$, or vice versa, the ranges on left and right-hand side respectively of the valley in Fig. 9 are considered. In the range on the left-hand side of the valley

there is a fairly large plateau, below which the favourable operating range is situated.

With adequate values of $R3$ and $R4$ we have determined how the electrode separations d_{S_2} of the control gap and the operating range vary as functions of the capacity of condenser C, the charging voltage U_C, and the analytical electrode separations d_F. The measurements were performed for the resistance values $R3 = 0{\cdot}02$ MΩ, and $R4 = 0{\cdot}5$ MΩ, and for the capacity values $C = 1000$, 5000, 10,000 pF and 20,000 pF. The results of the measurements are summarized in Figs. 10, 11, 12, and 13.

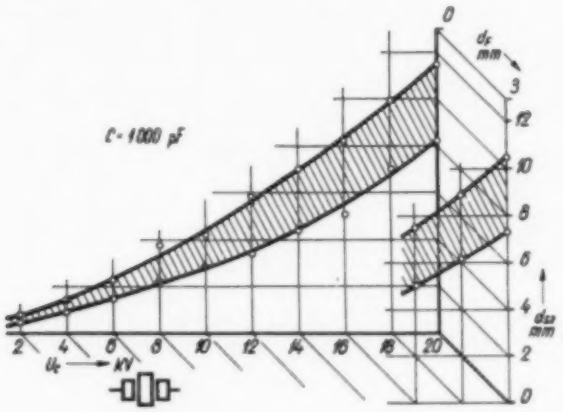

Fig. 10. Operating range of the double control-gap type spark source as a function of the charging voltage U_C and the analytical electrode separation d_F. $C = 1000$ pF, $R3 = 0{\cdot}02$ MΩ; $R4 = 0{\cdot}5$ MΩ; sparking frequency = 50/sec. The operating ranges are hatched.

In all the figures the curves marked $d_F = 0$ were taken with the analytical spark gap F short-circuited. These curves show that, at adequately small electrode separations, the circuit is still capable of operation at 2000 volts. This fact is important for the electronically controlled spark sources producing igniting sparks. In the case of an analytical spark gap $d_F = 3$ mm, the source ceases to work at about 12 kV for condenser values of 5000, 10,000, and 20,000 pF (Figs. 11, 12, and 13), while in Fig. 10, for a capacity value of 1000 pF, it does so already at about 16 kV. The operating range still decreases at $d_F = 6$ and 9 mm. In general, the lower the value of C, the higher the voltage values at which the system still operates. At the capacity value $C = 1000$ pF and $d_F = 6$ and 9 mm, no operation is possible. With decreasing capacity values the operating range also narrows and is shifted towards the smaller analytical electrode separations.

Here we should like to refer briefly to a property of the spark source in question which has not yet been mentioned. This is that the sparks start with a jitter of a few tenths of a microsecond in contrast to the control signal falling, on the grid of thyratron tube $V1$. This circumstance makes possible the production, by means of a rotating mirror, of time-resolved spark spectra of microsecond resolution or better. We shall return to this question elsewhere.

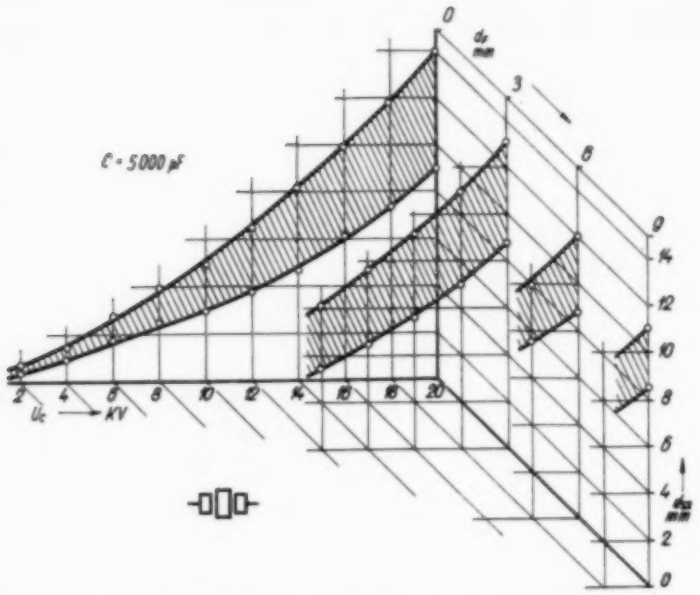

Fig. 11. Operating range of the double control-gap type spark source as a function of the charging voltage U_c and the analytical electrode separation d_r. $C = 5000$ pF; $R3 = 0{\cdot}02$ MΩ; $R4 = 0{\cdot}5$ MΩ; sparking frequency = 50/sec. The operating ranges are hatched.

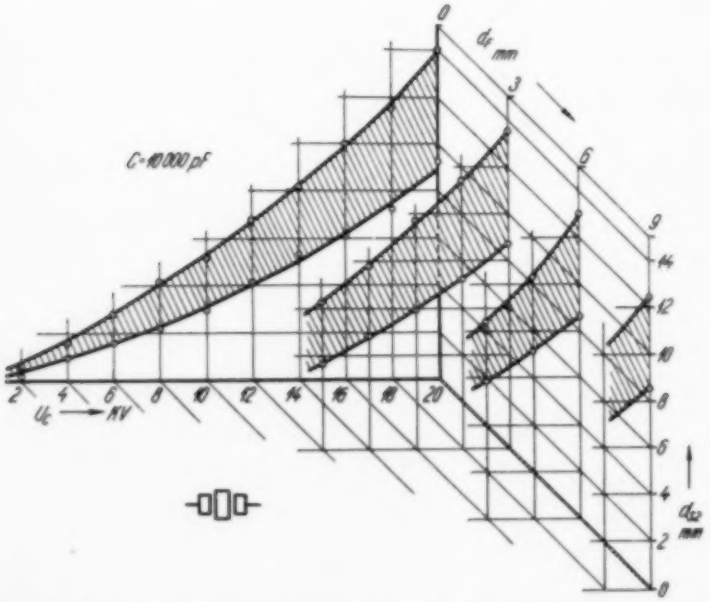

Fig. 12. Operating range of double control-gap type spark source as a function of the charging voltage U_c and the analytical electrode separation d_r. $C = 10{,}000$ pF; $R3 = 0{\cdot}02$ MΩ; $R4 = 0{\cdot}5$ MΩ; sparking frequency = 50/sec. The operating ranges are hatched.

Electronically controlled spark source producing 100 sparks/sec

Owing to the nature of the electronic arrangement, the spark sources in Figs. 1 and 2 can produce spark discharges at a maximum rate corresponding to the mains frequency. This sparking rate is quite satisfactory in most cases at the control of interrupted-arc and low-voltage spark sources, but it is not in the case of high-voltage condensed sparks. In the circuit of Fig. 14 the sparking rate can be raised to twice the mains frequency by comparatively simple means. The part of the circuit on the right-hand side of condenser C is identical with the circuit in Fig. 2; it can however, be formed according to Fig. 1. Between the parts on the left-hand

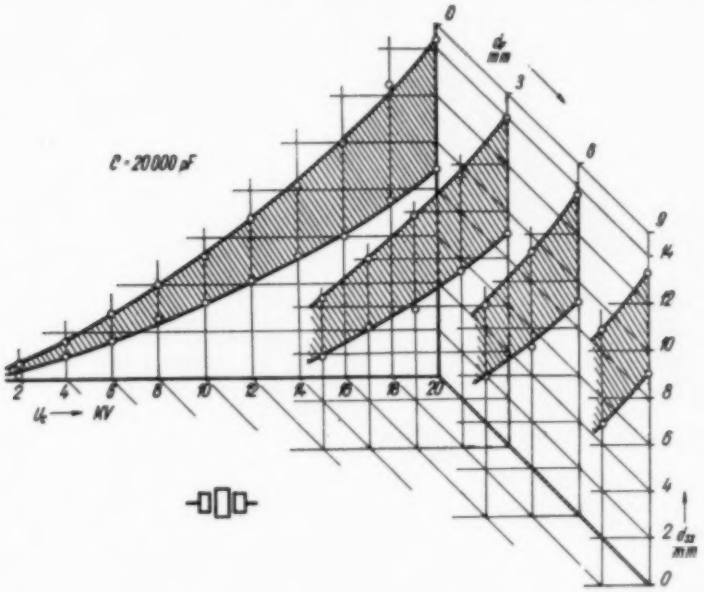

Fig. 13. Operating range of the double control-gap type spark source as a function of the charging voltage U_c and the analytical electrode separation d_r. C = 20,000 pF; $R3$ = 0·02 MΩ; $R4$ = 0·5 MΩ; sparking frequency = 50/sec. The operating ranges are hatched.

side of condenser C of Figs. 1 and 2, and that of Fig. 14, the difference is that in the latter case we have full-wave rectification with the aid of a Graetz circuit. If with a 50-Hz mains frequency the phase of the positive voltage signal controlling the grid of the thyratron tube is such that the spark is always produced at zero value of the transformer voltage, and if the signal frequency is 100 Hz, a spark series of 100-Hz frequency is obtained. Such discharge conditions are illustrated in the oscillogram of Fig. 17.

In the sources of Figs. 1 and 2, if the setting is correct the interval between the sparks is 0·02 sec during about 0·01 sec of which no voltage is on condenser C. Though in the circuit of Fig. 14 the discharge of condenser C takes place at zero value of the transformer voltage, almost simultaneously with the discharge the voltage begins to rise on the terminals of the condenser. With a small inductance

in the discharge circuit, and conventional values of the circuit elements, the system operates regularly. If, however, the discharge circuit contains a higher inductance and thus the duration of the discharge is longer, the spark gaps do not extinguish. In such cases air-blast must be applied to the control gap. In

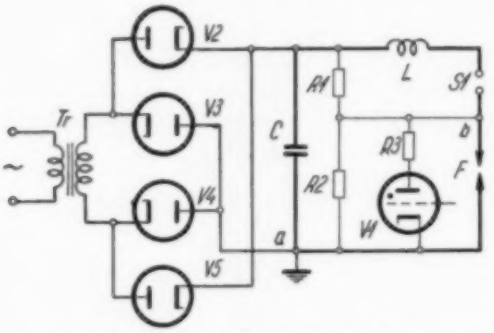

Fig. 14. Wiring diagram of the electronically controlled spark source producing 100 sparks/sec. C = condenser; F = analytical spark gap; L = self-inductance; $R1$, $R2$ = voltage divider ohmic resisters; $R3$ = ohmic resister; $S1$ = controlling spark gap; Tr = high-voltage transformer; $V1$ = thyratron tube; $V2$, $V3$, $V4$, $V5$ = rectifying diodes. The thick-line part is the discharge circuit.

the case of the double control gap $S2$ it suffices to blow air at the upper spark gap of Fig. 1, generally speaking at the spark gap which is not connected in parallel to the thyratron tube $V1$.

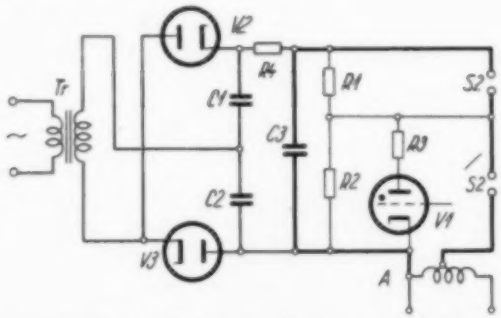

Fig. 15. Wiring diagram of the spark source producing ignitor sparks. A = Tesla transformer; $C1, C2, C3$ = condensers; $R1$, $R2$ = voltage divider ohmic resistors; $S2$ = double control gap; Tr = high-voltage transformer; $V1$ = thyratron tube; $V2$, $V3$ = rectifying diodes. The thick-line part is the discharge circuit.

With a 50-Hz mains frequency, sparks of a frequency of 100 Hz can also be produced by means of the circuit in Fig. 15, which is primarily suited to produce low-energy discharges. Thus it can be well used for the control of interrupted arcs and low-voltage condensed sparks. In Fig. 15, Tr, $V2$, $V3$, $C1$, and $C2$ denote the elements of a usual voltage-doubling circuit. The actual working condenser is marked by $C3$, which is charged by $C1$ and $C2$ through the ohmic resister $R4$. The other parts of the circuit are left unchanged, with the difference that the primary part of the Tesla autotransformer A is also contained in the discharge

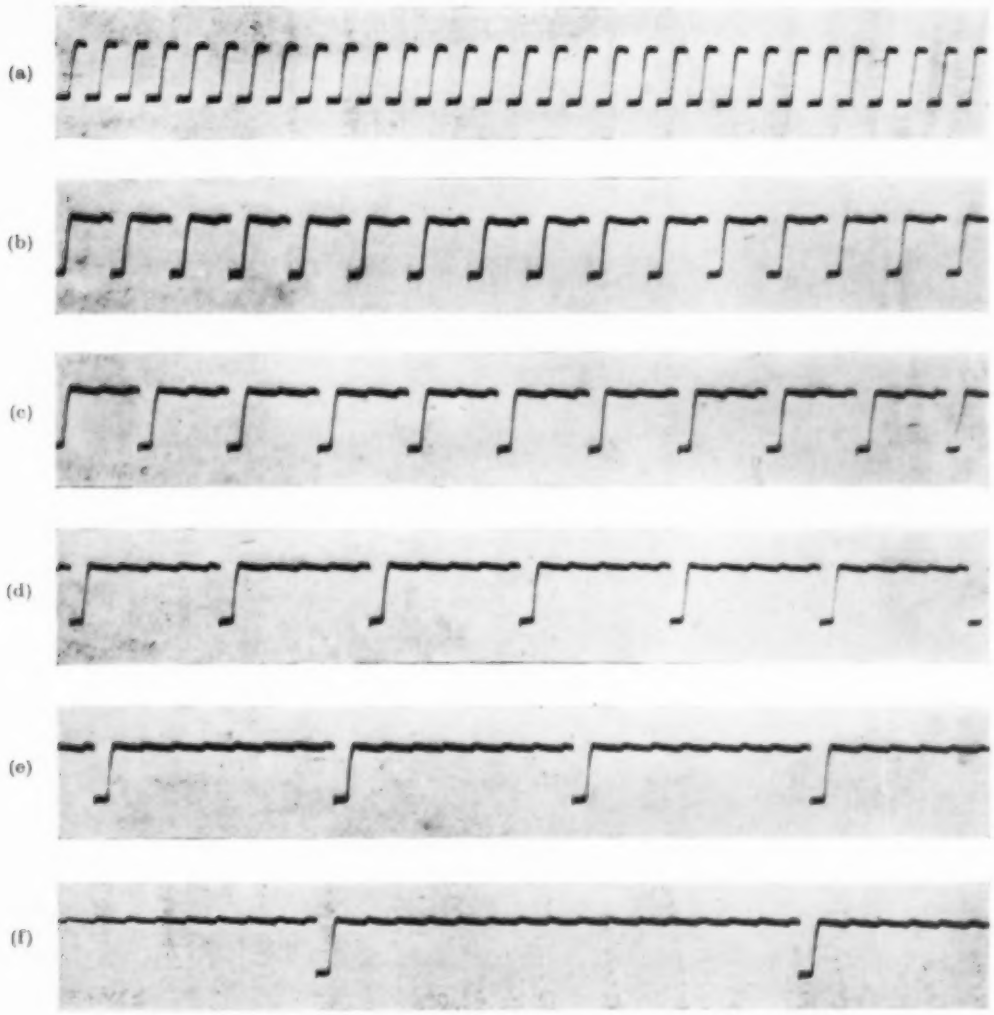

Fig. 16. Voltage course on the terminals of condenser C in Fig. 2 for various sparking frequencies. The oscillograms were taken by a fibre oscillograph. C = 10,000 pF; U_c = 18,000 volts. The respective sparking frequencies in the pictures a–f are 50, 50 × 1/2, 50 × 1/3, 50 × 1/5, 50 × 1/8, 50 × 1/16.

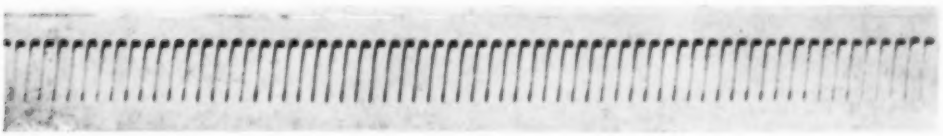

Fig. 17. Voltage course on the terminals of condenser C of Fig. 14. C = 10,000 pF; U_c = 18,000 volts; sparking frequency is 100/sec.

VOL
7
1955/

circuit. The high-frequency discharges produced in the circuit $C3$–$S2$–A are transformed by the Tesla autotransformer A, which also produces the igniting spark.

In ignitor-spark sources the d.c. supply has a definitive advantage. If condenser $C3$ of Fig. 15 is supplied by a.c., especially in the ignition of the low-voltage condensed spark, the peak value of the charging voltage of the low-voltage condenser, and that of the condenser $C3$, would not coincide in phase. The most efficient excitation and ignitor sparks are obtained, however, when the discharge takes place at the peak values of the charging voltage of the two condensers. In the case of a.c. supply it is difficult to make the two phases coincide. However, if condenser $C3$ is charged by d.c., the ignition can be easily made to conform to the desired phase of the working condenser, as the phase of the positive-voltage pulse controlling the grid of the thyratron tube can be easily set.

The basic system of the electronically controlled spark source described here is also suitable to produce sparks at a rate more than twice the mains frequency. This problem will be dealt with later.

Operation of the electronically controlled spark source

To illustrate the operation of the spark source, some oscillograms are shown in Figs. 16 and 17. The oscillograms in Fig. 16 show the voltage course on the terminals of condenser C of Fig. 2 if the grid of the thyratron tube $V1$ is controlled by positive voltage signals of various frequencies. The oscillograms were taken by a Siemens fibre oscillograph. In Figs. 16a–f the numbers of sparks/sec are 50, $50 \times 1/2$, $50 \times 1/3$, $50 \times 1/5$, $50 \times 1/8$, and $50 \times 1/16$ respectively. The small irregularities of the oscillograms are due to the self-oscillations of the oscillograph fibre.

The oscillogram of Fig. 17 taken with the circuit in Fig. 14 also gives the voltage variation on the terminals of condenser C, at a sparking frequency of 100 Hz.

Some remarks

The characteristic curves of the circuits in Figs. 2 and 1 exhibited in Figs. 4–7 and 10-13 show that the new electronically controlled spark source offers very stable electrical conditions, if condenser C is free of voltage after the discharge and the spark gaps have time enough for de-ionization. The stability is shown by the fact that the control-gap separations d_{S1} and d_{S2} can be varied within comparatively wide limits without affecting the regularity of operation. Owing to this, slight changes in the control-gap electrode separation hardly affect the operation from the spectroscopic point of view. Within the operating range the length of the control gap does not affect the charging voltage of condenser C. At the same time, the control gap being fixed, the ratio of the discharge energy distributed between the analytical and the control gap remains constant.

The characteristic curves of Figs. 4–7 and 10–13 are not valid for the circuits in Figs. 14 and 15 because, the condensers C and $C3$ being discharged, voltage appears on the spark gaps immediately, before they could have been de-ionized. If, however, the circuits in Figs. 14 and 15 are modified, so that a control charging tube is placed in the charging circuit of condenser C and $C3$, the conditions are quite the same as those of the circuits in Figs. 1 and 2.

Comparing the single control-gap spark source with the double control-gap type we can state the following:

The use of the single control-gap type electronically controlled spark source is limited, because the length d_F of the analytical spark gap F cannot be set independently of the charging voltage U_C of condenser C. The shortest length d_F of the analytical spark gap is necessarily the one which does not break down at the voltage on the terminals of resister $R2$. As can be seen from Figs. 4, 5, 6, and 7, this fact has practically no inconvenient effect up to 20,000 volts charging voltage, if the conventional analytical electrode separations are employed. However, inconveniences may result at such charging voltages with very small electrode separations, or with the conventional electrode separations at higher charging voltages.

Comparing the characteristic curves shown in Figs. 4–7 of the single control-gap circuit in Fig. 2, with those of the double control-gap circuit in Fig. 1 shown in Figs. 10–13, it can be stated that, with the analytical gap length $d_F = 3$ mm, the operating range of the double control-gap arrangement is wider than that of the single control-gap type. At electrode separations greater than that, the operating ranges of the two systems are generally equal. However, the characteristic curves in Figs. 4–7 cover a wider voltage range for all the electrode separations than in the case of Figs. 10–13.

In every case when conventional electrode separations and operating voltage are employed, the single control-gap type spark source is used to satisfaction.

Acknowledgements—Our thanks are due to Á. KLATSMÁNYI for his work in developing the electronically controlled spark source; to K. BERTA, A. BORONKAY, S. EDER, F. MANCZ, and Z. SIBALSZKY for their co-operation in the experiments and for carrying out the measurements.

References

[1] FOWLER, R. G., and WOLFE, R.A., *J. Opt. Soc. Amer.* 1945, **35**, 170.
[2] ENNS, J. H., and WOLFE, R. A., Symposium on spectrographic light sources. Spec. Tech. Publ. Am. Soc. Test. Mat., Philadelphia 1948.
[3] ENNS, J. H., and WOLFE, R. A., *J. Opt. Soc. Amer.* 1949, **39**, 298.
[4] KACZOR, E., and CHAMBERLAIN, K., *J. Opt. Soc. Amer.* 1949, **39**, 637.
[5] MALPICA, J. T. M., and BERRY, T. M., *Gen. Elec. Rev.* 1941, **44**, 563.
[6] CRAGGS, J.D., HAINE, M. E., and MEEK, J. M., *J. Inst. Electrical Engng.* 1946, **93**, III A, 963.
[7] BRAUDO, C., and CLAYTON, H. R., *Nature* 1946, **157**, 622.
[8] BRAUDO, C., and CLAYTON, H. R., *J. Soc. Chem. Ind.* 1947, **66**, 259.
[9] BARDÓCZ, Á., *Nature* 1953, **171**, 1156.
[10] BARDÓCZ, Á., *J. Opt. Soc. Amer.* 1952, **42**, 357.
[11] BARDÓCZ, Á., *Acta Phys. Hungarica* 1953, **2**, 265.
[12] BARDÓCZ, Á., *Spectrochim. Acta* 1953, **5**, 397.

Note added in proof—

In this journal (*Spectrochim. Acta*, 1955, **6**, 134) BUNGE described a spectrographic igniter circuit which contains, as controlling elements, two spark gaps and an electronic tube. In BUNGE's paper no reference is made to a paper by the author (*Nature*, 1953, **171**, 1156) where the principle of electronic tube-spark gap combination has been first applied for the control of spectrographic spark sources.

Spectrochimica Acta, 1956, Vol. 7, pp. 321 to 348. Pergamon Press Ltd., London

Analytical studies of the fluorescence of samarium in calcium tungstate*

C. Gordon Peattie† and L. B. Rogers
Department of Chemistry and Laboratory for Nuclear Science,
Massachusetts Institute of Technology, Cambridge 39, Mass.

(*Received* 9 *July* 1954; *accepted for publication* 22 *September* 1955)

Abstract—A quantitative fluorimetric procedure for samarium, based upon the preparation of a slurry from calcium tungstate and a solution containing trivalent samarium, has been developed. Amounts of samarium as small as 2 μg per gram of calcium tungstate can be detected after drying and igniting the slurry. If one employs 2536-Å radiation rather than 3650-Å for excitation, the tungstate will fluoresce and can be used as an internal standard. The fluorescence of samarium is severely quenched by the presence of other rare earths, and this will limit the applicability of the method.

Introduction

For nearly fifty years fluorescence has been used for the qualitative detection of samarium. A wide variety of solids ranging from reagent-grade salts such as alkali and alkaline earth halides, oxides, sulphides, borates, phosphates, sulphates, and tungstates [1–21] to minerals such as scheelite [3] have been used as media in which the samarium was held. The spectra were usually produced by irradiation with selected mercury lines, though sometimes with cathode rays, and were frequently examined with the aid of a spectrograph. The highest sensitivity, 1 μg of samarium (III) per gram of flux was reported by Servigne [15], who placed the fluorophor within the mercury lamp. A tenfold greater sensitivity (0·1 μg/g) was obtained by other investigators who worked with divalent samarium [12, 13]. Throughout the remainder of the present paper we shall assume, on the basis of the extensive work in the literature, that we are concerned only with trivalent samarium.

From the point of view of the analytical chemist, reports in the literature often proved disappointing after careful scrutiny. Frequently the details of the preparation of the fluorophors were scanty, and sometimes they were omitted completely, or else the procedures were too cumbersome to be practical for routine analytical use. On occasion, the quantitative claims were unsupported by data [16]. Moreover, the fluorescence spectra were often obtained at low resolution with rare earths of undetermined purity. For these reasons a critical comparison of the different fluxes appeared highly desirable.

Although the final goal of the study was a simple procedure that would require only a filter fluorophotometer, study of the fluoresence was made with a spectrograph because of the additional information that could be obtained. Much of that information has been included below in greater detail than required for analytical

* This paper was presented in part before the Pittsburgh Conference on Analytical Chemistry and Applied Spectroscopy on 2 March 1953. This paper was taken from a thesis submitted by C. G. Peattie in June 1952, in partial fulfilment of the requirements for the degree of Doctor of Philosophy.

† Present address: Shell Development Company, Exploration and Production Research, 3737 Bellaire Boulevard, Houston 25, Texas.

purposes, because it is felt that the data might be useful to those interested in the fundamental theory of fluorophors.

Experimental details

Reagents and solutions

Water was purified by passing ordinary distilled water through an ion-exchange column containing two parts of anion-exchange resin, IRA-410, to one part of cation exchange resin, IR-120, both from Rohm and Haas. The resulting water had a specific conductance of $0{\cdot}8–1{\cdot}2 \times 10^{-6}$ ohm^{-1} cm^{-1}.

The stock solutions of rare earths were made from rare-earth oxides, which were converted to the sulphates by fuming (four times) with sulphuric acid, then dissolved, and diluted to volume. As for the purity of the rare-earth oxides, the following information was received from the vendor (Research Chemicals Inc., Burbank, California):

(a) Samarium(III) oxide (99·9 per cent minimum). Principal impurities: europium, gadolinium.
(b) Europium(III) oxide (99·8 per cent minimum). Principal impurity: samarium.
(c) Gadolinium(III) oxide (98 per cent minimum). Principal impurities: "approximately 1 per cent terbium, plus fractional percentages of samarium, europium, and yttrium earths."
(d) Neodymium(III) oxide (99·9 per cent minimum). Principal impurities: samarium, praseodymium.

All the samples contained traces of calcium, silicon, and magnesium. All other reagents were Mallinckrodt analytical reagents and were used as received.

Preparation of fluorophors (general)

The fluorophors were prepared in two ways. In one, the solution of rare earth was added to the dry base material and a homogeneous slurry was formed by stirring. The slurry was then dried and ignited. In the second method of preparation coprecipitation was employed.

In both procedures, ignitions and measurements were carried out in circular platinum dishes, 3 mm deep, which had been punched out of platinum sheet, 0·5–1·0 mm thick. Each had an outer diameter of 17·5 mm and an inner diameter of 15·0 mm, a flat lip accounting for the difference.

Ignitions of the fluorophors between 200°C and 900°C were carried out in an electric furnace which had pyrometric control of a selected temperature. A second furnace having manual control of temperature was used for exploratory ignitions above 900°C. The temperatures were measured with a thermocouple of platinum and platinum-rhodium.

Excitation and measurement of fluorescence

The source of mercury 2536-Å excitation, a Sylvania germicidal lamp (Type B, 4-watt), was used in conjunction with a filter consisting of a solution of nickel sulphate hexahydrate (240 g/l) and cobalt sulphate heptahydrate (45·0 g/l), contained in a 5-cm quartz cell [21, 22]. This arrangement was placed as close to the fluorophor as possible, so as to obtain maximum intensity of irradiation.

The source of 3650-Å excitation was a combination of a General Electric AH-4 mercury light and a Corning filter (No. 5970). When using this excitation, the spectra of the fluorophors contained a continuous band which started abruptly at 5892 Å, extended to 6107 Å with essentially constant intensity, except for a peak at 5910 Å, and then fell off gradually to 6436 Å. This undesirable feature, which was not present in the spectrum of the 2536-Å excitation, made necessary a significant blank correction for all intensity measurements made in this region.

The spectrograph used in this study was designed by Professor R. C. Lord and assembled under his supervision by Sangster [23]. It was an automatic recording instrument that employed a motor-driven 4 in. × 6 in. echelette grating which was ruled with 15,000 lines per inch and blazed in the second-order ultra-violet. The energy receiver was an RCA-7140CA photomultiplier (large end-window type), which could be cooled with solidified carbon dioxide. The output of the photomultiplier was amplified and recorded by a modified Brown potentiometer. The spectra were recorded with a rate of rotation of the grating of 200 Å/min. At this

VOL 7 1955/

speed of rotation, the reciprocal linear dispersion, as determined from the recorded spectra, was 13·7 Å/mm.

The dishes containing the fluorophors were mounted in a concavity in an aluminium cylinder, which sat on a strip heater. After a steady-state temperature had been reached, the temperature of the fluorophor was assumed to be the same as that read on a thermometer inserted in a well in the cylinder.

In addition to the fluorescence bands of the fluorophor, the spectrum also contained mercury lines, reflected by the fluorophor. Except for two lines, the positions of these mercury lines were most fortuitous in that they were adjacent to but not superimposed on the fluorescence bands. The wavelengths of the fluorescence bands were determined by interpolation between mercury lines of known wavelength. An indication of the accuracy of the determination of wavelengths of strong, sharp bands is shown by the value of 6045·2 $\pm$ 2·9 Å, obtained as an average for the second-order reflection of the Hg 3023·5-Å line in eighteen different spectra.

The intensities of the fluorescence bands were measured by use of the baseline density method [25]. Successive runs on one sample, which stayed in the same position for all runs, showed that the intensity of the same band would not vary by more than 0·5 per cent.

A few measurements were made, using a filter fluorophotometer, which employed 3650-Å excitation from a General Electric AH-4 lamp and a photomultiplier (RCA 1P-21) for reception. Corning-glass filters were used in measurements of fluorescence intensity. These filters passed most of the visible wavelengths and the near infra-red to the cut off by glass just beyond 1 micron. The output of the photomultiplier was amplified and the signal read as the deflection of a microammeter.

VOL. 7 55/56

Exploratory survey of base materials

This survey was made because, in the majority of cases, the information in the literature was insufficient to permit comparison of the suitabilities of the different substances as base materials for a quantitative method. The slurry technique was used with all of these materials, 25 mg of base material being used in each case. The co-precipitation technique was used with calcium sulphate, strontium sulphate, barium carbonate, calcium fluoride, and calcium tungstate. In the case of co-precipitation, the sample was filtered by suction, washed with water previously saturated with the base material, removed from the filter paper to a platinum dish, and ignited. In order to avoid the possibility of self-quenching from the use of too high a concentration of samarium, five concentrations of samarium were prepared in nearly every base material: 0·015, 0·15, 1·5, 15, and 150 μg/g. Also, because the optimum temperature of ignition was not expected to be the same for all base materials, the samples were ignited successively at 200, 400, 600, 800, and 1000°C for 15-minute intervals. After ignition at each temperature, the intensity of the fluorescence relative to an appropriate blank was measured by means of the fluorophotometer, using 3650-Å excitation, while visual observation was also made of the behaviour of most of the mixtures under 2536-Å excitation, though, of course, fluorescence falling outside the visible region could not be detected in this way. Some data on tungstates and molybdates were obtained on the spectrograph, so that details of their fluorescence spectra could be compared with that of samarium in the calcium tungstate. These data have been combined with the others in Table 1. In the cases of strontium tungstate, barium tungstate, lead tungstate, cadmium tungstate, magnesium tungstate, calcium molybdate, strontium molybdate, and barium molybdate, the lowest samarium concentration used was 600 μg/g, and only one ignition temperature, 400°C, was employed. These materials were made by the method described later for calcium tungstate.

The results of the slurry procedure showed that potassium sulphate-sodium tungstate, strontium fluoride, calcium tungstate, strontium tungstate, cadmium tungstate, and calcium molybdate should be given further consideration. All of these base materials gave samarium fluorophors which were fluorescent under 3650-Å excitation. The first two were not fluorescent under 2536-Å excitation, so they were discarded. Of the four remaining base materials, the calcium tungstate offered the greatest sensitivity, the lower limit of detection of samarium in it being 20, 25, and 30 times lower than that in strontium tungstate, calcium molybdate, and cadmium tungstate, respectively. A choice based on the desire to use the fluorescence of the base material as an internal standard eliminated strontium tungstate and calcium molybdate from consideration. In strontium tungstate, the tungstate fluorescence was quenched at 20°C, while in calcium molybdate, the main molybdate band lay under the first group of samarium bands between 5461 Å and 5770 Å. Both cadmium tungstate and calcium tungstate had tungstate maxima well separated from the samarium bands, but the greater sensitivity to be achieved with the calcium tungstate resulted in its selection as the base material for fluorophors prepared by the slurry technique. Thus this portion of the survey confirmed an evaluation of the literature which indicated that calcium tungstate would be most suitable for fluorophors prepared by the slurry technique.

The co-precipitation method showed only two substances that might be considered as promising base materials for samarium fluorophors. These were calcium and barium sulphates, of which the former appeared to be the more favourable. In addition to offering greater sensitivity than barium sulphate, calcium sulphate filtered much faster and could be removed from the paper more quickly (and in one piece), while the barium sulphate had to be scraped off. Moreover, the calcium sulphate remained fibrous on being dried at 128°C and, consequently, was much more easily handled than the more brittle barium sulphate.

VOL.
7
1955/

The fluorophor: $CaWO_4$—Sm(III)

Preparation

An attempt was made to prepare this fluorophor by co-precipitation at room temperature. A stoichiometric amount of a saturated solution of sodium tungstate was added to a saturated solution of calcium nitrate (pH 3–5) containing samarium sulphate. After ignition at 850°C for fifteen minutes, the product was not fluorescent under 3650-Å excitation up to concentrations of 100 μg of samarium per g (assuming complete co-precipitation of all the samarium in the solution). Under 2536-Å excitation, only the blue tungstate fluorescence was observed. Hence, co-precipitation was abandoned and all further efforts devoted to slurries.

A large amount of the pure base material, calcium tungstate, was prepared by adding 50 per cent calcium nitrate solution to 37 per cent sodium-tungstate solution at room temperature, using stoichiometric amounts of each substance. The precipitate was filtered at once by suction and was not washed. It was then dried overnight at 128°C, and ground to about 200-mesh with an agate mortar and pestle.

Fluorophors prepared by slurrying 25 mg of calcium tungstate with 0·1 ml of samarium sulphate solution were satisfactory. The ignited product gave a uniform pink fluorescence under 3650-Å excitation. After ignition, the fluorophors

Table 1. Summary of exploratory survey of base materials for samarium(III) fluorophors

No.	Base material	Colour of fluorescence		Lower limit of detection (μg Sm/g)	Remarks
		2536-Å excitation	3650-Å excitation		
1	K_2SO_4	Not tried	Brilliant orange	—	A fluorescent product was obtained only when the sample was exposed *directly* to the gas flame. The product obtained by sintering in an electric oven or in a large platinum dish over a gas flame was not fluorescent. Since blanks gave the same fluorescence, the activator was not samarium.
2	K_2SO_4—Na_2WO_4 (1 : 1)	N.F.*	Pink	150	The base material was made by grinding equal weights of K_2SO_4 and Na_2WO_4 to 100–200 mesh, and mixing. Fusion occurred at 850°C.
3	$CaSO_4$	N.F.*	Pink	900	This fluorophor is discussed in detail in a second paper because it is the precursor to an excellent samarium(II) luminophor.
		N.F.†	Pink	150	
4	$SrSO_4$	N.F.*	N.F.	—	
		N.F.†	N.F.	—	
5	$BaSO_4$	N.F.*	N.F.	—	The precipitate was hard to remove from the filter paper; on drying it became brittle.
		Orange-pink†	Pink	150	
6	$CaCO_3$	N.F.*	N.F.	—	
		N.F.†	N.F.	—	
7	$SrCO_3$	Blue*	Blue	—	The samples could not be distinguished from the blanks.
		Blue†	Blue	—	
8	$BaCO_3$	N.F.*	N.F.	—	
		N.F.†	N.F.	—	
9	CaF_2	N.F.*	N.F.	—	The precipitate was difficult both to filter and to remove from the filter paper.
		N.F.†	N.F.	—	
10	SrF_2	N.F.*	Pink	15	The fluorescence excited by 3650 Å was not uniform, seeming to come from cracks in the surface.

* Prepared by slurry technique.
† Prepared by co-precipitation.
N.F. Not fluorescent.

Table 1—*continued*

No.	Base material	Colour of fluorescence		Lower limit of detection (μg Sm/g)	Remarks
		2536-Å excitation	3650-Å excitation		
11	$CaWO_4$	Blue-pink*	Pink	2 (2536 Å)	Heating the sample to 100°C increased the pink fluorescence of samarium excited by 2536 Å, while decreasing the blue fluorescence of tungstate. Heating to 100°C failed to produce any visible effect on the fluorescence excited by 3650 Å. Samples made by co-precipitation showed only the blue tungstate fluorescence under 2536-Å excitation, and no fluorescence under 3650 Å.
12	$SrWO_4$	Pink*	Pink	40 (2536 Å)	The samarium fluorescence excited by 2536 Å consisted of twelve bands, while the tungstate fluorescence was already quenched at 20°C. Heating to 80°C increased the intensity of seven samarium bands, but decreased that of the other five.
13	$BaWO_4$	N.F.*	N.F.	—	Neither samarium nor tungstate fluorescence was noted. Heating to 100°C produced no fluorescence.
14	$MgWO_4$	Light green-blue*	N.F.	—	The spectrum showed no samarium bands and only a weak tungstate band ($\lambda_{max} \sim 5616$ Å), which decreased by 50 per cent when the sample was heated to 100°C.
15	$PbWO_4$	White*	Green-white	150 (2536 Å)	Only a suggestion of these samarium bands appeared in the spectrum at 100°C.
16	$CdWO_4$	Light green-blue*	Light green-blue	60 (2536 Å)	The samarium spectrum consisted of eleven well-defined bands. In general appearance, the spectrum looked very much like that of samarium in calcium tungstate. There was a slight decrease in intensity of the samarium bands on heating the fluorophor from 20°C to 100°C. Under the same conditions, the two tungstate bands, located at about 4903 Å and 5461 Å, decreased by 93 per cent and 91 per cent, respectively.
17	$CaMoO_4$	White-orange (20°C); more orange at 60°C*	Pink-white at 20°C; pinker at 60°C	50 (2536 Å)	Samarium bands in spectra excited by 2536 Å seemed to coincide with those appearing in the spectrum of calcium tungstate containing samarium. The relative intensities of the samarium bands appeared to be the same in both

VOL 7 1955/

Table 1—*continued*

No.	Base material	Colour of fluorescence		Lower limit of detection (μg Sm/g)	Remarks
		2536-Å excitation	3650-Å excitation		
					spectra, but the absolute intensities of the prominent samarium bands at 5629, 5957, and 6072 Å were about four times as great in the tungstate as in the molybdate. On heating the two systems to 60°C, these three bands increased in intensity by 31, 40, and 46 per cent, respectively, in the molybdate system, while the increase of the same bands in the tungstate system was 37, 43, and 33 per cent, respectively. The molybdate fluorescence consisted of two maxima, one of which was poorly defined and located at 4860 Å, while what seemed to be the main molybdate peak lay under the first group of samarium bands between 5461 Å and 5770 Å. On heating to 60°C, the molybdate maximum at 4860 Å decreased by 62 per cent, compared with a decrease of 46 per cent for the tungstate maximum in the other sample. Under the same conditions, the main molybdate band decreased by 53 per cent.
18	$SrMoO_4$	Orange*	Pink	400 (2536 Å)	The spectra obtained under 2536-Å excitation showed weak, poorly defined samarium bands which remained unchanged on heating to 100°C. No molybdate fluorescence appeared in the spectrum at either temperature.
19	$BaMoO_4$	Orange*	Pink	600 (2536 Å)	Heating to 60°C produced no visible change under either exciting wavelength. The spectrum excited by 2536 Å was very poorly defined.
20	$PbMoO_4$	—	—	—	This substance underwent photochemical decomposition during air-drying which caused its initially white surface to become brown. This checked with the observation by KRÖGER [20] that irradiation of lead molybdate by wavelengths less than 3600 Å blackened the sample.

were kept in a desiccator over calcium sulphate, and were quite stable. Even after being held at −40°C or 100°C for as long as an hour at a time, the fluorescence regained its original intensity at room temperature.

Individual samples of calcium tungstate containing 600 μg of samarium/g were ignited for fifteen minutes at 200, 400, 600, 800, or 1140°C. The spectrum of each sample as excited by 2536 Å was then recorded. The observed intensities of the tungstate band and of the samarium bands, listed in Table 2, showed that the fluorophor ignited at 400°C was the most intensely fluorescent.

Table 2. Observed intensities* of tungstate and samarium fluorescence in samples of 600 μg Sm/g $CaWO_4$. Ignited for fifteen minutes at different temperatures (excitation: 2536 Å)

Wavelength (Å)	Temperature of ignition (°C)						
	200	300†	400‡	600	800	850§	1140
4613 $(WO_4)^=$	11	82·5–105	70	41	31	66	65
5555	ab	11·8–14·6	11·0	ab	ab	8·1	4·8
5629	12·4	42·4–59·1	46·5	13·0	11·4	36·2	18·0
5667	ab	22·6–32·7	25·6	9·7	8·0	ab	14·8
5883	8·0	18·6–25·3	20·5	6·7	4·9	16·4	9·0
5957	15·4	60·4–83·5	72·7	15·4	14·2	50·4	26·0
5995	16·3	46·7–61·6	56·6	15·0	13·6	37·2	21·3
6072	14·5	47·7–66·6	59·6	14·7	18·8	43·1	23·6
6422	7·7	31·4–38·8	37·0	11·0	9·6	26·7	14·0
6463	9·7	40·5–50·4	48·9	12·6	11·6	35·6	18·0
6511	5·4	17·7–23·5	22·7	8·8	9·8	15·6	12·1
6554	3·0	14·0–15·2	14·6	6·1	5·9	10·2	7·8

* "Observed intensities" have *not* been corrected to "true relative intensities" by correcting for energy losses within the spectrograph or for the response curve of the receiver.

ab: Absent.

† Range of three samples heated for 20 hours to test effect of longer periods of heating at low temperatures.

‡ Includes a fifteen-minute ignition from 200–400°C.

§ Prepared at an earlier time from a different batch of calcium tungstate.

Also included in Table 2 are the band intensities for a sample made from another batch of calcium tungstate (using the same batches of starting materials) and ignited at 850°C. The intensities were about three times as intense as those for a sample ignited at 800°C, while they are almost as intense as the bands of the 400°C sample. Thus, the data in Table 2 showed that ignition at a low temperature could produce as intensely luminescent fluorophors as ignition at high temperatures, and that variations in the preparation of the base material could be quite significant. Furthermore, although no special precautions were necessary for the preparation of satisfactory calcium tungstate, heat treatment of the calcium tungstate, prior to its being slurried with samarium, could apparently affect the intensity of the samarium fluorescence. One batch of calcium tungstate, after ignition at 850°C for fifteen minutes, could not be made to produce fluorophors showing samarium fluorescence. Presumably, the first ignition of the calcium tungstate had caused

VOL. 7 1955/5

the growth of crystals which could not subsequently incorporate samarium to form a fluorescent product.

Additional studies of the effect of ignition temperature on intensity of fluorescence indicated that a long ignition at comparatively low temperatures tended to produce somewhat more intensely luminescent fluorophors than short heating at higher temperatures. Thus, the intensities of the tungstate and samarium bands in the spectra of three samples of calcium tungstate containing 600 μg of samarium per g that had been ignited at 300°C for twenty hours were greater than those of the most intensely fluorescent sample that had been heated for fifteen minutes. It should be obvious, however, that if the temperature gets too low, the opposite result should be encountered. Thus, samples ignited overnight at 128°C showed no fluorescence, either of tungstate or samarium.

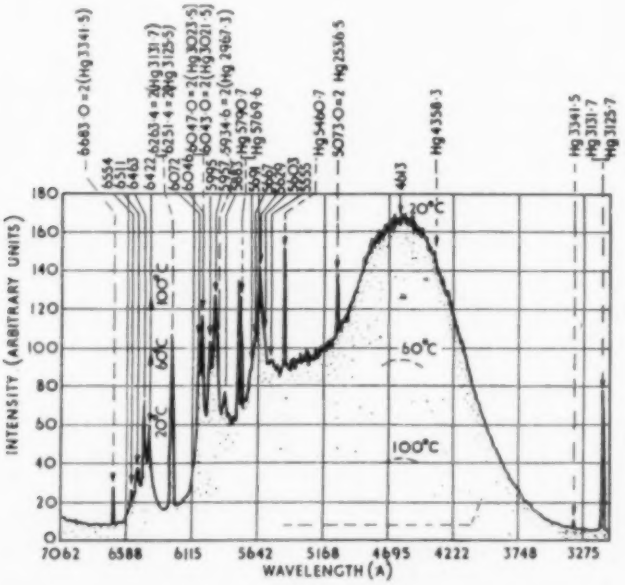

Fig. 1. The fluorescence spectrum of a calcium tungstate fluorophor, containing 600 μg of samarium per gram, when excited by 2536 Å. The dashed line represents, for a limited region, the spectrum obtained with 3650-Å excitation.

Fluorescence spectrum under 2536-Å *excitation*

The fluorescence consisted of a broad blue band due to the tungstate group, and fourteen relatively narrow bands of samarium which lay in the yellow, orange, and red. At room temperature, the predominantly blue fluorescence of samples containing up to 240 μg of samarium per g was due to the tungstate group, as shown in Fig. 1. Samples containing 600 μg of samarium per g or higher emitted predominantly the pink fluorescence of the samarium ion. Heating a fluorophor suppressed the blue fluorescence and enhanced the pink. Hence, a sample containing only 120 μg of samarium per g was blue at room temperature, but pink at 100°C. Fig. 1 indicates the effect of temperature on the intensities of the tungstate band

at 4613 Å, and the samarium band at 6422 Å at 60°C and 100°C. The increases in intensity observed for the other samarium bands were of the same order of magnitude as those indicated for the band at 6422 Å. The dashed line close to and parallel with the wavelength axis shows that 3650 Å excited only the samarium fluorescence.

For different batches of calcium tungstate, made from the same starting materials, the wavelengths of the samarium fluorescence were found to remain essentially unchanged. This is shown by the presentation in Table 3 of the

Table 3. Comparison of wavelengths of samarium bands obtained in this study with those reported in the literature for the sample, $CaWO_4$—Sm (excitation: 2536 Å)

Band	Wavelength (Å)		
	de Rohden	Servigne	This study†
$(WO_4)^=$	not reported	•	4613 ± 29
Sm(III)	5300	•	absent
	5545	•	5555 ± 4
	—	•	5603 ± 4 (pr)§
	5628	•	5629 ± 2
	—	•	5667 ± 2
	5689	•	5691 ± 4 (pr)
	5885	•	5883 ± 2
	5952	•	5957 ± 2
	5994	•	5995 ± 3
	6050	•	6046 ± 1‡
	6072	•	6072 ± 2
	6124	•	absent
	6368	—	absent
	6420	6420	6422 ± 3
	6460	6466	6463 ± 2
	—	6514	6511 ± 2
	6544	6557	6554 ± 2
	7100	7065	—
	7900	7908	—

pr: Poorly resolved.

• Wavelengths less than about 6000 Å were filtered out.

† Average wavelengths and average deviations of maxima in twenty-one samples made from three different batches of calcium tungstate (prepared from the same starting materials).

‡ Interference by second-order reflections of 3021·5-Å and in 3023·5-Å lines is bad. A glass slide was put in front of the slit of the spectrograph to filter out the mercury lines.

§ Interference by second-order reflection of 2803·5 Å is negligible.

wavelengths of the samarium bands in three batches of calcium tungstate. These same data showed that the positions of the tungstate and samarium bands were independent of fluorophor temperature over the range, 20–100°C, and of samarium concentration over the range, 60–3600 μg of samarium per g.

The wavelengths of the samarium bands were also independent of the conditions

of ignition, as shown by the data in Table 4, which lists the results for five fluorophors ignited for fifteen minutes at different temperatures. Considering that some of the spectra were poorly defined, it can be seen that the differences in the wavelengths were negligible. For all ignitions, except that at 200°C, this was roughly true for the tungstate maximum also.

Table 4. Wavelengths (Å) of maxima of samarium and tungstate bands in samples containing 600 μg Sm/g. $CaWO_4$ ignited at different temperatures (excitation: 2536 Å)

200°C—15 min	200°C—15 min plus 400°C—15 min	600°C—15 min	800°C—15 min	1140°C—15 min
4718*	4520*	4586*	4577*	4632*
ab	5562	ab	ab	ab
5633	5638	5633	5637	5628
ab	5668	5673	5664	5664
ab	5694	5687	ab	ab
5882	5880	5888	5892	5885
5953	5954	5951	5951	5955
5984	5994	5996	5996	5991
6074	6071	6074	6071	6075
6422	6422	6425	6428	6427
6465	6463	6460	6461	6463
6519	6510	6510	6501	6512
ab	6554	6553	ab	6553

* Tungstate maximum.
ab: Absent.

As can be seen from Table 3, many of the samarium wavelengths determined in this work agreed closely with those reported by DE ROHDEN [3] and by SERVIGNE [17]. Bands at 5300, 6124, 6368, 7100, and 7900 Å, which were found by DE ROHDEN with cathode-ray excitation, were not found in the present work, although SERVIGNE, who used Hg 1850-Å excitation, in addition to Hg 2536-Å excitation, reported the last two. It is possible that they are present at samarium concentrations higher than those used in this work. On the other hand, DE ROHDEN did not report the bands found in the present study at 5603, 5667, and 6511 Å.

The average relative intensities of the samarium bands, as determined for four separate samples, each containing 600 μg of samarium/g of calcium tungstate, are given in Table 5. Both the measured intensity values and those corrected for the variation in response of the photomultiplier with wavelength and the blaze of the grating* have been listed.

While the wavelengths of the tungstate and of the samarium bands were independent of the temperature of the fluorophor, the intensities of these bands were not [18]. The effect on intensity is shown in Table 6 for three fluorophors. It can be seen that the percentage increase was less at higher samarium concentrations; in fact, the two samarium bands at 6463 Å and 6511 Å decreased in intensity, on the temperature going to 93°C, in the sample containing 3600 μg of samarium per g, thus indicating the start of temperature quenching.

* SANGSTER, R. C., and IRVINE, J. W., JR., unpublished studies (1951).

Table 5. Average relative intensities of the samarium bands in four samples of calcium tungstate containing 600 μg Sm/g (excitation: 2536 Å)

Samarium band wavelength (Å)	Average relative intensity	
	Uncorrected	Corrected*
5555	17 ± 1	18 ± 1
5603	36 ± 1	37 ± 1
5629	70 ± 2	72 ± 2
5667	37 ± 1	37 ± 1
5691	23 ± 1	23 ± 1
5883	31 ± 1	39 ± 1
5957	100†	145
5995	74 ± 2	121 ± 3
6046	76 ± 2‡	146 ± 4
6072	81 ± 2	157 ± 4
6422	49 ± 3	245 ± 17
6463	63 ± 5	356 ± 25
6511	26 ± 3	172 ± 18
6554	20 ± 2	152 ± 14

* Corrected for losses within the spectrograph and changes in response of the receiver with wavelength through the use of a standard illuminant [26].
† Arbitrary.
‡ Calculated from intensity measurements made on spectra obtained free from interfering second-order reflections of Hg 3021·5 Å and Hg 3023·5 Å.

Table 6. Per cent change in intensity of fluorescence of the tungstate band and of the samarium bands in $CaWO_4$—Sm on increasing the temperature from 20°C to 93°C (excitation: 2536 Å)

Wavelength (Å)	3600 μg Sm/g (%)	600 μg Sm/g (%)	60 μg Sm/g (%)
4613*	−76·8	−74·2	−66·6
5555	29·2	63·4	—†
5629	36·5	104	157
5667	57·8	46·7	—†
5883	50·4	113	580
5957	19·0	102	196
5996	28·4	114	197
6072	5·7	78·6	153
6422	14·2	119	226
6463	−0·9	77·3	162
6511	−2·0	73·8	110
6554	—‡	56·0	150

* Tungstate band.
† Absent at this samarium concentration.
‡ Wiped out by automatic standardization of the recording potentiometer.

VOL 7 1955/

Quantitative aspects

Correlation of band intensity with concentration

Four samples of calcium tungstate containing 24, 60, 120, and 240 μg of samarium per g were prepared by ignition at 875°C for seventeen minutes. The spectra of the resulting fluorophors were recorded at temperatures of 20, 60, and 100°C, and the intensities of the samarium bands measured. Then, for each band, the logarithm of the intensity was plotted against the logarithm of the corresponding

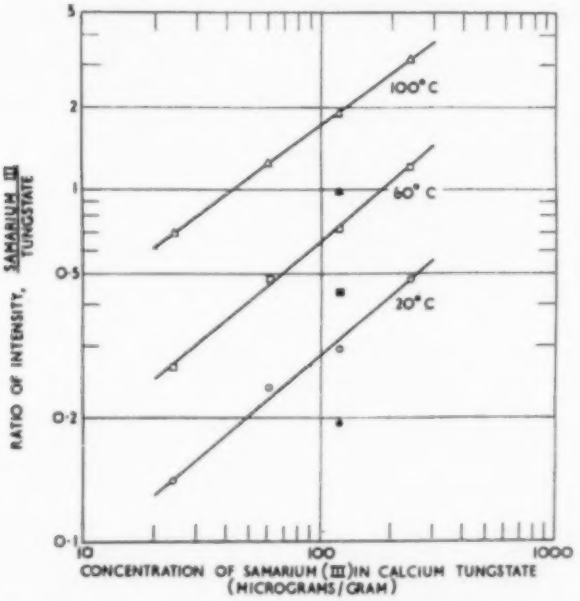

Fig. 2. Calibration curves for the samarium band at 5629 Å excited by 2536 Å. The solid points show the approximate relative positions on an intensity scale of certain measurements before correction by the intensity-ratio procedure.

concentration. The resulting calibration curves for samarium bands at 5629, 5667, 5883, 5957, 5995, 6072, 6422, 6463, and 6554 Å were satisfactorily linear at all three temperatures. In fact, in this concentration range, measurement of almost any samarium band could be used from 20–100°C as a measure of samarium concentration. Although the ordinates in Fig. 2 are plotted as intensity ratios rather than as intensities, the three curves are typical of the calibration curves obtained by simply measuring the intensities.

A number of investigators were using the spectrograph for different studies, so it was impossible to keep constant pre-slit optics. Unfortunately, this procedure showed an undesirable dependence upon both the pre-slit optics and the conditions of fluorophor preparation. The solid points in Fig. 2 show the approximate deviations obtained for the sample containing 120 μg of samarium when it was measured with an inferior arrangement of lenses before the slit of the spectrograph. The lower curve in Fig. 3, a complication of intensities for three sets of samples

prepared under different conditions and measured with different pre-slit optics, emphasized this undesirable situation. While the points within each set showed a linear relationship between intensity and concentration, the agreement among sets was very poor. To avoid this critical dependence upon conditions of sample preparation and upon pre-slit optics, an internal standard method was devised.

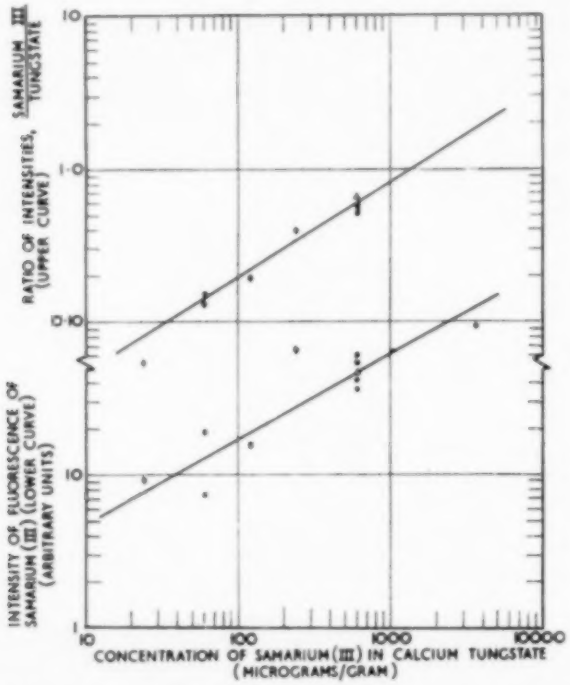

Fig. 3. Variations in intensity of the samarium fluorescence, excited by 2536-Å radiation, resulting from differences in the preparation of the fluorophor and in the pre-slit optics. Note the improvement due to the use of the intensity-ratio procedure.

Internal standard method

Using the intensity of the tungstate fluorescence as the internal standard, the procedure was to plot the ratio, intensity of samarium band divided by the intensity of tungstate band, against the corresponding samarium concentration. The result is shown in Fig. 2 for the 5629-Å band, where the degree of compensation afforded by use of the internal standard procedure is shown by comparing the solid points, which mark the approximate relative deviations of the original intensity values on an intensity scale, with the corresponding points obtained after applying the internal standard method. Similar results were obtained for the bands at 5667, 5883, 5957, 5995, 6072, 6422, and 6463 Å. In the case of the 6554-Å band, only partial compensation was obtained. As far as the samples containing 24, 60, and 240 μg of samarium per g (Fig. 2) were concerned, use of the internal-standard principle did not improve the 20°C and 60°C curves, most of which were excellent

already; in fact, the curves yielded by the internal-standard method were occasionally slightly worse. This was not true for the data at 100°C, all of which were improved by the use of the internal-standard method.

An example of the efficacy of the internal standard is given in Table 7, which

Table 7. Improvement factors* using an internal standard procedure for data on a calcium tungstate sample which contained 120 μg Sm/g and was measured at different times with different pre-slit optics (excitation: 2536 Å)

Wavelength (Å)	20°C	60°C	100°C
5629	5·9	13·0	34·9
5667	—†	9·3	25·5
5883	17·8	49·2	22·5
5957	9·8	8·9	5·2
5995	6·8	11·5	8·6
6072	4·2	6·2	3·7
6422	1·4	3·0	2·8
6463	3·2	3·0	2·5
6511	3·5	3·4	2·9
6554	1·8	2·4	3·6

* Internal standard improvement factor:

$$\frac{\text{Per cent deviation of } I_{Sm} \text{ from calibration curve of intensities}}{\text{Per cent deviation of } \frac{I_{Sm}}{I_{WO_4^{=}}} \text{ from calibration curve of intensity ratios}}$$

† This band was absent from the spectrum at 20°C.

lists for each samarium band of the sample containing 120 μg of samarium per g what is called the "internal-standard improvement factor." This factor, a ratio, is a convenient measure of the degree of compensation introduced by use of the internal-standard principle. It is defined as the percentage deviation of the intensity of a samarium band (I_{Sm}) of the sample containing 120 μg of samarium per g from the calibration curve of intensity against concentration, divided by the percentage deviation of the intensity ratio (I_{Sm}/I_{WO_4}) for the same band from the calibration curve of the intensity ratio against concentration. A value of less than 1 for the improvement factor means that use of the internal-standard method made the situation worse; a value greater than 1, better. The values listed in Table 7 are all greater than 1, in most cases by substantial amounts.

The internal-standard method was also applied successfully, as shown in the upper curve of Fig. 3, to the divergent data from three different batches of fluorophors shown in the lower curve of the same figure. Similar curves, obtained for the other samarium bands (5883, 5957, 5995, 6072, 6422, 6463, 6511, and 6554 Å) were either the same as, or slightly better than, that for the 5629-Å band. Thus, one can conclude that application of the internal-standard principle will produce calibration curves that are much less dependent upon changes in pre-slit optics and variations in preparative conditions than use of samarium intensity alone.

Lower limit of detection

Using the sample containing 24 μg of samarium per g of calcium tungstate, the intensities observed for the 5957-Å samarium band at fluorophor temperatures of 20, 60, and 100°C were 11·3, 21·6, and 33·3, respectively. Since there was an uncertainty of about one unit, the calculated lower limit of detection with the available equipment was about 2 μg of samarium per g of calcium tungstate, or 0·05 μg of samarium in the 25 mg of base material used.

Interferences

The evaluation of interferences was confined to neodymium, europium, and gadolinium. Samples were made up containing three concentrations of the possible

Table 8. The effect of varying amounts of neodymium upon the observed intensity of fluorescence of 600 μg Sm/g $CaWO_4$ at 20°C (2536-Å excitation)

Band	(Å) Wavelength	Neodymium concentration (μg/g)							
		3616		362		36		None	
		I	I.R.*	I	I.R.*	I	I.R.*	I	I.R.*
$(WO_4)^=$	4615	13·0	—	48·0	—	52·0	—	62·5	—
Sm(III)	5555	0	0	8·0	0·17	5·8	0·11	10·0	0·16
	5629	0	0	14·2	0·30	24·6	0·47	49·0	0·78
	5667	0	0	10·4	0·22	13·5	0·26	26·1	0·42
	5883	0	0	8·3	0·17	9·4	0·18	21·8	0·35
	5957	0	0	15·9	0·33	35·1	0·67	74·1	1·20
	5995	0	0	14·2	0·30	28·0	0·54	57·8	0·92
	6072	0	0	13·5	0·28	28·6	0·55	59·1	0·95
	6422	0	0	9·2	0·19	19·3	0·37	36·3	0·58
	6463	0	0	11·5	0·24	24·5	0·47	42·9	0·69
	6511	0	0	6·2	0·13	12·2	0·23	19·4	0·31
	6554	0	0	4·0	0·08	6·6	0·13	11·6	0·19

* I.R. intensity ratio for samarium to tungstate.

interferer, plus 600 μg of samarium per g, in ratios of about 6 : 1, 1 : 2, and 1 : 20. The actual concentrations of each interfering element were:

europium: 4228, 423, and 42 μg/g
gadolinium: 3632, 363, and 36 μg/g
neodymium: 3616, 362, and 36 μg/g

These samples, together with ones to which only samarium had been added, were ignited (20–400°C for fifteen minutes; 400°C for fifteen minutes), and their spectra measured at 20°C. The results for each of the three rare earths are summarized in Table 8.

Table 8 shows that a six-fold excess of neodymium completely wiped out the samarium bands, while the lower concentrations decreased the samarium bands by

VOL 7 1955/

30–40 per cent. Use of the internal-standard method produced negligible improvement; in fact, the intensity ratios for the samples containing the two lower concentrations were widely divergent. These results indicated that neodymium introduced a serious interference even when present in a concentration only 5 per cent that of samarium. It should also be noted that the neodymium simultaneously suppressed the intensity of the tungstate fluorescence.

It can be seen in Table 9 that a seven-fold excess of europium completely quenched the samarium spectrum and almost totally quenched the tungstate fluoresence. The two other europium concentrations also caused partial suppression of both samarium and tungstate fluorescence. The presence of europium in an amount about 5 per cent of that of samarium decreased the intensity of the samarium bands by approximately 67 per cent. However, data obtained for a sample containing 600 μg of samarium per g and only 6·0 μg of europium(III) per g showed no detectable interference by europium. It is interesting to note that the

Table 9. The effect of varying amounts of europium upon the observed intensities of tungstate and samarium fluorescence of 600 μg/g $CaWO_4$ (at 20°C) (2536-Å excitation)

Band	Wavelength (Å)	Europium concentration (μg/g)							
		4228		423		42		None	
		I	I.R.	I	I.R.	I	I.R.	I	I.R.
$(WO_4)^=$	4615	7·0	—	24·5	—	35·5	—	62·5	—
Sm(III)	5555	0	0	2·3	0·09	3·6	0·10	10·0	0·16
	5629	0	0	9·3	0·40	18·9	0·53	49·0	0·78
	5667	0	0	5·0	0·21	9·0	0·25	26·1	0·42
	5583	0	0	4·8	0·20	8·0	0·22	21·8	0·35
	5957	0	0	16·7	0·71	25·2	0·71	74·1	1·20
	5995	0	0	10·0	0·42	19·3	0·54	57·8	0·92
	6072	0	0	13·4	0·57	22·8	0·64	59·1	0·95
	6422	0	0	7·2	0·30	14·2	0·40	36·3	0·58
	6463	0	0	8·7	0·37	17·9	0·50	42·9	0·69
	6511	0	0	4·0	0·17	9·0	0·25	19·4	0·31
	6554	0	0	2·8	0·12	5·9	0·17	11·6	0·19

internal-standard method did improve somewhat the values for the samples containing 423 and 42 μg of europium per g.

The data in Table 10 show that a six-fold excess of gadolinium decreased the intensities of the samarium bands to about one-fourth of their values. A marked decrease was still observed when the gadolinium concentrations were about 50 per cent and 5 per cent of that of samarium. However, the data indicated that the two lower concentrations of gadolinium resulted in a nearly constant effect. This was shown by the good agreement between the values of the internal standard ratios for the two lower gadolinium concentrations.

From Tables 8, 9, and 10 calculations were made of the decrease in intensity of

the samarium bands at 5629 Å and 5957 Å produced by europium, gadolinium, and neodymium on a concentration basis (micrograms of interferer divided by the grams of calcium tungstate). The degrees of suppression produced by the intermediate concentration of interferer were, for the 5957-Å band in the ratio, Gd : Eu : Nd = 1·0 : 1·7 : 2·0; for the 5629-Å band, 1·0 : 2·3 : 2·3. The degrees of suppression produced by the lowest concentration of interferer were in the ratio, Gd : Eu : Nd = 1·0 : 1·2 : 1·2 for the 5957-Å band: 1·0 : 1·2 : 1·2 for the 5629-Å band.

Table 10. The effect of varying amounts of gadolinium upon the observed intensity of fluorescence of 600 μg Sm/g $CaWO_4$ at 20°C (2536-Å excitation)

Band	Wavelength (Å)	Gadolinium concentration (μg/g)							
		3632		363		36		None	
		I	I.R.	I	I.R.	I	I.R.	I	I.R.
$(WO_4)^=$	4615	35·5	—	57·0	—	54·5	—	62·5	—
Sm(III)	5555	abs.	—	6·2	0·11	6·8	0·12	10·0	0·16
	5629	13·1	0·37	34·0	0·60	28·0	0·51	49·0	0·78
	5667	8·7	0·24	17·5	0·31	14·7	0·27	26·1	0·42
	5883	5·5	0·16	14·7	0·26	13·0	0·24	21·8	0·35
	5957	19·4	0·55	44·9	0·79	40·3	0·74	74·1	1·20
	5995	15·9	0·45	35·0	0·61	29·6	0·54	57·8	0·92
	6072	16·8	0·47	38·8	0·68	35·5	0·65	59·1	0·95
	6422	10·3	0·29	25·8	0·45	21·9	0·40	36·3	0·58
	6463	14·1	0·40	34·2	0·60	27·9	0·52	42·9	0·69
	6511	6·0	0·17	16·5	0·30	12·4	0·23	19·4	0·31
	6554	3·7	0·10	9·8	0·17	8·4	0·15	11·6	0·19

Thus, gadolinium produced the least suppression of samarium intensity, while europium and neodymium both suppressed more and to about the same extent.

Fluorescence spectrum excited by 3650-Å *excitation*

The visual appearance of the fluorophor was pinker than when excited by 2536 Å, due to the absence of blue tungstate fluorescence (Fig. 1). The positions of the samarium bands were the same for both types of excitation, and were insensitive to changes in concentration of samarium and temperature.

Comparison of the relative intensities of the samarium bands produced by 2536-Å and 3650-Å excitation in samples containing the same concentration of samarium indicated that relative intensities of the samarium bands lying within the wavelength interval 5882–6068 Å were greater when excited by 3650 Å than by 2536 Å, while the remainder were less. These results are given in Table 11.

The behaviour of the samarium bands, upon being heated from 20° to 100°C. was quite different when they were excited by 3650 Å instead of 2536 Å. Table 12 shows that only the three bands, 5559 Å, 5666 Å, and 5698 Å, increased in intensity, while the rest decreased. Whether or not this change in intensity with temperature

Table 11. Comparison of the relative intensities* at 20°C of the samarium bands produced in different samples of 600 μg Sm/g $CaWO_4$ by 2536-Å and 3650-Å excitation

Band wavelength (Å)	Relative intensities of bands*		Range of per cent differences
	2536-Å excitation (4 samples)	3650-Å excitation (1 sample)	
5559	17	7	−56 to −61
5603	36	23	−35 to −36
5630	70	66	−2 to − 8
5666	37	26	−28 to −33
5698	23	14	−35 to −40
5882	31	39	+22 to +26
5954	100†	100†	—
5993	74	83	+9 to +14
6046	76	83	+6 to +12
6068	81	84	+2 to + 8
6417	49	41	−10 to −22
6459	63	53	−9 to −23
6507	26	21	−10 to −27
6547	20	11	−39 to −50

* Observed intensity; not corrected by comparison with a standard illuminant.
† Arbitrary.

Table 12. Per cent change in intensity of samarium bands in 3600 μg/g $CaWO_4$ on increasing the temperature from 20°C to 100°C (excitation: 3650 Å)

Wavelength (Å)	Per cent change	Wavelength (Å)	Per cent change
5559	+12	5993	−23
5603	no data	6046	−35
5630	−16	6068	−37
5666	+3	6417	−20
5698	+18	6459	−33
5882	−10	6507	−37
5954	−23	6547	−37

varied with samarium concentration, as it did for 2536-Å excitation, was not determined.

Quantitative aspects

Correlation of band intensity with concentration

Satisfactory calibration curves were obtained over the concentration range. 60–3600 μg of samarium per g, at 20°C for the bands at 5630, 5666, 5882, 6417, 6459, 6507, and 6547 Å. Typical of these calibration curves are those shown in

Fig. 4 for the 5630-Å band. The two curves were obtained under quite different optical conditions; hence, they were displaced from each other along the intensity axis, although still lying parallel to one another. Unfortunately, the internal-standard method could not be used here to compensate for differences in pre-slit optics, because of the absence of tungstate fluorescence.

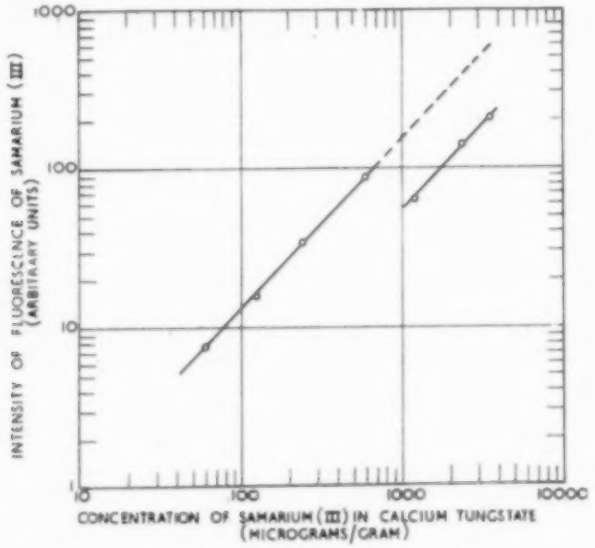

Fig. 4. Calibration curve for the samarium band at 5630 Å excited by 3650 Å.

Lower limit of detection

Using the sample containing 60 μg of samarium per g of calcium tungstate, the observed intensity for the most sensitive samarium band (5957 Å) at a fluorophor temperature of 20°C was 13·0. This indicated that the lower limit of detection on the spectrograph was about 15 μg of samarium per g of calcium tungstate, or 0·38 μg of samarium per g in the 25 mg of base material used. This sensitivity was 2·5 times less than that for excitation with 2536 Å at a fluorophor temperature of 20°C; 7·5 times less than at a fluorophor temperature of 100°C.

Studies of related fluorophors

$CaWO_4$—$PbWO_4$—Sm(III)

On the basis of reflectance data reported by Kroger [20], it appeared that addition of lead tungstate to calcium tungstate should result in increased absorption of Hg 2536 Å. If this additional absorbed energy could be transferred to samarium with an efficiency comparable to that obtained in $CaWO_4$—Sm, an increased intensity of fluorescence, with concomitant increase in sensitivity, should result. An analogous sensitization of samarium fluorescence was reported by Rothschild [21], who obtained a marked increase in the intensity of samarium fluorescence, excited by "3660-Å" radiation in CaS—Sm upon the introduction of lead or bismuth.

The base material was prepared by adding sodium tungstate solution to a solution containing calcium nitrate and lead nitrate to make a total volume of 90 ml. Stoichiometric amounts of reagents were used. Enough lead ion was present in solution to give a precipitate containing 10 per cent lead tungstate, providing all the lead was precipitated.* The precipitate was filtered without washing, dried overnight at 128°C, then ground to about 200-mesh. The fluorophors were prepared by slurrying 25 mg of base material in a platinum dish with 0·10 ml of samarium sulphate solution, drying under infra-red lamps, and igniting at 500°C for fifteen minutes.

The fluorophor gave a brilliant orange fluorescence under 2536-Å excitation and a bright pink fluorescence under 3650-Å excitation. The spectrum for 600 μg of samarium per g of mixed tungstates, when excited by 2536 Å, differed in three ways from the spectrum of samarium in calcium tungstate alone:

1. The tungstate maximum in the mixture was at 4862 $\pm$ 18 Å; in calcium tungstate, at 4613 $\pm$ 14 Å.
2. At 100°C, the spectrum of the mixed tungstates contained a small peak at 4212 Å, at about the start of the tungstate band. This peak, not present in the spectrum in calcium tungstate, was attributed to the presence of lead tungstate.
3. The spectrum of the mixture contained a band at 6055 $\pm$ 6 Å which was not otherwise present. This band represented the greatest difference in the spectra for the two-base materials.

The intensity of the tungstate fluorescence was 2·6-fold greater in the calcium tungstate fluorophor than in the calcium-lead mixture when both contained 600 μg of samarium per g, though the area under the tungstate band was about the same for each base material. The intensities of the samarium bands relative to one another in calcium tungstate and in calcium tungstate-lead tungstate were approximately the same; however, the magnitudes of the intensities for a given line in the two-base materials were not the same. At 20°C, a given samarium band was more intense in the mixture than in the most intensely fluorescent calcium tungstate fluorophor. For example, the intensities of the samarium bands at 5630, 5955, 5993, 6071, 6422, and 6458 Å increased by 29·3, 29·3, 34·4, 19·3, 36·8, and 40·7 per cent respectively. The wavelength values for samarium in the $CaWO_4$—$PbWO_4$—Sm fluorophor agreed with those obtained in calcium tungstate alone, except for the 6055 band, which is not in the spectrum of $CaWO_4$—Sm. Thus, the use of mixed tungstates produced greater sensitivity at 20°C under 2536-Å excitation. However, this superiority was limited to 20°C, because the samarium bands for equal samarium concentrations (600 μg/g) were about as intense in $CaWO_4$—Sm fluorophors at 60°C as in mixed tungstate fluorophors at 20°C; they were about 50 per cent more intense at 100°C.

The spectrum obtained under 3650-Å excitation differed from that excited by 2536 Å in that it lacked the 6055-Å band. The relative intensities of the samarium bands were the same as those excited in the calcium tungstate fluorophor by 3650 Å, but the magnitudes were less. In addition, there appeared to be a real difference

* The amount of lead tungstate dissolved in 100 ml of water at 25°C is 0·0250 g, as compared with 0·0006 g of calcium tungstate [26].

between the relative intensities of some of the samarium bands excited by 2536 Å and those excited by 3650 Å, specifically those of the bands at 6422, 6458, 6505, and 6552 Å.

$CaWO_4$—Eu(III)

Fluorophors containing 4228, 2114, 846, 423, and 211 μg of europium per gram were prepared by the slurry technique, followed by ignition at 450°C for thirty minutes. Visual observation of these fluorophors under 2536-Å radiation showed

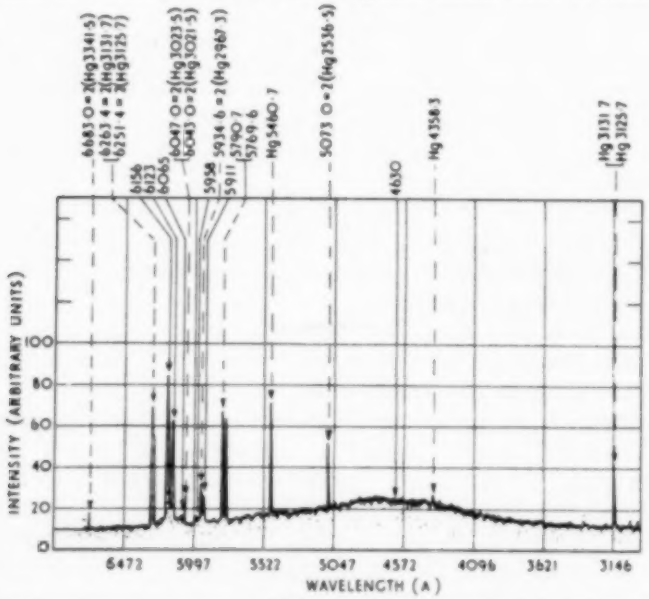

Fig. 5. The fluorescence spectrum at 20°C of a calcium tungstate fluorophor containing 2114 μg of europium per gram of calcium tungstate and excited by 2536 Å.

the fluoresence to be orange-pink for the two highest concentrations, predominantly pink for the intermediate concentration, blue with a pink tinge for the next-to-lowest concentration, and blue for the lowest concentration. No phosphorescence was noted in any of these samples. In the case of another fluorophor containing 362 μg of europium per gram, the sample showed a brilliant orange phosphorescence for some minutes after removal of the 2536-Å excitation. This phosphorescence was stronger at 60°C than at 20°C.

The spectrum of a europium fluorophor is shown in Fig. 5; the wavelengths and relative intensities of the bands are given in Table 13. These values are the averages of twenty-one spectra of samples having temperatures of 20, 60, and 100°C, and the five concentrations given above. Hence, there was no shift of europium bands over these ranges of temperature and concentration, nor was there any significant change in relative intensities of the bands. There was, however, a decrease in the intensities of the europium bands with temperature. For example, the intensities of the 6123-Å and 6156-Å bands decreased by 10 to 20 per cent on heating of the fluorophor to 60°C. Heating to 100°C effected a further decrease of about the same amount.

The tungstate fluorescence was a fairly flat band, its plateau starting at 4568 ± 102 Å and ending at 4827 ± 70 Å. Its intensity decreased with increasing concentration of europium and with increasing temperature. The intensity of tungstate fluorescence in the sample containing 42 μg of europium per g was 36

Table 13. Average wavelengths and intensities of europium(III) in calcium tungstate (2536-Å excitation)

Average wavelength*	Average relative intensity* (observed)	Corrected (26)
5911 ± 1	15	20
5958 ± 2†	66	96
6065 ± 3	67	131
6123 ± 2	59	127
6156 ± 3	100‡	236

* Average of twenty-one spectra.
† Because the intensity did not increase with temperature, the band was assigned to europium instead of samarium.
‡ Arbitrary assignment to the most sensitive band under the prevailing experimental conditions.

divisions, which was a third to a half the average tungstate intensity recorded for samarium fluorophors. At a europium concentration of 6·0 μg/g, the intensity of tungstate fluorescence was almost normal (81 divisions); at 0·6 μg/g, normal

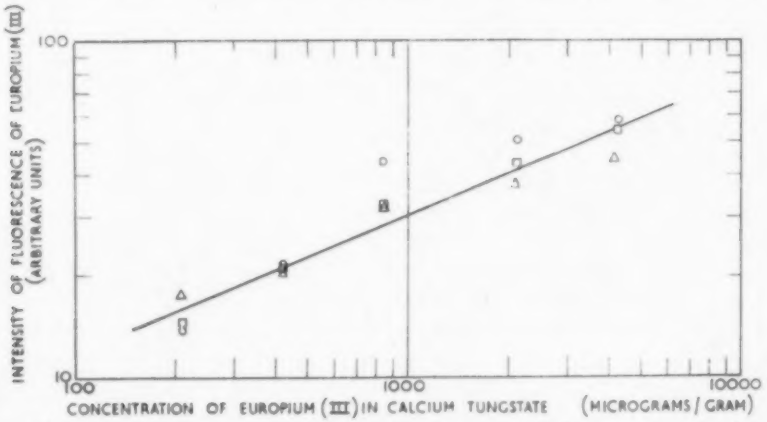

Fig. 6. Calibration curve for the europium band at 6156 Å excited by 2536 Å.
Circles: 20°C
Squares: 60°C
Triangles: 100°C

(92 divisions). The rate of decrease of the intensity of tungstate fluorescence upon heating the fluorophor from 20°C to 100°C was about the same as in the case of the samarium fluorophors. The overall decrease was 65 to 75 per cent.

The result of plotting intensity of europium fluorescence against europium concentration at 20°C, 60°C, and 100°C is shown in Fig. 6. The crowding of the

three curves was due to the small changes in intensity that occurred in the europium bands on heating. When the intensity of the tungstate fluorescence was used as an internal standard, the results shown in Fig. 7 were obtained.

The lower limit of detection was calculated to be 21 μg of europium per g of calcium tungstate. This estimate was based upon the intensity of the 6156-Å band as excited by 2536 Å in a sample containing 211 μg of europium per g of calcium tungstate.

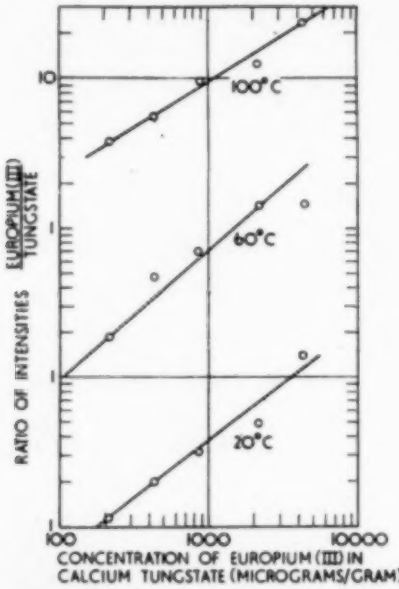

Fig. 7. Calibration curves for the europium band at 6156 Å excited by 2536 Å.

On the basis of a sample containing 600 μg of samarium per g and 42 μg of europium per g, the lower limit of detection of europium was calculated to be 10 μg of europium per g. Thus the intensity of the europium fluorescence seemed to be enhanced by the presence of samarium. This was confirmed by studies which showed that, in the presence of 600 μg of samarium per g, 423 μg of europium per g showed an intensity of 64·3 divisions at 6123 Å, while the intensity at the same wavelength for a fluorophor containing only the 423 μg of europium per g was 40·1 divisions. A ten-fold increase in europium resulted in an intensity of 120 divisions at 6123 Å, while its samarium-free partner had an intensity of 88. In the case of the first two samples, use of the intensity of the tungstate fluorescence as internal standard gave a value of 2·6 for the fluorophor containing both samarium and europium, and a value of 1·2 for the fluorophor containing only europium. As for the two samples containing 4228 μg of europium per g, the one containing samarium gave an internal standard ratio of 16, and the one containing no samarium a value of 15. An idea of the relative mutual interference of samarium and europium was shown by the fact that a seven-fold excess of europium (4228 μg/g) completely quenched the fluorescence of samarium (600 μg/g), while europium (42 μg/g) in the

presence of a fifteen-fold excess of samarium (600 μg/g) had an intensity of 14·3 divisions at 6123 Å.

$SrWO_4$—Sm(III)

One sample of this fluorophor containing 3600 μg of samarium per g was prepared by ignition at 875°C for seventeen minutes. The spectrum of the samarium fluorescence excited by 2536-Å radiation was very much like that of samarium in calcium tungstate. As for the tungstate fluorescence, it was completely suppressed at 20°C.

The samarium spectrum consisted of twelve bands, which are listed in Table 14

Table 14. Average wavelengths and average relative intensities of samarium in strontium tungstate (3600 μg Sm/g; 2536-Å excitation)

Average wavelength* (Å)	Average relative intensity* (observed)	Corrected (26)
5538	70	74
5613	55	57
5669	23	23
5876	86	107
5956	100†	145
5977	88	132
6027	66	112
6328	46	181
6416	54	262
6440	63	340
6479	27	164
6516	16	106

* Averages of six spectra at 20°C and 80°C.
† Arbitrary.

together with the relative intensities. Heating to 80°C did not cause any detectable shift in the wavelengths of the samarium bands, though it did affect the intensities. The bands at 5613, 5669, 5876, 5956, 5977, 6416, and 6440 Å were enhanced by 10, 24, 13, 5·0, 4·4, 16, and 2·8 per cent respectively. The 6027-, 6479-, and 6516-Å bands were decreased by 0·85, 2·5, and 21 per cent, respectively, while the 5538- and 6328-Å bands were completely suppressed.

On the basis of the intensity of the 5956-Å band, the lower limit of detection of samarium in strontium tungstate under 2536-Å excitation was estimated to be 40 μg of samarium per g.

$CaWO_4$—Sm(III)—Gd

This fluorophor was prepared by the slurry technique, followed by ignition from 40°C to 450°C for thirty minutes. Three samples were prepared. All three contained the same concentration of samarium, namely 600 μg/g, and different

concentrations of gadolinium. Of these three samples, the one containing 3632 μg of gadolinium per g had a white fluorescence under 2536-Å excitation, while the other two, which contained 363 and 36 μg of gadolinium per g of calcium tungstate, showed only the blue tungstate fluorescence.

In addition to the usual tungstate band and samarium bands, the spectrum contained four weak bands which were grouped closely and rather symmetrically about the Hg 5460·7-Å line. These four bands were attributed to gadolinium. The wavelengths and relative intensities of these bands are listed in Table 15. There was no shift of these wavelengths or of relative intensities of these bands when the fluorophor was heated to 60°C and to 100°C, though the intensities of

Table 15. Average wavelengths and average relative intensities of gadolinium in calcium tungstate (3632 μg Gd/g; 2536-Å excitation)

Average wavelength* (Å)	Average relative intensity*	
	Observed	Corrected (26)
5434 ± 1	73	87
5447 ± 1	100†	117
5483 ± 1	77	89
5501 ± 1	31	34

* Averages of six spectra at 20, 60, and 100°C.
† Arbitrary.

the bands increased by about 10 per cent in going from 20°C to 100°C. This group of bands was not present in the spectrum of the sample containing 363 μg of gadolinium per g of calcium tungstate, although linear extrapolation from the intensities in the spectrum of the sample containing 3632 μg of gadolinium per g had indicated the lower limit of detection to be about 363 μg/g. Hence, the lower limit of detection probably lay not far above 363 μg of gadolinium per g.

$CaWO_4$—Sm(III)—Nd(III).

Three samples were prepared by the slurry technique, each containing 600 μg of samarium per g and 3616, 362, and 36 μg of neodymium per g. The samples were ignited at 45°C for thirty minutes. Under 2536-Å excitation, the products had an olive-drab appearance. The tungstate band and the samarium bands appeared in the spectra of the samples containing 36 and 363 μg of neodymium per g. Only the tungstate band appeared in the spectrum of the sample containing 3632 μg of neodymium per g. In none of the three spectra did any band appear which could have been attributed to neodymium.

Discussion

The analytical advantages offered by calcium tungstate as a base material in the preparation of samarium fluorophors were that it permitted use of the tungstate fluorescence as an internal standard, that the preparative techniques were simple

and few, and that satisfactory samples could be prepared by ignition at a relatively low temperature (400°C). A disadvantage was that the fluorescence of samarium was very susceptible to interference by small concentrations of europium, neodymium, and gadolinium. Presumably other rare earths would also interfere seriously.

Excitation by 2536 Å was preferable to 3650 Å, because it excited tungstate fluorescence, which could be used as an internal standard, and because the intensity of the samarium fluorescence excited by it increased on heating of the sample. However, there is ample evidence to indicate that a method based on measurement of the absolute samarium intensities excited by 3650 Å would be quite satisfactory if the conditions for obtaining the intensities were standardized. Such standardization was impossible in the present study, because the spectrometer was being employed intermittently by other investigators for unrelated studies that required partial dismantling of the optical set-up from time to time.

In those cases where it would be preferable to measure the intensity of samarium fluorescence at room temperature rather than at 100°C, the increased intensity gained by utilizing a calcium-tungstate-lead-tungstate base material might be used to advantage. There is no reason to believe that the amount of lead used in preparing the fluorophor described here was optimal; a still further increase in intensity of samarium fluorescence might result upon changing the lead-tungstate content of the fluorophor. The fact that the samarium intensities excited by 3650-Å radiation were less than those in fluorophors not containing lead tungstate showed that the advantage to be gained by incorporating lead tungstate into a fluorophor was limited to 2536-Å excitation.

The spectrum of europium in calcium tungstate was marked by the sharpness of the two most intense europium bands, which were located at 6123 and 6156 Å. These two bands were the most suitable for the quantitative determination of europium in calcium tungstate in the range of concentrations used in this work. A second notable feature of the spectrum of europium in calcium tungstate was the marked decrease in tungstate fluorescence effected by the europium. Among the four rare earths, samarium, europium, gadolinium, and neodymium, only europium caused a striking decrease in the intensity of tungstate fluorescence.

The fluorophor, $CaWO_4$—Eu, was like the $CaWO_4$—Sm fluorophor in that the intensity of the europium fluorescence excited by 2536 Å was proportional to the concentration of europium. Another similarity was that the intensity of tungstate fluoresence could be used as an internal standard. This was more interesting in view of the inhibiting effect which europium exerted on tungstate fluorescence.

Three ways in which the europium fluorophor differed from that of samarium were: (a) the inhibition of the tungstate fluorescence by europium; (b) the decrease in intensity of the europium bands on heating of the fluorophor; and (c) the apparent increase in the intensity of europium fluorescence in the presence of samarium.

Acknowledgements—The authors are very grateful to the Office of Naval Research and to the Atomic Energy Commission for jointly supporting part of the expense of this study, and are indebted to Prof. R. C. Lord for making available his recording spectrograph.

References

[1] Urbain, G.; *Ann. chim. phys.* 1909 **18** (8), 229, 362
[2] Bruninghaus, L.; *Ann. chim. phys.* 1910 **21** (8), 210, 519
[3] Rohden, A. de; *Ann. chim. phys.* 1915 **3** (9), 338
[4] Tomaschek, R.; *Ann. phys.* 1924 **75,** 109
[5] Tomaschek, R.; *Ann. phys.* 1927 **84,** 329
[6] Tomaschek, R.; *Z. Phys.* 1933 **82,** 309
[7] Lenard, P., Schmidt, F., Tomaschek, R.; *Handbuch der Experimental Physik* 1928 **23,** 468
[8] Przibram, K.; *Nature* 1935 **135,** 100
[9] Przibram, K.; *Z. Phys.* 1937 **107,** 709
[10] Przibram, K.; *Nature* 1937 **139,** 329
[11] Przibram, K.; *Mikrochim. Acta* 1938 **3,** 68
[12] Karlik, B., and Przibram, K.; *Sitz. ber. Akad. Wiss. Wien.* 1937 **146** (IIa), 209
[13] Merkader, S.; *Sitz. ber. Akad. Wiss. Wien.* 1940 **149** (IIa), 349
[14] Haberlandt, H.; *Mikrochem. Mikrochim. Acta* 1951 **38/37,** 1075
[15] Servigne, M.; *Compt rend.* 1936 **203,** 1234
[16] Servigne, M., and Vassy, M.; *Compt. rend.* 1937 **204,** 1566
[17] Servigne, M.; *Compt. rend.* 1938 **207,** 905
[18] de Groot, W.; *Physica* 1940 **7,** 438
[19] Botden, Th. P. J., and Kröger, F. A.; *Physica* 1949 **15,** 747
[20] Kröger, F. A.; *Some Aspects of the Luminescence of Solids,* Elsevier Pub. Co., New York, 1948
[21] Rothschild, S.; *Phys. Z.* 1936 **37,** 757
[22] Bäckström, H. L. J.; *Naturwissenschaften* 1933 **21,** 251
[23] Kasha, M.; *J. Opt. Soc. Amer.* 1948 **38,** 929
[24] Sangster, R. C.; *A Study of Organic Scintillators,* Ph.D. Thesis, Massachusetts Institute of Technology, 1951
[25] Wright, N.; *Ind. Eng. Chem., Anal. Ed.* 1941 **13,** 1
[26] Gmelin; *Handbuch der Anorganischen Chemie,* Verlag Chimie, Leipsig, 1926

VOL.
7
1955/5

Spectrochimica Acta, 1956, Vol. 7, pp. 349 to 357. Pergamon Press Ltd., London

Contrast changes of Eastman Kodak Spectrum Analysis No. 1 Emulsion during cold storage, and their effect on observed intensity ratios

CYRUS FELDMAN and JANUS Y. ELLENBURG
Oak Ridge National Laboratory,
Oak Ridge, Tennessee

(*Received* 15 *November* 1954; *accepted for publication* 15 *March* 1955)

Abstract—This emulsion showed 0–4 per cent decreases in contrast at various wavelengths when stored one year at −17·8°C, and 4–12 per cent increases in contrast when stored for the same period at 4·4°C.

I. Introduction

IN order to minimize the need for emulsion calibration, spectrographers usually purchase substantial quantities of a given emulsion at a time, specifying that all plates or rolls of film must come from the same emulsion batch. The quantity purchased is limited by the fact that it is inadvisable to store such materials for long periods: both sensitivity and contrast are commonly known to undergo gradual changes during storage.

Manufacturers have long recommended that these changes be retarded by the use of low storage temperatures. The Eastman Kodak Company suggests the following conditions [1]:

Table 1

For storage periods up to	2 months	6 months	12 months
Keep plates and films below	75°F (23·9°C)	60°F (15·6°C)	50°F (10·0°C)

The same source also recommends storage in moisture-proof containers, pointing out that the benefits of low storage temperature are greatly reduced if this temperature is accompanied by high relative humidity in the atmosphere surrounding the emulsion.

Unpublished work by L. E. OWEN has indicated that the benefits of low temperature might be retained or increased by storage at freezing temperatures. It was expected that the exchange of moisture between the ambient atmosphere and the emulsion would be greatly retarded under these conditions, especially if the emulsion were stored in the unopened original moisture-proof container. The present paper is a response to Mr. OWEN'S suggestion to the authors that a statistical study of the effects of freezing on a spectrochemical emulsion might be of general interest.

An experimental study was made comparing the stability of Eastman Kodak SA1 emulsion contrast factors at −17·8°C and 4·4°C over a period of one year. This study is described in Section II.

II. Experimental

1. *Procedure*

Three 100-ft rolls were selected at random from a newly arrived shipment of 35 mm Eastman Kodak Spectrum Analysis No. 1 film. All rolls in this shipment were from the same emulsion batch. Roll I was calibrated immediately. Roll II, still sealed in its moisture-proof shipping container, was placed in a freezer at 0°F (−17·8°C). Roll III, in a similar container, was placed in a refrigerator at 40°F (4·4°C). These containers consisted of metal cans having tight-fitting lids, sealed

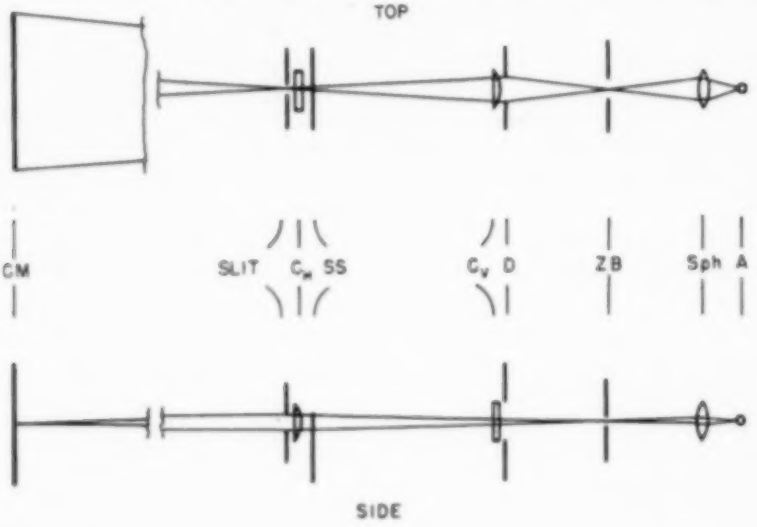

Fig. 1.

with two thicknesses of surgical adhesive tape. Unpublished work by E. H. S. VAN SOMEREN has indicated that this constitutes a satisfactory seal against moisture if the temperature does not fluctuate during storage.

One year later, rolls II and III were removed from storage and calibrated. In every case, the portions of film used were obtained from several positions along the length of a roll. Each of the emulsion characteristics listed in Tables 4–7 was obtained by pooling data from at least four such locations.

All exposures were made on a Jarrell-Ash 3·4 m Wadsworth grating spectrograph. Calibrations were performed by the two-step method [2], using the centre two steps of a logarithmic step sector. This sector was located at the slit, and was rotated at approximately 1000 r.p.m. No data were used unless tests run on the same film with the experimental exposure showed that intensity of illumination was uniform to within 2 per cent along the length of line used.

The illumination system is shown schematically in Fig. 1. An intermediate image of a 2·0 ampere iron bead arc A was formed on a diaphragm ZB held in an optical bench rider. The opening in the diaphragm was rectangular and admitted only the centre 20 per cent of the arc image. A 45 cm focal length horizontal-axis cylindrical lens C_H, located at the slit, formed an image of this opening on the

VOL 7 1955/

collimating mirror CM, filling the mirror vertically. A 10-cm focal length vertical-axis cylindrical lens C_V was used to focus the intermediate image on the slit. The width of this lens was reduced by diaphragm D until the beam of light coming through the slit exactly filled the collimating mirror horizontally. The width of the beams as shown in Fig. 1 is determined by the limiting aperture in each case; i.e., by the width of the opening in diaphragm D in the "Top" view, and by the height of the slit-opening in the "Side" view.

In accordance with the suggestion of SCHMIDT [3], results were expressed in terms of the Seidel function Δ, where

$$\Delta = \log\left(\frac{T_0}{T} - 1\right),$$

and T and T_0 are the transmittances of the line and an unexposed region of the emulsion, respectively.

This combination of procedures was chosen because it possesses the following advantages:

(1) The standard intensity ratio (the step ratio of the rotating sector) can be accurately reproduced from exposure to exposure, and is independent of wavelength.

(2) Vertical uniformity of illumination is only required over the height of two sector steps.

(3) When densitometric data are plotted in terms of the Seidel function, the preliminary curve is a straight line. (See next section.) This makes it possible to use an objective procedure (the least-squares method) for drawing the preliminary curve. The straightness of the preliminary curve also makes it possible to describe the shape of a calibration curve over the entire range of measured density values in terms of two parameters—the slope a and intercept b of its preliminary curve.

The schematic preliminary and calibration curves (Seidel function) shown in Fig. 2 are typical of the results obtained with the present emulsion.

Details of the procedures used for aligning optics and reducing data have been given elsewhere [4].

All films were developed three minutes at 20°C in Eastman Kodak D-19 developer. The developing solution was prepared immediately before use as follows: 150 ml of developing solution was removed from a 500-ml bottle which had previously been used to develop approximately 6 ft of film, and discarded. The bottle was then refilled with unused developer. Each portion of developing solution prepared in this way was used for no more than 6 ft of film, and was kept tightly stoppered in a full bottle. Development was carried out in a 500 ml capacity roll-film developing tank; agitation was intermittent.

Photometric readings were made on a National Spectrographic Laboratories "SpecRecorder" recording projection microdensitometer.

2. *Results*

SCHMIDT [3] and subsequent authors have stated that the preliminary curve is always a straight line when results are plotted in terms of Seidel function. In

order to test this assumption in the present case, a straight-line curve was calculated for each group of points by the least-squares method. The graph was then examined to find the highest number of consecutive points lying on the same side of the least-squares line. A statistical calculation was then performed to find the probability P that this large a group of consecutive points might by pure chance

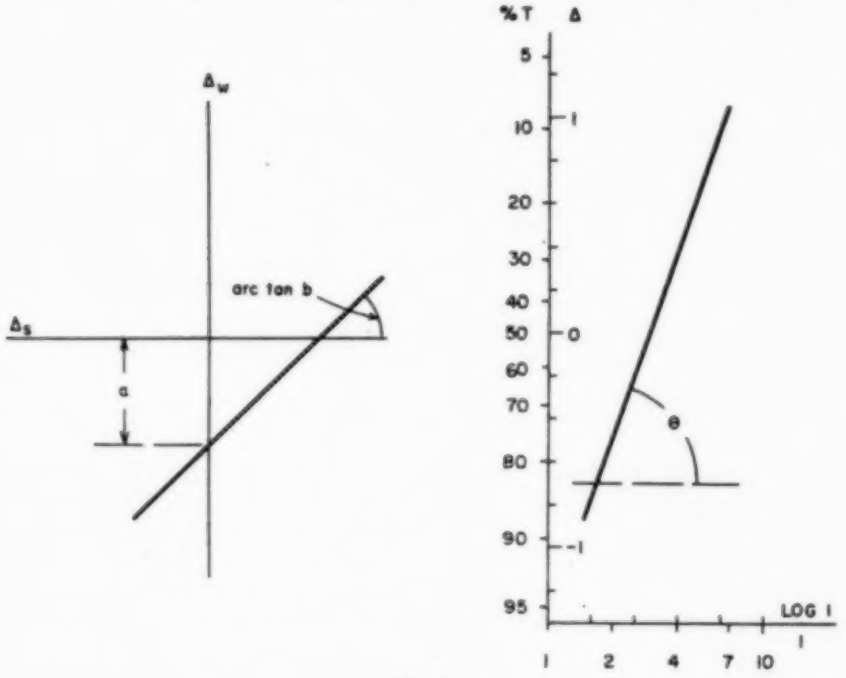

Fig. 2.

lie on the same side of the least-square line if the data truly represented a linear function. Details of the method used for calculating P have been given by KIMBALL [5]. For deciding the present question, it is necessary only to examine the distribution of P values. These were as follows:

Table 2. Distribution of P values

Value of P:	0	0·1	0·2	0·3	0·4	0·5	0·6	0·7	0·8	0·9	1·0
Number of preliminary curves having P in indicated range	2	2	2	2	0	0	0	3	0	3	10

Chances are excellent in most cases that the observed consecutive groupings could have occurred by chance in a truly linear distribution; furthermore, since the individual curves in this group of twenty-four were based on sixteen to twenty-four experimental points, it is also probable that a few low P values might occur by chance even if all twenty-four distributions were truly linear.

It has therefore been assumed that the present Seidel function preliminary curves are straight lines completely definable in terms of intercept and slope. (See Fig. 2.) The intercept a of the preliminary curve on the vertical (Δ_w) axis represents the density of the weak (high transmittance) step of the image in Seidel units when that of the strong step is zero. The negative of this intercept, divided by the logarithm of the sector step ratio (0·200 in this case) gives the slope of the Seidel function calibration curve (tan θ in Fig. 2) over the corresponding range of intensities. If the calibration curve is a straight line, tan θ is, of course, the slope of the entire calibration curve. The slope b of the preliminary curve characterizes the degree and sign of the curvature of the calibration curve derived from it. If this slope is greater or less than unity, the calibration curve is concave downward or upward, respectively. If this slope is unity, the calibration curve is a straight line. Table 3 summarizes the significance of the signs of changes in a and b in terms of changes in the calibration curve. Subscripts f, r, and o refer to "frozen" (stored at −17·8°C), "refrigerated" (stored at 4·4°C), and original emulsions, respectively.

Table 3. Significance of signs of changes in a and b

		If $(b_f - b_o)$ or $(b_r - b_o)$ is	
		+	−
If $(a_f - a_o)$ or $(a_r - a_o)$ is	+	Second curve less steep and more convex upward than original	Second curve less steep and more concave upward than original
	−	Second curve steeper and more convex upward than original	Second curve steeper and more concave upward than original

Table 4 compares the contrast of the original emulsion with that of the emulsion stored for one year at −17·8°C. The comparison is made in terms of $(a_f - a_0)$, the difference between the intercepts of the respective Seidel function preliminary curves. The standard error $s_{(a_f - a_0)}$ of this difference was calculated from the formula

$$s_{(a_f - a_0)} = \sqrt{s^2_{a_f} + s^2_{a_0}}$$

where s_{a_f} and s_{a_0} are the standard errors of intercept for the two curves. The level of significance LS was obtained by applying STUDENT's t test to these data [6]. A value of $LS = 96$ per cent, for example, means that there are only 4 chances in 100 that this difference would have been observed by chance if no real difference existed between a_f and a_0. The $(\tan \theta_f / \tan \theta_0)$ column gives the ratio of the slope of the frozen emulsion calibration curve to that of the original calibration curve. Tan θ = −(a/log step ratio); therefore, $(\tan \theta_f / \tan \theta_0) = a_f / a_0$.

Table 5 shows a similar comparison between intercept values and calibration curve slopes obtained for the refrigerated and original emulsions. Symbol definitions are analogous to those in Table 4.

Table 4. Comparison of contrast between original emulsion and emulsion stored one year at −17·8°C. Contrast measured in terms of "a" (intercept of Seidel function preliminary curve) and tan θ (slope of Seidel function calibration curve)

λ (in Å)	Stored at −17·8°C				Original				Difference			Calibr. curve slope ratio $\frac{\tan\theta_f}{\tan\theta_o}$
	Intercept a_f	No. of obs.	Std. error of intercept s_{a_f}		Intercept a_o	No. of obs.	Std. error of intercept s_{a_o}		Difference of intercepts $(a_f - a_o)$	Std. error of difference $s_{(a_f - a_o)}$	Level of signif. of difference *LS* (in %)	
			Absolute	Rel. (%)			Absolute	Rel. (%)				
2600	−0·6795	20	0·0087	1·3	−0·6675	14	0·0155	2·3	−0·0120	0·0178	50	1·018
2800	−0·6675	16	0·0055	0·8	−0·6662	18	0·0098	1·5	−0·0013	0·0113	50	1·012
3000	−0·6350	16	0·0079	1·2	−0·6529	16	0·0022	0·3	+0·0179	0·0082	96	0·970
3200	−0·6739	22	0·0045	0·7	−0·6871	21	0·0054	0·8	+0·0132	0·0070	95	0·981
3400	−0.6989	21	0·0178	2·5	−0·7403	18	0·0074	1·0	+0·0414	0·0193	96	0·944
3600	−0·6774	21	0·0078	1·2	−0·7091	21	0·0062	0·9	+0·0317	0·0099	>99	0·955
3900	−0·8111	17	0·0141	1·7	−0·8107	19	0·0134	1·6	−0·0004	0·0194	50	1·000
4300	−0·8125	17	0·0221	2·7	−0·8340	21	0·0095	1·1	+0·0215	0·0240	70	0·974

Table 5. Comparison of contrast between original emulsion and emulsion stored one year at 4·4°C, in terms of "a" (intercept of Seidel function preliminary curve) and tan θ (slope of Seidel function calibration curve)

λ (in Å)	Stored at 4·4°C				Original				Difference			Calibr. curve slope ratio $\frac{\tan\theta_r}{\tan\theta_o}$
	Intercept a_r	No. of obs.	Std. error of intercept s_{a_r}		Intercept a_o	No. of obs.	Std. error of intercept s_{a_o}		Difference of intercepts $(a_r - a_o)$	Std. error of difference $s_{(a_r - a_o)}$	Level of signif. of difference *LS* (in %)	
			Absolute	Rel. (%)			Absolute	Rel. (%)				
2600	−0·7031	22	0·0047	0·7	−0·6675	14	0·0155	2·3	−0·0356	0·0162	>99	1·053
2800	−0·6925	23	0·0059	0·9	−0·6662	18	0·0098	1·5	−0·0263	0·0114	>99	1·039
3000	−0·7144	20	0·0049	0·7	−0·6529	16	0·0022	0·3	−0·0615	0·0055	>99	1·102
3200	−0.7392	20	0·0126	1·7	−0·6871	21	0·0054	0·8	−0.0521	0·0137	>99	1·085
3400	−0·8154	21	0·0123	1·5	−0·7403	18	0·0074	1·0	−0·0751	0·0143	>99	1·101
3600	−0·7915	24	0·0143	1·8	−0·7091	21	0·0062	0·9	−0·0824	0·0156	>99	1·116
3900	−0·8871	19	0.0093	1·0	−0·8107	19	0·0134	1·6	−0·0764	0·0163	>99	1·094
4300	−0·9123	17	0·0161	1·7	−0·8340	21	0·0095	1·1	−0·0783	0·0187	>99	1·094

VOL
7
1955/

Table 6 compares the slopes b of the preliminary curves between the frozen and original emulsions; Table 7 makes a similar comparison between the refrigerated and original emulsions. Both comparisons are, of course, equivalent to comparisons of curvature of the corresponding calibration curves. Notation is analogous to that of Tables 4 and 5.

Table 4 shows the effect of one year of storage at −17·8°C on the Seidel contrast factor of Eastman Kodak SA1. This table indicates that the greatest change occurring under these conditions took place at 3600 Å, for which $\tan \theta_r/\tan \theta_0 = 0{\cdot}944$. Calculations of the type described by FAST [7] were performed to find the magnitude of the error which would be introduced by using the original calibration curve for this wavelength on data obtained from the stored emulsion.

It was found that the distortion would be approximately 4 per cent for a line intensity ratio of 8, and correspondingly less for smaller ratios. At other wavelengths where the changes appear real (3000–3400 Å), the maximum possible errors would be even smaller. At the remaining wavelengths, no measurable distortion should be introduced by storage at −17·8°C. It is interesting to note that at this temperature, the only statistically reliable changes are decreases in contrast.

Table 5 shows the effects of one year of storage at 4·4°C on the same emulsion. This storage increased the contrast at all wavelengths. The smallest change occurred at 2800 Å, where $\tan \theta_r/\tan \theta_0 = 1{\cdot}039$; the largest occurred at 3600 Å, where $\tan \theta_r/\tan \theta_0 = 1{\cdot}116$. At 2800 Å, therefore, the intensity ratio of a line pair in the range $0{\cdot}125 < L_2/L_1 < 8{\cdot}000$ imprinted on stored film, but read on the original calibration curve, would be 0–4 per cent high (depending on the value of the ratio) if greater than unity, and 0–4 per cent low if smaller than unity. The corresponding error would be approximately 0–12 per cent at 3600 Å, again depending on the value of the ratio itself. Maximum errors for a given intensity ratio at other wavelengths would lie between these limits.

Table 6 reveals three cases (2600, 3200, and 4300 Å) in which the calibration curves became more convex upwards during one year of storage at −17·8°C. No definite change was noted at other wavelengths. Table 7 shows that changes in curvature probably occurred at most wavelengths during one year of storage at 4·4°C; since the b values themselves ranged from 0·9565 to 1·0371, however, the changes were relatively slight.

The values of the standard errors of slope and intercept given in Tables 4–7 indicate that little variance could have been introduced by the pooling of data from several positions along the length of a roll. This indicates a corresponding degree of uniformity of contrast along the length of the roll.

No visible fogging occurred during storage at either temperature; i.e., the transmittance of unexposed emulsion compared to that of clear glass was the same for all three rolls of film.

III. Conclusion

Eastman Kodak SA1 emulsion showed fewer and smaller changes in contrast when stored for one year at −17·8°C than when stored for the same period at 4·4°C.

In the case of this emulsion, the application of calibration curves made at the time of receipt to film stored one year at −17·8°C would lead to maximum errors

Table 6. Comparison of curvature of Seidel function calibration curves between original emulsion and emulsion stored one year at −17·8°C. Curvature measured in terms of "b" (slope of Seidel function preliminary curve)

	Stored at −17·8°C				Original				Difference		
λ (in Å)	Slope b_f	No. of obs.	Std. error of slope s_{b_f}		Slope b_0	No. of obs.	Std. error of slope s_{b_0}		Difference of slopes $(b_f - b_0)$	Std. error of difference $s_{(b_f - b_0)}$	Level of signif. of diff. LS (in %)
			Absolute	Rel.(%)			Absolute	Rel.(%)			
2600	1·0296	20	0·0106	1·0	0·9565	14	0·0195	2·0	+0·0731	0·0222	>99
2800	0·9918	16	0·0067	0·7	0·9830	18	0·0108	1·1	+0·0088	0·0127	50
3000	1·0368	16	0·0114	1·1	1·0371	16	0·0031	0·3	−0·0003	0·0118	<50
3200	0·9830	22	0·0060	0·6	1·0295	21	0·0066	0·7	−0·0465	0·0089	>99
3400	0·9873	21	0·0207	2·1	1·0020	18	0·0098	1·0	−0·0147	0·0228	50
3600	1·0109	21	0·0096	0·9	1·0090	21	0·0084	0·8	+0·0019	0·0128	<50
3900	1·0051	17	0·0169	1·7	1·0039	19	0·0173	1·7	+0·0012	0·0242	<50
4300	0·9813	17	0·0271	2·7	1·0356	21	0·0112	1·1	−0·0543	0·0293	92

Table 7. Comparison of curvature of Seidel function calibration curves between original emulsion and emulsion stored one year at 4·4°C. Curvature measured in terms of "b" (slope of Seidel function preliminary curve)

	Stored at 4·4°C				Original				Differences		
λ (in Å)	Slope b_r	No. of obs.	Std. error of slope s_{b_r}		Slope b_0	No. of obs.	Std. error of slope s_{b_0}		Difference of slopes $(b_r - b_0)$	Std. error of difference $s_{(b_r - b_0)}$	Level of signif. of diff. LS (in %)
			Absolute	Rel.(%)			Absolute	Rel.(%)			
2600	0·9917	22	0·0063	0·6	0·9565	14	0·0195	2·0	+0·0352	0·0205	90
2800	0·9582	23	0·0082	0·8	0·9830	18	0·0108	1·1	−0·0248	0·0136	92
3000	1·0203	20	0·0065	0·7	1·0371	16	0·0031	0·3	−0·0168	0·0063	>99
3200	1·0060	20	0·0180	1·8	1·0295	21	0·0066	0·6	−0·0235	0·0191	77
3400	1·0064	21	0·0147	1·5	1·0020	18	0·0098	1·0	+0·0044	0·0176	<50
3600	0·9891	24	0·0184	1·9	1·0090	21	0·0084	0·8	+0·0199	0·0203	70
3900	0·9811	19	0·0117	1·2	1·0039	19	0·0173	1·7	+0·0228	0·0209	80
4300	0·9801	17	0·0204	2·1	1·0356	21	0·0112	1·1	+0·0555	0·0232	97

VOL. 7
1955/1

of 0–4 per cent in the apparent intensity ratio, depending on the wavelength and the value of the ratio. If these curves were used on the same emulsion stored for one year at 4·4°C, the corresponding maximum errors would range from 4 to 12 per cent.

Acknowledgements

The authors wish to express their gratitude to Dr. A. W. KIMBALL for his valuable advice on statistical treatment of data, and to Mr. GEORGE J. ATTA, who carried out most of the statistical calculations reported in Section II.

References

[1] EASTMAN KODAK CO.; "Materials for Spectrum Analysis" (Booklet) (1947) Rochester, N.Y.
[2] CHURCHILL, J. R., *Anal. Chem.* 1944 **16** 653.
[3] SCHMIDT, R., *Rec. trav. chim. Pays Bas* 1948 **67** 737.
[4] Suggested Practice E-2 SM 2-2, Sections 1–7 and 9 in "Methods for Emission Spectrochemical Analysis," American Society for Testing Materials, Philadelphia, 1953.
[5] KIMBALL, A. W.; Doctoral Thesis, North Carolina State College, Raleigh, N.C. (1950). Also published as Proj. No. 21-49-003, Report No. 3, U.S. Air Force School of Aviation Medicine, Randolph Field, Texas.
[6] SNEDECOR, G. W., *Statistical Methods*, Iowa State College Press, Ames, Iowa (1946).
[7] FAST, E., *J. Opt. Soc. Amer.* 1946 **36** 424.

OL.
7
5/56

Spectrochimica Acta, 1956, Vol. 7, pp. 358 to 366. Pergamon Press Ltd., London

Spectrographic analysis of copper-making and lead-making slags for major constituents

N. LOUNAMAA
Boliden Mining Company, Central Laboratory, Skelleftehamn, Sweden*

(*Received September* 1954; *revised version September* 1955)

Abstract—A method for the spectrographic determination of Cu, Pb, ZnO, Al_2O_3, CaO, FeO, MgO, and SiO_2 in copper- and lead-making slags has been developed. The method involves sample preparation by fusion with a mixture of lithium borate and boric acid which contains several internal standard elements, the use of a high-voltage spark in the excitation of the pellet and photographic recording of the spectra. The precision of the method is, expressed by a coefficient of variation, of 1·5 to 3·5 per cent for the different elements. No systematic errors have been revealed.

1. Introduction

As is well known, the chemical composition of the copper- and lead-making slags must be rigorously controlled in order to avoid excessive losses of valuable metals in slags. This control has been carried out in the Boliden Mining Company by wet chemical analysis. Since successful spectrographic methods for the control of steel-making slags have been published (HASLER [1] and PRICE [2]) it seemed desirable to find a corresponding method for the analysis of copper- and lead-making slags.

2. Development of the method

Of the steps inherent in every spectrographic analysis, only sample preparation and excitation will be dealt with in greater detail, because they generally contribute the major part of the total error of the whole procedure.

2.1 *Sample preparation*

Proper treatment of the sample prior to spectrographic analysis for major constituents, is the most important factor to be considered. To be effective, sample preparation should bring about chemical homogenization, elimination of structural differences, elimination or at least reduction of the effect of other elements, dilution, and incorporation of internal standard elements.

CARLSSON [3] as well as EECKHOUT and GILLIS [4] have obtained a somewhat low but nevertheless adequate accuracy merely by powdering the sample to below 100 mesh, and mixing with powdered graphite. However, they point out that difficulties arise in the analysis of samples of widely different origin, which accordingly are of different physical structure. AHRENS [5] and KVALHEIM [6] have been able to obtain good precision when applying d.c.-arc excitation to the analysis of silicate rocks without any extensive sample preparation, but they emphazise the use of standards which resemble the sample as much as possible. Both these examples thus indicate the importance of elimination of structural differences.

* Present address: Fagersta Bruks Aktiebolag, Central Laboratory, Fagersta, Sweden.

Of the two possible methods to obtain ideal homogenization, dissolving the sample to give an aqueous solution or fusing with a flux to obtain a glassy solid, the latter offers the greater possibilities in the analysis of silicates and oxides. The following chemicals have been tried as fluxing reagents: sodium carbonate, potassium carbonate, acid potassium sulphate, lithium fluoride, and borax by CARLSSON [3], lithium carbonate and boric acid by DUNER [7], lithium carbonate and boric oxide by HASLER *et al.* [1], and borax by PRICE [2]. In addition, potassium nitrate, sodium fluoride and boric acid have been used as fluxes in the preparation of samples of similar type prior to analysis by ordinary "wet" methods.

Of the chemicals listed above, borates seemed to be much superior to the others, as they easily give homogeneous melts with all metal oxides and silica. The author carried out fusion tests with several mixtures of lithium carbonate as well as borax with boric acid. A mixture in the weight-ratio lithium carbonate/boric acid = 1/3 has given the best results. The fusion bead was completely homogeneous and easy to remove from the crucible by pouring out the fused melt. The melting temperature was lower than that of stoichiometric borates. This is important as the temperature of fusion should be kept as low as possible, especially when determination of zinc and lead is desired. Borax was nearly as good as this mixture, but the bead was somewhat difficult to remove from the graphite crucible.

The sample-to-flux ratio chosen must necessarily be a compromise. Mixtures containing sample in amounts from 0·5 per cent (PRICE) to 20 per cent (HASLER) have been used. Low sample-to-flux ratio is advantageous as regards self-absorption of the lines of the elements to be determined, as well as effective homogenization in the fusion also. On the other hand, the heterogeneity of the sample, the impurities in the flux chemicals, and also the detectability requirements would favour a high ratio. The time of fusion is of lesser importance, provided it is kept constant. The author used a time of 5 min $\pm$ 15 sec.

It had been proved experimentally that serious losses of lead and zinc are not likely to occur, as long as the temperature of the fusion remains below 900°C. Visible fuming can be observed at 1000°C and when the sample-to-flux ratio is high (see Section 2·2).

As might be expected, the fusion method cannot be applied to samples containing sulphides, because these tend to form a separate phase.

2.2. *Internal standards*

The internal standards are, of course, incorporated during the process of sample preparation. In the present case their chemical properties have been considered at least as important as their emission properties. In the text to follow the internal standards for some of the commonest of the elements occurring in slags are discussed. The known chemical and physical properties are taken into account together with the information attained from spectrographical reproducibility tests, the numerical results of which are presented in Table 1. As this discussion is intended to give a more general review about the choice of internal standards for major constituents, the requirements of the present case are not strictly followed. The elements and lines used as internal standards in the final procedure have thus not been emphasized here, but have been summarized in Table 3 later on.

Silicon: From the chemical point of view the element bearing the greatest resemblance to silicon is germanium. However, the volatility of germanium compounds makes its use impossible in most cases. In experiments carried out by the author, the repeatability of the intensity ratio of the line pairs Si-2514/Ge-2651 and Si-2881/Ge-3039 was excellent within one pellet, but the values varied erratically from sample to sample. This received a satisfactory explanation when the fumes from a melt—fused at 1000°C—were analysed. The fumes contained mainly germanium, together with traces of lead, tin, and zinc.

Tin, titanium, and beryllium have also been tested as internal standards for silicon, but since no substantial improvement over cobalt could be registered, the latter has been preferred. Chemically cobalt is not ideal, but it is easily soluble in borates and yields spectral lines in the vicinity of the strong silicon lines, with excitation potentials nearly identical to those of the silicon lines.

The lithium line Li-4971 has been used as internal standard for silicon by HASLER [1]. In the present case only the line Li-3232 could be used, and the results were far from encouraging, obviously because this line exhibits a very strong self-absorption.

Iron: Cobalt is an ideal internal standard for iron in almost every respect. Suitable line pairs are easily found when the excitation potentials of the lines are taken into account. Reagent-grade cobalt seldom contains any harmful amounts of iron. When a determination of cobalt is desired, or the use of cobalt is otherwise considered impracticable, chromium, nickel, and titanum are acceptable as internal standards for iron.

Calcium and Magnesium: Chemically any one of the elements beryllium, strontium, and barium could be used to advantage. The author used beryllium with considerable success, this being probably due to the spectral similarity of the lines Be-3130, Ca-3179, and Mg-2802. Very likely cobalt might serve as an internal standard, if only suitable lines are chosen.

Aluminium: Since almost all the aluminium lines of sufficient sensitivity have a low excitation potential, Be-3131 cannot be used. The beryllium line 2348, on the other hand, is not acceptable photometrically. The line pair Al-3092/Li-3232 has so far given the best results, but the reproducibility cannot be considered satisfactory (cf. silicon).

Copper, Lead, and Zinc: These elements were of particular interest for the present work. For use with copper the best internal standard was shown to be cobalt. Silver, although spectrally an ideal element, gave erratic results, obviously because of its reduction to metallic silver in the fusion. Lead and especially zinc have low boiling-points, and accordingly losses can be anticipated in the fusion procedure. If the temperature is below 900°C, no losses are evident, whereas cadmium, which was tested as an internal standard for zinc, fumed vigorously at this temperature. Of the other elements tested, tin has given the best results.

In quantometric work the use of a single line as an internal standard is possible and even desirable. HASLER *et al.* [1] have used a single lithium line as an internal standard for iron, silicon, calcium, etc. Although the chemical properties of the metals have not been similar, the results of HASLER *et al.* have been quite satisfactory—even in the case of iron. This is partly due to the spectral similarity of

the lines used (Li-4971·9, E.P. 4·3 V; Fe-4404·8, E.P. 4·5 V), and also the better precision obtainable with the recording system compared to the photographic plate. When spectra are recorded photographically, the use of several internal standard lines is almost unavoidable. These may all be lines of the same element. An excellent example of this principle is the work of PRICE [2].

However, the discussion above shows that it is desirable to use different internal standards for different elements, as in the final procedure in the present work. Naturally the incorporation of so many internal standard elements as those dealt with above might be considered tedious. Since these elements can be mixed as oxides with the flux prior to analysis and are thus weighed together with the flux, the extra work in the daily routine analysis is small compared with the increase of the reproducibility of the results.

Table 1. Reproducibility tests with different internal standards

Line pair	Spark I		Spark II		Spark III	Line pair	Spark I		Spark II		Spark III
	N	*C.V.*	*N*	*C.V.*	*C.V.*		*N*	*C.V.*	*N*	*C.V.*	*C.V.*
Si-2881/Be-3130	7	3·2	9	6·7	—	Cu-3273/Sn-3262	10	3·7	9	3·5	—
Si-2881/Co-3044	7	2·3	9	3·9	—	Cu-3273/Ag-3280	10	2·9	10	3·6	—
Si-2881/Cr-2843	10	3·4	9	5·6	—	Cu-3273/Co-3283	—	—	—	—	2–3*
Si-2514/Ge-2651	10	2·5	11	2·8	—						
Si-2519/Co-2521	—	—	—	—	2–3*	Pb-2833/Sn-2839	9	3·1	10	3·6	2·5–3·5*
Si-2514/Ti-2644	—	—	—	—	4–5*	Pb-2833/Bi-3067	6	5·0	10	5·3	—
Si-2519/Sn-2839	10	4·6	10	4·9	—	Pb-2833/Cd-3261	6	7·2	9	5·3	—
Si-2519/Co-2530	—	—	—	—	2·5–3·5*	Pb-2833/Co-3044	6	4·3	9	4·6	—
						Pb-2833/Cr-2835	6	6·5	10	7·6	—
Fe-3020/Be-3130	8	4·5	8	7·5	—	Pb-2833/Be-3130	6	6·8	10	8·8	—
Fe-3020/Cr-2843	8	3·4	8	5·3	—						
Fe-3020/Co-3044	8	2·5	8	3·2	—	Zn-3345/Cd-3261	10	6·9	8	5·8	—
Fe-2599/Be-3130	8	3·4	7	7·0	—	Zn-3345/Sn-3262	10	5·5	8	3·2	2·5–3·5*
Fe-2599/Cr-2843	8	5·0	8	7·0	—	Zn-3303/Co-3385	10	8·6	10	6·8	—
Fe-3440/Co-3385	8	2·1	8	2·7	2·5–3·5*	Zn-3303/Bi-3067	10	5·6	10	5·5	—
						Zn-3303/Be-3130	10	8·4	9	8·5	—
Ca-3158/Li-3232	10	6·1	—	—	—	Zn-3303/Cd-3261	10	6·8	9	5·2	—
Ca-3158/Cr-2843	9	2·9	9	2·7	—	Zn-3345/Co-3385	10	6·2	8	8·0	—
Ca-3179/Co-3044	10	4·5	10	5·9	—						
Ca-3158/Be-3130	9	3·5	9	4·0	—	*N* = Number of determinations					
Ca-3179/Be-3130	9	—	9	—	1·5–2·5*	*C.V.* = Coefficient of variation					

Spark I: $V = 15{,}000$ V; $C = 0{\cdot}0037\ \mu$F; $L = 0{\cdot}1$ mH; $I_r = 3{\cdot}8$ amp
Spark II: $V = 15{,}000$ V; $C = 0{\cdot}0074\ \mu$F; $L = 0{\cdot}9$ mH; $I_r = 3{\cdot}2$ amp
Spark III: $V = 15{,}000$ V; $C = 0{\cdot}015\ \mu$F; $L = 0{\cdot}9$ mH; $I_r = 4{\cdot}0$ amp
The values marked with an asterisk are the limits of the *C.V.* in several sets of experiments.

The results of some reproducibility tests are presented in Table 1. These tests are carried out only in order to test the spectrographic suitability of various internal standards when excited from the same homogeneous lithium borate—boric acid mixture. The figures quoted express thus only the variation of the spectrographic procedure, and do not include the variation of the sample preparation.

2.3. *Excitation*

Notwithstanding the very high accuracy obtained with d.c.-arc excitation, by, for instance, AHRENS [3] and KVALHEIM [4] when determining major constituents in rocks, a greater reproducibility can be obtained by using sparklike conditions of

excitation. The d.c. arc is, of course, less sensitive to structural differences of the samples, but it cannot compete with the homogenization effected by fusion prior to excitation. The d.c. arc gives a better sensitivity, but sufficient sensitivity may be obtained with the spark as well, modified so as to give a more arc-like discharge. Traces must in any case be determined from separate samples—preferably undiluted—and this is when the d.c. arc, or its equivalent, is indispensable.

Several comprehensive studies deal with the investigation of the most suitable spark source for the analysis of slags and related materials. If it is supposed that the sample preparation has been entirely successful, and the pellets produced really are homogeneous, the amount of sample need not be very large. Of course, a statistically better sampling is obtained if the spark is more "consuming," but on the other hand an arc-like source is more liable to produce lines with self-absorption. When it is considered that adequate sensitivity is essential, it is obvious that the type of excitation chosen must necessarily be a compromise. In the present work low-voltage and high-voltage sparks from the source unit "Emitator" (manufactured by the Boliden Mining Company) have been tested. These experiments have shown that the difference between the different types of sparks as regards the reproducibility of the intensity ratios was insignificant.

Table 2. Spectrographic data for analytical lines cited

Element	*I.P.*	Wavelength	*E.P.*	Element	*I.P.*	Wavelength	*E.P.*
Ag	7·5	3280·683	3·8	Fe	7·8	3440·610	3·6
Al	6·8	3092·713	4·0	Fe	7·8	4404·752	4·5
B	8·3	2496·778	4·9	Ge	7·8	2651·178	4·8
Be	9·3	3130·072	13·2	Ge	7·8	3039·064	4·9
Bi	8·0	3067·716	4·0	Li	5·4	3232·61	3·8
Ca	6·1	3158·863	13·1	Li	5·4	4971·90	4·3
Ca	6·1	3179·332	13·1	Mg	7·6	2802·695	12·0
Ca	6·1	4318·652	4·7	Na	5·1	3302·323	3·7
Cd	8·9	3261·057	3·8	Pb	7·4	2833·063	4·4
Co	7·8	2521·363	4·9	Si	8·1	2514·331	4·9
Co	7·8	2530·13	5·4	Si	8·1	2519·207	4·9
Co	7·8	3044·005	4·0	Si	8·1	2881·578	5·1
Co	7·8	3283·462	5·5?	Sn	7·3	2839·989	4·8
Co	7·8	3385·224	4·1	Sn	7·3	3262·328	4·8
Cr	6·7	2835·633	12·6	Ti	6·8	2644·264	4·7
Cr	6·7	2843·252	12·6	Tl	6·1	2767·87	4·5
Cu	7·7	3273·962	3·8	Zn	3·4	3282·333	7·8
Fe	7·8	2599·396	12·4	Zn	3·4	3302·588	7·8
Fe	7·8	3020·640	4·1	Zn	3·4	3345·020	7·8

3. The spectrographic procedure. Results and discussion

3.1. *Standard analytical conditions*

As a result of the preliminary studies presented above, the following procedure has been developed for the determination of Cu, Pb, ZnO, Al_2O_3, FeO, CaO, MgO, and SiO_2 in slags.

Sample preparation: The sample is received by the laboratory as a powder of less than 100

mesh. 250·0 ± 0·2 mg are taken and mixed in a small beaker with 2250 ± 1 mg of buffer (see below). The mixture is transferred as completely as possible to a graphite crucible of the following dimensions: inside dia. 18 mm, height 16 mm, wall thickness 2·5 mm. The crucibles are reclaimed after use by turning on a lathe. The crucible is placed in an electric furnace and kept there for five min at 900°C (±25°C) and then immediately emptied on a stainless-steel plate. Normally the contents of the crucible come off completely and form a globule on the steel plate. The bead, which by now should be homogeneous throughout, is crushed in a Plattner mortar and passed through a 200-mesh stainless-steel sieve with the aid of a vibrator. Stainless steel as sieve material is much superior to the usual phosphor bronze, which has to be repaired very often, and in addition leaves about 0·001 per cent copper in the sample. The finely divided material (about 0·5 g) is mixed with graphite in a mechanical mixer and pressed to pellets of 12-mm diameter (pressure 7000 kg/cm^2). The preparation of four samples takes about one hour, and the preparation of eight samples an hour and a half.

The *buffer* is prepared as follows: Reagent-grade Li_2CO_3 and H_3BO_3 are mixed in the ratio 1 : 3, distilled water is added to form a thin paste of the mixture, whereupon the water is evaporated. Carbon dioxide is liberated during the evaporation. The mixture is dried at 200°C and crushed in a ball-mill. Cobalt oxide, beryllium oxide, and tin oxide are added in such amounts as to give reference-line intensities suitable for the samples to be analysed. The percentages used in this work have been: cobalt oxide (Co_3O_4) 10 to 15 per cent, tin oxide (SnO_2) 0·3 to 1 per cent, and beryllium oxide 0·01 to 0·1 per cent.

Standards are prepared from spectrographically and chemically standardized oxides and carbonates by mixing them in a small ball-mill. Any further treatment of the sample, such as sintering, is completely unnecessary.

Excitation:

Source: A high-voltage spark with the following settings:
$V_s = 15{,}000$ V, $C = 0{\cdot}015$ μF, $L = 0{\cdot}9$ mH, $I_r = 4{\cdot}0$ amp, $R_s = 2$ ohms.
Electrode separation: 3 mm.
Exposure time: 20 sec with a 10-sec pre-spark period.
Weight of sample consumed: 4–6 mg.

Spectrograph: A Zeiss "Q-24" with the Zeiss external optical system and the slit-width = 0·025 mm. Adjustment of exposure: As required, with a wire-gauze screen or with a step-filter in front of the slit.

Photographic plates: Ilford Process.

Plate processing: As usual, but with very rigorous adherence to the given conditions.

Densitometry: Densitometer: The Hilger "non-recording microphotometer." Optical density–intensity curves established by means of iron lines of known intensity in the wavelength region 3100–3150 Å. Only one curve is used, as the lines of the line pairs used for analysis lie closely together.

Calculations: "Respectra" calculating board. Background corrections are not made, as the line densities are selected to fall between $D = 0{\cdot}6$ and $D = 1{\cdot}2$, and background density is less than 0·05; moreover, the background is included in the working curve.

Analytical lines: Line pairs are given in Table 3.

3.2. *Results*

(a) *Reproducibility.* The spectral reproducibility of the present procedure—i.e., the overall precision of the excitation and the photometric process—is presented in Table 3.

The reproducibility of the procedure of fusion is shown in Table 4. The sample was prepared five times over, i.e., by fusion of five separate batches and making one pellet from each. The pellets were analysed four to eight times each.

Simple statistical calculations indicate that the differences between the separate melts—and the pellets prepared from them—is insignificant. In other words, the errors which arise from variations in sample preparation are smaller than those of the spectrographic procedure.

Table 3. Reproducibility of repeat determinations of the same sample (=pellet).

	Sample I								Sample II		
Component	Al_2O_3	CaO	Cu	FeO	MgO	Pb	SiO_2	ZnO	CaO	Cu	SiO_2
Line pair	Al-3092 / Li-3232	Ca-3179 / Be-3130	Cu-3273 / Co-3283	Fe-3440 / Co-3385	Mg-2802 / Be-3130	Pb-2833 / Sn-2839	Si-2519 / Co-2521	Zn-3282 / Sn-3263	Ca-3179 / Be-3130	Cu-3273 / Co-3283	Si-2519 / Co-2521
Mean per cent	4·34	32·7	0·135	15·6	5·87	2·98	28·5	7·38	3·65	0·322	37·7
C.V.	3·5	1·8	3·5	1·9	3·6	2·6	4·5	1·8	1·5	2·3	3·0
n	12	12	12	12	12	12	12	12	17	18	18

C.V. = Coefficient of variation n = number of spectra

Table 4. Reproducibility of the sample preparation

Pellet No. (=melt No.)	Number of spectra of each	Si-2519/Co-2521		Ca-3179/Be-3130		Cu-3273/Co-3283	
		Mean per cent	S.D.	Mean per cent	S.D.	Mean per cent	S.D.
1	7	40·7	0·81	4·21	0·077	0·280	0·00445
2	8	39·9	1·06	4·23	0·077	0·279	0·00743
3	6	39·6	1·03	4·16	0·086	0·276	0·00675
4	4	40·0	2·14	4·12	0·109	0·281	0·00917
5	4	41·4	1·04	4·18	0·089	0·276	0·00961

Table 5. Repeatability under routine conditions

		Cu	CaO	SiO_2
	Mean per cent	0·274	3·92	39·04
Sample No.	*C.V.*	3·1	2·48	3·3
SpS-2-3-2-2-10	*C.V.* $\sqrt{2}$	4·4	3·5	4·6
	n	46	46	46
	Mean per cent	0·416	3·61	34·66
Sample No.	*C.V.*	2·7	2·4	4·2
SpS-2-3-2-2-17	*C.V.* $\sqrt{2}$	3·8	3·4	5·9
	n	42	45	45

C.V. = coefficient of variation *n* = number of daily analyses

The reproducibility of a larger set of determinations is shown in Table 5. During a period of about two months the values for two control samples—which were analysed in duplicate on each of the daily "slag plates"—were collected, the mean values calculated for each duplicate, and the coefficient of variation calculated for these, and also the mean of all values.

(b) *Accuracy.* As in most cases of spectrographic analysis, there are difficulties in establishing the accuracy of the spectrographic procedure, owing to the lack of

samples of exactly known composition. As a result of this, the problem had to be approached by various means, each of which contributes to the knowledge of the accuracy of the method.

Before this new analytical method could be approved for slag control, it had to be compared with the old, well established, chemical methods. A comparison of both methods was conducted over a period of one month, with independent analyses of the same samples daily by the spectrographic and the chemical method. Over two hundred samples of copper-making slag were thus analysed for copper, lime, and silica. A statistical study of all the results showed that as regards copper no significant difference existed, whereas the values for lime and silica showed a significant difference. Control, by the most accurate chemical methods which were available, showed that the chemical values for silica were on the average 0·5 per cent too low, and that the spectrographic values for lime were correct to within the precision attainable with the chemical methods used for checking the results. The same policy of comparison of both analytical methods has also been applied for the analysis of the lead-making slags. In this case a statistical study indicated that the differences between the figures of both methods were statistically significant for all constituents determined.

As the thorough statistical study of the large amounts of results obtained by routine chemical and spectrographical methods had revealed some systematic differences, as mentioned above, a further control was necessary. This was done in the following way. The precisely weighed aliquots of all the samples were mixed together into one large sample, the composition of which was calculated on the basis of both the chemical routine and spectrographic values. This sample was then analysed independently, using accurate chemical methods, as opposed to routine methods. One "average sample" of both copper- and lead-making slag was controlled. The values obtained are presented in Table 6.

Table 6. Comparison of spectrographic, routine chemical, and accurate chemical values

	Lead-making slag					Copper-making slag			
	Pb per cent	ZnO per cent	CaO per cent	SiO_2 per cent	FeO per cent		Cu per cent	CaO per cent	SiO_2 per cent
Routine chem. mean, $n = 32$	2·57	9·68	31·54	23·27	20·14	$n = 22$	0·326	3·88	36·2
Accurate chemical	2·76	10·2	30·2	24·0	19·7		0·312	3·8	36·5
Spectrographic mean, $n = 32$	2·90	10·05	30·68	23·75	19·58	$n = 22$	0·309	3·85	36·4

3.3. *Discussion*

The relatively great difference in reproducibility between values obtained from a sample on a single plate and from the sample photographed on different plates during a longer period (see Tables 4 and 6). has been shown to depend on the fact that the optical density–intensity curve has not been measured for every plate.

It is thought, however, that since the errors of the values for the actual samples are less when the values are corrected in accordance with the control samples included on every plate, it is not advisable to calibrate every plate separately. According to experiments carried out in this connection, considerable time is required if the emulsion is to be calibrated with an accuracy of better than 1 per cent at different wavelengths and over large intensity intervals.

As regards the overall accuracy, the present method has proved satisfactory. No systematic errors have been detected. Owing to great dilution with the flux, and the small separation between analytical lines, not even background effects have been observed.

A reproducibility of 1·5 to 3·5 per cent has been obtained by the spectrographic method for the different elements. Accordingly, at a concentration of 30 per cent the results will be accurate to within $\pm 0{\cdot}3$ to $\pm 0{\cdot}6$ per cent when three spectra from the same pellet are measured. Since this relative accuracy can be maintained over the entire range of concentration occurring in the samples, the method has been considered adequate for the control of slags. In the case of most elements, probably with the exception of copper and iron, it would be difficult to obtain this accuracy by "wet" chemical means under routine conditions, if the content is less than say 5 per cent.

As regards the time required for analyses, two samples may be analysed for six constituents and four samples for three constituents in a time of five hours (man hours). This time is considered to be satisfactory in the case of control analyses of copper-making and lead-making slags, and it is shorter indeed than the time required by chemical methods.

Speaking of the reproducibility and the accuracy of a method, the author would like to include the reliability in the hands of the user as a third characteristic of a method. This property is, although often neglected or insufficiently tested, of prime importance in the industrial laboratory, where unskilled labour must be employed. The method presented here has been in use daily during a year, and in this time 1400 samples have been analysed, corresponding to over 6400 determinations of elements.

Acknowledgements—The author is greatly indebted to Mr. ALLAN DANIELSSON, Head of the Physical Department of the Central Laboratory of Boliden Mining Company, for many helpful discussions and assistance during the development of the method. Thanks are also due to the management of Boliden Mining Company for permission to publish this paper.

References

[1] HASLER, M. F., and BARLEY, F., *Applied Research Laboratories* 1952.
[2] PRICE, W. J., *Spectrochim. Acta*, 1953, **6**, 26.
[3] CARLSSON, C. G., *Jernkontorets Ann.*, 1951, **135**, 607.
[4] GILLIS, J., and EECKHOUT, J., *Spectrochim. Acta*, 1950, **4**, 284.
[5] DENNEN, N. H., AHRENS, L. H., and FAIRBAIRN, H. W. Geological Survey Bulletin 980, 1951.
[6] KVALHEIM, A. J., *J. Opt. Soc. Amer.*, 1947, **37**, 585.
[7] DUNÈR, B., *Metallografiska Inst. Spektralkommittes handlingar* No. 1029, 1951.

VOL
7
1955/

Spectrochimica Acta, 1956, Vol. 7, pp. 367 to 372. Pergamon Press Ltd., London

Über den Nachweis von Oxydationsvorgängen in der Funkenstrecke*

ALBERT KEIL
Laboratorium der Platinschmelze Dr. E. Dürrwächter K. G., Pforzheim

(*Received* 30 *July* 1955)

Abstract—The oxidation of the surface of a metal electrode during sparking may influence the total brightness of the spectrum as well as the relative intensity of the lines of different elements. Evidence is produced that during the sparking of silver under certain conditions an oxide phase can be detected. The course of the sparking-off effects of silver alloys depends on whether the alloying elements are really in solution in the silver, or are segregated as oxide in intercrystalline films; this has been tested for Cd and Mn. In either case, the spectra after prolonged sparking tend to reach similar conditions. For alloys of silver and molybdenum, thermochemical reactions between the two elements can be identified in the spark.

CHEMISCHE Reaktionen zwischen Luftsauerstoff und Elektrodenoberfläche unter der Einwirkung einer elektrischen Entladung sind bisher nur in Einzelfällen in ihrem Ablauf exakt erfasst worden. Die grundsätzliche Bedeutung dieses Problemes für die praktische Spektralanalyse ist in jüngerer Zeit von F. TWYMAN [1] nach kritischer Sichtung des von zahlreichen Autoren erarbeiteten Materials besonders hervorgehoben worden. Eine Ordnung der verschiedenartigen Einzelbeobachtungen, unter denen beispielsweise die Arbeiten von J. VAN CALKER [2] und O. LEUCHS [3] zu nennen sind, nach einheitlichen Gesichtspunkten ist jedoch zur Zeit noch nicht möglich. Es soll daher auch nicht die Aufgabe des vorliegenden Berichtes sein, einen Überblick über das Gesamtgebiet zu geben. Die zu beschreibenden Versuche beziehen sich vielmehr auf einige Einzelbeobachtungen an Silber-Legierungen, bei denen besonders übersichtliche Verhältnisse einen Beitrag für die Diskussion der folgenden beiden Fragen ermöglichen:

(1) Kann die Bildung oxydischer Phasen an der Elektrodenoberfläche die Materialüberführung in den Entladungsraum und damit die Gesamthelligkeit des Spektrums beeinflussen?

(2) Lassen sich bei Legierungen Intensitätsverschiebungen zwischen den Linien der Partnerelemente—z.B. beim Abfunkeffekt—eindeutig mit Oxydationserscheinungen erklären?

Von entscheidender Bedeutung für das "chemische Verhalten" einer elektrischen Entladung in Bezug auf die Elektrodenoberfläche ist die thermische Beständigkeit der dabei durch Reaktion mit dem Luftsauerstoff entstehenden Oxyde. Liegt die Funken-oder Bogenansatztemperatur über der Dissoziationsgrenze bzw. dem Sublimationspunkt der gebildeten Oxyde, so bleibt die Oxydbildung auf periphere Zonen der Bogenbahn beschränkt, die Elektrodenoberfläche selbst wird beim Wandern der Bogenansatzstelle "gereinigt." Liegt hingegen die Dissoziationsgrenze der gebildeten Oxyde über der Funken-oder Bogenansatztemperatur,

* Ein Teil der Resultate wurde bereits beim 4. internationalen Colloquium für Spektroskopie, Münster (Westfalen), September 1953 vorgetragen.

verschlackt die gesamte Elektrodenoberfläche. Dieser letztere Fall ist der allgemeiner bekannte, er gilt insbesondere für alle sehr unedlen Metalle wie z.B. Aluminium, Magnesium und ihre Legierungen. Der erste Fall ist am Beispiel des Kupfers beschrieben worden [1]. Die Materialüberführung in die Bogensäule erfolgt demnach an einer Kupferkathode über die Zwischenstufe der Bildung von Kupferoxydul, das zunächst eine flüssige Phase auf der Elektrodenoberfläche bildet. Da es nun eine besondere Eigenschaft mancher Edelmetalle ist, in abgegrenzten Temperaturbereichen beständige Oxyde zu bilden, die bei höheren Temperaturen, jedoch noch wesentlich unterhalb des Metallschmelzpunktes, zerfallen bzw. flüchtig sind, ist der Nachweis derartiger Erscheinungen bei ihnen besonders aussichtsreich.

Im Gegensatz zu einigen Metallen der Platingruppe, bei denen durch kurzzeitige Lagerung in einem Temperaturgefälle mit nachfolgendem Abschrecken der Probe in Wasser das Gebiet beständiger Oxyde leicht sichtbar gemacht werden kann, ist allerdings ein ähnlicher Nachweis für das hier interessierende Silber mit einfachen Mitteln nicht möglich. Immerhin ist die Beständigkeit von Silberoxyden bei Temperaturen unterhalb 300°C bekannt und ihre Entstehung unter den Bedingungen der Glimmentladung ist neben Silbernitrit von F. E. Haworth [4] quantitativ nachgewiesen worden. Die folgenden Experimente sollten daher zunächst darüber Aufschluß geben, ob auch unter den Bedingungen einer Funkenentladung mit derartigen Reaktionen zu rechnen ist.

Kondensation von Oxyden aus der Funkenbahn

Für die Untersuchung wurden Elektroden aus verschiedenen Metallen in den Entladungskreis eines Feußner-Funkenerzeugers geschaltet ($C = 2100$ pF, $L = 0{,}08$ mH) und unmittelbar an die Funkenstrecke ein Objektträger aus Glas angebracht [5]. Die elektrische Entladung folgt dann als Gleitfunken der Glasoberfläche und die auf ihr niedergeschlagenen Kondensationsprodukte können anschließend mikroskopisch untersucht werden. Bild 1 zeigt das für unedle Metalle charakteristische Ergebnis bei der Verwendung von Al-Elektroden. Es bilden sich am Ansatzpunkt der Entladung Höfe von kondensierten Oxyden. Ein anderes Bild ergibt sich bei der Verwendung von Silberelektroden (Bild 2). In diesem Fall entsteht zwischen den Elektroden eine Brücke von metallischem Silber. Sie wird seitlich von graubraunen Zonen begrenzt, die unter dem Mikroskop keine kristalline, sondern eine glasflußartige Struktur zeigen. Im Gegensatz zum metallischen Brükkenkern ist diese Randzone in Ammoniak löslich, sie kann durch Wärmebehandlung oberhalb 300°C unter Bildung von metallischem Silber zersetzt werden. Der Schluß, daß es sich bei dieser Randzone um kondensierte oxydische Mischphasen des Silbers handelt, hat demnach eine hohe Wahrscheinlichkeit für sich. Es ist nun einleuchtend, daß beim seitlichen Abwandern der Funkenansatzstelle auf der Probenoberfläche immer wieder Stellen erfaßt werden, auf denen sich vorher Oxyde niedergeschlagen hatten. Diese zerfallen dabei und ihre Atome treten leichter in den Entladungsraum über, als die im Kristallgitter der Elektrode gebundenen. Wenn diese Deutung richtig ist, müßte demnach der Verdampfungsmechanismus des Silbers durch die Anwesenheit von unedlen Legierungskomponenten beeinflußt werden, sofern diese den Sauerstoff bevorzugt an sich binden.

VOL 7 1955/

VOL.
7
55/56

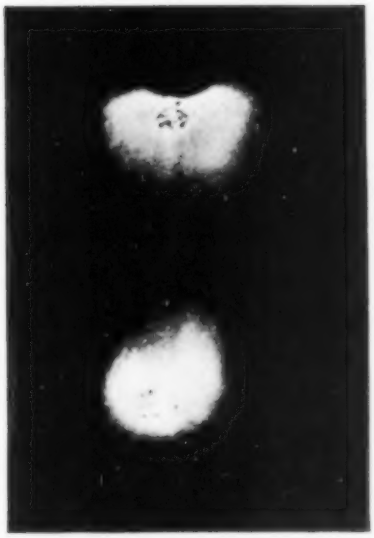

Bild 1. Kondensat an Aluminium-Elektroden. Vergrößerung = 9.

Bild 2. Silberkondensat nach 2′ Funkenübergang. Vergrößerung = 9.

VOL.
7
1955/

Veränderungen von Abfunkkurven durch den Sauerstoffgehalt der Proben

Für den Nachweis der Existenz derartiger Effekte sollen im folgenden einige Abfunkkurven herangezogen werden, bei denen nach Unterschieden in den Intensitätsverhältnissen gesucht wurde und zwar für echte Legierungen und für Werkstoffe gleicher Zusammensetzung, bei denen die Oxydation der unedlen Komponenten vorweggenommen war. Nun ist allerdings die naheliegende Verwendung pulvermetallurgisch hergestellter Sinterkörper aus Metall-Metalloxyd-Gemischen für derartige Zwecke nicht unbedenklich. Bild 3 zeigt nämlich einen solchen Vergleich

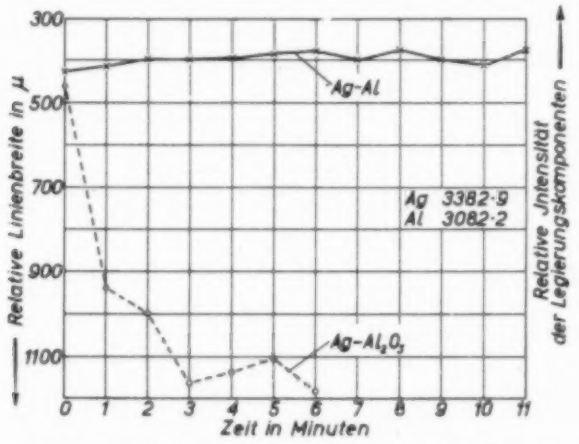

Bild 3. Abfunkkurven einer Ag-Al-Legierung und eines Ag-Al_2O_3-Sinterkörpers mit jeweils 4% Al-Gehalt.
Die Zahlenwerte der Ordinate sind fallend aufgetragen, denn die gemessene "Breite" der Linie des Grundmetalls (Ag 3382·9), bezogen auf die Schwärzung der Linie des Zusatzmetalles (Al 3082·2), wird kleiner für wachsende Intensität der Linie des Zusatzmetalles.

zwischen einer Ag-Al-Gußlegierung und einer aus Silberpulver und feinkörnigem Korund hergestellten Ag-Al_2O_3-Sinterprobe mit gleichem Al-Gehalt (4%). Entscheidend für die Verdampfung des Oxyds in der zweiten Probe ist augenscheinlich sein Dispersionsgrad. Nur kleine Partikel werden in die Funkenbahn überführt, die größeren im Kristallverband fest verankerten Al_2O_3-Körner werden bei relativ niedrigen Bogenansatztemperaturen nicht mehr zum Verdampfen gebracht, sodaß im Spektrum des Sinterkörpers die Al-Linien rasch schwächer werden. Die Auswertung der Spektrogramme erfolgte dabei nach dem Verfahren der relativen Linienbreite von W. Gerlach und W. Rollwagen [6], da bei diesem nahe benachbarte Linien sehr verschiedener Intensität in Beziehung gesetzt werden können.

Nun bietet das Silber als Legierungsbasis eine metallurgische Möglichkeit, in gewissen Fällen derartige störende Nebeneffekte auszuschließen. Es gibt nämlich ein Verfahren, durch eine Glühbehandlung in Luft bei 700–800°C in homogenen Silberlegierungen, die beispielsweise 5–10% Cd oder Mn enthalten, durch die Eindiffusion von Luftsauerstoff die in dieser Legierung enthaltenen unedlen

Elemente durch "innere Oxydation" heterogen im Kristallgefüge quantitativ auszuscheiden. In Bild 4 ist eine Übergangszone zwischen homogenen Silbermischkristallen und dem durch ausgeschiedene CdO-Partikel heterogenisierten Werkstoff in starker Vergrößerung im Querschliff dargestellt. Das CdO liegt demnach in außerordentlich feiner Verteilung vor, so daß sein Dispersionsgrad

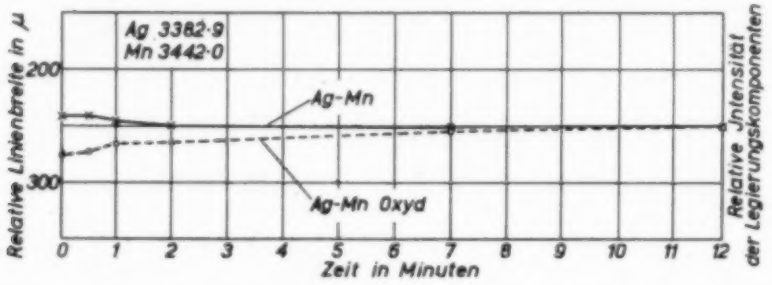

Bild 5. Abfunkkurven von einer Ag-Cd-Legierung mit 5% Cd und einer durchoxydierten Probe des gleichen Materials.

gegenüber dem ursprünglichen Mischkristall kaum verändert erscheint. Vergleicht man nun die Abfunkkurven einer echten Ag-Cd-Legierung und einer aus ihr hergestellten, vollständig durchoxydierten Probe (Bild 5), so zeigt sich, daß deren Verlauf durch den Sauerstoffgehalt in der ersten Minute des Funkenübergangs erheblich beeinflußt wird. Dann stellt sich auf der Elektrodenoberfläche ein Oxydations-Reduktionsgleichgewicht ein, das jedoch in keinem der beiden Fälle

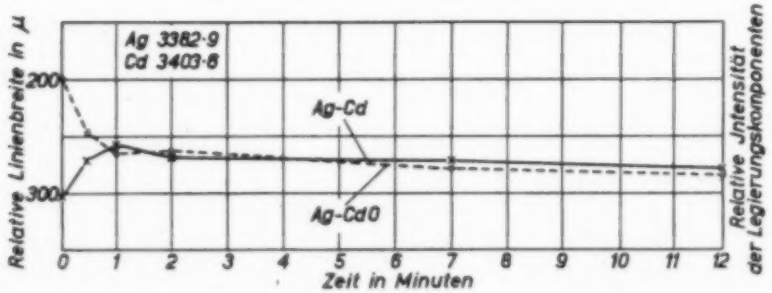

Bild 6. Abfunkkurven von einer Legierung mit 5% Mn und einer durchoxydierten Probe des gleichen Materials.

dem durch das Elektrodenmaterial vorgegebenen Zustand entspricht. Führt man den Versuch mit einem thermisch beständigeren Oxyd durch (CdO sublimiert bezw. dissoziiert nämlich bereits bei Temperaturen oberhalb 1000°C), so scheint z.B. im Falle des Mangans als Legierungspartner (Bild 6) die Einstellung des Gleichgewichtes einen erheblich längeren Zeitraum (7 Minuten) zu benötigen.

Zum Schluss sei noch ein Beispiel einer direkten chemischen Reaktion zwischen den Metallen der Elektroden besprochen. Schaltet man in zwei parallelen Versuchen jeweils eine flächenhafte Elektrode aus Molybdän gegen einen Draht aus Gold,

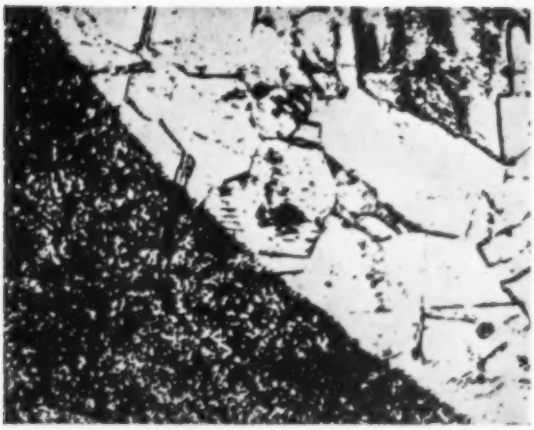

Bild 4. Querschliff durch eine Probe (geätzt); rechts oben homogener Ag-Cd-Mischkristall, links unten heterogenisiert durch innere oxydation des Kadmiums Vergrößerung = 200.

VOL.
7
65/56

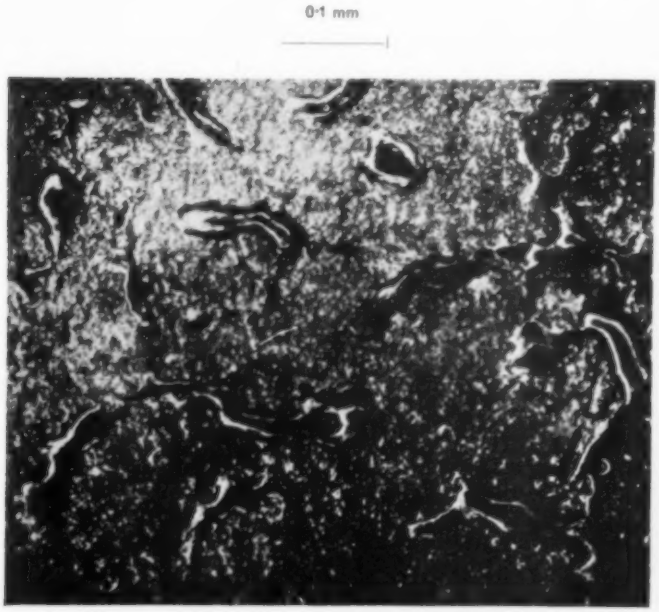

Bild 7. Oxydische Schmelzperlen auf einer Elektrodenoberfläche aus Mo nach dem Funkenübergang bei Schaltung gegen eine Elektrode aus Ag.

VOL.
7
1955/5

bezw. aus Silber, so lassen sich nach dem Funkenübergang auf der Molybdän-Elektrode typische Unterschiede erkennen. Bei dem Versuch mit der Goldgegenelektrode hat sich im Zentrum des Funkenansatzes eine Zone gebildet, die von metallischem Gold bedeckt ist. Sie ist umgeben von einem Hof dunkel gefärbten Metallstaubes. Bei dem Versuch mit der Silbergegenelektrode ist hingegen kein metallisches Kondensationsprodukt auf der Molybdänfläche zu erkennen, sondern es haben sich auf ihr glasflussartige Schmelzperlen gebildet (Bild 7). Dieser Vorgang ist mit einer Abnahme der Gesamthelligkeit des Spektrums im Verlaufe der ersten Minuten des Funkenüberganges verbunden (was bei dem Versuch mit der Goldgegenelektrode nicht so ausgeprägt beobachtet wird), sowie mit einer Tendenz zur Glimmentladung. In Analogie zu Zunderversuchen an reinen Pulvergemischen von Silber und Molybdän [7] ist es wahrscheinlich, dass es sich dabei um die Bildung von Silbermolybdaten handelt, die entweder unter Hinzutritt von Sauerstoff nach dem Reaktionsschema

$$2\,Ag + MoO_3 + \tfrac{1}{2}\,O_2 \rightarrow Ag_2MoO_4$$

oder unter Reduktion von ursprünglich gebildeter Molybdänsäure nach der Gleichung

$$2\,Ag + 4\,MoO_3 \rightarrow Ag_2MoO_4 + Mo_3O_8$$

verlaufen kann. Es handelt sich demnach um den Ablauf einer thermo-chemischen Reaktion, durch die das Silber im Gegensatz zum Gold, beidem der Effekt nicht auftritt, in dem durch die elektrischen Entladungsbedingungen gegebenen Temperaturbereich seinen Charakter als Edelmetall verliert und in ein thermisch beständiges Mischoxyd übergeführt wird, wodurch sich wiederum die Entladungsbedingungen und die Intensitätsverhältnisse im Spektrum ändern.

Schlussfolgerung

Bei der Aufstellung von Analysenvorschriften können neben physikalischen und metallurgischen Überlegungen gelegentlich auch thermo-chemische Erwägungen von Bedeutung sein. Die Versuche an einigen Silberlegierungen lassen dafür als mitbestimmende Faktoren erkennen:

(1) Die Lage der Zersetzungs—bezw. Sublimationstemperatur der entstehenden Oxyde in Bezug auf die Funken—oder Bogenansatztemperatur und den Schmelzpunkt der Metalle.

(2) Den Dispersionsgrad der im Metall eingeschlossenen Oxyde oder nichtmetallischen Verbindungen.

(3) Oxydations-Reduktionsgleichgewichte zwischen den Legierungskomponenten, wobei der vorgegebene Sauerstoffgehalt der Proben von erheblichem Einfluss sein kann.

(4) Direkte thermo-chemische Reaktionen zwischen den Elementen und ihren Oxyden.

Zusammenfassung—Oxydationserscheinungen an den Elektrodenoberflächen unter der Einwirkung einer Funkenentladung können sich sowohl auf die Gesamthelligkeit des Spektrums als auch auf den Abfunkeffekt auswirken. Zunächst wird gezeigt, daß bei dem Edelmetall Silber unter üblichen Anregungsbedingungen eine Entstehung oxydischer Mischphasen nachweisbar ist. Der Verlauf von

Abfunkkurven ist weiterhin bei Silberlegierungen verschieden, jenachdem, ob die in diesen enthaltenen unedlen Komponenten (z.B. Cd, Mn) im Mischkristall gelöst sind oder zuvor als Oxyd interkristallin ausgeschieden wurden. Für beide Modifikationen des Materials streben jedoch nach Ablauf einer gewissen Zeit die Abfunkkurven dem gleichen Endwert zu. Schließlich wird an dem Metallpaar Silber/Molybdän auch die Möglichkeit direkter, thermochemischer Reaktionen zwischen den Partnerelementen im Funken nachgewiesen.

Schrifttum

[1] TWYMAN, F., *Metal Spectroscopy*, Griffin & Co., London, 1951, 237
[2] VAN CALKER, J., *Spectrochimica Acta*, 1944, **2**, 340
[3] LEUCHS, O., *Spectrochimica Acta*, 1950, **4**, 237
[4] HAWORTH, F. E., *Journ. appl. Phys.*, 1951, **22**, 606
[5] KEIL, A., *Metall.*, 1952, **6**, 674
[6] GERLACH, W., und ROLLWAGEN, W., *Metallwirtschaft*, 1937, **16**, 1083
[7] KEIL A., und MEYER C.-L., *E.T.Z.*, 1952, **73**, 31

VOL.
7
1955/5

Spectrochimica Acta, 1956, Vol. 7, pp. 373 to 386. Pergamon Press Ltd., London

A comparison of three methods of plate calibration and evaluation for routine spectrographic analysis of low-alloy steels

H. T. SHIRLEY, A. OLDFIELD, and H. KITCHEN
Brown-Firth Research Laboratories, Sheffield, England

(*Received April* 1954; *in revised form, October* 1955)

Abstract—A comparative study has been made of the use of three procedures for plate-response calibration and general evaluation of low-alloy steel spectrograms—

(a) based on the direct relation of densitometer readings to log-relative intensity,
(b) using the Kaiser-Seidel-transformation (P-value) technique for straightening the plate-response curve,
(c) by means of the $-f(\tau)$ transmittance table of J. W. ANDERSON.

For this work, a series of ten working plates, taken over a period of a year, provided a total of fifty spectrograms for each of two low-alloy steel standard samples.

It is shown that an improvement in analytical accuracy (standard error), of the order of 20 per cent, may be expected from the use of methods (b) and (c) with individual plate calibration, as compared with method (a) and batch calibration. About one-third of this improvement was from individual plate calibration.

Speed and ease of working is considered generally similar for the three methods, but plate-response calibration is considerably simplified by the straight-line relationships of methods (b) and (c).

Introduction

ACCURATE spectrographic analysis through photographically recorded spectra requires some form of correction for non-linearity and variability in the response of the photographic plates. A sufficient degree of accuracy can in some cases be achieved by careful standardization of procedure, with incorporation of spectrograms from a number of standard samples of known analysis on each plate. Non-linearity of plate response will then be included in the form of the composition curves, and may considerably restrict permissible variation in overall density or response of the plates. Such a system is obviously less flexible, and in general less satisfactory, than one in which individual- or batch-plate calibration permits a more direct relation of composition to line intensity. Mention should be made of the "two line-pair" methods of SANDERS [1] and of ARGYLE and PRICE [2], which introduce a considerable measure of correction by geometric treatment of readings from two line-pairs, without direct-plate calibration, but the present work is concerned only with the more usual single line-pair technique.

Speed, reliability, and simplicity of operation are the most important desiderata in routine analysis, and much thought has been devoted to various forms of calculating board and other means of applying plate calibration with these ends in view. Reference may particularly be made to papers by KAISER [3] in Germany, by CHURCHILL [4] and KING [5] in America, and by BROMMELLE and CLAYTON [6] in this country. CARLSSON [7] has made a useful survey of the principal types of calculating board and of plate calibration by selected iron lines of known relative

intensity. Detailed consideration of methods of plate calibration, including recommended series of iron lines suitable for this purpose, is given in the report on the Spectrographic Analysis of Low-alloy Steels prepared by the B.I.S.R.A. Spectrographic Analysis Sub-committee [8]. More recently, a paper by Anderson [9] introduces a new form of exposure-transmittance table as a means of converting densitometer readings to relative line intensities.

General consideration of methods of plate calibration

In the authors' laboratory, plate calibration is normally based on a time-scale using spark exposures and reading lines from the series of iron spark lines selected for stability of relative intensity and recommended by the B.I.S.R.A. Sub-committee [8]. This method provides a calibrating intermittent light source closely comparable with that used for the actual analyses, and once the relative "intensities" of the various lines have been determined for the operating conditions, a single spectrogram can be used to check the plate calibration. Initial calibration is usually based on duplicate spectrograms for each of four exposure times, and the curve drawn relates densitometer readings R directly to log-relative intensity based on the exposure-time scale. It has the "S" form shown in curve R of Fig. 2.

Some straightening of this curve is possible by plotting density as ordinate in place of transmittance, but the effectively straightened portion is confined to densitometer readings below about 15 cm on the 50-cm scale (density 0·5) for the Ilford thin-film half-tone plates used in the present work (Fig. 1).

Kaiser [3a] showed that much more effective straightening could be effected by substitution of the Seidel density for the simple density of Fig. 1. This is expressed as

$$W = \log\left[\left(\frac{d_0}{d}\right) - 1\right]$$

where d is the densitometer reading for a clear-glass reading of d_0, the ordinary density, D, being given by $\log d_0/d$. A still better result was obtained by use of appropriate values of "l" in the generalized Seidel transformation,

$$P = lD + (1 - l)\,W.$$

and for process type plates "l" may be taken as 0·5, giving

$$P = \frac{D + W}{2}$$

A comparison of the three types of curve is given in Fig. 2 for an Ilford thin-film half-tone plate.

Tables for conversion of densitometer readings to values of D and W have been published by Mitchell [11]. The straight-line relation between P and relative intensity greatly simplifies individual-plate calibration, particularly for calculating board applications.

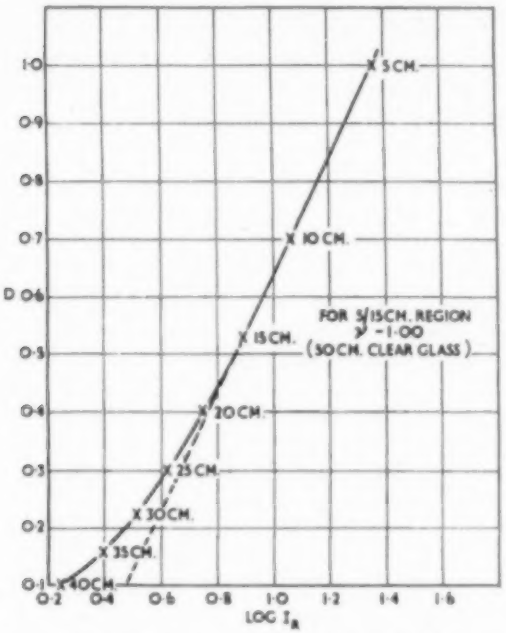

Fig. 1. Density/log I_R curve for Ilford thin-film half-tone plate.

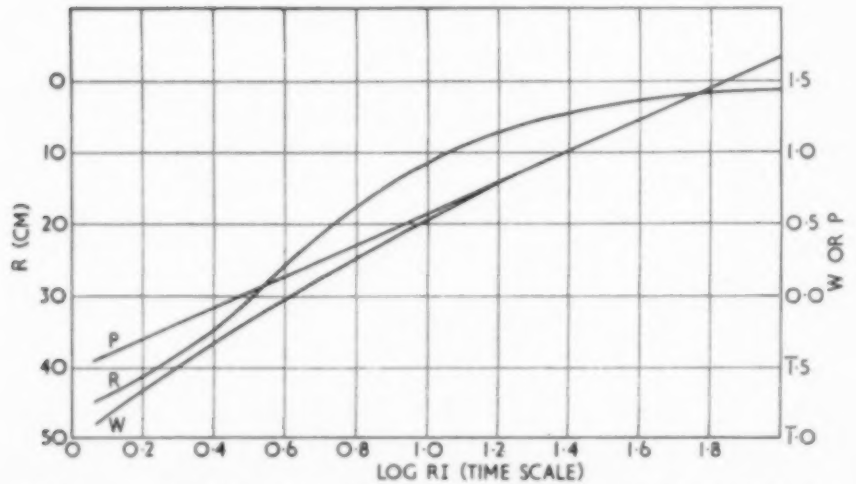

Fig. 2. Comparison of three types of calibration curve (Ilford thin-film half-tone plates).
R = Densitometer reading; $W = \log\left(\frac{d_0 - 1}{d}\right)$; $P = \frac{D + W}{2}$ where $D = \log\frac{d_0}{d}$.

The method described by Anderson [9] requires no calibration curve. Instead, use is made of the work of Murphy and Hughes [10] to derive an exposure-transmittance table relating densitometer readings to a function $-f(\tau)$. This function provides a linear relation between the fractional transmittance (τ) and log exposure, the basic relationship being given as

$$\gamma = \frac{S \times \Delta[-f(\tau)]}{\Delta \log E}$$

where γ is the gamma, or contrast factor of the plate, and S a scaling constant of value 0·993 calculated from observations. By reading the transmittance values for two lines of known relative intensity, it is thus readily possible to calculate γ for any plate or specific region of a plate. Once this value is determined, log-relative intensity values can be deduced from densitometer readings according to the expression

$$\log I_R = \Delta \log E = \frac{0{\cdot}993}{\gamma} \Delta[-f(\tau)].$$

Such an operation can be carried out directly with a slide-rule, or if desired can be worked from an appropriate series of log $I_R/\Delta[-f(\tau)]$ curves on a calculating board as with the P values.

VOL. 7 1955/5

Scope of the present investigation

It was considered of interest to study the accuracy of working of the following procedures:—

(a) The method employing densitometer reading/log "intensity" tables constructed from type R curve of Fig. 2.
(b) The use of a simple calculating-board technique, with plate calibration based on the P values of Kaiser, i.e., using the P line of Fig. 2.
(c) By using the exposure transmittance tables of Anderson.

In all three cases calibration was based on transmittance readings for lines from the B.I.S.R.A. spark-line series [8].

Since methods (b) and (c) greatly simplify individual plate calibration, their use would make it practicable to consider inclusion of such treatment in place of the batch calibration normally used by the authors. Comparison of accuracy for the two types of standardization was, therefore, included.

Details of plates used

A series of ten plates was already available from an earlier reproducibility study. These were all of the Ilford thin-film half-tone type, and each plate included five spectrograms from each of two of the B.I.S.R.A. standards (3 and 6) giving a total of fifty spectrograms per sample. Appropriate plate-response and composition-calibration plates were also available.

Details of the plates were as follows.

(a) *Plate-response calibration*

One plate was used for the primary standardization work. Four exposures were made in duplicate covering 19, 38, 75, and 150 seconds, arrangements being generally as for the analytical work, except for the use of a pure iron specimen. This plate was exposed in October 1950.

(b) *Composition-curve calibration plate*

On this plate triplicate exposures were made for each of the eight B.I.S.R.A. standard low-alloy steels. Each complete exposure consisted of two superimposed 45-sec periods without pre-spark. Two pure iron, plate calibrating spectrograms were included at 1 × 75 sec exposure. The plate was prepared in November 1950.

(c) *Working plates*

These were exposed at intervals over a period of a year, four during October–November 1949 and six during October–November 1950. The first seven were from one box and the remaining three, with plates (a) and (b) above, from the second box, both boxes being from a single delivery.

All these plates contained a pure iron spectrogram, before and after the set of ten spectrograms, five from each of the working samples. Exposure for the pure iron spectrograms was 1 × 75 sec, and for the working spectrograms, two superimposed 45 sec periods, without pre-sparking, using a Hilger large quartz spectrograph with a slit-width of 0·015 mm. A Hilger condensed-spark unit was employed for excitation, with a nominal 15-kV output, using no added inductance and a condenser of 0·005-μF capacity. Auxiliary electrodes were $\frac{1}{4}$-in.-diameter graphite rods with 80° points sparking against a flat steel surface.

The plates were processed for $3\frac{1}{2}$ min in quarter-strength Kodak D19b developer at 18°C, using Kodak "squeegee-type" agitation [12], followed by normal fixing and washing, with unheated shelf-drying.

Working samples

The two working samples were B.I.S.R.A. standards 3 and 6, of the following chemical analyses [8], in respect of the elements used:—

	Mn	Ni	Cr	Mo	V	Cu
No. 3	0·36	2·92	0·35	0·95	0·22	0·50
No. 6	1·21	0·18	2·34	0·54	0·36	0·23

Line-pairs

The line-pairs were selected from the recommended series in the B.I.S.R.A. Sub-committee Report [8], shown at top of p. 378.

Photometry was carried out with a Hilger non-recording densitometer using the linear galvo-scale attachment.

		Sample 3	Sample 6
Manganese	Mn	2933·06	3441·99
	Fe	2936·90	3443·88
Nickel	Ni	3101·55	3414·76
	Fe	3100·67	3417·84
Chromium	Cr	3132·06	3408·76
	Fe	3116·66	3407·46
Molybdenum	Mo	2816·15	2816·15
	Fe	2813·61	2813·61
Vanadium	V	3102·30	3102·30
	Fe	3100·67	3100·67
Copper	Cu	3273·96	3273·96
	Fe	3277·35	3277·35

Details of evaluation methods

Method (a)

A curve as R of Fig. 2 was deduced from readings for the selected iron lines. Duplicate spark spectrograms were prepared for exposure times of 19, 38, 75, and 150 seconds.

Using the eight recommended spark lines from the B.I.S.R.A. Sub-committee's report [8], mean densitometer readings for each exposure-time were plotted against values of log-time, as shown in Fig. 3. The resulting curve fragments were then moved horizontally to link up into a single curve.

In this connection it must be understood that the spark illumination provides an intermittent light source with a frequency of the order of 300–400 sparks per second [13]. Under these conditions, complications from reciprocity failure in connection with the exposure-time scale do not arise.

A table was constructed from the composite curve for conversion of densitometer readings to log I_R values in steps of 0·05 cm.

From the curve it is also possible to deduce log ($I_R \times 10$) and relative intensity values I_R, for the calibrating iron lines, for calibration of the working plates. Values obtained were:—

Fe line	log ($I_R \times 10$)	I_R
2783·696	1·839	6·90
2831·562	1·632	4·29
2793·888	1·146	1·40
2828·634	1·033	1·08
2799·286	1·000	1·00
2827·434	0·645	0·44
2819·337	0·301	0·20
2812·493	0·204	0·16

For "batch calibration" work, the primary conversion table was used throughout. For individual plate calibration the above iron-line log ($I_R \times 10$) values were used to sketch in the individual plate curve. An auxiliary correction table was prepared, indicating the desired correction over various ranges of the primary table, the appropriate correction being added when reading off values from the primary table for the plate in question. This was not found to present any serious difficulty, though fixing the appropriate correction would be expected to be less certain with a curve of this type (R of Fig. 2) than for a straight line relation.

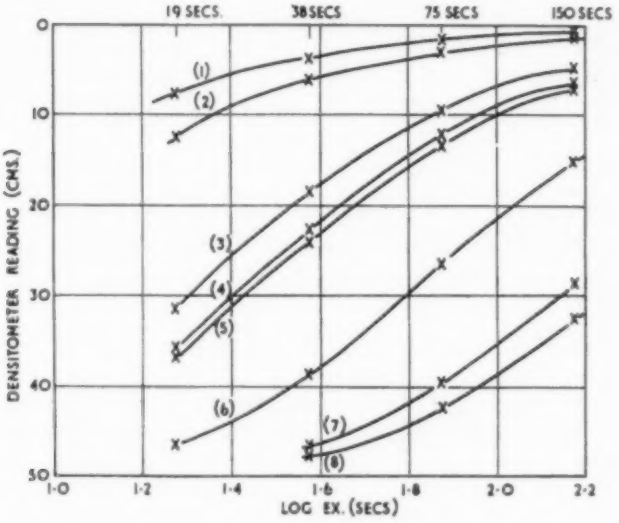

Fig. 3. Derivation of plate-calibration curve from Fe spark lines.
Fe lines used:

(1) 2783·696	(5) 2799·286
(2) 2831·562	(6) 2827·434
(3) 2793·888	(7) 2819·333
(4) 2828·634	(8) 2812·493

Method (b)

The derivation of P values has already been discussed. Since these have a fixed relation to densitometer readings, a single table of conversion values covers all requirements. This can readily be prepared from the Mitchell tables [11]. The working table so produced covered the range 1 cm to 45 cm of a 50-cm densitometer scale in steps of 0·05 cm. To illustrate this, Table 1 summarizes the figures in steps of 1 cm.

From the plate characteristic curve of method (a), values of equivalent log I_R were read at intervals of 2·5 cm on the ordinate scale. These values were used to plot the P/log I_R curve of Fig. 4, which shows the very effective straightening achieved by the P transformation. P curves were then prepared for the working plates from readings given by the standard iron lines, assuming the relative intensity values deduced under method (a). No great differences were found,

Table 1. P values from 1–45 cm of the 50-cm densitometer scale.

cm	P	cm	P	cm	P	cm	P
1	1·695	12	0·561	23	0·204	34	1·920
2	1·389	13	0·520	24	0·177	35	1·893
3	1·208	14	0·481	25	0·150	36	1·864
4	1·078	15	0·445	26	0·125	37	1·889
5	0·977	16	0·412	27	0·100	38	1·809
6	0·893	17	0·379	28	0·072	39	1·779
7	0·822	18	0·348	29	0·047	40	1·747
8	0·757	19	0·317	30	0·024	41	1·714
9	0·701	20	0·287	31	1·999	42	1·679
10	0·650	21	0·259	32	1·973	43	1·640
11	0·605	22	0·231	33	1·947	44	1·597

gamma values for the various plates falling between 0·97 and 1·06 (deduced from P-curve slope, as indicated in Fig. 5). Three working P curves adequately covered the series, and these were employed with a simple calculating board for conversion of ΔP to composition.

Method (c)

This method uses the relation between fractional transmittance (τ) and log-exposure (log E), described by ANDERSON [9] and discussed in the introduction to the present paper.

$$\gamma/S = \frac{\Delta[-f(\tau)]}{\Delta \log E}$$

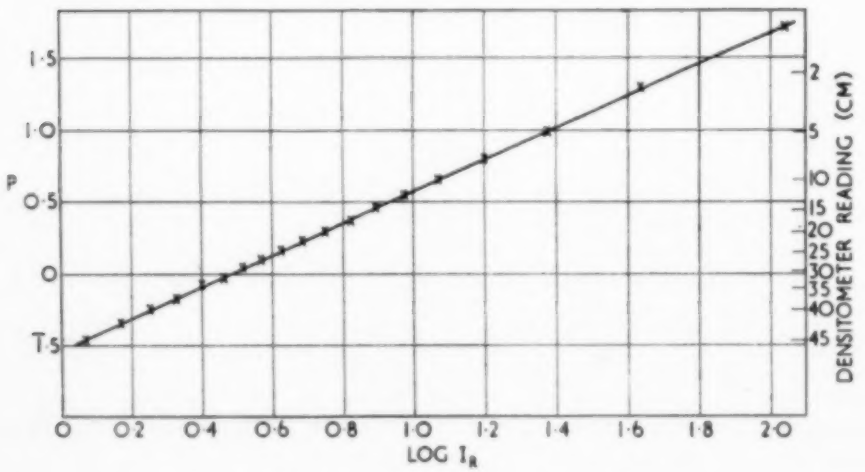

Fig. 4. P/log I_R curve for composition curve plate.

The values of $-f(\tau)$ were taken from ANDERSON's table, adding duplicate values from the 50 cm scale densitometer readings to obtain the required percentage transmittance figures.

Preliminary check of applicability to the plates used was made by determining exposure ratios across a wide density range from the plate-calibration data. Three

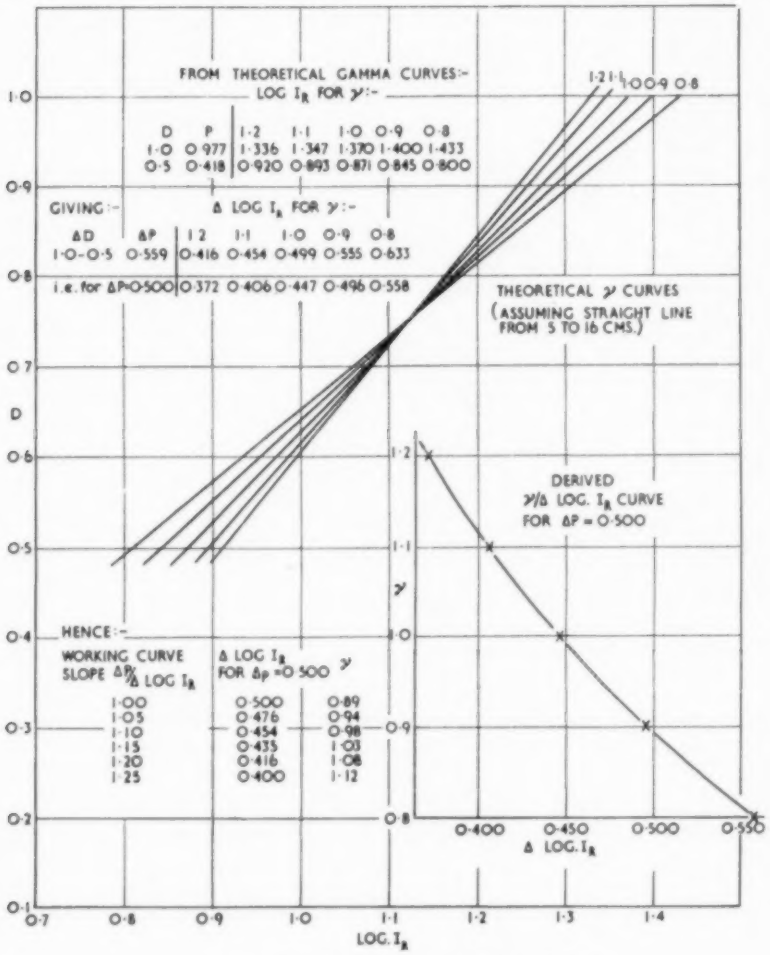

Fig. 5. Relation of slope of $P/\log I_R$ curve to α.

of the standard iron lines were selected, covering a 10/1 intensity range. γ/S was determined for each line by inserting values from the longest and shortest exposures in the above equation. Using these values of γ/S, the process was reversed to calculate intermediate exposure ratios. The results, given in Table 2, show a very satisfactory correspondence.

The relative intensities of the three iron lines were next determined from the

Table 2. Preliminary check on applicability of Anderson table by calculation of exposure ratios*

Fe lines		2831·56	2799·29	2827·43	Mean
Relative intensities, method (a)		4·29	1·00	0·44	—
γ/S from E_{19}–E_{150} (or E_{38}–E_{150})		1·04	1·01	1·00	1·02
Calculated exposure ratios	From E_{38}–E_{19} (i.e., 2·00)	2·09	1·92	too weak	2·00
	From E_{75}–E_{38} (i.e., 1·97)	2·01	2·10	1·93	2·01
	From E_{150}–E_{75} (i.e.,.2·00)	1·93	1·96	2·03	1·97
	Mean (1·99)	2·01	1·99	1·98	—

* Using data from four exposure times from the plate-calibration plate, i.e., 19, 38, 75, and 150 sec, as indicated by E_{19}, etc.

calibration-plate data for 38-, 75-, and 150-sec exposures. Values of γ/S were first determined from the 38- and 150-sec exposures, and the mean γ/S used to calculate relative intensities from the relation

$$\log I_R = S/\gamma \times \Delta[-f(\tau)].$$

The results are given in Table 3, and the relative intensities will be seen to be in close agreement with those taken from the B.I.S.R.A. Sub-committee's report. $\Delta \log I_R$ for the lines 2827·43 and 2831·56 is 1·014, and this value was used to calculate the S/γ for each of the ten working plates. It will be noted that the mean γ for the calibration plate works out at 1·01.

For the purposes of the present study, the working plates were evaluated by means of $\log I_R$/composition curves, using slide-rule conversion of $\Delta[-f(\tau)]$ values to $S/\gamma \times \Delta[-f(\tau)]$. It is evident that, if desired, a series of lines could be drawn for different values of S/γ to permit the use of $-f(\tau)$ values on the calculating board as for method (b), with essentially similar working procedure.

Assessment and consideration of results

Comparison of accuracies is made in Table 4 in terms of coefficient of variation, calculated according to:—

$$\text{C.V.} = \frac{100}{c}\sqrt{\frac{\Sigma d^2}{n}}$$

where c is composition per cent, d indicates difference between spectrographic result and chemical figure, and n is the total number of results, i.e., 50. Values of C.V. were obtained in the case of each element for the three methods, using both batch- and individual-plate calibration.

To assist in drawing broad conclusions, a mean figure for all elements has been included in the table for each procedure. There is indication of an overall improvement of the order of 20 per cent in analytical accuracy (standard errors) as between the original method, using the densitometer reading-log I_R curve with batch-plate

Table 3. Derivation of relative intensity of iron lines used for plate calibration by Anderson method.

Line	Sum of duplicate densitometer readings			$-f(\tau)$			γ*	γ/S	$\log RI = S/\gamma\ \Delta[-f(\tau)]$†				Relative intensities	
	38 sec	75 sec	150 sec	38 sec	75 sec	150 sec			38 sec	75 sec	150 sec	Mean	Found	BISRA report
2827·4	77·8	52·6	30·15	—0·116	0·175	0·483	1·00	1·00	—0·333	—0·368	—0·354	—0·352	0·44	0·44
2799·3 (reference line)	48·5	26·3	14·0	0·224	0·550	0·844	1·03	1·04	0·000	0·000	0·000	—0·000	1·00	1·00
2831·6	12·15	6·0	3·05	0·908	1·220	1·515	1·01	1·02	0·671	0·657	0·658	0·662	4·59	4·62

* $\gamma = \dfrac{S \times \Delta\,[-f(\tau)]}{\Delta \log E}$. Values for the 38- and 150-sec. exposures were used, making $\Delta \log E = 0{\cdot}596$, while the constant S was taken at Anderson's value of 0·993.

† Using $\gamma/S = 1{\cdot}02$.

Table 4. Values of coefficient of variation (C.V.) for the various methods

Sample	Element	Element content per cent				C.V. for batch-plate calibration			C.V. for individual-plate calibration		
		Chemical analysis	Spectro mean (I.P.C.)								
			Method (a)	Method (b)	Method (c)	Method (a)	Method (b)	Method (c)	Method (a)	Method (b)	Method (c)
3	Manganese	0·36	0·36	0·36	0·36	4·6	4·5	4·2	4·3	3·9	3·7
	Nickel	2·92	2·88	2·84	2·86	3·9	3·9	3·7	3·9	3·5	4·0
	Chromium	0·35	0·37	0·36	0·37	6·0	6·2	6·0	5·1	4·8	5·7
	Molybdenum	0·95	0·96	0·95	0·96	3·2	3·3	3·1	2·9	2·1	2·4
	Vanadium	0·22	0·22	0·22	0·22	2·8	2·4	2·1	2·9	2·3	1·7
	Copper	0·50	0·49	0·49	0·48	7·0	5·0	5·1	6·2	4·8	4·7
6	Manganese	1·21	1·23	1·23	1·22	3·1	3·2	2·9	2·9	2·9	2·7
	Nickel	0·18	0·19	0·18	0·18	8·7	6·5	7·9	8·4	7·8	7·4
	Chromium	2·34	2·29	2·31	2·31	2·8	2·5	2·2	2·6	2·3	2·0
	Molybdenum	0·54	0·54	0·54	0·54	2·7	2·8	2·8	2·6	2·2	3·0
	Vanadium	0·36	0·37	0·36	0·36	4·7	4·4	3·4	3·9	2·8	2·8
	Copper	0·23	0·24	0·23	0·23	6·1	3·7	4·9	5·9	4·5	4·5
Mean values (arithmetic) for C.V.						4·6	4·0	4·0	4·3	3·7	3·7

Methods:— (a) Using densitometer reading-log I_R curve.
(b) Using P curve.
(c) Using $-f(r)$ tables.

VOL 7 1955/

calibration, and the newer methods with individual-plate calibration. This improvement may be broken down into roughly two-thirds from change in method and one-third from individual-plate calibration.

There remain questions of speed and ease of working. It is customary in the authors' laboratory to carry out photometric work with two operators; one taking densitometer readings, the other recording, with conversion to $\Delta \log I_R$, P, or $[-f(\tau)]$, according to the method used. The work here is very much the same in the three cases, and no difficulty has been experienced in keeping pace with the normal speed of reading on the densitometer. $\Delta \log I_R$ readings obtained under method (a) are used directly with the composition curves. ΔP or $\Delta[-f(\tau)]$ readings require the use of the calculating board technique, or a slide-rule correction for γ, before reading from the curves. The slide-rule technique requires an extra operation, but it can be carried out very rapidly with a constant initial setting of the slide-rule for any given plate. The general impression is that there is little practical difference in overall speed for the three methods. Personal preference can, therefore, be allowed to decide as to the exclusive use of tables, or the inclusion of slide-rule and calculating-board techniques, without introducing any major differences of speed and ease of working. On the other hand, the straight-line relationships of methods (b) and (c) have obvious advantage in ease of plate calibration, particularly when individual-plate calibration is desired.

VOL. 7 55/56

Conclusions

For routine working with batch calibration, the three methods used have been found generally similar in respect of speed and ease of working. For individual-plate calibration, or where a calculating-board technique is desired, the use of P curves, or the $-f(\tau)$ transmittance table, offers advantage from effective straightening of the plate-response curve for the Ilford thin-film half-tone plates used.

In regard to analytical accuracy, there is indication of an improvement of the order of 20 per cent in standard error from the use of individual-plate calibration with P curves, or $-f(\tau)$ transmittance table, as compared with batch calibration and the densitometer reading-log I_R type of curve. About a third of this improvement resulted from the use of individual as against batch calibration of the plates.

It is considered that no great differences are likely to be found in overall speed or ease of working as between the three methods, but the straight-line relation underlying plate-response calibration by the P and $-f(\tau)$ procedures considerably simplifies this operation.,

Acknouledgements—The authors wish to thank Dr. C. Sykes, F.R.S., Managing Director of Thos. Firth & John Brown Ltd., for permission to publish this paper.

References

[1] Sanders, C.; *J. Soc. Chem. Ind.* 1948 **67** 185.
[2] Argyle, A. and Price, W. J.; *J. Soc. Chem. Ind.* 1948 **67** 187.
[3] (a) Kaiser, H.; *Spectrochimica Acta* 1948 **3** 158–190.
(b) Kaiser, H.; *Spectrochimica Acta* 1951 **4** 351–365.
[4] Churchill, H. V. and Churchill, J. R.; *Ind. and Eng. Chem.* (Anal. Ed.) 1945 **17** 751–754.

[5] King, C.; *J. Opt. Soc. Amer.* 1942 **32** 112–115.
[6] Brommelle, N. S. and Clayton, H. R.; *J. Soc. Chem. Ind.* 1944 **63** 83–89.
[7] Carlsson, C. G.; *Jernkontorets Annaler* 1948 **132** 467–484.
[8] Spectrographic Analysis of Low Alloy Steels. *Iron and Steel Inst. Special Report No.* 47, Sept. 1952.
[9] Anderson, J. W.; *Applied Spectroscopy* 1953 **7** 121–124.
[10] Hughes, H. K. and Murphy, R. W.; *J. Opt. Soc. Amer.* 1949 **39** 501.
[11] The Spectrographic Analysis of Soils, Plants and Related Materials. Mitchell, R. L., Communication No. 44 of Commonwealth Bureau of Soil Science (1948), pp. 172–175.
[12] Shirley, H. T., Elliott, E., and Meeds, J. C.; *J. Iron and Steel Inst.* 1947 **157** 391–409.
[13] Shirley, H. T., Oldfield, A., and Kitchen, H.; *J. Iron and Steel Inst.* 1950 **166** 329–338.

VOL
7
1955/

Spectrochimica Acta, 1956, Vol. 7, pp. 387 to 394. Pergamon Press Ltd., London

Die Infrarot und Ramanspektren hochsymmetrischer Molekule

Mitteilung: Das Infrarotspektrum und die Schwingungsanalyse des Urotropins (1,3,5,7-Tetraazaadamantan)

R. Mecke und H. Spiesecke
Institut für physikalische Chemie der Universität, Freiburg i. Br.

(*Received* 18 *October* 1955)

Abstract—The infra-red spectrum of urotropin (1, 3, 5, 7,-tetra-aza-adamantan) has been recorded from 1–25μ. With the help of published Raman data obtained by other workers an assignment of the vibrational spectrum has been worked out. Four basic vibration frequencies of the inactive forbidden class F_1 have been calculated from combination vibration frequencies.

Angeregt durch eine Zusammenstellung der Verbindungen mit Urotropinstruktur von H. Stetter [1], haben wir damit begonnen, die IR- und Ramanspektren dieser Substanzen zu untersuchen. Dies schien lohnend, da trotz der großen Atomzahl infolge der hohen Symmetrie der Moleküle, übersichtliche Spektren zu erwarten waren.

Wir beginnen diese Reihe mit der Untersuchung des Urotropins ($C_6N_4H_{12}$), dessen IR-Spektrum bisher noch nicht veröffentlicht worden ist. Es kristallisiert in einem kubisch-raumzentrierten Gitter, was bereits auf eine hochsymmetrische Form seiner Molekel schließen läßt. Die sechs C-Atome bilden ein reguläres Oktaeder, während sich die vier N-Atome in den Ecken eines Tetraeders befinden. Das letztere ist so in das Oktaeder eingelagert, daß sich seine Ecken in den Flächenmitten gegenüberliegender Oktaederseiten befinden. Es ensteht so ein Gerüst von vier Sechsringen, die in der Sesselform starr miteinander verbunden sind.* Bereits Decker [2] nannte es die "eigentliche Zelle" des Diamanten.

Die Konstitution wurde von Duden und Scharff [3] aus chemischen Gründen intuitiv erschlossen und später durch zahlreiche Röntgenanalysen bestätigt [4, 5, 6, 7, 8].

Die Anzahl der möglichen Schwingungen berechnet sich bei 22 Atomen zu $3 \times 22 - 6 = 60$. Die hohe Symmetrie und die damit verbundenen Schwingungsentartungen, reduziert ihre Zahl jedoch auf 25 Frequenzen, von denen 7 inaktiv und verboten sind. 18 Banden beobachtet man im Ramaneffekt und 9 im IR-Spektrum. Nach den bekannten Abzählvorschriften [9] erhält man folgende Tabelle, in der die Auswahlregeln und die Aufschlüsselung der Grundschwingungen in Valenz- und Deformationsschwingungen des Molekülskelettes und der CH_2-Gruppen enthalten sind (Tab. 1).

Das Ramanspektrum des Urotropins wurde wiederholt von mehreren Autoren im festen Zustand und in Lösung aufgenommen [10, 11, 12, 13]. Wir beziehen uns in dieser Arbeit hauptsächlich auf die Werte von Couture-Mathieu, Mathieu, und Mitarbeitern [13].

Da in der Symmetriegruppe T_d nur die Schwingungen der Klasse F_2 in

* Die Projektion der Formel in die Ebene verleitet zur Annahme von nur drei Ringen. Diese irrtümliche Auffassung trifft man noch häufig an.

Absorption erlaubt sind, sind im IR-Spektrum vier Skelettschwingungen und fünf Schwingungen der CH_2-Gruppen zu erwarten. Die Aufnahme der Spektren in den verschiedenen Aggregatzuständen bestätigte diese Annahme. Gleichzeitig wurde dadurch bewiesen, daß die Auswahlregeln beim Uebergang vom Gas zur Lösung und zum Festkörper gültig bleiben. Die Rotationsstruktur der Banden

Tabelle 1. Grundschwingungen des Urotropins ($C_6N_4H_{12}$)

T_d			Ring		CH_2-Gruppen					
	Ra	IR	ω	Δ	ν	δ	ρ_1	τ	ρ_2	n
A_1	p	ia	1048	782	2933	(1428)	—	—	—	4
A_2	v	ia	—	—	—	—	—	(?)	—	1
E	dp	ia	1350	460	2914	1455	—	1020	—	5
F_1	v	ia	1315	378	(?)	—	(?)	1078	925	6
F_2	dp	M	1009	672	2890	1462	1372	—	812	9
			1238	511	2967	—	—	—	—	
n	18	9	5	5	5	3	2	3	2	25

im Gasspektrum entspricht der bei einem Kugelkreisel—einem Molekül mit drei gleichen Trägheitsmomenten—zu erwartenden Form mit einem starken Q- und zwei eng anschließenden P- und R-Zweigen. Die Ringvalenzschwingungen fallen durch ihre große Intensität auf. Sie wird durch die Polarität der C-N Bindung bedingt. Die Banden der Gerüstdeformationsschwingungen sind dementsprechend nicht so intensiv, da bei einem derartigen starren Molekülskelett die Deformation des Winkels C-N-C und damit die Aenderung des Dipolmoments der C-N Bindung nur sehr klein ist.

Die niedrigste Skelettdeformationsfrequenz der Klasse F_2 liegt bei 511 cm^{-1}. Sie stimmt mit dem von Couture-Mathieu, Mathieu berechneten Wert überein. Bei 672 cm^{-1} folgt dann die zweite Deformationsschwingung des Molekülskelettes. Eine Gerüstvalenzschwingung liegt bei 1009 cm^{-1}. Größere Schwierigkeiten bereitete die Zuordnung der zweiten Ringvalenzschwingung, da zwischen den Werten 1238 und 1372 cm^{-1} nicht eindeutig entschieden werden konnte. Die Lösung dieser Frage brachte dann das IR-Spektrum des Adamantans ($C_{10}H_{16}$) (Abb. 2) [14]. Beide Verbindungen unterscheiden sich durch den Austausch des Stickstoffs durch isoelektronische CH-Gruppen. Dabei gehen die C-N Bindungen in einfache C-C Bindungen über, deren Kraftkonstante etwas kleiner ist [15]. Dementsprechend muß im Adamantan die Ringvalenzschwingung einen merklich niedrigeren Wert haben, während sich die Werte für die CH_2-Pendelschwingungen in beiden Verbindungen nicht wesentlich unterscheiden werden. Tatsächlich fanden wir beim Adamantan bei 1357 cm^{-1} eine Bande, die nur um 15 cm^{-1} niedriger liegt, als die entsprechende des Urotropins. Eine zweite Bande ist dagegen um 137 cm^{-1}, von 1238 cm^{-1} im Hexamethylentetramin auf 1101 cm^{-1} im Adamantan gefallen, so daß wir mit Sicherheit die Skelettvalenzschwingung der Bande

VOL 7 1955/

bei 1238 cm^{-1} zuordnen können. Die Einordnung der vier restlichen Banden bereitet keinerlei Schwierigkeiten mehr. Sie sind eindeutig den Valenz- (2890, 2967 cm^{-1}), Kipp- (812 cm^{-1}), und Spreizschwingungen (1372, 1462 cm^{-1}) der

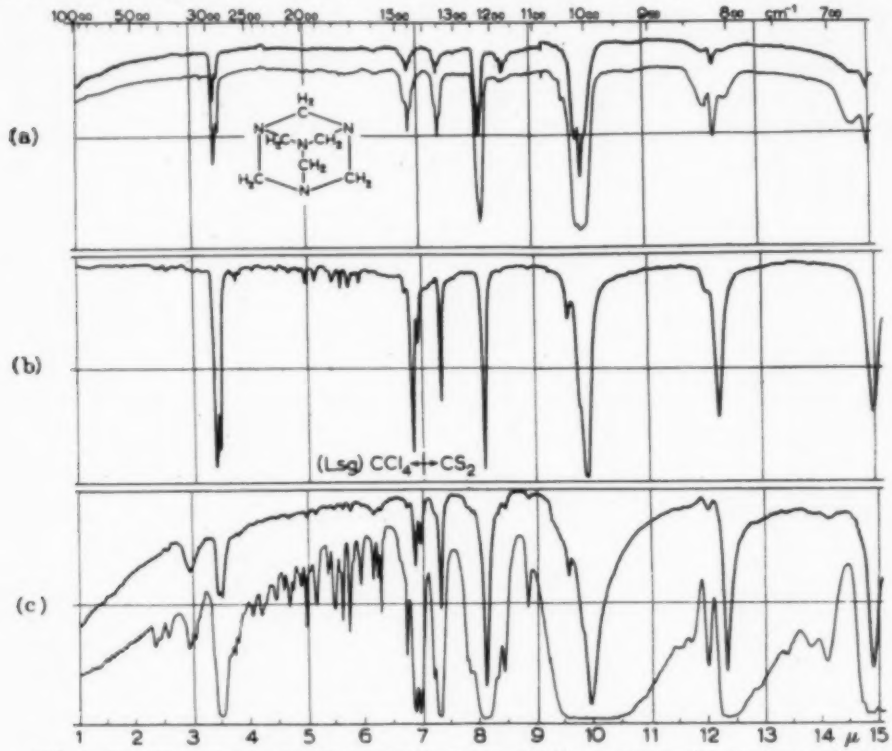

Abb. 1. Das IR-Spektrum des Urotropins in den verschiedenen Aggregatzuständen von 1–25 μ. (a) Gas, (b) Lösung, (c) fest in KBr.

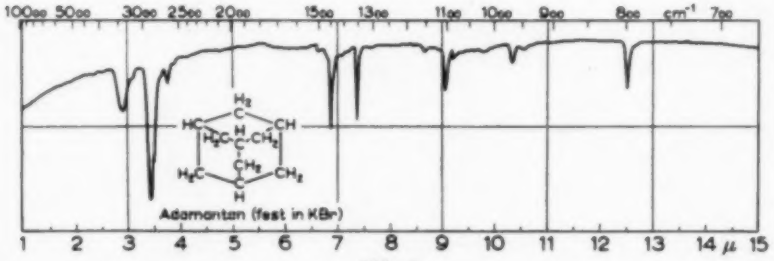

Abb. 2.

Methylengruppen zuzuordnen (siehe Tab. 1). Wir haben es bewußt vermieden, bei den Skelettschwingungen von charakteristischen Frequenzen der C-N Bindung zu reden, da es bei einem solchen kompakten und starren Ringsystem wenig Sinn hat, die Schwingung einer isolierten Bindung zu betrachten. Selbstverständlich sind diese Kopplungskräfte nicht so groß, daß die Banden ihrer Frequenzlage

nach nicht mehr mit den entsprechenden Schwingungen der C-N Gruppe in einfachen Molekülen wie den Methylaminen verglichen werden könnten.

Erhöht man die Konzentration der Lösungen bzw. die Einwaagen in den KBr-Tabletten, so treten im Spektrum eine ganze Anzahl von Kombinationsbanden auf. Um sie zuordnen zu können, haben wir mit den Eigenschwingungen des Moleküls alle möglichen Kombinationen berechnet. Für sie gelten nun ebenfalls gewisse Auswahlregeln, die wir in Tabelle 2 zusammengestellt haben. Alle Kombinationen, die eine Komponente der Symmetrieklasse F_2 enthalten, müssen im Spektrum gesucht werden. Umgekehrt lassen sich so auch inaktive bzw. verbotene Grundschwingungen auffinden.

Tabelle 2. Auswahlregeln der Ober- und Kombinationsschwingungen

$a_1^2 = A_1$	$e^2 = A_1 + E$	$f_1^2 = A_1 + E + F_2$	Oberschwingungen
$a_2^2 = A_2$		$f_2^2 = A_1 + E + F_2$	

	a_1	a_2	e	f_1	f_2
f_2	F_2	F_1	$F_1 + F_2$	$A_2 + E + F_1 + F_2$	$A_1 + E + F_1 + F_2$
f_1	F_1	F_2	$F_1 + F_2$	$A_1 + E + F_1 + F_2$	
e	E	E	$A_1 + A_2 + E$		
a_2	A_2	A_1			
a_1	A_1				

Kombinationsschwingungen

Es gelang uns so, vier Frequenzen der Klasse F_1 rückwärts aus ihren beobachteten Kombinationsbanden zu berechnen. Die Werte 925 und 1315 cm^{-1} sind allerdings ungewiß.

Im Gebiet von 2500–3000 cm^{-1} fanden Kahovec [11] und auch Couture-Mathieu, Mathieu [13] eine Anzahl von Banden mit einem nahezu gleichen Abstand von 40 cm^{-1}, Kahovec nimmt ein Rotationsschwingungsspektrum der CH_2-Gruppen um eine Raumdiagonale des Oktaeders an, während Couture-Mathieu, Mathieu eine Schwingung in Richtung dieser Achse zur Diskussion stellen. Wir neigen dazu, diese Serie allein als eine Folge von Kombinationsbanden anzusehen, nämlich:

ν (Kahovec, Couture)	ν (Verfasser)	Zuordnung
2631 cm^{-1}	2632 cm^{-1}	$2 \times 1315 = 2630$
2650	2652	$1238 + 1428 = 2666$
2698	2695	$1238 + 1455 = 2698$
2738	2744	$2 \times 1372 = 2744$
2786	—	$1315 + 1462 = 2777$
2828	—	$1372 + 1462 = 2834$
2994	—	?

Tabelle 3. Frequenzwerte und Zuordnung des IR- und Ramanspektrums des Urotropins

Gas			Flüssig				Fest			Zuordnung
Wellenzahl	Int	IR	Wellenzahl	Int	IR/Ra	Pol	Wellenzahl	Int	IR/Ra	
—			265	—	Ra	*dp*	—			782 − 511 = 271
—			299	—	Ra	*dp*	—			812 − 511 = 301
—			398	—	Ra	*dp*	—			782 − 378 = 404
—			*456*	9	Ra	*dp*	*465*	8	Ra	E
512	1	IR	*511*	5	IR/Ra	*dp*	*511*	9	IR/Ra	F_2
—			—				630	4	IR	1009 − 378 = 631
669	6	IR	*668*	7	IR/Ra	*dp*	*672*	9	IR/Ra	F_2
—			—				696	*tf*	Ra	
—			—				711	7	IR/Ra	1078 − 378 = 700
—			—				727	6	IR	1238 − 511 = 727
—			—				756	*tf*	Ra	2 × 378 = 756
—			*783*	13	Ra	*p*	*782*	19	Ra	A_1
825	5	IR	*818*	7	IR/Ra	*dp*	*812*	10	IR/Ra	F_2
—			834	1	IR		834	7	IR	460 + 378 = 838
—			—				855	1	IR	1238 − 378 = 860
—			885	1	IR		—			511 + 378 = 889
—			952	f	Ra		—			1462 − 511 = 951
1013	9	IR	*1010*	10	IR/Ra	*dp*	*1009*	10	IR/Ra	F_2
—			1022	*sh*	IR/Ra	*dp*	1020	4	Ra	2 × 511 = 1022
1047	2	IR	1048	4	IR		1048	4	IR	672 + 378 = 1050
—			*1050*	10	Ra	*p*	*1041*	10	Ra	A_1
—			1090	—	Ra	*dp*	1100	*tf*	Ra	1462 − 378 = 1084
—			1129	0	IR		1134	5	IR	672 + 460 = 1132
—			1195	0	IR		1190	7	IR	672 + 511 = 1183
—			—				1206	*sh*	IR	812 + 378 = 1190
1239	10	IR	*1236*	9	IR/Ra	*dp*	*1238*	10	IR/Ra	F_2
—			—				1275	6	IR	460 + 812 = 1272
—			—				1288	6	IR	511 + 782 = 1293
—			—				1307	*tf*	Ra	F_1??
—			*1349*	10	Ra	*dp*	*1354*	7	Ra	E
1364	5	IR	*1364*	6	IR		*1372*	10	IR	F_2
—			—				1397	7	IR	1020 + 378 = 1398
—			—				1428	1	Ra	(E) (A_1)??
—			1440		Ra		1433	*sh*	IR/Ra	511 + 925 = 1436
—			1441	7	IR		1441	9	IR	672 + 782 = 1454
—			*1455*	7	Ra	*dp*	*1454*	7	Ra	E
1466	5	IR	*1462*	8	IR		*1456*	9	IR	F_2
—			1490	0	IR		1490	7	IR	672 + 812 = 1484
—			—				1517	*sh*	IR	1009 + 511 = 1520
—			—				1585	*sh*	IR	1078 + 511 = 1589
—			1603	1	IR		1595	4	IR	782 + 812 = 1594
—			—				1608	2	IR	1238 + 378 = 1616
—			1639	1	IR		1631	2	IR	2 × 812 = 1624
—			1698	1	IR		1692	3	IR	460 + 1238 = 1698
—			1721	4	IR		—			672 + 1048 = 1720
—			—				1730	*sh*	IR	1350 + 378 = 1728
										1372 + 378 = 1750
—			1754	1	IR		1748	6	IR	1238 + 511 = 1749

Tabelle 3 (*continued*)

Gas			Flüssig				Fest			Zuordnung
Wellenzahl	Int	IR	Wellenzahl	Int	IR/Ra	Pol	Wellenzahl	Int	IR/Ra	
—			1789	1	IR		1789	5	IR	1009 + 782 = 1791
—			—				1805	*sh*	IR	1350 + 460 = 1810
—			1838	7	IR		1831	4	IR	1462 + 378 = 1840
—			1862	3	IR		—			511 + 1350 = 1861
										812 + 1048 = 1860
—			—				1873	2	IR	1372 + 511 = 1883
—			—				1945	4	IR	1009 + 925 = 1934
—			1961	1	IR		1957	4	IR	1455 + 511 = 1966
—			1976	1	IR		1986	*tf*	Ra	1462 + 511 = 1973
—			—				1992	0	IR	
—			2024	1	IR		2024	5	IR/Ra	1009 + 1020 = 2029 2 × 1009 = 2018
—			2066	4	IR		2062	2	IR/Ra	1009 + 1048 = 2057
							2075	0	IR	1009 + 1078 = 2087
—			2105	2	IR		—			672 + 1428 = 2100
—			—				2114	1	IR	672 + 1455 = 2127
—			—				2137	*sh*	IR	672 + 1462 = 2134
—			2146	5	IR		2150	3	IR	1372 + 782 = 2154
										1050 + 1078 = 2156
—			2188	3	IR		—			1372 + 812 = 2184
—			2198	0	IR		2193	2	IR	1020 + 1078 = 2198
—			2252	3	IR		2252	*tf*	IR/Ra	1009 + 1238 = 2247
—			2257	1	IR		2268	2	IR	1455 + 812 = 2267
—			2342	0	IR		2347	*sh*	IR	1009 + 1338 = 2353
—			—				2387	3	IR	1009 + 1372 = 2381
—			2481	4	IR		2481	2	IR	2 × 1238 = 2476
—			2494	0	IR		—			1462 + 1020 = 2482
—			2513	1	IR		2513	2	IR	1048 + 1462 = 2510
—			—				2563	*tf*	Ra	1238 + 1315 = 2553
—			2632	5	IR		2631	*f*	Ra	2 × 1315 = 2630
—			—				2652	1	IR/Ra	1428 + 1238 = 2666
—			2688	7	IR		—			1315 + 1372 = 2687
—			2695	1	IR		2695	1	IR/Ra	1238 + 1455 = 2698
—			2732	5	IR		2738	*f*	Ra	2 × 1372 = 2744
							2744	0	IR	
—			—				2828	*tf*	Ra	1462 + 1372 = 2834
2890	3	IR	*2899*	6	IR/Ra	*p*	*2890*	5	IR/Ra	F_2
—			2914	*f*	Ra	*p*	2908	*f*	Ra	1462 + 1455 = 2917
			—				2933		Ra	A_1
2959	4	IR	*2967*	8	IR/Ra	*p*	*2967*	5	IR/Ra	F_2
—			2989		Ra	*dp*	2994	*sh*	IR/Ra	
—			3344	5	IR		3333	2	IR	2890 + 460 = 3350
—			—				3460	3	IR	2967 + 511 = 3478
—			3717	5	IR		—			2890 + 812 = 3702
—			—				3906	*sh*	IR	2890 + 1009 = 3899
—			—				3968	2	IR	2890 + 1078 = 3968
—			3984	4	IR		—			2967 + 1009 = 3976
—			4184	1	IR		4184	1	IR	2933 + 1238 = 4171
—			4292	*sh*	IR		4310	*sh*	IR	2967 + 1350 = 4317
—			—				4386	3	IR	2967 + 1428 = 4395

VOL 7 1955/

VOL. 7
55/56

Tabelle 4. Kombinationshäufigkeit der Grundschwingungen

				ΔR	ΔR	ΔR	ΔR	ΔR	$\rho_2\,CH_2$	ωR	$\tau\,CH_2$	ωR	$\tau\,CH_2$	ωR	ωR	ωR	$\rho_1\,CH_2$	$\delta\,CH_2$	$\delta\,CH_2$	$\delta\,CH_2$
				378	456	511	668	782	812	1009	1020	1050	1078	1238	1315	1350	1372	1428	1455	1462
				F_1	E	F_2	F_2	A_1	F_2	F_2	E	A_1	F_1	F_2	F_1	E	F_2	A_1	E	F_2
F_1	378	v	ia	749																
E	456	dp	ia	834	ia															
F_2	511	dp	M	—	—	1022														
F_2	668	dp	M	1048	1134	1190	—													
A_1	782	p	ia	v	ia	1288	1456	ia												
F_2	812	dp	M	1190	1275	—	1490	1595	1631											
F_2	1009	dp	M	1391	1462	1511	—	1789	1831	2024										
E	1020	dp	ia	1391	—	—	1692	1799	1831	2024	ia									
A_1	1050	p	ia	v	ia	—	1721	ia	1873	2062	ia	ia								
F_1	1078	v	ia	1456	—	1595	1748	v	—	—	—	2150	2150							
F_2	1238	dp	M	1608	1692	1748	—	2024	2062	2252	2252	2294	—	2481						
F_1	1315	v	ia	1692	—	1831	1992	—	2137	—	2347	—	2387	—	—					
E	1350	dp	ia	1730	ia	1873	2024	2137	2164	2358	—	—	—	—	2652	ia				
F_2	1372	dp	M	1748	1831	1873	2024	2150	2193	2387	2387	—	—	—	2695	—	2747			
A_1	1428	p	ia	v	ia	1945	2193	ia	2252	—	—	v	2513	—	v	ia	—	v		
E	1455	dp	ia	1831	ia	1957	2114	ia	2286	—	2481	2513	—	2695	—	ia	—	ia	ia	
F_2	1462	dp	M	1831	—	—	2137	2252	2294	2481	2481	2513	—	2695	—	—	—	—	—	—

Eine vollständige Aufklärung dürfte erst die (restlose) Festlegung aller F_1-Frequenzen bringen. Wir untersuchen z. Zt. Additionsverbindungen des Urotropins mit den Halogenen und den Halogenwasserstoffsäuren. Diese Verbindungen besitzen niedrigere Symmetrie. Die entarteten Schwingungen des Hexamethylentetramins müssen daher in zwei bzw. drei Komponenten aufspalten. Sind alle im IR-Spektrum erlaubt, so kann man auch die verbotenen Banden der Klasse F_1 beobachten.

In Tabelle 3 haben wir unsere IR Messungen mit den Ramanwerten von COUTURE-MATHIEU, MATHIEU (s.o.) und KAHOVEC (s.o.) zusammengestellt. Tabelle 4 soll über die "Kombinationsfreudigkeit" der einzelnen Grundschwingungen Auskunft erteilen. Sie enthält die gefundenen Werte, ohne Wiederholungen auszuschließen.

Experimentelles—Die Spektren wurden mit einem Doppelstrahlgerät Perkin Elmer Mod. 21 mit NaCl- und KBr-Prisma aufgenommen. Als Untersuchungsmaterial diente uns Urotropin p.a. der Firma E. Merck, Darmstadt. Beim Gasspektrum zeigte sich überraschenderweise, daß Urotropin bis 220°C thermisch völlig stabil ist. Die Zersetzungsprodukte, NH_3 und CH_2O, hätten sich an Hand ihres Spektrums leicht nachweisen lassen.

Zusammenfassung

Das IR-Spektrum des Urotropins (1,3,5,7-Tetraazaadamantan) wurde von 1–25 μ aufgenommen. Unter Benutzung der von Couture-Mathieu, Mathieu, und Mitarbeitern veröffentlichten Ramanwerte wurde eine Zuordnung des Schwingungsspektrums gegeben. Aus Kombinationsschwingungen wurden vier Grundschwingungen der inaktiven und verbotenen Klasse F_1 berechnet.

Literatur

[1] STETTER, H.; *Z. angew. Chem.*, 1954, **66**, 217.
[2] DECKER, H.; *Z. angew. Chem.*, 1924, **37**, 795.
[3] DUDEN, P., and SCHARFF, M.; *Liebigs Ann. Chem.*, 1895, **288**, 218.
[4] DICKINSON, R. G., and RAYMOND, A. L.; *J. Amer. chem. Soc.*, 1922, **45**, 22.
[5] GONNELL, MARK; *Z. phys. Chem.*, 1923, **107**, 181.
[6] WYCKOFF, R. W. G., and COREY, R. B.; *Z. Krist.*, 1934, **89**, 462.
[7] GRIMM, H. G.; *Naturwissenschaften*, 1939, **27**, 1.
[8] SHAFFER, P. A., JR.; *J. Amer. chem. Soc.*, 1947, **69**, 1557.
[9] HERZBERG, G.; *Infrared and Ramanspectra of Polyatomic Molecules*. Vol. II, 126ff, New York, 1945.
[10] KRISHNAMURTI, P.; *Ind. J. Phys.*, 1931, **6**, 309.
[11] KAHOVEC, L., KOHLRAUSCH, K. W. F., REITZ, A. W., und WAGNER, J.; *Z. phys. Chem.*, 1938, **39B**, 431.
[12] SUNANDA BAI, K.; *Proc. Ind. Acad. Sci.*, 1944, **20**, 71.
[13] COUTURE-MATHIEU, L., MATHIEU, J. P., CREMER, J., und POULET, H.; *J. Chim. Phys.*, 1951, tome **48**, Nos. 1–2.
[14] MECKE, R., und SPIESECKE, H.; *Chem. Berichte* 1955, **88**, 1997-2002
[15] KOHLRAUSCH, K. W. F.; *Der Smekal-Ramaneffekt*, Berlin 1931 und 1938.

Spectrochimica Acta, 1956, Vol. 7, pp. 395 and 397. Pergamon Press Ltd., London

SPECTROCHEMICAL NOTES

Determination of tin in bismuth

ILANA LEVITAN
Weizmann Institute of Science, Rehovoth, Israel

(*Received* 10 *October* 1955)

Abstract—A method is described for the determination of 0·01 to 1·00 per cent of tin in bismuth. Analyses may be carried out with samples as small as 0·02 g.

VOL. 7 55/56

Introduction

A RELIABLE and rapid method for the determination of tin in bismuth was called for in connection with studies of conductivity and galvanomagnetic effects in single crystals of bismuth-tin. The crystals were prepared in the Solid State Laboratory of the Weizmann Institute. They took the form of rods, normally about 1 mm diameter by 5 mm in length, but occasionally only half this size.

The range of concentrations of interest was from 0·01 to 1·00 per cent of tin in bismuth. RAIKHBAUM [1] has reported on the analysis of lead-bismuth-tin alloys. His method involved total combustion of the sample in a d.c. arc, and gave satisfactory results for concentrations of tin between 3 and 97 per cent in the alloy. However, the method is not applicable to alloys containing a very small tin content.

Experimental

The spectrum was excited by a high-voltage condensed spark with the sample supported on a 6·5-mm diameter graphite electrode. Considerable attention had to be paid to the form of the latter. If the electrode had the usual shape of a shallow cup, it was found that the force of the discharge ejected the specimen before it had properly melted. If, on the other hand, the specimen were placed in a deep cup in order to avoid this, it would not melt, and the spectrum would not appear. Accordingly for each individual sample a separate electrode was prepared, having a shallow cylindrical recess of a diameter slightly less than the length of the crystal. The latter was then placed horizontally on the electrode and forced into the recess by applying pressure. By these means it was held firmly until fused by the discharge. The counter electrodes were of the same diameter, 6·5 mm, and pointed. The spark-gap was 4 mm. The exposures were 20 sec in duration. Samples melted in as little as one second after the initiation of the discharge, and accordingly exposures were made without preliminary sparking.

Standards were prepared from spectroscopically pure bismuth and tin. The metals were placed in small pyrex tubes and fused in an induction furnace. In order to assure a homogeneous alloy and to avoid crystallization, the specimen was agitated vigorously during the entire period of fusion and resolidification. The process was carried out in vacuum to avoid oxidation.

A satisfactory pair of analysis lines was found to be Sn-3034·12 Å and Bi-3034·87 Å.

The lines were of equal intensity for an alloy containing about 0·14 per cent tin, under the experimental conditions used. This value fell neatly within the range of concentrations of interest to us. The plate calibration was carried out with a six-step neutral filter. A working curve is shown in Fig. 1.

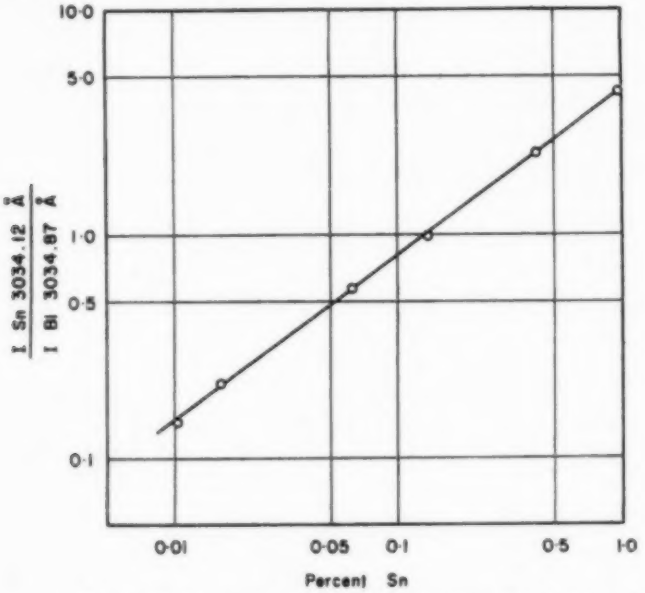

Fig. 1. Working curve for the determination of tin in bismuth.

The principal items of the equipment were as follows:
Source: ARL spark unit Model 4.
Spectrograph: Hilger E-478 Littrow, with quartz prism.
Photographic plate: Ilford ordinary.

Reference

[1] Raikhbaum, Ya. D.; *Zavodskaya Lab.* 1939, **8** 1101.

Eine Kapillarelektrode aus Metall zur direkten, spektrochemischen Untersuchung von Lösungen

H. J. Eichhoff und K. Picard*
Anorganisch-Chemisches Institut der Universität Mainz

Abstract—Description of a simple arrangement of metal electrodes for direct spectrochemical investigations of solutions.

Die direkte, spektrochemische Untersuchung von Lösungen mit relativ hohem Salzgehalt durch Eindampfen eines Lösungsvolumens auf einer Metallelektrode und anschliessende Anregung im Funken, Abreissbogen oder Dauerbogen stösst im allgemeinen auf Schwierigkeiten, da die entstandenen Salzkrusten nicht fest auf den Elektroden haften und bei der

* This paper was completed in 1953, but has been withheld until now, for technical reasons

VOL
7
1955/

VOL.
7
55/56

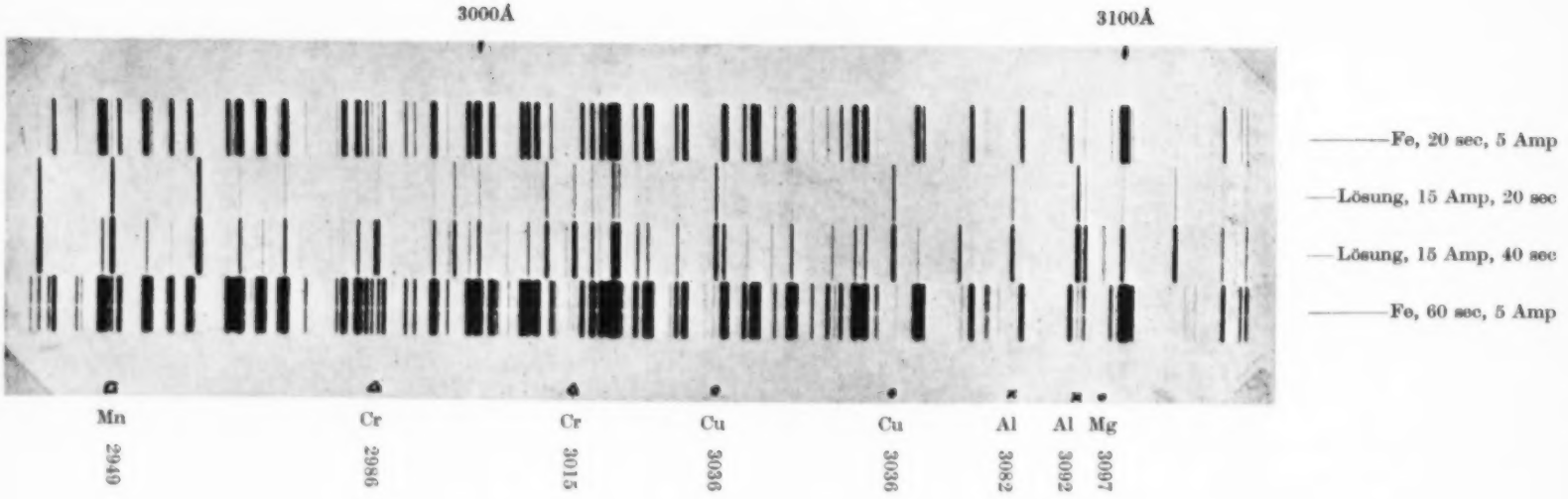
3000Å
3100Å
Fe, 20 sec, 5 Amp
Lösung, 15 Amp, 20 sec
Lösung, 15 Amp, 40 sec
Fe, 60 sec, 5 Amp
Mn 2949
Cr 2986
Cr 3015
Cu 3036
Cu 3036
Al 3082
Al 3092
Mg 3097

VOL.
7
1955/5

Anregung abspringen. Die "Porous Cup"-Methode [1] kann in manchen Fällen den schwerwiegenden Nachteil haben, dass die auftretenden Cyanbanden das Spektrum stören. Die im Folgenden beschriebene Kapillarelektrode, welche zur Bestimmung von Rubidium mit der Linie 4201,8 Å in Alkalichloridlösungen verwendet wurde, vermeidet diese Nachteile und wird sich in manchen Fällen mit Vorteil verwenden lassen.

Abb. 1

In Abb. 1 ist die Elektrodenanordnung schematisch dargestellt. Ein Cu-Stab von 5 mm Durchmesser (an Stelle von Cu kann auch ein anderes, geeignetes Elektrodenmetall verwendet werden) mit runder Kuppe wird mit einer etwa 10 mm tiefen, zentralen Bohrung von 0,7 mm Durchmesser versehen und erhält entsprechend Abb. 1 eine unter etwa 60° zur Elektrodenachse verlaufende Bohrung von 1,5 mm Durchmesser, in welche die zu untersuchende Losung mit einer Kapillarpipette eingefüllt wird. Durch Absaugen der Lösung mit einem Filtrierpapierstreifen von der Kuppe her lässt sich die Kapillare leicht blasenfrei füllen. Die Gegenelektrode, aus einem gleichen Cu-Stab gefertigt, trägt eine unter etwa 60° verlaufende Spitze, welche genau auf die Kapillare zentriert wird. Der Elektrodenabstand beträgt 2 mm. Zur Kühlung wird die Kapillarelektrode in ein mit Wasser von Zimmertemperatur gefülltes Rohr von 10–20 cm^3 Inhalt eingesetzt. Die Anregung erfolgt im Wechselstrom-Abreissbogen mit Hochfrequenzzündung nach *Pfeilsticker* bei einer Kurzschlussstromstärke von 10 A, einer Zündzahl von 1/sec und einem Brennrythmus von 1 : 3 [2]. Durch ein Nachfüllen des Lösungsvorrates in der Kapillarelektrode nach 25–30 Zündungen wird dafür gesorgt, dass die Kapillare selbst stets vollständig mit Lösung gefüllt ist. Die Entladung erfolgt sehr gleichmässig ohne ein störendes Verspritzen der Lösung. Der P_H-Wert der Lösungen wird durch Zugabe von Säure auf 3 gebracht, da die Intensitätsverhältnisse in der Nähe des Neutralpunktes P_H-abhängig sind.

Bei 3 Parallelbestimmungen und Verwendung einer geeigneten Vergleichslinie lassen sich mit der angegebenen Methode Intensitätsverhältnisse auf $\pm$5–10% genau messen, wie an den Linienpaaren Rb^I4201,8 In^I4101,7 in Alkalichloridlösungen, enthaltend etwa 24 mg Na, 120 mg K, 4 mg Cs, 4 mg Rb, und 0,08 mg In (als $In_2(SO_4)_3$) pro cm^3, und an den Linienpaaren Mn^{II}2576, 1–2593, 7–2605, 7/Cr^{II}2835,6; Mg^{II}2795,5–2802,7/Mn^{II}2605,7; Mg^I2852,1/Al^I3082,2; Cr^{II}2835,6–2849,8/Mg^{II}2802,7 in einer Lösung, enthaltend pro cm^3 je 2 mg Cr, Fe, Mg, Al, und Mn, festgestellt wurde.

In Abb. 2 wird ein Spektrum der letztgenannten Lösung wiedergegeben, das bei einem Öffnungsverhältnis des Spektrographen von 1 : 50 auf Perutz-Silbereosin-Platte (12/10 DIN) aufgenommen wurde. Bis auf schwache OH-Banden bei 3063 Å sind die Spektren frei von Untergrund.

Herrn Prof. Dr. F. Strassmann danken wir für die Möglichkeit zur Durchführung dieser Untersuchung, der deutschen Forschungsgemeinschaft für die Zuteilung von ERP-Mitteln zur Anschaffung der optischen Ausrüstung.

Literatur

[1] Feldman, Cyrus *Analyt. Chem.*, 1949 **21** 1041-1046.
[2] Kaiser, H., und Sohm M. *Spectrochim. Acta*, 1944 **2** 81-91.

Book review

A. MAYER and W. J. PRICE: **Chemical and Spectrographic Analysis of Magnesium and Its Alloys**, Magnesium Elektron Ltd. London, 1954. 63/-

THIS book at once attracts attention by its open recognition of the continuous development of analytical methods, in that it has been published in loose-leaf binding, with a promise of supplements to follow included in the original price.

About one-third of its pages deal with spectrographic methods; and besides dealing thoroughly with the estimation of every possible element in magnesium alloys, they include a brief and practical description of apparatus, photographic technique, photometric procedures, and the statistical evaluation of results. Except for the section on apparatus, it is all adequate as a textbook for the beginner in routine metallurgical analysis; and the whole book will be essential to every analyst of magnesium alloys.

ERNEST VAN SOMEREN

ANNOUNCEMENT

Notices of Meetings

FROM the U.S.A. we hear that the Society for Applied Spectroscopy is planning meetings in New York in 1956 on January 3, February 7, March 6, April 3, and May 1; details may be obtained from C. A. JEDLICKA, c/o Lucius Pitkin Inc., 47 Fulton Street, New York 38, N.Y. The Philadelphia section will meet on January 17, March 20, and April 17; details from E. D. HALLER, c/o Arthur H. Thomas Co., P.O. Box 779, Philadelphia 5, Pa.

In Memoriam

Franz Xaver Mayer

IN September 1955 we lost our friend and colleague Dr. Franz Mayer, who died in Vienna at the age of fifty-one. Most of us did not know him as a professor of the University of Vienna, but as the moving spirit of the Spectroscopic and Colorimetric Group of the Austrian Association of Chemists. His interest in spectroscopy developed out of his studies in organic chemistry and forensic medicine, and he took part in the second, third, and fourth International Spectroscopy Colloquia; the fifth Colloquium owed its special success to his devotion and leadership, and the summary of its proceedings which he edited is evidence of his wide knowledge of spectroscopy and all its applications. Many of our readers will mourn the loss to Austria, or rather to Europe, by his death.

E. v. S.

VOL.
7
55/56